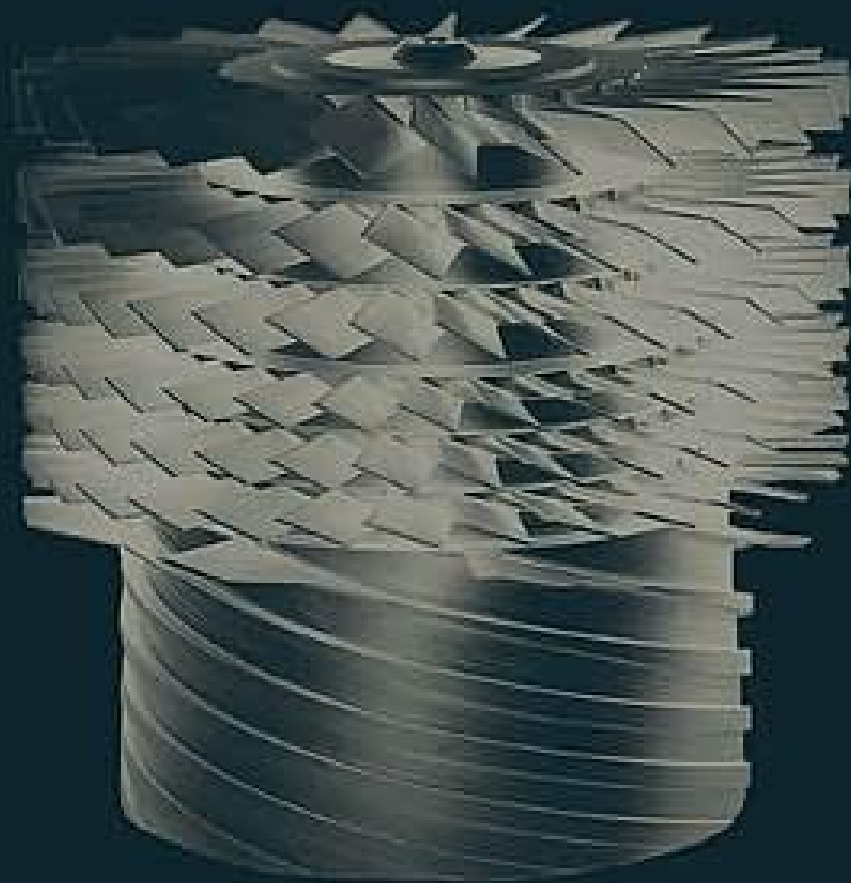


A User's Guide to Vacuum Technology

Third Edition

John F. O'Hanlon



A User's Guide to Vacuum Technology

Third Edition

A User's Guide to Vacuum Technology

Third Edition

John F. O'Hanlon

**Professor Emeritus of Electrical and Computer Engineering
The University of Arizona**



A JOHN WILEY & SONS, INC., PUBLICATION

Copyright © 2003 by John Wiley & Sons, Inc. All rights reserved.

Published by John Wiley & Sons, Inc., Hoboken, New Jersey.

Published simultaneously in Canada.

No part of this publication may be reproduced, stored in a retrieval system or transmitted in any form or by any means, electronic, mechanical, photocopying, recording, scanning or otherwise, except as permitted under Section 107 or 108 of the 1976 United States Copyright Act, without either the prior written permission of the Publisher, or authorization through payment of the appropriate per-copy fee to the Copyright Clearance Center, Inc., 222 Rosewood Drive, Danvers, MA 01923, (978) 750-8400, fax (978) 750-4470, or on the web at www.copyright.com. Requests to the Publisher for permission should be addressed to the Permissions Department, John Wiley & Sons, Inc., 111 River Street, Hoboken, NJ 07030, (201) 748-6011, fax (201) 748-6008, e-mail: permreq@wiley.com.

Limit of Liability/Disclaimer of Warranty: While the publisher and author have used their best efforts in preparing this book, they make no representation or warranties with respect to the accuracy or completeness of the contents of this book and specifically disclaim any implied warranties of merchantability or fitness for a particular purpose. No warranty may be created or extended by sales representatives or written sales materials. The advice and strategies contained herein may not be suitable for your situation. You should consult with a professional where appropriate. Neither the publisher nor author shall be liable for any loss of profit or any other commercial damages, including but not limited to special, incidental, consequential, or other damages.

For general information on our other products and services please contact our Customer Care Department within the U.S. at 877-762-2974, outside the U.S. at 317-572-3993 or fax 317-572-4002.

Wiley also publishes its books in a variety of electronic formats. Some content that appears in print, however, may not be available in electronic format.

Library of Congress Cataloging-in-Publication Data:

Library of Congress Cataloging-In-Publication Data is available:
0-471-27052-0

Printed in the United States of America.

10 9 8 7 6 5 4 3 2 1

For Jean, Carol, Paul, and Amanda

Preface

This book is intended for the vacuum system user—the university student, technician, engineer, manager, or scientist—who wishes a fundamental understanding of modern vacuum technology and a user's perspective of modern laboratory and industrial vacuum technology.

Vacuum technology is largely secondary; it forms part of other technologies that are central to analysis, research, development, and manufacturing. It is used to provide a process environment. Many advances in vacuum technique have resulted from the demands of other technologies, although scientists and engineers have studied vacuum for its own sake. The average user is process-oriented and becomes immersed in vacuum technique only when problems develop with a process or when new equipment purchases become necessary.

A *User's Guide to Vacuum Technology, 3rd Edition* focuses on the operation, understanding, and selection of equipment for processes used in semiconductor, optics, and related technologies. It emphasizes subjects not adequately covered elsewhere, while avoiding in-depth treatments of topics interesting only to the designer or curator. Residual gas analysis is an important topic whose treatment differs from the usual explanation of mass filter theory. Components such as the turbomolecular and helium gas refrigerator cryogenic pumps are now widely used but not well understood. The discussion of gauges, pumps, and materials is a prelude to the central discussion of systems. System designs are grouped according to their function. Current designs are either single-chamber or multichamber; the details of each design are determined by the requirements of an industrial or research application.

In this edition, the discussion of gauges, pumps, and materials has been updated, where relevant, to reflect changes in practice. Spinning rotor gauges are no longer a laboratory curiosity. Ultrahigh vacuum gauges, though limited in their availability, will be a necessity in next-generation production deposition systems. Ultraclean, low dead volume metrology and valves, along with superior materials and cleaning techniques, have made contamination-free manufacturing a reality.

Ultraclean vacuum, once the domain of the researcher, is now routinely used for high-volume production of semiconductor chips and storage

media. However, methodologies for reaching low pressures in a clean manner have changed significantly. No longer are single-chamber systems baked for twenty-four hours. Rather, cassette-based load/unload chambers serve as high-volume interfaces between atmosphere and ultraclean process chambers. These chambers, which can be accessed in serial or random order, are only exposed to atmosphere during maintenance.

Large, efficient multichamber medium and highvacuum systems are used in high-speed coating of numerous consumer products such as window glass, solar cells, video tape, printer paper, eyeglass lenses, automobile headlamps, plastic films and security devices.

The gap in knowledge and training between those who manufacture and those who use vacuum equipment continues to widen. It is from this perspective that the previous edition of this book has been revised. Important formulas have been denoted with a ► for emphasis. Easy questions have been emphasized with a †.

Thanks are due to countless researchers who, individually and collaboratively, have advanced this field by creative solutions to real problems; I also thank Dr. Bruce Kendall for his insightful comments and thoughtful review.

J. F. O'Hanlon

Tucson, Arizona

Contents

ITS BASIS

1. Vacuum Technology	3
1.1 Units of Measurement	6
References	8
2. Gas Properties	9
2.1 Kinetic Picture of a Gas	9
2.1.1 Velocity Distribution	10
2.1.2 Energy Distribution	11
2.1.3 Mean Free Path	12
2.1.4 Particle Flux	13
2.1.5 Monolayer Formation Time	14
2.1.6 Pressure	14
2.2 Gas Laws	15
2.2.1 Boyle's Law	15
2.2.2 Amonton's Law	16
2.2.3 Charles' Law	16
2.2.4 Dalton's Law	16
2.2.5 Avogadro's Law	16
2.2.6 Graham's Law	17
2.3 Elementary Gas Transport Phenomena	18
2.3.1 Viscosity	18
2.3.2 Thermal Conductivity	20
2.3.3 Diffusion	21
2.3.4 Thermal Transpiration	22
References	23
Problems	24
3. Gas Flow	25
3.1 Flow Regimes	25
3.2 Throughput, Mass Flow, and Conductance	27
3.3 Continuum Flow	28
3.3.1 Orifices	29
3.3.2 Long Round Tubes	30

3.3.3	Short Round Tubes	32
3.4	Molecular Flow	32
3.4.1	Orifices	33
3.4.2	Long Round Tubes	34
3.4.3	Short Round Tubes	34
3.4.4	Other Short Structure Solutions	36
	Analytical Solutions	37
	Monte Carlo Technique	38
3.4.5	Combining Molecular Conductances	39
	Parallel Conductances	39
	Series Conductances	39
	Exit and Entrance Effects	44
	Series Calculations	45
3.5	The Transition Region	49
3.6	Models Spanning Several Pressure Regions	50
3.7	Summary of Flow Regimes	51
	References	52
	Problems	53

4. Gas Release from Solids

57

4.1	Vaporization	57
4.2	Diffusion	58
4.2.1	Reduction of Outdiffusion by Vacuum Baking	60
4.3	Thermal Desorption	61
4.3.1	Desorption Without Readsorption	62
	Zero-Order Desorption	62
	First-Order Desorption	62
	Second-Order Desorption	63
4.3.2	Desorption from Real Surfaces	65
	Outgassing Measurements	65
	Outgassing Models	67
	Reduction of Outgassing by Baking	68
4.4	Stimulated Desorption	70
4.4.1	Electron-Stimulated Desorption	70
4.4.2	Ion-Stimulated Desorption	70
4.4.3	Stimulated Chemical Reactions	70
4.4.4	Photodesorption	71
4.5	Permeation	71
4.5.1	Molecular Permeation	71
4.5.2	Dissociative Permeation	73
4.5.3	Permeation and Outgassing Units	73
4.6	Pressure Limits	74
	References	77
	Problems	77

MEASUREMENT

5. Pressure Gauges	81
5.1 Direct-Reading Gauges	81
5.1.1 Diaphragm and Bourdon Gauges	82
5.1.2 Capacitance Manometers	83
5.2 Indirect-Reading Gauges	87
5.2.1 Thermal Conductivity Gauges	87
Pirani Gauge	88
Thermocouple Gauge	91
Stability and Calibration	92
5.2.2 Spinning Rotor Gauge	92
5.2.3 Ionization Gauges	94
Hot Cathode Gauges	94
Hot Cathode Gauge Errors	100
Cold Cathode Gauge	103
Gauge Calibration	104
References	105
Problems	106
 6. Flow Meters	 109
6.1 Molar Flow, Mass Flow, and Throughput	109
6.2 Rotameters and Chokes	112
6.3 Differential Pressure Techniques	114
6.4 Thermal Mass Flow Meter Technique	115
6.4.1 Mass Flow Meter	115
6.4.2 Mass Flow Controller	120
6.4.3 Mass Flow Meter Calibration	120
References	121
Problems	121
 7. Pumping Speed	 123
7.1 Pumping Speed	123
7.2 Mechanical Pumps	124
7.3 High Vacuum Pumps	125
7.3.1 Measurement Techniques	125
Pump Dependence	126
Measurement of Water Vapor Pumping Speed	126
Pumping Speed at the Chamber	127
7.3.2 Measurement Error	128
References	130
Problems	130

8. Residual Gas Analyzers	133
8.1 Instrument Description	133
8.1.1 Ion Sources	134
Open Ion Sources	135
Closed Ion Sources	136
8.1.2 Mass Filters	139
Magnetic Sector	139
RF Quadrupole	141
Resolving Power	145
8.1.3 Detectors	145
Discrete Dynode Electron Multiplier	147
Continuous Dynode Electron Multiplier	148
8.2 Installation and Operation	150
8.2.1 High Vacuum Operation	150
Mounting	150
Stability	151
8.2.2 Medium and Low Vacuum Sampling	153
Differentially Pumped Sampling	153
Miniature Quadrupoles	156
8.3 RGA Calibration	156
8.4 RGA Selection	158
References	159
Problems	160
9. Interpretation of RGA Data	161
9.1 Cracking Patterns	161
9.1.1 Dissociative Ionization	161
9.1.2 Isotopes	162
9.1.3 Multiple Ionization	163
9.1.4 Combined Effects	163
9.1.5 Ion Molecule Reactions	165
9.2 Qualitative Analysis	166
9.3 Quantitative Analysis	172
9.3.1 Isolated Spectra	172
9.3.2 Overlapping Spectra	173
References	177
Problems	178
PRODUCTION	
10. Mechanical Pumps	183
10.1 Rotary Vane Pump	183
10.2 Rotary Piston Pump	187

10.3 Lobe Pump	189
10.4 Claw Pump	193
10.5 Scroll Pump	194
10.6 Screw Pump	195
10.7 Diaphragm Pump	196
10.8 Mechanical Pump Operation	198
References	199
Problems	199
11. Turbomolecular Pumps	201
11.1 Pumping Mechanism	201
11.2 Speed-compression Relations	203
11.2.1 Maximum Compression Ratio	203
11.2.2 Maximum Speed	206
11.2.3 General Relation	207
11.3 Ultimate Pressure	209
11.4 Turbomolecular Pump Designs	210
11.5 Turbomolecular Drag Pumps	213
References	214
Problems	215
12. Diffusion Pumps	217
12.1 Pumping Mechanism	217
12.2 Speed-Throughput Characteristics	219
12.3 Boiler Heating Effects	223
12.4 Backstreaming, Baffles, and Traps	224
References	227
Problems	228
13. Pump Fluids	229
13.1 Fluid Properties	229
13.1.1 Vapor Pressure	229
13.2.2 Other Properties	233
13.2 Pump Fluid Types	234
13.2.1 Mineral Oils	234
13.2.2 Synthetic Fluids	235
Esters	236
Silicones	236
Ethers	237
Fluorochemicals	237
13.3 Fluid Selection	238
13.3.1 Rotary Vane, Piston, and Lobe Pumps	238
13.3.2 Turbomolecular Pumps	240

13.3.3	Diffusion Pumps	241
13.4	Reclamation	244
	References	244
	Problems	245
14.	Getter and Ion Pumps	247
14.1	Getter Pumps	247
14.1.1	Titanium Sublimation Pumps	248
14.1.2	Nonevaporable Getter	258
14.2	Ion Pumps	256
	References	260
	Problems	261
15.	Cryogenic Pumps	263
15.1	Pumping Mechanisms	264
15.2	Speed, Pressure, and Saturation	267
15.3	Refrigeration Techniques	271
15.4	Cryogenic Pump Characteristics	276
15.4.1	Medium Vacuum Sorption Pumps	276
15.4.2	High Vacuum Gas Refrigerator Pumps	279
15.4.3	High Vacuum Liquid Pumps	283
	References	284
	Problems	286
MATERIALS		
16.	Materials in Vacuum	289
16.1	Metals	290
16.1.1	Vaporization	290
16.1.2	Permeability	290
16.1.3	Outgassing	291
	Dissolved Gas	292
	Surface and Near-Surface Gas	295
16.1.4	Structural Metals	299
16.2	Glasses and Ceramics	300
16.3	Polymers	306
	References	309
	Problems	311
17.	Joints, Seals, and Valves	313
17.1	Permanent Joints	313
17.1.1	Welding	314
17.1.2	Soldering and Brazing	318

- 17.1.3 Joining Glasses and Ceramics 319
- 17.2 Demountable Joints 321
 - 17.2.1 Elastomer Seals 322
 - 17.2.2 Metal Gaskets 328
- 17.3 Valves and Motion Feedthroughs 329
 - 17.3.1 Small Valves 330
 - 17.3.2 Large Valves 332
 - 17.3.3 Special Purpose Valves 335
 - 17.3.4 Motion Feedthroughs 337
- References 341
- Problems 342

18. Lubrication 345

- 18.1 Lubrication Processes 345
- 18.2 Rheology 347
 - 18.2.1 Absolute Viscosity 347
 - 18.2.2 Kinematic Viscosity 348
 - 18.2.3 Viscosity Index 348
- 18.3 Lubrication Techniques 349
 - 18.3.1 Liquid Lubrication 349
 - 18.3.2 Grease Lubrication 352
 - 18.3.3 Dry Lubrication 353
- References 355
- Problems 356

SYSTEMS

19. Rough Vacuum Pumping 359

- 19.1 Pumping Rate 360
 - 19.1.1 Pump Size 360
 - 19.1.2 Aerosol Formation 362
- 19.2 Crossover 365
 - 19.2.1 Oil Backstreaming 366
 - 19.2.2 Overload Criteria 369
- Diffusion Pumps 369
- Turbomolecular Pumps 371
- Cryogenic Pumps 373
- Ion Pumps 374
- References 375
- Problems 376

20. High Vacuum Systems 379

- 20.1 Diffusion-Pumped Systems 379

20.1.1	System Operation	382
20.1.2	Operating Concerns	383
20.2	Turbomolecular-Pumped Systems	385
20.2.1	System Operation	388
20.2.2	Operating Concerns	389
20.3	Ion-Pumped Systems	391
20.3.1	System Operation	391
20.3.2	Operating Concerns	393
20.4	Cryogenic-Pumped Systems	394
20.4.1	System Operation	394
20.4.2	Regeneration	394
20.4.3	Operating Concerns	396
20.5	High Vacuum Chambers	397
20.5.1	Managing Water Vapor	
	References	400
	Problems	400
21.	Ultraclean Vacuum Systems	403
21.1	Ultraclean Pumps	405
21.1.1	Turbomolecular Pumps	405
21.1.2	Cryogenic Pumps	406
21.1.3	Sputter-Ion, TSP, and NEG Pumps	406
21.2	Ultraclean Chambers	407
21.2.1	Chamber Materials and Components	407
21.2.2	Chamber Pumping	409
21.2.3	Pressure Measurement	412
	References	412
	Problems	413
22.	High Flow Systems	415
22.1	Mechanically Pumped Systems	417
22.2	Throttled High Vacuum Systems	419
22.2.1	Process Chambers	419
22.2.2	Turbo Pumped	421
22.2.3	Cryo Pumped	424
	References	429
	Problems	429
23.	Multichamber Systems	431
23.1	Flexible Substrates	432
23.2	Rigid Substrates	434
23.2.1	Inline Systems	435
23.2.2	Cluster Systems	440

23.3 Instrumentation Systems	443
References	444
Problems	444

24. Leak Detection **447**

24.1 Instruments	448
24.1.1 Forward-Flow Leak Detector	448
24.1.2 Counter-Flow Leak Detector	449
24.2 Performance	450
24.2.1 Sensitivity	450
24.2.2 Response Time	452
24.2.3 Sampling Pressurized Chambers	453
24.3 Leak-Hunting Techniques	453
References	457
Problems	457

Symbols **459**

APPENDIXES

A. Units and Constants **463**

A.1 Physical Constants	463
A.2 SI Base Units	463
A.3 Conversion Factors	464

B. Gas Properties **466**

B.1 Mean Free Paths of Gases as a Function of Pressure	466
B.2 Physical Properties of Gases and Vapors at $T = 0^{\circ}\text{C}$	467
B.3 Cryogenic Properties of Gases	468
B.4 Gas Conductance and Flow Formulas	469
B.5 Vapor Pressure Curves of Common Gases	475
B.6 Appearances of Discharges in Gases and Vapors at Low Pressures	477

C. Material Properties **478**

C.1 Outgassing Rates of Vacuum Baked Metals	478
C.2 Outgassing Rates of Unbaked Metals	479
C.3 Outgassing Rates of Unbaked Ceramics and Glasses	480
C.4 Outgassing Rates of Elastomers	480
C.5 Permeability of Polymeric Materials	481
C.6 Vapor Pressure Curves of Solid and Liquid Elements	482
C.7 Outgassing Rates of Polymers	485
C.8 Austenitic Stainless Steels	486

D. Isotopic Abundances	488
E. Cracking Patterns	492
E.1 Cracking Patterns of Pump Fluids	492
E.2 Cracking Patterns of Gases	494
E.3 Cracking Patterns of Common Vapors	495
E.4 Cracking Patterns of Common Solvents	496
E.5 Cracking Patterns of Semiconductor Dopants	497
F. Pump Fluid Properties	498
F.1 Compatibility of Elastomers and Pump Fluids	498
F.2 Vapor Pressures of Mechanical Pump Fluids	499
F.3 Vapor Pressure of Diffusion Pump Fluids	500
F.4 Kinematic Viscosity of Pump Fluids	501
F.5 Kinematic Viscosity Conversion Factors	502
References	503
Index	505

Its Basis

An understanding of how vacuum components and systems function begins with an understanding of the behavior of gases at low pressures. Chapter 1 discusses the nature of vacuum technology. Chapter 2 reviews basic gas properties. Chapter 3 describes the flow of gases at reduced pressures, and Chapter 4 discusses how gas is evolved from the surfaces of materials. Together, these chapters form the basis of vacuum technology.

CHAPTER 1

Vacuum Technology

Torricelli is credited with the conceptual understanding of the vacuum within a mercury column by 1643. It is written that his good friend Viviani actually performed the first experiment, perhaps as early as 1644 [1,2]. His discovery was followed in 1650 by Otto von Guericke's piston vacuum pump. Interest in vacuum remained at a low level for more than 200 years, when a period of rapid discovery began with McLeod's invention of the compression gauge. In 1905 Gaede, a prolific inventor, designed a rotary pump sealed with mercury. The thermal conductivity gauge, diffusion pump, ion gauge, and ion pump soon followed, along with processes for liquefaction of helium and refinement of organic pumping fluids. They formed the basis of a technology that has made possible everything from light bulbs to space simulation. The significant discoveries of this early period of vacuum science and technology have been summarized in a series of historical review papers [2–7].

A vacuum is a space from which air or other gas has been removed. All gas cannot be removed. The amount removed depends on the application, and is done for many reasons. At atmospheric pressure molecules constantly bombard surfaces. These molecules can bounce from surfaces, attach themselves to surfaces, or perhaps chemically react with surfaces. Air or other surrounding gas quickly contaminates a cleaned surface. A clean surface—for example, a freshly cleaved crystal—will remain clean in an ultrahigh vacuum chamber for long periods of time, because the rate of molecular bombardment is low.

Molecules are crowded closely together at atmospheric pressure and travel in every direction much like people in a crowded plaza. It is impossible for a molecule to travel from one wall of a chamber to another without colliding with many molecules. By reducing the pressure to a suitably low value, a molecule from one wall can travel to another without a collision. Many effects become possible if molecules can travel long distances between collisions. Metals can be evaporated from a pure source without reacting in transit. Molecules or atoms can be accelerated to a high

energy and sputter away, or be implanted in the bombarded surface. Electrons or ions can be scattered from surfaces and be collected. The energy changes they undergo on scattering or release from a surface can be used to probe or analyze the surface or underlying layers. For convenience the subatmospheric pressure scale has been divided into several ranges. Table 1.1 lists these ranges.

The required vacuum level depends on the application. Epitaxial growth of semiconductor films (reduced pressure epitaxy) and laser etching of metals are two processes that are performed in the low vacuum range. Sputtering, plasma etching and deposition, low-pressure chemical vapor deposition, ion plating, and gas filling of encapsulated heat transfer modules are examples of processes performed in the medium vacuum range.

Pressures in the high vacuum range are needed for the manufacture of traditional low- and high-tech devices such as microwave, power, cathode ray and photomultiplier tubes, light bulbs, architectural and automotive glazing, decorative packaging, degassing of metals, vapor deposition, and ion implantation. A number of medium technology applications including medical, microwave susceptors, electrostatic dissipation films, and aseptic packaging use films fabricated in a vacuum environment [8]. Retail security, bank note security, and laser and inkjet paper have joined this group.

The background pressure must be reduced to the very high vacuum range for electron microscopy, mass spectroscopy, crystal growth, and x-ray and electron beam lithography, and storage media production. For ease of reading, we call the very high vacuum region "high vacuum" and call the pumps "high vacuum pumps."

Pressures in the ultrahigh vacuum range were formerly the domain of the surface analyst, materials researcher, or accelerator technologist. Critical high-volume production applications, such as semiconductor devices, thin-

Table 1.1 Vacuum Ranges

Degree of Vacuum	Pressure Range (Pa) ^a		
Low	10^5	$> P >$	3.3×10^3
Medium	3.3×10^3	$\geq P >$	10^{-1}
High	10^{-1}	$\geq P >$	10^{-4}
Very high	10^{-4}	$\geq P >$	10^{-7}
Ultrahigh	10^{-7}	$\geq P >$	10^{-10}
Extreme ultrahigh	10^{-10}	$> P$	

Source: Reprinted with permission from *Dictionary for Vacuum Science and Technology*, M. Kaminsky and J. M. Lafferty, Eds., American Vacuum Society, New York, 1980.

^a 101323.3 Pa = 1 atmosphere.

film media heads, and extreme UV lithography systems, require ultrahigh vacuum base pressures to improve yield by reducing gaseous impurity contamination. Additionally, processes carried out in these systems must be free of particle contamination, so we call them ultraclean vacuum systems.

A vacuum system is a combination of pumps, valves, and pipes, which creates a region of low pressure. It can be anything from a simple mechanical pump or aspirator for exhausting a vacuum storage container to a complex system such as an underground accelerator with miles of piping that is maintained at ultrahigh vacuum.

Removal of air at atmospheric pressure is usually done with a displacement pump. A displacement pump is one that removes the air from the chamber and expels it to the atmosphere. Rotary vane and piston pumps are examples of pumps used to exhaust gases at atmospheric pressure. Liquid nitrogen capture pumps or sorption pumps have also been designed for exhausting gases at atmospheric pressure. They are used only on small chambers because of their finite gas sorption.

Rotary vane, piston and sorption pumps have low-pressure limits in the range 10^{-1} – 10^{-3} Pa. Pumps that will function in a rarefied atmosphere are required to operate below this pressure range. Several displacement and capture pumps can remove air at these low pressures. The diffusion pump was the first high vacuum pump. It is a displacement pump. Its outlet pressure is below atmosphere. The turbomolecular pump, a system of high-speed rotating turbine blades, can also pump gas at low pressures. The outlet pressures of these two pumps need to be kept in the range 0.5–50 Pa, so they must exhaust into a rotary vane or piston “backing” pump, or “fore” pump. If the diffusion or turbomolecular pump exhaust gas flow would otherwise be too great, a lobe blower will be placed between the exhaust of the diffusion or turbomolecular pump and the inlet of the rotary pump to pump gas at an increased speed in this intermediate pressure region.

Capture pumps can effectively remove gas from a chamber at low pressure. They do so by freezing molecules on a wall (cryogenic pump), chemically reacting with the molecules (getter pump), or accelerating the molecules to a high velocity and burying them in a metal wall (ion pump). Capture pumps are more useful as high vacuum pumps than as atmospheric exhaust pumps because the number of molecules to be captured at high vacuum is less than the number removed during initial evacuation from atmosphere.

Air is the most important gas to understand, because it is in every vacuum system. It contains at least a dozen constituents, whose major constituents are described in Table 1.2. The differing ways in which pumps remove air, and gauges measure its pressure, can be understood in terms of the partial pressures of its components. The concentrations listed in Table 1.2 are those of dry atmospheric air at sea level (total pressure

Table 1.2 Components of Dry Atmospheric Air

Constituent	Content		Pressure (Pa)
	(vol. %)	(ppm)	
N ₂	78.084 ± 0.004		79,117
O ₂	20.946 ± 0.002		21,223
CO ₂ ^a	0.037		37.5
Ar	0.934 ± 0.001		946.357
Ne		18.18 ± 0.04	1.842
He		5.24 ± 0.004	0.51
Kr		1.14 ± 0.01	0.116
Xe		0.087 ± 0.001	0.009
H ₂		0.5	0.051
CH ₄		2.	0.203
N ₂ O		0.5 ± 0.1	0.051

Source: Reprinted with permission from *The Handbook of Chemistry and Physics*, 59th ed., R. C. Weast, Ed., copyright 1978, The Chemical Rubber Publishing Co., CRC Press, Inc., West Palm Beach, FL 33409.

^a Carbon dioxide data from Mauna Kea, Hawaii, 2000. Data since 1955 are available as: <http://stratus.mlo.hawaii.gov/Projects/GASES/co2graph.htm>.

101,323.2 Pa or 760 Torr). The partial pressure of water vapor is not given in this table, because it constantly changes. At 20°C a relative humidity of 50% corresponds to a partial pressure of 1165 Pa (8.75 Torr), making it the third largest constituent of air. The total pressure changes rapidly with altitude, as shown in Fig. 1.1, whereas its proportions change slowly but significantly. In outer space the atmosphere is mainly H₂ with some He [6].

In the pressure region below 10 Pa, gases evolving from material surfaces contribute more molecules per second to the total gas load than do the gases originally filling the chamber. The correct pump is not the only requirement needed to reach low pressures—the materials of construction, techniques for joining components, surface cleaning techniques, and operational procedures are all critically important. In the remaining chapters the pumps, gauges, and materials of construction and operational techniques are described in terms of fundamental gas behavior. The focus is on the understanding and operation of vacuum systems for a variety of technological applications.

1.1 UNITS OF MEASUREMENT

Units of measurement present problems in many disciplines and vacuum technology is no exception. The use of noncoherent vacuum units has been common in the US long after the adoption of System International.

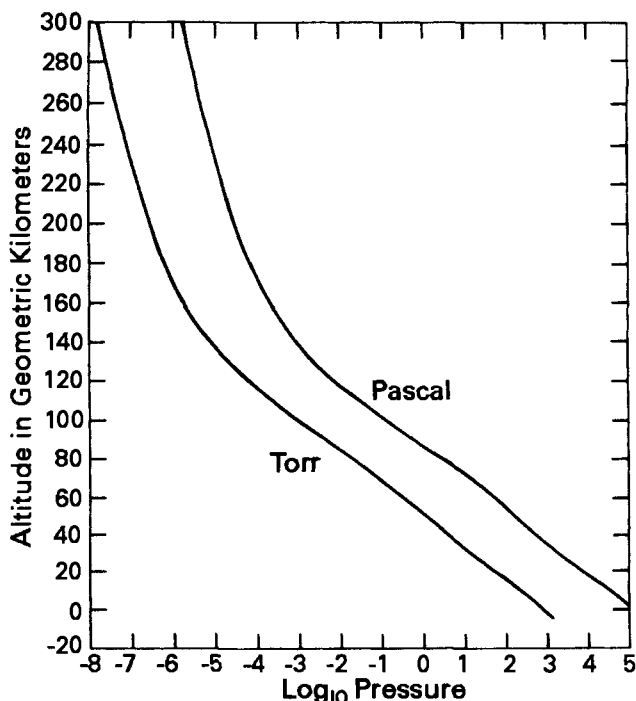


Fig. 1.1 Relation between the atmospheric pressure and the geometric altitude. Reprinted with permission from *The Handbook of Chemistry and Physics*, 59th ed., R. C. Weast, Ed. copyright 1978, The Chemical Rubber Publishing Co., CRC Press, Inc., West Palm Beach, FL 33409.

The meter-kilogram-second (MKS) system was first introduced over a half-century ago; its use became commonplace only after a decade or more of classroom education by instructors committed to change. In a similar manner, those who teach vacuum technique will lead the way to routine use of SI units. Instruments are manufactured for use in a global economy and their readings can be displayed in several formats. The advantages of using a coherent unit system are manifold. Calculations become straightforward and logical and the chance for error is reduced. Incoherent units such as permeation constant, the volume of gas (at standard temperature and pressure) per material thickness per material area per sec pressure difference, are cumbersome. Additionally, these permeation units mask their relation to solubility and diffusion. Ultimately, SI units will be routinely used. To assist with this change, dual labels have been added throughout the text. Basic SI units for pressure (Pa), time (s) and length (m) will be assumed in all formulas, unless noted differently within a formula statement.

REFERENCES

1. W. E. K. Middleton, *The History of the Barometer*, Johns Hopkins Press, Baltimore, 1964.
2. P. A. Redhead, *Vacuum*, **53**, 137 (1999).
3. T. E. Madey, *J. Vac. Sci. Technol. A*, **2**, 110 (1984).
4. M. H. Hablanian, *J. Vac. Sci. Technol. A*, **2**, 118 (1984).
5. J. H. Singleton, *J. Vac. Sci. Technol. A*, **2**, 126 (1984).
6. P. A. Redhead, *J. Vac. Sci. Technol. A*, **2**, 132 (1984).
7. T. E. Madey and W. C. Brown, Eds., *History of Vacuum Science and Technology*, American Institute of Physics, New York, 1984.
8. P. R. Johansen, *J. Vac. Sci. Technol. A*, **8**, 2798 (1990).
9. D. J. Santeler, et al., *Vacuum Technology and Space Simulation*, NASA SP 105, National Aeronautics and Space Administration, Washington, DC, 1966, p. 34.

CHAPTER 2

Gas Properties

In this chapter we discuss the properties of gases at atmospheric and reduced pressures. The properties developed here are based on the kinetic picture of a gas. Kinetic theory has its limitations, but with it we are able to describe particle motion, pressure, effusion, viscosity, diffusion, thermal conductivity, and thermal transpiration of ideal gases. We will use these ideas as the starting point for discussing gas flow, gauges, pumps and systems.

2.1 KINETIC PICTURE OF A GAS

The kinetic picture of a gas is based on several assumptions. (i) The volume of gas under consideration contains a large number of molecules. A cubic meter of gas at a pressure of 10^5 Pa and a temperature of 22°C contains 2.48×10^{25} molecules, whereas at a pressure of 10^{-7} Pa, a very high vacuum, it contains 2.5×10^{13} molecules. Indeed, any volume and pressure normally used in the laboratory will contain a large number of molecules. (ii) Adjacent molecules are separated by distances that are large compared with their individual diameters. If we could stop all molecules instantaneously and place them on the coordinates of a grid, the average spacing between them would be about 3.4×10^{-9} m at atmospheric pressure (10^5 Pa). The diameter of most molecules is of order $2\text{--}6 \times 10^{-10}$ m and their separation distances are $\sim 6\text{--}15$ times their diameter at atmospheric pressures. For extremely low pressures, say 10^{-7} Pa, the separation distance is about 3×10^{-5} m. (iii) Molecules are in a constant state of motion. All directions of motion are equally likely and all velocities are possible, although not equally probable. (iv) Molecules exert no force on one another except when they collide. If this is true, then molecules will be uniformly distributed throughout the volume and travel in straight lines until they collide with a wall or with one another.

Using these assumptions, many interesting properties of ideal gases have been derived. Some elementary properties are reviewed here.

2.1.1 Velocity Distribution

As the individual molecules move about they collide with elastic collisions. Elastic collisions conserve energy, whereas the colliding particle's velocity is changed after each collision. We stated that all velocities are possible, but not with equal probability. The distribution of particle velocities calculated by Maxwell and Boltzmann is

$$\frac{dn}{dv} = \frac{2N}{\pi^{1/2}} \left(\frac{m}{2kT} \right)^{3/2} v^2 e^{-mv^2/(2kT)} \quad (2.1)$$

m is the particle mass and T is the Kelvin temperature. The relation between the Kelvin scale and the Celsius scale is $T(K) = 273.16 + T(^{\circ}C)$. In (2.1) N is the total number of particles, and k is Boltzmann's constant. Figure 2.1 illustrates (2.1) for nitrogen molecules (air) at three temperatures. It is a plot of the relative number of molecules between velocity v and $v + dv$. We see that there are no molecules with zero or infinite velocity, and that the peak or most probable velocity v_p , is a function of the average gas temperature. The particle velocity also depends on the molecular mass, the peak velocity can be expressed as $v_p = (2kT/m)^{1/2}$. The arithmetic mean or average velocity \bar{v} is useful when describing particle flow.

$$\bar{v} = \left(\frac{8kT}{\pi m} \right)^{1/2} \quad \blacktriangleright (2.2)$$

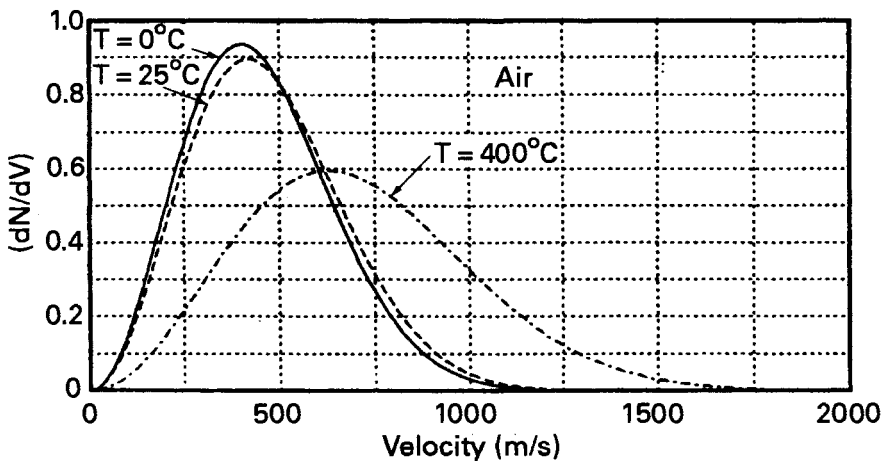


Fig. 2.1 Relative velocity distribution of air at 0°C, 25°C, and 400°C.

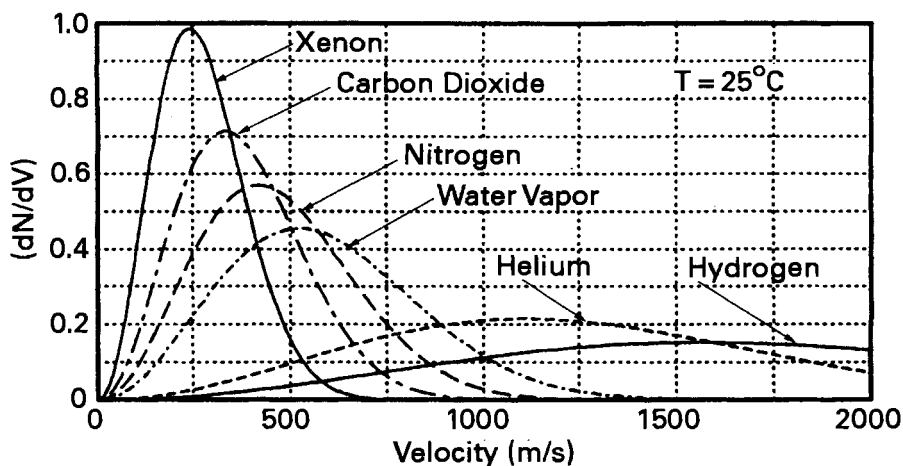


Fig. 2.2 Relative velocity distribution of several gases at 25°C.

The average velocities of several gas and vapor molecules are given in Appendix B.2. The root of the mean square velocity, is $v_{\text{rms}} = (3kT/m)^{1/2}$. The rms velocity is the square root of the average or mean of each velocity squared times the number of particles with that velocity. For Maxwell-Boltzmann statistics the average velocity is always 1.128 times as large as v_p , while $v_{\text{rms}} = 1.225v_p$. In Fig. 2.1 we illustrated the temperature dependence of the velocity distribution. As the temperature is increased the peak is broadened and shifted to a higher velocity. We may also plot (2.1) for different gases having the same temperature. Figure 2.2 illustrates the velocity distribution for H_2 , He, H_2O , N_2 , CO_2 , and Xe. There are two concepts illustrated in Figs. 2.1 and 2.2. First the average velocity of a particle is proportional to $(T/m)^{1/2}$. An increase in temperature or decrease in mass causes an increase in a particle's velocity and the frequency with which it collides with other particles or nearby walls. Second, not all the particles in a distribution have the same velocity. The Maxwell-Boltzmann distribution is quite broad—over 5% of the molecules travel at velocities greater than two times the average velocity.

2.1.2 Energy Distribution

Maxwell and Boltzmann also derived an energy distribution, which is based on the same assumptions as the velocity distribution. It is

$$\frac{dn}{dE} = \frac{2N}{\pi^{1/2}} \frac{E^{1/2}}{(kT)^{3/2}} e^{-E/(kT)} \quad (2.3)$$

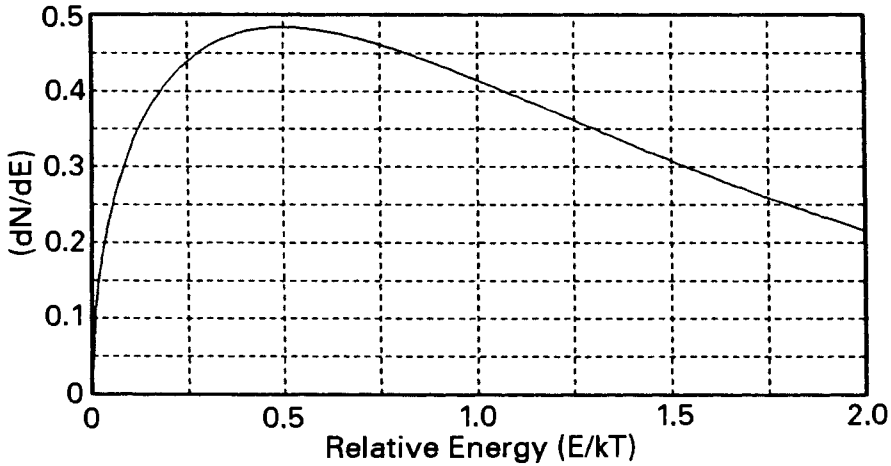


Fig. 2.3 Relative energy distribution of a gas at 25°C.

From this expression the average energy can be calculated as $E_{ave} = 3kT/2$, and the most probable energy as $E_p = kT/2$. Notice that neither the energy distribution nor the average energy is a function of the molecular mass. Each is only a function of temperature, as shown in Fig. 2.3. For example, all the gases depicted in Fig. 2.2 have the same energy distribution, because they all have the same average temperature. See Fig. 2.3.

2.1.3 Mean Free Path

The fact molecules are randomly distributed and move with different velocities implies that each travels a different straight-line distance, known as a *free path* before suffering a collision. As illustrated in Fig. 2.4, not all free paths are the same length. The average, or mean, of the free paths λ , is found from kinetic theory

$$\lambda = \frac{1}{2^{1/2} \pi d_0^2 n} \quad \blacktriangleright (2.4)$$

where d_0 is the molecular diameter in meters, and n is the gas density in molecules per cubic meter. The mean free path is clearly gas density dependent. If the temperature is constant, it is also pressure dependent. See (2.12). For air at room temperature the mean free path is most easily remembered by one of the following expressions

$$\lambda \text{ (cm)} = \frac{0.67}{P \text{ (Pa)}} \quad \text{or} \quad \lambda \text{ (cm)} = \frac{0.005}{P \text{ (Torr)}} \quad \blacktriangleright (2.5)$$

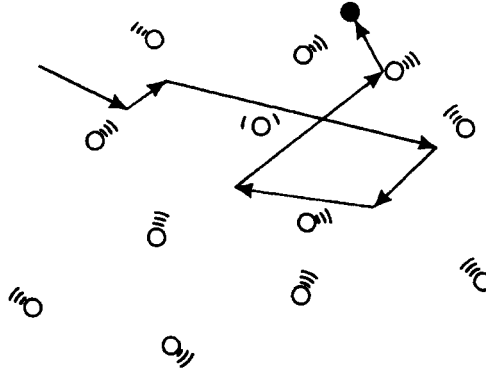


Fig. 2.4 Individual molecular paths.

where λ has units of cm, and P is the pressure in Pascal or Torr, respectively. Kinetic theory also describes the distributions of free paths.

$$N = N' e^{-x/\lambda} \quad (2.6)$$

N' is the number of molecules in the volume and N is the number of molecules that traverse a distance x before suffering a collision. Equation 2.6 states that 63% of the collisions occur in a distance $0 \leq x \leq \lambda$, whereas about 37% of the collisions occur in range $\lambda \leq x \leq 5\lambda$. Only about 0.6% of the particles travel distances greater than 5λ without suffering a collision.

For the case of two gases, a and b , the mean free path of a in b is

$$\lambda_a = \frac{1}{\left[2^{1/2} \pi n_a d_a^2 \left(1 + \frac{v_b^2}{v_a^2} \right)^{1/2} n_b \frac{\pi}{4} (d_a + d_b)^2 \right]} \quad (2.7)$$

2.1.4 Particle Flux

The concept of particle flux is helpful in understanding gas flow, pumping, and evaporation. According to kinetic theory the flux Γ of an ideal gas striking a unit surface or crossing an imaginary plane of unit area from one side is

$$\Gamma(\text{particles} \cdot \text{m}^2 \cdot \text{s}^{-1}) = n v / 4 \quad \blacktriangleright (2.8)$$

where n is the particle density and v , the average velocity. On substituting (2.2) we see that

$$\Gamma = n \left(\frac{kT}{2\pi m} \right)^{1/2} \quad (2.9)$$

The particle flux is directly proportional to the particle density and the square root of T/m .

2.1.5 Monolayer Formation Time

The time to saturate a surface with one layer of molecules is a function of the molecular arrival rate Γ , an molecular size. Assuming each molecule sticks and occupies surface area d_o^2 , the time to form a monolayer is

$$t_{ml} = \frac{1}{\Gamma d_o^2} = \frac{4}{nvd_o^2} \quad (2.10)$$

At ambient temperature, a monolayer of air ($d_o = 0.372$ nm, $v = 467$ m/s) will form in about 2.5 s at a pressure of 10^{-4} Pa. The formation time will be longer, if the sticking coefficient is less than unity.

2.1.6 Pressure

The absolute pressure on a surface is defined as the rate at which momentum mv , is imparted to a unit surface. A molecule incident on a surface at an angle ϕ from the normal will impart a total impulse or pressure of $2mv \cos \phi$. By integrating over all possible angles in the half-plane we find that the pressure is

$$P = \frac{1}{3} n m v_{rms}^2 \quad (2.11)$$

The total energy of a molecule, however, is proportional to its temperature

$$E = \frac{mv_{rms}^2}{2} = \frac{3}{2} kT \quad (2.12)$$

Equations (2.11) and (2.12) may be combined to form the ideal gas law.

$$P = nkT \quad \blacktriangleright (2.13)$$

If n is expressed in units of m^{-3} , k in joules per kelvin, and T in kelvin, then P will have units of pascal (Pa). A pascal is a newton per square meter and the fundamental unit of pressure in System International (SI). Simply divide the number of pascals by 133.32 to convert to units of Torr, or divide by 100 to convert to units of millibars. A conversion table is included in Appendix A.3. Values of n , d' , λ , and Γ for air at 22°C are

Table 2.1 Low Pressure Properties of Air^a

Pressure (Pa)	n (m ⁻³)	d' (m)	λ (m)	Γ (m ⁻² -s ⁻¹)
1.01×10^5 (760 Torr)	2.48×10^{25}	3.43×10^{-9}	6.5×10^{-8}	2.86×10^{27}
100 (.75 Torr)	2.45×10^{22}	3.44×10^{-8}	6.6×10^{-5}	2.83×10^{24}
1 (7.5 mTorr)	2.45×10^{20}	1.6×10^{-7}	6.6×10^{-3}	2.83×10^{22}
10^{-3} (7.5×10^{-6} Torr)	2.45×10^{17}	1.6×10^{-6}	6.64	2.83×10^{19}
10^{-5} (7.5×10^{-8} Torr)	2.45×10^{15}	7.41×10^{-6}	664	2.83×10^{17}
10^{-7} (7.5×10^{-10} Torr)	2.45×10^{13}	3.44×10^{-5}	6.6×10^4	2.83×10^{15}

^a Particle density n ; average molecular spacing d' ; mean free path λ ; and particle flux on a surface Γ , for $T = 22^\circ\text{C}$.

tabulated in Table 2.1 for pressures ranging from atmospheric to ultrahigh vacuum. The pressure dependence of the mean free path is given for several gases in Appendix B.1.

2.2 GAS LAWS

Kinetic theory, as expressed in (2.13), summarizes all the earlier experimentally determined gas laws. However, we review several of the experimentally verified laws here, because they are especially helpful to those with no experience in gas kinetics. When using kinetic theory, we need to remember that the primary assumption of a gas at rest in thermal equilibrium with its container is not always valid in practical situations. For example, a pressure gauge close to and facing a high vacuum cryogenic pumping surface will register a lower pressure than when it is close to and facing a warm surface in the same vessel [1]. This and other non-equilibrium situations will be discussed as required.

2.2.1 Boyle's Law

In 1662 Robert Boyle demonstrated that the volume occupied by a given quantity of gas varied inversely as its pressure, when the gas temperature remained the same.

$$P_1 V_1 = P_2 V_2 \quad (N, T \text{ constant}) \quad (2.14)$$

This is easily derived from the general law by multiplying both sides by the volume V and noting that $N = nV$.

2.2.2 Amontons' Law

Amontons discovered the pressure in a confined chamber increased as the temperature increased. Amontons' law can be expressed as

$$\frac{P_1}{T_1} = \frac{P_2}{T_2} \quad (N, V \text{ constant}) \quad (2.15)$$

In 1703 he constructed an air thermometer based on this relationship. This later came to be known as the law of Gay-Lussac.

2.2.3 Charles' Law

The French chemist Charles found in 1787 that gases expanded and contracted to the same extent under the same changes of temperature provided that no change in pressure occurred. Again by the same substitution in (2.13) we obtain

$$\frac{V_1}{T_1} = \frac{V_2}{T_2} \quad (N, P \text{ constant}) \quad (2.16)$$

2.2.4 Dalton's Law

Dalton discovered in 1801 that the total pressure of a mixture of gases was equal to the sum of the forces per unit area of each gas taken individually. By the same methods for a mixture of gases, we can develop the relation

$$P_t = nkT = n_1kT + n_2kT + n_3kT + \dots \quad (2.17)$$

which reduces to

$$P_t = P_1 + P_2 + P_3 + \dots \quad (2.18)$$

pressures and densities, respectively. Equation (2.18) is called Dalton's law of partial pressures and is valid for pressures below atmospheric [2].

2.2.5 Avogadro's Law

In 1811 Avogadro observed that pressure and number of molecules were proportional for a given temperature and volume:

$$\frac{P_1}{N_1} = \frac{P_2}{N_2} \quad (T, V \text{ constant}) \quad (2.19)$$

Two terms, "standard temperature and pressure" and "mole" often cause confusion. Standard temperature and pressure (STP) conditions refer to a

gas with a temperature of 0°C , at pressure of 1 atmosphere. However, in Chapter 6, we note that some manufacturers of thermal mass flow controllers assume a temperature of 20°C when calibrating flow meters; this is called NTP, or normal temperature and pressure. In SI, Avogadro's number of any gas species is $N_0 = 6.02252 \times 10^{26}$ and occupies a molar volume of $V_0 = 22.4136 \text{ m}^3$. Avogadro's number of molecules is known as a mole. In SI, the unit of volume is the m^3 and the unit of mass is the kg. To avoid confusion with cgs units, we will use "kg-mole." For example one kg-mole of oxygen contains 6.02252×10^{26} molecules and weighs 32 kg. Its density at STP is therefore $32 \text{ kg}/22.4136 \text{ m}^3$ or $1.45 \text{ kg}/\text{m}^3$.

2.2.6 Graham's Law

In the nineteenth century Graham studied the rate of effusion of gases through very small holes in porous membranes. He observed the rate of effusion to be inversely proportional to the square root of the density of the gas provided that the pressure and temperature were held constant. Since the density of a gas is proportional to its molecular weight, Grahams' law can be stated as

$$\frac{\text{effusion rate}_a}{\text{effusion rate}_b} = \left(\frac{M_b}{M_a} \right)^{1/2} \quad (P, T \text{ constant}) \quad (2.20)$$

Grahams' law describes how a helium-filled balloon loses its gas more quickly than an air-filled balloon.

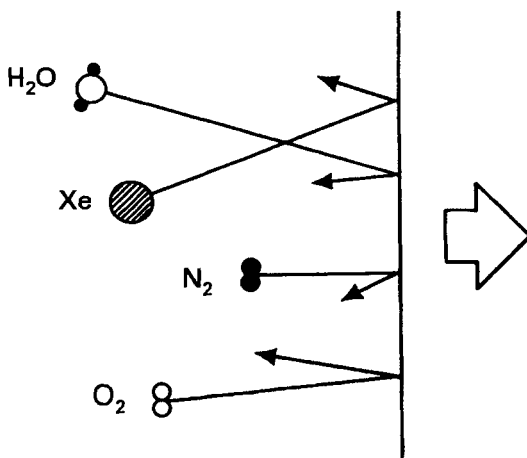


Fig. 2.5 Dalton's law states that the total pressure is the sum of the partial pressures.

2.3 ELEMENTARY GAS TRANSPORT PHENOMENA

In this section approximate views of viscosity, thermal conductivity, diffusion, and thermal transpiration are discussed. We state results from kinetic theory without derivation.

2.3.1 Viscosity

A viscous force is present in a gas when it is undergoing shear. Figure 2.5 illustrates two plane surfaces, one fixed and the other traveling in the x direction with a uniform velocity. The coefficient of absolute viscosity η is defined by the equation

$$\frac{F_x}{A_{xz}} = \eta \frac{du}{dy} \quad (2.21)$$

where F_x is the force in the x direction, A_{xz} is the surface area in the x - z plane, and du/dy is the rate of change of the gas velocity at this position between the two surfaces. Because the gas stream velocity increases as the moving plate is approached, those molecules crossing the plane A_{xz} from below (1 in Fig. 2.5) will transport less momentum across the plane than will those crossing the same plane from above (2 in Fig. 2.5). The result is that molecules crossing from below the plane will, on the average, reduce the momentum of the molecules from above the plane, in the same manner molecules crossing from above the plane will increase the momentum of those molecules below the plane. To an observer this viscous force appears to be frictional; actually it is not. It is merely the result of momentum transfer between the plates by successive molecular collisions. Again, from kinetic theory the coefficient of viscosity is

$$\eta = \frac{1}{3} nmv\lambda \quad (2.22)$$

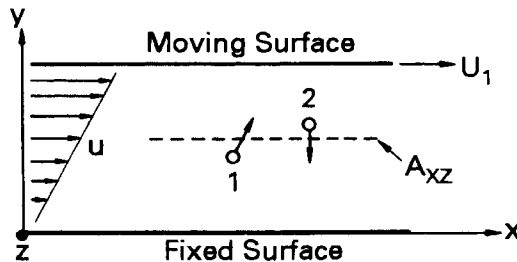


Fig. 2.6 Origin of the viscous force in a gas.

When the gas density is measured in units of m^{-3} , the molecular mass in kg, the velocity in m/s and the mean free path in m, η will have units of $(\text{N}\cdot\text{s})/\text{m}^2$, or Pa-s. One Pa-s is equal to 10 poise. A more rigorous treatment of viscosity [3] yields a result with a slightly different numerical coefficient:

$$\eta = 0.499nmv\lambda \quad \blacktriangleright (2.23)$$

Substituting (2.2) and (2.4) into this result yields

$$\eta = \frac{0.499(4mkT)^{1/2}}{\pi^{3/2}d_o^2} \quad (2.24)$$

From (2.24) we see that kinetic theory predicts that viscosity should increase as $(mT)^{1/2}$ and decrease as the square of the molecular diameter. An interesting result of this simple theory is that viscosity is independent of gas density or pressure. This theory, however, is valid only in a limited pressure range. If there were a perfect vacuum between the two plates, there would be no viscous force because there would be no mechanism for transferring momentum from one plate to another. This understanding leads to the conclusion that (2.24) is valid as long as the distance between the plates is greater than the mean free path—for example, the gas is viscous.

For a rarefied gas in which the ratio of the mean free path to plate separation $\lambda/y \gg 1$ the viscous force can be expressed as

$$\frac{F}{A_{xz}} = \left(\frac{Pmv}{4kT} \right) \frac{U_1}{\beta} \quad (2.25)$$

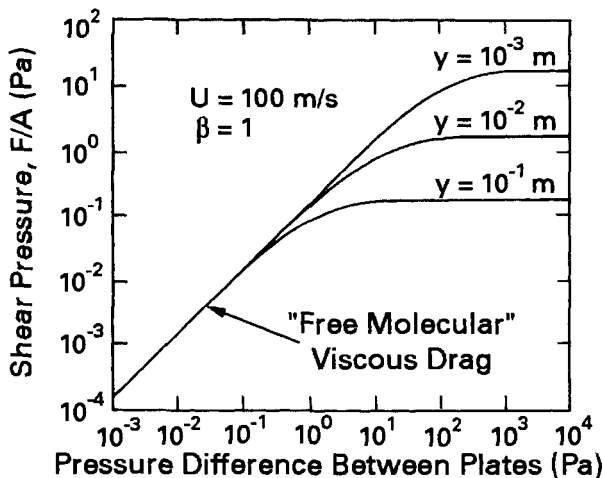


Fig. 2.7 Viscous shear force between two plates at 22°C.

where the term in parentheses is referred to as the free-molecular viscosity. The free-molecular viscosity is directly proportional to the molecular density ($n = P/kT$) available to transfer momentum between the plates. It is valid in the region $\lambda \gg y$. The constant β in (2.25) is related to the slip of molecules on the plate surfaces. For most vacuum conditions $\beta \sim 1$.

Figure 2.6 illustrates the magnitude of the viscous force caused by air at 22°C between two plates moving with a relative velocity of 100 m/s for three plate separations. Equation (2.24) was used to calculate the asymptotic value of the viscous drag at high pressures and (2.25) was used to calculate the free molecular limit. A more complete treatment of the intermediate or viscous slip region is given elsewhere [4]. The viscous shear force is independent of the plate spacing as long as the mean free path is larger than the spacing. This idea was used by Langmuir [5] to construct a viscosity gauge in which damping was proportional to pressure.

2.3.2 Thermal Conductivity

Heat conductivity between two infinite parallel plates is explained by kinetic theory in a manner analogous to that used to explain viscosity. The diagram in Fig. 2.6 could be relabeled to make the top plate stationary at temperature T_2 , and the lower plate a stationary plate at a temperature T_1 , where $T_1 < T_2$. Heat conduction can be modeled by noting that the molecules moving across the plane toward the hotter plate carry less energy than those moving across the plane toward the cooler surface. The heat flow can be expressed as

$$H = AK \frac{dT}{dy} \quad (2.26)$$

where H is the heat flow and K is the heat conductivity. The simple theory predicts that the heat conductivity K is expressed by $K = \eta c_v$, where η is the viscosity and c_v is the specific heat at constant volume. This simple theory is correct only to an order of magnitude. A more detailed analysis, which accounts for molecular rotational and vibrational energy, yields

$$K = \frac{1}{4}(9\gamma - 5)\eta c_v \quad \blacktriangleright (2.27)$$

where γ is the ratio of specific c_p/c_v . When η has the units of Pa-s and c_v has units (J/kg)/K, then K will have units of (W/m)/K. At room temperature, the heat conductivity and viscosity both increase as $(mT)^{1/2}/d^2$. For infinite parallel plates, K does not depend on pressure, as long as the mean free path is smaller than the plate spacing. In the low-pressure region, the heat transfer between parallel plates [6] has been calculated as

$$E_o = \alpha \Lambda P (T_2 - T_1)$$

where

$$\alpha = \frac{\alpha_1 \alpha_2}{\alpha_1 + \alpha_2 - \alpha_1 \alpha_2} \quad \Lambda = \frac{1}{8} \frac{(\gamma + 1) v_1}{(\gamma - 1) T_1} \quad (2.28)$$

This equation has the same general form as (2.25) for free-molecular viscosity. Λ is the free-molecular heat conductivity and α_1 , α_2 , α are the accommodation coefficients of the cold surface, hot surface, and system, respectively. If molecules can thermally equilibrate with the surface, say by making many small collisions on a rough surface, α will have a value that approaches unity. If however, the same surface is smooth and the molecule recoils without gaining or losing energy, α will approach zero. The kinetic picture of heat conductivity is rather like viscosity except that *energy transfer* determines the thermal conductivity, and *momentum transfer* determines the viscous drag. Even so, Fig. 2.5 can be sketched for the thermal conductivity of a gas between two parallel plates, where the vertical axis has dimensions of heat flow. In SI Λ has units of $\text{W}\cdot\text{m}^{-2}\cdot\text{K}^{-1}\cdot\text{Pa}^{-1}$, whereas E_o has units of W/m^2 . Tables of the accommodation coefficient are given elsewhere [3,7]. The accommodation coefficient of a gas is not only dependent on the material but on its cleanliness, surface roughness, and gas adsorption as well.

When the heated parallel plate is replaced by a heated fine wire, the situation changes. In the case of a heated fine wire, the upper “knee” of the curve is not dependent on the ratio of λ to plate separation, but rather on the ratio of λ to hot wire diameter [8,9]. Both thermocouple and Pirani gauges operate in a region in which the heat conduction from the heated wire is linearly dependent on pressure. However, the “knee” in their linear range begins at a mean free path equal to a few multiples of the wire diameter and not at a mean free path related to the wire-envelope distance.

2.3.3 Diffusion

Diffusion is a complex phenomenon. This discussion has been simplified by restricting it to the situation in a vessel that contains two gases whose compositions vary slowly throughout the vessel but whose total number density is everywhere the same. The coefficient of diffusion D , of two gases is defined in terms of their particle fluxes $\Gamma_{1,2}$

$$\Gamma_1 = -D \frac{dn}{dx} \quad \Gamma_2 = -D \frac{dn_2}{dx} \quad (2.29)$$

These fluxes result from the partial pressure gradient of the two gases. The result from kinetic theory, when corrected for the Maxwellian distribution of velocities and for velocity persistence, is [9]

$$D_{12} = \frac{8 \left(\frac{2kT}{\pi} \right)^{1/2} \left(\frac{1}{m_1} + \frac{1}{m_2} \right)^{1/2}}{3\pi(n_1 + n_2)(d_{o1} + d_{o2})^2} \quad \blacktriangleright (2.30)$$

where D_{12} is the constant of inter-diffusion of the two gases. In SI it has units of m^2/s . For the case of self diffusion, the coefficient is

$$D_{11} = \frac{4}{3\pi n d_o^2} \left(\frac{kT}{\pi m} \right)^{1/2} \quad \blacktriangleright (2.31)$$

If the density n is replaced by P/kT , it becomes apparent that the diffusion constant is approximately proportional to $T^{3/2}$ and P^{-1} .

The diffusion equation, $dC/dt = -Dd^2C/dt^2$, whose solutions we do not describe here, contains the term $(Dt)^{1/2}$. This term has the dimensions of length and is called “diffusion length.” For long times the diffusion “front” moves through the gas in proportion to $(Dt)^{1/2}$. Values of the diffusion constant for several gases in air are given in Appendix B.2.

Examination of (2.31) shows the diffusion coefficient will become infinitely large as the density of molecules goes to zero. This does not happen. When the pressure becomes low enough so that the mean free path is much larger than the dimensions of the container, say the diameter of a pipe, gas diffusion is limited by molecules recoiling from walls, rather than from collisions with each other. At low pressures, where $\lambda \gg d$, the diffusion coefficient is given by

$$D = \frac{2}{3} r v \quad \blacktriangleright (2.35)$$

where r is the radius of the pipe and v is the thermal velocity. This is called the Knudsen diffusion coefficient for a long capillary [10].

2.3.4 Thermal Transpiration

When a tube or orifice connects two chambers of different temperatures, their relative pressures depend on the nature of the gas flow in the connecting tubing. The nature of the gas flow in the tubing or orifice is characterized by (λ/d) , where d is the diameter of the connecting tube or orifice. For $\lambda \ll d$ the pressure is everywhere the same in both chambers, $P_1 = P_2$. The densities in the two chambers are related by

$$\frac{n_2}{n_1} = \frac{T_1}{T_2} \quad \blacktriangleright (2.36)$$

When the orifice diameter is such that $\lambda \gg d$, the flux of gas through the orifice is given by (2.8).

$$\Gamma_{1,2} = \frac{n_{1,2}}{4} \left(\frac{8kT_{1,2}}{\pi m} \right)^{1/2} = \frac{P_{1,2}}{(2kT\pi m)^{1/2}} \quad \blacktriangleright (2.37)$$

In steady state the net flux between the two chambers must be zero—for example, $(\Gamma_{1 \rightarrow 2} = \Gamma_{2 \rightarrow 1})$ —with the result

$$\frac{P_1}{P_2} = \left(\frac{T_1}{T_2} \right)^{1/2} \quad \blacktriangleright (2.38)$$

Equations (2.36) and (2.38) can be used to calculate the pressures within furnaces or cryogenic enclosures when the pressure gauge is located outside the enclosure at a different temperature. Equation (2.36) is used at high pressure ($\lambda < d/10$), and (2.38) is used at low pressure ($\lambda > 10d$).

Thermal transpiration was discovered by Neumann [11] and studied by Maxwell [12], who predicted the square-root dependence given in (2.38). The geometry and reflectivity from walls of the connecting tubing introduce deviations from the theory. Siu [13] has studied these effects and has predicted that (2.38) is obtained in short tubes only for specular reflection and in long tubes only for diffuse reflection.

REFERENCES

1. R. W. Moore, Jr., *Proc. 8th Nat'l. Vac. Symp. 1961*, **1**, Pergamon, New York, 1962, p. 426.
2. E. H. Kennard, *Kinetic Theory of Gases*, McGraw-Hill, New York, 1938, p. 9.
3. Ref. 2, pp. 135–205 and 291–337.
4. S. Dushman, *Scientific Foundations of Vacuum Technique*, 2nd ed., J. M. Lafferty, Ed., Wiley, New York, 1962, p. 35.
5. Langmuir, *Phys. Rev.*, **1**, 337 (1913).
6. Ref. 4, p. 6.
7. Ref. 4, p. 68.
8. H. von Ubisch, *Vak. Tech.*, **6**, 175 (1957).
9. M. Pirani and J. Yarwood, *Principles of Vacuum Engineering*, Reinhold, New York, 1961, p. 100.
10. For example, see L. M. Lund and A. S. Berman, *J. Appl. Phys.*, **37**, 2489 (1966).
11. C. Neumann, *Math Phys. K.*, **24**, 49 (1872).
12. J. C. Maxwell, *Philos. Trans. R. Soc. London*, **170**, 231 (1879).
13. M. C. I. Siu, *J. Vac. Sci. Technol.*, **10**, 368 (1973).

PROBLEMS

- 2.1 † State the assumptions that form the basis of kinetic theory.
- 2.2 Consider a 1-cm-diameter pipe 10 meters long. (a) Sketch the self-diffusion constant of air in this pipe over the pressure range 0.01 Pa to 10^5 Pa. (b) Knowing that the diffusion front moves as $d^2 \propto Dt$, estimate the time required for air to diffuse to the end of the 10-meter-long pipe over the pressure range given in (a).
- 2.3 The diffusion constant for gas (1) in gas (2), D_{12} describes how gas a gas of one molecular weight diffuses in the background of a second gas. For the case where the diffusing gas (1) is light ($m_1 \ll m_2$), and is present in a small concentration ($n_1 \ll n_2$), derive a simplified relationship for (2.30). This happens during helium leak checking.
- 2.4 † Room temperature N_2 molecules are directed toward a surface 100-cm distant. To what pressure must a chamber be evacuated in order that the molecules reach the surface, on average, without first colliding with another N_2 molecule?
- 2.5 † What is the advantage of low-pressure chemical vapor deposition over atmospheric pressure chemical vapor deposition?
- 2.6 Explain why the viscosity of a gas should increase with increasing particle mass and temperature. (The viscosity of a liquid decreases with increasing temperature.)
- 2.7 † The air surrounding it cools an object that is heated by a constant-power source. What would happen to its temperature, if the surrounding air were replaced (a) by helium and (b) by argon?
- 2.8 What is the heat flow by thermal conduction between two 0.1 m^2 sheets of copper with a temperature difference of 100°C and which are separated by 0.1 cm of CO_2 at pressures of (a) 10^5 Pa, (b) 10^3 Pa, and (c) 100 Pa.
- 2.9 A 0.5-cm-diameter tube interconnects two chambers. The left-hand chamber is heated to a temperature of 250°C , while the right-hand chamber remains at room temperature. Over what pressure range is the pressure in the two chambers the same? Over what pressure range does the transpiration equation apply? Sketch a plot of $P_{\text{hot}}/P_{\text{cold}}$ versus the pressure of the cold chamber. Assume diffuse scattering.
- 2.10 In Problem 2.9, nitrogen is replaced by helium. Sketch a plot of $P_{\text{hot}}/P_{\text{cold}}$ versus the pressure of the cold chamber in the transition region. How does this compare to the curve in Problem 2.9 for helium?

CHAPTER 3

Gas Flow

In this chapter we discuss the flow of gas at reduced pressures, as it is encountered in a vacuum system. Gas flow is complex and the nature of the solution depends on the flow rate and gas properties as well as the geometry and surface properties of the duct. We begin by defining the flow regimes and introducing the concepts of throughput, mass flow and conductance. We describe the gas throughput and conductance for several kinds of flow. We show how approximation techniques and probability methods are used to solve complex problems, such as flow in ducts containing entrance and exit orifices, aperture plates, or other irregular shapes.

3.1 FLOW REGIMES

Gas flow regimes are characterized by the *nature* of the gas and by the *relative quantity* of gas flowing in a pipe. The nature of the gas is determined by examining Knudsen's number, whereas Reynolds' number describes the relative flow. In the viscous gas region (high pressures) the flow is called continuum flow. The flow can be further described as turbulent or viscous. Turbulent flow is chaotic, like the flow behind a moving vehicle or the rising smoke some distance from a cigarette. Laminar or stream flow occurs when the velocity and surface irregularities are small enough for the gas to flow gently past obstructions in laminar streamlines. In the molecular gas region, the mean free path is so long in comparison to the pipe size that the flow is entirely determined by gas-wall collisions. The flow in this region is called molecular flow. Between the continuum flow region and the molecular flow region is the transition region. In this region gas molecules collide with each other and with walls.

A viscous gas is characterized by a Knudsen number of < 0.01 . Knudsen's number Kn , is a dimensionless ratio of the mean free path to a characteristic dimension of the system, say, the diameter of a pipe:

$$Kn = \frac{\lambda}{d} \quad \blacktriangleright (3.1)$$

In continuum flow the diameter of the pipe is much greater than the mean free path and the character of the gas flow is determined by gas–gas collisions. The flow has a maximum velocity in the center of the channel and zero velocity at the wall. Continuum flow can be either turbulent or laminar viscous. The boundary between turbulent and viscous flow can be expressed in terms of Reynolds' dimensionless number R for round pipes:

$$R = \frac{Upd}{\eta} \quad (3.2)$$

where ρ is the mass density (kg/m^3), of the gas of viscosity η flowing with stream velocity U in a pipe of diameter d . Reynolds' number is used to characterize the relative quantity of gas flow. It is a ratio of the shear stress due to turbulence to the shear stress due to viscosity. Alternatively, it tells something about the forces necessary to drive a gas system in relation to the forces of dissipation due to viscosity. Reynolds [1] found two flow situations dynamically similar when this dimensionless number was the same. When $R > 2200$, the flow was always turbulent and when $R < 1200$ the flow was always viscous [2]. In the region $1200 < R < 2200$ the flow was viscous or turbulent, depending on the geometry of the inlet and outlet and on the nature of the piping irregularities.

Laminar viscous flow, the ordered flow of a gas in streamlines, occurs in the region bounded by a Reynolds' number lower than 1200 and a Knudsen number less than 0.01.

When the mean free path is equal to or greater than the pipe diameter, say $Kn > 1$, and when $R < 1200$, the gas is said to be a molecular gas, and the flow is called molecular flow. To be precise, Reynolds' number does not have any meaning for a gas in the free-molecular regime, because classical viscosity cannot be defined. The nature of molecular flow is very different from laminar viscous flow. Gas–wall collisions predominate and the concept of viscosity is meaningless. For most surfaces, diffuse reflection at the wall is a good approximation; that is, each particle arrives, sticks, rattles around in a surface imperfection, and is re-emitted in a direction independent of its incident velocity. Thus there is a chance that a particle entering a pipe in which $\lambda \gg d$ will not be transmitted, but will be returned to the entrance. In molecular flow, gas molecules do not collide with one another, and gases can flow in opposite directions without interaction.

In the region $1 > Kn > 0.01$ the gas is neither viscous nor molecular. Flow in the transition region is difficult to treat theoretically. In this range,

called the transition, or slip flow range, where the pipe is several mean free paths wide, the velocity at the wall is not zero, as in viscous flow and the reflection is not diffuse, as in free molecular flow. Now let us define throughput, mass flow and conductance and develop some practical gas flow formulas.

3.2 THROUGHPUT, MASS FLOW, AND CONDUCTANCE

Throughput is the quantity of gas (the volume of gas at a known pressure) that passes a plane in a known time; $d/dt(PV) = Q$. In SI throughput has units of Pa-m³/s. Because 1 Pa = 1 N/m², and 1 J = 1 N-m, the units could be expressed as J/s or watts (1 Pa-m³/s = 1 W). Throughput is the energy per unit time crossing a plane. The energy in question is not the kinetic and potential energy contained in the gas molecules, but rather the energy required to transport the molecules across a plane. Expressing gas flow in units of watts is awkward and not used, but it helps to explain the concept that throughput is energy flow. Throughput is a volumetric dimension (volume of gas/unit time). Throughput cannot be converted to mass flow unless the temperature is specified. It is in many ways unfortunate that vacuum technologists have chosen to use a volumetric unit, which conveys incomplete information. Volumetric flow does not conserve mass.

Mass flow, molar flow, or molecular flow are, respectively, the quantity of substance in units of kg, kg-moles, or molecules that passes a plane in a known time. Equation (3.3) describes the relationship between molar flow and throughput.

$$N'(\text{kg - mole/s}) = \frac{Q}{N_o kT} = \frac{Q}{RT} \quad (3.3)$$

In a similar fashion, mass flow is related to throughput by $N'(\text{kg/s}) = MQ/N_o kT$. Throughput can be related to molar or mass flow, only if the temperature is constant and known. A spatial change in the temperature can alter the throughput without altering the mass flow. We discuss applications of mass flow in Chapter 6 (flow meters) and in Chapter 15 where we describe cryogenically pumped systems.

The flow of gas in a duct or pipe is dependent on the pressure drop across the object as well as its cross-sectional geometry. Division of the throughput by the pressure drop across a duct held at constant temperature yields a property known as the conductance of the duct.

$$C = \frac{Q}{P_2 - P_1} \quad \blacktriangleright (3.4)$$

In SI the unit of throughput is the $\text{Pa}\cdot\text{m}^3/\text{s}$ and the unit of conductance or pumping speed is the m^3/s ; however, related throughput units of $\text{Pa}\cdot\text{L}/\text{s}$ and conductance units of L/s are widely used. Unless explicitly stated, all formulas in this chapter use the cubic meter as the volumetric unit.

The pressures P_1 and P_2 in (3.4) refer to the pressures measured in large volumes connected to each end of the channel or component. According to (3.4) conductance is the property of the object between the points at which the two pressures are measured. For those whose first introduction to flow was with electricity (3.4) is analogous to an electrical current divided by a potential drop. As with electrical charge flow, there are situations (transition, viscous and choked flow) in which the gas conductance is nonlinear, that is, a function of the pressure in the tube. Unlike electrical charge flow, there are cases in which the molecular conductance depends not only on the object, but also on the nature of adjacent objects and how they allow particles to be diffusely scattered from their surfaces. We will explore this last issue in detail when we describe methods for combining conductances in the molecular flow regime.

3.3 CONTINUUM FLOW

A gas is called a viscous gas when $\text{Kn} < 0.01$. The flow in a viscous gas can be either turbulent $\text{R} > 2200$, or viscous $\text{R} < 1200$. Equation (3.2) can be put in a more useful form by replacing the stream velocity with

$$U = \frac{Q}{AP} \quad (3.5)$$

If we replace the mass density, using the ideal gas law, (3.2) becomes

$$\text{R} = \frac{4m}{\pi k T \eta} \frac{Q}{d} \quad \blacktriangleright (3.6)$$

For air at 22°C , this reduces to

$$\text{R} = 8.41 \times 10^{-4} \frac{Q(\text{Pa} \cdot \text{L}/\text{s})}{d} \quad (3.7)$$

In ordinary vacuum practice turbulent flow occurs infrequently. Reynolds' number can reach high values in the piping of a large roughing pump during the initial pumping phase. For a pipe 250 mm in diameter connected to a 47-L/s pump, R at atmospheric pressure is 16,000. Turbulent flow will exist whenever the pressure is greater than $1.5 \times 10^4 \text{ Pa}$ (100 Torr). In practice, roughing lines are often throttled during the initial portion of the roughing cycle to prevent the sudden out-rush of gas from scattering

process debris that may reside on the chamber floor. The flow in the throttling orifice is turbulent at high pressures.

In the high flow limit of the turbulent flow region the velocity of the gas may reach the velocity of sound in the gas. Further reduction of the downstream pressure cannot be sensed at the high-pressure side so that the flow is choked or limited to a maximum or critical value of flow. The value of critical flow depends on the geometry of the element, for example, orifice, short tube, or long tube, and the shape of the entrance. A detailed discussion of critical flow has been given by Shapiro [3].

Rather than divide the discussion of continuum flow into viscous, turbulent and critical, it is easier to discuss the flow in terms of the geometry of the pipe. We divide this discussion into orifice flow, long tube flow, and short tube flow, and we give equations for each region.

3.3.1 Orifices

For tubes of zero length (an extremely thin orifice) the flow versus pressure is a rather complicated function of the pressure. Consider a fixed high pressure, say atmospheric pressure, on one side of the orifice with a variable pressure on the downstream side. As the downstream pressure is reduced, the gas flowing through the orifice will increase until it reaches a maximum. At this ratio of inlet to outlet pressure (the critical pressure ratio), the gas is flowing at the speed of sound in the gas. The gas flow through the orifice is given by

$$Q = AP_1 C^* \left(\frac{2\gamma}{\gamma-1} \frac{kT}{m} \right)^{1/2} \left(\frac{P_2}{P_1} \right)^{1/\gamma} \left[1 - \left(\frac{P_2}{P_1} \right)^{(\gamma-1)/\gamma} \right]^{1/2} \quad \blacktriangleright (3.8)$$

for $P_2 / P_1 \geq (2/(\gamma+1))^{\gamma/(\gamma-1)}$

The factor C^* accounts for the reduced cross-sectional area as the high-speed gas stream continues to decrease in diameter, after it passes through the orifice. This phenomenon is called the vena contracta. For thin, circular orifices, C^* is ~ 0.85 . If the downstream pressure P_2 is further reduced, the gas flow will not increase, because the gas in the orifice is traveling at the speed of sound and cannot communicate with the high-pressure side of the orifice to tell it that the pressure has changed. In this region P_2 cannot influence the flow so long as $P_2/P_1 < (2/(\lambda+1))^{\lambda/(\lambda-1)}$. The ratio of specific heats is λ whose values are given in Appendix B.4. The flow is given by

$$Q = AP_1 C^* \left(\frac{kT}{m} \frac{2\gamma}{\gamma+1} \right)^{1/2} \left(\frac{2}{\gamma+1} \right)^{\gamma/(\gamma-1)} \quad \blacktriangleright (3.9)$$

for $P_2 / P_1 \leq (2/(\gamma+1))^{\gamma/(\gamma-1)}$

This value is called critical, or choked, flow. See Fig. 3.1. This limit is important in describing flow restrictors (devices that control gas flow and the rate of pumping or venting in a vacuum system), choked flow in air-to-air load locks, and flow through small leaks from atmosphere. In any of these relationships, the conductance can be found from $C = Q/(P_1 - P_2)$. For air at 22°C, $\lambda = 1.4$ and $P_2/P_1 = 0.525$; the choked-flow limit is

$$Q(\text{Pa} \cdot \text{m}^3/\text{s}) = 200 P_1 A C' \quad \blacktriangleright (3.10)$$

for air at 22°C, when $P_2 / P_1 \leq 0.52$

$$Q(\text{Pa} \cdot \text{L/s}) = 2 \times 10^5 P_1 (\text{Pa}) A (\text{m}^2) C' \quad \blacktriangleright (3.11)$$

for air at 22°C, when $P_2 / P_1 \leq 0.52$

3.3.2 Long Round Tubes

A general mathematical treatment of viscous flow results in the Navier-Stokes equations, which are most complex to solve. The simplest and most familiar solution for long straight tubes is the equation due to independently to Poiseuille and Hagen, and called the Hagen-Poiseuille equation:

$$Q = \frac{\pi d^4}{128 \eta l} \frac{(P_1 + P_2)}{2} (P_1 - P_2) \quad \blacktriangleright (3.12)$$

The gas flow for air at room temperature becomes

$$Q(\text{Pa} \cdot \text{m}^3/\text{s}) = 718.5 \frac{d^4 (P_1 + P_2)}{l} (P_1 - P_2) \quad (3.13)$$

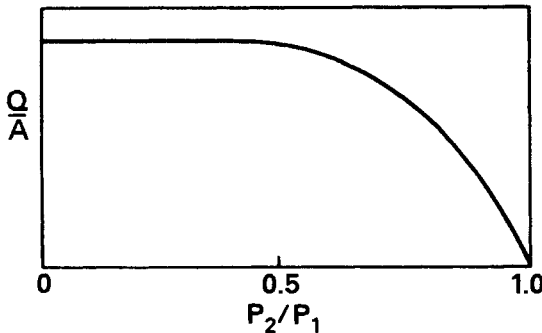


Fig. 3.1 Throughput versus pressure ratio in a circular orifice.

This specific solution is valid when four assumptions are met: (1) fully developed flow (the velocity profile is not position-dependent), (2) laminar flow, (3) zero wall velocity, and (4) incompressible gas. Assumption 1 holds for long tubes in which the flow lines are fully developed. The criterion for fully developed flow was determined by Langhaar [4] who showed that a distance of $l_e = 0.0568dR$ was required before the flow streamlines developed into their parallel, steady-state profile. For air at 22°C this reduces to l_e (meters) = $0.0503Q$ when Q is given in units of Pa·m³/s. Assumptions 2 and 3 are satisfied if $R < 1200$ and if $Kn < 0.01$. The assumption of incompressibility holds true, provided that the Mach number U , the ratio of gas-to-sound velocity, is < 0.3 .

$$U = \frac{U}{U_{\text{sound}}} = \frac{4Q}{\pi d^2 P U_{\text{sound}}} < \frac{1}{3} \quad (3.14)$$

For the special case of air at 22°C we have

$$Q(\text{Pa} \cdot \text{L/s}) < 9.0 \times 10^5 d^2 P \quad \blacktriangleright (3.15)$$

This is a value of flow that may be exceeded in many cases and would render the results of the Poiseuille equation incorrect.

Relationships for viscous flow between long, coaxial cylinders and long tubes of elliptical, triangular and rectangular cross section have been tabulated by Holland et al. [5]. Williams et al. [6] give the relation for flow in a long rectangular duct for air at 20°C

$$Q(\text{Pa} \cdot \text{L/s}) = 4.6Y \frac{b^2(\text{cm}^2)h^2(\text{cm}^2)}{l(\text{cm})} \frac{(P_1 + P_2)}{2} (P_1 - P_2) \quad (3.16)$$

where the duct cross-section dimensions b and h and the length l are given in cm. The function $Y(h/b)$ is obtained from the following table:

h/b	Y	h/b	Y	h/b	Y
1.0	0.4217	0.4	0.30	0.05	0.0484
0.8	0.41	0.2	0.175	0.02	0.0197
0.6	0.31	0.1	0.0937	0.01	0.0099

In the limit $h \ll b$, the air flow reduces to the one-dimensional solution of Sasaki and Yasunaga [7]

$$Q(\text{Pa} \cdot \text{L/s}) = 4.6Y \frac{h^3(\text{cm}^3)b(\text{cm})}{l(\text{cm})} \frac{(P_1 + P_2)}{2} (P_1 - P_2) \quad (3.17)$$

Again h , b , and l are given in cm. The flow in (3.16) and (3.17), like (3.13), is inversely proportional to viscosity and may be accordingly scaled for other gases. These relations for long tubes are of limited use. They are of use in components such as mass flow meter tubes, controlled leaks, and piping that connects chambers with remotely located pumps and gas tanks. In most practical cases we connect chambers with as short a duct as possible to reduce unwanted pressure drops, and we need to know relationships which are valid for these cases.

3.3.3 Short Round Tubes

As we noted above, the flow in short tubes does not obey the Poiseuille equation. The flow may switch from viscous to critical flow without there being any pressure region in which the Poiseuille equation is valid. This problem has been treated in several ways. Dushman [8] gives a non-linear relation for flow in short round tubes. It is valid only for unchoked flow. Santeler [9] devised a technique in which he models the short tube as an aperture in series with a short tube of length l . The problem is formulated by assuming an unknown pressure P_x between the “tube” and the “aperture.” This is the pressure that would be measured by a gauge just inside the end of the tube that was pointing upstream. Figure 3.2 illustrates an application of this technique—calculating the pressure drop and airflow through a 100- μm -diameter leak in a 1-cm-thick vacuum wall. Santeler’s model uses (3.13) with P_1 replaced by P_x . The flow through the aperture was modeled using (3.10) with P_x as its inlet pressure, and “high vacuum” ($P = 0$) as its outlet pressure. Since the two flows are in series, they are equal; the solution is $P_x = 44,560$ Pa. The answer can be checked to ensure that the assumption of choked flow in the aperture is valid; if not, then (3.8) must be used in place of (3.10). This model predicts Poiseuille leak flow with significant gas expansion at the vacuum side.

3.4 MOLECULAR FLOW

A gas is called a molecular gas when $\text{Kn} > 1.0$. This is equivalent to stating that $Pd < 6.6$ Pa-mm (4.95 Torr-mm) for air at 22°C. In this region the flow is called molecular flow. For completeness we could say that $\text{Re} < 1200$; however, we cannot define a Reynolds number in the region where viscosity cannot be defined. The molecular flow region is theoretically the best understood of any flow type. This discussion focuses on orifices, infinite tubes, finite tubes, and other shapes, including combinations of components in molecular flow.

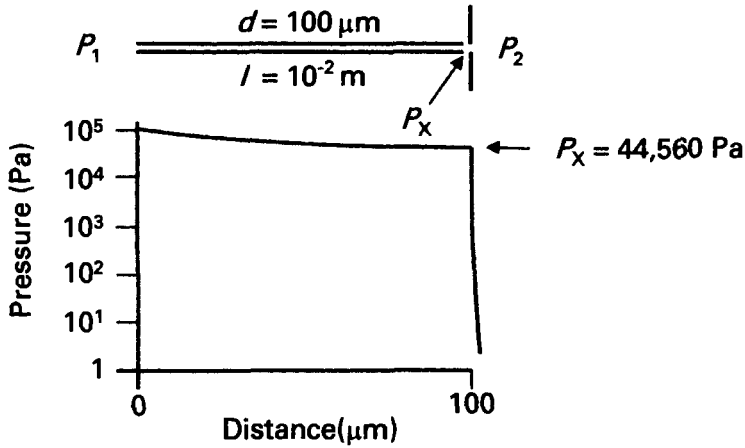


Fig. 3.2 Pressure profile through a fine leak in a vacuum wall, as calculated with Santeler's model. This model assumes Poiseuille flow through the tube with a precipitous drop in pressure immediately within the vacuum vessel caused by choked flow at the exit.

3.4.1 Orifices

If two large vessels are connected by an orifice of area A and the diameter of the orifice is such that $Kn > 1$, then the gas flow from one vessel (P_1, n_1) to the second vessel (P_2, n_2) is given by

$$Q = \frac{kT}{4} v A (n_1 - n_2) = \frac{v}{4} A (P_1 - P_2) \quad (3.18)$$

and the conductance of the orifice is

$$C = \frac{Q}{P_1 - P_2} = \frac{v}{4} A \quad \blacktriangleright (3.19)$$

which for air at 22°C has the value

$$C(\text{m}^3/\text{s}) = 116A(\text{m}^2) \quad (3.20)$$

or

$$C(\text{L/s}) = 11.6A(\text{cm}^2) \quad \blacktriangleright (3.21)$$

From (3.18) we note an interesting property of the molecular flow regime. Gas can flow from vessel 2 to vessel 1; at the same time gas is flowing from vessel 1 to vessel 2 without either of the gases colliding with gas that originated in the other vessel.

3.4.2 Long Round Tubes

The diffusion method of Smoluchowski [10] and the momentum transfer method of Knudsen [11] and Loeb [12] were the first used to describe gas flow through very long tubes in the free molecular flow region. For circular tubes both derivations yield conductances of

$$C_{\text{tube}} = \frac{\pi}{12} v \frac{d^3}{l} \quad (3.22)$$

For air at 22°C this becomes

$$C_{\text{tube}} (\text{m}^3/\text{s}) = 121 \frac{d^3}{l} \quad (3.23)$$

Conductance relations for long noncircular tubes have been derived [13].

3.4.3 Short Round Tubes

The flow equation for long tubes (3.22) indicates the conductance becomes infinite as the length tends toward zero, whereas in Section 3.4.1 we showed the conductance actually becomes $vA/4$. Dushman [14] developed a solution to the problem of short tubes by considering the total conductance to be the sum of the reciprocal conductances of an aperture and a section of tube of length l .

$$\frac{1}{C_{\text{total}}} = \frac{1}{C_{\text{tube}}} + \frac{1}{C_{\text{aperture}}} \quad (3.24)$$

As $l/d \rightarrow 0$, (3.24) reduces to (3.19), and as $l/d \rightarrow \infty$ it reduces to (3.22). Although this equation gives the correct solution for the extreme cases, it is not correct for the intermediate. It can be in error by as much as 12–15%.

The difficulty in performing calculations for short tubes lies in the nature of the gas–wall interaction. Lorentz [15] assumed the walls of a pipe are molecularly rough; that is, molecules are scattered according to the cosine law (diffuse reflection). Molecules hit a wall, oscillate in potential wells, and recoil in a direction that is independent of their arrival angle. In diffuse reflection, scattered molecules have the greatest probability of recoiling at an angle of 90° from the surface. Particles not scattering at 90° have as much likelihood of going forward through the tube as going backward toward the source. See Fig. 3.3. Clausing [16] solved this problem by calculating the probability that a molecule entering the pipe at one end will escape at the other end after making diffuse collisions with the walls. Clausing's solution is in the form of an integral that is difficult to evaluate. For simple cases such as round pipes, Clausing and others have generated approximate solutions. The solution has been tabulated in many standard

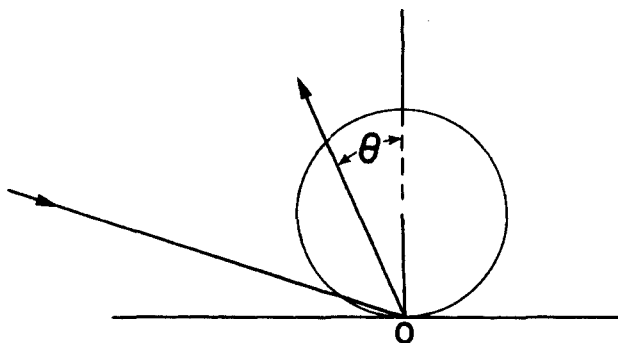


Fig. 3.3 A molecule making diffuse collisions with a wall is scattered in a direction independent of its original path. A molecule forgets its original direction and is emitted with a probability proportional to $\cos \phi$ from the normal. The most probable angle is $\phi = 0^\circ$. A molecule has an equal probability of going forward as it does backward.

texts, and it is usually given in the form of a transmission probability a that a molecule entering the pipe will leave the pipe at the other end. The conductance of a pipe is then found from (3.25), where A is the cross-sectional area of the pipe and v is the thermal velocity of the gas.

$$C = a \frac{v}{4} A \quad \blacktriangleright (3.25)$$

For the special case of very long round tubes ($l \gg d$), the expression given in (3.22) can be written in the form of (3.25) to reveal that the transmission probability a of a long tube is $(4d/3l)$ as shown in Table 3.1.

$$C = \left(\frac{4d}{3l} \right) \frac{v}{4} \left(\frac{\pi d^2}{4} \right) \quad (3.26)$$

For air at 22°C the conductance can be simplified to read

$$C \text{ (L/s)} = 1.16 \times 10^5 a A \text{ (m}^2\text{)}$$

$$C \text{ (L/s)} = 1.16 a A \text{ (cm}^2\text{)} \quad \blacktriangleright (3.27)$$

Equation (3.27) describes the molecular conductance per unit area of any structure in molecular flow has a maximum value [$11.6 \text{ L/(s-cm}^2\text{)}$ for air at 22°C] and that any structure (thicker than a thin aperture) will have a conductance less than this value.

DeMarcus [17] used a variational principle to solve the Clausing integral with improved accuracy. Berman [18] made a polynomial fit to DeMarcus' solution, and extended it to larger l/d values. Values of the transmission

Table 3.1 Transmission Probability a for Round Pipes

l/d	a	l/d	a
0.00	1.00000	1.6	0.40548
0.05	0.95240	1.7	0.39195
0.10	0.90922	1.8	0.37935
0.15	0.86993	1.9	0.36759
0.20	0.83408	2.0	0.35658
0.25	0.80127	2.5	0.31054
0.30	0.77115	3.0	0.27546
0.35	0.74341	3.5	0.24776
0.40	0.71779	4.0	0.22530
0.45	0.69404	4.5	0.20669
0.50	0.67198	5.0	0.19099
0.55	0.65143	6.0	0.16596
0.60	0.63223	7.0	0.14684
0.65	0.61425	8.0	0.13175
0.70	0.59737	9.0	0.11951
0.75	0.58148	10.0	0.10938
0.80	0.56655	15.0	0.07699
0.85	0.55236	20.0	0.05949
0.90	0.53898	25.0	0.04851
0.95	0.52625	30.0	0.04097
1.0	0.51423	35.0	0.03546
1.1	0.49185	40.0	0.03127
1.2	0.47149	50.0	0.02529
1.3	0.45289	500.0	0.26479×10^{-2}
1.4	0.43581	5000.0	0.26643×10^{-3}
1.5	0.42006	∞	$4d/3l$

probability for round pipes obtained from his equations are given in Table 3.1 for a range of l/d values. The DeMarcus-Berman results agree with very precise calculations done by Cole [19] to between 4 and 5 decimal places. These values of a can be used in (3.25) and (3.27). "Exit effects", which we shall discuss shortly, are included in these tabulations of probability values.

3.4.4 Other Short Structure Solutions

The calculation of molecular conductance in an arbitrarily complex short tube structure is not possible in closed form. The molecular conductance has been solved analytically for noncircular cross sections in only a few cases. Where exact solutions are not possible, probabilistic methods have been used. Tanigouchi et al. [20] have simulated the effects of varying accommodation coefficient and sticking coefficient on probability.

**Table 3.2 Transmission Probability a
for Thin, Rectangular, Slit-like Tubes**

l/h	a	l/h	a
0.0	1.00000	15	0.18664
0.1	0.95245	20	0.15425
0.2	0.90958	30	0.11648
0.3	0.87097	40	0.09471
0.4	0.83617	50	0.08035
0.5	0.80473	60	0.07008
0.6	0.77620	70	0.06234
0.7	0.75021	80	0.05627
0.8	0.72643	90	0.05136
0.9	0.70457	100	0.04731
1.0	0.68438	200	0.02722
2.0	0.54206	500	0.01276
3.0	0.45716	1000	0.70829×10^{-2}
4.0	0.39919	2000	0.38914×10^{-2}
5.0	0.35648	5000	0.17409×10^{-2}
6.0	0.32339	10000	0.94000×10^{-3}
7.0	0.29684	20000	0.50472×10^{-3}
8.0	0.27496	50000	0.22023×10^{-3}
9.0	0.25655	100000	0.11705×10^{-3}
10	0.24080	200000	0.61994×10^{-4}

Analytical Solutions

A geometry that is not circular in cross section is the thin, rectangular, slit-like pipe. This geometry is often encountered in differentially pumped feedthroughs and joints between differentially pumped chambers. It consists of a thin gap of thickness h , length l , and width b , with the condition $h \ll b$, where b , h , and l are defined in Fig. 3.8. Berman [18] developed a polynomial fit to solutions for the transmission coefficient and values calculated with the use of his formula are given in Table 3.2. His results agree with those of Neudachin et al. [21]. The conductance of a slit can be calculated from (3.25) using the transmission probability from Table 3.2 and an inlet area of bh . "Exit conductance" drops are also included in these transmission probabilities. The transmission probability has been experimentally shown to decrease with increased surface roughness [22].

In addition to the short round pipe and the slit-like tube discussed above, solutions exist for the annular cylindrical pipe [23], the rectangular pipe [24], the elliptical tube, and the triangular tube [5]. Other short tube cross

sections and complex structures have been treated with statistical techniques such as the Monte Carlo technique described here.

Monte Carlo Technique

The Monte Carlo statistical methods developed for the calculation of molecular flow conductance by Davis [25] and by Levenson et al. [26] were a major breakthrough in the calculation of complex, but practical, vacuum system elements such as elbows, traps, and baffles. The Monte Carlo technique uses a computer to simulate the individual trajectories of a large number of randomly chosen molecules. Figure 3.4 is a computer graphical model of the trajectories of 15 random molecules entering an elbow. It yielded a transmission probability of 0.222. When a large number of particles was used, the transmission probability of 0.31 was calculated. This points to one difficulty of the Monte Carlo technique; its accuracy depends on the number of molecular trajectories used in the calculation. A great deal of computational time is required for accurate solutions to complex problems. Figures 3.5 through 3.12 contain examples of the Monte Carlo technique for some structures of interest [25–27]. The molecular conductance is the product of the probability and conductance of

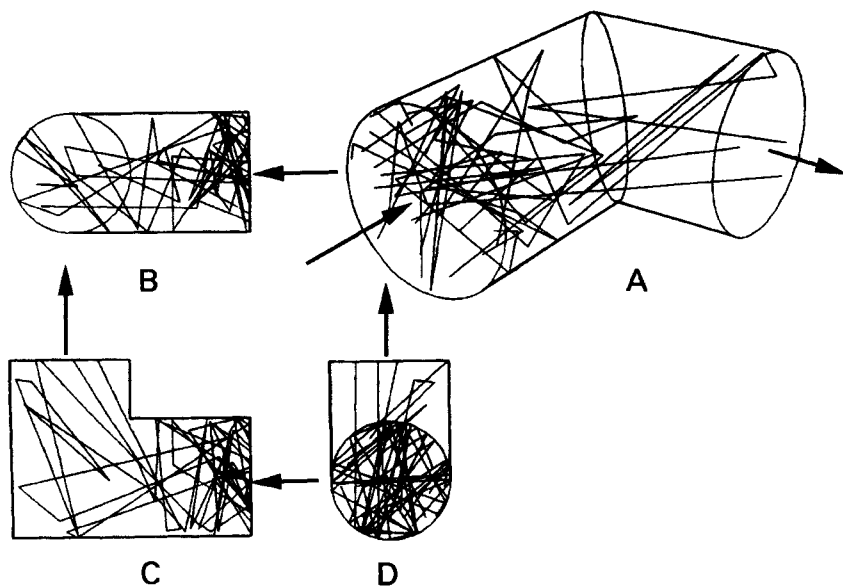


Fig. 3.4 A computer graphical display of the trajectories of 15 molecules entering an elbow in free molecular flow. Courtesy of A. Appel, IBM T. J. Watson Research Center.

an aperture identical in shape to the entrance of the structure under consideration. End effects are included in these formulas as well. The great computational time required to perform a transmission probability calculation by the Monte Carlo technique, has driven others to approximate complex systems by combining cylindrical tubes, orifices, and baffle plates. See, for example, Füstöss and Töth [28], Harries [29], Steckelmacher [30], Oatley [31], Haefer [32], and Ballance [33]. However, molecular conductances must be combined in series with great care. The increased capability of desktop computing has made possible direct simulation with Monte Carlo methods [34].

3.4.5 Combining Molecular Conductances

Implicit in the definition of conductance (3.4) is the understanding that molecules will arrive at the entrance to the component distributed in a Maxwell-Boltzmann fashion, and depart into a void without colliding with another surface. This is possible only if there are no other walls in the vicinity of the entrance and exit of the component. It can be accomplished by connecting the component between two large reservoirs so that the pressures in the vessels will be unaffected by the flow through the component. In practice this condition is rarely met. Typically the shortest possible lengths of pipe are used to interconnect pumps, chambers, traps, and baffles or elbows (whose length is of the order of the pipe diameter).

Parallel Conductances

The conductance of tubes connected in parallel can be obtained from the simple sum and is independent of any end effects.

$$C_T = C_1 + C_2 + C_3 + \dots \quad \blacktriangleright (3.28)$$

Series Conductances

Series conductances of truly independent elements in molecular flow will yield a total conductance of

$$\frac{1}{C_T} = \frac{1}{C_1} + \frac{1}{C_2} + \frac{1}{C_3} + \dots \quad \blacktriangleright (3.29)$$

Equation (3.29) gives the value of conductance we would measure if the elements were isolated from each other by large volumes. See Fig. 3.13a. The large volume provides a place for the distribution of molecules exiting the prior conductance to completely randomize, or assume the distribution of a rarefied Maxwell-Boltzmann gas.

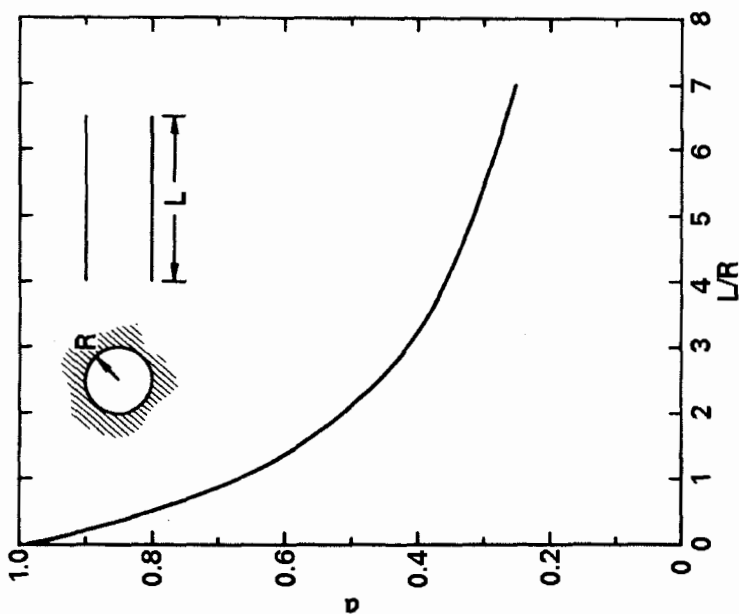


Fig. 3.5 Molecular transmission probability of a round pipe. Reprinted with permission from *Le Vide*, No. 103, p. 42, L. L. Levenson et al. Copyright 1963, Société Française des Ingénieurs et Techniciens du Vide.

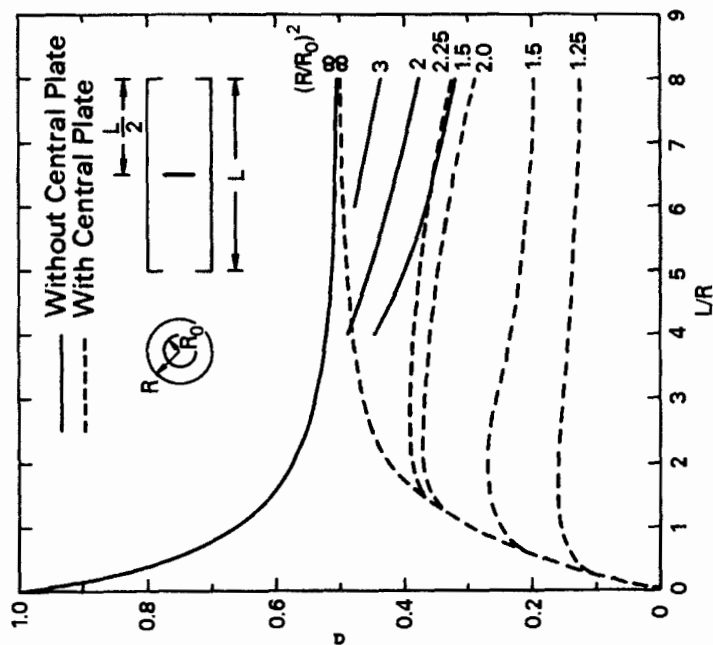


Fig. 3.6 Molecular transmission probability of a round pipe with entrance and exit apertures. Reprinted with permission from *J. Appl. Phys.*, 31, p. 1169, D. H. Davis. Copyright 1960, The American Institute of Physics.

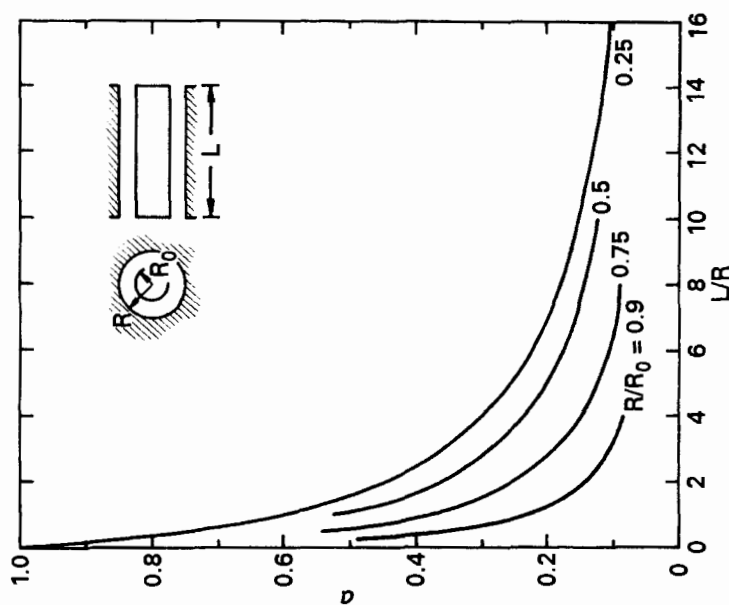


Fig. 3.7 Molecular transmission probability of an annular cylindrical pipe. Reprinted with permission from *Le Vide*, No. 103, p. 42, L. L. Levenson et al. Copyright 1963, Société Française des Ingénieurs et Techniciens du Vide.

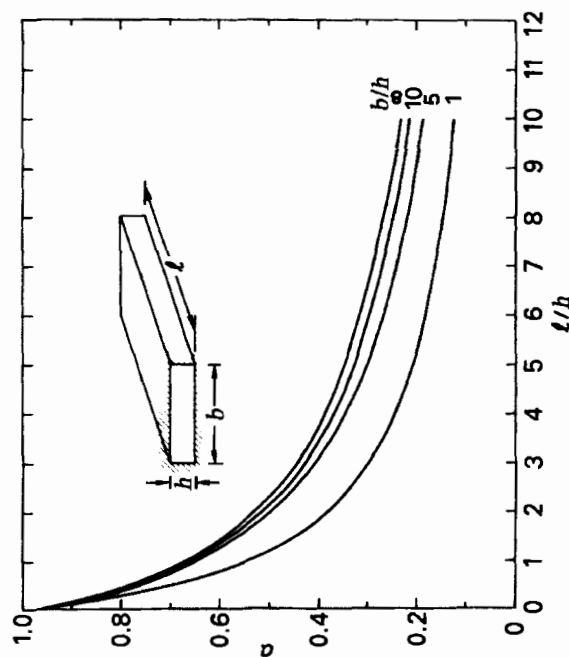


Fig. 3.8 Molecular transmission probability of a rectangular duct. Reprinted with permission from *Le Vide*, No. 103, p. 42, L. L. Levenson et al. Copyright 1963, Société Française des Ingénieurs et Techniciens du Vide.

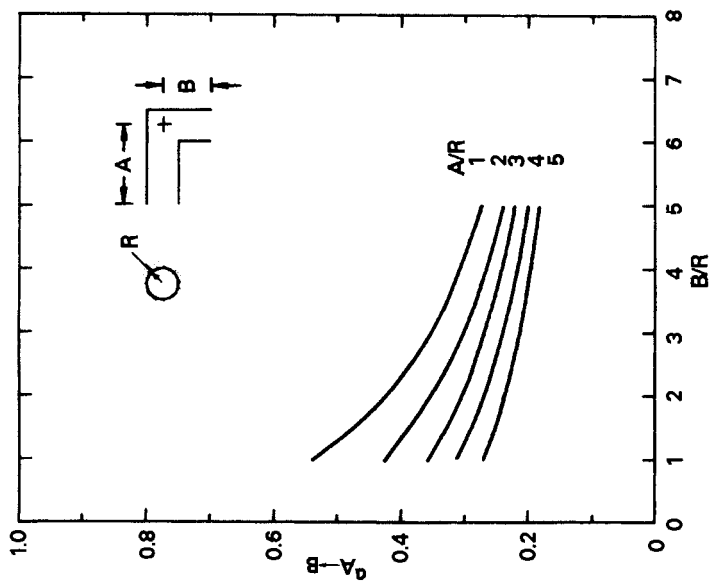


Fig. 3.10 Molecular transmission probability of an elbow. Reprinted with permission from *J. Appl. Phys.*, 31, p. 1169, D. H. Davis. Copyright 1960, The American Institute of Physics.

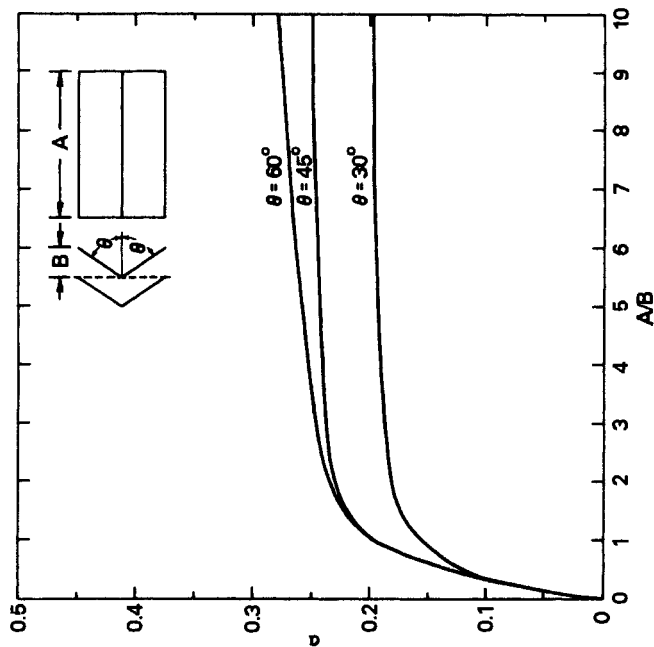


Fig. 3.9 Molecular transmission probability of a chevron baffle. Reprinted with permission from *Le Vide*, No. 103, p. 42, L. L. Levenson et al. Copyright 1963, Société Française des Ingénieurs et Techniciens du Vide.

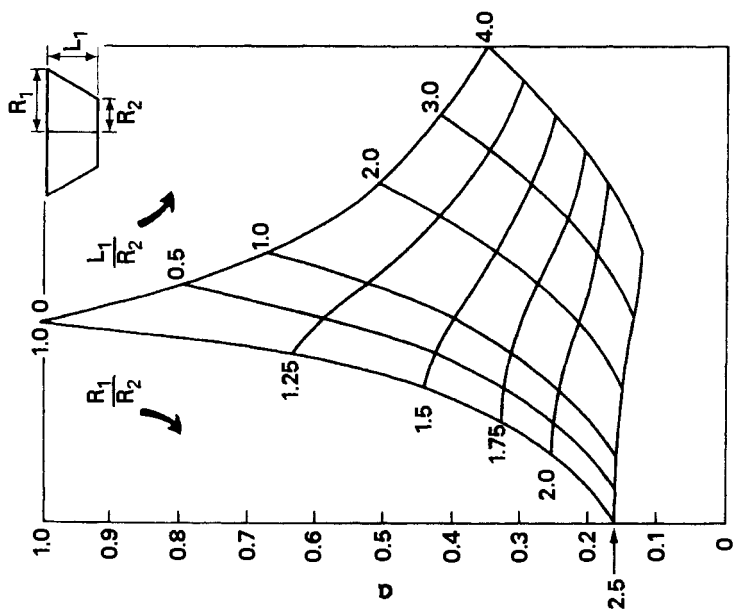


Fig. 3.11 Molecular transmission probability of a frustum of a cone. Reprinted with permission from *Trans. 9th Natl. Vac. Symp.*, J. D. Pinson and A. W. Peck. Copyright 1962, Macmillan, New York, p. 407.

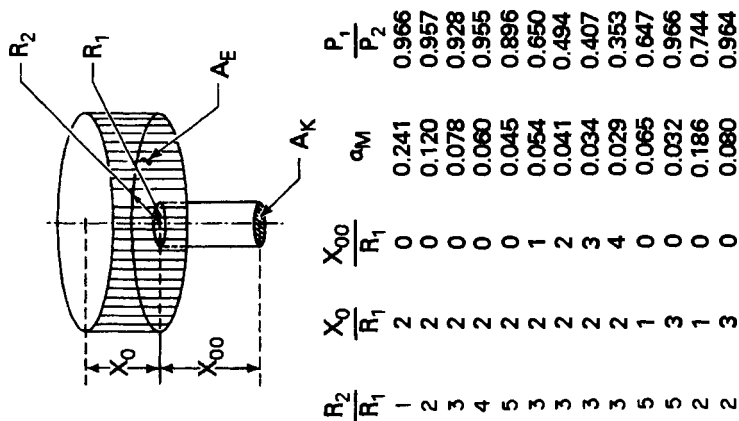


Fig. 3.12 Molecular transmission probability of a parallel plate model. Reprinted with permission from *Trans. 9th Natl. Vac. Symp.*, J. D. Pinson and A. W. Peck. Copyright 1962, Macmillan, New York, p. 407.

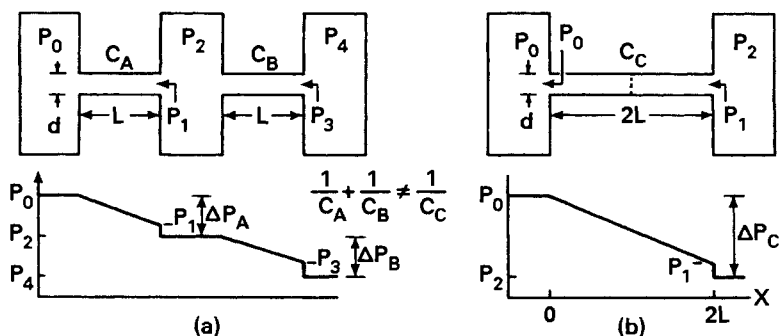


Fig. 3.13 Series conductance of two elements: (a) the pipes are isolated by a large volume, and (b) the pipes are connected directly together. The pressure readings are those measured by a gauge in the gas stream pointing upstream and parallel to the flow direction.

Exit and Entrance Effects

The simple reciprocal rule does not work where we combine two conductances directly. See Fig. 3.13b. Let us consider two tubes each of length-to-diameter ratio $l/d = 1$. From Table 3.1 we obtain the transmission probability of each tube as $a = 0.51423$. If we combine them according to the reciprocal rule in (3.29) we will obtain a net transmission probability of $a = 0.25712$. We know that the transmission of this structure (tube with $l/d = 2$) can be found from the data in Table 3.2 as $a = 0.35685$. The error in using the simple reciprocal rule is 27.9%. Why do we have this large error? The reason is the pressure distribution in the two tubes is not the same. For the case of the isolated conductances, the pressure in the (imaginary) large chamber between the two pipes can be defined. It is single-valued and could be measured with a gauge in the chamber. If we were to point a directional gauge in any direction in this chamber, we would measure the same pressure. In an analogous fashion, we could measure a voltage at the junction of two series resistors, which are carrying a current.

When we combine two pipes in series without the large volume in between, the situation changes drastically. The pressure at the exit of the first tube and the entrance to the second tube are now the same but not easy to define. If we were to place a directional gauge at the junction of the two pipes and point it upstream, it would read higher than downstream. Also, were it to face sideways, it would also depend on whether it were in the center of the tube or off-axis. The pressure is anisotropic. This is to be contrasted to the case of the two tubes connected by a chamber, which has a known pressure. In that case the only place where the pressure will differ is at the exit of the first tube as it enters the chamber as measured with a gauge looking upstream. That pressure will be higher than in the chamber.

Recall the definition of conductance given in (3.3). If we examine Fig. 3.13a, we see that the pressure difference in (3.3) is measured in the large chambers at each end of the tube. By measuring the pressure in this way we include the pressure drop schematically shown at the end of the tube. When we connect the two tubes directly, we have eliminated the pressure drop at the exit of the tube that would be measured by an upstream-directed gauge. For this reason we say the conductances tabulated here and in other sources include what Santeler [35] called the *exit loss*.

There is another effect, which is present to a small extent—gas beaming. Note that the gas entering the second tube in Fig. 3.13a is randomly distributed, while the gas entering the second half of the tube in Fig. 3.13b is beamed. See for example the molecular exit angles depicted in Fig. 3.14. In normal cases this is a small correction—a few percent—which we will describe shortly. Beaming effects (entrance effects) in most real molecular flow situations do not introduce major errors, because real systems are made up of short tubes connected by elbows, traps, and so on. We observe in Fig. 3.14 that short tubes have near-cosine exit flux. Any component containing an elbow, baffle, chevron, or the like will also scatter molecules and shift the distribution toward cosine.

Series Calculations

Harries [29], Steckelmacher [30], Oatley [31] and Haefer [32] have each used the concept of a probability factor a , to calculate the conductance of a

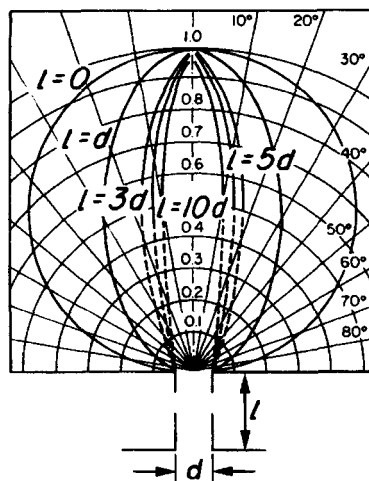


Fig. 3.14 Angular distribution of particles exiting tubes of various ratios of length to diameter. Reproduced with permission from *Atom and Ion Sources*, 1977, p. 86, L. Vályi. Copyright 1977, Akadémiai Kiadó, Budapest.

series combination of vacuum elements in free molecular flow. We examine here the method developed by Oatley. Figure 3.15 illustrates the concept with a single component; Γ molecules per second enter at the left-hand side, Γ molecules per second exit at the right-hand side, and $(1 - a)\Gamma$ molecules per second are returned to the source vessel. The conductance is expressed by

$$C = a \frac{v}{4} A \quad (3.30)$$

For two tubes in series, Oatley developed a technique for calculating a combined probability, the results of which are illustrated in Fig. 3.16. Among the Γ molecules per second that enter the first tube $a_1\Gamma$ enter the second; $\Gamma(1 - a_2)a_1$ of these are returned to the first tube and $\Gamma a_1 a_2$ enter the second. From the group $\Gamma(1 - a_2)a_1$ molecules returned the first tube $\Gamma a_1(1 - a_2)(1 - a_1)$ are returned to the second, and so on, until an infinite series expression was developed that simplified to

$$\frac{1}{a} = \frac{1}{a_1} + \frac{1}{a_2} - 1 \quad (3.31)$$

The last term represents the exit pressure drop, which is subtracted in this formula. When generalized to several elements in series, this becomes

$$\frac{1-a}{a} = \frac{1-a_1}{a_1} + \frac{1-a_2}{a_2} + \frac{1-a_3}{a_3} + \dots \quad \blacktriangleright (3.32)$$

Now let us use (3.31) or (3.32) and calculate the series conductance of the two pipes of $l/d = 1$ described earlier. We obtain a value $a = 0.3460$. Note that this is closer to the Clausing value of $a = 0.35685$ obtained from Table 3.1. It is in error by 2.93%, because it cannot account for beaming effects.

Oatley's formula, as given in (3.32), applies directly to elements of the same diameters, but it can be extended to elements of differing diameters. If the series components are of different diameters, or of increased complexity, the addition theorem developed by Haefer provides the easiest solution.



Fig. 3.15 Model for calculating the transmission probability of a single element.

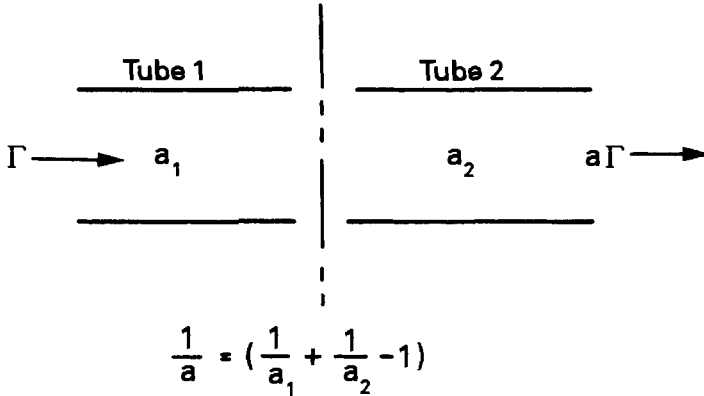


Fig. 3.16 Model for calculating the transmission probability of two elements in series. Reprinted with permission from *Br. J. Appl. Phys.*, **8**, p. 15, C. W. Oatley. Copyright 1957, The Institute of Physics.

Haefer [32] developed a useful addition theorem for elements in the molecular flow regime. It relates the total transmission probability of n elements a_{1n} , to the transmission probability a_i and the inlet area A_i of each component. Extra terms are included in the equation whenever a cross-sectional area decreases upon entering the next element but not when the area increases. It is given here without proof.

$$\frac{1}{A_1} \left(\frac{1 - a_{1 \rightarrow n}}{a_{1 \rightarrow n}} \right) = \sum_1^n \frac{1}{A_i} \left(\frac{1 - a_i}{a_i} \right) + \sum_1^{n-1} \left(\frac{1}{A_{i+1}} - \frac{1}{A_i} \right) \delta_{i,i+1} \quad \blacktriangleright (3.33)$$

where $\delta_{i,i+1} = 1$ for $A_{i+1} < A_i$, and $\delta_{i,i+1} = 0$ for $A_{i+1} \geq A_i$

The use of this formula is demonstrated with the example given in Fig. 3.17. Shown is a combination of three pipe sections of inlet areas A_1 , A_2 , and A_3 . The pipes have corresponding transmission probabilities a_1 , a_2 , and a_3 . By use of (3.33), one obtains

$$\frac{1}{A_1} \left(\frac{1 - a_{1 \rightarrow 3}}{a_{1 \rightarrow 3}} \right) = \frac{1}{A_1} \left(\frac{1 - a_1}{a_1} \right) + \frac{1}{A_2} \left(\frac{1 - a_2}{a_2} \right) + \frac{1}{A_3} \left(\frac{1 - a_3}{a_3} \right) + \left(\frac{1}{A_3} - \frac{1}{A_2} \right) \quad (3.34)$$

after some simplification (3.34) becomes

$$\frac{1}{a_{1 \rightarrow 3}} = \frac{1}{a_1} + \left(\frac{A_1}{A_2} \right) \frac{1}{a_2} + \left(\frac{A_1}{A_3} \right) \frac{1}{a_3} - \left(\frac{A_1}{A_2} \right) 2 \quad (3.35)$$

From (3.35) it can be seen that this answer reduces to (3.32) when the pipe areas are all the same. Haefer's method must be applied with consistency

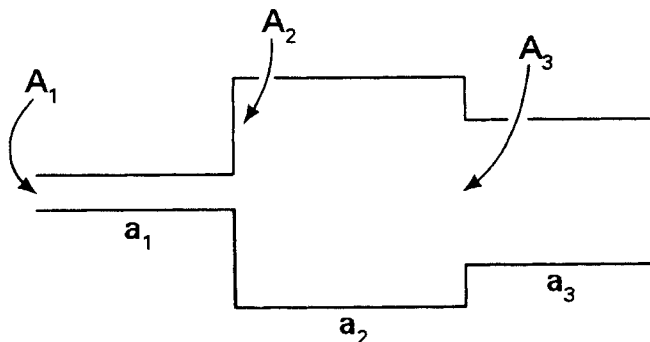


Fig. 3.17 Sample conductance to be evaluated with Haefer's addition theorem.

because the total transmission coefficient one calculates is a function of the end of the structure chosen as the origin. If the transmission probability were calculated from right to left, a_{n-1} , we would have to use an inlet area of A_n in calculating the conductance. However, this does not affect the total conductance of a structure as

$$C = (a_{1 \rightarrow n}) \frac{v}{4} A_1 = (a_{n \rightarrow 1}) \frac{v}{4} A_n \quad (3.36)$$

We can also see that the answer would have been different if the order of the second and third pipes were interchanged. Interchanging the order of components in a series configuration will affect the total transmission probability. As a rule, the conductance of the actual configuration should be calculated, because errors can creep in when components are mathematically rearranged to simplify calculation [36]. It is generally true that a complex structure made up of several series elements has the maximum conductance when the elements are arranged in increasing or decreasing order because the exit losses are the smallest and the beaming is the greatest. Arranging conductances in alternating large and small diameters introduces wall scattering, which makes the input to the following sections more like a Maxwell-Boltzmann gas, with a cosine distribution of scattered molecules.

Problems arise in conductance calculations because (3.29), which is valid for independently defined C 's, is indiscriminately applied to series elements *not isolated* from one another, for example, in which the exit effect is not subtracted, and the inlet gas does not obey a cosine distribution. The most serious error is the introduction of the exit impedance of the tube multiple times. In all tabulated transmission coefficients, the exit term has been included. Therefore it is necessary to

remove it when combining conductances, and for this reason we use formulas like (3.32) or (3.33). The choice between an exact or approximate formula for the conductance of an individual pipe segment is usually less important than the correction for the exit effect. The Oatley and Haefer formulas remove the biggest error in calculating the conductance of combinations—the exit conductance drop at the end of each junction of equal diameter—but neither formula corrects for entrance effects, that is, non-cosine or beamed entrance flux.

Pinson and Peck [27] discuss beaming errors for pipe sections with and without baffles and show the difference between a calculation and Monte Carlo technique is $\leq 10\%$ with the greatest differences seen when a baffle is not used. Beaming corrections for tube combinations have been developed by Santeler [35]. Components like chevron baffles and elbows tend to scatter the gas. For example, the conductance of a nondegenerate elbow can be calculated by using the conductances of the individual arms, obtained from Fig. 3.5, and summing these conductances with (3.31). Saksaganski [37] discusses efficient methods for analyzing complex systems and shows the angular coefficient and integral kinetic methods as alternatives to the Monte Carlo method.

The formulas developed by Haefer and Oatley may be used to calculate the pumping speed at the inlet of pipes connected to a pump. In this case the pump is characterized by its inlet area and H_0 coefficient (defined in Chapter 7). The pump is simply considered to be a conductance of entrance area A and transmission probability α_p equal to its H_0 coefficient.

3.5 THE TRANSITION REGION

The theory of gas flow in the transition region is not well developed. Thomson and Owens [38], and Loyalka et al. [39], have reviewed the state of the theory. DeMuth and Watson [40] have done additional work on the transition between molecular and isentropic flow in orifices. The simplest treatment of this region, due to Knudsen, discussed in many texts states

$$Q = Q_{\text{viscous}} + Z' Q_{\text{molecular}} \quad \blacktriangleright (3.37)$$

where for long circular tubes Z' is given by

$$Z' = \frac{1 + 2.507 \left(\frac{d}{2\lambda} \right)}{1 + 3.095 \left(\frac{d}{2\lambda} \right)} \quad (3.38)$$

3.6 MODELS SPANNING SEVERAL PRESSURE REGIONS

Flow relations that span different pressure regions are difficult to construct. Two examples have already been given in this chapter. In addition to Dushman's model for the transition region discussed above, we have discussed Santeler's model for flow in a short tube in the viscous and choke regions. Santeler's [9] model for a short tube separates the tube component from the exit effect. Therefore, it can be applied to a series of tubes by modeling the system as a series of tubes with one exit loss after the last tube section. Tison [41] developed an empirical fit with a form similar to Knudsen's that described the flow through a metal capillary from the molecular to the viscous region. Other relations have been developed for specialized geometrical shapes. One is a relation developed by Kieser and Grundner [42] for the thin, slit-like tube. The thin, rectangular slit-like tube with one side in a rarefied gas and the other at atmospheric pressure is encountered in atmosphere-to-vacuum continuous feed systems and reel-to-reel coating systems known as web, or roll, coaters. This relation, which is valid in the molecular, transition and viscous flow regions, combines the ideas of Dushman and Knudsen. It is valid for any inlet pressure but only for low exhaust pressures ($P_o < 0.52P_i$). Kieser and Grundner begin with Dushman's relationship, which assumed a duct to be composed of a pipe and an entrance aperture. The conductance of the series combination is

$$\frac{1}{C_{\text{total}}} = \frac{1}{C_{\text{pipe}}} + \frac{1}{C_0} \quad (3.39)$$

or, for air at 20°C,

$$\frac{1}{C_{\text{total}}} = \frac{1}{(0.1106eP_i + Z')C_M} + \frac{1}{C_0} \quad (3.40)$$

C_0 and C_M in (3.40) are given by

$$C_0 (\text{L/s}) = 11.6ew \left[\frac{10 + 0.5(e/\lambda)^{3/2}}{10 + 0.3412(e/\lambda)^{3/2}} \right] \quad (3.41)$$

$$C_M (\text{L/s}) = 11.6ew \left(\frac{a}{1-a} \right) \quad (3.42)$$

In the above relationships, e is the channel thickness, and w is the channel width. The form of (3.41) allows the (air) conductance of the aperture to vary from 11.6 L/s in molecular flow to 17 L/s in the choked limit. Equation (3.41) is an experimental fit to the transition region for air [42].

The pipe conductance given in (3.39) is due to Knudsen and is a superposition of continuum and molecular flow. Since the aperture is

included in the C_0 term, we have removed it from (3.42) [43]. The pipe conductance C_M , calculated by Berman already contains an end effect C_0 . Also the premise on which (3.38) is based, that is, the representation of the total conductance as a series combination of a “pipe conductance” and an “aperture conductance”, is known to be in error by 10–15% in the region $l/e = 1$ –5. For longer pipes there is another small error. Equation (3.40) implicitly lets the average pressure in the “pipe” portion of the conductance be $P_i/2$. This forces the pressure across the viscous conductance to an incorrect value. However, the pipe conductance is in series with a choked orifice, so any error in the “pipe” conductance is greatly attenuated by the series combination. (It is like putting a large resistor in parallel with a very small one—the parallel combination isn’t greatly affected by the value of the larger resistor.)

There are few papers on flow relations, which are valid over several regions. For example, Schumacher [44] summarized the flow through small round tubes in graphical form, while Levina [45] developed nomographs for the same problem.

3.7 SUMMARY OF FLOW REGIMES

The values of gas flow, pressure, and pipe size discussed in the previous sections each extend over a wide range. We summarize this discussion by sketching a plot of flow divided by pipe size (Q/d) versus pressure times distance (Pd). Figure 3.18 depicts the various regions discussed in this section. Molecular flow occurs in the region $R < 1200$, and $Kn > 1$. The flow is proportional to the first power of the pressure (slope = 1). When $Kn < 0.01$ the gas is viscous, and the flow is either turbulent, fully developed (Poiseuille), undeveloped, or choked. Observe that fully developed flow is proportional to the square of the pressure (slope = 2). The boundary between turbulent and laminar viscous is determined by the Reynolds’ number. Langhaar’s number and the Mach number determine the boundary between fully developed and undeveloped flow. We illustrate how a short tube can go from molecular to choked without ever having the Poiseuille equation apply. The region between molecular and viscous flow is the transition region. We see the transition from completely free molecular flow to completely viscous flow can take place over a two-decade pressure range.

In this chapter we have considered the equations of flow in each region. The equations developed here relate flow to pressure drop in several pressure regions and for several geometric cross sections. When we combine these with the dynamical equations of gas flow from a chamber, we can calculate the time required to reach a particular pressure.

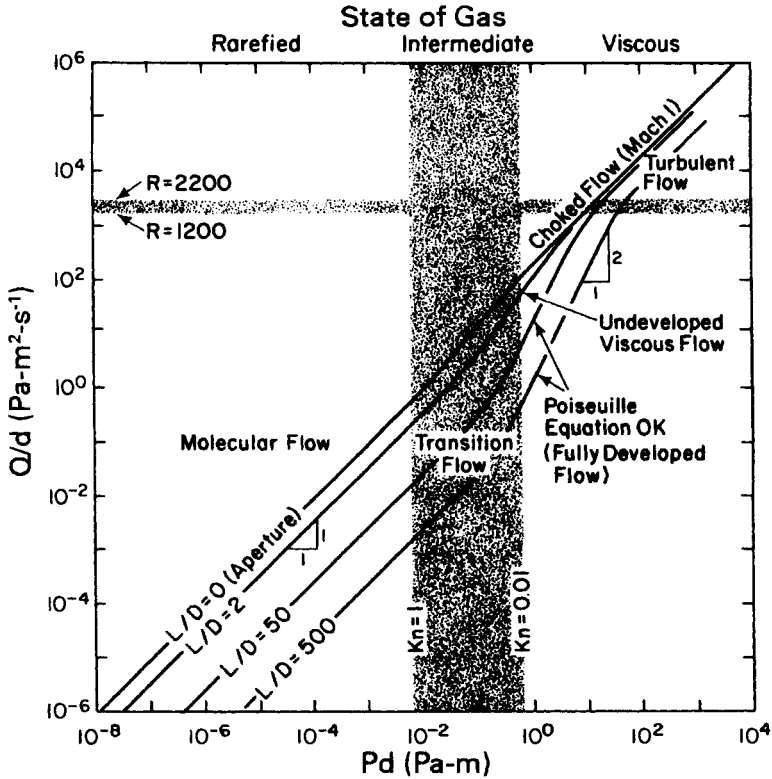


Fig. 3.18 Gas flow-pressure regimes.

REFERENCES

1. O. Reynolds, *Philos. Trans. R. Soc., London*, **174** (1883).
2. A. Guthrie and R. K. Wakerling, *Vacuum Equipment and Techniques*, McGraw-Hill, New York, 1949, p. 25.
3. A. H. Shapiro, *Dynamics and Thermodynamics of Compressible Fluid Flow*, Ronald, New York, 1953.
4. H. L. Langhaar, *J. Appl. Mech.*, **9**, A-55 (1942).
5. L. Holland, W. Steckelmacher, and J. Yarwood, *Vacuum Manual*, E. & F. Spoon, London, 1974, p. 26.
6. B. J. Williams, B. Fletcher, and J. A. A. Emery, *Proceedings of the 4th International Vacuum Congress, 1968*, Institute of Physics and the Physical Society, London, 1969, p. 753.
7. S. Sasaki and S. Yasunaga, *J. Vac. Soc. Japan*, **25**, 157 (1982).
8. S. Dushman, *Scientific Foundations of Vacuum Technique*, 2nd ed., J. M. Lafferty, Ed., Wiley, New York, 1962, p. 35.
9. D. J. Santeler, *J. Vac. Sci. Technol. A*, **4**, 348 (1986).
10. M. von Smoluchowski, *Ann. Phys.*, **33**, 1559 (1910).
11. M. Knudsen, *Ann. Physik*, **28**, 75 (1909); **35**, 389 (1911).
12. L. B. Loeb, *The Kinetic Theory of Gases*, 2nd ed., McGraw-Hill, New York, 1934, Chapter 7.

13. W. Steckelmacher, *J. Phys. D: Appl. Phys.*, **11**, 473 (1978).
14. Ref. 5, p. 91.
15. H. A. Lorentz, *Lectures on Theoretical Physics*, **1**, Macmillan, London, 1927, Chapter 3.
16. P. Clausing, *Ann. Phys.*, **12**, 961 (1932), English Translation in *J. Vac. Sci. Technol.*, **8**, 636 (1971).
17. W. C. DeMarcus, Union Carbide Corp. Report K-1302, Part 3, 1957.
18. A. S. Berman, *J. Appl. Phys.*, **36**, 3365 (1965), and erratum, *ibid.*, #37, 4598 (1966).
19. R. J. Cole, *Rarefied Gas Dynamics*, **51**, Part 1, of *Progress in Astronautics and Aeronautics*, J. L. Potter, Ed., (10th International Symposium Rarefied Gas Dynamics), Am. Inst. of Aeronautics and Astronautics, 1976, p. 261.
20. H. Tanigouchi, M. Ota, and M. Aritomi, *Vacuum*, **47**, 787 (1996).
21. I. G. Neudachin, B. T. Porodnov and P. E. Suetin, *Soviet Physics, Technical Physics*, **17**, 1036 (1972).
22. W. Sugiyama, T. Sawada, and K. Nakamori, *Vacuum*, **47**, 791 (1996/)
23. A. S. Berman, *J. Appl. Phys.*, **40**, 4991 (1969).
24. D. J. Santeler, and M. D. Boeckmann, *J. Vac. Sci. Technol. A*, **9**, 2378 (1992).
25. D. H. Davis, *J. Appl. Phys.*, **31**, 1169 (1960).
26. L. L. Levenson, N. Milleron, and D. H. Davis, *Le Vide*, **103**, 42 (1963).
27. J. D. Pinson and A. W. Peck, *Transactions of the 9th National Vacuum Symposium*, Macmillan, New York, 1962, p. 407.
28. L. Füstöss and G. Töth, *J. Vac. Sci. Technol.*, **9**, 1214 (1972).
29. W. Harries, *Z. Angew. Phys.*, **3**, 296 (1951).
30. W. Steckelmacher, *Proc. 6th Int. Vacuum Cong.*, Kyoto, *Jpn. J. Appl. Phys.*, Suppl. #2, Pt.1, 117 (1974).
31. C. W. Oatley, *Br. J. Appl. Phys.*, **8**, 15 (1957).
32. R. Haefer, *Vacuum*, **30**, 217 (1980).
33. J. O. Ballance, *Transactions of the 3rd. International Vacuum Congress*, **2**, Pergamon, Oxford, 1967, p. 85.
34. A. Pace and A. Poncet, *Vacuum*, **41**, 1910 (1990).
35. D. J. Santeler, *J. Vac. Sci. Technol. A*, **4**, 338 (1986).
36. D. J. Santeler et al., *Vacuum Technology and Space Simulation*, NASA SP-105, National Aeronautics and Space Administration, Washington, DC, 1966, p. 115.
37. G. L. Saksaganski, *Molecular Flow in Complex Systems*, Gordon and Breach, New York, 1988.
38. S. L. Thomson and W. R. Owens, *Vacuum*, **25**, 151 (1975).
39. S. K. Loyalka, T. S. Storvick, and H. S. Park, *J. Vac. Sci. Technol.*, **13**, 1188 (1976).
40. S. F. DeMuth and J. S. Watson, *J. Vac. Sci. Technol. A*, **4**, 344 (1986).
41. S. A. Tison, *Vacuum*, **44**, 1171 (1993).
42. J. Kieser and M. Grundner, *Proc. VIII Intl. Vac. Congr., Suppl. Rev. Le Vide*, **201**, 376 (1978).
43. J. F. O'Hanlon, *J. Vac. Sci. Technol. A*, **5**, 98 (1987).
44. B. W. Schumacher, *Proceedings of the 8th National Vacuum Symposium 1961*, Vol. 2, Pergamon, New York, 1962, p. 1192.
45. L. E. Levina, *Sov. J. Nondestruct. Test.*, **16**, 67 (1980).

PROBLEMS

- 3.1 † Describe the molecular, transition, laminar viscous and turbulent gas flow regimes.
- 3.2† Calculate Reynolds' and Knudsen's numbers for the following cases:
(a) 80 Pa·m³/s of air through a 2-mm-diameter choked orifice at a

a pressure of 101,000 Pa, (b) an air flow of 5×10^6 Pa-L/s (1 atm at 50 L/s) in a 5-cm-diameter mechanical pumping line at the time the pump is started, and (c) a flow of 0.1 Pa-L/s of water vapor in a 20-cm-diameter high vacuum pumping line. Assume room temperature. Characterize the flow in each case.

- 3.3 (a) Calculate the maximum gas flow in a 1-mm-diameter tube, which is 15 mm long, with atmospheric pressure on one end and 1 Pa on the other end using the Poiseuille equation. (b) Calculate the maximum choked flow through a 1-mm-diameter orifice. Explain the difference between two answers.
- 3.4 † What is the lowest average pressure necessary to keep the room temperature air flow predominantly viscous laminar in a 5-cm-diameter line?
- 3.5 † A 15-cm-diameter pipe, 15 cm long connects a high vacuum chamber and a pumping system. Which of the following modifications will give the greatest increase in conductance in the molecular flow region? (a) Reducing the length of the tube to 7.5 cm, (b) increasing the diameter to 17.5 cm from 15 cm.
- 3.6 A 1-cm-diameter tube, 10 cm long, interconnects two very large vessels. The vessel A contains nitrogen at 10^{-2} Pa, and vessel B contains nitrogen at 10^{-4} Pa. (a) What is the flow rate of the nitrogen molecules originally in vessel A from vessel A to vessel B? (b) Is there any flow from vessel B to A? If so, how much? (c) What is the net nitrogen flow from vessel A to vessel B?
- 3.7 The piston in Fig. 3.19 is moved to the right at a uniform, linear velocity U , so that the nitrogen flow Q through the leak remains constant at 1×10^{-6} Pa-m³/s. (a) Assume that the pressure in the chamber remains constant at 10 Pa during this motion. Calculate the velocity of the piston. (b) Assume that the piston moves to the right at a velocity of $U = 3$ mm/s whereas the value of the leak remains unchanged. Calculate the rate of pressure rise of dP/dt in the chamber.

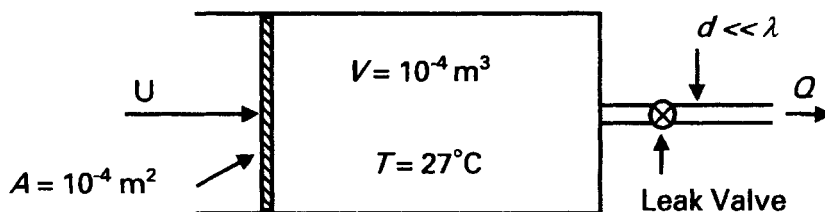


Fig. 3.19

- 3.8 †Kurtz [*Proc. 4th Int. Vac. Cong.* (1968), Inst. of Phys. and The Phys. Soc., London, 1969, p. 817]. published a clever, simplified Monte Carlo probability generator using six-sided dice. His method helps us to visualize the nature of molecular flow. It is easily applied to any two-dimensional structure. First, we divide the entrance to a structure in 6 equal areas and number them serially. We cast a (six-sided) die and randomly determine an entrance position. Second, we cast a pair of six-sided dice and determine the angle, or direction of particle motion (explanation below). We draw a ray from the starting point along that angle to a point where the particle “collides” with a wall. See Fig. 3.20a. We cast the dice again, determine a new angle, and repeat the procedure until the particle either leaves the structure at the exit or returns to the entrance. After a number of attempts, the transmission probability can be calculated. It is the ratio of particles successfully navigating the structure divided by the total number of particles entering the structure.

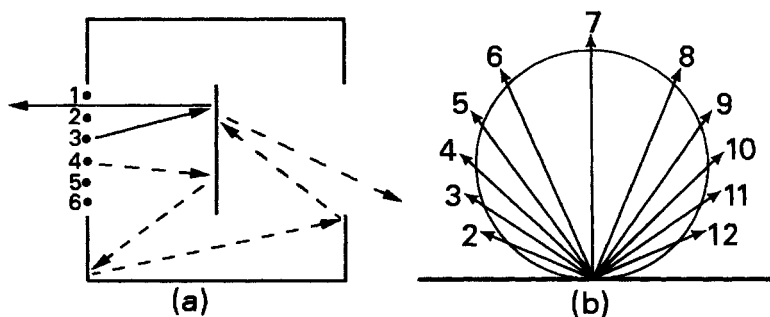


Fig. 3.20

We can determine the angle of escape with the template depicted in Fig. 3.20b. Seven is the most probable sum obtained when casting two dice; it occurs 6/36 times. Six and 8 each will be obtained on average 5/36 times, or 5/6 of the probability of obtaining a 7. A sum of 7 is equated with an escape angle of 0° from the normal. A sum of 6 or 8 corresponds to $\cos \phi = 5/6$, or $\phi = \pm 34^\circ$, and so on, as sketched in Fig. 3.20b.

† (a) Determine the probabilities for each of the other possible combinations (2 through 12) and make a template of escape angle versus sum of the dice as sketched in Fig. 3.20b.

† (b) Draw a two-dimensional “cold trap” like that sketched in Fig. 3.20a. Draw the length and diameter equal ($L = 2R$) and draw the

entrance and plate diameter as half the outer diameter ($R = 2R_0$). Determine the transmission probability by Kurtz' technique for a gas that does not stick to the walls. This transmission probability is analogous to that of nitrogen or oxygen as it passes through a cold trap to the pump.

† (c) Calculate the transmission probability of this structure for a vapor like water, that is frozen on the interior plate. Do this by re-examining the individual paths of each molecule you traced, and only counting those that successfully traversed the trap without hitting the center (LN_2 -cooled) plate. This transmission probability is analogous to the trapping probability of water vapor in this kind of a cold trap.

† (d) Why does the Monte Carlo technique require many attempts to calculate the transmission probability accurately?

- 3.9 † Under what conditions does the gas flux have a cosine distribution at the entrance to a vacuum component in the molecular flow regime?
- 3.10 Using the addition method for molecular flow developed by Haefer, calculate the transmission probability of a 10-cm-diameter round pipe that is 20 cm long and terminated in a 5-cm-diameter diaphragm.

CHAPTER 4

Gas Release from Solids

All the gas could be pumped from a vacuum chamber in a very short time, if it were located in the volume of the chamber. Consider a 100-L chamber previously roughed to 10 Pa and just connected to a 1000 L/s high vacuum pump. Equation (19.1) states that the pressure would drop from 10 Pa, when the high vacuum valve is opened, to 4.5×10^{-4} Pa in 1 s. In practice this will never happen, because gases and vapors residing on and in the interior walls desorb slowly. The surface gas adds to the volume gas that is to be removed by the pump. For this example 15–60 min will be required to reach the mid- 10^{-4} -Pa range in an unbaked, but clean system.

This chapter discusses the mechanisms of gas evolution from solid surfaces and explains how they affect the pumping rate and ultimate pressure in vacuum chambers. Gas is dissolved in and adsorbed on solids. This gas release, collectively referred to as outgassing, is actually a result of several processes. Figure 4.1 shows the possible sources of gas in addition to the gas located in the volume of the chamber. Gases and vapors released from the surface are a result of vaporization, thermal desorption, diffusion, permeation, and stimulated desorption.

4.1 VAPORIZATION

A vapor is a gas above its condensation temperature and vaporization is the thermally stimulated entry of molecules into the vapor phase. In dynamic equilibrium the rate at which molecules leave the surface of a solid or liquid equals the rate at which they arrive at the surface. The pressure of the vapor over the surface in dynamic equilibrium is the vapor pressure of the solid or liquid, provided that the solid or liquid and the vapor are at the same temperature. In Chapter 2 we stated the molecular flux of vapor crossing a plane was $nv/4$. In equilibrium, this is therefore the rate of molecular release from the surface. For the case of free evaporation of a solid from a heated source, (2.9) given here in a different form

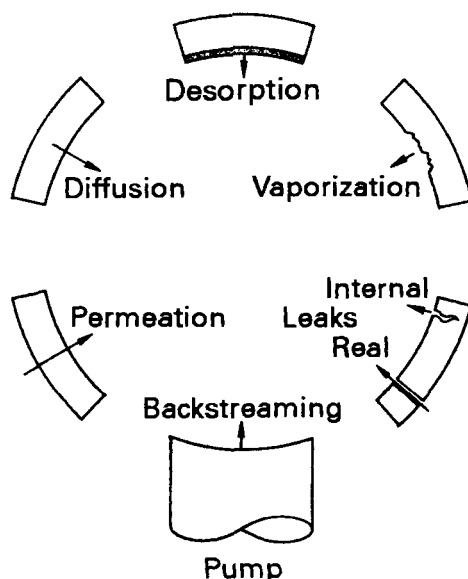


Fig. 4.1 Potential sources of gases and vapors in a vacuum system.

may be used to calculate the maximum rate of evaporation of a solid based on knowledge of its temperature, vapor pressure, surface area, and molecular weight:

$$\Gamma(\text{molecules/s}) = 2.63 \times 10^{24} \frac{PA}{(MT)^{1/2}} \quad \blacktriangleright (4.1)$$

The vapor-pressure-temperature curves for many gases are given in Appendixes B.5 and B.6. Appendix C.7 provides the vapor pressures of the solid and liquid elements.

4.2 DIFFUSION

Diffusion is the transport of one material through another. Gas diffusion to the interior wall of a vacuum system followed by desorption into the chamber contributes to the system outgassing. The gas pressure in the solid establishes a concentration gradient that drives molecules or atoms to the surface, where they desorb. Because diffusion is often a much slower process than desorption, the rate of transport through the bulk to the surface will usually govern the rate of release into the vacuum. A concentration gradient moves the atoms or molecules to the surface with a flux given by (2.29). The outgassing rate from a solid wall containing gas

at an initial concentration C_o is obtained from the diffusion equation [1]. One solution for a uniform initial concentration of dissolved gas is

$$q = C_o \left(\frac{D}{\pi t} \right)^{1/2} \left[1 + 2 \sum_{n=1}^{\infty} (-1)^n \exp \left(-\frac{n^2 d^2}{Dt} \right) \right] \quad (4.2)$$

where D is the diffusion constant in m^2/s and $2d$ is the thickness of the material. C_o , the internal pressure of the gas dissolved in the solid, is given in units of Pa, q has units of $(\text{Pa} \cdot \text{m}^3)/(\text{m}^2 \cdot \text{s})$ or in less physically recognizable terms, W/m^2 . We do not have to derive or solve this equation in order to understand some basic ideas about diffusion. We only need to know its value for short and long times. Let's examine the solutions for these two limits. In the limit as we approach $t = 0$, the terms in the sum become zero and the rate of gas release from the surface is given by

$$q = C_o \left(\frac{D}{\pi t} \right)^{1/2} \quad \blacktriangleright (4.3)$$

Equation (4.3) describes the slow decrease in outdiffusion that is experimentally observed. The initial outdiffusion from a solid containing a uniform gas concentration varies as $t^{1/2}$. This gas release rate is much slower than first order desorption.

For long times the infinite series (4.2) does not converge rapidly. By the maneuver of placing the mathematical origin at one surface, instead at the center of the solid, the diffusion equation can be solved again to yield

$$q = \frac{2DC_o}{d} \sum_{n=0}^{\infty} \exp \left[-\frac{(2n+1)^2 \pi^2 Dt}{4d^2} \right] \quad (4.4)$$

Equations (4.2) and (4.4) are equivalent but (4.4) converges rapidly for large values of t . Only the first term is significant for long times, and the solution reduces to

$$q = \frac{2DC_o}{d} \exp \left(-\frac{\pi^2 Dt}{4d^2} \right) \quad \blacktriangleright (4.5)$$

Equation 4.5 states that the outdiffusion rate decreases as $\exp(-aDt)$ at long times. This rapid exponential decrease in outdiffusion is experimentally observed and corresponds to the near depletion of the dissolved gas in the solid. Figure 4.2 describes the rate at which nitrogen diffuses from one side of a two-dimensional silicone rubber surface that is immersed in vacuum. We first observe the rate to decrease slowly as $t^{1/2}$, and after some time decrease as $\exp(-aDt)$, when the solid is nearly exhausted of its gas supply. The transition from the slow decay to the rapid decay occurs at $t \sim d^2/6D$.

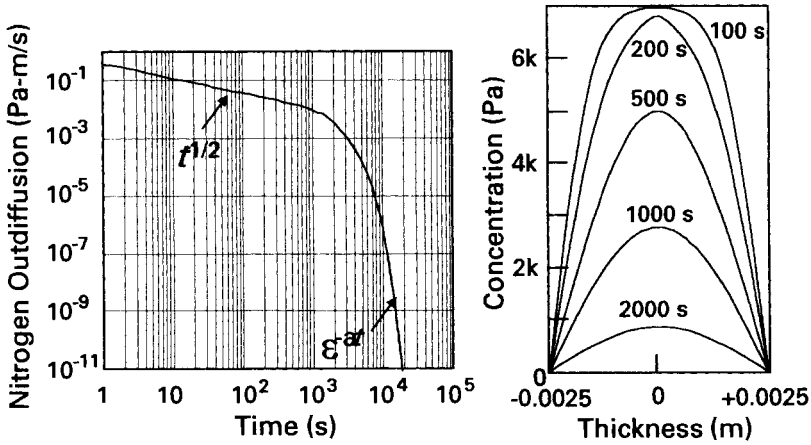


Fig. 4.2 (Left) The outdiffusion rate of nitrogen from one surface of a 0.005-m-thick silicone rubber sheet, $T = 25^\circ\text{C}$. (Right) The internal nitrogen concentration profile.

4.2.1 Reduction of Outdiffusion by Vacuum Baking

The diffusion constant is a function of the thermal activation energy of the diffusing gas in the solid and is given by

$$D = D_0 e^{(-E_D/kT)} \quad (4.6)$$

Because of this exponential dependence on temperature, a rather modest increase in temperature will sharply increase the initial outdiffusion rate and reduce the time necessary to unload the total quantity of gas dissolved in the solid.

Figure 4.3 illustrates how vacuum baking reduces the final outdiffusion rate to a level far below that which is possible in the same time without baking. A solid exposed to vacuum at ambient temperature T_1 outdiffuses along the initial portion of the lower curve with a slope of $t^{-1/2}$, as given by (4.3). At a time corresponding to point A, the temperature is increased to temperature T_2 . Because the gas concentration in the solid cannot change instantaneously, the outdiffusion rate increases to the value given by point B on the high temperature diffusion curve but shifted in time to point C. The dotted line connecting A and B is a line of constant concentration. It has a slope of -1 and the value of q_B is given by $q_A t_A = q_B t_B$. Outdiffusion continues along the high temperature curve but is displaced in time. The plot looks curved near point C, because of the logarithmic axis. At a time corresponding to point D the baking operation is terminated and the temperature is reduced to T_1 . The outdiffusion rate is reduced to a value corresponding to point E on the low-temperature curve but at an earlier

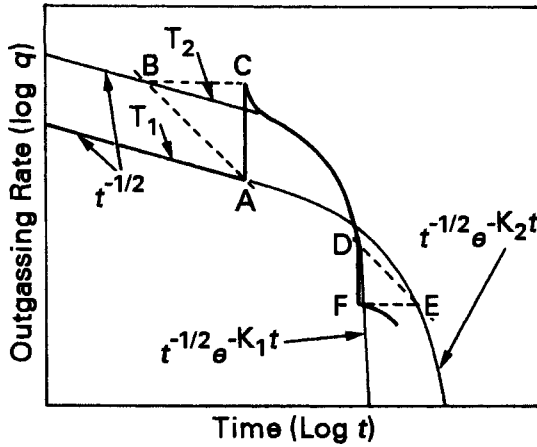


Fig. 4.3 Change in outdiffusion rate for an increase in temperature from T_1 to T_2 for a diffusion process. Reprinted with permission from *Vacuum Technology and Space Simulation*, D. J. Santeler et al., SP-105, 1966. National Aeronautics and Space Administration, Washington, DC.

time given by point F . Outdiffusion continues at a rate given by the low-temperature curve, but shifted to an earlier point in time. The new pressure at point F is given by [2]

$$P_f = (D_1 / D_2) P_d \quad (4.7)$$

where $D_{1,2}$ are the diffusion coefficients at temperatures $T_{1,2}$ respectively. The net effects of baking are the reduction in the outgassing rate and the reduction of the time required to remove the initial concentration of gas dissolved in the solid.

4.3 THERMAL DESORPTION

Thermal desorption is the heat-stimulated release of gases or vapors previously adsorbed on the interior walls of the system. They may have been adsorbed on the chamber surface, while it was exposed to the environment and then slowly released as the pump removed gas from the chamber. Alternatively, they may have reached the inner surface by diffusion from within, or permeation from the outside. The rate of desorption is a function of the molecular binding energy, the temperature of the surface, and the surface coverage. Gas is bound on surfaces by physisorption and chemisorption. Physisorbed molecules are bonded to the surface by weak van der Waals forces of energy < 40 MJ/(kg-mole). Adsorption at energies greater than this value is known as chemisorption.

Weakly physisorbed molecules are removed quickly from solid surfaces at ambient temperature and do not hinder pumping. Chemisorbed particles desorb slowly unless external energy is provided in the form of phonons, photons, or charged particles. The effects of readsorption must be included in real vacuum systems, when determining the net or measured thermal desorption rate. If readsorption is significant, the true outgassing rate will be much higher than the measured outgassing rate.

In this section we will first consider desorption without readsorption. Our discussion of readsorption will focus on the practical issue of pumping adsorbed water vapor, a most important concern in the performance of both quick-cycle, unbaked vacuum systems, and well baked accelerator systems.

4.3.1 Desorption Without Readsorption

Zero-Order Desorption

Surfaces covered with multilayers of molecules, such as water vapor will desorb at a constant rate [3].

$$\frac{dn}{dt} = \alpha e^{\frac{E_v}{kT}} \quad (4.8)$$

This process is called zero order desorption; n is molecular surface density, E_v is the latent heat of vaporization, and α is a constant. It describes the rate at which molecules depart from a surface saturated with large quantities of vapor. $E_v \sim 40,600$ MJ/(kg-mol) or 9.7 kcal/g-mol for water.

First Order Desorption

When the surface coverage becomes less than one monolayer, molecules that do not dissociate on adsorption depart without return at a rate proportional to their surface concentration. This can be expressed mathematically

$$\frac{dC(t)}{dt} = -K_1 C(t) = \frac{e^{-E_d/(N_o kT)}}{\tau_o} C(t) \quad (4.9)$$

Desorption with a rate $dC(t)/dt$, which is proportional to the concentration of atoms or molecules on the surface C , is called first-order desorption. This is a description of how monoenergetic atoms of, for example, helium or argon desorb from a metal or glass, or how water vapor desorbs from itself or a glass. The rate constant K_1 is strongly dependent on desorption energy E_d and the temperature. It can be described by the equation

$$\frac{1}{K_1} = \tau_r = \tau_o e^{E_d/(N_o kT)} \quad \blacktriangleright (4.10)$$

where τ_0 is the vibrational frequency of a molecule or atom in an adsorption site and is typically 10^{13} s. K_1 is also the reciprocal of the average residence time τ_r that a molecule or atom spends on the surface. The desorption rate will also decrease with time as the surface layer becomes depleted. By integrating (4.3) we can show

$$\frac{dC(t)}{dt} = C_0 K_1 e^{-K_1 t} = C_0 K_1 e^{-t/\tau_r} \quad (4.11)$$

Equation (4.11) shows the manner in which desorption rate decreases with time. This equation predicts rapid (exponential) decay of the desorption rate in a few τ_r .

Table 4.1 shows the strong dependence of the residence time on the temperature and desorption energy for three representative gas-metal systems: Water weakly bonded to itself, hydrogen strongly bonded to molybdenum, and the intermediate case was water bonded to a metal. These residence times assume, of course, that the molecule accommodated to the surface after its arrival. Not all molecules do so; or said another way, the sticking coefficients may be < 1 . Reliable sticking coefficients are lacking. These residence times were calculated using desorption energies given by Ehrlich [4], and Moraw and Prasol [5]. The room temperature residence time for water adsorbed on itself is less than a microsecond and baking is not necessary to remove the bulk of this physisorbed water—it is removed quickly beginning at about 2330 Pa (17.5 Torr), the vapor pressure of water at 20°C. Hydrogen is strongly chemisorbed at energies of 160 MJ/(kg-mole) or 40,000 cal/(g-mole). It cannot be removed without a high temperature bake or the use of stimulated desorption. One monolayer of water is chemisorbed on a metal with energies in the range 92–100 MJ/(kg-mole) or 22,000–24,000 cal/(g-mole) [5]. It is a problem because it is bound just strongly enough to stick at room temperature. Although it is hard to remove at room temperature, it is easily desorbed by baking at temperatures over 250°C. Cooling the surface has a dramatic effect on the residence time of all molecules—physisorbed and chemisorbed. Residence times become very long as cooled surfaces become traps.

Water is the most troublesome vapor to remove without baking, because the last monolayer desorbs over a long time period, ranging from hours to days at room temperature. Desorption of the remaining monolayer is difficult without some form of baking or nonthermal radiation. Hydrogen is the dominant gas that desorbs from stainless steel surfaces.

Second-Order Desorption

First-order desorption does not describe the situation where a gas dissociates on adsorption and recombines before desorption. Diatomic

Table 4.1 Average Residence Time of Chemisorbed Molecules

System	Desorption Energy (10^6 J/(kg-mole))	Residence Time at		
		77 K (s)	22°C (s)	450°C (s)
H ₂ O/H ₂ O	40.6	10^{15}	10^{-5}	10^{-9}
H ₂ O/metal	96	—	10^5	10^{-5}
H ₂ /Mo	160	—	10^{17}	1

gases on metals, for example hydrogen on steel or molybdenum, dissociate on adsorption. The atoms must recombine on the surface before desorbing ($H + H = H_2$). A reaction that is proportional to the concentration of each of two species is called a second-order reaction; the rate equation is given by

$$\frac{dC(t)}{dt} = -K_2 C^2(t) \quad (4.12)$$

This equation can be solved to yield

$$\frac{dC(t)}{dt} = \frac{-K_2 C_o^2}{(1 + C_o K_2 t)^2} \quad \blacktriangleright (4.13)$$

We see from (4.13) that the time to clean up a surface is longer than for first order because the rate decays as $1/t^2$. Remember that K_2 also contains the energy and temperature dependent term $\exp(-E_d/kT)$ so that second-order desorption, like first-order desorption, can proceed rapidly at high temperatures and weak binding energies.

Figure 4.4 shows a sketch of desorption rate versus time for a first and a second order process. Knize and Cecchi [6] performed an experiment, which nicely illustrates the two processes. Their vacuum system contained Zr-Al getters whose surfaces were contaminated with a small amount of deuterium. Since two deuterium atoms need to recombine and form D₂ before desorption can occur, surfaces with a low concentration of deuterium desorbed as a second order process according to (4.13). By flooding the chamber with a high, constant pressure of hydrogen, they created a surface in which the small number of deuterium atoms was flooded with H atoms. Since an H atom was frequently hitting each D atom, H-D was formed and desorbed at a rate proportional to the concentration of D atoms. Their data showed the deuterium desorption rate to decrease as $1/t^2$ without the addition of hydrogen gas. With the addition of hydrogen, the HD desorption rate decreased exponentially; a second-order process was converted into a first order process described by (4.11).

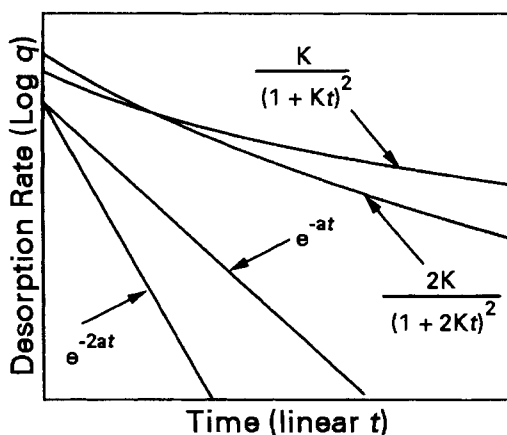


Fig. 4.4 Desorption rate (log) versus time (linear) for first order desorption K_1 , and second order desorption K_2 . Two activation energies are shown for each type of desorption. In both cases the rate constants are energy dependent, but after long times second order desorption is always slower than first order.

4.3.2 Desorption from Real Surfaces

If atoms and molecules simply desorbed from a surface and exited to the pump in a single bounce—never to return again—the relationships described in Section 4.3.1 would accurately characterize their rate of removal. Unfortunately, real vacuum systems cannot be characterized in this manner. In the molecular flow regime, molecules leaving a surface make myriad collisions with other surfaces before encountering the pump entrance. During some of those collisions, a molecule will re-adsorb or stick, whereas the molecule will be merely scattered, usually diffusely, after the remainder of the collisions. The sticking coefficient s represents the fraction of collisions in which the molecules re-adsorbs at an available surface site. It remains at a surface for a residence time τ_r . The picture is further complicated by the variation of the sticking coefficient with the number of available adsorption sites, and by the ability of molecules to diffuse to the surface from complex, porous, near-surface regions.

Here we discuss experimental outgassing, practical baking of vacuum chambers and models for thermal desorption.

Outgassing Measurements

Outgassing may be measured by several methods [7]. The throughput method, where the gas is pumped through a known conductance, is one commonly used method. Gas accumulation or rate of rise, where the pressure

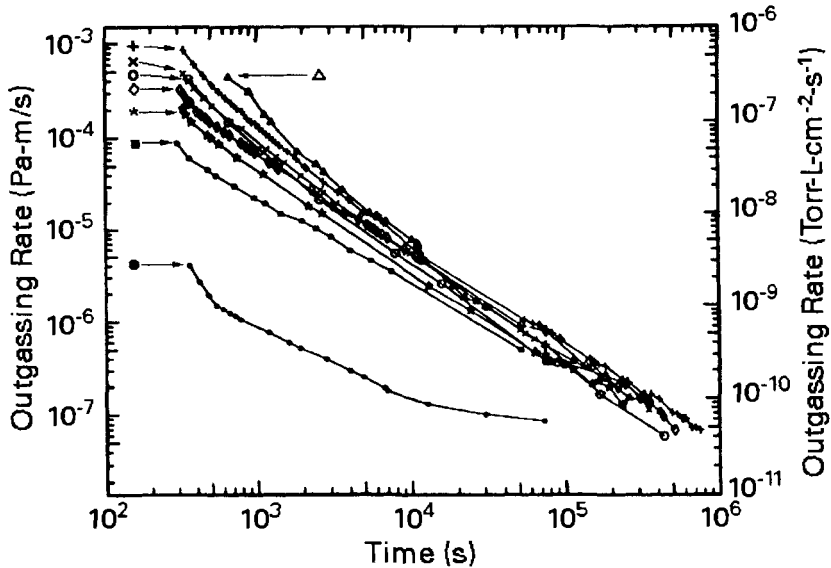


Fig. 4.5 Outgassing measurements for different H_2O exposures during venting of a 304 stainless steel chamber of inner surface area 0.4747 m^2 . \circ Ambient air exposed, 7.8 ml absorbed; Δ 600 ml exposed, 16.8 ml absorbed; $+$ 400 ml exposed, 9.2 ml absorbed; \times 200 ml exposed, 7.2 ml absorbed; \diamond 100 ml exposed, 3.6 ml absorbed; \star 10 ml exposed, 2.3 ml absorbed; \blacksquare N_2 gas with <10 ppm H_2O exposed, 0.7 ml absorbed; \bullet dry N_2 gas exposed, 0.017 ml absorbed; Reprinted with permission from *J. Vac. Sci. Technol. A*, **11**, p. 1702, M. Li and H. F. Dylla. Copyright 1993, AVS—The Science and Technology Society.

rise is measured after the chamber has been isolated, is another common method. Typical results are displayed in Fig. 4.5 for the outgassing of 304L stainless steel with differing initial water vapor exposures [8].

Room temperature outgassing data for most gases sorbed on metals, including water vapor, show the outgassing rate to vary inversely with time, at least for the first 10 h of pumping [8–10]. This can be expressed as

$$q_n = \frac{q}{t^{\alpha_n}} \quad \blacktriangleright (4.14)$$

where the subscript n denotes the time in hours for which the data apply. See Fig. 4.6. The exponent α will range from 0.7–2 with 1 the most common value. Equation (4.14) is often misinterpreted to be an equation by which outgassing data, such as given in Appendixes C.1–4, C.7, can be determined for all time. That is not its intent. The values given in the appendixes and other publications are points and slopes at discrete times. Tabulated experimental data are usually given for one or two representative times—for example, 1 and 4 hours, or 1 and 10 hours. To

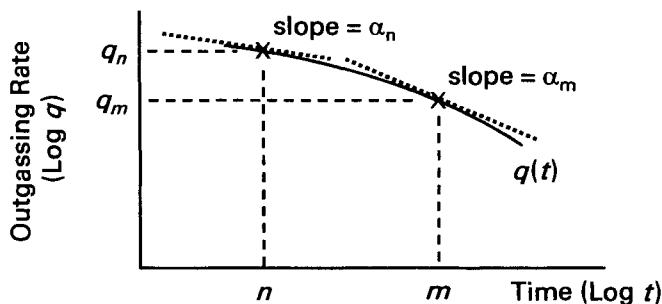


Fig. 4.6 Outgassing data notation, as used in Appendix C.

further confuse the situation, published studies may not have all chosen the same $t = 0$. This starting time is best chosen as the time at which the chamber pressure equals the saturation vapor pressure of water. Outgassing data for engineering surfaces typically show wide variation, representative of both the methods used to accumulate data, and by which samples were prepared. We will discuss this in detail in Chapter 16.

Outgassing Models

The mathematical modeling of outgassing from stainless steel has been studied by numerous investigators. There are two distinct models. Gas can be assumed to originate in the near-surface region and be released after diffusing to the surface [8–10]. In this model, readsorption is not included. Alternatively, gas can be assumed to originate in an adsorbed layer on the surface [3,5,11,12]. As Redhead pointed out, both adsorption and diffusion occur and the two models differ in their assumption of which process is the rate limiting step [3]. Both models are able to predict the $1/t$ dependence experimentally observed for water on 304 stainless steel.

Dayton [9] modeled this $1/t$ behavior as the sum of the successive out diffusion of molecules of a range of energies. He proposed a uniform distribution of activation energies like that found in a surface oxide containing pores of varying diameters will result in a sum of individual outgassing curves. It will appear as one curve with a slope of about -1 on a log-log plot of outgassing rate versus pumping time, as sketched in Fig. 4.7. Each one of the curves in Fig. 4.7 is an outgassing curve whose shape we discussed previously. Redhead [3] assumed the short-term sub-monolayer outgassing of water from stainless steel was dominated by desorption from a reversible phase. He used an extended Temkin isotherm to describe the surface coverage–pressure relation, and with it, he closely modeled experimental data using a sticking coefficient of $s = 0.1$.

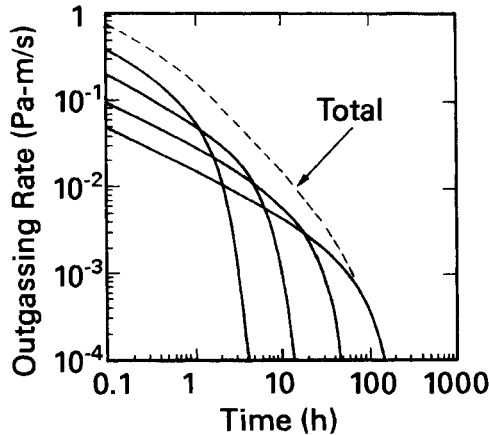


Fig. 4.7 Total outgassing rate as a sum of four rates, each resulting from a single outgassing time constant whose value depends on the shape of the surface oxide pores and the activation energy for desorption. Reprinted with permission from *Trans. 8th Vac. Symp.* (1961), p. 42, B. B. Dayton. Copyright 1962, Pergamon Press, Ltd.

Experimental measurements of the sticking coefficient of water on stainless steel at less than one monolayer coverage are not in agreement, but do show the same trend—the sticking coefficient increases as the number of available sites increases. Tuzi et al. [11], showed the sticking coefficient to increase from $s < 0.001$ at 5×10^{-3} Pa to $s = 0.04$ at $P \leq 10^{-8}$ Pa. Moraw and Prasol [5] found s varied from 0.0018 at $P = 10^{-4}$ Pa to 0.003 at $P = 10^{-6}$ Pa. A pulsed laser desorption experiment [12] yielded $s = 0.2$ for clean surfaces and $s = 0.01$ at a coverage of 2×10^{17} molecules/m².

Reduction of Outgassing by Baking

Recalling that surface desorption was modeled by Dayton [9] as the sum of diffusive release of gas from the surface oxide pores, we find that baking will reduce the outgassing time in the same manner as it reduces the outdiffusion time. The rate of gas release from the surface of a solid containing dissolved gas is slow, because the rate is determined by the mobility of the gas in the solid. When the solid is nearly exhausted, the slope becomes much greater (exponential).

Readsorption of molecules leaving a surface will lengthen the time a molecule remains in the chamber. The average number of collisions a molecule makes with a surface before departing the chamber depends on the pump speed S , the internal surface area A , and the average velocity [5].

$$f = \frac{v}{4} \left(\frac{1}{S/A} \right) \quad (4.15)$$

This results in an increased residence time τ_c in a chamber of

$$\frac{t_c}{t_r} = \left(1 + \frac{v}{4} \frac{s}{S/A} \right) \quad (4.16)$$

When baking vacuum systems, it is imperative that all surfaces be baked, as any area not baked will contribute an exceedingly large gas flux, relative to the baked area. For example, if 10% of the area were not baked, and its outgassing rate were 1000 \times that of the baked area, then the unbaked area would contribute 90% of the desorbed gas flux.

Alternatively, one can draw the same conclusion using a residence time model. Consider two surfaces, as shown on the left side of Fig. 4.8. In this cartoon, a water molecule is shown bouncing from two stainless steel surfaces on its sojourn to the pump. One surface is unheated (295K or 22°C) whereas the other surface is heated to 80°C. This cartoon would be representative of a vacuum system in which only half the wall area was heated. Half the molecular bounces would be from heated surfaces and half would be from unheated surfaces. In constructing this model, we have assumed that the sticking coefficients were the same for both surfaces. Using (4.10) and the sorption energy for H₂O on stainless steel given in Table 4.1, residence times of 9800 s and 16 s were calculated for the cold and warm surfaces, respectively, near one monolayer water coverage. The right-hand illustration in Fig. 4.8 shows that a uniform temperature of 27.3°C will result in the same net residence time. Were the water molecules to have bounced from a system with 1/3 cooled walls and 2/3 heated (80°C) walls, the equivalent uniform baking temperature would have been 30.5°C. We see that baking a fraction of the chamber (1/2–2/3 in this example) to a high temperature is equivalent to baking the entire system to just a few degrees (5–8°C in this example) above ambient!

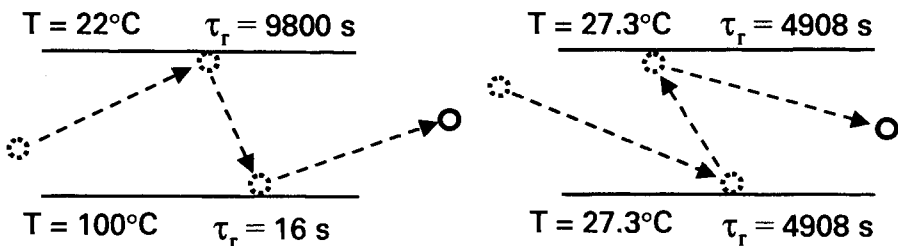


Fig. 4.8 The total residence time for a water molecule after two bounces from a metal surface is shown to be the same for two sets of surface temperatures; a sticking coefficient of one was assumed. This example illustrates the necessity of baking all surfaces within a vacuum chamber. Unbaked surfaces dominate the behavior of the system.

4.4 STIMULATED DESORPTION

Electrons, atoms, molecules, ions, or photons incident on solid surfaces can release adsorbed gases and generate vapors in quantities large enough to limit the ultimate pressure in a vacuum chamber. Many reactions are possible when energetic particles collide with a surface [13]. Among them are electron-stimulated desorption, ion-stimulated desorption, electron- or ion-induced chemical reactions, and photodesorption.

4.4.1 Electron-Stimulated Desorption

An energetic electron incident on the surface gas layer excites a bonding electron in an adsorbate atom to a nonbonding level. This produces a repulsive potential between the surface and atom, which allows the atom to desorb as a neutral or an ion [14–17]. The electron stimulated desorbed neutral gas flux can be as high as 10^{-1} atom per electron, whereas the desorbed ion flux is of order 10^{-5} ion/e. This desorption process is specific; it depends on the manner in which a molecule is bonded to the surface. These gas release phenomena have been shown to cause serious errors in pressure measurement with the Bayard-Alpert gauge [18,19] and residual gas analyzer [20] and to increase the background pressure in systems that use high-energy electron or ion beams.

4.4.2 Ion-Stimulated Desorption

Ion stimulated desorption has been studied by Winters and Sigmund [21] and Taglaier and Heiland [22]. Winters and Sigmund studied desorption of previously chemisorbed nitrogen on tungsten by noble gas ions in the range up to 500 V. They also showed that the adsorbed atoms were removed by a sputtering process as a result of direct knock-on collisions with impinging and reflecting noble gas ions. Ion-stimulated desorption is responsible for part of the gas release observed in sputtering systems, Bayard-Alpert gauges, and glow discharge cleaning.

Edwards [23] has measured the electron- and ion-stimulated desorption yields of 304 stainless steel and aluminum as a function of cleaning technique. Table 4.2 shows his results for degreased stainless and aluminum samples. The methane desorption is most likely caused by an electron- or ion-induced chemical reaction.

4.4.3 Stimulated Chemical Reactions

Ion- and electron-stimulated chemical reactions may also occur at solid surfaces. For example, hydrogen and oxygen can react with solid carbon to

Table 4.2 Desorption Yields for Stainless Steel and Aluminum^a

Gas	1000 eV Ar ⁺ ions		500 eV electrons	
	304 SS	Aluminum	304 SS	Aluminum
H ₂	2.13	2.38	0.15	0.18
CO	3.22	3.00	0.06	0.05
CO ₂	1.55	1.35	0.21	0.16
CH ₄	0.075	0.07	0.0025	0.003

Source: Reprinted with permission from *J. Vac. Sci. Technol.*, **16**, p. 758, D. Edwards, Jr. Copyright 1979, The American Vacuum Society.

^a Cleaned by a soap wash, water rinse, acetone rinse, methanol rinse, and air dried followed by 200°C, 60-h bake, and 2-day equilibration.

produce methane and carbon monoxide. An ion-stimulated chemical reaction is responsible for rapid etch rates observed in reactive-ion etching. In reactive-ion etching of silicon high-energy ions in a collision cascade greatly enhance the reaction of neutral F with Si and produce a much greater yield of volatile SiF₄ than is possible without ion bombardment.

4.4.4 Photodesorption

Lichtman et al. [24] observed greater than band gap desorption. The effect occurs in semiconductors (CrO₂ on stainless steel). However, one should be aware that the fraction of the energy greater than band gap, available from a mercury arc lamp, is insufficient to clean a vacuum chamber. Most desorption results from optically induced surface heating. Gröbner et al., [25], Mathewson [26] and Ueda et al., [27] measured the energetic photon-induced desorption of H₂, CO₂, CO, and CH₄ from aluminum, copper, and stainless steel used in high-energy accelerators. They measured desorption efficiencies of 0.1–0.001 molecules per photon.

4.5 PERMEATION

Permeation is a three-step process. Gas first adsorbs on the outer wall of a vacuum vessel, diffuses through the bulk, and lastly desorbs from the interior wall. Permeation through glass, ceramic, and polymeric materials is molecular. Molecules do not dissociate on adsorption. Hydrogen does dissociate on metal surfaces and diffuses as atoms that recombine before desorption on the vacuum wall.

4.5.1 Molecular Permeation

The time-dependence of the permeation rate of a nondissociating gas through a solid wall is described by [28]

$$q(\text{Pa} \cdot \text{m/s}) = \frac{DS'P}{d} \sum_{m=1}^{\infty} 2(-1)^m \exp\left(\frac{-m^2\pi^2 Dt}{d^2}\right) \quad (4.17)$$

where D is the diffusion constant, S' is the gas solubility, and d is the thickness of the material through which the gas permeates. Equation 4.14 converges slowly for short times. The alternative relationship for short times, given in (4.15), can be obtained by the same method as used for (4.10).

$$q(\text{Pa} \cdot \text{m/s}) = 2S'P \left(\frac{D}{\pi t}\right)^{1/2} \sum_0^{\infty} \exp\left(\frac{d^2}{4dt}(2m+1)^2\right) \quad (4.18)$$

Figure 4.9 illustrates the permeation of helium through 7740 glass at 300K for glass that is initially devoid of helium. In time, equilibrium will be established and helium will permeate the glass at a constant rate. Steady-state permeation therefore behaves like a constant leak. The product of the diffusion constant and the solubility is the permeation constant K_p .

$$K_p = DS' \quad (4.19)$$

In SI, both permeation constant and diffusion constant have units of m^2/s . Solubility is the dimensionless ratio of the gas-to-solid volume at the temperature of the measurement. For example, the experimentally determined solubility of He in 7740 glass described in Fig. 4.9 is 0.0065. The concentration inside the glass surface C , the solubility S' , and the external gas pressure P are related through Henry's law, $C = S'P$. The solubility of many materials is not strongly temperature-dependent. Because of this, the activation energies for permeation and diffusion are similar for many engineering materials. Consequently, both quantities increase rapidly with temperature.

The steady-state permeation flux of an atom or molecular that does not dissociate on adsorption can be expressed as

$$Q_k = q_k A = \frac{K_p P A}{d} \quad \blacktriangleright (4.20)$$

where q_k is the flux in units of $(\text{Pa} \cdot \text{m}^3)/(\text{s} \cdot \text{m}^2)$ and P is the pressure drop across the solid of thickness d . This is the characteristic steady-state flux for all gases that permeate glass, ceramic, and polymeric materials.

Since the initial gas load must traverse a solid (devoid of gas) before it reaches the vacuum wall, a period of time will pass before it is first observed in the vacuum chamber. The time to reach the steady state is known as the critical time t_c and is given by [28]

$$t_c = \frac{d^2}{6D} \quad (4.21)$$

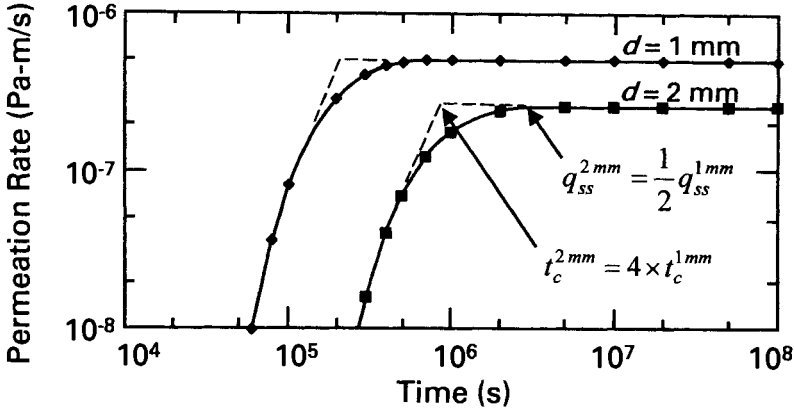


Fig. 4.9 Permeation of helium through $d = 1$ -mm- and 2-mm-thick 7740 glass at 27°C that was initially free of helium. The steady-state permeation rate varies inversely with the glass thickness. The critical time increases with the square of the glass thickness.

Solubility S' and diffusion D play distinct roles in gas permeation. The product of $S'D$ (4.17) determines the steady-state flux, whereas the time to reach steady state is only dependent on the diffusion constant (4.18). See Fig. 4.9. Doubling the glass thickness reduced the steady-state flux by 2 \times , but increased the critical time to reach steady state by 4 \times .

4.5.2 Dissociative Permeation

Diatomic gases frequently dissociate when they adsorb on metals. The steady-state permeation rate of hydrogen through metal proceeds by a slightly different route than discussed in the previous section. First, the molecule dissociates on the surface with equilibrium constant k_1 , then each atom is incorporated into the solid with equilibrium constant k_2 . The total concentration within the metal is found to be $[H]_{\text{solid}} = k_2 \sqrt{k_1 [H_2]_{\text{gas}}}$. Thus, the driving force for diffusion of hydrogen in metals is $P^{1/2}$; the permeation flux can be expressed as

$$Q_k = q_k A = \frac{K_p (P_2^{1/2} - P_1^{1/2}) A}{d} \quad \blacktriangleright (4.22)$$

The permeability K_p for gases that dissociate has units of $\text{Pa}^{1/2} \cdot \text{m}^2/\text{s}$.

4.5.3 Permeation and Outgassing Units

Permeation units recorded in the literature are inconsistent. They are not standardized in gas quantity, surface area, thickness, or pressure drop. Some researchers used a differential pressure of 10 Torr. Others used 1

Torr, or 1 cm Hg or 1 atmosphere; some researchers normalized data to 1-mm-thick samples; others reported data per cm thickness. The “scc” and “standard atmosphere” of gas quantity are traditionally referenced to 0°C, whereas the volumetric flow units for permeation flux are referenced to the measurement temperature, thus permeation measurements recorded at high temperature should be corrected for density change $273/T_{meas}$ [28]. Non-coherent units are as cumbersome to convert between each other as they are to SI. Converting older units directly to m^2/s facilitates comparison.

Permeability is a measure of gas transport through a solid by diffusion. It is the product of a dimensionless number (solubility) and diffusion constant. We routinely use units of cm^2/s or m^2/s (SI) for diffusion constant, so it is hard to explain the origin of such cumbersome permeability units. If the permeability and the diffusion constant are stated in SI units of m^2/s , the distinct roles of solubility and diffusion in determining steady-state flux q and critical time t_c are obvious. We will revisit this topic when we discuss the very important topic of gas permeation through elastomer O-rings.

Total flux Q permeating through an object is given in units of $\text{Pa}\cdot\text{m}^3/\text{s}$ or $\text{mbar}\cdot\text{L}/\text{s}$. The older English unit is the Torr-L/s. One $\text{Pa}\cdot\text{m}^3/\text{s} = 1 \text{ W}$. Measuring permeation flux in watts is not useful, but it illustrates that gas release from a surface has the dimensions of energy flow. The permeation per unit surface area is given in units of $\text{Pa}\cdot\text{m}/\text{s}$, or $\text{mbar}\cdot\text{m}/\text{s}$. Conversion factors between older units and SI are given in Appendix A.3.

4.6 PRESSURE LIMITS

In the introduction to this chapter we alluded to the fact that outgassing, not volume gas removal determined the final pressure in the high vacuum region. We know this to be true from another viewpoint. One monolayer of gas on the interior of a 1-L sphere, if desorbed instantly, would result in a pressure of 2.5 Pa (18 mTorr). This is a pressure far above high vacuum. Diffusion, permeation, and stimulated desorption are also important. In the previous section we made no attempt to relate numerically these various rates to a real vacuum system. The relative roles of surface desorption, diffusion, and permeation are a function of the materials used for construction (steel, aluminum, ceramic, or glass), the seals (metal gaskets, or single- or differentially-pumped elastomer gaskets), and the system history (newly fabricated, unbaked, chemically cleaned, or baked). The mathematical description of this pumping problem can be solved easily with certain approximations. The mathematical description of this pumping problem can be solved easily with certain approximations. The solution is

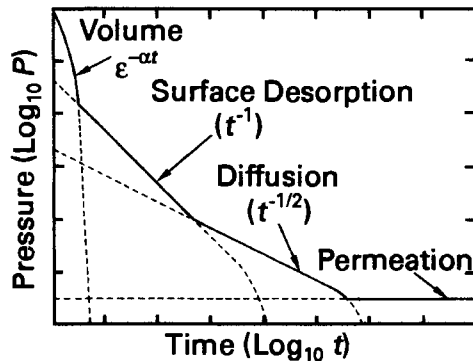


Fig. 4.10 Rate limiting steps during the pumping of a vacuum chamber.

$$P = P_0 e^{-St/V} + \frac{Q_o}{S} + \frac{Q_D}{S} + \frac{Q_k}{S} \quad \blacktriangleright (4.23)$$

The first term in the solution (4.23) represents the time-dependence of the pressure that is due to the gas in the chamber volume. The remaining terms represent the contribution of other gas sources. These terms represent outgassing, diffusion and permeation. They are slowly varying functions and become dominant after the initial pumping period has passed. After some time the first term on the right-hand side is zero and the pressure is determined by outgassing, diffusion, desorption, and permeation. The first term (outgassing) decays slowly, often as t^{-1} . The second term is the diffusion term. It decays initially as $t^{-1/2}$ and at long times as $\exp(-aDt)$. The last term in (4.20) is due to permeation and is constant. From this equation we can construct a composite pump-down curve that will illustrate the relative roles of these phenomena. Figure 4.10 shows the high vacuum pumping portion of an unbaked system sealed with metal gaskets. In the initial stages the pressure is reduced exponentially with time as the volume gas is removed. This portion of the pumping curve takes only a short time because a typical system time constant is only seconds. It is expanded here for clarity. In the next phase surface desorption controls the rate of pressure decrease. In a typical unbaked system, most of the gas load is water vapor, however nitrogen, oxygen, carbon oxides, and hydrocarbons are also present. The material and its history determine the total quantity of gas released. Glass or steel that has been exposed to room ambient for extended periods may contain up to 100 monolayers of water vapor, whereas a carefully vented chamber may contain little water vapor. A slow decrease in pressure is to be expected, if the system has a number of large elastomer O-rings, or a large interior surface area. Unbaked, rapidly cycled systems are never pumped below the outgassing-limited range.

If the system is allowed to continue pumping without baking, the surface gas load will ultimately be removed and the outdiffusion of gases in solution with the solid walls will be observed. The slope of the curve will change from t^{-1} to $t^{-1/2}$. For example, hydrogen that diffuses into steel in a short time at high fabrication temperatures outdiffuses from near surface regions exceedingly slowly at room temperatures. The system would now be at its ultimate pressure given by $P = Q_k/S$. Particular gases are known to permeate materials. Hydrogen perhaps from water vapor is a potential permeation source through stainless steel. Helium permeates glass walls, and water and air permeate elastomers. In a real system, the time required to achieve the ultimate pressure depends strongly on the materials and cleaning procedures used.

The order of importance of the processes is not always as shown in Fig. 4.10. Elastomer gaskets have a high permeability for atmospheric gases and if the system contained a significant amount of these materials, it would be the dominant permeation source.

The level of outgassing resulting from various electron- and ion-stimulated desorption processes is not shown in Fig. 4.10. These processes play a variable but important role in determining the ultimate pressure in many instances because they are desorb atoms that are not removed by baking. The desorption yield from energetic electrons and ions is a function of incident particle's energy, the material and its cleaning treatment, and the time under vacuum.

Electron-stimulated desorption in an ion gauge is easily observable during gauge outgassing. A 10-mA electron flux can desorb 6×10^{14} neutrals/s. Because a gas flux of 2×10^{17} atoms/s is equivalent to 1 Pa-L/s at 22°C, this electron flux can initially provide a desorption flux of 2×10^{-3} Pa-L/s. If the system is pumping on the ion gauge tube at a rate of 10 L/s, this desorption peak can reach a pressure of an order of 10^{-4} Pa in the gauge tube. The scattered electrons from Auger and LEED systems can stimulate desorption in a similar manner, with an increase in background pressure when the beam is operating. Electron-induced desorption is a first-order process that should produce a simple exponential decay of the desorbed species. If readsorption is included, the initial rate will decay exponentially to a steady-state level [29]. A 20-mA ion beam can desorb surface gas at an initial rate of 10^{-3} Pa-L/s, assuming a desorption efficiency of two atoms per incident ion.

REFERENCES

1. H. S. Carslaw and J. C. Jaeger, *Conduction of Heat in Solids*, 2nd ed., Oxford, New York, 1959, p. 97.
2. D. G. Bills, *J. Vac. Sci. Technol.*, **6**, 166 (1969).
3. P. Redhead, *J. Vac. Sci. Technol.*, **13**, 2791 (1995).
4. G. Ehrlich, *Trans. 8th Natl. Vac. Symp. and Proc. 2nd Intl. Vac. Congr. on Vac. Sci. Technol. (1961)*, **1**, Pergamon, New York, 1962, p. 126.
5. M. Moraw and H. Prasol, *Vacuum*, **49**, 353 (1998).
6. R. J. Knize and J. L. Cecchi, *J. Vac. Sci. Technol. A*, **1**, 1273 (1993).
7. P. A. Redhead, *J. Vac. Sci. Technol. A*, **20**, 1667 (2002).
8. M. Li and H. F. Dylla, *J. Vac. Sci. Technol. A*, **11**, 1702 (1993).
9. B. B. Dayton, *Trans. 8th Nat. Vac. Symp. and Proc. 2nd Intl. Congr. on Vac. Sc. Technol. (1961)*, **1**, Pergamon, New York, 1962, p. 42.
10. B. B. Dayton, *Trans. 7th Vac. Symp. (1960)*, Pergamon, New York, 1961, p. 101.
11. Y. Tuzi, K. Kurokawa, and K. Takeuchi, *Vacuum*, **44**, 477 (1993).
12. Y. Shiohara, and M. Ichikawa, *J. Vac. Sci. Technol. A*, **16**, 1131 (1998).
13. See, for example, P. A. Redhead, J. P. Hobson, and E. V. Kornelsen, *The Physical Basis of Ultrahigh Vacuum*, Chapman and Hall, London, 1968, Chapter 4.
14. M. J. Drinkwine and D. Lichtman, *Progress in Surface Science*, Vol. 8, Pergamon, New York, 1977, p. 123.
15. D. Menzel and R. Gomer, *J. Chem. Phys.*, **41**, 3311 (1964).
16. P. Redhead, *Can. J. Phys.*, **42**, 886 (1964).
17. M. L. Knotek and P. J. Feibelman, *Phys. Rev. Lett.*, **40**, 964 (1978).
18. P. A. Redhead, *Vacuum*, **12**, 267 (1962).
19. T. E. Hartman, *Rev. Sci. Instr.*, **34**, 1190 (1963).
20. P. Marmet and J. D. Morrison, *J. Chem. Phys.*, **36**, 1238 (1962).
21. H. F. Winters and P. Sigmund, *J. Appl. Phys.*, **45**, 4760 (1974).
22. E. Taglauer and W. Heiland, *J. Appl. Phys.*, **9**, 261 (1976).
23. D. Edwards Jr., *J. Vac. Sci. Technol.*, **16**, 758 (1979).
24. G. W. Fabel, S. M. Cox and D. Lichtman, *Surface Sci.*, **40**, 571 (1973).
25. O. Gröbner, A. G. Mathewson, and P. C. Marin, *J. Vac. Sci. Technol. A*, **12**, 846 (1994).
26. A. G. Mathewson, *Vacuum*, **44**, 479 (1993).
27. S. Ueda, M. Matsumoto, T. Kobari, T. Ikeguchi, M. Kobayashi, and Y. Hori, *Vacuum*, **41**, 1928 (1990).
28. W. A. Rogers, R. S. Buritz and D. Alpert, *J. Appl. Phys.*, **25**, (7) 868 (1954).
29. M. J. Drinkwine and D. Lichtman, *J. Vac. Sci. Technol.*, **15**, 74 (1978).

PROBLEMS

- 4.1 † (a) By what mechanisms does gas dissolved in a solid enter a vacuum chamber?
- 4.2 The measured outgassing rate Q_m is the flux exiting a chamber through the pumping orifice. For the case where the chamber pumping speed is determined by the orifice dimension, derive a relationship between the ratio of measured-to-intrinsic outgassing rates Q_m/Q_I and the orifice area a and the sticking coefficient of the chamber walls s .

- 4.3 Nitrogen is collected in a beaker inverted over a water bath held at 25°C. The nitrogen is added until the water level inside the beaker equals that of the water outside the beaker. What is the pressure of the nitrogen in the bath if the external pressure is 101,323 Pa (760 Torr)?
- 4.4 Aluminum is sputtered from an rf-coupled plasma source at a rate of 2×10^{-9} m/s (1.2×10^{20} atoms/s). Background gas, assumed to be air, also strikes the substrate. Calculate the ratio of Al atoms-to-air-molecules incident on the surface for background gas pressures of (a) $P = 10^{-3}$ Pa (decorative metallurgy), (b) $P = 10^{-5}$ Pa (metallization of a first surface mirror), and (c) $P = 10^{-7}$ Pa (metallization of a silicon microprocessor wafer). Assume 22°C.
- 4.5 A 1-L cubical chamber has been pumped (ideally) of all the volume gas; however, the internal surfaces remain covered with one monolayer of nitrogen, corresponding to $\sim 10^{19}$ molecules/m². Assume all the monolayer instantly desorbs into the empty volume. (a) Calculate the resulting pressure in the chamber. (b) What fraction of atmospheric pressure is this? (c) In what pressure region is surface cleaning most important?
- 4.6 Verify the temperature obtained in the right-hand illustration of Fig. 4.8. Recalculate this uniform temperature, if the lower surface in the left-hand illustration of Fig. 4.8 were increased from 100°C to 200°C.
- 4.7 A noble nonsticking gas, such as Ar, passes through a very long, small, round tube ($d \ll \lambda$) in molecular flow. This flow can be described by (3.26). Show that the precisely the same result can be obtained when starting with (4.17).
- 4.8 † Define equilibrium vapor pressure.
- 4.9 † In what way does the permeation of a molecular gas through glass differ from hydrogen through steel?
- 4.10 † What role do solubility and diffusivity have in determining the steady-state permeation, and the critical time to reach steady state?

CHAPTER 5

Pressure Gauges

In this chapter we discuss common pressure gauges. To discuss in detail each existing pressure gauge would result in a reduced presentation of those gauges that are the most important. Descriptions of the less frequently used gauges are contained in other texts [1–3]. Descriptions of ultrahigh vacuum gauges have been added to this discussion, as they are needed in production systems with ultrahigh vacuum base pressures.

Many techniques have been developed for the measurement of reduced pressures. Gauges are either direct- or indirect-reading. Those that measure pressure by calculating the force exerted on the surface by incident particle flux are called direct reading gauges. Indirect gauges record the pressure by measuring a gas property that changes in a predictable manner with gas density. Figure 5.1 sketches a way of classifying many pressure gauges. Their operating ranges are illustrated in Fig. 5.2.

5.1 DIRECT-READING GAUGES

Diaphragm, Bourdon, and capacitance manometers are the most commonly used direct-reading gauges. Two rather well known gauges which have a necessary place in pressure measurement, the U-tube manometer and the McLeod gauge, are not described in detail because they are not routinely used by the average vacuum-system operator. In its simplest form a manometer consists of a U-tube that contains a low vapor pressure fluid such as mercury or oil. One arm is evacuated and sealed, the other is connected to the unknown pressure. The unknown pressure is read as the difference in the two liquid levels. The McLeod gauge is a mercury manometer in which a volume of gas is compressed before measurement; for example, compressing a small volume of gas at 10^{-2} Pa by 10,000 \times results in a measurable pressure of 100 Pa. The U-tube manometer, which is used in the 10^2 -to- 10^5 Pa range, and the McLeod gauge, which is a primary standard in the 10^{-3} -to- 10^2 Pa pressure range, are described elsewhere [1–3].

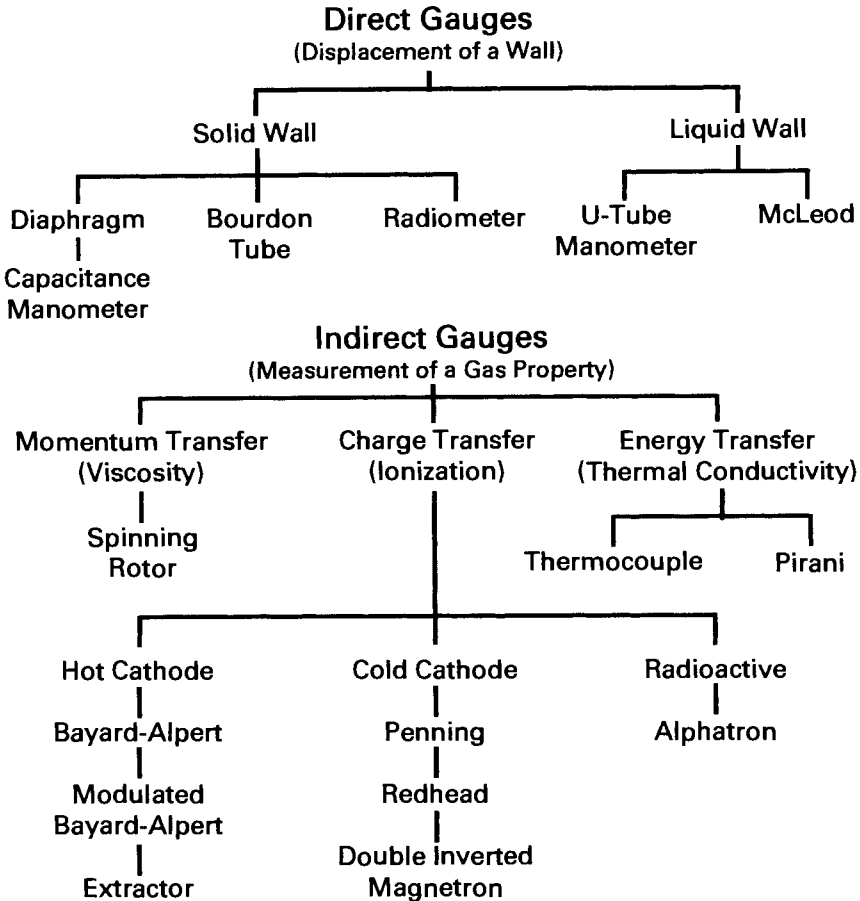


Fig. 5.1 Classification of pressure gauges

5.1.1 Diaphragm and Bourdon Gauges

The simplest mechanical gauges are diaphragm and Bourdon gauges. Both use gears and levers to transmit the deflection of a solid wall to a pointer. The Bourdon tube is a coiled tube of elliptical cross section, fixed at one end and connected to the pointer mechanism at the other end. Evacuation of the gas in the tube causes rotation of the pointer. The diaphragm gauge contains a pressure-sensitive element from which the gas has been evacuated. By removing gas from the region surrounding the element, the wall is caused to deflect, and in a manner similar to the Bourdon tube, the linear deflection of the wall is converted to angular deflection of the pointer.

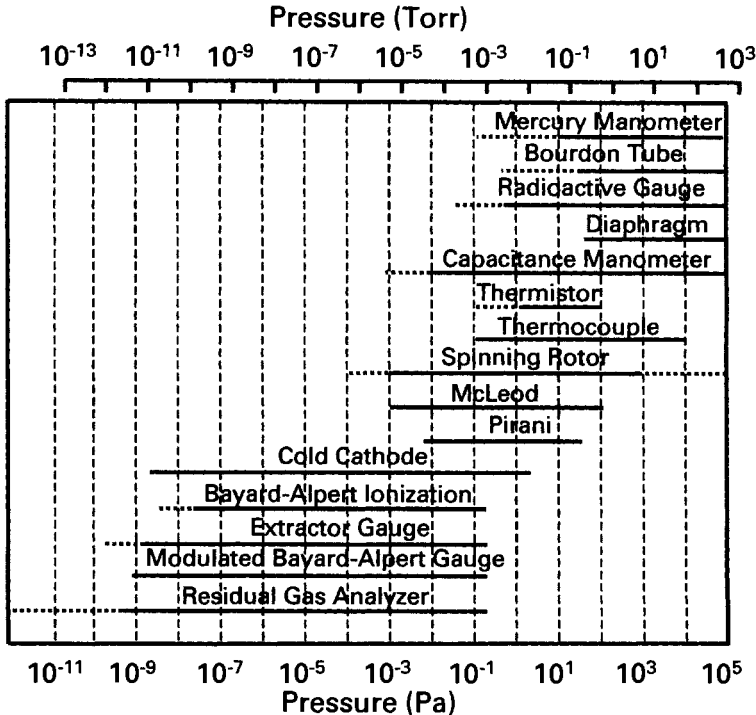


Fig. 5.2 Pressure ranges for various gauges. Adapted with permission from *Scientific Foundations of Vacuum Technique*, 2nd ed., J. M. Lafferty, Ed., p. 350. Copyright 1962, John Wiley & Sons.

Simple Bourdon or diaphragm gauges—for example those of the 50-mm-diameter variety—will read from atmospheric pressure to a minimum pressure of about 10^3 – 5×10^3 Pa (10–40 Torr). They are inaccurate and used only as a rough indication of pressure.

Diaphragm and Bourdon gauges, which are more accurate than those described above, are available in a variety of ranges from 10^3 -to- 2×10^5 Pa (10–760 Torr) and with sensitivities of order 25 Pa (0.2 Torr). The differential Bourdon gauge is quite suitable for rough pressure measurement of clean systems when fabricated from 316 stainless steel. When made from Inconel, it can be designed to measure corrosive gases.

5.1.2 Capacitance Manometers

A capacitance manometer is simply a diaphragm gauge in which the deflection of the diaphragm is measured by observing the change in capacitance between it and a fixed counterelectrode. Alpert, Matland, and

McCoubrey [4] described the first gauge in 1951. They used a differential gauge head as a null reading instrument between the vessel of unknown pressure and another whose pressure was independently adjustable and monitored by a U-tube manometer.

The capacitance of the diaphragm-counter-electrode structure is proportional to geometry (area/gap) and the dielectric constant of the measured gas relative to air. For most gases the pressure may be calculated from the geometry and the observed capacitance change; this is a true, absolute-pressure measurement. A few gases have relative dielectric constants significantly different from air—for example, certain conductive and heavy organic vapors, or gases ionized by radioactivity. For these gases, a 1% difference in dielectric constant will result in a 0.5% error. A single-sided structure is not dependent on the dielectric constant of the measuring gas, because both electrodes are on the vacuum (reference) side.

Capacitance manometers consist of two components, a transducer and an electronic sense unit that converts the membrane position to a signal linearly proportional to the pressure. A common transducer design is shown in Fig. 5.3. The flexible metal diaphragm, which has been stretched and welded in place, is located between two fixed electrodes. The differential transducer shown in Fig. 5.3 may be a null detector or a direct reading gauge. When used as a null detector, the pressure at the reference

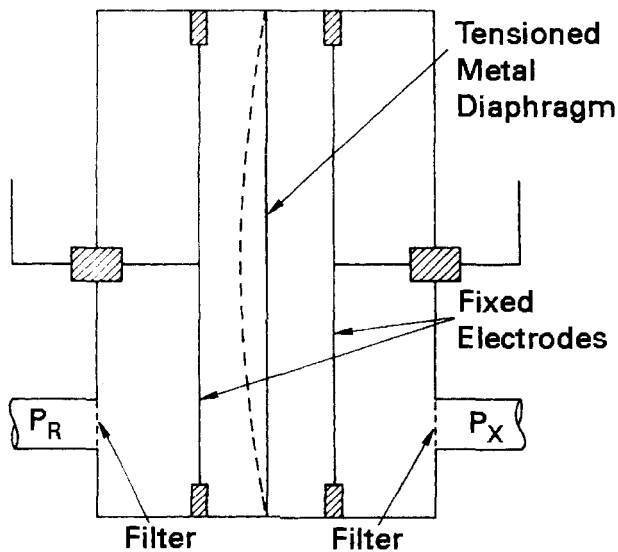


Fig. 5.3 Double-sided capacitance manometer head assembly. Reprinted with permission from *Industrial Research/Development*, January 1976, p. 41. Copyright 1976, Technical Publishing Co.

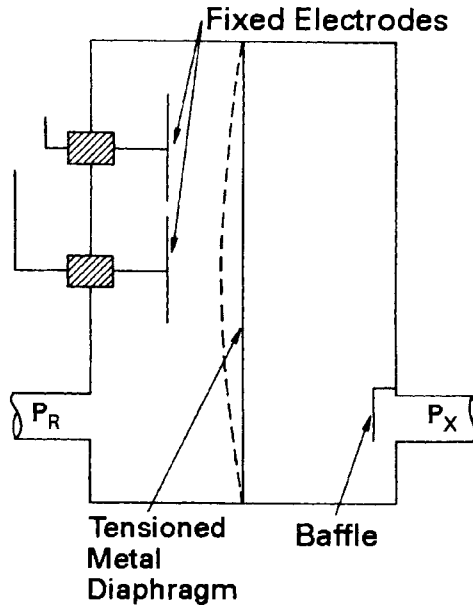


Fig. 5.4 Single-sided capacitance manometer head assembly. The outer electrode is an annular ring. Reprinted with permission from *Industrial Research/Development*, January 1976, p. 41. Copyright 1976, Technical Publishing Co.

side P_r is adjusted until the diaphragm deflection is zero. In this mode a second gauge is necessary to read pressure. To use as a direct reading gauge the reference side must be pumped to about 10^{-5} Pa. After calibration the instrument may be used directly over the pressure range for which it was designed. Transducers are available with the reference side open for evacuation, or evacuated and permanently sealed with a copper pinch seal; a gettering surface is activated inside the tube at the time of manufacture.

Care should be taken in attaching the transducer to a system. It is generally advisable to have a bellows section in series with one tube, if the transducer is to be permanently welded to a system with short tube extensions. Even though some transducers contain filters to prevent particles from entering the space between the diaphragm and the electrodes, it is advisable to force argon through a small diameter tube placed inside the tube or bellows extension during welding. The end of this small tube should be pushed beyond the weld location to allow the argon flow to flush particles out of the tube and away from the sensor during welding. This procedure stops oxide formation on the tube's interior walls.

Because the transducer contains ceramic insulators, cleanliness is in order; a contaminated head is difficult to clean. Cleaning solvents are difficult to remove from the ceramic and may cause contamination of the

system at a later time. To avoid this problem one transducer has been designed with a single sided sensor. Both electrodes are on the reference side. See Fig. 5.4. One electrode is placed at the center of the diaphragm and the second is an annular ring located around the center electrode. For zero deflection of the membrane the circuit is adjusted for zero output signal. The deflection or bowing of the diaphragm causes a capacitance imbalance, which is converted to a voltage proportional to pressure. A proper choice of materials results in a transducer suitable for service in corrosive environments without head damage or in extremely clean environments without contamination by the head.

The electronic sensing unit applies an ac signal to the electrodes. The changes in signal strength produced by the diaphragm are amplified and demodulated in phase to minimize the noise level. The dc output is then used to drive an analog or digital read-out. Because the resolution of the instrument is limited by system noise, the system bandwidth must be stated when specifying resolution; noise is proportional to the half-power of the bandwidth. Typical capacitance manometers have a resolution of 1 part per million (ppm) full scale, at a bandwidth of 2 Hz.

Just as low electronic noise is of prime importance in obtaining high resolution, thermal stability of the head is necessary for stable, accurate, and drift-free operation. The diaphragm deflection in the transducer can be as low as 10^{-9} cm; therefore motion of parts due to temperature change becomes a large source of error. Transducers are available with heaters that maintain the ambient temperature at about 50°C and avoid some of the problems of ambient temperature change. Many transducers can be operated at temperatures as high as 250°C. At high temperatures, the readings must be corrected for thermal transpiration. See Section 2.3.4. Stable operation of a transducer requires that the thermal expansion coefficients of the diaphragm and electrode assemblies be well-matched. Practical designs must make a trade-off between expansion coefficient and corrosion resistance. Without proper temperature regulation a transducer may have zero and span coefficients of 5–50 ppm full scale and 0.004–0.04% of reading per degree Celsius, respectively, at ambient temperature [5]. Proper temperature regulation can result in an order of magnitude improvement in the zero and span coefficients.

Capacitance manometers can be operated over a large dynamic range, a factor of 10^4 – 10^5 for most instruments. The overall system accuracy deteriorates at small fractions of full head range, as illustrated in Fig. 5.5 for the 1.3×10^5 Pa (1000-Torr) head. Transducers with a full-scale deflection of 130 Pa (1 Torr) have been checked in the 2.5×10^{-2} -to- 6.5×10^{-4} Pa (1.5×10^{-4} -to- 5×10^{-6} Torr) pressure range by volumetric division. They have been found to be linear to the lowest pressure and in agreement within 0.6% plus 5.3×10^{-5} Pa [6].

5.2 INDIRECT-READING GAUGES

In this section, we describe the most useful indirect reading gauges. Indirect gauges report pressure by measuring a pressure-dependent property of the gas. In the pressure range above 0.1 Pa, energy and momentum transfer techniques can be used for pressure measurement. Thermal conductivity gauges incorporate the principle of energy transfer between a hot wire and a room temperature gauge wall. A Pirani [7] or a thermocouple [8] gauge is found on every vacuum system for measuring pressure in the medium vacuum region. The spinning rotor gauge [9,10] operates on the principle of momentum transfer. Ionization gauges, which measure gas density, have found wide acceptance. Hot and cold cathode gauges are based on the principle of ionization. The Bayard-Alpert [11] and extractor [12] hot cathode gauges and the cold cathode [13] gauge span the range $0.1\text{--}10^{-10}$ Pa.

5.2.1 Thermal Conductivity Gauges

Thermal conductivity gauges are a class of pressure-measuring instruments that operates by measuring the rate of heat transfer between a hot wire and its surroundings. In the low-pressure range, free molecular heat flow increases linearly with pressure. It is first observable when the pressure is large enough for the heat flow from the wire to be larger than the end and radiation losses. It is not related to the tube diameter. In the high-pressure limit von Ubisch [14,15] found heat flow from the wire to become nonlinear at a $\lambda \sim 1$ wire diameter, and saturate at 9–12 wire diameters [16]. Molecules leaving the heated wire collided with nearby gas molecules and returned heat to the wire. von Ubisch varied the tube diameter from 0.25-to-10 cm with little significant change in the characteristic response [17]. Ultimately, at very high pressures, the heat flow from wire to tube would become constant, were it not for convection currents within the gauge causing increased heat flow to the wall. See Fig. 5.5. Thermocouple gauges using serpentine heaters fabricated in a planar thin-film structure [18] would begin to saturate at a pressure corresponding to a value where the distance between the heater and thermal sink is a few mean free paths. In the lowest pressure region radiation and conduction to the supports account for most of the heat flow losses.

$$H = A\sigma\epsilon_1(T_2^4 - T_1^4) + \text{end losses} \quad (5.1)$$

To extend the range of a gauge to its lowest possible pressure limit it is necessary to reduce both radiation losses and conduction losses. End losses dominate when the wire is short, (in thermocouple tubes), whereas radiation losses (and sensitivity) increase with wire temperature. Two commonly

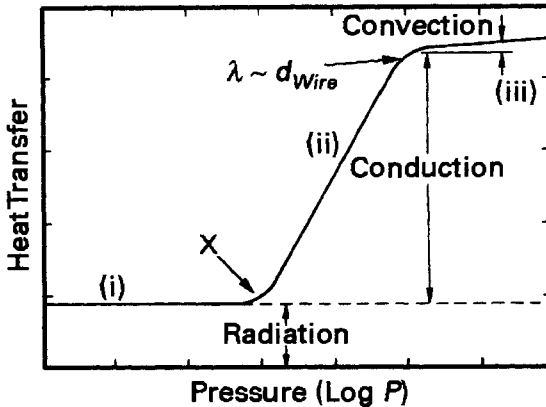


Fig. 5.5 Heat transfer regimes in thermal conductivity gauges, such as thermocouple gauges or Pirani gauges constructed from fine, heated wires. Three regions are illustrated: (i.) $\lambda \gg d_{Wire}$, (iii.) $\lambda \ll d_{Wire}$, and (ii.) intermediate. The location of the upper knee will differ, if the heated element is fabricated in a planar or coiled geometry. X = low-pressure limit; it is reached when the heat transfer is equals the radiation and end conduction losses.

manufactured sensors have upper pressure limits of 15 and 150 Pa (0.1 and 1 Torr). Sensors reading to 10^5 Pa (760 Torr), which take advantage of the pressure-dependent convection losses, are commercially available [19].

The sensitivity of the gauge is determined by tube construction and gas as well as by the technique for sensing the change in heat flow with pressure. Tungsten is commonly used for the heater wire because it has a large thermal resistance coefficient. (When a semiconductor is used as the heat sensitive element, the device is referred to as a thermistor gauge, even though it is configured identically to a Pirani gauge). The accommodation coefficient α for clean materials can be of an order 0.1, but for contaminated surfaces it can be as high as unity. For most cases, α is stable but not known. With all other factors well controlled, changes in emissivity and accommodation coefficient are large enough to allow thermal conductivity gauges to be used as only rough indicators of vacuum.

The change in wire temperature can also be detected by monitoring the resistance of the heated wire. When a Wheatstone bridge circuit is used to measure the resistance change, the device is termed a Pirani gauge. Alternatively, the temperature change can be measured directly with a thermocouple, in which case it is called a thermocouple gauge.

Pirani Gauge

The term Pirani gauge is given to any type of thermal conductivity gauge in which the heated wire forms one arm of a Wheatstone bridge. A simple

form of this circuit is shown in Fig. 5.6. The gauge tube is first evacuated to a suitably low pressure, say 10^{-4} Pa and R_1 is adjusted for balance. A pressure increase in the gauge tube will unbalance the bridge because the increased heat loss lowers the resistance of the hot wire. By increasing the voltage, more power is dissipated in the hot wire, which causes it to heat, increase its resistance, and move the bridge toward balance. In this method of gauge operation, called the constant temperature method and the most sensitive and accurate technique for operating the bridge, each pressure reading is taken at a constant wire temperature. To correct for temperature-induced changes on the zero adjustment, an evacuated and sealed compensating gauge tube is used in the balance arm of the bridge. Bridges with a compensating tube can be used to 10^{-3} Pa.

The constant voltage and constant current techniques were devised to simplify the operation of the Pirani gauge. In each case the total bridge voltage or current is kept constant. The constant voltage method is widely used in modern instruments because no additional adjustments need to be made after the bridge is nulled at lower pressures. The out-of-balance current meter is simply calibrated to read the pressure.

The constant temperature method is the most sensitive and accurate because at constant temperature the radiation and end losses are constant. Because the wire temperature is constant, the sensitivity is not diminished in the high-pressure region. This method does not lend itself to easy operation; balancing is required before each measurement. A sudden drop in pressure can also cause overheating of the wire if the bridge is not immediately re-balanced. Direct reading constant-temperature bridges that need only a zero adjustment are now commercially available, although at

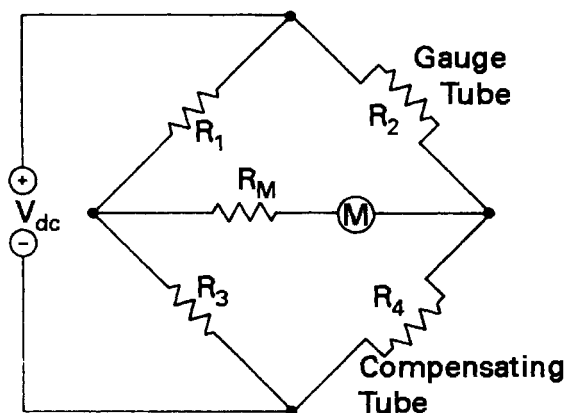


Fig. 5.6 Basic Pirani gauge circuit. Adapted with permission from *Vacuum Technology*, A. Guthrie, p. 163. Copyright 1963, John Wiley & Sons.

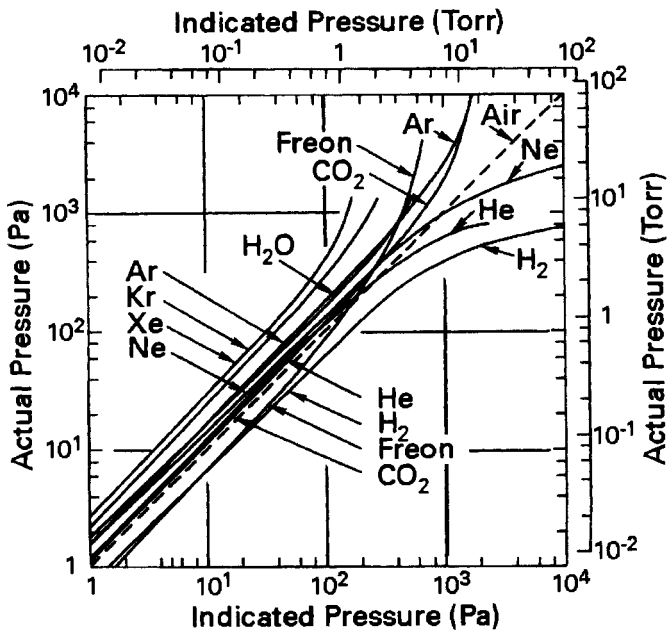


Fig. 5.7 Calibration curves for the Leybold TR201 Pirani gauge tube. Reprinted with permission from Leybold-Heraeus GmbH, Köln, Germany.

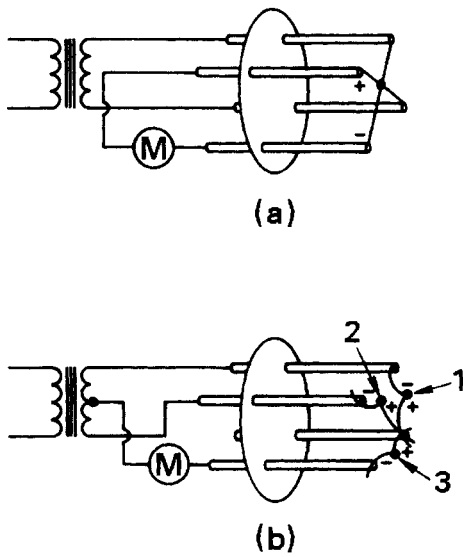


Fig. 5.8 Thermocouple gauge tube commonly used in the 0-to-100 Pa (0-to-1000 Torr) range. (a) Uncompensated gauge tube and (b) compensated gauge tube (thermocouple No. 3 is the compensating couple).

somewhat greater expense than a constant voltage or current bridge. Modern circuitry has eliminated tedious bridge balancing. Because the heat conductivity varies considerably among gases and vapors, the calibration of the gauge is dependent on the nature of the gas. Most instruments are calibrated for air; therefore a chart like the one shown in Fig. 5.7 is needed for each specific gauge, when the pressure of other gases is to be measured.

Thermocouple Gauge

The thermocouple gauge measures pressure-dependent heat flow. Constant current is delivered to the heated wire, and a tiny Chromel-Alumel thermocouple is carefully spot welded to its midpoint. As the pressure increases heat flows to the walls and the temperature of the wire decreases. A low-resistance dc microammeter is connected to the thermocouple, and its scale is calibrated in pressure units.

Figure 5.8 shows the four-wire and three-wire versions of the gauge tubes. The four-wire gauge tube uses a dc meter to read the temperature of the thermocouple, whereas the power supply is regulated to deliver a constant current to the wire. The current can be ac or dc. The three-wire gauge circuit reduces the number of leads between the gauge tube and

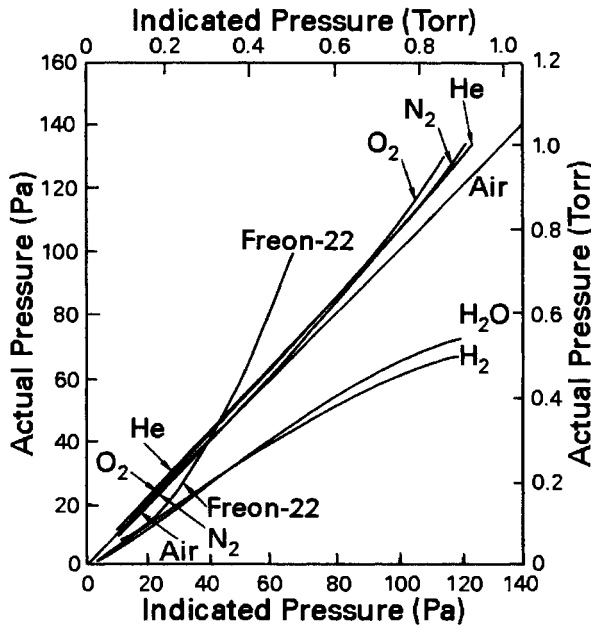


Fig. 5.9 Calibration curves for the Hastings DV-6M thermocouple gauge tube. Reprinted with permission from Hastings Instruments Co, Hampton, VA.

controller. It reduces the number of vacuum feed-throughs by using ac to heat the wires, and a dc microammeter to read the voltage between one thermocouple wire and the center tap of the transformer, which is a dc connection to the other junction. In both tubes the power delivered is not constant; instead the wire current is constant. Because the resistance of the wire is temperature-dependent, the power delivered decreases slightly at high pressures. Both gauge forms are rugged and reliable but inaccurate. Calibration curves for one thermocouple gauge are given in Fig. 5.9.

Stability and Calibration

A detailed review of the properties of thermal conductivity gauges determined its critical parameters for stability [20]. It concluded that the critical parameter in the low-pressure portion of their operating range was the wire emissivity. The mid-range accuracy was found strongly dependent on the thermal accommodation coefficient—a function of surface contamination. The full-scale region of the thermal conductivity gauge had no critical parameter; good stability was predicted and observed.

Thermal conductivity gauges can be calibrated by direct comparison to standard reference gauges, such as capacitance manometers or spinning rotor gauges. Detailed recommended practices and procedures for calibrating thermal conductivity vacuum gauges have recently been published by the American Vacuum Society [21].

5.2.2 Spinning Rotor Gauge

The spinning rotor gauge [9,10] measures pressure by measuring the rate at which a rotating ball slows due to the viscosity of the surrounding gas. Gas molecules collide with the ball, causing its angular momentum to decrease. At high pressure, the rotating ball slows rapidly; at low pressures, slowly. The spinning rotor gauge is an indirect gauge—it does not measure pressure on a wall. However, it has been proven so accurate and stable that it has found use as a secondary or transfer standard [22,23].

The rate at which a rotating ball loses angular velocity is given by

$$-\frac{\omega}{\omega_0} = \sigma \left(\frac{10}{\pi} \right) \left(\frac{1}{rd} \right) \frac{P}{v_{ave}} \quad (5.2)$$

where σ is the coefficient of tangential momentum transfer, ω is the rotational velocity, ω_0 is the rotational velocity at time zero—typically 400 revolutions per second, r is the ball radius, and d is the ball density. An illustration of a commercial sensing head is shown in Fig. 5.10. Only the rotating ball is located within the vacuum system; it is levitated inside a

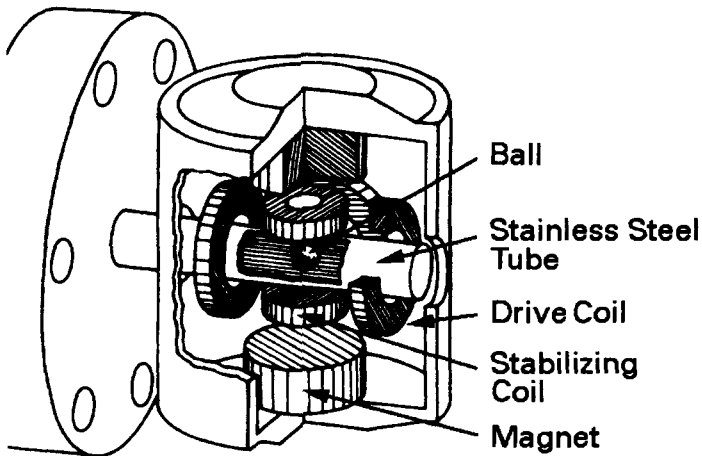


Fig. 5.10 Spinning rotor gauge sensor. Reprinted with permission from MKS Instruments, 6 Shattuck Road, Andover, MA 01810.

small stainless steel closed-end tube that is welded to a 70-mm-diameter metal flange. Equation (5.2) shows that the rate of decay is proportional to the \sqrt{m} of the measured gas. The user is required to know the gas being measured and its calibration factor. Hinkle and Jacobs [24] have shown that the effective mass of a gas mixture can be entered into the spinning rotor gauge software as

$$m_{eff} = \left(\sum_{i=1}^n a_i \sqrt{m_i} \right)^2 \quad (5.3)$$

They note that simultaneous use of a capacitance manometer and spinning rotor gauge allows the user to observe changes in gas mixtures.

The fundamental property that makes this instrument so stable, is the constancy of the quantity σ , the coefficient of tangential momentum transfer. Long-term studies have shown that this variable remains constant for long periods of time and shows little variation between similar rotor balls. In one sequence of measurements on eight instruments in three national laboratories, σ ranged from 0.9927-to-1.0075, with standard deviations between 0.0003-to-0.0012 in the values reported for individual instruments [25].

As the pressure tends to zero, there is a fixed “offset” rate at which the ball slows. This rate is due to eddy currents induced in the ball by the rotor fields and by coulomb forces developed by the magnets. Thus, to read the lowest pressure possible, this offset rate must be subtracted. It is claimed that commercial instruments can read to 10^{-5} Pa (10^{-7} Torr) [26]; however,

care is required. The ball requires spinning for approximately five hours at a pressure one decade lower than the lowest pressure to be measured in order to achieve equilibrium and obtain a precise measurement of the residual drag [27]. Even after that measurement, the residual drag must be measured frequently during use. At high pressures, the rate at which the ball velocity decreases is a constant and is determined by the properties of the (viscous) gas in which it is immersed. This rate has been calculated to be 50 Pa, but the real device becomes non-linear above 0.1 Pa. Algorithms contained within commercial instruments attempt to correct for this non-linearity and thermal changes introduced at high pressure. With refined algorithms the gauge can measure pressures of 100 Pa (1 Torr) to $\pm 1\%$ [28]; it can measure pressures of ~ 1000 Pa (10 Torr) with less accuracy.

The spinning rotor gauge is an excellent instrument when used by a trained operator in a laboratory setting. It is the instrument of choice for calibrating other indirect gauges within its pressure range; it can be used by a skilled operator to identify gas mixture problems.

5.2.3 Ionization Gauges

In the high and ultrahigh vacuum region, where the particle density is extremely small it is not possible, except in specialized laboratory situations, to detect the minute forces that result from the direct transfer of momentum or energy between the gas and a solid wall. For example, at a pressure of 10^{-8} Pa the particle density is only $2.4 \times 10^{12}/\text{m}^3$. This may be compared with a density of $3 \times 10^{22}/\text{m}^3$ at 300 K, which is required to raise a column of mercury 1 mm. Even a capacitance manometer cannot detect pressures lower than 10^{-4} Pa.

In the region below 10^{-3} Pa, pressure is measured by ionizing gases, then counting and amplifying the ion signal. Each ionization gauge has its own lower pressure limit at which the ionized particle current is equal to a residual or background current. Ionization gauges normally used in the high vacuum region have a background limit of $\sim 10^{-8}$ Pa (10^{-10} Torr). Both hot and cold cathode gauges have been developed for pressure measurement. Each technique has its own operating range, advantages, and disadvantages.

Hot Cathode Gauges

The operation of the ion gauge is based on electron impact ionization. The ionized molecular current to the collector electrode is proportional to pressure, provided that all other parameters, including temperature, are held constant. The number of positive ions formed is actually proportional to the number density, not the pressure; the ion gauge is not a true pressure

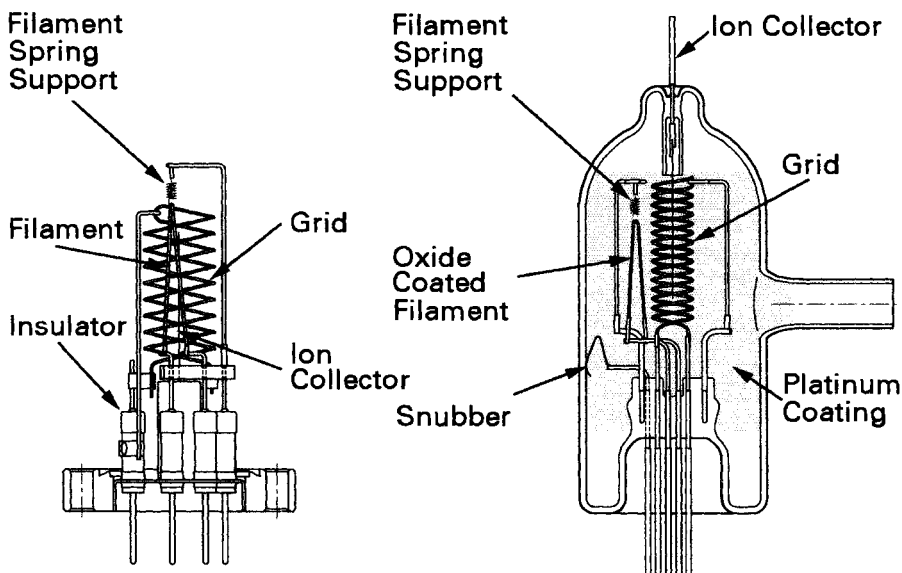


Fig. 5.11 Cross sectional views of two Bayard-Alpert sensors. Left: Bakeable, flange-mounted nude gauge. Right: Glass-encapsulated gauge. Reprinted with permission from Televac/ETI, a Fredericks Company, 2400 Philmont Ave., Huntingdon Valley, PA 19006.

measuring instrument, but rather it is a particle-density gauge. Its reading is proportional to pressure only when the temperature is constant.

The earliest form of ion gauge, the triode gauge, consisted of a filament surrounded by a grid wire helix and a large-diameter, solid cylindrical ion collector. This gauge, which is not illustrated here, looked a lot like a triode vacuum tube. Electrons emitted by the heated filament were accelerated toward the grid wire, which was held at a positive potential of about 150 V. The large area external collector was biased about -30 V with respect to the filament; it collected the positive ions generated in the space between the filament and the ion collector. This gauge recorded pressures as low as 10^{-6} Pa; it would not give a lower reading, even if indirect experimental evidence indicated the existence of lower pressures. Further progress was not made until after 1947, when Nottingham [29] suggested that the cause of this effect was x-ray-generated photocurrent. Nottingham proposed that soft x-rays generated by the electrons striking the grid wire collided with the ion collector cylinder and caused photoelectrons to flow from the collector to the grid. Some photo emission is also caused by ultraviolet radiation from the heated filament. As they leave the collector, these photoelectrons produce a current in the external circuit, which is not distinguishable from the positive ion flow toward the ion collector, and mask the measurement of reduced pressures.

In 1950 Bayard and Alpert [11] designed a gauge in which the large area collector was replaced with a fine wire located in the center of the grid (Fig. 5.11a). Because of its smaller area of interception of x-rays, this gauge could measure pressures as low as 10^{-8} Pa. Today this gauge is the most popular design for the measurement of high vacuum pressures.

The proportionality between the collector current and pressure is given by

$$i_c = S' i_e P$$

or

$$P = \frac{1}{S'} \frac{i_c}{i_e} \quad \blacktriangleright (5.4)$$

where i_c and i_e are the collector and emission currents, respectively, and S' is the sensitivity of the gauge tube. This sensitivity has dimensions of reciprocal pressure, which in SI is 1/Pa. The sensitivity is dependent on the tube geometry, grid and collector voltages, the type of control circuitry, and the nature of the gas being measured. For the standard Bayard-Alpert tube with external control circuitry, a grid voltage of +180 V, and filament bias voltage of +30 V, the sensitivity for nitrogen is typically 0.07/Pa. See Fig. 5.12. Variations in tube design, voltage, and control circuitry can cause it to range from 0.05-to-0.15/Pa. The tube's sensitivity for other gases varies with ionization probability. Alpert [30] suggested that the relative sensitivity (the ratio of the absolute sensitivity of an unknown gas to nitrogen) should be independent of structural and electronic variations and therefore be more meaningful to tabulate than absolute sensitivity.

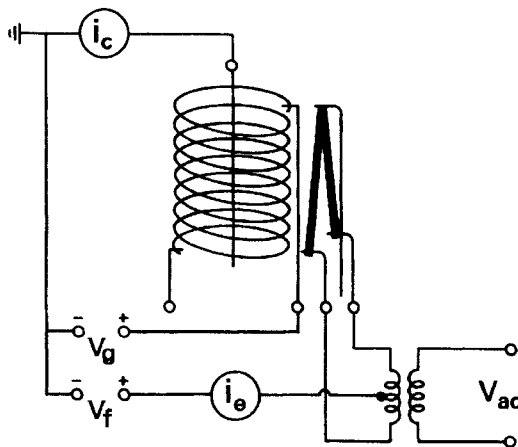


Fig. 5.12 Control circuit for a Bayard-Alpert ionization gauge tube.

**Table 5.1 Approximate Relative Sensitivity
of Bayard-Alpert Gauge Tubes to
Different Gases^a**

Gas	Relative Sensitivity
H ₂	0.42–0.53
He	0.18
H ₂ O	0.9
Ne	0.25
N ₂	1.00
CO	1.05–1.1
O ₂	0.8–0.9
Ar	1.2
Hg	3.5
Acetone	5

Source: Adapted with permission from *J. Vac. Sci. Technol.*, 8, p 661, T. A. Flaim and P. D. Owenby. Copyright 1971, The American Vacuum Society.

^a The pressure of any gas is found by dividing the gauge reading by the relative sensitivity.

The relationship between the pressure of an unknown gas $P(x)$ and the meter reading is

$$P(x) = \frac{S(N_2)}{S(x)} P(\text{meter reading}) \quad (5.5)$$

or after normalizing the gas sensitivities, by dividing each sensitivity by that of nitrogen: $S(x)_{\text{relative}} = S(x)/S(N_2)$ we obtain

$$P(x) = \frac{P(\text{meter reading})}{S(x)_{\text{relative}}} \quad \blacktriangleright (5.6)$$

By use of (5.6) and Table 5.1 [31] the pressure of gases other than nitrogen can be measured with an ion gauge, even though all ion gauges are calibrated for nitrogen.

Gauge sensitivity is often given in units of microamperes of collector current per unit of pressure per manufacturer's specified emission current; for example, a typical nitrogen sensitivity is $(100/\mu\text{A}/\text{mTorr})/10 \text{ mA}$. This is a confusing way of saying the sensitivity is 10/Torr, but it does illustrate an important point; not all gauge controllers operate with the same emission current and not all gauge tubes have the same sensitivity. Checking the instruction manual can avoid potential embarrassment.

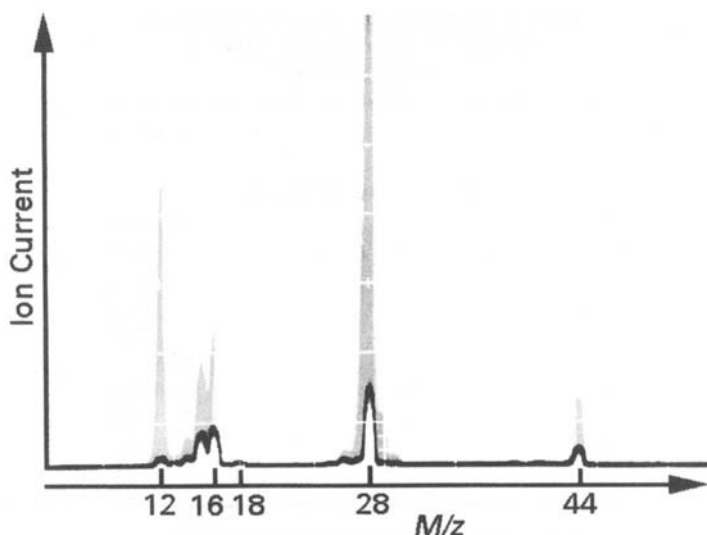


Fig. 5.13 Transient desorption during degassing a glass-encapsulated Bayard-Alpert ion gauge tube as recorded by a storage tube oscilloscope. The gray traces indicate the transient release of carbon monoxide along with some methane and carbon dioxide on grid heating. The solid black line represents the background spectrum.

The classical control circuit is designed to stabilize the potentials and emission current while measuring the plate current. The plate current meter is then calibrated in appropriate ranges and units of pressure. The accuracy of the gauge is dependent in part on moderately costly, high-quality, emission current regulation.

Tungsten and thoriated iridium (ThO_2 on iridium) are two commonly used filament materials. Thoriated iridium filaments are not destroyed when accidentally subjected to high pressures—an impossible feat with fine tungsten wires—but they do poison in the presence of some hydrocarbon vapors. The remarks in Section 8.2 about filament reactivity with gases in the residual gas analyzer ionizer also pertain to the ion gauge.

Ion gauge grids are outgassed by direct or electron bombardment heating. The grid wire can be directly heated by connecting it to a low-voltage, high-current transformer. Alternatively, the grid and plate wire can be connected to a high-voltage transformer and heated by electron bombardment. It is best to wait until the pressure is on a suitably low scale ($\sim 10^{-4}$ Pa) before outgassing. An unbaked glass encapsulated gauge should be outgassed until the glass has desorbed. (The pressure may be monitored during outgassing of gauges with resistance-heated grids.) The time for this initial outgassing is variable, but 15–20 min is typical. After the initial outgassing the tube should be left on. Subsequently, only short outgassing

times, say 15 s, are periodically needed to clean the electrodes. Figure 5.13 illustrates the gas release from a grid during electron bombardment. Notice the large transients at $M/z = 28$, 16, 12, and to a lesser extent, 44. This identifies the desorbed gases as CO, CO₂ and some CH₄. If the outgassing power supply is inadequately designed, desorption will not be complete [32]; see the discussion of electron stimulated desorption in the following subsection.

Extending the operating region of the hot cathode gauge below 10^{-8} Pa (10^{-10} Torr) is not so easy. Few ultrahigh vacuum hot cathode gauges are commercially available at the time of this writing. This presents a problem to designers and users of state-of-the-art UHV advanced vacuum processing systems that require ultrahigh vacuum base pressures. The Extractor gauge [12] and uhv-24 Bayard-Alpert sensor and are two commercially available ultrahigh vacuum gauges. The modulated Bayard-Alpert gauge is worthy of reconsideration. The efficient Bayard-Alpert design, known as the uhv-24, increased the sensitivity of the gauge tube by capping the end of the grid to prevent electron escape [33]. It reduced the x-ray limit by use of a fine, 125- μm -diameter collector wire. This sensor has a sensitivity of 0.15/Pa (20/Torr) [34]. It is mounted on a 70-mm-diameter metal flange and can be baked to 450°C. See Fig. 5.11 (left). One Extractor gauge is illustrated in Fig. 5.14. The hemispherical ion reflector, maintained at grid potential, reflects ions to the collector wire. The sensitivity of a similar IE511 gauge

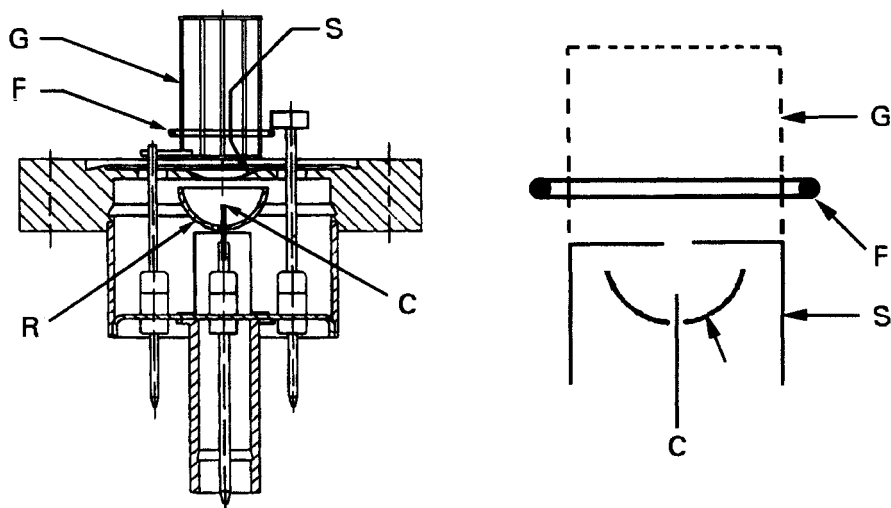


Fig. 5.14 IE514 Extractor gauge. Left: Sensing head. Right: Expanded detail of the electrode structure. G, grid; F, filament; S, suppressor; R, reflector; C, collector. Reprinted with permission from INFICON AG, 9496 Balzers, Liechtenstein

tube was reported as 0.045/Pa (6/Torr) [35]. It is a stable gauge with a low x-ray limit. It is less sensitive to electron-stimulated grid desorption than a standard Bayard-Alpert Gauge.

The modulated Bayard-Alpert gauge was constructed like a standard Bayard-Alpert gauge, but had a modulator wire located within the grid region [36]. When a potential was applied to the modulator wire located that equaled that of the collector, some of the gas phase ion flux was diverted to the modulator and the collector current decreased. However, the x-ray-generated charge flow remained constant. By measuring this fractional decrease at pressures far above the x-ray limit, the modulation factor was determined and the gauge calibrated. Its sensitivity was measured to be 0.9/Pa (12/Torr) [37].

Hot Cathode Gauge Errors

Despite its deceptively simple operating principle, measurement of pressure in the ultrahigh vacuum region with a hot cathode gauge must be done with considerable care. Numerous effects can alter the indicated ion current [32,38,39]. The previously described x-ray generated photocurrent, electron-stimulated grid (and ion collector) desorption, wall outgassing caused by thermal heating from the hot cathode, chemical effects on heated cathodes, controller errors, wall diameter, and cathode evaporation can each introduce measurement error.

Historically, the most attention has been paid to reducing the x-ray limit; it was the most significant limiting factor; indeed it remains a concern. The uhv-24 sensor has x-ray limit of 4×10^{-9} Pa (2.8×10^{-11} Torr) [34]. The Leybold IE511 was found to have an x-ray limit of 2×10^{-10} Pa (1.5×10^{-12} Torr) [35], whereas its original version had an x-ray limit 25 times less [38]. The modulated Bayard Alpert gauge was shown to have an x-ray limiting pressure of 9×10^{-9} Pa (7×10^{-12} Torr) [37].

Electron-stimulated desorption is a significant, but a variable and an unpredictable source of error; in many cases ESD errors can be significantly larger than those caused by x-rays. Electrons striking the grid and ion collector release previously adsorbed gases. Prior exposures to oxygen results in desorption of CO formed by a reaction of dissociated oxygen and carbon impurities in metals. Other studies point to enhanced ESD in systems containing small amounts of water vapor or other oxygen containing gases. Using optical metrology (with no heated filaments), Looney [40] has demonstrated ESD of carbon monoxide from Bayard Alpert gauges and RGA sensors. Figure 5.15 illustrates the decrease and increase of the CO signal as hot filaments in the RGA and Bayard-Alpert gauges were first turned off, then on. The instantaneous change in signal levels indicated that CO released from surfaces was not due to the slow

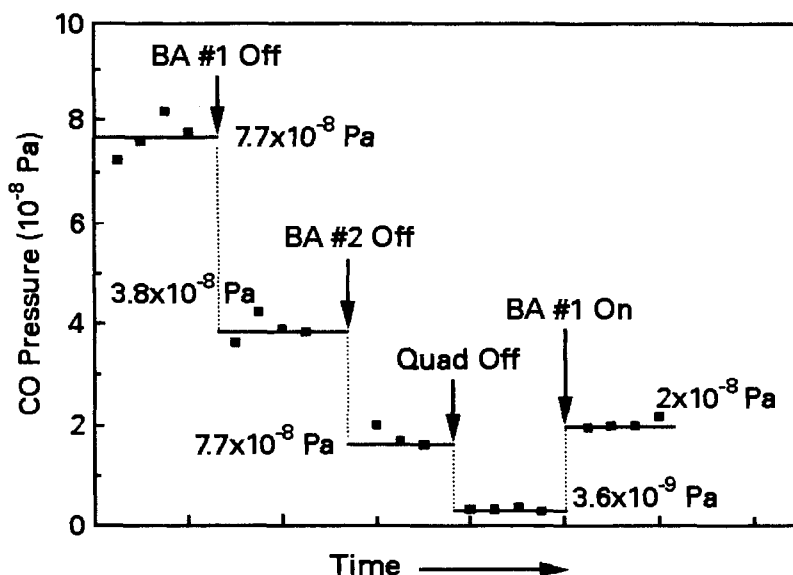


Fig. 5.15 Carbon monoxide concentration in an ultrahigh vacuum system as measured optically (no hot filament). The CO partial pressure is seen to decrease as hot filament devices are turned off. Reprinted with permission from *J. Vac. Sci. Technol. A*, 11, p. 3111. J. P. Looney, J. E. Harrington, K. C. Smyth, T. R. O'Brian, and T. B. Lucatorto. Copyright 1993, AVS-The Science and Technology Society.

heating or cooling of nearby surfaces. For decades, many researchers have inferred CO to be an artifact of hot filaments and not a true ultrahigh vacuum background gas. These data unambiguously confirm our earlier suspicions. Kendall [32] observed that ESD disappeared when a Bayard-Alpert grid was heated above ~ 800 K. He concluded that gases could not adsorb on grids at this temperature. Watanabe's careful ESD measurements agree [39]. Figure 5.16 shows the magnitude of the ESD signal in an experimental gauge capable of distinguishing gas phase ions from their energetically different ESD counterparts. Since some new ionization gauge controllers operate at emission currents of 4 mA or less, they may not heat the grid to a sufficiently high temperature to prevent ESD. There was a reason ionization gauges were designed to operate at 10 mA; a reason which may have been forgotten.

Wall outgassing caused by heating of the gauge walls, or surfaces near nude gauges, will introduce measurement errors. Watanabe noted that stainless steel, surrounding a typical ultrahigh vacuum gauge, had two undesirable characteristics—high emissivity and low thermal conductivity. The nearby walls are hot, because they absorb heat easily and dissipate it poorly. Watanabe used these concepts to construct an experimental gauge

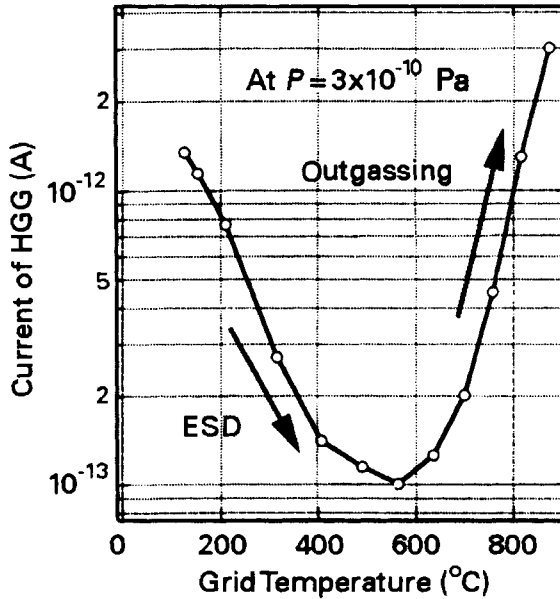


Fig. 5.16 Ion current versus grid temperature in a hot cathode UHV ion gauge. Electron stimulated desorption of the grid decreases with temperature up to a temperature of ~ 800 K. The increased signal at high grid temperatures is believed to be caused by the outdiffusion of hydrogen from the grid wire. Reprinted from *Vacuum*, 53, F. Watanabe, 151–157, copyright 1999, with permission from Elsevier.

using a gold-plated copper fixture, which operated with reduced heater power and reduced wall outgassing [40].

Kendall observed that mounting flange virtual leaks and dimensional manufacturing tolerances, as well as inaccurate electrometer and voltage divider resistors contributed to gauge error [32]. Surface chemical effects can synthesize ions not part of the system background. The gauge envelope is also part of the measurement circuit. Glass charges to a floating potential. Redhead demonstrated that the sensitivity factor for a Bayard-Alpert gauge was strongly dependent on the filament distance and the electric fields near the filament [42]. The diameter of the glass or metal envelope affects electron orbits [43]. Filippelli demonstrated that envelope diameter changes could produce sensitivity changes as large as 50% with some Bayard-Alpert sensors [44]. He found that extractor gauges were less susceptible to wall diameter changes, because of the sensor's low profile—much of the gauge was located within its mounting flange.

Measurement of pressure in the ultrahigh vacuum range requires care; it is essential that those who are serious about this subject begin by reading papers by Kendall [32], Redhead [38] and Watanabe [39].

Cold Cathode Gauge

The cold cathode gauge, developed by Penning in 1937 [13], provides an alternative to the hot cathode gauge, which in many respects is superior to a Bayard-Alpert gauge. A commercial sensor tube is illustrated in Fig. 5.17. This gauge is based on the inverted magnetron geometry [45]. The arrangement of the electric and magnetic fields causes electrons to travel long distances in spiral paths before finally colliding with the anode. Long electron trajectories enhance the ionization probability and improve sensitivity. The discharge begins when one electron or ion gains sufficient energy to ionize a gas molecule. The electron density increases until it is space charge limited. The time required for a gauge to reach steady state decreases as pressure increases. This can be described by a starting parameter, typically of order 50–500 $\mu\text{Pa}\cdot\text{s}$ (0.5–5 $\mu\text{Torr}\cdot\text{s}$) for gauges without auxiliary starting sources [46]. Starting the gauge at low pressures can be difficult unless the gauge contains an auxiliary source; radioactive sources, photo emitters, hot filaments, and field emitters have been used to provide additional starting electrons. The range of operation of the cold

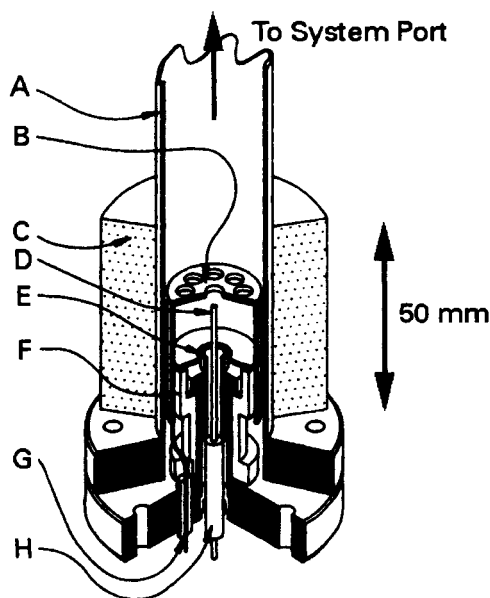


Fig. 5.17 Cold cathode gauge: A, envelope; B, cathode; C, magnet; D, anode; E, guard electrode; F, ceramic support; G, cathode current feedthrough; H, high voltage feedthrough. Reproduced with permission from *J. Vac. Sci. Technol. A*, 9, p. 1977, R. N. Peacock, N. T. Peacock, and D. S. Hauschulz. Copyright 1991, AVS-The Science and Technology Society.

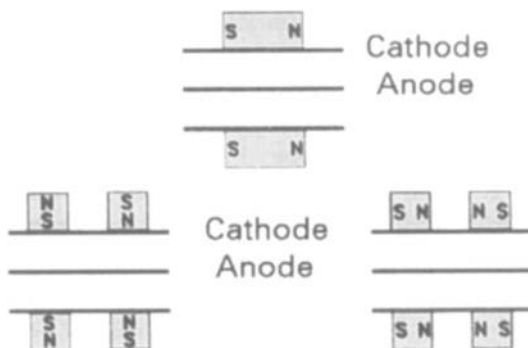


Fig. 5.18 Simplified view of the magnet configurations in modern inverted magnetron cold cathode gauges. Top: Conventional single inverted magnetron. Lower left: Radial double magnets. Lower right: Axial double magnets. Reprinted with permission from *J. Vac. Sci. Technol. A*, **18**, p. 1724. B. R. F. Kendall and E. Drubetsky. Copyright 2000, AVS—The Science and Technology Society.

cathode gauge is $1\text{--}10^{-9}$ Pa ($10^{-2}\text{--}10^{-11}$ Torr). It is a viable option to the hot cathode gauge for systems with 10^{-9} -Pa-range base pressures, if it is not mounted immediately adjacent to a hot cathode gauge or residual gas analyzer. Cold and hot cathode gauges have sensitivities that vary with gas species and in a similar manner. Like hot cathode gauges, cold cathode gauges measure gas density. Unlike hot cathode gauges, they have no x-ray limit and have little electron-stimulated desorption or thermally induced wall outgassing; they do not have filaments to change. Gas release from a cold cathode gauge was observed after the gauge had been contaminated [47]. The magnetic field surrounding a cold cathode gauge is a concern in some applications. Fringing fields have been reduced with alternative magnetic configurations [46]. Figure 5.18 illustrates a conventional and two “double magnetron” designs; one uses opposing radial magnets whereas the other uses opposing longitudinal magnets.

Cold cathode gauges can pump; however, their pumping speeds have been found similar to those of a hot cathode gauge [48]. They should not be connected to a system with tube of a smaller diameter or a pressure drop will result. Cold cathode gauges should be mounted in a way that will not allow metal particles to fall inside the tube.

Gauge Calibration

Direct comparison, static expansion, and continuous expansion are techniques used to calibrate high vacuum gauges against primary standards. Direct comparison is performed by comparing standard and

unknown gauges on the same chamber. The static expansion method uses Boyle's law to calculate the known quantity of gas, as it expands from one chamber to a second. By repeating this process, successively lower pressures can be reached. In the continuous expansion method, gas from a vessel of known pressure flows to a calibration chamber through an orifice of known size. From the calibration chamber, the gas flows through another known orifice into the pump. Knowing the dimensions of the calibration chamber, the temperature, and the difference between the two flow rates, one can calculate the pressure of the intermediate chamber. Series expansion is claimed to be the most accurate method [49]. The AVS Standards [50], published in 1969, described direct calibration of ion gauges only to a low-pressure value of 10^{-3} Pa (10^{-5} Torr). German standards were adopted in 1976, whereas an ISO draft was published in 1974 [51]. Calibration must be done with care. The equipment necessary for calibrating high vacuum gauges is usually to be found only in the laboratories of government standards institutions and gauge manufacturers. The average user does not have the resources to calibrate high vacuum gauges, but may wish single point comparison to a secondary standard such as a spinning rotor gauge or a capacitance manometer. Ion gauges have been found to be linear to low pressures [52], so that direct comparison with a standard in their upper range is valid. Cold cathode gauges often exhibit a small "kink" in their response current-pressure response at low pressure [48]. Hot cathode gauge tubes tend to be more repeatable than accurate; however, the issues discussed in the previous section can affect accuracy. Reducing errors generated by improper use or mounting can be as significant as calibration.

REFERENCES

1. J. H. Leck, *Pressure Measurement in Vacuum Systems*, 2nd ed., Chapman and Hall, London, 1964.
2. J. P. Roth, *Vacuum Technology*, North-Holland, Amsterdam, 1982.
3. A. Berman, *Total Pressure Measurements in Vacuum Technology*, Academic Press, New York, 1985.
4. D. Alpert, C. G. Matland, and A. C. McCoubrey, *Rev. Sci. Instrum.*, **22**, 370 (1951).
5. J. J. Sullivan, *Ind. Res. Dev.*, January 1976, p. 41.
6. G. Lorient and T. Moran, *Rev. Sci. Instrum.*, **46**, 140 (1975).
7. M. Pirani, *Verhandl. Dent. Physik. Ges.*, **8**, 686 (1906).
8. W. Voegt, *Physik Zs.*, **7**, 498 (1906).
9. J. W. Beams, D. M. Spitzer, Jr., and J. P. Wade Jr., *Rev. Sci. Instrum.*, **33**, 151 (1962).
10. J. K. Fremerey, *J. Vac. Sci. Technol.*, **9**, 108 (1972).
11. R. T. Bayard and D. A. Alpert, *Rev. Sci. Instrum.*, **21**, 571 (1950).
12. P. A. Redhead, *J. Vac. Sci. Technol.*, **3**, 173 (1966).
13. F. M. Penning, *Physica*, **4**, 71 (1937).

14. H. von Ubisch, *Arch. F. Mat. Astro och fysik*, **36A**, 4, (1948); *Nature* [London], **161**, 927 (1948).
15. H. von Ubisch, *Vak. Tech.*, **6**, 175 (1957).
16. M. Pirani and J. Yarwood, *Principles of Vacuum Engineering*, Reinhold, New York, 1961. pp. 100–101.
17. J. H. Leck, *Pressure Measurement in Vacuum Systems*, Chapman and Hall, London, 1957. pp. 33–38.
18. W. J. Alvesteffer, D. C. Jacobs, and D. H. Baker, *J. Vac. Sci. Technol. A*, **13**, 2980 (1995).
19. For example, the Granville-Phillips Convector Gauge, Series 275, Granville Phillips Co, Boulder CO. The Leybold TR201, TR211 or TTR90 gauges, (Leybold GmbH, Köln, Germany), as well as the HPS-MKS Series 317 and 907 gauges, (HPS Division of MKS Instruments, 5330 Sterling Drive, Boulder, CO, 80301) can also measure pressure to one atmosphere by use of the convection principle.
20. W. Jitschin and M. Ruschitzka, *Vacuum*, **44**, 607 (1993).
21. R. E. Ellefson and A. P. Miiller, *J. Vac. Sci. Technol. A*, **18**, 2568 (2000).
22. G. Comsa, J. K. Fremerey, B. Lindenau, G. Messer, and P. Röhl, *J. Vac. Sci. Technol.*, **17**, 642 (1980).
23. G. Reich, *J. Vac. Sci. Technol.*, **20**, 1148, (1982).
24. L. D. Hinkle and R. P. Jacobs, *J. Vac. Sci. Technol. A*, **11**, 261 (1993).
25. K. Jousten, A. R. Filippelli, and C. R. Tilford, *J. Vac. Sci. Technol. A*, **15**, 2395 (1997).
26. E. Ueda, Y. Hirohata, T. Hino, and T. Yamashina, *Vacuum*, **44**, 587 (1993).
27. K. E. McCulloh, S. D. Wood, and C. R. Tilford, *J. Vac. Sci. Technol. A*, **3**, 1738 (1985).
28. J. Setina and J. P. Looney, *Vacuum*, **44**, 577 (1993).
29. W. B. Nottingham, *7th Ann. Conf. on Phys. Electron.*, M.I.T., 1947.
30. D. Alpert, *J. Appl. Phys.*, **24**, 7 (1953).
31. T. A. Flaim and P. D. Ownby, *J. Vac. Sci. Technol.*, **8**, 661 (1971).
32. B. R. F. Kendall, *J. Vac. Sci. Technol. A*, **17**, 2041 (1999).
33. W. B. Nottingham, *1954 Vacuum Symp. Trans., Comm. Vacuum Techniques*, Boston, 1955, p. 76.
34. H. C. Hseuh and C. Lanni, *J. Vac. Sci. Technol. A*, **5**, 3244 (1987).
35. F. Watanabe, *J. Vac. Sci. Technol. A*, **9**, 2744 (1991).
36. P. A. Redhead, *Rev. Sci. Instrum.*, **31**, 343 (1960).
37. A. R. Filippelli, *J. Vac. Sci. Technol. A*, **5**, 3234 (1987).
38. P. A. Redhead, *Vacuum*, **44**, 559 (1993).
39. F. Watanabe, *Vacuum*, **53**, 151 (1999).
40. J. P. Looney, J. E. Harrington, K. C. Smyth, T. R. O'Brian, and T. B. Lucatorto, *J. Vac. Sci. Technol. A*, **11**, 3111 (1993).
41. F. Watanabe, *J. Vac. Sci. Technol. A*, **11**, 1620 (1993).
42. S. Suginuma and M. Hirata, *Vacuum*, **53**, 177 (1999).
43. P. Redhead, *J. Vac. Sci. Technol.*, **6**, 848 (1969).
44. A. R. Filippelli, *J. Vac. Sci. Technol. A*, **14**, 2953 (1996).
45. J. P. Hobson and P. A. Redhead, *Can. J. Phys.*, **36**, 271 (1958).
46. B. R. F. Kendall and E. Drubetsky, *J. Vac. Sci. Technol. A*, **18**, 1724 (2000).
47. K. Mukugi, H. Tsuchidate, and N. Oishi, *Vacuum*, **44**, 591 (1993).
48. R. N. Peacock, N. T. Peacock, and D. S. Hauschulz, *J. Vac. Sci. Technol. A*, **9**, 1977 (1991).
49. W. Jitschin, J. K. Migwi, and G. Grosse, *Vacuum*, **41**, 1799 (1990).
50. AVS Tentative Standard 6.4 (1969), *J. Vac. Sci. Technol.*, **7**, 370 (1970).
51. See references 1 and 2 in: K. Jousten, *Vacuum*, **49**, 81, (1998).
52. A. R. Filippelli and S. Dittmann, *J. Vac. Sci. Technol. A*, **9**, 2757 (1991).

PROBLEMS

- 5.1 † Indicate whether the following gauges will or will not be damaged if they are turned on at atmospheric pressure: (a) thermocouple, (b) Pirani, (c) cold cathode (d) hot cathode ion with tungsten filament, (e) capacitance manometer, spinning rotor.
- 5.2 The following relation has been given for the capacitance between the tensioned diaphragm and the fixed electrode of a capacitance manometer (*Methods of Experimental Physics 14, Vacuum Physics and Technology*, G. W. Weissler and R. W. Carlson, eds., Academic Press, New York, 1979, p. 50.)

$$C = \frac{\epsilon_0 A E t^3}{D E t^3 - K r_2 P}$$

A is the area of the diaphragm of radius r , thickness t , and elastic constant E . D is the diaphragm-counter electrode spacing at $P = P_{\text{ref}} = 0$. Show that, to first order, the change in capacitance is not dependent on a small change in either disk thickness or elastic constant at low pressures.

- 5.3 A capacitance manometer and a McLeod gauge monitor the pressure in a very large chamber. The McLeod gauge uses mercury and, therefore, is trapped with liquid nitrogen. The McLeod gauge reads 1000 Pa, and the capacitance manometer reads 1100 Pa. What can you tell about the nature of the molecules being measured?
- 5.4 A capacitance manometer head is heated to 50°C with a small oven. What thermal transpiration correction is required for $P < 0.2$ Pa in a head with 0.03-m-diameter tubing? Assume air at 20°C.
- 5.5 What thermal transpiration correction is required for a differential capacitance manometer heated to 50°C in which one side is referenced to 100 Pa and the gauge reads 0.2 Pa? Assume the same geometry and ambient as the last problem.
- 5.6 † What mechanisms account for the inaccuracy of thermocouple gauges?
- 5.7 If a thermal conductivity gauge contains an automatic re-zero feature that resets the zero when the chamber pressure reaches 10^{-2} Pa (10^{-4} Torr), what has been done to the instrument's calibration?
- 5.8 A Bayard-Alpert ion gauge mounted in a glass envelope is mounted on a flange above a diffusion pump near a nude Bayard-Alpert ion

gauge mounted on metal flange. The gauge with the glass envelope reads 5×10^{-6} Pa, while the nude gauge reads 1×10^{-5} Pa. Why do the gauges indicate different pressures?

- 5.9 An “artificial load” that looks like a “pressure reference” is attached to a Bayard-Alpert ion gauge controller for the purpose of calibration. Precisely what is being calibrated with this device? What is not being calibrated?
- 5.10 A small chamber containing an ion gauge is connected to a vacuum system with an intervening cold trap. Two-cm-diameter tubes connect the main chamber to the cold trap, and the cold trap to the gauge. The temperature in the main chamber is 200°C , in the cold trap 77 K, and in the gauge chamber 25°C . Assume that the gases in the system do not condense at the temperature of the liquid nitrogen trap. Does the presence of the cold trap affect the accuracy with which the gauge can read the system pressure?

Measurement

In these five chapters we discuss the tools used to characterize gases in a vacuum system: pressure gauges, flow meters, and residual gas analyzers. Pressure gauges are used to monitor routine system performance and discover problems. Flow meters are now a necessary part of any deposition or etching system. Residual gas analyzers add a considerable degree of sophistication to our analytical capability. RGA's can single out a gas or vapor that is limiting the system pressure or causing a process problem. They greatly reduce the difficulty in trouble shooting large and complex systems.

Chapter 5 is devoted to a discussion of commonly used pressure gauges. Chapter 6 describes the operation of flow meters especially the thermal mass flow meter. Chapter 7 describes pumping speed measurement techniques. Pumping speed is a quantity derived from pressure and flow, so both instruments are needed. Chapter 8 discusses the operation and installation of residual gas analyzers. Chapter 9 concludes this section with a description of qualitative and quantitative methods for interpreting the information contained in an RGA spectrum.

CHAPTER 6

Flow Meters

Flow measurements are performed to characterize components and to monitor and control systems. Pump manufacturers and some users measure the speed of pumps; they require measurement of gas flow to determine pumping speed. Process engineers control the gas flow in systems for plasma deposition or etching, chemical vapor deposition, reactive sputtering, or ion milling. Scientists measure the gas flow into a chamber to calibrate systems used for studying gas desorption kinetics. For some applications, accuracy is important; however, repeatability is important for other applications.

At atmospheric pressure a moderately large 50-L/s (100-cfm) mechanical pump has a gas throughput of 5×10^6 Pa-L/s (3.75×10^4 Torr-L/s). A small 100-L/s ion pump operating at 10^{-5} Pa pumps 10^{-3} Pa-L/s (7.5×10^{-6} Torr-L/s)—a range of more than nine orders of magnitude. Figure 6.1 illustrates the flow ranges of several pumps and processes, along with the capabilities of some flow meters. No one gauge covers the entire range. Old techniques such as moving oil or mercury pellets, and time to exhaust a reservoir, and so on [1–3], are still used to measure the very low flows needed to make pumping speed measurements.

In this chapter we define molar flow and mass flow, relate them to throughput, and review several methods and devices for flow measurement.

6.1 MOLAR FLOW, MASS FLOW AND THROUGHPUT

Gas flow can be expressed in two ways. It is frequently expressed in units of throughput, such as Pa-m³/s or Torr-L/s. It may also be expressed in term of the conservable quantities kg-moles/s or kg/s. Confusion arises because the two ways of expressing flow are not dimensionally the same and throughput does not conserve energy. In SI, throughput has units of Pa-m³/s. Although we do not express it in these dimensions, throughput has the dimensions of power and $1 \text{ Pa-m}^3/\text{s} = 1 \text{ J/s} = 1 \text{ W}$. This is the power

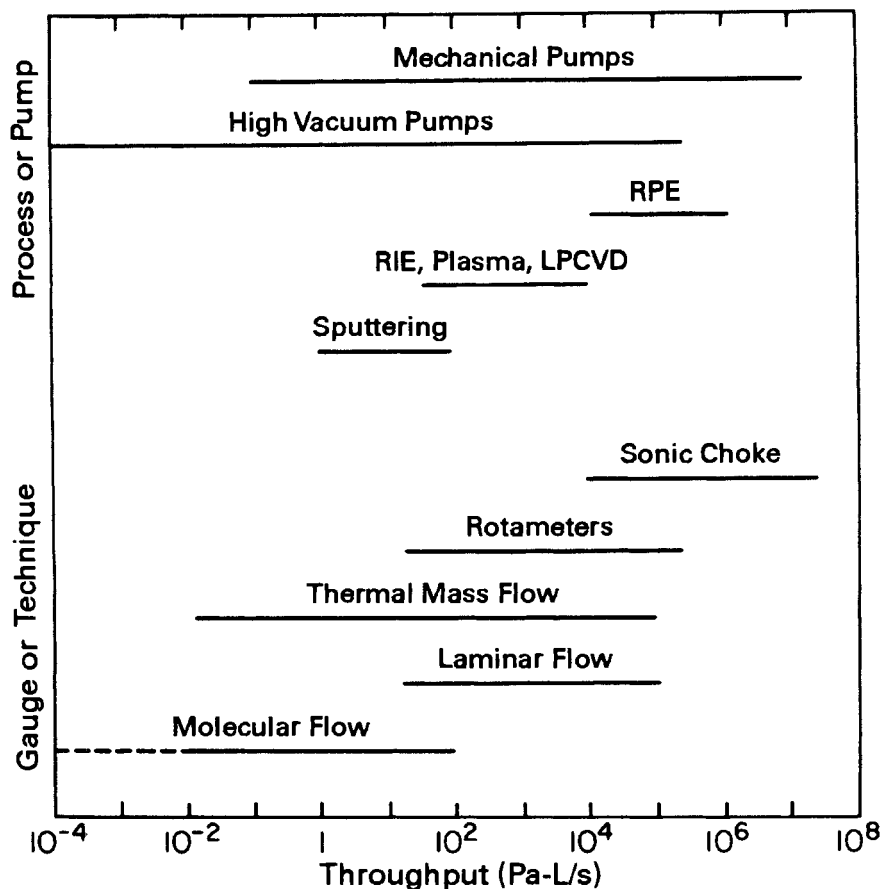


Fig. 6.1 Gas flow requirements and instrument ranges: Top: Gas flow ranges of some pumps and flow requirements for several processes. Bottom: Gas flow ranges of flow measuring instruments and devices.

required to *transport* the gas. One $\text{Pa}\cdot\text{m}^3$ is the quantity of gas contained in 1 m^3 at a pressure of 1 Pa. Molar flow and mass flow have dimensions of $\text{kg}\cdot\text{moles}/\text{time}$ or mass/time , respectively. These can be related to throughput, only if the temperature of the gas is known.

Mass conservation is a second distinction between mass flow and throughput. Throughput is not a conservable quantity. The numerical value of $\text{Pa}\cdot\text{m}^3$ does not uniquely define the number of molecules. One $\text{Pa}\cdot\text{m}^3$ of air could contain 2.45×10^{20} molecules/ m^3 at 300 K, or it could contain 1.225×10^{20} molecules/ m^3 at 600 K. Moles and mass are conservable quantities. Knowledge of the number of moles/s, or kg/s, flowing through a system allows us to perform calculations when the system temperature is

not uniform. We need to know when it is appropriate to use molar flow or throughput, and how to convert from throughput to mass or molar flow.

The molar flow rate N' has SI units of (kg-moles)/s and represents the total number of kg-moles of gas passing a plane in one second. Molar flow and throughput are related through the ideal gas law. If we replace n in (2.13) with N/V , we get

$$PV = NkT = \frac{N}{N_o}(N_o k)T = N' RT \quad (6.1)$$

where N' is the molar quantity (kg-moles) of gas, and $R = N_o k = 8314.3$ kJ/(K·kg mole). The molar flow rate at constant temperature is obtained by taking the time derivative of (6.1).

$$\begin{aligned} \frac{d}{dt}(PV) &= Q = RT \frac{dN'}{dt} \\ \frac{dN'}{dt} \text{ (kg - moles/s)} &= \frac{Q}{RT} = 1.21 \times 10^{-4} \left(\frac{Q}{T} \right) \end{aligned} \quad \blacktriangleright (6.2)$$

Sometimes we wish to express the flow as mass flow. Its units will be kg/s in SI; we recall that each kg-mole has a mass of M kg.

$$\frac{dm}{dt} \text{ (kg/s)} = \left(\frac{MQ}{RT} \right) = 1.21 \times 10^{-4} \left(\frac{MQ}{T} \right) \quad \blacktriangleright (6.3)$$

M is the molecular weight and Q has units of Pa·m³/s at temperature T . The flow may be expressed alternatively as the number of molecules per second passing a plane: Γ (molecules/s) = $N_o dN'/dt$. Using these relationships, we can convert from throughput Q to molar flow rate dN'/dt , mass flow rate dm/dt , or molecular flow rate Γ . Ehrlich [4] notes that it is customary to label standard leaks with units of “atm-cc/s at T .” He reminds us that the value given is numerically equal to Q and not to kg-moles/s. The statement “at T ” is included to allow conversion from throughput to molar flow. Some of the equations given here have flow given with dimensions of throughput and others with molar or mass flow.

Throughput, mass flow, or molar flow can be used in calculations. Throughput is a convenient term to use when the system is at a constant temperature for measurements such as pumping speed calculations. Molar flow is best used for studying reaction kinetics and for calculations, which would otherwise have to be referred to several temperatures. For example, a calibrated leak labeled in “Pa·m³/s at 23°C” is connected to a system whose chamber is at 35°C and pump is at 50°C. In this example it would be much easier to have the leak labeled in kg-moles/s. The important concept to remember is the fundamental difference between throughput Q and molar flow dN'/dt . Throughput is dimensionally distinct from molar

flow and is not a quantity that is conserved. A kg-mole of gas is a fixed, known number of molecules that does not change with temperature.

6.2 ROTAMETERS AND CHOKES

A rotameter [5] is a flow-measuring device constructed from a precision tapered bore that contains a ball of accurately ground diameter and known mass. See Fig. 6.2a. The gas flow through the tube raises the ball to a height proportional to the throughput or mass flow. The general equation for continuum flow in an orifice is

$$Q = AP_1 C' \left(\frac{2\gamma}{\gamma-1} \frac{kT}{m} \right)^{1/2} \left(\frac{P_2}{P_1} \right)^{1/\gamma} \left[1 - \left(\frac{P_2}{P_1} \right)^{(\gamma-1)/\gamma} \right]^{1/2} \quad (6.4)$$

The equation for continuum flow in a rotameter with a low pressure drop can be obtained from this by letting $P_2 = (P_1 - \Delta P)$. When ΔP is small compared to P_1 or P_2 , we get

$$Q = \left(\frac{2kT\Delta P P_1}{m} \right)^{1/2} A \quad (6.5)$$

Except for a geometrical factor, which accounts for the nonzero thickness of the orifice, (6.5) describes gas flow through a rotameter. The gas flow is a function of the inlet pressure P_1 , gas temperature, molecular weight, height h , and mass of the ball. The mass of the ball is constant and creates a constant pressure difference ΔP .

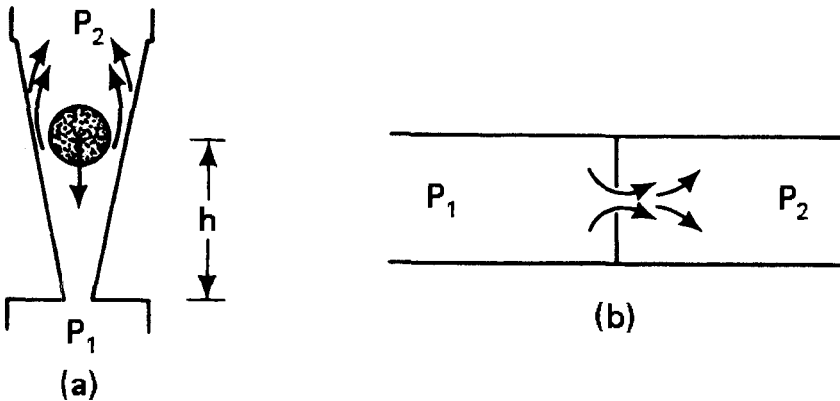


Fig. 6.2 (a) Rotameter, and (b) choke flow element.

$$Q \propto \left(\frac{T}{M} \Delta P P_1 \right)^{1/2} f(h) \quad (6.6)$$

The mass flow rate can be expressed as

$$m' \propto \left(\frac{M}{T} \Delta P P_1 \right)^{1/2} f(h) \quad (6.7)$$

From (6.6) and (6.7) we see that the inlet pressure and temperature must be known to calibrate the throughput and mass flow. Rotameters are initially calibrated for one gas and must be recalibrated for use with any other gas. Rotameters are made for flows ranging from 5×10^3 -to- 5×10^6 Pa-L/s. The accuracy of these instruments is of order 10–20% full scale, whereas repeatability is about 2–3%.

Chokes [6,7] (Fig. 6.2b) are used to measure, or more commonly set, the throughput in the range 5×10^4 to 10^7 Pa-L/s. After the flow through an orifice reaches its sonic limit ($P_2/P_1 < 0.52$), it is practically independent of outlet pressure and is expressed as

$$Q = A P_1 C' \left(\frac{kT}{m} \frac{2\gamma}{\gamma+1} \right)^{1/2} \left(\frac{2}{\gamma+1} \right)^{1/(\gamma-1)} \quad (6.8)$$

for air at 22°C,

$$Q(\text{Pa} \cdot \text{L/s}) = 2 \times 10^5 P_1 C' A (\text{m}^2) \quad (6.9)$$

The mass flow rate is given by

$$\frac{dm}{dt} = A P_1 C' \left(\frac{m}{kT} \frac{2\gamma}{\gamma+1} \right)^{1/2} \left(\frac{2}{\gamma+1} \right)^{1/(\gamma-1)} \quad (6.10)$$

for air at 22°C,

$$\frac{dm}{dt} (\text{kg/s}) = 2.58 \times 10^{-3} P_1 C' A (\text{m}^2) \quad \blacktriangleright (6.11)$$

Again the throughput is dependent on the area, inlet pressure, temperature, and gas species. These devices are not accurate in small sizes (less than 1-mm diameter), because the nature of the choke is critically dependent on the length of the hole as well as the radius and shape of the entrance edge. Van Atta [7] discusses large radius orifices, which are designed to make the flow more uniform and repeatable. Chokes are useful as flow restricting devices where accuracy and repeatability are not necessary. Chokes are used to limit flow from gas cylinders and to control turbulence during venting and rough pumping.

6.3 DIFFERENTIAL PRESSURE TECHNIQUES

Rotameters and chokes measure gas flow at a known inlet pressure and an essentially constant pressure drop. They do not operate in the flow ranges below 5×10^3 Pa-L/s (50 Torr-L/s). Low flow rates are easily measured in the molecular or laminar viscous flow region by measuring the pressure drop across a known conductance. The concept is the same for low, medium, and high vacuum. Only the form of the conductance and the pressure gauge differ. High and ultrahigh vacuum flow measurements are almost always limited to pumping speed measurements and are treated separately in Chapter 7.

A molecular or laminar viscous element is used in combination with a capacitance manometer to measure the gas flow in the low and medium vacuum range. A laminar flow element [8] is incorporated into a flow meter as sketched in Fig. 6.3a. It is simply a capillary tube long enough to satisfy the Poiseuille equation. See Section 3.3.

$$Q = \frac{\pi d^4}{128 \eta l} P_{\text{ave}} \Delta P \quad (6.12)$$

The flow is proportional to ΔP and the average pressure in the tube. Flow measurement with a long capillary requires two pressure gauges and knowledge of the temperature as well as the gas species. This is an accurate technique, but not the most convenient. It is most often used for calibration of thermal mass flow meters.

Molecular-flow elements [9] are constructed from a parallel bundle of capillaries, v-grooves or similar shapes. See Fig. 6.3b. The diameter of each channel must be kept small for the flow to remain molecular at usably high pressures, say 100 Pa. Typically, a single channel will have a diameter of a fraction of a millimeter. The conductance of one channel is of order 10^{-4} L/s so that a large number of parallel channels ($>10,000$) are necessary to achieve a practical device. The flow through such an element can be expressed as

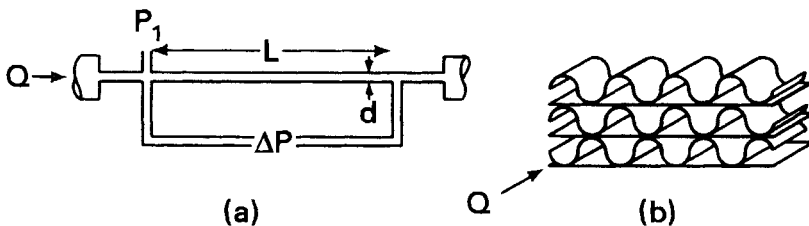


Fig. 6.3 Differential pressure flow elements, (a) laminar and (b) molecular.

$$Q = C\Delta P = xa' \frac{v}{4} \Delta P \quad (6.13)$$

where x is the number of channels and a' is the transmission probability of one channel. We see the flow to be proportional to $(T/M)^{1/2}$. As long as the line pressure is less than 100 Pa, it is not necessary to know its value. These devices are available commercially for use in the range 0.01–100 Pa-L/s, attitude-insensitive, stable and easy to use. However, the holes can become clogged. They have a slow response time (5–60 s), can have a high pressure drop; they cannot be used at inlet pressures greater than 100 Pa. The output of the capacitance manometer that measures ΔP can be used to control the opening and closing of an adjacent valve and achieve closed loop flow control.

6.4 THERMAL MASS FLOW TECHNIQUE

Mass flow can be calculated from the quantity of heat per unit time required to raise the temperature of a gas stream a known amount. Flow meters have been constructed which are sensitive to either thermal conductivity [10–12] or heat capacity [13,14]. Devices sensitive to heat capacity have become widely accepted, because of their accuracy and ability to measure large gas flows with low power input. When combined with a rapidly acting valve, they become mass flow controllers.

6.4.1 Mass Flow Meter

The concept of the Thomas thermal mass flow meter [15] is illustrated in Fig. 6.4. We can measure the gas flow by applying constant power to the

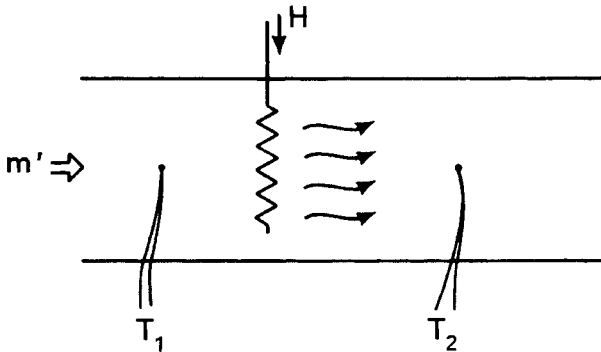


Fig. 6.4 Principle of thermal mass flow measurement

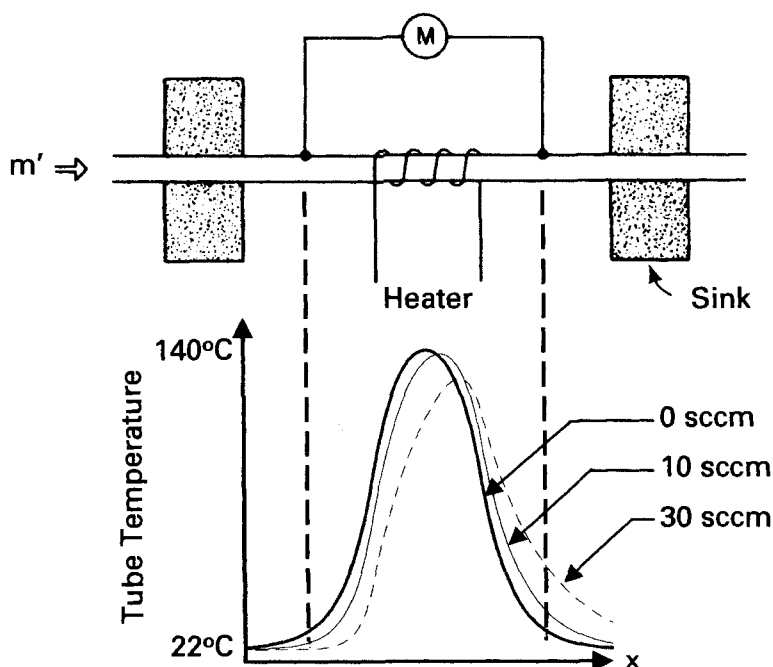


Fig. 6.5 Thermal mass flow sensor and temperature profile. Upper: Cross-sectional view of the sensor tube, resistance thermometers, and heat sinks. Lower: Temperature profile. Temperature profile reproduced with permission from *An Improved Thermal Mass Flow Controller for Hazardous and Precision Applications*, William J. Alvesteffer, M. S. Thesis, Old Dominion University. Copyright 2000, William J. Alvesteffer.

uniformly spaced grid and observing the temperature rise of the gas on the downstream side of the grid. The amount of heat that is required to warm the gas stream is linearly dependent on the mass flow and the specific heat

$$\frac{dm}{dt} = \frac{H}{C_p(T_2 - T_1)} \quad (6.14)$$

For example, if we apply a nitrogen mass flow of 0.001 kg/s to this device we will observe a temperature rise of 10°C for each 8.1 J/s of heat input to the grid. The change in thermal capacity with temperature is small and has only a slight effect on the measurement of mass flow. Typical thermal coefficients due to heat capacity variations range from +0.075%/°C (CO₂) to +0.0025%/°C (Ar).

Operation of a thermal mass flow meter is based on (6.14). One early form of the device is sketched in Fig. 6.5. Heat is externally applied at the center of the tube. While there is no gas flow, the temperature profile is

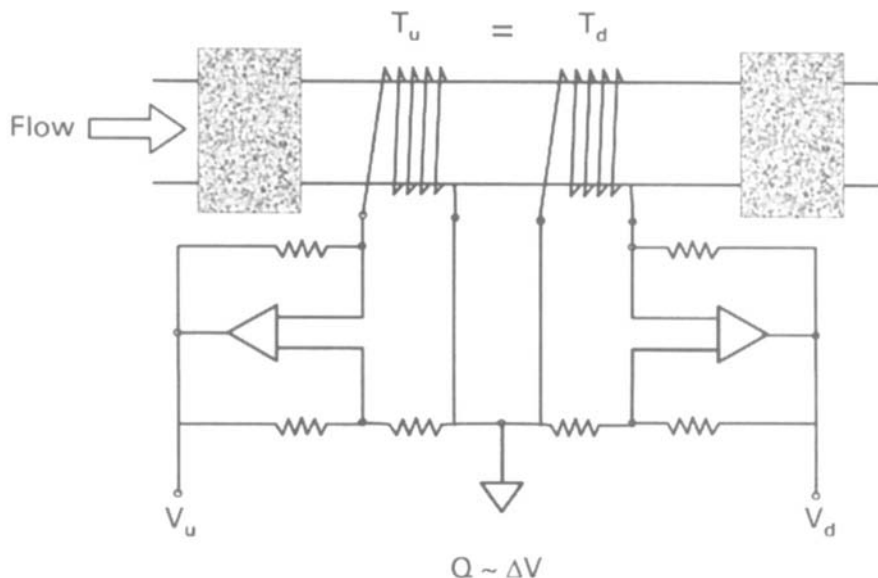


Fig. 6.6 Constant power mass flow controller circuit. Reproduced with permission of Luke Hinkle, Copyright 2000, Luke Hinkle.

symmetrical. With gas flow, the thermal profile is skewed. Two thermocouples (or resistance thermometers) measure the change in temperature profile between the no-flow and flow condition. The meter must be mounted in the position shown, as the heat distribution is attitude sensitive. Another form of the device is illustrated in Fig. 6.6. It uses a bridge circuit to keep the temperatures constant. With this technique, the mass flow is proportional to the amount of power required to maintain constant temperatures. Sampling tubes of 0.2–0.8-mm internal diameter are usually made from stainless steel; however, Inconel or Monel can be used for corrosive gases. Flow meter manufacturers prefer units of standard cubic centimeters per minute (sccm) for display of small flows and standard liters per minute for large gas flows. Flow meters are manufactured with full-scale deflections ranging from 1 sccm (1.6 Pa-L/s) to 500 standard liters per minute ($\sim 10^6$ Pa-L/s). Devices that measure flows greater than 10–200 sccm (~ 20 –3500 Pa-L/s) use a laminar flow bypass, which diverts a fixed percentage of the flow to the small tube. Hinkle and Marino have shown that the linearity of the flow bypass is design-dependent; the bypass ratio was affected by end effects. The thermal properties of the system are dependent on the Nusselt number, which varied with flow; if the boundary conditions vary, it is also a function of position [16]. These effects can be addressed by software algorithms.

Table 6.1 Thermal Mass Flow Meter Correction Factors^a

Gas	Heat Capacity J/(kg·°C)	Density (kg/m ³) at 0°C	Correction Factor f^b
Air	1004.2	1.293	1.00
NH ₃	2058.5	0.760	0.73
Ar	520.5	1.782	1.45
AsH ₃	488.3	3.478	0.67
BCl ₃	535.1	5.227	0.41
CCl ₄	692.5	6.86	0.31
Cl ₂	478.7	3.163	0.86
CF ₄	692.0	3.926	0.42
B ₂ H ₆	2125.5	1.235	0.44
SiH ₂ Cl ₂	627.6	4.506	0.40
C ₂ H ₆	1714.2	1.342	0.50
He	5192.3	0.1786	1.45
H ₂	1430.0	0.0899	1.01
HBr	360.0	3.61	1.00
HF	1455.6	0.893	1.00
Kr	2481.5	3.793	1.54
CH ₄	2229.2	0.715	0.72
Ne	1029.3	0.9	1.46
NO	974.0	1.339	0.99
N ₂	1039.7	1.250	1.00
NO ₂	808.8	2.052	0.74
NF ₃	751.9	3.168	0.48
O ₂	917.6	1.427	1.00
PH ₃	993.3	1.517	0.76
SiH ₄	1334.3	1.433	0.60
SiCl ₄	531.4	7.58	0.60
SF ₆	666.1	6.516	0.26
CCl ₂ FCClF ₂	673.6	8.36	0.20 ^c
WF ₆	338.9	13.28	0.25
Xe	158.2	5.856	1.32

^a Reproduced with permission from MKS Instruments, 6 Shattuck Road, Andover, MA 01810.

^b $Q_x = f Q_{\text{meter}}$

^c at 60°C.

A thermal mass flow meter directly measures the amount of heat absorbed by the gas stream, and therefore indirectly measures the mass flow. However, the gauge scales are normally calibrated in units of throughput—usually air. We can convert throughput to mass flow with the aid of (6.3). A gauge calibrated in units of throughput has a different temperature coefficient than one calibrated in units of mass flow, because throughput is density-dependent. According to (6.3), a mass flow of 10^{-6} kg/s (air) at a temperature of 20°C corresponds to a throughput of 83.64

Pa-L/s. If the gas were heated to 30°C, a mass flow of 10^{-6} kg/s would correspond to a throughput of 86.5 Pa-L/s. Heated air is less dense than room temperature air. Near room temperature the temperature coefficient due to density changes is about $-0.33\%/^{\circ}\text{C}$. The temperature coefficient for throughput is therefore slightly less than this because of the small positive temperature coefficient of the heat capacity previously discussed. Temperature stability is improved by use of an insulation layer. Adding insulation increases the response time from 1–2 s to 6–10 s.

The mass flow sensor will have to be readjusted for gases other than air. We can purchase a sensor especially calibrated for one gas, or we can multiply the meter reading by a correction factor. To first order, the meter deflection is proportional to the gas density and heat capacity, so we can make an approximate correction with the aid of (6.15).

$$Q_x = \left(\frac{\rho(\text{air})C_p(\text{air})}{\rho(x)C_p(x)} \right) Q_{\text{meter}} = f_x Q_{\text{meter}} \quad \blacktriangleright (6.15)$$

The factor in parentheses is known as the meter correction factor f . This factor is approximate. The actual correction may differ due to small changes in gas viscosity, specific heat with temperature, or the rate at which a gas transfers heat to and from the tube wall. Example correction factors are given in Table 6.1. Hinkle and Marino [16] have shown that a function, not a factor is required for some gases. The factors were found to

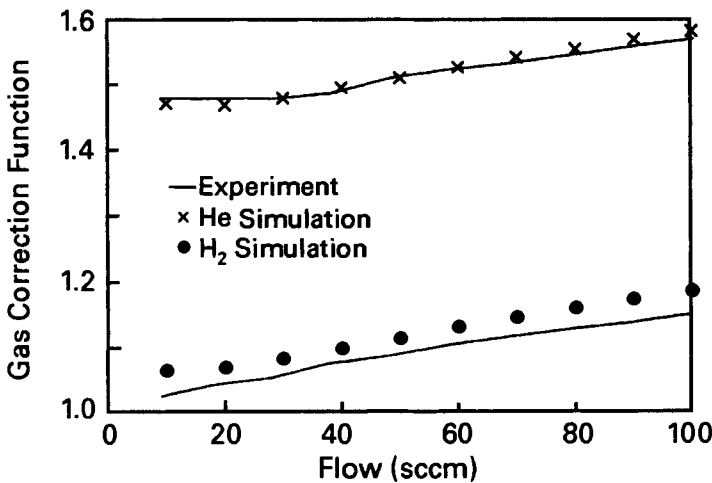


Fig. 6.7 Simulation and experimental gas correction functions for He and H₂ relative to N₂. Reproduced with permission from *J. Vac. Sci. Technol. A*, 9, 2043, L. D. Hinkle and C. F. Marino. Copyright 1991, AVS—The Science and Technology Society.

be correct for small gas flows. For high flows, they demonstrated that significant error could be introduced when measuring gases with different thermal diffusion constants. Figure 6.7 illustrates this error for two gases, helium and hydrogen, when measured in a flow sensor calibrated for nitrogen. A flow of 100 sccm introduced a 7% error in the helium correction factor, whereas the same flow of hydrogen introduced a 12% error in the correction factor.

Thermal mass flow sensors have the advantages of convenience, stability, accuracy ($<1\%$) and moderately short response time. These sensors are attitude-sensitive and have a high temperature coefficient. Designs using very-small-diameter tubes can clog, especially when reactive gases contact minute impurities of water vapor.

6.4.2 Mass Flow Controller

A thermal mass flow controller (MFC) consists of a thermal mass flow sensor, a rapidly acting valve, and an electronic control system. In its basic form, a mass flow controller can maintain a constant, operator-set flow. Complex instruments can maintain ratios of gas flows or be integrated into process control systems. Flow valves may be controlled by a solenoid, a piezoelectric stack. For ultraclean applications, a piezoelectric controller with a metal diaphragm will produce the fewest particles.

The maximum flow and the pressure drop across the flow sensor and valve must be known to choose the proper size combination. We first determine the equivalent air throughput from $Q_{\text{meter}} = Q_x / f_x$. We then choose a flow meter with the next largest full-scale meter deflection. From the manufacturer's data we determine the pressure drop ΔP across the meter and valve combination at maximum flow. The value of ΔP is little concern, if the delivery pressure is above atmosphere. Vapors e.g., CCl_4 , which are liquid at room temperature, have vapor pressures below atmospheric pressure. If the gas or vapor source is at a reduced pressure, we must size the meter and valve so that the pressure drop is less than the difference between P_1 and P_2 , the delivery and chamber pressures, respectively. $\Delta P < (P_1 - P_2)$. The pressure drop can be reduced by choosing a low conductance valve or, if necessary, a somewhat larger flow meter than might otherwise be desired.

6.4.3 Mass Flow Meter Calibration

Calibration of a mass flow meter can be done by comparison with primary or secondary standards. Primary standards are most often maintained at National laboratories. They determine flow by comparison with independently calibrated fundamental measurements. Secondary standards

are instruments that have been calibrated against primary standards. Secondary standards are found in the laboratories of large research institutions or manufacturing firms. Volumetric piston and rate of rise techniques are used as primary standards, whereas the pressure drop across a laminar flow element or another mass flow meter can be used as secondary standards. No AVS recommended practices have been published for calibration of mass flow meters. Methods for low throughput measurement are found in the AVS recommended procedure for pumping speed measurement [3]. Hinkle and Uttaro have reviewed primary and secondary standards and presented some data on long-term mass flow meter stability [17].

REFERENCES

1. C. E. Normand, *1961 Trans. 8th. Nat'l Vac. Symp.*, L. E. Preuss, ed., Pergamon Press, Elmsford, NY, 1962, p. 534.
2. D. J. Stevenson, *1961 Trans. 8th. Vac. Symp.*, L. E. Preuss, ed., Pergamon Press, Elmsford, NY, 1962, p. 555.
3. M. Hablarian, *J. Vac. Sci. Technol. A*, **5**, 2552 (1987). (American Vacuum Society Recommended Procedure for Measuring Pumping Speeds; see Appendix A).
4. C. Ehrlich, *J. Vac. Sci. Technol. A*, **4**, 2384, 1986.
5. C. M. Van Atta, *Vacuum Science & Engineering*, McGraw-Hill, New York, 1965, Chapter 7.
6. R. W. Kuzara, in *Flow—Its Measurement and Control in Science and Industry*, Vol. 2, W. W. Durgin, Ed., Instrument Society of America, Research Triangle Park, NC, 1981, p. 741.
7. Flow Measurement, PTC 19.5.4 *American Society of Mechanical Engineers*, New York, 1959, Chapter 4.
8. D. A. Todd, Jr., in *Flow—Its Measurement and Control in Science and Industry*, Vol. 2, W. W. Durgin, Ed., Instrument Society of America, Research Triangle Park, NC, 1981, p. 695.
9. R. M. Kiesling, J. J. Sullivan, and D. J. Santeler, *J. Vac. Sci. Technol.*, **15**, 771 (1978).
10. C. E. Hastings and C. R. Weislo, *AIEE*, March, 1951.
11. F. Mac Donald, *Instrum. and Control Syst.*, October (1969).
12. J. H. Laub, *Electrical Engineering*, December 1947.
13. J. M. Benson, W. C. Baker, and E. Easter, *Instrum. Control Syst.*, p. 85 (1970).
14. C. E. Hawk and W. C. Baker, *J. Vac. Sci. Technol.*, **6**, 255 (1969).
15. C. C. Thomas, *J. Franklin Institute*, **152**, 411 (1911).
16. L. D. Hinkle and C. F. Marino, *J. Vac. Sci. Technol. A*, **9**, 2043 (1992).
17. L. D. Hinkle and F. L. Uttaro, *Vacuum*, **47**, 523 (1996).

PROBLEMS

6.1 † What is the basic difference between mass flow and throughput?

- 6.2 (a) What is the mass flow rate in kg/s of 1000 Pa-L/s of air at 20°C? Express this as (b) a molecular flow rate and (c) a molar flow rate.
- 6.3 What is the limiting flow of 20°C atmospheric pressure air through a sonic choke whose diameter is 3.5 mm?
- 6.4 † A 0.5-L/s molecular flow element is used with a capacitance manometer with a range of 0.01 to 100 Pa. (a) What range of flow can it measure (a) for air and (b) for argon?
- 6.5 A laminar flow tube is being used to calibrate a 0–200 SCCM thermal mass flow meter for air. The tube is 1 mm in diameter and 5 cm long. The room temperature air supply has a maximum pressure of 10^5 Pa, and the differential capacitance manometer has a full-scale reading of 200 Pa. Does this calibrated source provide enough air flow to calibrate the flow meter?
- 6.6 † What are two advantages and disadvantages of a thermal mass flow meter?
- 6.7 How much power is absorbed from a heater that causes air (heat capacity of 1004.16 J/(kg-K)) flowing at the rate of 0.06 kg/min to rise 2°C?
- 6.8 A thermal mass flow sensor with a full-scale value of 100 sccm reads 0 sccm at 20°C with no pressure drop across the sensor. At a temperature of 30°C the indicated flow through the device is +0.16 sccm. What is the zero flow temperature coefficient in units of parts per million (ppm) of full scale per degree Celsius.
- 6.9 The sketch of sensor tube temperature versus position illustrated in Fig. 6.5 indicates that the maximum tube temperature decreases as the gas flow increases. Why is this true?
- 6.10 1,1,2-Trichloro-1,2,2-trifluoroethane ($\text{CCl}_2\text{FCClF}_2$) is a liquid with a vapor pressure of 37,730 Pa (288 Torr) at 20°C. (a) What is the maximum flow that can be read on a thermal flow meter that is calibrated for a full-scale nitrogen flow of 500 SCCM (844 Pa-L/s)? (b) This flow meter is used in series with a control valve to regulate the flow into a vacuum chamber held at a pressure of 10 Pa. For trichlorotrifluoroethane the flow in the meter-valve combination can be expressed as $Q(\text{Pa-L/s}) = 2 \times 10^{-7} P_{\text{ave}} \Delta P$. Can this meter-valve combination provide a trichlorotrifluoroethane flow equal to the full-scale value of the flow meter?

CHAPTER 7

Pumping Speed

Pumping speed is a quantity few of us measure. We are usually content with published data; however, we should know how speed is measured, so that we can meaningfully interpret data. Pumping speed is measured by established, standard techniques. Recommended practices have been improved; however, much data taken in old test domes pervades the literature. We should know the accuracy of the available data. We may also wish to measure the pumping speed to check for proper pump operation, or to provide specialized information. For example, the pumping speed may be needed for a specific gas, pump temperature, or pump fluid. If we know the correct pumping speed at the inlet of a pump and the correct connecting conductance, we can calculate the pumping speed at the chamber entrance with reasonable accuracy.

We begin by defining pumping speed and then describe its measurement in mechanical and high vacuum pumps. We include a simplified technique for checking an operating system, and we discuss the measurement of water pumping speed in high vacuum pumps. We conclude with a discussion of the errors inherent in standard test fixtures.

7.1 PUMPING SPEED

Pumping speed is the volumetric rate at which gas is transported across a plane. In mathematical terms speed is the gas throughput divided by the pressure at the plane of the pressure gauge.

$$S = \frac{Q}{P} \quad \blacktriangleright (7.1)$$

Like conductance, it has dimensions of volume per unit time, and in SI it is expressed in units of m³/s. Units of L/s or m³/h are also used. Unlike conductance, pumping speed is not a property of a passive component like

a length of pipe or a baffle. Recall the definition of conductance from (3.3). It is the gas throughput divided by the pressure drop across a component. Pumping speed is the gas throughput divided by the pressure at the point of pressure measurement.

Equation (7.1) implies independent measurements for the throughput Q and pressure P . Pressure gauges are described in Chapter 5. For measuring permanent gas pressures, liquid nitrogen cold traps may be used between the gauge and test dome to avoid errors due to condensable gas impurities. Several flow-measuring devices are needed to span the range of flows necessary to characterize mechanical and high vacuum pumps. All of these with the exception of the conductance (also called the orifice) method are described in Chapter 6; the conductance method is described in Section 7.3.1.

7.2 MECHANICAL PUMPS

The test dome used for measuring mechanical pump speeds is illustrated in Fig. 7.1 (right). The dome and pump diameters are equal, unless the pump diameter is less than 50 mm. For pumps whose inlet diameter is less than 50 mm, a conical adapter flange is used to make the transition from test dome to pump. This flange is described in the AVS Recommended procedures for measuring the performance of positive displacement mechanical pumps [1]. Several pressure gauges are required. Gauge accuracy must be within $\pm 5\%$ above 0.1 Pa, and $\pm 10\%$ in the range 0.001–0.1 Pa. The capacitance manometer, spinning rotor, and ion gauge (≤ 0.01 Pa) may be used. The recommended procedures require flow-measuring devices with 2% accuracy. Thermal mass flow meters may be used in the range 10–10,000 Pa-L/s, whereas the conductance method is appropriate for flows less than 0.1 Pa-L/s. The intermediate range may be covered by a differential capacitance flow meter. After the gas has been flowing into the test dome for at least 3 min, the equilibrium pressure is recorded and the speed is calculated from (7.2), where P is the measured pressure and P_b is the base pressure with zero gas flow.

$$S = \frac{Q}{(P - P_b)} \quad (7.2)$$

Three pumping speed measurements per decade are made over the pump's operating range. The ambient temperature, barometric pressure, rotation speed, and type of oil in the pump should be recorded. Pumping speed measurements are typically performed with nitrogen; liquid-nitrogen-cooled cold traps are used between the gauge sensor and system to eliminate the effects of pump oil vapors.

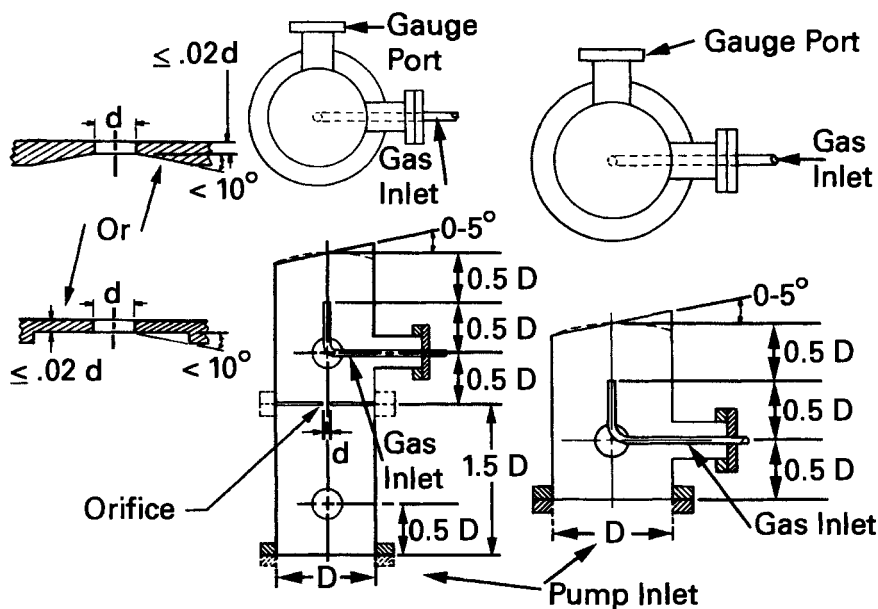


Fig. 7.1 Test domes for the measurement of mechanical and high vacuum pumps. Right: Flowmeter method test dome. This dome is used for speed measurement in pumps with a diameter greater than 50 mm. Left: Conductance (orifice) test dome. This dome is used for speed measurement at low gas flows. Reprinted with permission from *J. Vac. Sci. Technol. A*, 5, p. 2552, M. Hablanian, Copyright 1987, The American Vacuum Society.

7.3 HIGH VACUUM PUMPS

Measurement of high vacuum pumping speed requires flow measurements considerably below the range of the techniques discussed in Chapter 6. Speed measurements are further complicated by the anisotropic gas flow patterns in the test dome, and a flowing gas stream. Here we examine two techniques for measuring the speed of a pump and examine one technique for estimating speed at the entrance to the working chamber.

7.3.1 Measurement Techniques

Volumetric pumping speed is measured with a standard metering dome. Myriad early dome designs have been replaced by a design similar to that described in the new AVS Recommended procedure for measuring pumping speeds [2] and described in Fig. 7.1.

The flowmeter method uses a dome described in Fig. 7.1 (right). Pumping speed is calculated in the same manner as given in (7.2). For very low flows, the orifice method described in Fig. 7.1 (center) is used. Use of

this technique requires molecular flow. The numerical value of the flow is determined by the pressure drop across a known conductance $C(P_1 - P_2)$; the resulting speed is calculated from

$$S = C \left(\frac{P_1 - P_{01}}{P_2 - P_{02}} - 1 \right) \quad (7.3)$$

Pump Dependence

The ISO standard specifies the use of nitrogen; however, speed can be and is measured for many other gases. Turbo, ion, getter, and cryo pumps behave differently from diffusion pumps, as their speed versus mass dependence's are not the same. Diffusion pumps pump all gases; ideally, their speed should vary as $1/m^{1/2}$. In Chapter 12 we show the light gas pumping speeds to be somewhat higher than the speeds for air, or nitrogen, but not as great as predicted $1/m^{1/2}$. Ion, getter, and cryogenic pumps do not pump all gases. Consequently, capture pumps are characterized with specific gases, because their speed is a function of gas composition as well as prior history.

Some time may be required for a capture pump to reach equilibrium after admitting gas at a fixed flow rate [2]. This is particularly true for ion pumps at low pressure [3]. If pumping-speed data are recorded too quickly, data taken in order of decreasing pressure will yield an incorrectly small value of speed, while those taken in order of increasing pressure will yield an incorrectly large value of speed. It may also be necessary to erase the pump's memory for one or more gases pumped before measurement. This can be accomplished by pumping for 1 h at a pressure of 10^{-3} Pa with the gas under study [2].

The operating characteristics of each pump should be recorded with the speed measurements. The type of fluid, the size of forepump and foreline pressure in compression pumps, the boiler power in a diffusion pump, the rotating frequency of a turbomolecular pump, and the refrigeration capacity of cryogenic pumps are some of the factors which need to be reported with speed data.

Measurement of Water Vapor Pumping Speed

Few measurements of water vapor pumping speed have been made because of the experimental problems. Water is difficult to degas: It can freeze on evaporation, boil at room temperature, and plug valves. It will sorb on the test dome at very low pressures. Landfors et al. [4] have measured the water pumping speed of a diffusion pump with and without a liquid nitrogen cold trap and the speed of a cryogenic pump. They constructed a chamber for admitting known amounts of degassed water vapor at constant pressure into an ISO test dome. Speed was measured at pressures greater

than 10^{-2} Pa to avoid sorption effects. They found the water pumping speed to be the essentially the same as air for a diffusion pump without an LN_2 trap. The water pumping speed for an LN_2 -trapped diffusion pump was approximately the same as that for a cryo pump of the same throat area. They concluded the pumping speed for water should be given by the projected area of the cold surface at the inlet of the trap as reduced by the conductance of the intervening tubing. AVS Recommended Practices for measuring performance of closed-loop helium cryopumps describe methods for measuring speed of cryopumps [5]. Although cryopumps have a higher Ho coefficient than other pumps, the variations allowed in the recommended practice have little impact on the pumping speed results [6].

Pumping Speed at the Chamber

Only pump manufacturers and large projects will have the necessary test domes for measuring pumping speed, so it is necessary to have an approximate method anyone can use on an existing system. The approximate pumping speed at the entrance to the chamber can be measured without the trouble of attaching an elaborate dome and metering system. The speed can be deduced approximately if it is assumed to be independent of pressure in the region of interest. If this is true, then it follows that

$$S = \left(\frac{Q_2 - Q_1}{P_2 - P_1} \right) \quad (7.4)$$

where Q_1 is the flow that results in P_1 , and so on. It can be shown that this flow is equivalent to

$$S = V \frac{\left(\frac{dP_2}{dt} \right) - \left(\frac{dP_1}{dt} \right)}{(P_2 - P_1)} \quad \blacktriangleright (7.5)$$

To measure the pumping speed, the system is first pumped to its base pressure P_1 and the high vacuum valve is closed. At this time the pressure rise dP_1/dt is plotted over at least a one-decade pressure increase. The high vacuum valve is opened and the system pumped to its original base pressure. A gas is then admitted through a leak valve until the pressure rises to a value P_2 , which is several times that of the base pressure. The high vacuum valve is closed and dP_2/dt is recorded. The system volume is then estimated and the speed is calculated by use of (7.5). This method, called the rate of rise or constant volume method, is only approximate, because gas flow at the base pressure Q_1 is, in general, background desorption and not the same gas species as admitted through the leak.

Fixing the starting pressure P_2 at a value of at least 10 times P_1 will ensure reasonable accuracy.

The pressure at the pump throat can be estimated by subtracting the impedance drop of the conducting pipe and trap located between the gate valve and the pump.

7.3.2 Measurement Error

High vacuum pumping speed measurement error arises from three sources. First, the definition of speed given by (7.1) requires Q and P to be measured at the same surface. This is not true for the dome described in Fig. 7.1. Second, the definitions of Q and P assume cosine distribution of molecular arrival and that is not the case when gas enters from a pipe. Third, the gas flow is sometimes measured inaccurately. All three sources of measurement error exist, because we do not completely compensate for the nonuniform gas distribution in the system. The nonuniform gas distribution affects both the capture coefficient (Ho coefficient of the pump) and the measurement of pressure. The Ho coefficient is the ratio of actual pumping speed to the maximum pumping speed of an aperture of the same size in which no molecules are reflected [7].

In Chapter 3 we defined the intrinsic conductance of a tube for cosine distribution of incoming molecules and noted this definition did not apply to beamed flow. The same effect occurs at the inlet of a pump. The capture probability is a function of arrival angle. When we place a pipe at the inlet of a pump, the capture coefficient will change, and the pump no longer has its “intrinsic” speed—that is, the speed it would have if appended to an extremely large chamber. Its speed may increase because molecules shot straight into the pump will have a greater probability of being captured than will those arriving in a cosine distribution [8], and because molecules bounce around—the “maze” effect [9]. Test domes constructed from pipes of the same diameter as the pump are criticized because the inlet flux is not cosine and the resultant speed is not what is measured on a large chamber. Proponents of equal-diameter test domes argue that the measured speed is meaningful because pumps are usually connected to a pipe of the same diameter.

Pressure measurement is our second consideration. The pressure in the dome is not isotropic or uniform. Mathematically, the pressure in the dome can be described by a tensor [10]. The pressure is a function of gauge location and orientation, and the surface temperature may not be uniform. Examine the pump and pipe sketched in Fig. 7.2. The pump is an ideal pump from which no molecules return ($\alpha = 1$). Gas is flowing to the pump inlet. Gauge 1 reads the pressure at the pump entrance, whereas gauge 2 reads a pressure corresponding to the flux incident on its opening. One-half the gas arriving at the entrance to gauge 2 will come from the top, and one-half

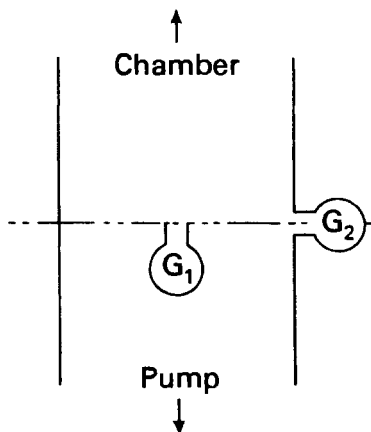


Fig. 7.2 The effect of orientation on pressure gauge readings.

from the bottom. Since there is no flow from the bottom, gauge 2 will read $P_1/2$. The speed we would calculate from the side-mounted gauge located in the plane of the pump inlet would be two times the actual speed. Side reading gauge error has been understood for quite some time and has been discussed by many authors [8, 10–13]. Projecting parts and low sticking coefficients will usually prevent a pump from capturing all molecules. A fraction $(1 - a)$ of them will be returned and gauge 2 will read $P_2 = P(1 - a/2)$, where a is the transmission coefficient. The error resulting from the use of a side reading gauge is a function of the Ho coefficient. The relation between the actual Ho coefficient a and the apparent Ho coefficient a' , due to the side reading gauge, is found to be [15]

$$a = \left(\frac{a'}{1 + \frac{a'}{2}} \right) \quad \blacktriangleright (7.6)$$

The apparent speed of a perfect pump ($a = 1$) is $2S$. The error will become less as the Ho coefficient goes to zero. Equation (7.5) is valid provided that the reflected gas obeys a cosine distribution. In general this is not true, but objects such as inlet screens and chevrons randomize the flow and minimize the deviation from a cosine distribution.

Feng and Xu [14] calculated the pumping speed measurement error of the new AVS / ISO test dome to be within 4% for Ho coefficients in the range 0.2–1.0. They found the error in the original AVS dome [15] to be greater than 10%. Measurement error was the reason for changing the gauge location in the new AVS Recommended Practice. This is sufficient

accuracy for the applications envisioned. Measuring pumping speed in the high vacuum region is complicated by the inhomogeneous gas flow patterns. But with the choice of a suitable dome we can measure a speed, which we can use to calculate the pumping rate of a chamber. It is not necessary to know the pumping speed to a fraction of a percent because we will use formulas for joining conductances, which are not corrected for beaming.

REFERENCES

1. B. R. F. Kendall, *J. Vac. Sci. Technol. A*, **7**, 2403 (1989).
2. M. Hablanian, *J. Vac. Sci. Technol. A*, **5**, 2552 (1987).
3. D. Andrew, *Vacuum*, **16**, 653 (1966).
4. A. A. Landfors, M. H. Hablanian, R. F. Herirck, and D. M. Vaccarello, *J. Vac. Sci. Technol., A* **1**, 150 (1983).
5. K. Welch, B. Andeen, J. E. de Rijke, C. A. Foster, M. H. Hablanian, R. C. Longworth, W. E. Millikin, Jr., Y. T. Sasaki, and C. Tzemos, *J. Vac. Sci. Technol. A*, **17**, 3081 (1999).
6. S.B. Nezterov, Y.K. Vassiliev, and R.C. Longworth, *J. Vac. Sci. Technol. A*, **19**, 2287 (2001).
7. T. L. Ho, *Physics*, **2**, 386 (1932).
8. W. Steckelmacher, *Vacuum*, **15**, 249 and 503 (1965).
9. R. Buhl and E. A. Trendelenburg, *Vacuum*, **15**, 231 (1965).
10. B. B. Dayton, *Ind. Eng. Chem.*, **40**, 795 (1948).
11. D. J. Santeler et al., *Vacuum Technology and Space Simulation*, NASA SP-105, National Aeronautics and Space Administration, Washington, DC, 1966, p.119.
12. B.B. Dayton, *Vacuum*, **15**, 53 (1965).
13. D. R. Denison, *J. Vac. Sci. Technol.*, **12**, 548 (1975).
14. Y. Feng and T. Xu, *Vacuum*, **30**, 377 (1980).
15. Apparatus of AVS Tentative Standard 4.1, 4.7, 4.8, *J. Vac. Sci. Technol.* **8**, 664 (1971).

PROBLEMS

- 7.1 † Define volumetric pumping speed.
- 7.2 † What is the distinction between volumetric pumping speed and conductance?
- 7.3 A 500-L/s high vacuum pump is operating at an inlet pressure of 2×10^{-3} Pa. What is the throughput of the pump? The pressure at the top of the cold trap above the pump is 2.1×10^{-3} Pa, what is the conductance of the trap?
- 7.4 † A chamber containing air at reduced pressure is connected to a perfect vacuum by a thin circular aperture of area A. What is the pumping speed of the aperture when the mean free path of the gas is much larger than the diameter of the aperture?
- 7.5 Sketch the speed and conductance of an aperture in molecular flow, as a function of the ratio of pressures P_1/P_2 across the aperture.

- 7.6 † For what reasons are pumping speed measurements more complex in high vacuum than in the low or medium vacuum regions?
- 7.7 The pumping speed of an oil-sealed rotary vane mechanical pump filled with mineral oil was measured using the test dome of Fig. 7.1 (right). The flow and pressure data were:

Gas Flow (Pa-L/s)	Gauge Reading (Pa)
84.4	13.3
7.33	1.33
0.67	0.133
0.149	0.27
0.069	0.0133
0.012	0.054
0.0017	0.027

Plot the pumping speed (L/s) versus inlet pressure (Pa). Estimate the blank-off pressure.

- 7.8 A 0.11-m³ chamber is connected by way of an adjacent gate valve, duct, and cold trap to a six-inch diffusion pump. The pump contains polyphenyl ether pump fluid. A rate of rise measurement is performed

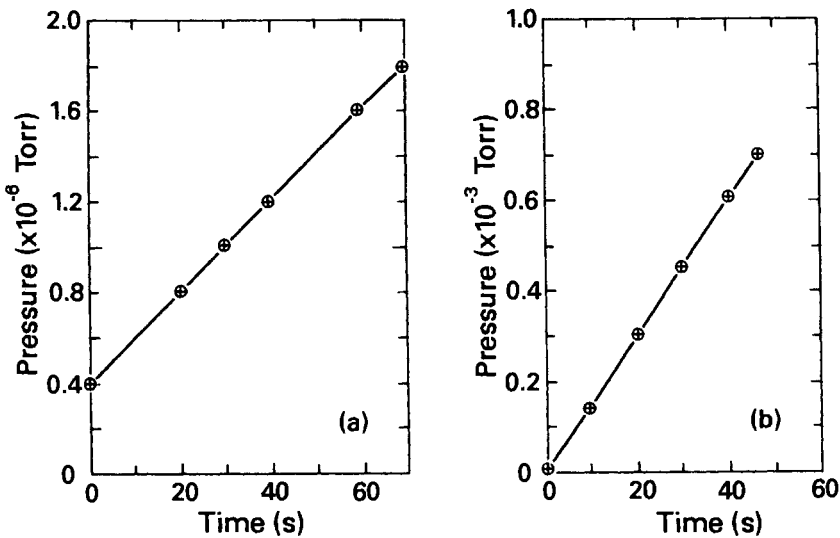


Fig. 7.3 Rate of rise data. Left: Without gas flow. Right: With argon flow.

on the system for the purpose of measuring the net system pumping speed. Figure 7.3, (left) shows the rate of rise of the background following valve closure. Residual gas analysis shows it to be mainly water vapor. At the end of this measurement the system was pumped to the base pressure and a constant but unknown argon flow was admitted to the chamber. The base pressure rose to 5×10^{-6} Torr. Figure 7.3 (right) shows the rate of rise after the gate valve was closed. Calculate the pumping speed for argon at the entrance to the chamber.

- 7.9 A six-inch (0.197-m-diameter) diffusion pump has been appended to the dome like that in Fig. 7.2 for measurement of the air pumping speed. The diameter of the connecting orifice is 1.97 cm. The lower ion gauge reads 8.3×10^{-5} Pa, while the upper gauge reads 4.8×10^{-3} Pa. (a) What is the pumping speed for air? (b) What is the Ho coefficient?
- 7.10 Calculate the pumping speed at the chamber for the pumping system sketched in Fig. 7.4. Assume the real pumping speed of the diffusion pump is 2100 L/s at the pump throat.

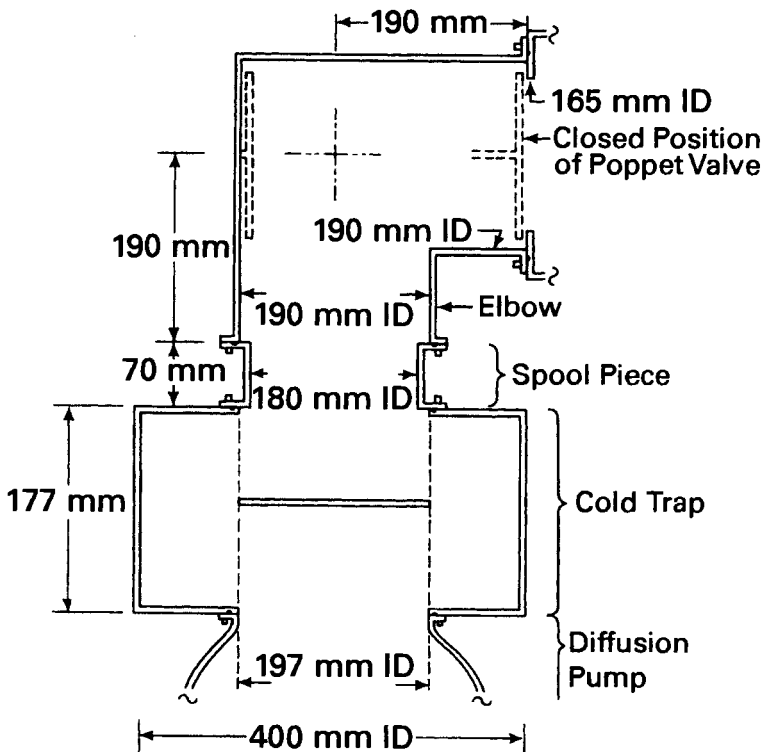


Fig. 7.4 System containing pump, cold trap, connecting pipe and poppet valve.

CHAPTER 8

Residual Gas Analyzers

The first 180° magnetic sector mass spectrometer was developed in 1918 by Dempster [1]. By 1943 Prof. A. O. C. Nier, an early developer of magnetic sector mass spectrometers [2], designed a metal version of his glass instrument to measure uranium isotope ratios [3] and to leak test separation equipment at Oak Ridge Laboratory [4]. In 1960 Caswell used the RGA to study the residual gases in vacuum evaporators, and he demonstrated that the performance of a vacuum system could be improved by Viton gaskets, Meissner traps, and getters [5]. Caswell also used the RGA to characterize the effects of residual gases on the properties of tin and indium films [6,7].

Since then RGAs have proved their value in the solution of many vacuum-related manufacturing problems. They have been used extensively to diagnose problems and verify environments. RGAs are being increasingly used as sophisticated process control instruments where they are used to measure gas purity, gas loads evolved from films and sputtering targets, vapor fluxes from physical vapor deposition sources, and background gas composition during sputtering and other plasma processes.

This chapter is concerned with the theory of the operation of magnetic sectors and rf quadrupoles, as well as installation methods and data collection on high vacuum and plasma processing chambers. The interpretation of RGA spectra is discussed in Chapter 9.

8.1 INSTRUMENT DESCRIPTION

Mass spectrometers are used to measure the ratio of mass-to-electric charge (M/z) of a molecule or atom. Mass measurement is based on the ^{12}C scale—that is, the weight of carbon is 12.0000 atomic mass units (AMU). The charge of the ion is ze , where z is the number electrons removed from the outer shell of the atom, and e is the charge of the electron. Figure 8.1 displays a mass spectrum recorded on an analytical quadrupole mass spectrometer [8]. Examination of this spectrum shows three well-resolved

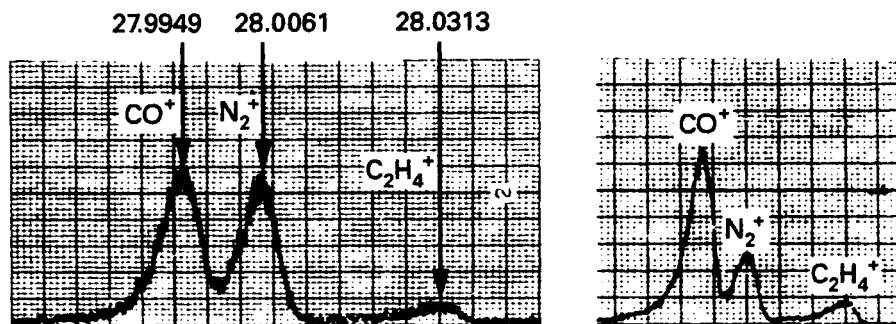


Fig. 8.1 Left: Expanded sweep over the $M/z = 28$ triplet showing resolution of CO^+ , N_2^+ , and C_2H_4^+ at a time shortly after pump down. Right: Expanded sweep over the $M/z = 28$ triplet after about 2 h of pumping showing the diminution of N_2 relative to CO and C_2H_4 . Reprinted with permission from *J. Vac. Sci. Technol.*, 11, 351, W. L. Fite and P. Irving. Copyright 1974, AVS—The Science and Technology Society.

peaks. The resolving power of this instrument permitted identification of the triplet CO^+ ($M/z = 27.9949$), N_2^+ ($M/z = 28.0061$), and C_2H_4^+ ($M/z = 28.0313$). The spectrum shown in Fig. 8.1 illustrates the capability of a precision analytical laboratory instrument. The small, portable, inexpensive instruments we describe here are called residual gas analyzers (RGAs). These instruments are capable of resolving approximately single mass units ($\Delta M/z \sim 1$), and they scan an M/z range of 1–50 or perhaps 1–400. In an RGA spectrum, each of the triplets illustrated in Fig. 8.1 would be displayed as one peak. Figure 8.1 (right) showed that the N_2 peak decreased after pumping, whereas the CO peak increased; we now know that CO is generated in the hot filaments used in RGAs and ion gauges.

All mass spectrometers have three parts: an ionizer, a mass filter, and a detector. See Fig. 8.2. The simplicity and reduced cost of an RGA results in an instrument with far less resolving power and sensitivity than is possible in an analytical laboratory instrument. Here we review two commonly used ion sources, two mass filters, and two detectors used in commercial RGAs.

8.1.1 Ion Sources

The only technique applicable to the production of positive ions in commercial residual gas analyzers is electron impact ionization. Other techniques such as field ionization and chemical ionization are useful in research instruments, such as the triple-quadrupole atmospheric pressure ionization mass spectrometer (APIMS) or tandem magnetic sector analytical mass spectrometer. In a modern RGA, the ion source is either

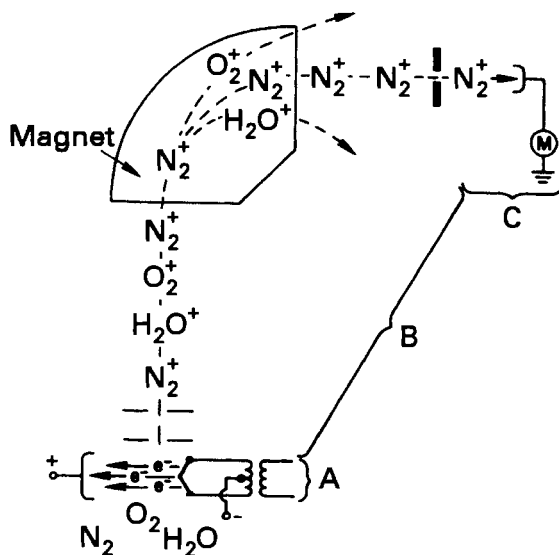


Fig. 8.2 Three stages of partial pressure analysis: (A) Ionizer—hot filament illustrated; (B) mass filter—magnetic sector illustrated; and (C) detector—Faraday cup illustrated.

immersed in the vacuum ambient or locally isolated by nearby walls from the source gas. These ion sources are referred to, respectively, as open and closed ion sources.

Open Ion Sources

Figure 8.3 sketches an open ion source that might be used in a residual gas analyzer. The electrons from the filament are drawn across the chamber to the anode. Some of the electrons collide with gas molecules, strip off one or more outer electrons, and create positive ions. Not all ionization chambers are geometrically similar to the one sketched in Fig. 8.3. One instrument looks very much like a Bayard-Alpert ionization gauge except for the absence of the wire collector and the addition of an electron reflector. These and other ionizers were designed to maximize ion production and sensitivity.

As in the ion gauge, positive ion production is not equal for all gases. The RGA differs from the ion gauge in that it sorts ions by their mass-to-charge ratio (M/z) and counts each ratio separately. For example, when measuring nitrogen, an ion gauge makes no distinction between current due to $^{14}\text{N}^+$ ($M/z = 14$), $^{15}\text{N}^+$ ($M/z = 15$), or $^{14}\text{N}_2^+$ ($M/z = 28$), whereas the RGA distinguishes each ion current. Table 8.1 gives total positive ion cross-sections, relative to N_2 , for several common gases at an ionizing

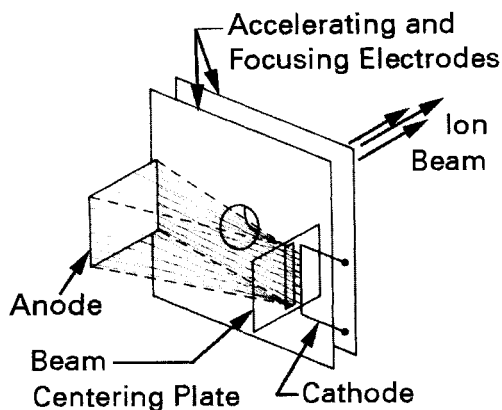


Fig. 8.3 One form of an open ion source.

energy of 70 V [9]. Although the ionization cross section does not peak at the same energy for all gases, it is generally the largest for most gases in the range 50–150 V. For this reason, many ionizers operate at an electron energy of 70 V. Some instruments make provision for adjustment of the electron energy, because it is sometimes desirable to reduce the potential in order to reduce the dissociation of complex molecules. This is essential in qualitative analysis.

The ion production of each species is proportional to its density or partial pressure. Consider a sample of a gas mixture containing only equal portions of nitrogen, oxygen, and hydrogen, whose total pressure is 3×10^{-5} Pa. A mass scan of this mixture would show three main peaks of unequal amplitudes. Since the sensitivity and gain are not constant for all masses, the peak ratios will not be in direct proportion to their partial pressures. If however, the total pressure of the gas mixture were increased to 6×10^{-5} Pa, the amplitudes of each of the three dominant peaks would double. In other words, the instrument is linear with pressure. Ionizers are linear to a pressure of $\sim 10^{-3}$ Pa (10^{-5} Torr). At higher pressures the effects of space charge and gas collisions become important. The ions produced in the space between the filament and anode are drawn out of that region, focused, and accelerated toward the mass filter. The acceleration energy depends on the type of mass analyzer; in a magnetic sector, ion acceleration is part of the mass filtering process.

Closed Ion Sources

Electron- and ion-stimulated desorption from an open source limits an RGA's sensitivity, when sampling gases through pressure reducing

**Table 8.1 Experimental Total Ionization
Cross Sections (70 V) for Selected
Gases Normalized to Nitrogen**

Gas	Relative Cross Section
H ₂	0.42
He	0.14
CH ₄	1.57
Ne	0.22
N ₂	1.00
CO	1.07
C ₂ H ₄	2.44
NO	1.25
O ₂	1.02
Ar	1.19
CO ₂	1.36
N ₂ O	1.48
Kr	1.81
Xe	2.20
SF ₆	2.42

Source. Reprinted with permission from *J. Chem. Phys.*, 43, p. 1464, D. Rapp and P. Englander-Golden. Copyright 1965, The American Institute of Physics.

components. Consider a process chamber operating at 1 Pa (10^{-2} Torr) connected through a pressure reducer to a differentially pumped RGA, whose ionizer and analyzer are operating at 10^{-4} Pa (10^{-6} Torr). In this example, imagine 10^{-7} Pa of water vapor was desorbed from the analyzer walls by stimulated desorption and thermal heating of nearby surfaces. This water vapor signal would be indistinguishable from 10^{-3} Pa of water vapor in the chamber, whose pressure is reduced to 10^{-7} Pa by the pressure reducer. The smallest partial pressure of water vapor from the process chamber that could be detected within the analyzer would therefore be 10^{-3} Pa or 0.1% of the process gas concentration. The closed ion source was developed to overcome the effects of stimulated desorption from walls when sampling from high-pressure chambers.

The sketch in Fig. 8.4 illustrates how gas flows through the small sample tube of one closed ion source. An external filament emits electrons, some of which pass through the hole in the sample tube, and ionize the gas within. The only electron-stimulated wall desorption is generated by the small local area inside the sample tube. The ionizer efficiency of a closed

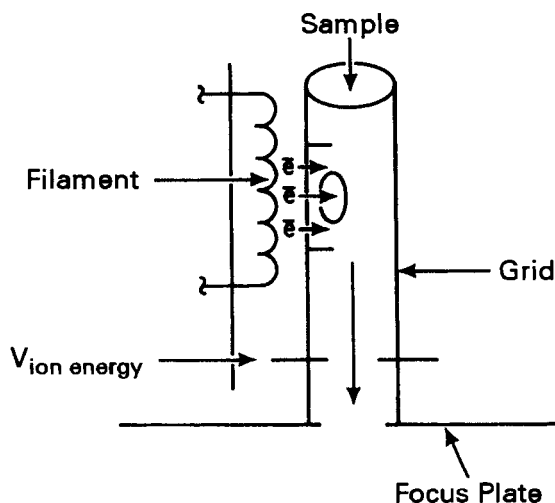


Fig. 8.4 Schematic view of a closed ion source. Gas enters the upper end of sample tube, which is at a higher pressure than the analytical chamber, before flowing into the analyzer. The filament is located outside this tube and is at the same pressure as the analyzer. Reprinted with permission from *J. Vac. Sci. Technol. A*, **11**, 694, B. S. Brownstein, D. B. Fraser, and J. F. O'Hanlon. Copyright 1993, AVS—The Science and Technology Society.

source will be less than that of an open source, because less than a quarter of the electron flux enters the hole in the sample tube. The closed ion source is particularly useful in sampling chambers operating at high pressures, which require differential pumping. We will discuss the use of this source in Section 8.2.2.

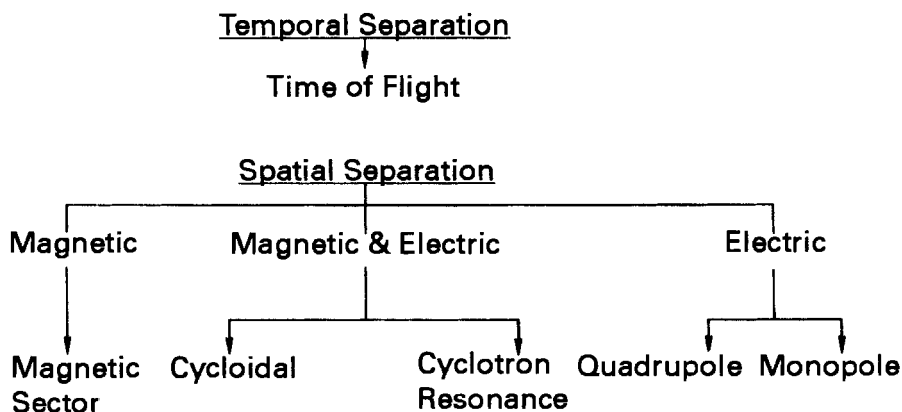


Fig. 8.5 Mass separation methods.

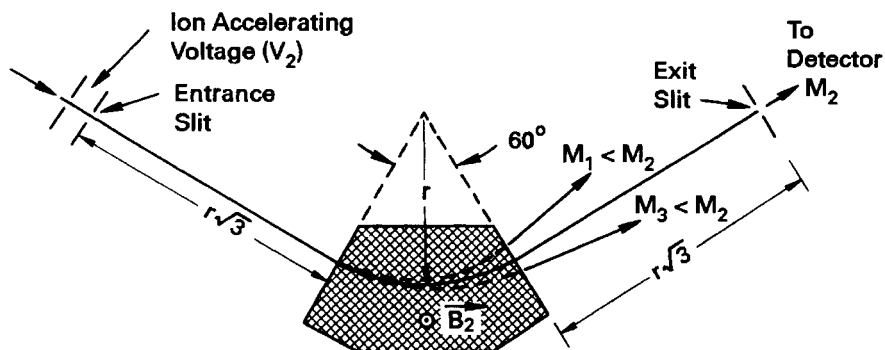


Fig. 8.6 A magnetic sector mass separator (60°) with symmetrical entrance and exit slits. Adapted with permission from *Mass Spectroscopy in Science and Technology*, p. 18, F. A. White. Copyright 1968, John Wiley & Sons.

8.1.2 Mass Filters

Numerous techniques have been developed for mass filtering. For various reasons only two—the magnetic sector and the rf quadrupole—have survived the test of commercial development. Those who are interested in a thorough discussion of all types of mass separation schemes are referred elsewhere [9]. The common methods are outlined in Fig. 8.5. This section discusses quadrupole and magnetic-sector mass filters.

Magnetic Sector

The magnetic sector mass filter separates ions of different mass-to-charge ratios by first accelerating the ions through a potential V_a and then directing them into a uniform magnetic field perpendicular to the direction of ion motion. While under the influence of this magnetic field the ions are deflected in circular orbits of radii r

$$r = \frac{1}{B} \left(\frac{2mV_a}{ze} \right)^{1/2} \quad \blacktriangleright (8.1)$$

If B is given in units of tesla, the ion accelerating energy V_a is given in volts, the mass M is given in atomic mass units, and z is the degree of ionization, the radius of curvature will be

$$r = \frac{1.44 \times 10^{-4}}{B} \left(\frac{MV_a}{z} \right)^{1/2} \quad (8.2)$$

A practical mass analyzer that uses magnetic separation is shown in Fig. 8.6 for a 60° magnetic sector. In principle, any angle will work, but angles of 180° , 90° , and 60° are common. The 60° sector is a common filter for RGA applications. It provides sufficient separation between source and collector, provides good focusing for divergent ions, and requires a minimum amount of magnetic material.

As illustrated in Fig. 8.6, the location of the exit and entrance slits determines the radius r at which the beam will be properly focused. With the radius so specified, the mass-to-charge ratio M/z of the beam in focus is determined by the accelerating potential and the magnetic field-strength. In the example shown, a singly ionized molecule $z = 1$ of mass M_2 is focused on the exit slit for $V_a = V_2$ and $B = B_2$. Masses $M_1 < M_2$ and $M_3 > M_2$ will be deflected through greater and lesser angles, respectively, than M_2 . To focus mass M_3 on the detector, B must be increased or V_a must be decreased. Commercial RGAs generally use permanent magnets and a variable acceleration voltage. Electromagnets are available to extend the range and provide magnetic scanning.

Equation (8.1) states that for constant r and B , MV_a/z is a constant. Sweeping a large M/z range, say 1–300, requires prohibitively large linear sweep voltages. Because of this limitation, permanent magnetic sector analyzers divide the instrument range into at least two scales by changing the magnet. For example, one M/z range might cover 2–50 with a magnet of about 0.1 T and a second M/z range of 12–300 with a magnet of 0.25 T. Traditionally, such instruments sweep the voltage linearly with time. Because MV_a/z is a constant, the resulting mass scan is not linear with time; as the mass number increases the peak separation decreases. Some instruments allow the accelerating potential to be held constant, while an electromagnet of 0–0.25 T sweeps the M/z range 1–100.

Differentiation of (8.1) reveals that the mass dispersion Δx of the instrument is mass dependent. For ions of equal energy traversing a uniform magnetic sector the mass dispersion, or spatial separation between adjacent peaks of mass m and $m + 1$, has been found to be [10]

$$\Delta x \propto \frac{r}{m} \quad \blacktriangleright (8.3)$$

Equation (8.3) illustrates why instruments of small radii cannot effectively separate adjacent massive peaks. The resolving power and sensitivity of a magnetic sector are dependent on mass and exit slit width.

Figure 8.7 shows two idealized mass peaks being scanned with slits of different widths and indicates that wide slits collect ions efficiently (high sensitivity), but resolve adjacent mass peaks poorly (low resolving power). To first order there are no mass-dependent transmission losses in a fixed-

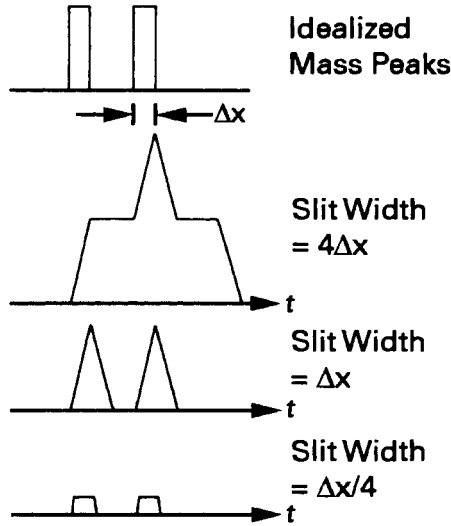


Fig. 8.7 Idealized mass peaks illustrate the relationship between sensitivity and resolution.

radius, magnetic-sector analyzer. This means that if equal numbers of, say, He and Xe atoms pass through the entrance slit, equal numbers will pass through the exit slit. It will be noted later that this is not always true of the quadrupole. Figure 8.8 shows an RGA trace taken with a small sector analyzer on a 35-in. oil diffusion pumped system [11]. This trace clearly illustrates the nonlinear nature of the sweep and the mass-dependent resolution. The slit width at the detector is fixed, but the distance between

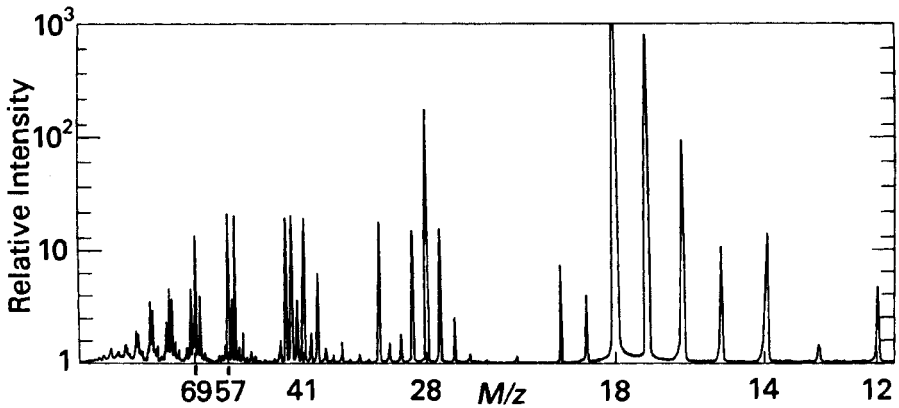


Fig. 8.8 Mass scan from a large diffusion pumped evaporator taken with a magnetic sector instrument with a permanent magnet and voltage sweep.

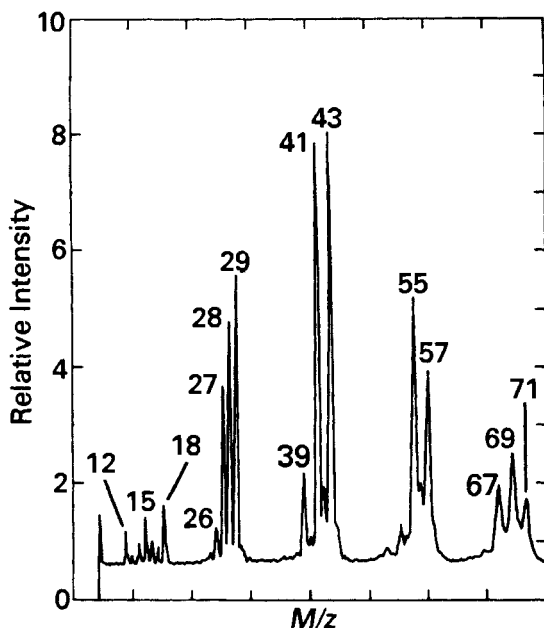


Fig. 8.9 Linear mass scan taken with an Aero Vac 700 series magnetic sector instrument. Reprinted with permission from High Voltage Engineering Corp., Burlington, MA.

adjacent mass peaks varies as $1/m$. Thus, the valley between two peaks of unit M/z difference is not so pronounced at high as at low M/z . Figure 8.9 was taken on an analyzer in which the magnetic field was varied to produce a linear scan. The same mass-dependent resolution is also evident here. More detailed discussions of magnetic sectors are presented in other sources [12,13].

RF Quadrupole

The rf quadrupole, developed by Paul [14] and coworkers, is currently the most popular mass filter. Its acceptance has been due, in part, to the development of the necessary stable, high-power quadrupole power supplies. Figure 8.10 illustrates the mass filter geometry and the path of a filtered ion. The ideal electrodes are hyperbolic in cross section. In practice, they are realized by four rods of cylindrical cross section located to provide the optimum approximation to the hyperbolic fields. Each of the rods is spaced a distance r_0 from the central axis. Mosharrafa [15] has provided a nonmathematical explanation of quadrupole operation. The two rods with positive dc potential, $+U$ in Fig. 8.11, create a potential valley near the axis in which positive ions are conditionally stable. The potential is

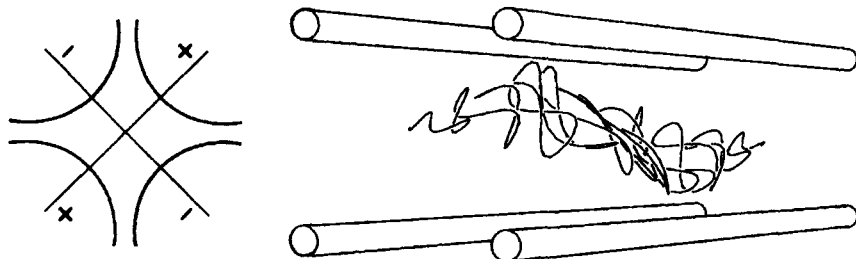
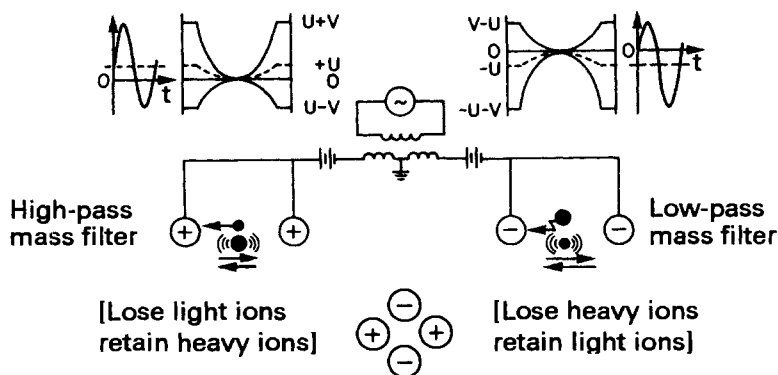


Fig. 8.10 Quadrupole mass filter. Left: Idealized hyperbolic electrode cross section. Right: Three-dimensional computer generated representation of a stable ion path. Courtesy of A. Appel, IBM T. J. Watson Research Center, Yorktown Heights, NY.

zero along the axis of symmetry, shown in the dashed curve of Fig. 8.11. This field is zero only if the potential $-V$ is simultaneously applied to the other pair of quadrupole rods. It is a property of a quadrupole, not a dipole, field. The addition of an rf field of magnitude greater than the dc field ($U + V \cos(\omega t)$) creates a situation in which positive ions are on a potential “hill” for a small portion of the cycle. Heavy ions have too much inertia to be affected by this short period of instability, but light ions are quickly collected by the rods after a few cycles. The lighter the ion, the fewer number of cycles required before ejection from the stable region. This rod pair acts as a “high-pass” filter.

The rod pair with the negative dc potential $-U$ creates a potential “hill” that is unstable for positive ions. However, the addition of the rf field creates a field $-(U + V \cos \omega t)$, which allows a potential “valley” to exist along the axis of the quadrupole for a small portion of the cycle, provided that $V > U$. In this field, light ions are conditionally stable and heavy ions drift toward the electrodes, because the potential “hill” exists for most of the cycle. This half of the quadrupole forms a “low-pass” filter.

Together the high- and low-pass filters form a band-pass filter that allows ions of a particular mass range to go through a large number of stable, periodic oscillations while traveling in the z direction. The width of the pass band is a function of the ratio of dc to rf potential amplitudes U/V . The “sharpness” of the pass band is determined by the electrode uniformity, electrical stability, and ion entrance velocity and angle. A detector is mounted on the z axis at the filter's exit to count the transmitted ions. Ions of all other M/z ratios will follow unstable orbits. The rods will collect them before exiting the filter. The stability limits for a particular M/z ratio are determined from the solutions of the equations of motion of an ion through the combined rf and dc fields. The solutions involve ratios of ω , M/z , and r_0^2 and the potentials U and V . A thorough discussion of the rf



Band-Pass Mass Filter

Fig. 8.11 Electric fields in a quadrupole mass filter. Reprinted with permission from *Industrial Research/Development*, March 1970, p. 24, M. Mosharrafa. Copyright 1970, Technical Publishing Co.

quadrupole has been given by Dawson [16]. By sweeping the rf and dc potentials linearly in time the analyzer can scan a mass range. Scan times as slow as 10–20 min and as fast as 80 ms are typically attainable in commercial analyzers with M/z ranges of 1–300. One noticeable distinguishing feature of the quadrupole is that no additional restriction other than linear sweeping of the rf and dc potentials is needed to obtain a graphical display that is linear in mass scan.

Although the stability of the trajectory of an ion may be calculated without consideration of the z component of the ion velocity or the beam divergence, experimentally the situation is more complicated. There is a reasonable range of velocities and entrance angles that yields stable trajectories. In the magnetic sector both the ion energy and the magnetic field determine the focus point of an ion. One of the advantages of the quadrupole is that ions with a range of energies or entrance velocities will focus, although not with the same resolution. The slow ions are resident in the filter for a longer time and therefore are subjected to a greater number of oscillations in the rf field than are those ions with larger z components of velocity. As a result, the slow ions are more finely resolved, but suffer more transmission losses than do the light ions. For this reason, quadrupole transmission usually decreases with increasing mass. In a typical instrument that can resolve mass peaks 1 AMU apart, the gain is constant to about $20 < M/z < 50$, after which it decays at the rate of approximately a decade per 150 AMU. See Fig. 8.12. This is only typical; there is considerable instrumental and manufacturer variation. By proper choice of the potentials U and V , the mass dependence of the transmission can be

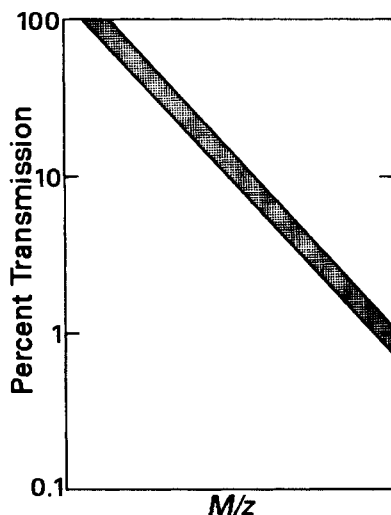


Fig. 8.12 Relative transmission of a typical rf quadrupole as a function of M/z , when adjusted for unity absolute resolution. This may be varied by changing the sensitivity.

considerably improved at the expense of resolution. If accurate knowledge of the transmission versus mass is desired, it must be measured for the particular filter and potentials in question. A typical mass scan taken on a small oil diffusion pumped system with a quadrupole adjusted for constant absolute resolution is displayed in Fig. 8.13.

Resolving Power

The resolving power of an RGA is a measure of the ion-separating ability of the instrument of a given mass-to-charge ratio M/z . The width of the peak at 10% of the peak height $\Delta(M/z)_{10}$ is one way to measure resolving power. The resolving power of an RGA is the dimensionless ratio of peak height to the peak width at 10% peak height, $(M/z)/\Delta(M/z)_{10}$. See the AVS Recommended Practice for the Calibration of Mass Spectrometers and Partial Pressure Analyzers [17]. Analytical spectroscopy requires the discrimination of mass peaks separated by extremely small fractional mass units. A resolving power of 2000 is needed to distinguish $^{32}\text{S}^+$ ($M/z = 31.9720$) from $^{16}\text{O}_2^+$ ($M/z = 31.9898$). RGAs or PPAs can resolve peaks separated by about 1 AMU.

8.1.3 Detectors

The ion current detector, located at the exit of the mass filter, must be sensitive to small ion fluxes. The ion current at mass n is related to the pressure in the linear region by

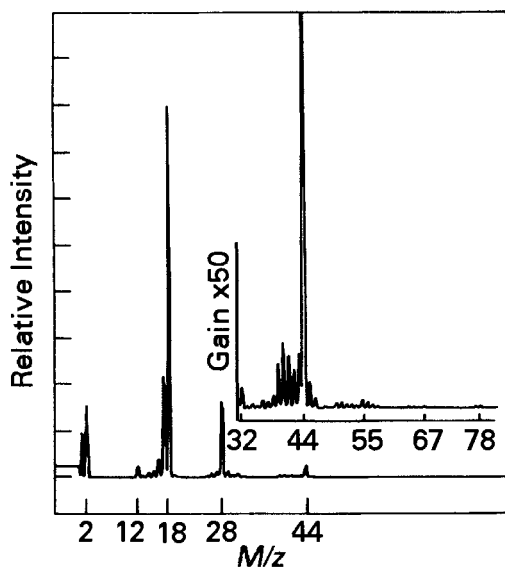


Fig. 8.13 Mass scan taken on a small oil diffusion pumped chamber with an rf quadrupole instrument.

$$i_n = S'_n P_n \quad (8.4)$$

where i_n , S'_n , and P_n are, respectively, the ion current, sensitivity of the ionizer and filter, and partial pressure of the n^{th} gas. A typical sensitivity for nitrogen is 5×10^{-6} A/Pa to 2×10^{-5} A/Pa. We might ask why the sensitivity is defined with dimensions of current per unit pressure, instead of reciprocal pressure, as in ion gauge tubes. The answer is that the ion sources used in RGAs are sometimes space charge controlled, and their ion current is not linearly proportional to their emission current. Some instruments with high sensitivity use high emission currents, up to 50 mA, but a typical ionizer with a nitrogen sensitivity of 7×10^{-6} A/Pa will have an emission current of 1–5 mA. For an emission current of 1 mA the sensitivity, defined as an ion gauge, would be 7×10^{-3} Pa⁻¹, which is an order of magnitude smaller than that of an ion gauge. The design of the mass analyzer is responsible for the low “ion gauge” sensitivity of the mass analyzer. Not all the ions generated in the ionizer are extracted through the focus electrode. Not all of these extracted ions traverse the mass filter. If we assume an average sensitivity of 10^{-5} A/Pa and a dynamic pressure range of 10^{-1} – 10^{-12} Pa, the ion current at the entrance to the detector can range from 10^{-6} to 10^{-17} A. For the upper half of this range a simple Faraday cup detector, followed by a stable, low-noise, high-gain FET amplifier will suffice. Below 10^{-12} A, an electron multiplier is required.

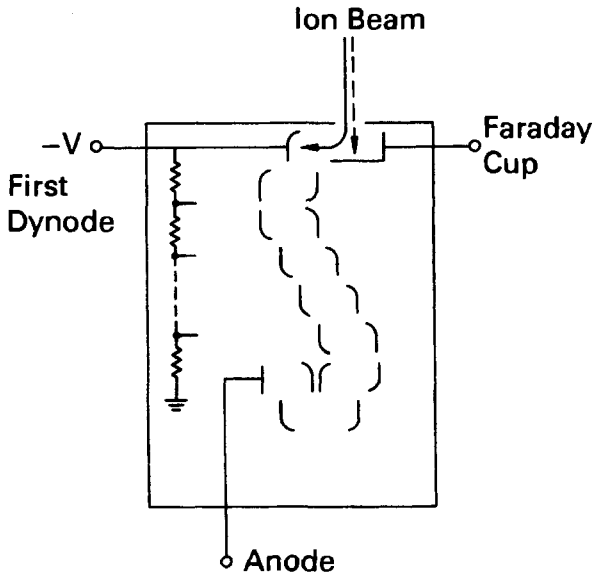


Fig. 8.14 Combination Faraday cup-electron multiplier detector. Reprinted with permission from Uthe Technology Inc., 325 N. Mathilda Avenue, Sunnyvale, CA 94086.

Discrete Dynode Electron Multiplier

Figure 8.14 illustrates a typical installation in which high gain is required—a combination Faraday cup-electron multiplier. When the Faraday cup is in operation, the first dynode is grounded to avoid interference. When the electron multiplier is used, the Faraday cup is grounded or connected to a small negative potential to improve the focus of the ions as they make a 90° bend toward the first dynode. In quadrupole analyzers the first dynode is generally located off-axis to avoid x-ray and photon bombardment.

Amplification in an electron multiplier is achieved when positive ions incident on the first dynode generate secondary electrons. Secondary electrons are amplified as they collide with each succeeding dynode. Multipliers are operated with a large negative voltage (–1000 to –3000 V) on the first dynode. The gain of the multiplier is given by

$$G = G_1 G_2^n \quad \blacktriangleright (8.5)$$

where G_1 is the number of secondary electrons generated on the first dynode per incident ion and G_2 is the number of secondary electrons per incident electron generated on each of the n succeeding dynodes. The values of G_1 and G_2 depend on the material, energy, and nature of the

incident ion. For a 16-stage multiplier, whose overall gain $G = 10^6$, $G_2 = 2.37$; for $G = 10^5$, G_2 would be 2.05.

The multiplier sketched in Fig. 8.14 typically uses a Cu-Be alloy, containing 2–4% Be, as the dynode material. When suitably heat-treated to form a beryllium oxide surface, it will have an initial gain as high as 5×10^5 . These tubes should be stored under vacuum at all times, because a continued accumulation of contamination will cause the gain to decrease slowly. If the tube has been contaminated with vapors, such as halogens or silicone-based pump fluids, the gain will drop below 10^3 ; at this point the multiplier must be cleaned or replaced. If the multiplier has had only occasional exposure to air or water vapor and has not been operated at high output currents near saturation for prolonged times, its gain can usually be restored. A typical treatment uses successive ultrasonic cleanings in toluene and acetone, followed by an ethyl alcohol rinse, air drying, and baking in air or oxygen for 30 min at 300°C. Tubes contaminated with silicones cannot be reactivated. Tubes contaminated with chemisorbed hydrocarbons or fluorocarbons often form polymer films on the final stages in which the electron current is great. Such contamination can be quickly removed by plasma ashing.

Continuous Dynode Electron Multiplier

A channel electron multiplier is illustrated in Fig. 8.15. The structure consists of a finely drawn $\text{PbO-Bi}_2\text{O}_3$ [18] tube, typically 5 mm OD and 1 mm ID. A high voltage is applied between the ends of the tube. The high

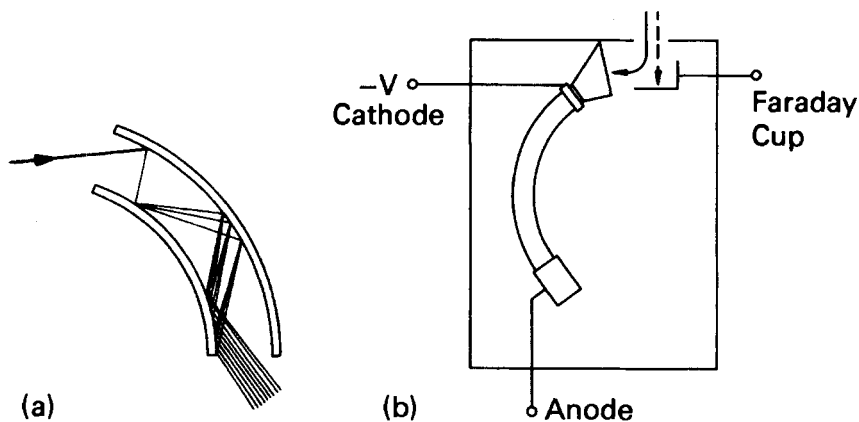


Fig. 8.15 Channeltron® electron multiplier: (a) Schematic detail of capillary; (b) Incorporation into mass analyzer. Reprinted with permission from Galileo Electro-Optics Corp., Galileo Park, Sturbridge, MA 01518.

resistivity of the glass makes it act like a resistor chain, which causes secondary electrons generated by incoming ions to be deflected in the direction of the voltage gradient. The tubes are curved to prevent positive ions generated near the end of the tube from traveling long distances in the reverse direction, gaining a large energy, colliding with the wall, and releasing spurious, out-of-phase secondary electrons [19,20]. If the tube is curved, the ions will collide with a wall before becoming energetic enough to release unwanted secondary electrons. An entrance horn can be provided if a larger entrance aperture is needed. A channel electron multiplier can be operated at pressures up to about 10^{-2} Pa and at temperatures up to 150°C ; it has a distinct advantage over the Be-Cu-type multiplier in that it is relatively unaffected by long or repeated exposure to atmosphere. Because the secondary emission material is a sub-oxide, its emission is adversely affected by prolonged operation at high oxygen pressures. It seems to be less affected by some contaminants than a Be-Cu multiplier. Under normal operating conditions the gain of either multiplier will degrade in one or two years to a point at which replacement or rejuvenation is necessary. Little increase in gain will be realized by increasing the voltage on a multiplier whose gain is less than 1000.

Although channel electron multipliers can be exposed to air, they saturate at a lower current than Be-Cu multipliers and cannot be operated with a linear output at high pressures, unless the operating voltage or the emission current is reduced. The manufacturer's literature should be consulted for the precise values of saturation current and range of linearity before any electron multiplier is used. The gain of a multiplier is not a single-valued function. Ions illuminate the first dynode and electrons collide with each succeeding dynode. The gain of the latter dynodes G_2 is dependent on the inter stage voltage and the dynode material, whereas the gain of the first dynode G_1 is complex. The gain of the first stage is primarily dependent on the material, mass, and the energy of the impinging ion. Ideally, the gain is proportional to $m^{1/2}$, but this is valid only for heavy, low energy ions. The gain of any multiplier is dependent on other factors. Stray magnetic fields can distort the path of the electrons and complex molecules may dissociate on impact, to produce more electrons than a simple compound or element of the same mass. Isotopes and doubly ionized molecules also react somewhat differently, because of the variations in outer electron binding energy [21].

If the gain of a specific electron multiplier needs to be accurately known, a calibration curve of gain versus mass must be experimentally measured for all gases and vapors of interest. The gain of an electron multiplier is never constant. It may be measured by taking the ratio of the currents from the Faraday cup and the electron multiplier output, a tedious process, done

only when semiquantitative analysis is required. Even then the gain of the multiplier must be periodically checked with one major gas to account for day-to-day aging of the tube. Only periodic checking of the gain at mass 28 with N₂ is necessary for routine gas analysis.

8.2 INSTALLATION AND OPERATION

RGAs may be mounted within high and ultrahigh vacuum chambers as well as process chambers operating below the 10⁻³ Pa range. Standard RGAs may be used to sample the gas in a medium vacuum chamber by extracting gas through an orifice or capillary tube into a low-pressure sample chamber. Alternatively, miniature quadrupoles can be installed directly in chambers that operate at pressures up to 1 Pa (10 mTorr). We first discuss RGA mounting and analysis within high vacuum chambers, and then we discuss gas sampling and miniature instruments for analyzing high-pressure process chambers.

8.2.1 High Vacuum Operation

RGAs are attached to chambers operating in the molecular flow region for leak detection and monitoring preprocess chamber conditions. They are extensively used for monitoring the partial pressures of background impurities and source vapor fluxes. Mounting and stability are two issues the user needs to understand in order to generate meaningful data.

Mounting

For routine leak detection or background gas analysis, the RGA head is mounted on a port immediately adjacent to the chamber. A valve is usually placed between the head and the process chamber to keep the electron multiplier clean, especially when the chamber is frequently vented to air. This is important with a Be-Cu electron multiplier. The head should be positioned to achieve maximum sensitivity in the volume being monitored. If the instrument is to monitor beams, a line-of-sight view is necessary. It is often worthwhile to mount the head inside the chamber and shield its entrance so that the beam impinges on a small portion of the ionizer. This shielding will reduce the contamination of the ionizer and associated ceramic insulators. It is counterproductive to mount the RGA in remote locations where it samples the chamber ambient through convoluted pathways.

An automated data collection system and printer simplify data analysis. On-line graphics are useful for observing the gas “fingerprint” and for leak

hunting. The electron multiplier may saturate at high gain, if the pressure is too high, say above 10^{-3} Pa; in this case one may reduce the electron multiplier voltage or switch to the Faraday cup. High-gain observation of very small signals should be done with low-speed scans, say 1 AMU/s, or the long time constant will mask the signal. The ground connection of a turbomolecular pump and other noise sources should be connected to the ground of the most sensitive input of the highest gain amplifier. That point should be connected to the nearest quiet ground.

Stability

Stable operation of an RGA in a high vacuum or ultrahigh vacuum chamber is a function of many variables. Some of these variables are related to the instrument design, whereas others are operator- or system-dependent. Stability is affected by materials of filament and ionizer construction, exposure to contaminants during prior use, ion currents and energies, electron-stimulated desorption, and operation of nearby hot filaments. Electron-stimulated desorption (ESD) is as much of a problem in the operation of RGAs as it is in Bayard-Alpert ion gauges. However, the ability to vary the ion energy allows the RGA operator to discern its presence, as the relative sensitivity is a function of ion energy [22]. If the ion energy is reduced and the spectrum changes, then ESD is a concern. The use of silicone-based pump fluids will result in the deposition of insulating films on nearby surfaces. Insulating films and polymer surfaces can store surface charge and alter the energy of the ions entering the mass filter and alter electron orbits. The absence of fluid fragments from the spectrum does not imply the surface is polymer free. Polyphenylether or perfluoropolyether diffusion pump fluids will dissociate as vapors under electron bombardment; they are recommended for use in RGAs and leak detectors.

Ceramic insulators will often exhibit a “memory effect” in which they continuously evolve fragments of hydrocarbons, fluorides, or chlorides after having been exposed to their vapors. This memory effect often confuses analysis when a mass head is moved from one system to another. Ion sources can be cleaned by vacuum firing at 1100°C.

Filaments made from tungsten, thoriated iridium, and rhenium are used in RGAs. Tungsten filaments are recommended for general-purpose work, although they generate copious amounts of CO and CO₂. Rhenium filaments do not consume hydrocarbons. Thoriated iridium filaments are used in oxygen environments, although their emission characteristics are easily changed after contamination by hydrocarbons or halocarbons. As in the ion gauge, the thoriated iridium or “non-burnout” filaments are advantageous when a momentary vacuum loss occurs. Thoriated iridium or

Table 8.2 Some Properties of RGA Filament Materials

Property	ThO ₂	W/3% Re	Re
CO production	Unknown	High	High
CO ₂ production	High	Moderate	Moderate
O ₂ consumption	Low	High	High ^a
H-C consumption	Unknown	High	Low
Water entrapment	Maybe high	Low	Low
Volatility in O ₂	Low	High	Very high ^b
Good filament for ...	Nitrogen oxides	Hydrogen	Hydrogen
	Oxygen	Hydrogen halides	Hydrocarbons
	Sulfur oxides	Halogens	Hydrogen halides
		Halocarbons ^c	Halocarbons ^c
			Halogens

Source. Reprinted with permission from Uthe Technology Inc., 325 N. Mathilda Ave., Sunnyvale, CA 94086.

^a Loss of one filament caused O₂/N₂ ratio to increase 17.6%.

^b Exposure to air at 10⁻⁴ Pa caused failures of the filament pair at 30 and 95 h.

^c Freons, etc.

rhodium filaments also operate at reduced temperature with less adjacent wall outgassing [23]. Preconditioning the filament by heating it above its normal operating temperature should eliminate less volatile materials [24]. Table 8.2 gives some of the properties of three filament materials as tabulated by Raby [25]. Molecular hydrogen dissociates at a temperature of 1100K [26]. This can be avoided by the use of a lanthanum hexaboride filament operating at 1000K [27]. Outgassing of nearby walls can be reduced by the use of EX-processed aluminum [28], or gold coated copper [29], because they are excellent thermal conductors.

Bayard-Alpert ion gauge tubes should be turned off when the RGA is operated. They can produce ion- and electron-stimulated desorption and increase thermally stimulated outgassing of nearby walls. In the ultrahigh vacuum region, inert gas ions may be pumped, whereas hydrogen and $M/z = 16, 28$ will be desorbed by electron bombardment [30]. Ion-stimulated desorption from the extraction plate has been observed; it was shown that the amount of desorption is gas- pressure- and ion-energy dependent [31]. Maintaining a positive filament potential with respect to ground has been shown to reduce outgassing rates of RGAs [32].

Mass heads and pressure gauges should be baked at the same or higher temperature than the chamber, and they should be cooled slowly to prevent the condensation of vapors. The maximum baking temperature will affect electron multiplier choice. Detectors with channel electron multipliers can be baked to 320°C and operated at temperatures up to 150°C. Detectors using a Be-Cu multiplier can usually be baked to about 400°C and operated at temperatures up to 185°C. These temperature limitations are due to the

materials used in channel electron structures and the glass encapsulated resistors in Be–Cu multiplier chains.

8.2.2 Medium and Low Vacuum Sampling

At pressures greater than $\sim 10^{-3}$ Pa (10^{-5} Torr), the standard RGA will not function. An atmospheric pressure ionization mass spectrometer (APIMS) [33], in which the gas is field ionized at high pressures, can sample impurities in process gas streams to the level of parts per trillion of one atmosphere ($\sim 10^{-7}$ Pa). This analytical laboratory technique is only suitable for specialized applications. For routine analysis of plasma systems at pressures as high as 1 Pa (10^{-2} Torr), one may sample the gas stream by means of a pressure reduction scheme or use a miniature quadrupole. Miniature quadrupoles have dimensions of order of the mean free path. Differentially pumped gas analysis and miniature quadrupoles are useful techniques for determining the time constants of contaminant decay during preprocessing and for sampling the background gases during processing.

Differentially Pumped Sampling

Analysis of gas in a plasma etching or deposition chamber can be done by differentially pumping the source gas. Honig [34] has given three primary conditions for gas analysis with a differentially pumped RGA: (1) The beam intensity should be directly proportional to the pressure of the gas in the sample chamber, but should be independent of its molecular weight. (2) In a gas mixture the presence of one component should not affect the peaks due to another component. (3) The gas flow through the orifice should be constant during the scan. These conditions are satisfied if there is good mixing in the chamber, the leaks are molecular, and the pump is throttled.

Unfortunately, it is not always possible to meet these conditions in all applications. Many references state that the superior method of sampling from high pressures is a two-stage reduction scheme, where the gas is first drawn through a long capillary tube to an intermediate chamber. A mechanical pump attached to this chamber removes most of the gas. A sample of that gas is then further pressure divided in the molecular flow regime. See Fig. 8.16. Fractionation can occur in either of these pressure dividers. Consider first the case of a short capillary not meeting the requirements of Poiseuille flow. Such a case was illustrated in Fig. 3.2. In that case, we showed the net flow was determined by equating Poiseuille flow in the tube to choked flow in the orifice. Poiseuille flow depends on viscosity and molecular diameter, whereas choked flow depends on the nonlinear ratio of specific heats. Contrary to popular belief, gas mixtures will fractionate. Consider next a long capillary tube connecting the high-

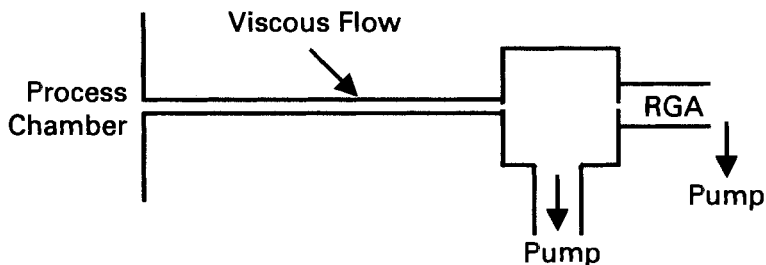


Fig. 8.16 Analysis of a differentially pumped residual gas analyzer using a long viscous flow capillary sampling tube, followed by a molecular flow pressure divider. Reprinted from *Vacuum*, 44, G. B. Bunyard, 633–638, copyright 1993, with permission from Elsevier.

pressure chamber to the intermediate chamber, as described in Fig. 8.16; flow in this tube is governed by (3.12). Fractionation of a gas mixture can result at the exit during expansion. Gas mixtures will not fractionate in the limit of small Knudsen numbers. If the flow is in the transition region, the mixture will be significantly dependent on the ratio of gases; barodiffusion and the diffusion baro effect are small but they do depend on the Knudsen number in viscous flow [35].

When sampling in molecular flow, the relative size of the pump and second orifice must be considered. Examine the model of the differentially pumped system sketched in Fig. 8.17 that operates in molecular flow. In this model, P_c is the pressure in the sputtering chamber, P_s is the pressure in the spectrometer chamber, and P_p is the pressure in the auxiliary pump whose speed is S_p . The conductances C_1 and C_2 , which connect these chambers, are schematically shown as capillary tubes, but in practice, C_1 may be a closed ion source or myriad small holes milled in a thin plate. The gas flow through the auxiliary system, which is everywhere the same, leads to the following equation:

$$C_1(P_c - P_s) = C_2(P_s - P_p) = S_p P_p \quad (8.6)$$

When P_p is eliminated, we obtain

$$P_s = \frac{P_c}{1 + \left(\frac{C_2}{C_1} \right) \left(\frac{S_p}{S_p + C_2} \right)} \quad (8.7)$$

Now consider two cases: Case 1: Let the conductance C_2 be much larger than the speed of the pump. The auxiliary pump is located in or immediately adjacent to the spectrometer chamber with no interconnecting conductance. Equation (8.7) then reduces to

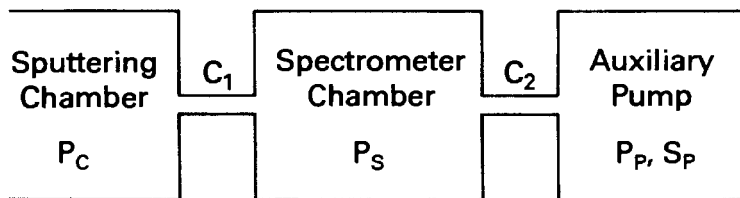


Fig. 8.17 Analysis of a differentially pumped residual gas analyzer using a molecular flow pressure divider.

$$P_s = \frac{P_c}{1 + (S_p / C_1)} \quad \blacktriangleright (8.8)$$

The conductance C_1 has a mass dependence that varies as $1/m^{1/2}$, whereas the pumping speed has a mass dependence that is a function of the pump type. For example, an ion pump has different speeds for noble and reactive gases. Diffusion pump speeds increase for light gases, but not as rapidly as $1/m^{1/2}$. The important result is that the ratio of the gas pressure in the spectrometer to the pressure in the chamber P_s/P_c is mass-dependent, when the auxiliary pump is appended directly to the chamber. Gases will not exit the spectrometer chamber in the same proportion as they exit the sputtering chamber. Honig's first criterion will not be satisfied.

Case 2 considers the situation in which a small conductance C_2 is placed between the spectrometer and pump, such that $C_2 \ll S_p$. Then (8.7) becomes

$$P_s = \frac{P_c}{1 + (C_2 / C_1)} \quad \blacktriangleright (8.9)$$

Light gases will still pass from the sputtering chamber to the spectrometer chamber more rapidly than heavy gases, but also they will exit to the pump. Stated another way, the mass dependence of C_1 and C_2 are the same and cancel each other so that (8.9) is mass independent. Therefore, to sample the ratios of gases in the sputter chamber accurately, the auxiliary pump should be throttled to about 1/10 of its speed. If this is done, the pressure ratio of two gases in the chamber, P_{ac}/P_{bc} will be the same as their ratio in the spectrometer chamber P_{as}/P_{bs} .

The flow ratio of two gases passing through an orifice in molecular flow is given by (2.20); this implies that the gas composition in the sputtering chamber would eventually change with time. However, the flow to the sampling system is so small that it cannot affect the process flow. Sullivan and Busser [36] noted that the time constant of the spectrometer chamber (V_s/C_2) must be equal to or less than the reaction time of the process to obtain accurate time-dependent information concerning the process.

When C_1 in Fig. 8.17 is a closed ion source, the gas pressure in the ionizer can be as high as 100 times that of the spectrometer chamber and this further increases the sensitivity for impurity detection. Using a closed ion source, one can detect ~100 ppm for H_2O and 200 ppb for other gases.

The background gases in the chamber should first be analyzed while the chamber is at its ultimate pressure, in order to ensure there are no leaks. One should save a background spectrum for later comparison. After initiating process gas flow to the chamber, a process flow background is recorded. Next a process spectrum is taken with the discharge operating. The large pressure reduction factor and ever-present background gases reduce the detection limit of the RGA, unless a closed ion source is used.

Miniature Quadrupoles

As early as 1973, Visser [37] demonstrated that miniature quadrupoles designed to operate at short mean free path could be operated directly in a process chamber at pressures up to 0.5 Pa. Commercial instruments have been constructed by scaling standard quadrupoles to operate at pressures as high as 1 Pa (10 mTorr) without any pressure reduction stages [38]. Gas scattering at pressures above 0.1 Pa required internal correction for the (nonlinear) sensitivity. Ion-molecule reactions occur in all instruments in which ions can collide with molecules and the collision probability increases linearly with pressure. Such reactions are observable downstream from the corona discharge ionizer in an APIMS, as well as in miniature quadrupoles when operated at pressures above 0.1 Pa. For example, N_3^+ can be formed from a collision between N_2^+ and N_2 . In turn, the N_3^+ can react with O_2 to form NO^+ or NO_2^+ . See Section 9.1.5.

8.3 RGA CALIBRATION

Calibration of an RGA is done for the purpose of checking the linearity over a wide pressure range, measuring the sensitivity at important M/z values, and verifying the electron multiplier gain. The gain of an electron multiplier can be checked quite simply by taking the ratio of an ion current at the electron multiplier exit to the electron current at the Faraday cup. The instrument sensitivity and linearity can be verified by direct comparison to a transfer standard, by use of a pressure dividing calibration chamber, or by use of an orifice flow system. Detailed descriptions of these techniques and test chambers are given in the AVS Recommended Practice for Calibration of Mass Spectrometers and Partial Pressure Analyzers [17].

Many users wish to have a quick, *in situ* method for verifying the RGA sensitivity and pumping speed. The pulse injection method was developed

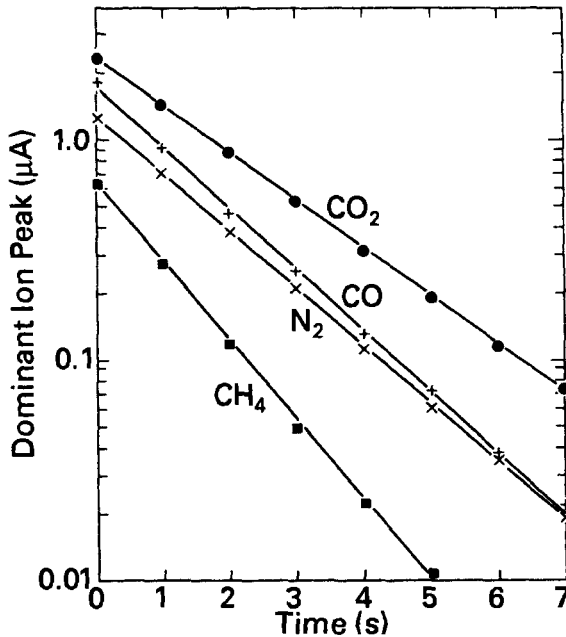


Fig. 8.18 Measurement of the sensitivity and pumping speeds of four gases using the pulsed injection technique. Reprinted with permission from *J. Vac. Sci. Technol. A*, 9, p. 1, J. F. O'Hanlon. Copyright 1991, AVS—The Science and Technology Society.

by Kendall [39]. In its original form, a small quantity of gas was isolated and injected into the vacuum system by means of a piston with two closely spaced O-ring gaskets. Alternatively a fuel injector was used to inject a series of extremely short pulses. The gas pulse ($P_i V_i$) can be approximated by isolating a small quantity of gas in a small pipe between two valves. This requires knowledge of the small volume V_i , and its pressure P_i . Knowing the chamber volume V_c one can calculate the instantaneous pressure rise of the chamber $P_c = (P_i V_i / V_c)$. The RGA sensitivity is found by dividing I_p the peak ion current at $t = 0$ by P_c . The sensitivity is $S' = I_p V_c / (P_i V_i)$. Figure 8.18 illustrates the instantaneous peaks and decay rates of four separate gases. In addition to determining the RGA sensitivity, one can determine the pumping speed for each test gas at the location of the RGA sensor. Since the ion current decays to a value of $1/\epsilon$ in time τ , the system time constant can be determined graphically from a plot like that given in Fig. 8.18. The time required for the ion current to decay to a value of I_p/ϵ can be determined from the semilog plot of $\log I$ versus linear t . Pumping speeds for individual gases are given by $S_i = V_c / \tau_i$. The advantage of this method is that the data are taken on the system and are representative of the system.

8.4 RGA SELECTION

The instrument chosen for residual gas analysis work must be simple, reliable, and have adequate resolution, adequate sensitivity, and mass range. A variety of instruments is available from elementary sector or quadrupole, with an M/z range of 1–50, a Faraday cup detector, and the capability to resolve 1 AMU. Other instruments have M/z ranges up to 800 AMU. The only differences are complexity and cost.

For simple monitoring of background gases in a cycled, unbaked high vacuum chamber, the simplest of instruments with a range of $M/z = 1$ –50 is adequate. With such an instrument, the dominant fixed gases up to $M/z = 44$ and hydrocarbons at $M/z = 39, 41, \text{ and } 43$ may be monitored. Units with Faraday cup detectors and a partial pressure limits of 10^{-8} Pa are commercially available. Most instruments have provisions for alarms to alert the operator when the ion current at a particular M/z value has been exceeded.

More detailed residual gas analysis with a sector or quadrupole requires increased sensitivity and mass range. Partial pressures of 10^{-12} Pa are detectable with an electron multiplier. An M/z range of at least 1–80 is necessary to distinguish most pump oils, but some solvents such as xylene have major peaks in the M/z range 104–106. An M/z range of 1–200 permits identification of many heavy solvents. The ability to detect partial pressures in the 10^{-10} – 10^{-12} Pa range is needed to leak check, to analyze the background of ultrahigh vacuum systems, and do serious semiquantitative analysis. An electron multiplier is necessary for differentially pumped systems. Instruments for these purposes need both Faraday cup and electron multiplier to measure the gain and function over a wide pressure range.

Analysis of gases in medium and low vacuum pressures can be done with either a closed source ionizer or a miniature quadrupole. The spectrum from a closed source instrument can be interpreted in a straightforward manner, whereas miniature quadrupoles operated at high pressure will always produce peaks generated by ion–molecule reactions.

Microprocessor-based instruments offer convenience and ease of storing and manipulating large quantities of data and interpretive displays. The operator convenience and databases are quite useful, but they cannot overcome the influences of instrument design, instrument history, cleanliness, and operating parameter adjustments, in particular they cannot compensate for instabilities caused by electron-stimulated desorption. Ignorance of these effects can seduce the user into believing that the data are representative. Do not accept partial pressure equivalent conversions of ion currents unless the instrument has been calibrated recently for several useful gas mixtures.

REFERENCES

1. J. Dempster, *Phys. Rev.*, **11**, 316 (1918).
2. A. O. C. Nier, *Rev. Sci. Instrum.*, **11**, 212 (1940).
3. F. A. White, *Mass Spectrometry in Science and Technology*, Wiley, New York, 1968, p. 11.
4. A. Nerkin, *J. Vac. Sci. Technol. A*, **9**, 2036 (1992)
5. H. L. Caswell, *J. Appl. Phys.*, **32**, 105 (1961).
6. H. L. Caswell, *J. Appl. Phys.*, **32**, 2641 (1961).
7. H. L. Caswell, *IBM J. Res. Dev.*, **4**, 130 (1960).
8. W. L. Fite, *J. Vac. Sci. Technol.*, **11**, 351 (1974).
9. D. Rapp and P. Englander-Golden, *J. Chem. Phys.*, **43**, 1464 (1965).
10. F. A. White, *Mass Spectrometry in Science and Technology*, Wiley, New York, 1968, p. 13.
11. AeroVac Model 610 Magnetic Sector, AeroVac Products, High Voltage Engineering Corporation, Burlington, MA.
12. G. P. Barnard, *Modern Mass Spectrometry*, The Institute of Physics, London, 1953.
13. A. McDowell, *Mass Spectrometry*, McGraw Hill, New York, 1963.
14. W. Paul and H. Steinwedel, *Zeitschrift für Naturforsch.*, **8A**, 448 (1953).
15. M. Mosharrafa, *Industrial Research/Development*, March 1970, p. 24.
16. P. H. Dawson, Ed., *Quadrupole Mass Spectrometry and Its Applications*, Elsevier, New York, 1976.
17. J. A. Basford, M. D. Boeckman, R. E. Ellefson, A. R. Filippelli, D. H. Holkeboer, L. Lieszkovszky, C. M. Stupak, *J. Vac. Sci. Technol. A*, **11**, A22 (1993).
18. U.S. Patent #3,492,523
19. J. G. Timothy and R. L. Bybee, *Rev. Sci. Instrum.*, **48**, 292 (1977).
20. E. A. Kurz, *Am. Lab.*, March 1979, p. 67.
21. M. G. Inghram and R. J. Hayden, National Academy of Science, National Research Council, Report #14, Washington, D.C., 1954.
22. L. Lieszkovszky and A. Filippelli, *J. Vac. Sci. Technol. A*, **8**, 3838 (1990).
23. S. Kurokouchi, S. Watanabe, and S. Kato, *Vacuum*, **47**, 763 (1996).
24. J. H. Batey, *Vacuum*, **43**, 15 (1992).
25. B. Raby, UTI Technical Note 7301, May 18, 1977.
26. T. W. Hickmott, *J. Vac. Sci. Technol.*, **2**, 257 (1965).
27. T. W. Hickmott, *J. Chem. Phys.*, **32**, 810 (1960).
28. H. Ishimaru, *J. Vac. Sci. Technol. A*, **7**, 2439 (1989).
29. F. Watanabe, *J. Vac. Sci. Technol. A*, **11**, 1620 (1993).
30. G. A. Rozgonyi and J. Sosniak, *Vacuum*, **18**, 1 (1968).
31. N. Müller, *Vacuum*, **44**, 623 (1993).
32. S. Kurokouchi and S. Kato, *J. Vac. Sci. Technol. A*, **19**, 2820 (2001).
33. K. Siefering, H. Berger, and W. Whitlock, *J. Vac. Sci. Technol. A*, **11**, 1593 (1993).
34. R. E. Honig, *J. Appl. Phys.*, **16**, 646 (1945).
35. F. Sharipov and D. Kalempa, *J. Vac. Sci. Technol. A*, **20**, 814 (2002)
36. J. J. Sullivan and R. G. Busser, *J. Vac. Sci. Technol.*, **6**, 103 (1969).
37. J. Visser, *J. Vac. Sci. Technol.*, **10**, 464 (1973).
38. D. H. Holkeboer, T. L. Karndy, F. C. Currier, L. C. Frees, and R. E. Ellefson, *J. Vac. Sci. Technol. A*, **16**, 1157 (1998).
39. B. R. F. Kendall, *J. Vac. Sci. Technol. A*, **5**, 143 (1987).

PROBLEMS

- 8.1 † What are the functions of the ionizer, mass filter, and detector in a residual gas analyzer.
- 8.2 † Can a residual gas analyzer determine the mass of an atom?
- 8.3 † Based on the carbon-12 scale (mass of $^{12}\text{C} = 12.0000$ AMU), verify the M/z ratios for CO^+ , N_2^+ , and C_2H_4^+ given in Fig. 8.1. Use the following precision mass measurements given in reference 3, p. 124: $^1\text{H} = 1.007825$ AMU, $^{14}\text{N} = 14.003074$ AMU, $^{16}\text{O} = 15.994915$ AMU.
- 8.4 What is the resolving power at $M/z = 28$ for the instrument used to record the spectrum shown in Fig. 8.1?
- 8.5 Describe a procedure for measuring the sensitivity of an electron multiplier at $M/z = 28$.
- 8.6 † State two advantages of a Be–Cu multiplier and two advantages of a channel electron multiplier.
- 8.7 A gas at a pressure of 100,000 Pa is to be sampled by an RGA with a maximum operating pressure of 0.001 Pa. An orifice designed by the method of Section 8.2.2 is too small to work. How would you do sample this gas?
- 8.8 Describe how gas sampling with a reducing orifice and a high speed pump affects the analysis of a mixture of argon, nitrogen and hydrogen when pumped independently by (a) an ion pump, (b) a turbomolecular pump, and (c) a diffusion pump. Begin by examining the pressure ratio as described in (8.8).
- 8.9 The calibration data shown in Fig. 8.18 were taken on a system whose volume was 4.0 L. Calculate the pumping speeds for CO_2 , CO , N_2 , and CH_4 .
- 8.10 What complications could result from the use of elastomer gaskets in connecting components of a differentially pumped RGA sampling systems shown in Fig. 8.16 or 8.17?

CHAPTER 9

Interpretation of RGA Data

The method of interpreting mass scans like those depicted in Figs. 8.8, 8.9, and 8.13 is based on detailed knowledge of the cracking or fragmentation patterns of gases and vapors found in the system. After becoming familiar with an RGA, qualitative analysis of many major constituents is rather straightforward, whereas precise quantitative analysis requires careful calibration and complex analysis techniques. This section discusses cracking patterns, some rules of qualitative analysis, and methods of determining the approximate partial pressures of the gases and vapors in the spectrum.

9.1 CRACKING PATTERNS

When molecules of a gas or vapor are struck by electrons whose energy can cause ionization, fragments of several mass-to-charge ratios are created. The mass-to-charge values are unique for each gas species, whereas the peak amplitudes are dependent on the gas and instrumental conditions. This pattern of fragments, called a cracking pattern, forms a fingerprint that may be used for absolute identification of a gas or vapor. The various peaks are primarily created by dissociative ionization, isotopic mass differences, and multiple ionization. In an ionizer operating at pressures greater than 0.1 Pa (10^{-3} Torr), ions and molecules may react to form new ionized radicals.

9.1.1 Dissociative Ionization

The cracking pattern of methane CH_4 , illustrated in Fig. 9.1, shows, in addition to the parent ion CH_4^+ , the electron dissociation of the molecule into lighter fragments, CH_3^+ , CH_2^+ , CH^+ , C^+ , H_2^+ , H^+ . Fragments containing ^{13}C are not shown. Except for H_2^+ , fragments shown in this cracking pattern were produced by dissociative ionization.

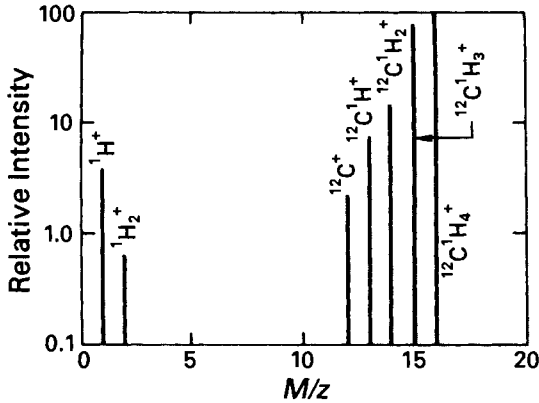


Fig. 9.1 This cracking pattern of methane illustrates the five largest dissociative ionization peaks.

9.1.2 Isotopes

Figure 9.2 illustrates several isotopic peaks in the mass spectrum of singly ionized argon. By comparing the peak heights of the isotopes with the relative isotopic abundance given in Appendix D, we see that this is a spectrum of naturally occurring argon. The relative isotopic peak heights observed on the RGA will generally mirror those given in Appendix D unless the source was enriched, or the sensitivity of the RGA was not constant over the isotopic mass range. Some compressed gas cylinders may contain gas in which a rare component has been selectively removed.

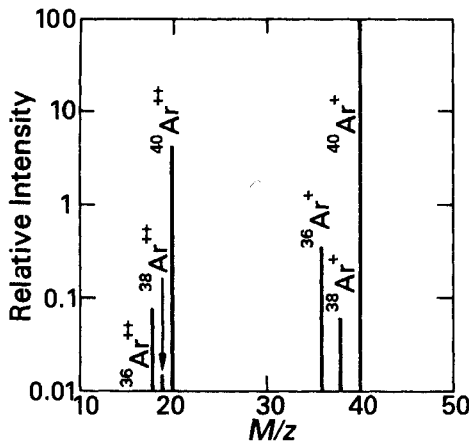


Fig. 9.2 The argon cracking pattern illustrates isotopic mass differences (three isotopes) and two degrees of ionization (single and double).

9.1.3 Multiple Ionization

Higher degrees of ionization are also visible in the argon spectrum. Argon has three isotopes of masses 36, 38, and 40; the doubly ionized peaks Ar^{++} show up at $M/z = 18, 19,$ and 20 . The cracking patterns of heavy metals used in filaments (W, Re, Mo, Ir) may show triply ionized states.

9.1.4 Combined Effects

The cracking pattern of a somewhat more complex molecule CO, given in Appendix E.2, is illustrated in Fig. 9.3 to show the combined effects of isotopes, dissociation, and double ionization. The amplitude of the largest line $^{12}\text{C}^{16}\text{O}^+$ has been normalized to 100, while the amplitude of the weakest line shown, $^{16}\text{O}^{++}$, is 10^6 times smaller. The spectrum, as sketched in Fig. 9.3, can be observed only under carefully controlled laboratory conditions. During normal operation of an RGA the spectrum will be cluttered with other gases and only the four or five most intense peaks will be identifiable as a part of the CO spectrum. Even then, some of the peaks will overlap the cracking patterns of other gases. Under the assumption that

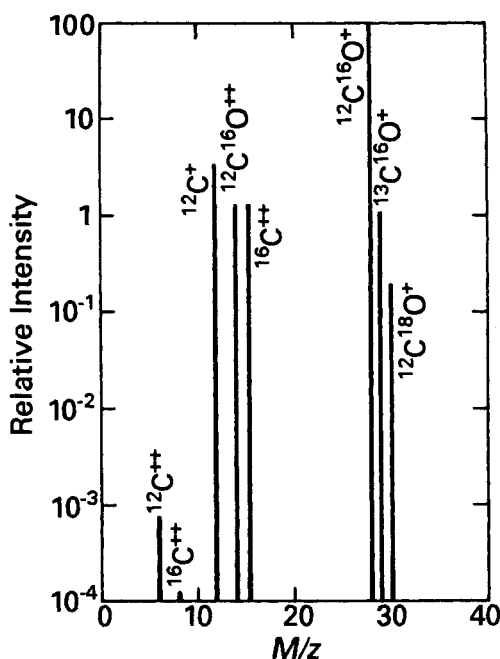


Fig. 9.3 The cracking pattern of CO contains peaks due to dissociative ionization, isotopic ionization, and double ionization.

this clean spectrum has been obtained, it is instructive to classify the eight lines according to their origin. The main peak at $M/z = 28$ is due to the single ionization of the dominant isotope $^{12}\text{C}^{16}\text{O}$. Energetic electrons decompose some of these molecules into two other fragments $^{12}\text{C}^+$, and $^{16}\text{O}^+$. Because carbon has two isotopes and oxygen three, several isotopic combinations are possible. The two most intense lines are $^{13}\text{C}^{16}\text{O}^+$ and $^{12}\text{C}^{18}\text{O}^+$. Isotopic fragments such as $^{13}\text{C}^+$ and $^{18}\text{O}^+$ are too weak to be seen here. Other complexes—for example, $^{12}\text{C}^{16}\text{O}^{++}$ ($M/z = 14$), $^{16}\text{O}^{++}$ ($M/z = 8$), and $^{12}\text{C}^{++}$ ($M/z = 6$)—have high enough concentrations to be seen.

The relative amplitudes of the eight lines of CO are determined by the source gas and instrument. If isotopically pure source gas were used (^{12}C and ^{16}O), only six peaks would be found. Changes in the operating conditions of the instrument also affect the relative peak heights. The ion temperature and electron energy affect the probability of dissociation and the formation of higher ionization states. Dissociation of a molecule into fragments also changes the kinetic energy of the ion fragment. This can be a serious problem in a magnetic sector instrument because the kinetic energy of the ion directly affects the focusing and dispersion of the instrument. Quadrupoles can focus ions with a greater range of initial energies and therefore are less sensitive to transmission losses of fragment ions than sector instruments.

Electron- and ion-stimulated desorption of atoms from surfaces [1,2] can also add to the complexity of the cracking pattern. Oxygen, fluorine, chlorine, sodium, and potassium are some of the atoms that can be released from surfaces by energetic electron bombardment. In a magnetic sector, instrument energetic oxygen or fluorine will often occur at fractional mass numbers of mass $16^{1/3}$ and $19^{1/2}$, respectively [3]. These peaks represent gas phase oxygen and fluorine that dissociated on adsorption, then desorbed from the walls. They occur at fractional mass numbers because they are formed at energies different from those corresponding to the ionized states of free molecules [1] and leave the surface with some kinetic energy [3]. The generation of gases resulting from the decarburization of tungsten filaments can add other spurious peaks to the cracking pattern.

Representative cracking patterns are given in the appendix. Appendixes E.2 and E.3 give the cracking patterns of some common gases and vapors, and Appendix E.4 contains the patterns of frequently encountered solvents. Appendix E.5 describes the patterns of gases used in semiconductor processing and partial cracking patterns of six pump fluids are given in Appendix E.1. The patterns in the appendices are intended to be representative of the substances; they are not unique. It cannot be emphasized too strongly that each pattern is quantitatively meaningful only to those who use the same instrument under identical operating conditions. Nonetheless, there are enough similarities to warrant tabulation.

9.1.5 Ion–Molecule Reactions

At pressures greater than 0.1 Pa (10^{-3} Torr), ion–molecule reactions will be large enough to be detectable. Ion–molecule reactions are visible in miniature quadrupoles operating at high pressure, because gas–gas collisions are linearly proportional to pressure. Ar_2^+ formed by Ar^+ and Ar gas collisions has an abundance of 500 ppm at 1 Pa and is within the operating region of a physical vapor deposition system. A standard RGA typically operates at pressures < 0.01 Pa, so the Ar dimer abundance predicted by the equation in Table 9.1 is only 5 ppm and is not normally observed in the spectrum. Table 9.1 shows representative ion–molecule reactions generated by collisions between of argon, nitrogen and wet or dry air. Spectra from air will yield NO. If oxygen is present, it dominates the reaction with nitrogen to produce NO; however, if water vapor is present instead of O_2 , it will react with nitrogen to produce NO. Charge exchange reactions ($\text{X} + \text{Y}^+ \rightarrow \text{X}^+ + \text{Y}$) can cause the apparent or observed ion ratios to differ from their actual concentration ratios. These and other reaction products can be as large as parts-per-thousand at a pressure of 1 Pa. One should understand that ion-molecule products would be generated in any ionizer operating at high pressure e.g., miniquadrupole, APIMS, standard closed-source ionizer, or micromechanical mass spectrometer.

Table 9.1 Common Ion–Molecule Reactions

<u>Plasma Constituents</u> Ion–Molecule Reaction(s)	Parent Ion	Reaction Product Ion	Reaction/Parent Ratio Pressure Dependence ^a
Argon:			
$\text{Ar}^+ + \text{Ar} \rightarrow \text{Ar}_2^+$	Ar^+	Ar_2^+	$5 \times 10^{-4} P(\text{Ar})$
Dry Nitrogen (300 ppm H_2O):			
$\text{N}_2^+ + \text{N}_2 \rightarrow \text{N}_3^+ + \text{N}$	N_2^+	N_3^+	$8 \times 10^{-4} P(\text{N}_2)$
$\text{N}_2^{++} + \text{H}_2\text{O} \rightarrow \text{NO}^+ + \text{H}_2 + \text{N}$	N_2^{++}	NO^+	$8 \times 10^{-5} P(\text{N}_2)$
Dry Air (400 ppm H_2O):			
$\text{N}_2^+ + \text{O}_2 \rightarrow \text{NO}^+ + \text{NO}$	N_2^+ N_2^{++}	NO^+ N_3^+	$2.1 \times 10^{-3} P(\text{N}_2)$ $5.3 \times 10^{-4} P(\text{N}_2)$
$\text{N}_2^+ + \text{N}_2 \rightarrow \text{N}_3^+ + \text{N}$			
$\text{N}_3^+ + \text{O}_2 \rightarrow \text{NO}^+ + \text{O} + \text{N}_2$			
$\quad \quad \quad \rightarrow \text{NO}_2^+ + \text{N}_2$			
$\text{N}_2^{++} + \text{H}_2\text{O} \rightarrow \text{NO}^+ + \text{H}_2 + \text{N}$			
Wet Air (2.7% H_2O):			
(same reactions as above for dry air)	N_2^+ N_2^{++}	NO^+ N_3^+	$2.2 \times 10^{-3} P(\text{N}_2)$ $5.1 \times 10^{-4} P(\text{N}_2)$

Source. Reprinted with permission from INFICON, Inc., 2 Technology Place, East Syracuse, NY 13057.

^a As taken on an INFICON Transceptor XPR2 miniature quadrupole mass spectrometer.

9.2 QUALITATIVE ANALYSIS

Perhaps the most important aspect of the analysis of spectra for the typical user of an RGA is qualitative analysis; that is, the determination of the types of gas and vapor in the vacuum system. In many cases the existence of a particular molecule points the way to fixing a leak or correcting a process step. The quantitative value or partial pressure of the molecular species in question usually does not need to be known because industrial process control is frequently done empirically. The level of a contaminant—for example, water vapor, which will cause the process to fail—is determined experimentally by monitoring the quality of the product. An inexpensive RGA tuned to the mass of the offending vapor is then used to indicate when the vapor has exceeded a predetermined partial pressure. With experience many gases, vapors, residues of cleaning solvents, and traces of pumping fluids will be recognizable without much difficulty.

The mass spectra shown in Figs. 8.8, 8.9, and 8.13 contain considerable information about the present condition as well as the history of the systems on which they were recorded. To help in their interpretation examine the hypothetical spectrum in Fig 9.4, which was constructed from five gases H_2O , N_2 , CO , O_2 , and CO_2 in the ratio (20:4:4:1:1) from the cracking patterns in Appendixes E.2 and E.3. Let us study this pattern under the assumption that its origin and composition are not known. Examination of the cracking patterns of common gases, like those tabulated in Appendixes E.2 and E.3, quickly verifies the presence of carbon dioxide, oxygen, and water vapor. Notice that the mass 32 peak is not due to the dissociation of carbon dioxide. The presence of oxygen at 32 AMU usually indicates an air leak unless it is being intentionally introduced. Analysis of the mass 28 peak is not so clear. Some of this peak is certainly due to the dissociation of CO_2 ; however, if we assume that the sensitivity of the instrument is reasonably constant over the mass range in question, that contribution cannot be very great. The majority of the peak amplitude would then be attributable to N_2 or CO or both. To distinguish these gases further the amplitudes of the peaks at $M/z = 16$ (O^+), $M/z = 14$ (N^+ , N_2^{++} , CO^+), and $M/z = 12$ (C^+) are examined. In practice it is difficult to conclude much from the presence of carbon because it originates from so many sources, both organic and inorganic. The $M/z = 14$ peak is largely due to N^+ . Therefore, nitrogen is present. Analysis of the $M/z = 16$ peak is complicated by the fact that there are other sources of atomic oxygen beside CO , namely O_2 and CO_2 , as well as electron-stimulated desorption of O^+ from the walls. Oxygen desorption is a common phenomenon. Referring to the cracking pattern tables, we see that the $M/z = 16$ peak looks too large to be accounted for totally by the dissociation of CO_2 and O_2 . The $M/z = 14$ peak looks too small to be only a fragment of nitrogen.

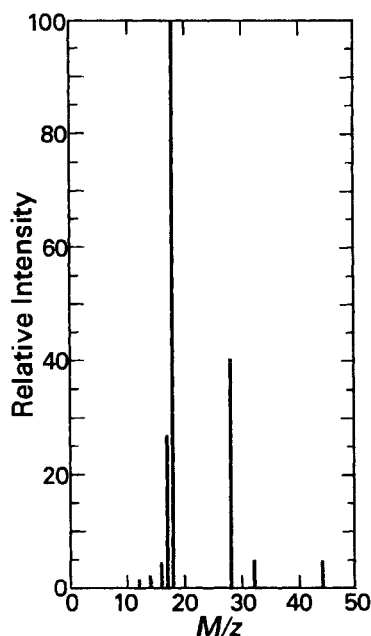


Fig. 9.4 Background spectrum constructed from a (20:4:4:1:1) mixture of H_2O , N_2 , CO , O_2 , and CO_2 .

We then conclude that both nitrogen and carbon monoxide are present but in undetermined amounts.

After some familiarity with the combined effects of these common background gases, they should be easily identifiable in the spectra shown in Figs. 8.8, 8.9, and 8.13. The large peaks 32, 28, and 14 AMU seen in Fig. 8.8 are an indication of an air leak. The fact that water vapor is the dominant gas load in an unbaked vacuum system is verified by the large 18 AMU peak shown in Figs. 8.8 and 8.13. These spectra also show fragments that are characteristic of organic compounds as well as fixed gases. One way to determine the nature of the organic in the system qualitatively is to become familiar with the cracking patterns of commonly used solvents, pump fluids, and elastomers.

The cracking patterns of several solvents are listed in Appendix E.4. A common characteristic of organic molecules is their high probability of fragmentation in a 70-eV ionizer. It is so great that the parent peak is rarely the most intense peak in the spectrum. The lighter solvents such as ethanol, isopropyl, and acetone have fragment peaks bracketing nitrogen and carbon monoxide at $M/z = 27$ and 29 , but each has a prominent peak at a different mass number. Methanol and ethanol each have a major fragment at $M/z = 31$; they can be distinguished by the methanol's absence of a fragment at

$M/z = 27$. Solvents that contain fluorine or chlorine have characteristic fragments at $M/z = 19, 20$ and $35, 36, 37, 38$, respectively. The extra fragments at $M/z = 20$ (HF) and $35-38$ (HCl) seem to be present, whether or not the solvent contains hydrogen. Fragments due to CF, CCl, CF₂, and CCl₂ are also characteristic of these compounds. As with all fragments, their relative amplitudes will vary with instrumental conditions. The fragments at $M/z = 27, 29, 31, 41$, and 43 are prominent in these solvents. They are also common fragments of many pump fluids, which further complicates the interpretation of a spectrum.

Appendix E.1 lists the partial cracking patterns of six common pump fluids. All the fragment peaks up to mass number 135 are tabulated. For the sector instrument the largest peak (100%) often occurs at a higher mass number and therefore is not shown. The complete spectra of the four fluids, which were taken on the sector instrument, were tabulated by Wood and Roenigk [4]. Most organic pump fluid molecules are quite heavy and the parent peaks are not often seen in the system because only the lighter fragments backstream through a properly operated trap. Saturated straight-chain hydrocarbon oils are characterized by groups of fragment peaks centered 14 mass units apart and coincide with the number of carbon atoms in the chain. Figure 9.1 shows the fragment peaks for group C₁ in the mass range 12 to 16. Higher carbon groups have similar characteristic arrangements; C₂ ($M/z = 24-30$), C₃ ($M/z = 36-44$), C₄ ($M/z = 48-58$), C₅ ($M/z = 60-72$), and so on. The spectrum of Apiezon BW diffusion pump oil taken by Craig & Harden [5], shown in Fig. 9.5, illustrates these

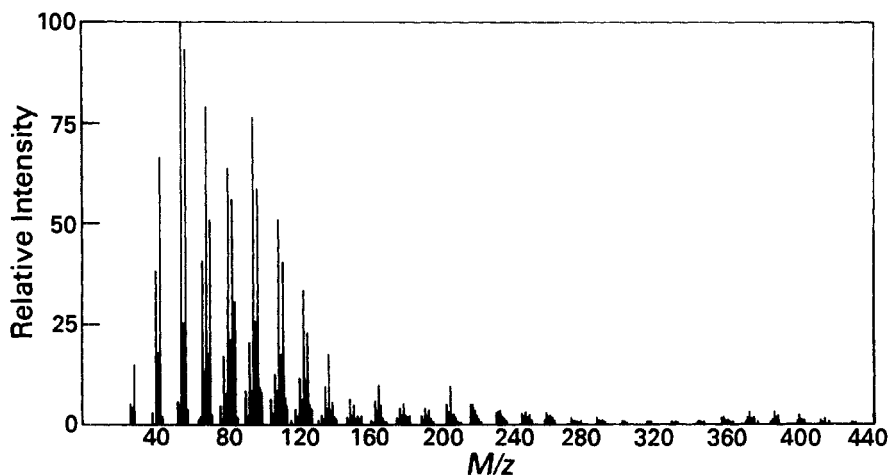


Fig. 9.5 Mass spectrum of Apiezon BW oil (obtained using MS9 sector spectrometer), source temperature 170°C. Reprinted with permission from *Vacuum*, 16, 67, R. D. Craig and E. H. Harden. Copyright 1966, Pergamon Press, Ltd.

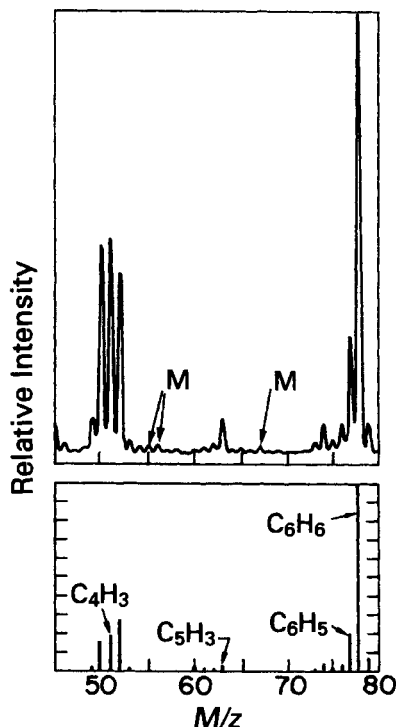


Fig. 9.6 Comparison of residual gas background in a system contaminated with DC-705 fluid (top) and (b) cracking pattern of benzene (bottom).

fragment clusters. In most hydrocarbon oils the fragments at $M/z = 39, 41, 43, 55, 57, 67,$ and 69 are notably stable and their presence is a guarantee of hydrocarbon contamination. These odd-numbered peaks, which are more intense than the even-numbered peaks in straight-chain hydrocarbons, clearly stand out in the scans shown in Figs. 8.8 and 8.9. Some traces of mechanical pump oil are seen in Fig. 8.13. Hydrocarbon oils are used in most rotary mechanical pumps, except those for pumping oxygen or corrosive gases, and in many diffusion pumps. Hydrocarbon diffusion pump oils are not resistant to oxidation and will decompose when exposed to air while heated. Their continued popularity for certain applications is due to their low cost.

Silicones are an important class of diffusion pump fluids. They have very low vapor pressures and also have extremely high oxidation resistance [6]. Cracking patterns for Dow Corning DC-704 and DC-705, given in Appendix E.1, show many of the characteristic fragments of benzene. By way of illustration, a partial spectrum taken in a contaminated diffusion pumped system using DC-705 fluid is compared with the cracking pattern

of benzene in Fig. 9.6. The peaks labeled M are due to mechanical pump oil. Systems that have been contaminated with a silicone pump fluid will always show the characteristic groups at $M/z = 77$ and 78 and usually those at $M/z = 50, 51$, and 52 . Notice the lack of these peaks in Fig 8.8, which was taken on a system with a straight chain hydrocarbon oil in the diffusion pump. Wood and Roenigk [4] observed fragments of DC-705 at $M/z = 28, 32, 40$, and 44 , all of which could naturally occur in a vacuum system. These peaks are due to dissolved gas.

Esters and polyphenylethers are also widely used pump fluids because they polymerize to form conducting layers. They find use in systems that contain mass analyzers, glow discharges, and electron beams. Octoil-S is characterized by its repeated C_mH_n groupings. Polyphenylether (Santovac 5, Convalex-10, and BL-10) also contains the characteristic fragments of the phenyl group which include the fragments at $M/z = 39, 41, 43, 44$, and 64 . Cracking patterns will vary greatly from one instrument to another and the inability to match the data exactly to the patterns in any table should not be considered evidence of the absence or existence of a particular pumping fluid in the vacuum system. In fact, the cracking pattern for DC-705 given in Appendix E.1 does not show the same relative intensities at $M/z = 50, 51, 52$, and 78 , as shown in Fig. 9.6a or seen by other workers. The spectrum taken from a gently heated liquid pump fluid source contains proportionally more high mass decomposition products than the spectrum of backstreamed vapors from a trapped diffusion pump because the trap is effective in retaining high molecular weight fragments. See Section 11.4. A liquid nitrogen trap is a mass-selective filter. These patterns cannot be used to differentiate between backstreamed DC-704 and DC-705. High-mass ion currents are severely attenuated when a quadrupole instrument is operated at constant absolute resolution. This built-in attenuation, sketched in Fig. 8.12, can easily lead to the conclusion that the environment is free of heavy molecules.

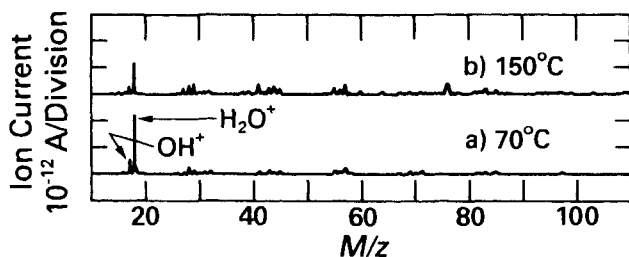


Fig. 9.7 Mass spectra obtained during the heating of Buna-N rubber. Reprinted with permission from *Trans. 7th Natl. Vacuum Symp.* (1960), p. 39, R. R. Addis, L. Pensak, and N. J. Scott. Copyright 1961, Pergamon Press, Ltd.

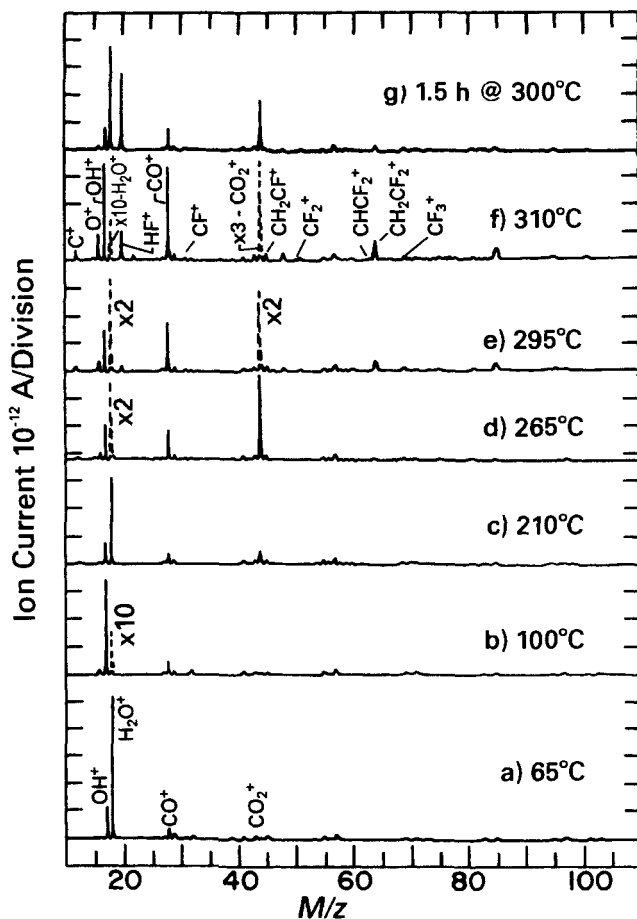


Fig. 9.8 Mass spectra obtained during the heating of Viton fluoro-elastomer. Reprinted with permission from *Trans 7th Natl. Vacuum Symp.* (1960), p. 39, R. R. Addis, L. Pensak, and N. J. Scott. Copyright 1961, Pergamon Press, Ltd.

Elastomers are found in all systems with demountable joints except those using metal gaskets. The most notable property of all elastomers is their ability to hold gas and release it when heated or squeezed. The mass spectrum of Buna-n is shown in Fig. 9.7 during heating [7]. Also shown is the initial desorption of water followed by the dissociation of the compound at a higher temperature. The decomposition temperature is quite dependent on the material. Mass spectra obtained during the heating of Viton fluoroelastomer, depicted in Fig. 9.8, show the characteristic release of water at low temperatures and the release of carbon monoxide and carbon dioxide at higher temperatures. At a temperature of 300°C the

Viton begins to decompose. Silicone rubbers have a polysiloxane structure. They are permeable, and their mass spectra usually show a large evolution of H_2O , CO , and CO_2 . At high temperatures they begin to decompose. Their spectra show groups of peaks at $\text{Si}(\text{CH}_3)_n$, $\text{Si}_2\text{O}(\text{CH}_3)_n$, and $\text{Si}_3\text{O}_2(\text{CH}_3)_n$; $n = 3, 5, 6$, respectively, are the largest [8]. Polytetrafluoroethylene (Teflon) is suitable for use up to 300°C , although it outgasses considerably. A spectrum taken at 360°C shows major fragments at $M/z = 31$ (CF), 50 (CF_2), 81 (C_2F_3), and 100 (C_2F_4) [8].

The potential limits of qualitative analysis become clear after some practice with an RGA. Knowledge of the instrument, the cleaning solvents, and the pumping fluids used in mechanical, diffusion, or turbomolecular pumps combined with periodic background scans will result in the effective use of the RGA in the solution of equipment and process problems.

9.3 QUANTITATIVE ANALYSIS

The RGA is not intended to be an analytical instrument. It cannot eliminate overlapping peaks, nor is it as stable as an analytical spectrometer. Quantitative analysis of a single gas or vapor or combination of gases and vapors with unique cracking patterns is a simpler task than the analysis of combinations that contain overlapping peaks. This section demonstrates approximation techniques for quickly obtaining quantitative partial pressures within a factor of 10 but points out that the acquisition of data accurate to, say, 10% requires careful calibration. Either crude data are obtained quickly or accurate data are obtained painstakingly—there is little middle ground. Let us consider techniques, both approximate and reasonably precise, for gases with isolated and overlapping cracking patterns.

9.3.1 Isolated Spectra

Approximate analysis techniques for gases with isolated spectra will yield results of rough accuracy with minimal effort. For example, a mixture of Ar , O_2 , N_2 , and H_2O would be reasonably easy to examine, because of unique peaks at $M/z = 40, 32, 28$, and 18 . An approximate measure of the partial pressures can be obtained by summing the heights of all peaks of significant amplitude that are caused by these gases, followed by the division of that number into the total pressure. The resulting sensitivity factor, expressed in units of pressure per unit scale division, is then applied to all the peaks without further correction. Some improvement in accuracy can be made if the ion currents are first corrected for the ionizer sensitivity by dividing by the values given in Table 8.1. There is an alternative

technique that is equally accurate and does not require the knowledge of the total pressure. It relates the partial pressure of a given gas to the ion current, sensitivity of the mass analyzer, and gain of the electron multiplier according to (9.1).

$$P(x) = \frac{\text{total ion current}(x)}{GS(N_2)} \quad \blacktriangleright (9.1)$$

The sensitivity is usually provided by the manufacturer for nitrogen and is typically of the order of 10^{-5} A/Pa. By taking the ratio of electron multiplier current to the Faraday cup current we can determine the gain G of the multiplier. From this information the partial pressure of the gas is obtained. These two techniques are accurate to within a factor of five.

A more accurate correction accounts for the gas ionization sensitivity and the mass dependencies of the multiplier gain and mass filter transmission. The mass dependence of the multiplier is often approximated as $M^{1/2}$, but this is not always valid. The transmission of a fixed radius sector with variable magnetic field is independent of mass, but the most common RGA, the quadrupole, has a transmission that is dependent on the energy, focus, and resolution settings. The more accurate correction may turn out to be less accurate unless a significant amount of calibration is done to obtain the mass dependence of the mass filter and electron multiplier accurately. The time spent in applying corrections is probably out of proportion to the information gained.

Accurate measurements of the partial pressures of gases with nonoverlapping spectra are best accomplished by calibrating the system for each gas of interest. The vacuum system must be thoroughly clean and baked if possible before the background spectrum is recorded. It is then backfilled with gas to a suitable pressure so that the cracking pattern can be recorded and the gas sensitivity, measured. The values of all the ionizer potentials and currents, the gain of the electron multiplier, and the pressure should be recorded at that time. The system should be thoroughly pumped and cleaned between each successive background scan and gas admission. Calibration procedures are discussed in Section 8.3. Calibration is a laborious process and is only done when precise knowledge of the partial pressure of a particular species is required. Even then a periodic check of the multiplier gain—for example at $M/z = 28$ —remains necessary.

9.3.2 Overlapping Spectra

Analysis of overlapping spectra is made more difficult by the fact that the peak ratios for a given gas may not be stable with time because of electron multiplier contamination and because trace contaminants in the system will

add unknown amounts to the minor peaks of gases under study. To gain an appreciation of the problems involved in determining partial pressures, two simplified numerical examples are solved here.

Consider a mass spectrum taken on a system that contains peaks mainly attributable to N_2 and CO. Peaks due to nitrogen appear at $M/z = 28$ and 14. Peaks due to CO appear at $M/z = 28$, 16, 14, and 12. Trace amounts of carbon present in the system from other sources dictate that the amplitude of the $M/z = 12$ peak cannot be relied on for accurate determination of the CO concentration. In a similar manner the $M/z = 16$ peak is of questionable value because of the surface desorption of atomic oxygen, methane, or other hydrocarbon contamination. Therefore the analysis in this simplified example is weighted heavily in favor of using the peaks at $M/z = 14$ and 28. From cleanly determined experimental cracking patterns the relative peak heights for nitrogen were found to be 0.09 and 1.00 for $M/z = 14$ and 28, respectively. Values of 0.0154 and 1.10 were measured at the same locations for CO. (The CO cracking patterns have been corrected for the difference in ionizer sensitivity; see Table 8.1). The sensitivity and multiplier gain of the instrument were $S = 10^{-5}$ A/Pa and $G = 10^5$. From the mass spectrum the ion currents were $i_{14} = 10.54 \mu\text{A}$, and $i_{28} = 210 \mu\text{A}$. The individual partial pressures were then found by solving the following two equations simultaneously:

$$\begin{aligned} i_{28} &= SG[a_{11}P(N_2) + a_{12}P(\text{CO})] \\ i_{14} &= SG[a_{21}P(N_2) + a_{22}P(\text{CO})] \end{aligned} \quad (9.2)$$

or

$$\begin{aligned} 210 \mu\text{A} &= 1 \text{ A/Pa}[1.00 \times P(N_2) + 1.10 \times P(\text{CO})] \\ 10.54 \mu\text{A} &= 1 \text{ A/Pa}[0.09 \times P(N_2) + 0.0154 \times P(\text{CO})] \end{aligned}$$

which yielded $P(N_2) = P(\text{CO}) = 10^{-4}$ Pa.

Now consider how a change unaccounted for in the cracking pattern would affect the accuracy of this calculation. The actual cracking pattern of nitrogen, and consequently the measured ion currents, could have changed without the knowledge of the operator, because of contamination in the first dynode or a change in the temperature of the ion source. If this had happened, an error would have been introduced into the calculation, because the coefficients a_{mn} in the right-hand side of (9.2) were not altered simultaneously. Figure 9.9a shows the calculated values of $P(N_2)$ and $P(\text{CO})$ that would be obtained for the example in (9.2) if the actual $M/z = 14$ fragment of nitrogen were changed from 9 to 5% of the $M/z = 28$ peak without our knowledge and therefore without our having made the corresponding change in the coefficient a_{21} . It can be seen that even with moderate changes in the cracking pattern the partial pressures of the two gases can still be determined within 25% for this example in which the N_2

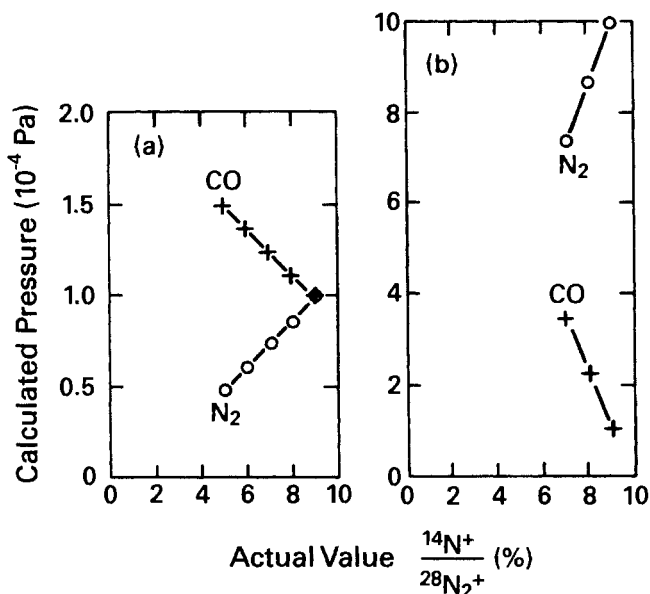


Fig. 9.9 Errors induced in the calculation of pressures of mixtures of N_2 and CO resulting from physical changes in the dissociation of nitrogen (the ratio of ^{14}N to $^{14}\text{N}_2$) which were not compensated for by appropriate changes in the coefficient a_{21} of the nitrogen cracking pattern. (a) 1:1 mixture of N_2 to CO , (b) 10:1 mixture of N_2 to CO .

and CO are present in equal amounts. If greater accuracy is desired, the cracking pattern of the gases should be taken frequently and the coefficients a_{mn} adjusted to account for these instrumental changes.

For unequal concentrations of the two gases the errors are far greater than when the gases are present in equal proportions. Figure 9.9b illustrates the pressure measurement error as a function of the cracking pattern change for a 10:1 ratio of N_2 : CO . Again, this represents an actual change in cracking pattern which was not accounted for by a corresponding change in the coefficient a_{21} . This demonstrates that even modest changes in the cracking pattern ratios of the major constituent can cause the error in partial pressure calculation of the minor constituent to be as great as 200% to 400% when the major and minor constituents have overlapping cracking patterns.

These two illustrations demonstrate that quantitative analysis of overlapping spectra requires accurate and often, frequent measurements of the cracking patterns and that accurate quantitative measurements of trace gases are difficult when the trace gas peaks overlap those of a major constituent.

The effects of certain cracking pattern errors in a residual gas spectrum have been illustrated by Dobrozemsky [9]. These data taken on an Orb-Ion pumped system are presented in Table 9.1. Column 1 shows the correctly analyzed partial pressures and their standard deviations, Column 2 and 3, respectively, show the effects of incorrectly interchanging the peaks at $M/z = 17$ and 18, and the effects of doubling the peak height at $M/z = 14$. Dobrozemsky's analysis demonstrates vividly the effects of cracking pattern errors in the accuracy of calculating trace gas compositions. Column 1, the correct analysis, shows a standard deviation for H_2O of 0.3%, while for a trace gas such as hydrogen the standard deviations is large enough to render the measurement useless. The standard deviation for hydrogen is large, because the signal at $M/z = 2$ arises from many sources. Literally any hydrocarbon that is ionized in the RGA has a fragment at $M/z = 2$ and the standard deviation of each fragment is additive. The result is that the hydrogen concentration, if any, is not known. It demonstrates the ease with which false data can be generated when cracking patterns are not accurately known. Note also that the incorrect analyses, shown in Column 2 and Column 3 of Table 9.2, yield unreasonably large standard deviations for all gases even when only one ion current was in error.

Even though only a limited number of low molecular weight gases are present in a vacuum system, the analysis procedure is complicated by the fact that there are often several gases that produce peaks at the same M/z values. For example, CO , N_2 , C_2H_4 , and CO_2 produce ion current at $M/z = 28$ and CO_2 , O_2 , CH_4 , and H_2O produce ion currents at $M/z = 16$. For a system containing n gases and m ion current peaks, (9.2) becomes

$$\begin{bmatrix} i_1 \\ i_2 \\ \bullet \\ i_m \end{bmatrix} = \begin{bmatrix} a_{11} & \bullet & \bullet & a_{1n} \\ a_{12} & \bullet & \bullet & a_{2n} \\ \bullet & \bullet & \bullet & \bullet \\ a_{m1} & \bullet & \bullet & a_{mn} \end{bmatrix} \begin{bmatrix} P_1 \\ P_2 \\ \bullet \\ P_n \end{bmatrix} \quad (9.3)$$

where i_m is the ion current at mass m , a_{mn} are the components of the cracking pattern matrix, and P_n is the partial pressure of the n^{th} gas. Most gases have more than one peak, so that $m > n$, and the system is over-specified. Least mean squares or some other smoothing criterion is then applied to the data to get the best fit. If the cracking patterns are carefully taken and if the standard deviations are measured as well, then accuracy of a few percent may be obtained for major constituents [9,10]. The matrix for a real problem would contain about 10×50 elements and would require the assistance of a computer in order to obtain a solution. In this case careful data acquisition, instrument control, and analysis are required [10].

Table 9.2 Analysis of Background Gases in an Orb-Ion Pumped System^a

Partial Pressures $\times 10^{-8}$ Torr			
Gas	1	2	3
H ₂	2.21 \pm 3.15	2.85 \pm 8.29	2.07 \pm 2.67
He	15.54 \pm 0.62	14.95 \pm 22.6	14.94 \pm 7.2
CH ₄	5.37 \pm 0.49	-13.50 \pm 5.13	9.64 \pm 1.63
NH ₃	2.64 \pm 0.89	49.56 \pm 6.83	5.03 \pm 2.17
H ₂ O	50.95 \pm 0.15	15.40 \pm 5.29	48.44 \pm 1.68
Ne	4.54 \pm 0.54	4.39 \pm 16.5	4.38 \pm 5.24
N ₂	-1.99 \pm 3.26	34.88 \pm 57.6	-13.60 \pm 18.3
CO	4.54 \pm 2.91	-30.70 \pm 51.4	15.38 \pm 16.4
C ₂ H ₆	3.42 \pm 0.74	8.44 \pm 18.4	1.89 \pm 5.84
O ₂	0.00 \pm 0.13	-0.99 \pm 4.87	0.30 \pm 1.55
Cl	-0.02 \pm 0.12	0.04 \pm 4.64	0.02 \pm 1.48
Ar	1.36 \pm 0.09	1.29 \pm 3.29	1.31 \pm 1.04
CO ₂	5.67 \pm 0.14	5.30 \pm 3.22	5.50 \pm 1.02
C ₃ H ₈	2.72 \pm 0.56	0.27 \pm 12.9	3.32 \pm 4.11
Acetone	2.99 \pm 0.31	7.94 \pm 6.91	1.33 \pm 2.2

Source. Reprinted with permission from *J. Vac. Sci. Technol.*, **9**, p. 220, R. Dobrozemsky. Copyright 1972, The American Vacuum Society.

^a The total pressure is 1.3×10^{-7} Torr. Column (1): Correct analysis. Column (2): Incorrect spectrum obtained by interchanging ion currents at mass numbers 17 and 18; Column (3): Incorrect spectrum obtained by doubling the ion current at mass number 14.

These experiments are expensive and time consuming and are only performed in situations where such precision is required. Beware of instruments that directly convert ion currents to partial pressures and generate graphical displays. Cleanliness, sensitivity, pressure, and gas mixture each affect cracking patterns. Simple algorithms cannot accurately determine pressure. One must run test mixtures of representative gases.

REFERENCES

1. P. Marmet and J. D. Morrison, *J. Chem. Phys.*, **36**, 1238 (1962).
2. P. A. Redhead, *Can. J. Phys.*, **42**, 886 (1964).
3. J. L. Robins, *Can. J. Phys.*, **41**, 1383 (1963).
4. G. M. Wood, Jr. and R. J. Roenigk Jr., *J. Vac. Sci. Technol.*, **6**, 871 (1969).
5. R. D. Craig and E. H. Harden, *Vacuum*, **16**, 67 (1966).
6. C. W. Solbrig and W. E. Jamison, *J. Vac. Sci. Technol.*, **2**, 228 (1965).
7. R. R. Addis, Jr., L. Pensak, and N. J. Scott, *Trans. 7th A.V.S. Natl. Vacuum Symp.* 1960, Pergamon, Oxford, 1961, p. 39.
8. H. Beck, *Handbook of Vacuum Physics*, Vol. 3, Macmillan, New York, 1964, p. 243.

9. R. Dobrozemsky, *J. Vac. Sci. Technol.*, **9**, 220 (1972).
10. D. L. Ramondi, H. F. Winters, P. M. Grant, and D. C. Clarke, *IBM J. Res. Dev.*, **15**, 307 (1971).

PROBLEMS

- 9.1 † Define dissociative ionization, multiple ionization, and isotopic ionization.
- 9.2 Examine the cracking pattern of CO_2 given in Appendix E.2. List the mass to charge ratios resulting from (a) dissociative ionization, (b) multiple ionization, and (c) isotopes.
- 9.3 Give an example of a peak in a mass spectrum, which might be caused by (a) atomic attachment and (b) dissociation-recombination.
- 9.4 The charge-to-mass ratio of a singly ionized benzene molecule is 78. A small peak at $M/z = 79$ is observed. What is the origin of this peak and what is the ratio of the two peak heights?
- 9.5 Mass scans shown in Fig. 9.10a and 9.10b were taken on the same system on adjacent days after, each time, reaching a base pressure. Describe the difference in the condition of the two systems.

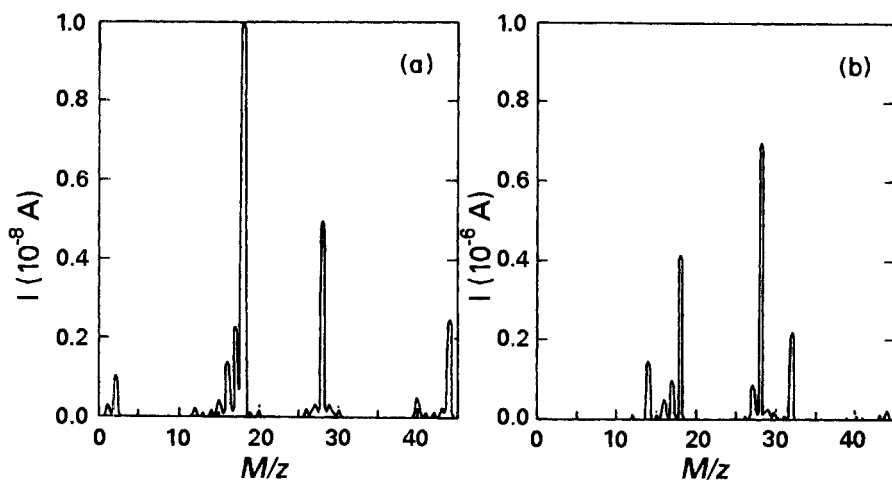


Fig. 9.10 Mass spectra of a baked, diffusion pumped vacuum system. (a) First scan, taken while the system was performing properly. (b) Second scan, taken after a performance problem was observed. Note the relative vertical axes in the two figures.

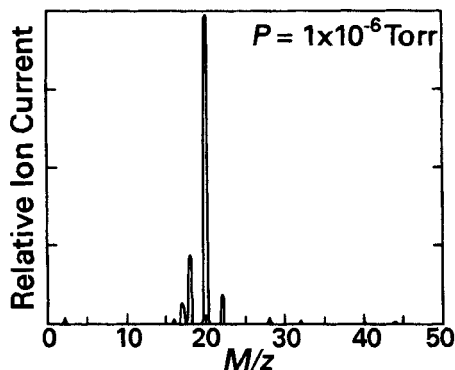


Fig. 9.11 Mass spectrum of a vacuum system containing an unidentified material.

- 9.6 † Identify the gas whose spectrum is given in Fig. 9.11, above.
- 9.7 In an ion beam system, which uses large amounts of argon, what will interfere with analyzing for trace amounts of water vapor?
- 9.8 What is the effect of operating an ion gauge near to a residual gas analyzer in the presence of (a) hydrogen, (b) argon, and (c) nitrogen?
- 9.9 Examine the spectrum in Fig. 9.12. What is this complex molecule that is frequently used to maintain vacuum system interiors?

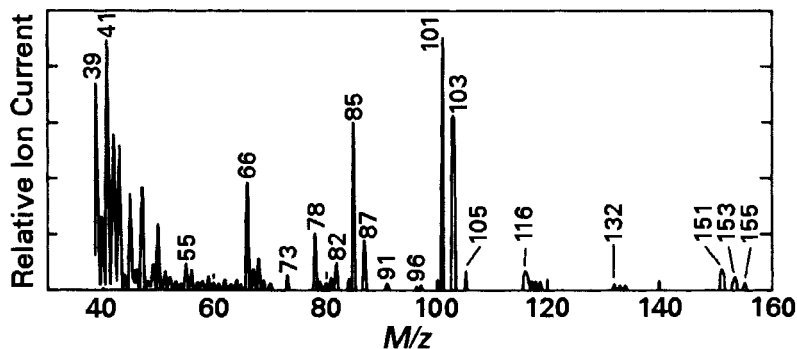


Fig. 9.12 Mass spectrum of compound for Problem 9.9.

- 9.10 The spectrum in Fig. 9.13 was taken on an diffusion pumped system that used DC-705 silicone oil in the diffusion pump. Can you identify which peaks resulted from the diffusion pump fluid? Is there any evidence of mechanical pump oil contamination in this spectrum? On what evidence is your conclusion based?

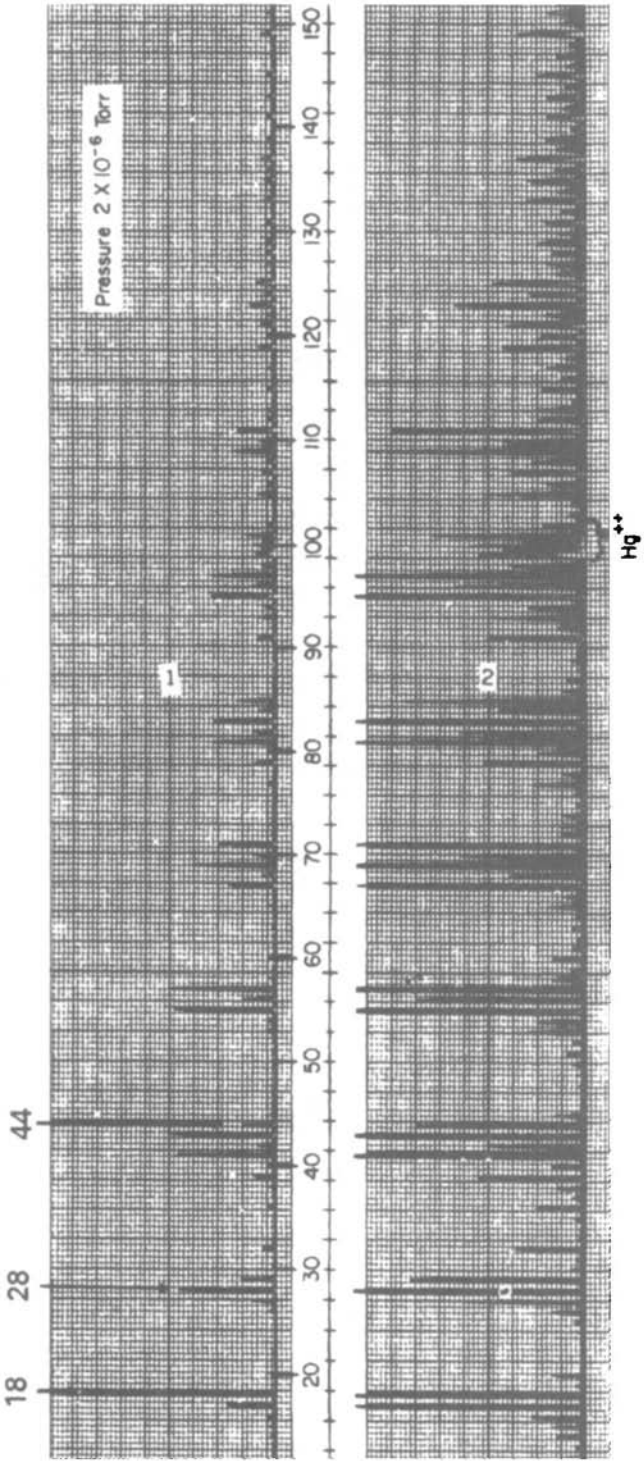


Fig. 9.13 Background spectrum from an oil diffusion pumped system. Reprinted with permission from *J. Vac. Sci. Technol.*, **11**, p. 351. W. L. Fite and P. Irving. Copyright 1974, AVS-The Science and Technology Society.

CHAPTER 10

Mechanical Pumps

In this chapter we review the operation of five low vacuum pumps (the rotary vane and piston, scroll, screw and diaphragm pump), and two medium vacuum pumps (the lobe or Roots pump and the claw pump). Vane and piston pumps are widely used for backing high vacuum pumps and for initial chamber evacuation. Lobe blowers are used with piston or vane pumps to rough large systems, to back large pumps, and to pump large quantities of gas in plasma processing systems. Screw, scroll, and diaphragm pumps are used in oil-free applications, and the claw pump is particularly well suited for pumping particulate-laden atmospheres.

10.1 ROTARY VANE PUMP

The rotary piston pump and the rotary vane pump are two oil-sealed pumps commercially available for pumping gas in the pressure range of $1\text{--}10^5$ Pa. Of the two, the rotary vane is the most commonly used in small to medium-sized vacuum systems. Rotary vane pumps of $10\text{--}200$ m³/h displacement are used for rough pumping and for backing diffusion or turbomolecular pumps.

In a rotary vane pump (Fig. 10.1), gas enters the suction chamber (A) and is compressed by the rotor (3) and vane (5) in region B and expelled to the atmosphere through the discharge valve (8) and the fluid above the valve. An airtight seal is made by one or more spring or centrifugally loaded vanes and the closely spaced sealing surfaces (10). The vanes and the surfaces between the rotor and housing are sealed by the low vapor-pressure fluid, which also serves to lubricate the pump and fill the volume above the discharge valve. Pumps that use a speed-reduction pulley operate in the 400–600 rpm range, whereas direct drive pumps operate at speeds of 1500–1725 rpm. The fluid temperature is considerably higher in the direct drive pumps than in the low-speed pumps, typically 80°C and 60°C, respectively. These values will vary with the viscosity of the fluid and the quantity of air being pumped.

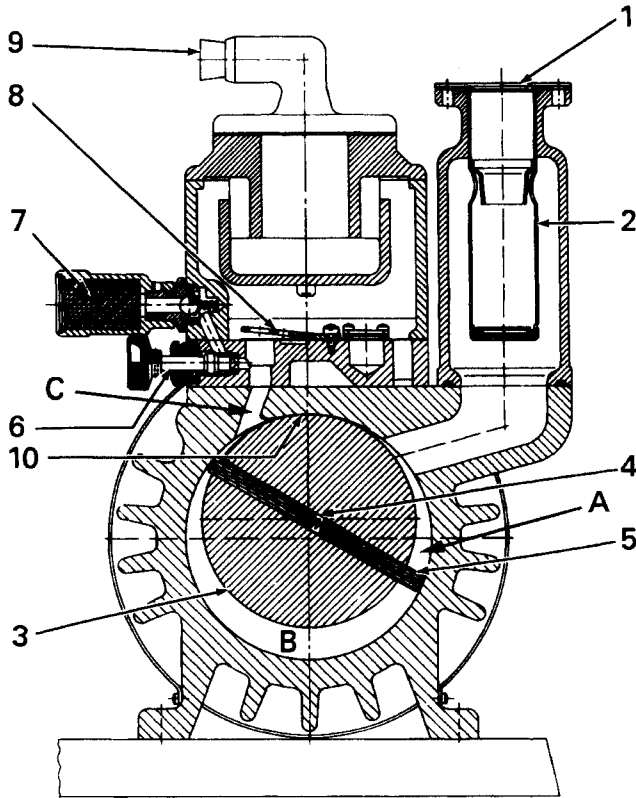


Fig. 10.1 Sectional view of the Pfeiffer DUO-35, 35 m³/h double-stage, rotary vane pump: (1) intake, (2) filter, (3) rotor, (4) spring, (5) vane, (6) gas ballast valve, (7) filter, (8) discharge valve, (9) exhaust, (10) sealing surface. Reprinted with permission from A. Pfeiffer Vakuumtechnik, GmbH, Wetzlar, Germany.

Single-stage pumps consist of one rotor and stator block (Fig. 10.1). If a second stage is added as shown schematically in Fig. 10.2, by connecting the exhaust of the first stage to the intake of the second, lower pressures may be reached. The ultimate pressure at the inlet of the second stage is lower than at the inlet to the first because the fluid circulating in the second stage is rather isolated from that circulating in the second stage. The fluid in the second stage contains less gas than the fluid in the reservoir. Physically, the second pumping stage is located adjacent to the first and on the same shaft. The pumping speed characteristics of single-stage and two-stage rotary vane pumps are shown in Fig. 10.3. The free-air displacement and the ultimate pressure are two measures of the performance of roughing pumps. The free air displacement is the volume of air displaced per unit time by the pump at atmospheric pressure with no pressure differential. For

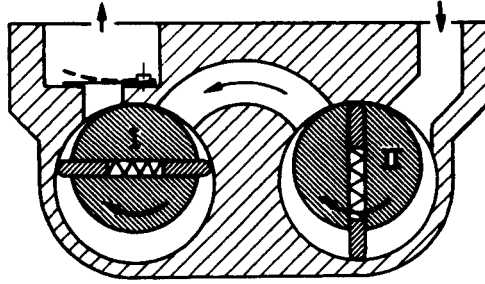


Fig. 10.2 Schematic section through a two-stage rotary pump. Reprinted with permission from *Vacuum Technology*, Leybold-Heraeus, GmbH, Köln, Germany.

the two pumps whose pumping speed curves are shown in Fig. 10.3, this has the value of $30 \text{ m}^3/\text{h}$ (17.7 cfm) at a pressure of 10^5 Pa (1 atm). At the ultimate pressure of the blanked-off pump, the net speed (forward flow – back flow) drops to zero because of dissolved gas in the fluid, leakage around the seals, and trapped gas in the volume below the valve. Rotary vane pumps have ultimate pressures in the 3×10^{-3} – 1 Pa range; the lowest ultimate pressures are achieved with two-stage pumps. The single- and two-stage pumps characterized in Fig. 10.3 have ultimate pressures of 1.4 and $1.5 \times 10^{-2} \text{ Pa}$, respectively. These ultimate pressures are obtained with a new pump using clean, low vapor pressure fluid. As the fluid becomes contaminated and the parts wear, the ultimate pressure will increase.

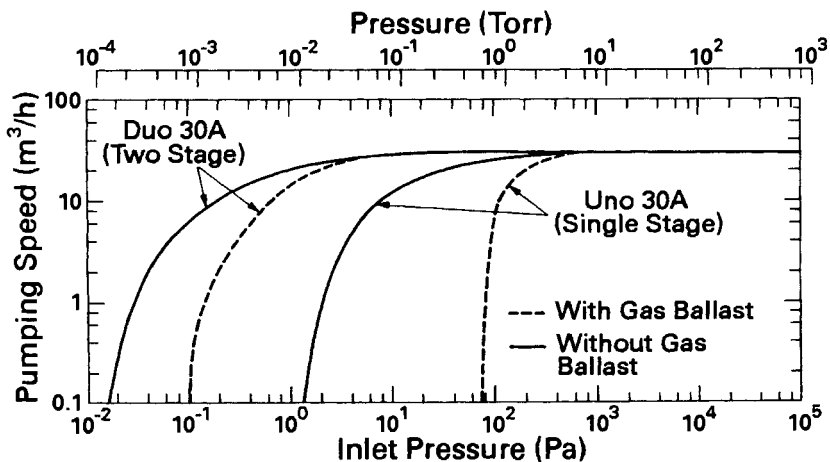


Fig. 10.3 Pumping speed curves for the Pfeiffer UNO 30A and DUO 30A rotary vane pumps. Reprinted with permission from A. Pfeiffer Vakuumtechnik, GmbH, Wetzlar, Germany.

Kendall [1] demonstrated the effect of dissolved gas in the fluid on the ultimate pressure of a two-stage rotary vane pump. He showed a rotary vane pump could reach an ultimate pressure of 4×10^{-5} Pa when the fluid reservoir was exhausted by another pump. Figure 10.4 shows the effect of prolonged outgassing and the effect of admitting CO_2 to the fluid reservoir after degassing the fluid.

When large amounts of water, acetone, or other condensable vapors are being pumped, condensation occurs during the compression stage after the vapor has been isolated from the intake valve. As the vapor is compressed, it reaches its condensation pressure, condenses, and contaminates the fluid before the exhaust valve opens. Condensation causes a reduction in the number of molecules in the vapor phase and delays or even prevents the opening of the exhaust valve. If condensation is not prevented, the pump will become contaminated, the ultimate pressure will increase, and gum deposits will form on the moving parts. Some compounds will eventually cause the pump to seize. To avoid condensation and its resulting problems, gas is admitted through the ballast valve. The open valve allows ballast, usually room air, to enter the chamber during the compression stage; the trapped volume is isolated from the intake and exhaust valves. This inflow of gas, which can be as much as 10% of the pump displacement, is

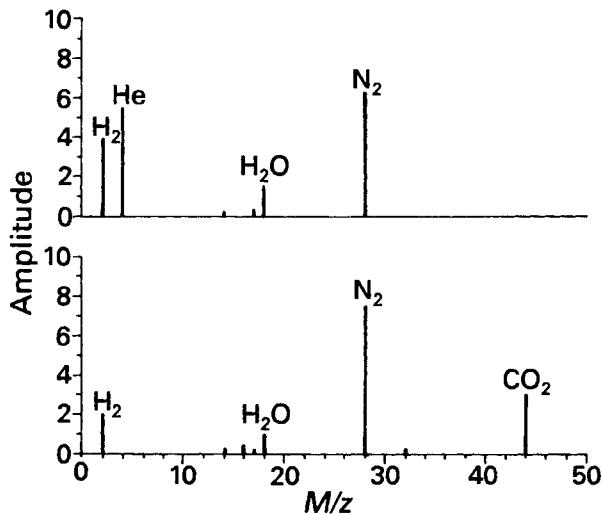


Fig. 10.4 Relative abundance of gases at pump ultimate: Top: After prolonged outgassing of oil and with zero pressure at the exhaust port. Helium pressurization applied intermittently to provide lubricating oil pressure ($P = 7 \times 10^{-7}$ Torr, 9.3×10^{-5} Pa). Bottom: After oil had been exposed to carbon dioxide and then exhaust pressure reduced to zero ($P = 3 \times 10^{-7}$ Torr, 4×10^{-5} Pa). Reprinted with permission from *J. Vac. Sci Technol.*, 21, p. 886, B. R. F. Kendall. Copyright 1982, The American Vacuum Society.

controlled by valve 6 (Fig. 10.1). The added gas causes the discharge valve to open before it reaches the condensation partial pressure of the vapor. In this manner the vapor is swept out of the pump and no condensation occurs. The ultimate pressure of a gas-ballast pump is not very low with the ballast valve open. Figure 10.3 shows the effect of full gas ballast on the performance of a single- and double-stage pump.

Gas ballast can be used to differentiate contaminated fluid from a leak. If the inlet pressure drops when the ballast valve is opened, but drifts upward slowly after the valve is closed, the fluid is contaminated with a high vapor pressure impurity. Additional gas ballast details are covered in reference [2], and Van Atta [3] describes alternative methods for pumping large amounts of water.

10.2 ROTARY PISTON PUMP

Rotary piston pumps are used as roughing pumps on large systems alone or in combination with lobe blowers. They are manufactured in sizes ranging from 30-to-1500 m³/h. A piston pump is a rugged and mechanically simple pump. There are no spring-loaded vanes to stick in a piston pump; all parts are mechanically coupled to a shaft that can be powered by a large motor.

Fig. 10.5 shows a sectional view of a rotary piston pump. As the keyed shaft rotates the eccentric (1) and piston (2), gas is drawn into the space A. After one revolution, this volume of gas has been isolated from the inlet, while the piston is closest to the hinge box. During the next revolution the isolated volume of gas (B) is compressed and vented to the exhaust through the poppet valve when its pressure exceeds that of the valve spring. Like the vane pump, the piston pump is manufactured in single and compound or multistage types.

The clearance between the piston and housing is typically 0.1 mm, but is three or four times larger near the hinge box. Because the clearance between moving and fixed parts is greater in a piston than in a vane pump, the piston pump is tolerant of particulate contamination. A lubricating fluid is used to seal and lubricate the spaces between fixed and moving parts. As in a vane pump, the fluid must have low vapor pressure and good lubricating ability. A rather viscous fluid is used in the piston pump.

The rotational speed of the piston pump is typically 400–600 rpm, although some run as slow as 300 rpm and others as fast as 1200 rpm. The maximum rotational speed of a piston pump is limited by vibration from the eccentric. Small piston pumps are air cooled in the same manner as rotary vane pumps. Large pumps are water-cooled.

The pumping speed curves for a 51-m³/h single-stage rotary piston pump are shown in Fig. 10.6 with and without gas ballast. The shaft power is also

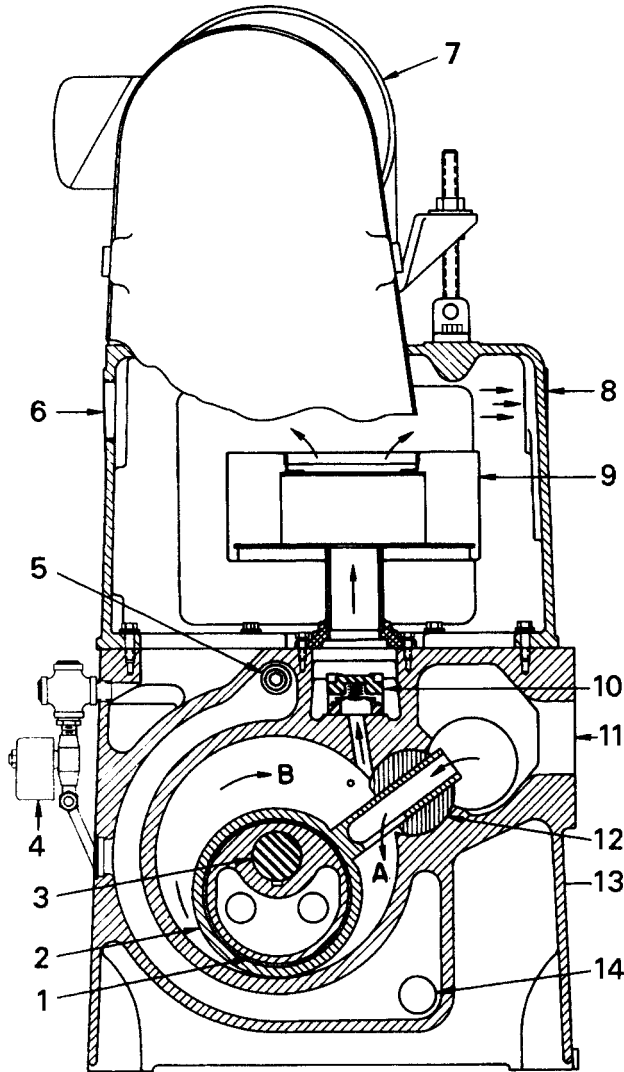


Fig. 10.5 Sectional view of a Stokes 212H, 255-m³/h rotary piston pump: (1) eccentric, (2) piston, (3) shaft, (4) gas ballast, (5) cooling water inlet, (6) optional exhaust, (7) motor, (8) exhaust, (9) oil mist separator, (10) poppet valve, (11) inlet, (12) hinge bar, (13) casing, (14) cooling water outlet. Reprinted with permission from Stokes Division, Pennwalt Corp., Philadelphia, PA.

given and it is seen to peak at a pressure of 4×10^4 Pa and is independent of ballast. At lower pressures operation of the pump with full gas ballast requires more than twice the shaft power as without the use of gas ballast. The ultimate pressure of the piston pump shown in Fig. 10.6 is 1 Pa.

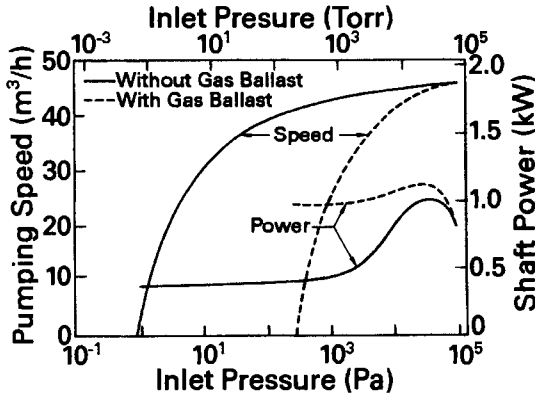


Fig. 10.6 Pumping speed and shaft power for the Stokes 146H, $51\text{-m}^3/\text{h}$ rotary piston pump. Reprinted with permission from Stokes Division, Pennwalt Corp., Philadelphia, PA.

10.3 LOBE PUMP

The positive displacement blower, or lobe blower is used in series with a rotary fluid-sealed pump to achieve higher speed and lower ultimate pressure in the medium vacuum region than can be obtained with a rotary mechanical pump alone. Lobe blowers, also known as Roots pumps, consist of two figure-eight-shaped rotors mounted on parallel shafts. The rotors have substantial clearances between themselves and the housing—typically about 0.2 mm. They rotate in synchronism in opposite directions at speeds of 3000 to 3500 rpm. These speeds are possible because a fluid is not used to seal the gaps between the rotors and the pump housing. A sectional view of a single-stage lobe blower is given in Fig. 10.7.

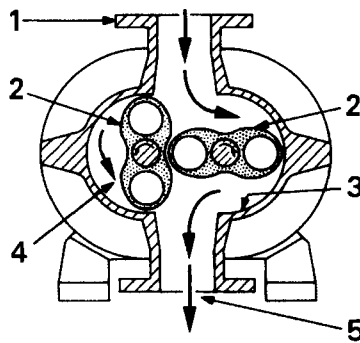


Fig. 10.7 Section through a single-stage lobe blower: (1) inlet, (2) rotors, (3) housing, (4) pump chamber (swept volume), (5) outlet. Reprinted with permission from *Vacuum Technology*, Leybold-Heraeus GmbH, Köln, Germany.

The compression ratio, or ratio of outlet pressure to inlet pressure, is pressure dependent and usually has a maximum near 100 Pa. At higher pressures the compression ratio should, theoretically, remain constant. In practice it decreases. Outgassing and the roughness of the rotor surfaces contribute to compression loss at low pressures. Each time the rotor surface faces the high-pressure side it sorbs gas. Some of this gas is released when the rotor faces the low-pressure side. The compression ratio K_{omax} , for air for a single-stage Lobe blower of 500-m³/h displacement is shown in Fig. 10.8. It has a maximum compression ratio of 44. Large pumps tend to have a larger compression ratio than small pumps, because they have a smaller ratio of gap spacing to pump volume. The compression ratio for a light gas such as helium is about 15–20% smaller than the ratio for air. The compression ratio K_{omax} is a static quantity and is measured under conditions of zero flow. The inlet side of the pump is sealed and a pressure gauge is attached. The outlet side is connected to a roughing pump and the system is evacuated. Gas is admitted to the backing line that connects the blower to the roughing pump. The backing pressure P_b , is measured at the blower outlet, and the pressure P_i is measured at the inlet. The compression ratio is given by P_b/P_i .

Lobe blowers generate considerable heat, when pumping gas at high pressures. Heat causes the rotors to expand; if unchecked, rotor expansion could destroy the pump. To avoid overheating, a maximum pressure difference between the inlet and outlet of a lobe blower is specified. This maximum pressure difference is typically 1000 Pa, but that value may be exceeded for a short time without harm to the pump. Lobe blowers are connected as compression or transport pumps.

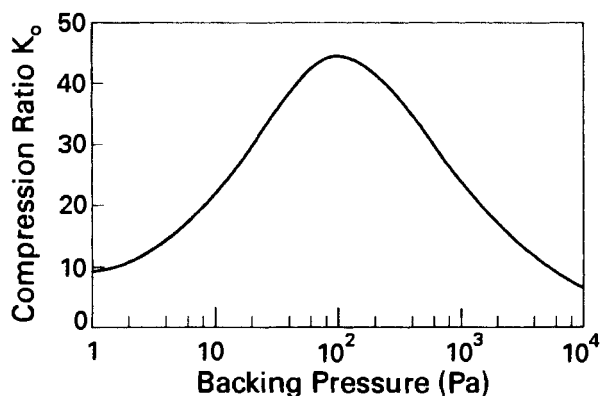


Fig. 10.8 Dependence of the air compression ratio K_{omax} of the Leybold WS500 lobe pump on the backing pressure. Values for helium are about 20% smaller. Reprinted with permission from *Vacuum Technology*, Leybold-Heraeus GmbH, Köln, Germany.

In compression pumping, the common method, a lobe pump is placed in series with a rotary pump whose rated speed is 2–10 times smaller than its own speed. When pumping is initiated at atmospheric pressure, a bypass line around the lobe pump is opened, or the pump is allowed to free wheel. All the pumping is done by the rotary pump until the backing pressure is below the manufacturer's recommended pressure difference, at which time the lobe blower is activated and the bypass valve is closed. Some lobe blowers have this bypass feature built into the pump housing; others are allowed to free-wheel until a pressure sensor activates a clutch between motor and blower. The net speed of a lobe blower of 500-m³/h capacity backed by a 100-m³/h rotary piston pump is shown in Fig. 10.9. The speed curve for the mechanical pump alone is shown for comparison. Such lobe blower–rotary pump combinations are often used when speeds of 170 m³/h or greater are required because the combination costs less than a rotary pump of similar capacity.

The second method, transport pumping, uses a lobe blower in series with a rotary pump of the same displacement. Figure 10.9 shows the pumping speed of a 60-m³/h lobe blower backed by a 60-m³/h rotary vane pump. The pumping speed of the rotary vane pump is shown for comparison. Both pumps are started simultaneously at atmospheric pressure because the critical pressure drop will never be exceeded.

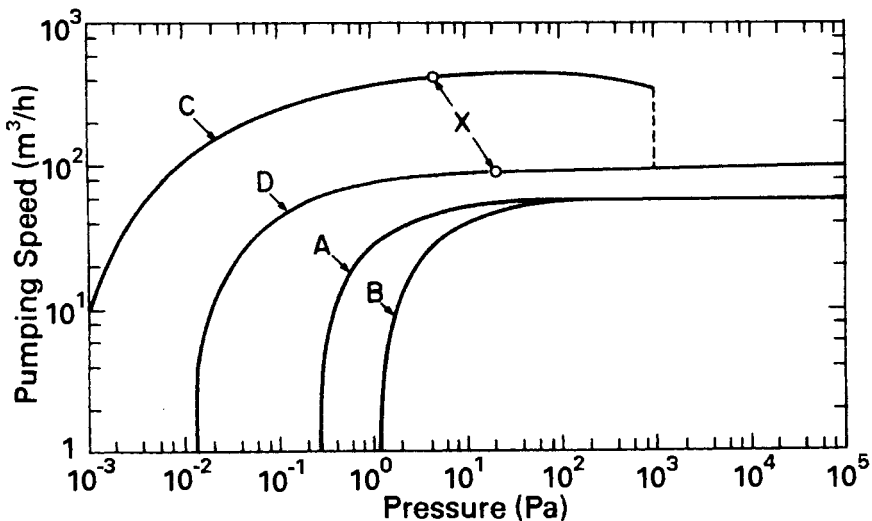


Fig. 10.9 Lobe blower–rotary pump combinations. Transport mode: (A) Leybold RUTA 60 lobe blower and S60 rotary vane; (B) S60 only. Compression mode: (C) Leybold WS500 lobe blower and DK100 rotary piston pump; (D) DK100 only. Reprinted with permission from *Vacuum Technology*, Leybold-Heraeus GmbH, Köln, Germany.

Detailed calculations of the effective pumping speed of the lobe blower have been carried out by Van Atta [3]. Here we give approximate formulas for the inlet pressure P_i , and the inlet speed S_i [2].

$$P_i = P_b \left(\frac{1}{K_{o\max}} + \frac{S_b}{S_D} \right) \quad \blacktriangleright (10.1)$$

$$S_i = \frac{S_b S_D K_{o\max}}{S_D + S_b K_{o\max}} \quad \blacktriangleright (10.2)$$

S_D is the pump displacement, or speed of the lobe blower at atmospheric pressure. With these approximate equations, the pumping speed curve for the rotary pump, the compression ratio $K_{o\max}$, and the lobe blower displacement, a curve of the speed of the lobe pump versus inlet pressure can be calculated. The point on the upper end of the line marked X in Fig. 10.9 is the result of applying (10.1) and (10.2). In this example the inlet pressure P_i , and the inlet speed S_i were calculated for a backing pressure of 20 Pa. At 20 Pa, $K_{o\max} = 30$ (Fig. 10.8), and $S_b = 90 \text{ m}^3/\text{h}$ (Fig. 10.9d). With (10.1), (10.2), and $S_D = 500 \text{ m}^3/\text{h}$, we get $P_i = 4.3 \text{ Pa}$ and $S_i = 422 \text{ m}^3/\text{h}$.

Lobe pumps are also used to back large diffusion or turbomolecular pumps. For example, a 35-in.-diameter diffusion pump used to evacuate a 2-m^3 chamber is backed by a series combination of a $1300\text{-m}^3/\text{h}$ lobe blower and a $170\text{-m}^3/\text{h}$ rotary piston pump.

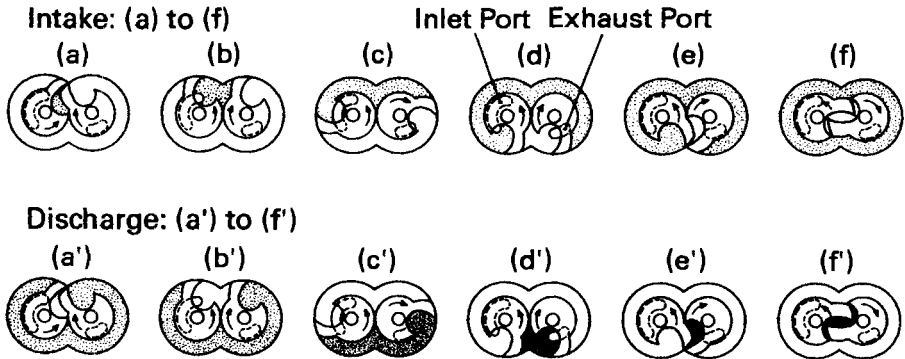


Fig. 10.10 Compression sequence for 1 revolution of a claw stage: (a)–(f) show the intake sequence with the inlet port open from (b)–(d). The compression and exhaust sequence is shown in (a')–(f') with the exhaust port open from (c')–(d'). The carryover volume, which limits the maximum obtainable compression, is shown in (f'). Reprinted with permission from *J. Vac. Sci. Technol. A*, 9, p. 2048, A. P. Troup and N. M. T. Dennis. Copyright 1991, AVS–The Science and Technology Society.

10.4 CLAW PUMP

The lobe or Roots design is one of many shapes into which a counter-rotating pair may be machined for vacuum pumping. The Northey hook and claw compressor is one design that has proven useful for particular applications. It has two irregularly shaped lobes or “claws” that counter-rotate in the same manner as a lobe blower. However, a lobe blower does not compress gas inside the pump—rather it transports the gas from the inlet to the foreline, where compression takes place. The claw pump does compress gas inside the pump, as described in the rotational sequence illustrated in Fig. 10.10. Each complete revolution of the claw pair compresses a volume of gas. Claw pumps are more efficient at compressing gas at high pressures than Roots pumps [5] and have at least equal compression ratios at low pressure [6]. The maximum compression is limited by the volume of gas depicted in illustration (f) of Fig. 10.10, which returns to the inlet at the end of the cycle. Claw and Roots stages are combined to form an efficient multistage pump that can effectively pump corrosive and abrasive gas [7]. One design uses a Roots inlet stage followed by three claw stages before exhausting to atmosphere; its pumping speed curve is depicted in Fig. 10.11 exhausting to atmosphere. Both Roots and claw pumps require cooling and gas purging [8]. Pumps with combined Roots–claw stages have ultimate pressures in the range 0.5–1 Pa (4–7 mTorr) when exhausting directly to atmosphere. They are used to provide oil-free backing for turbomolecular pumps in corrosive or

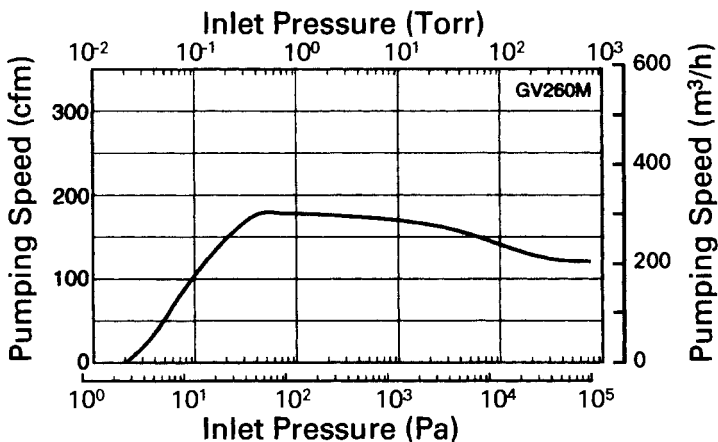


Fig. 10.11 Pumping speed curve for a four-stage booster pump exhausting directly to atmosphere. This pump contains a lobe inlet stage followed by three claw stages. Reprinted with permission from BOC Edwards, 301 Ballardvale Street, Wilmington, MA 01887.

abrasive etching and deposition systems. Because of their shape, claw stages efficiently remove deposited particles. As a result, maintenance intervals can be increased when using these pumps in chemically aggressive process environments.

10.5 SCROLL PUMP

The scroll pump is a relatively simple compressor consisting of two surfaces, one fixed and one orbiting. Note that the movable plate does not rotate, but rather it orbits. Mirror-image spiral grooves are cut in two facing, stator plates; in turn these plates mesh within a plate containing sets of complementary spiral ridges. Figure 10.12 illustrates cross-sectional and plan views of an orbiting scroll pump. Gas enters the chambers at the periphery, and is forced around in a spiral helical path until it reaches the exit port located at the pump center. The pump inlet is located at the periphery, which must be sealed with a bellows. The ultimate pressure of a scroll pump is ~ 1 Pa (10^{-2} Torr), see Fig. 10.13. These pumps are manufactured in small sizes of order 15–40 m³/h. They find application for backing turbomolecular drag pumps that have in-built molecular drag stages, and they find other applications where small oil-free pumps are needed. The polymer seal that prevents gas flow between the closely spaced edges of the orbiting seal plate and the stator will generate wear particles. One can

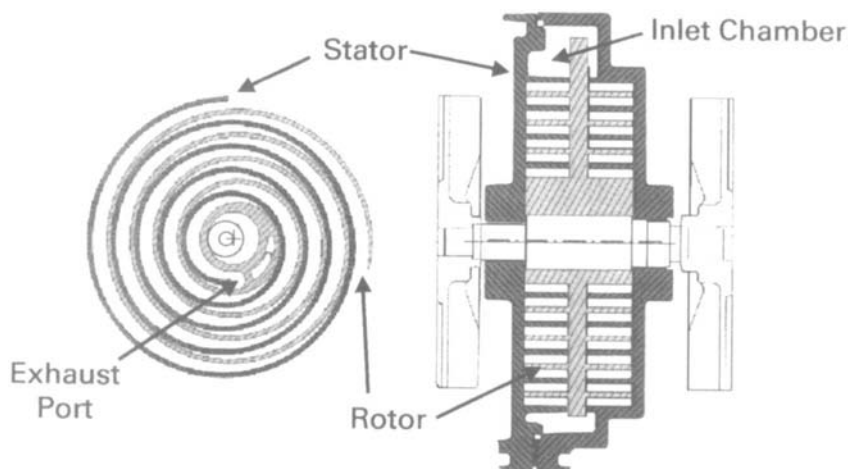


Fig. 10.12 Anest-Iwata orbiting scroll pump mechanism. Right: Plan view of orbiting scroll. Left: Cross-sectional view of stator and orbiting rotor. Reprinted with permission from Synergy Vacuum, P. O. Box 2084 Montrose, CO 81402.

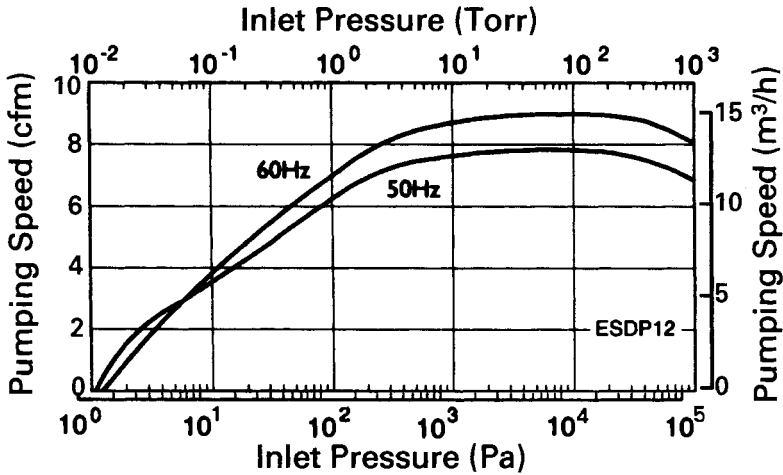


Fig. 10.13 Pumping speed of a model ESDP12 orbiting scroll pump, reprinted with permission from BOC Edwards, 301 Ballardvale Street, Wilmington, MA 01887.

trap these in a point-of-use $0.02\text{-}\mu\text{m}$ -diameter particle filter mounted on the pump inlet, and prevent them from migrating to the process chamber, where they can contaminate the process.

10.6 SCREW PUMP

The screw pump is another compressor with a long history of use in fields other than vacuum technology. Recently screw pumps have been manufactured for oil-free applications, and for pumping abrasive and corrosive gases. They are used for backing magnetic levitated turbomolecular pumps on reactive ion etching and low-pressure chemical vapor deposition systems. The basic design of a screw pump is illustrated in Fig. 10.14. The two uniquely shaped screws, located inside a closely fitting stator, are counter rotated at equal rotational velocities. Gas enters at the end of the rotating pair, and is transported along screws in a trapped region defined by the contact of the screws and the wall. It is expelled into the exhaust plenum at the right-hand end of the screw pair. The rotors may be coated for use in pumping corrosive gases. In some designs, asymmetrical screws rotate at different velocities, provided that the total number of turns is limited. Pumping speed curves for one family of pumps is shown in Fig. 10.15. The ultimate pressure of a screw pump is of order 0.7 Pa (5×10^{-3} Torr) with speeds as high as $2500\text{ m}^3/\text{h}$. Screw pumps are rugged and reliable.

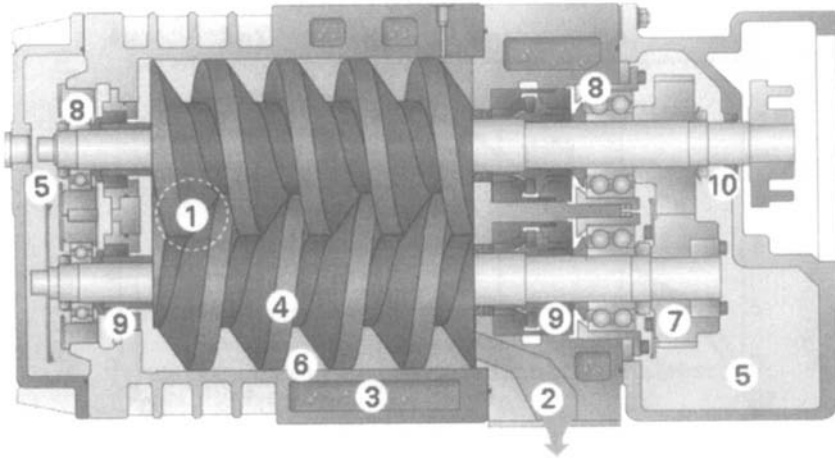


Fig. 10.14 Cross-sectional view of a screw vacuum pump. (1) Inlet, (2) discharge, (3) cooling jacket, (4) screws, (5) gear case, (6) stator housing, (7) drive gears, (8) shaft bearings, (9) shaft seals, (10) motor shaft seal. Reprinted with permission from Busch Semiconductor Vacuum Group, 18430 Sutter Blvd., Morgan Hill, CA 95037.

10.7 DIAPHRAGM PUMP

Diaphragm pumps, in the form of bellows, are one of the oldest known pumps. They consist of a small chamber designed to have minimal dead space containing a flexible diaphragm connected to a piston, such as illustrated in Fig. 10.16. The eccentric shaft moves the piston–diaphragm

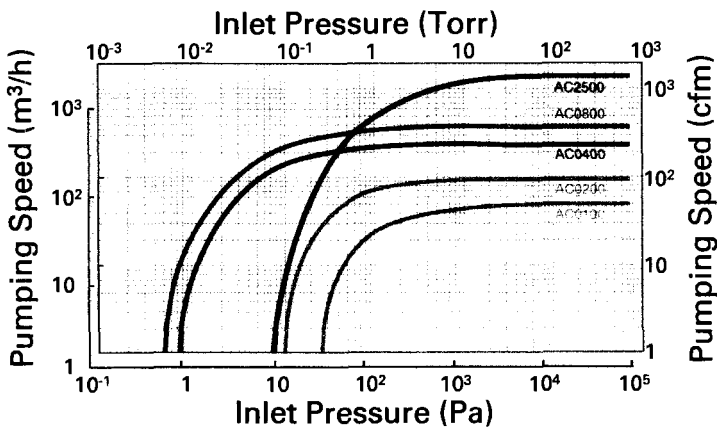


Fig. 10.15 Pumping speed curves for a family of screw pumps. Reprinted with permission from Busch Semiconductor Vacuum Group, 18430 Sutter Blvd., Morgan Hill, CA 95037.

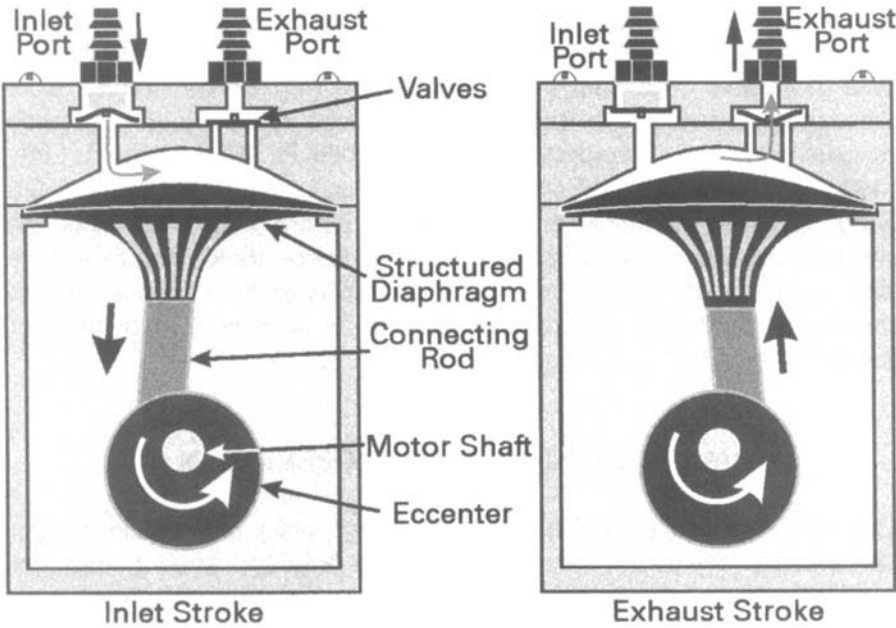


Fig. 10.16 Diaphragm pumping mechanism. Reprinted with permission from KNF Neuberger USA, Two Black Forest Road, Trenton, NJ, 08691.

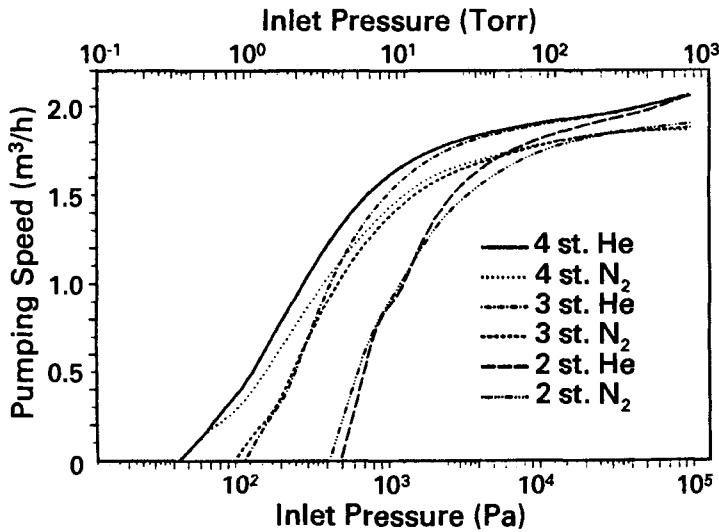


Fig. 10.17 Pumping speed curves for four-stage, three-stage, and two-stage diaphragm pumps for nitrogen and helium. Reprinted from *Vacuum*, 47, F. J. Eckle, P. Bickert, R. Lachenmann and B. Wortmann, 799–801, copyright 1996, with permission from Elsevier.

assembly in rocking, swinging manner so as to draw gas in through the left-hand inlet valve, and a half-stroke later expel the gas through the right-hand exit valve. The pumps are oil-free and may be constructed from chemically inert materials. Up to four stages can be combined to provide ultimate pressures of, respectively, 7000–20,000 Pa (50–150 Torr), 700–1400 Pa (5–10 Torr), 200–400 Pa (1.5–3 Torr), and 50–75 Pa (0.4–0.6 Torr). Sizes do not exceed several m^3/h . Figure 10.17 illustrates the nitrogen and helium pumping speeds for small two-, three-, and four-stage diaphragm pumps. Diaphragm pumps can be used for medium vacuum chemically aggressive applications and can be used as oil-free backing pumps for turbomolecular-drag pumps.

10.8 MECHANICAL PUMP OPERATION

There are several common rules for operating rotary mechanical pumps. The exhaust should be vented outside the building. Most pumps are supplied with an oil mist separator, but it does not adequately remove all the vapors. Most laboratories and plant safety rules require the use of an outside vent. The vent hose should not run vertically from the exhaust connection, because water or other vapors, which have condensed on cold pipe walls, will flow into the pump exit and contaminate the fluid. A satisfactory solution to this problem is the addition of a sump at the exhaust connection to collect the vapors before they can flow into the pump. A vane pump must also be vented at the time it is stopped to prevent fluid from being forced back into the vacuum system by external air pressure. Venting is done automatically in most pumps, and it can be achieved in others by the addition of a vent valve above the inlet port. The fluid level in mechanical pumps should be checked frequently, especially those that are used on systems regularly cycled to atmosphere. Small rotary pumps of capacity less than $30 \text{ m}^3/\text{h}$ have fluid consumption rates (cm^3/h) of about $10^{-6} - 10^{-5}PS$ where P is the inlet pressure and S is the inlet speed in m^3/h [4]. Larger pumps will use more fluid. The fluid should be changed when the pump performance deteriorates or when it becomes discolored or contaminated with particles. Poor fluid maintenance is the major cause of mechanical pump failure. Flushing the pump and changing the fluid can solve ninety-five percent of all pump problems. A discussion of mechanical pump fluids is given in Chapter 13. Vapor pressure and kinematic viscosity of mechanical pump fluids are given in Appendixes F.1 and F.3.

REFERENCES

1. B. R. F. Kendall, *J. Vac. Sci. Technol.*, **21**, 886 (1982).
2. Leybold-Heraeus Publication HU152, Leybold-Heraeus, GmbH, Köln, Germany.
3. C. M. Van Atta, *Vacuum Science and Engineering*, McGraw-Hill, New York, 1965, Chapter 5.
4. Reference 2, p. H-B 61.
5. A. P. Troup and N. T. M. Dennis, *J. Vac. Sci. Technol. A*, **9**, 2048 (1991).
6. H. Wycliffe, *J. Vac. Sci. Technol. A*, **5**, 2608 (1987).
7. P. Bachmann and M. Kuhn, *Vacuum*, **41**, 1827 (1990).
8. M. Hablanian, *Vacuum*, **41**, 1814 (1990).

PROBLEMS

- 10.1 † A simple mechanical piston has a displacement of 1 L. It is connected to a chamber of 10 L. If pumping commences at 1 atmosphere, what is the pressure in Pa after four complete strokes?
- 10.2 Define free air displacement. Give a formula for the free air displacement SD , in terms of rotational speed n and swept volume V , of (a) a piston pump and (b) a two-stage vane pump.
- 10.3 Rank the following pumps in order of increasing physical size for equal displacements: (a) Rotary vane pump, two-vane belt drive; (b) rotary piston pump; (c) rotary vane pump, two-vane direct drive.
- 10.4 † What are three functions of the fluid in a rotary vane or piston pump?
- 10.5 Plot throughput versus pressure for the single-stage and two-stage mechanical pumps whose no-ballast pumping speed curves are given in Fig. 10.3.
- 10.6 What is the staging ratio of a lobe-piston pump set? What performance differences would you expect between a set with a staging ratio of 10:1 and one of 2:1, provided that the two sets use the same mechanical pump?
- 10.7 † What will happen if the mechanical pump exhaust hose runs vertically in a direct line from the pump to a connection in the exhaust plenum?
- 10.8 † What is the most important step in ensuring long, trouble free operation of a rotary pump?
- 10.9 The piston pump whose speed characteristic is shown in Fig. 10.9d is connected to a chamber by a 400-cm length of 4-cm-diameter

pipe. When the pressure at the inlet of the pump is 1 Pa, what is the pressure in the chamber?

- 10.10 † What is the hazard in discharging mechanical pump exhaust fumes into the work area? What will happen if the exhaust hose forms a loop like a sink trap, before being connected to the exhaust plenum?

Production

Vacuum pumps are often classified according to the physical or chemical phenomena responsible for their operation. In practice this is a bit awkward because some pumps combine two or more principles to pump a wide range of gases or to pump over a wide pressure range. In this section the discussion of pump operation is divided into six chapters. Chapter 10 discusses mechanical vacuum pumps. Rotary vane, rotary piston, and Roots pumps operate by displacing gas from the work chamber to the pump exhaust. Rotary vane and piston pumps operate in the low vacuum region, whereas the Roots pump operates in the medium vacuum region. Scroll and screw pumps are nominally "oil-free" and are used in particulate or chemically reactive applications. The turbomolecular pump is a mechanical high vacuum pump, which is the subject of Chapter 11. It transports gas from regions of low pressure to high pressure by momentum transfer from high-speed blades. Molecular drag pumps are combined with magnetically levitated turbomolecular pumps to provide "oil-free" high vacuum pumps for particular applications.

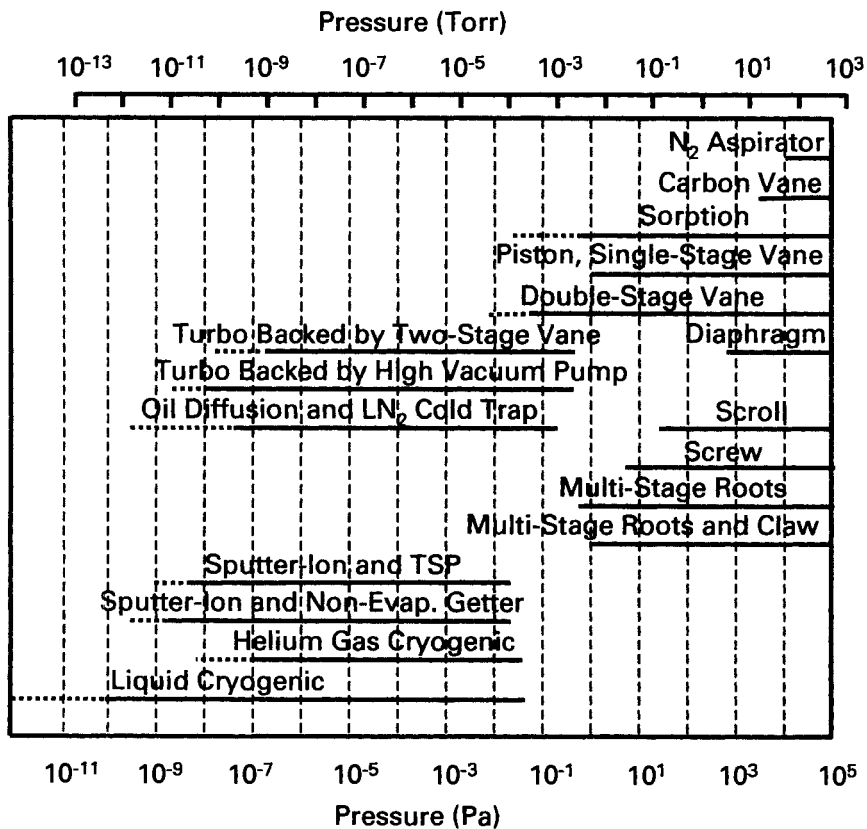
Chapter 12 is devoted to the diffusion pump, which, like the turbomolecular pump, is a momentum transfer pump. The diffusion pump has been the mainstay of the vacuum industry for many applications and is now being supplanted by cryogenic and turbomolecular pumps for many applications.

Vacuum pump fluids are common to all of the above pumps. In Chapter 13, we describe properties of the fluids needed for correct operation of each pump.

Capture pumps or entrainment pumps bind particles to a surface instead of expelling them to the atmosphere. Chapter 14 describes getter and ion pumps. Getter pumps, such as the titanium sublimation pump, remove gases by chemical reactions that form solid compounds; ion pumps ionize gas molecules and imbed them in a wall. The sputter-ion pump combines getter pumping with ion pumping. Other entrainment pumps are based on condensation and sorption. Sorption pumps physisorb gas molecules in materials of high surface area. These surfaces are usually cooled to enhance their pumping ability. Another capture pump, the cryogenic pump, is the subject of Chapter 15. A cryogenic pump uses at least two stages of

cooling. The warmer stage pumps by condensation or adsorption on a cooled metallic surface, and the colder stage uses in addition an adsorbate such as charcoal or zeolite. Shown below are the operating pressure ranges of many pumps and pump combinations.

These chapters do not cover all of the many techniques by which high vacuum may be achieved. Their purpose is to review the operation of commonly used pumps in a concise manner and to amplify the treatment of turbomolecular and cryogenic pumps. The latter warrant expanded treatment in view of the rapidity with which they have replaced older pumps in many high and ultrahigh vacuum applications.



Vacuum pump operating ranges

CHAPTER 11

Turbomolecular Pumps

The axial-flow turbine, or turbomolecular pump as it is known, was introduced in 1958 by Becker [1]. His design originated from a baffling idea with which he had experimented a few years earlier—a disk with rotating blades mounted above a diffusion pump [2]. When it was introduced commercially, the pump had low speed and high cost, as compared to a diffusion pump. It did not backstream hydrocarbons and did not require a trap of any kind. Since its introduction, the turbomolecular pump has undergone rapid development both theoretically and experimentally. The important early theoretical development was the work on blade geometry at MIT in the group headed by Shapiro [3,4]. Practical advances in lubrication drive motors, and fabrication techniques have improved the quality and reliability of turbomolecular pumps. Modern turbomolecular pumps have high pumping speeds, large hydrogen compression ratios, and low ultimate pressures. They do not backstream hydrocarbons, have high exhaust pressures, and can be backed by oil-free pumps. They are well-suited to pump gas cleanly at high flow rates or low pressures.

This chapter reviews the pumping mechanism in the free molecular pressure range, and it discusses the relations between pumping speed, compression ratio, backing pump size, and gas flow. Vacuum lubrication techniques are discussed in Chapter 18. The operation and performance of pumps in a variety of applications is discussed in the Systems chapters.

11.1 PUMPING MECHANISM

The turbomolecular pump is a molecular turbine that compresses gas by momentum transfer from high-speed rotating blades to gas molecules. It is a high-speed molecular bat. The pump operates at rotor speeds in the range 24,000–80,000 rpm and is driven by solid-state power supplies or motor-generator sets. The relative velocity between the alternate slotted rotating

blades and slotted stator blades makes it probable that a gas molecule will be transported from the pump inlet to the pump outlet. Each blade is able to support a pressure difference. Because this compression ratio or pressure ratio is small for a single stage, many stages are cascaded. For a series of stages the compression ratio for zero flow is approximately the product of the compression ratios for each stage. Figure 11.1 shows a sectional view of a dual-rotor, horizontal-axis, turbomolecular pump. The blades impart momentum to the gas molecules most efficiently in the molecular flow region. The pump exhaust pressure must remain in the molecular or transition regime, therefore it cannot exhaust to atmosphere. For this reason, a backing pump—typically a rotary vane, screw, scroll, or diaphragm pump—is required.

If the foreline pressure is allowed to increase to a point at which the rear blades are in viscous flow, the rotor will be subjected to an additional torque. The power required to rotate a shaft in steady state is proportional to the product of the rotor speed and the torque. The available power in many pumps is limited by the supply, so that too large an increase in foreline pressure (increase in torque) will cause a sudden reduction in the rotor speed and a loss in gas pumping speed. One design used a constant-speed motor whose power consumption increased in proportion to the gas load or increase in torque. Effects of backing pump size and rules for selecting backing pumps are discussed later in this section.

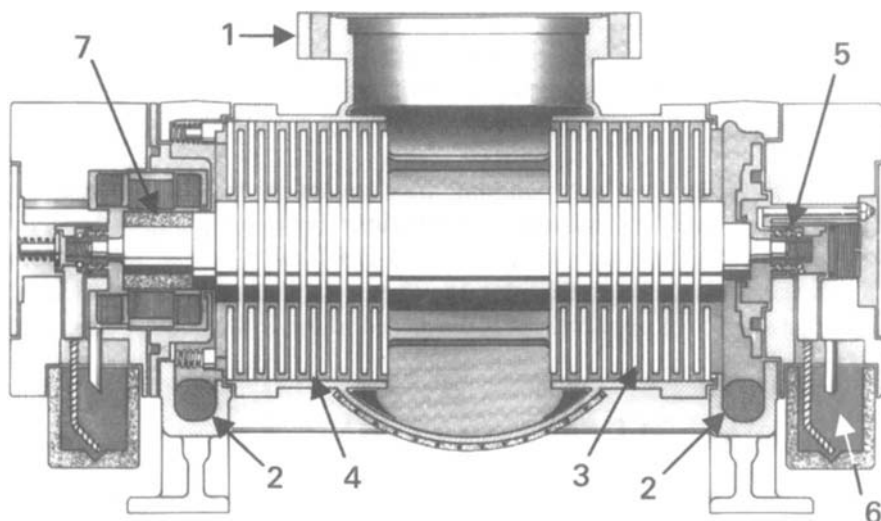


Fig. 11.1 Section view of Pfeiffer TPU-200 turbomolecular pump: (1) inlet, (2) outlet, (3) rotor disk, (4) stator disk, (5) bearing, (6) oil reservoir, (7) motor. Reprinted with permission from A. Pfeiffer Vakuumtechnik, GmbH, Wetzlar, Germany.

11.2 SPEED-COMPRESSION RELATIONS

Continuum methods that give a reasonable account of pump performance have been developed [2]; later, Monte Carlo analysis of single-blade rows provided Kruger and Shapiro [3–5] with design insights. Their probabilistic methods were valid for all no-flow situations. The model used to analyze a single rotor disk is shown in Fig. 11.2. This disk, which rotated with a tip velocity near the thermal velocity of air, imparted a directed momentum to a gas molecule on collision. The blades were slotted at an angle to make the probability of a gas molecule being transmitted from the inlet to the outlet much greater than in the reverse direction. The stator disks are slotted in the opposite direction. Γ_1 and Γ_2 are, respectively, the number of molecules incident on the disk per unit time at the inlet and at the outlet. a_{12} is the fraction of Γ_1 transmitted from the inlet (1) to the outlet (2) and a_{21} is the fraction of Γ_2 transmitted from the outlet to the inlet. Now define the net flux of molecules through the blades to be a function of the Ho coefficient W , the ratio of net flux to incident flux. Assuming mass conservation and zero-flow conditions, one obtained

$$\Gamma_1 W = \Gamma_1 a_{12} - \Gamma_2 a_{21} \quad (11.1)$$

or by rearrangement,

$$\frac{\Gamma_2}{\Gamma_1} = \frac{a_{12}}{a_{21}} - \frac{W}{a_{21}} \quad (11.2)$$

If the gas temperature and the velocity distributions are the same everywhere, the ratio Γ_2/Γ_1 will be equal to the pressure ratio P_2/P_1 . The ratio of outlet to inlet pressure is called the compression ratio K . Again, for zero-flow conditions, this becomes

$$\frac{P_2}{P_1} = K = \frac{a_{12}}{a_{21}} - \frac{W}{a_{21}} \quad (11.3)$$

Maximum compression occurs at zero flow, while unity compression occurs at maximum speed or mass flow. This is a general property of a fan. Envision the compression and flow in a household vacuum cleaner as you hold your hand over the inlet (zero flow) and release it (maximum flow). Let us now examine the maximum compression, maximum flow, and the intermediate case for the region between these extremes.

11.2.1 Maximum Compression Ratio

Assuming zero flow, $W = 0$, (11.3) reduces to

$$K = K_{\max} = \frac{a_{12}}{a_{21}} \quad \blacktriangleright (11.4)$$

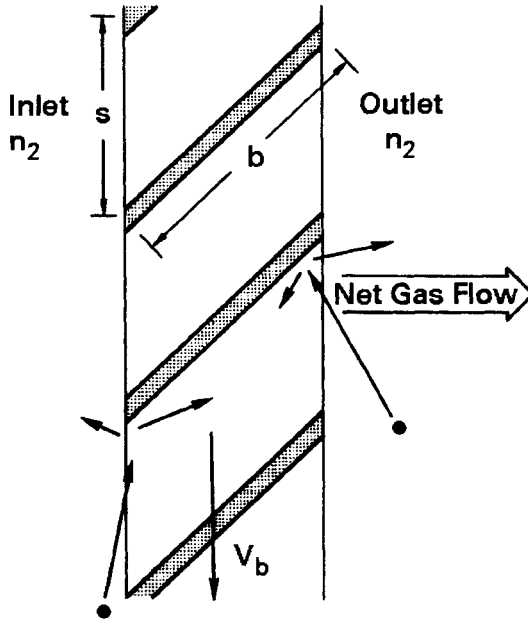


Fig. 11.2 Sectional view of a flat-bladed disk.

Equation (11.4) states the maximum compression ratio is the ratio of forward to reverse transmission probabilities. To maximize the compression ratio, the ratio a_{12} to a_{21} is maximized. Kruger and Shapiro calculated these forward and reverse transmission probabilities by Monte Carlo techniques. They solved for the transmission probabilities as a function of the blade angle ϕ , the blade spacing-to-chord ratio s/b , and the blade speed ratio $s_r = V_b(M/2kN_oT)^{1/2}$. Figure 11.3 sketches the results of a calculation for the single-stage compression ratio at zero flow. From this curve we observe the logarithm of the compression ratio is approximately linear with blade speed ratio for $s_r \leq 1.5$ or

$$K_{\max} \propto \exp \left[\frac{V_b \sqrt{M}}{\sqrt{2kN_oT}} \right] \quad \blacktriangleright (11.5)$$

The compression ratio is exponentially dependent on rotor speed and $M^{1/2}$. The constant of proportionality is dependent on the blade angle and s/b . In particular, hydrogen will have a compression ratio much smaller than that for any other gas. For a blade tip velocity of 400 m/s the speed ratio for argon is about unity, and for hydrogen it is about 0.3. From Fig. 11.3 for $\phi = 30^\circ$ we find this blade velocity corresponds to compression ratios $K(\text{H}_2) = 1.6$

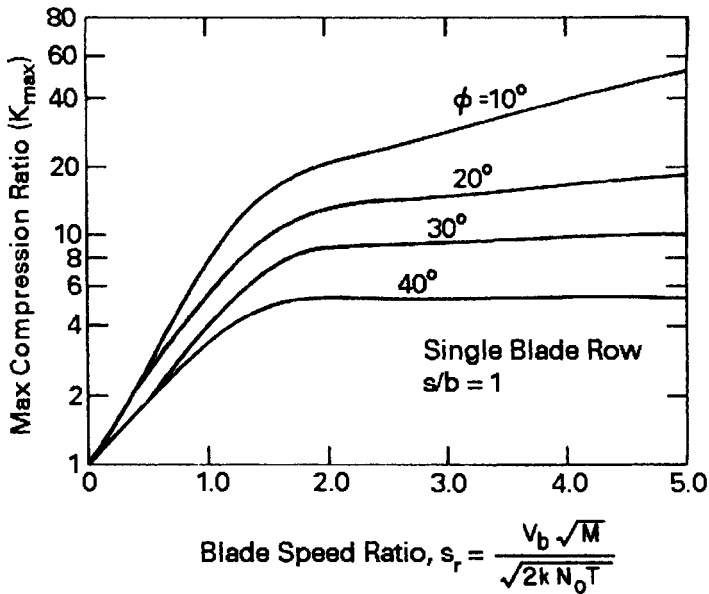


Fig. 11.3 Calculated curve of the compression ratio at zero flow for a single blade row with $s/b = 1$. Reprinted with permission from *Trans. 7th Nat. Vac. Symp.* (1960), p. 6, C. H. Kruger and A. H. Shapiro. Copyright 1961, Pergamon Press.

and $K(\text{Ar}) = 4$. If two disks (five rotors and five stators) are cascaded, the net compression ratios are approximately 100 and 10^6 , respectively. A total of 15 disks would raise $K(\text{H}_2)$ to 1000. A stator blade has the same compression ratio and transmission as a rotor. An observer sitting on a stator sees blades moving with the same relative velocity as an observer sitting on a rotor. The linear blade velocity is proportional to the radius and the rotor angular frequency ($V_b = r\omega$). An area closer to the center of the rotor will have a smaller speed ratio and blade spacing-to-chord ratio. The data of Kruger and Shapiro show that the net effect of these changes is a low compression ratio for the region closest to the rotor axis. Blades designed to have a high $K(\text{H}_2)$ should be slotted to a depth of only about 30% of the radius.

Experimental compression ratios are given for a horizontal-axis, dual-rotor pump in Fig. 11.4. These data were taken in a manner identical to lobe blower compression curves, or diffusion pump forepressure tolerance curves. Gas is admitted to the foreline of a blanked-off pump and the measured compression ratio is the ratio of forepressure to inlet pressure. As the foreline or backing line pressure is increased, the rear blades first go into transition flow and then into viscous flow, the rotor speed decreases, and the compression ratio decreases.

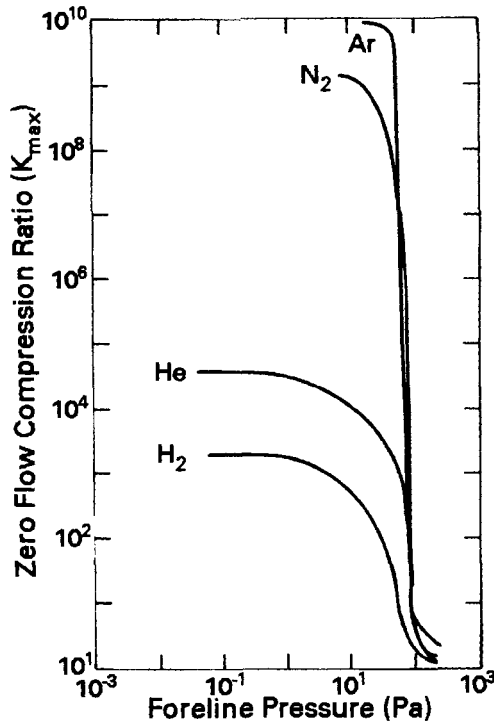


Fig. 11.4 Measured compression ratio for zero flow in a Pfeiffer TPU-400 turbomolecular pump. Reprinted with permission from A. Pfeiffer Vakuumtechnik, GmbH, Wetzlar, Germany.

11.2.2 Maximum Speed

Maximum speed is achieved when the compression ratio across a blade is unity. However, the model assumed by Kruger and Shapiro holds only for the zero flow case. Recently, Chang and Jou [6] derived an analytic expression for the maximum speed factor with gas flow in terms of transmission probabilities. They predicted the maximum speed factor to be

$$W_{\max} = \frac{a_{12} - a_{21}}{1 - a_{21}} \quad \blacktriangleright (11.6)$$

This value is greater than that predicted ($W_{\max} = a_{12} - a_{21}$) by Kruger and Shapiro. To maximize W , a_{12} (forward transmission probability) must be maximized and a_{21} (reverse transmission probability) minimized. The Ho coefficient W for a single blade is given in Fig. 11.5 as a function of blade-speed ratio for a spacing-to-chord ratio $s/b = 1$ and three blade angles. For s_r small, W is reasonably linear with s_r , so that one could write

$$W \propto \left[\frac{V_b \sqrt{M}}{\sqrt{2kN_o T}} \right] \quad \blacktriangleright (11.7)$$

Because the molecular arrival rate is proportional to thermal velocity $(kT/m)^{1/2}$, the net pumping speed of the blade is approximately independent of the mass of the impinging molecules, therefore

$$S \propto V_b \quad (11.8)$$

Monte Carlo methods can be used for calculating the net Ho coefficient for a series of blades. These calculations show the Ho coefficient to increase with the number of stages [7], with a saturation in speed after several blades are operated in series.

11.2.3 General Relation

The maximum compression ratio (11.4) occurs only when the pump is pumping no gas (the pump is at base pressure), whereas maximum speed occurs when the pressure ratio is near 1. An operating pump works throughout the region between these extremes. Chang and Jou [6] derived an

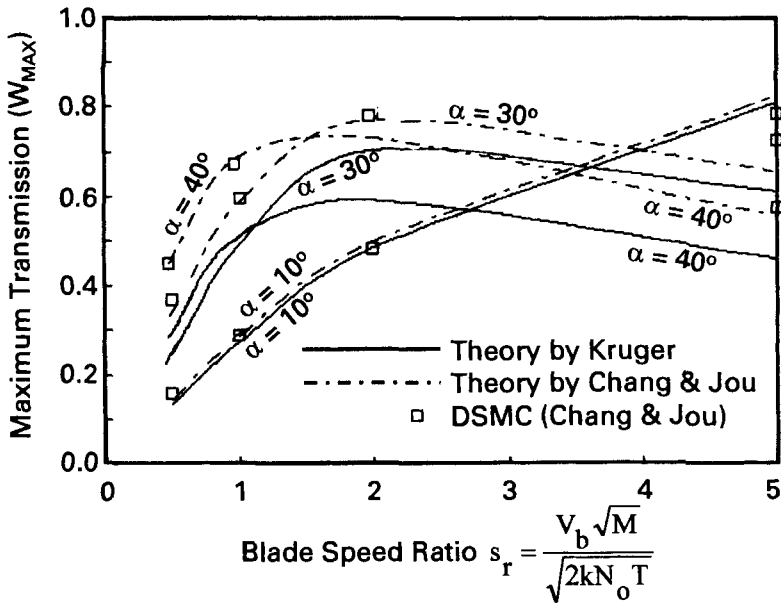


Fig. 11.5 Maximum speed factor (Ho coefficient), single blade row with $s/b = 1$, for three different blade angles. Reprinted with permission from *J. Vac. Sci. Technol. A*, **19**, p. 2900, Y-W. Chang and R-Y. Jou. Copyright 2001, AVS-The Science and Technology Society.

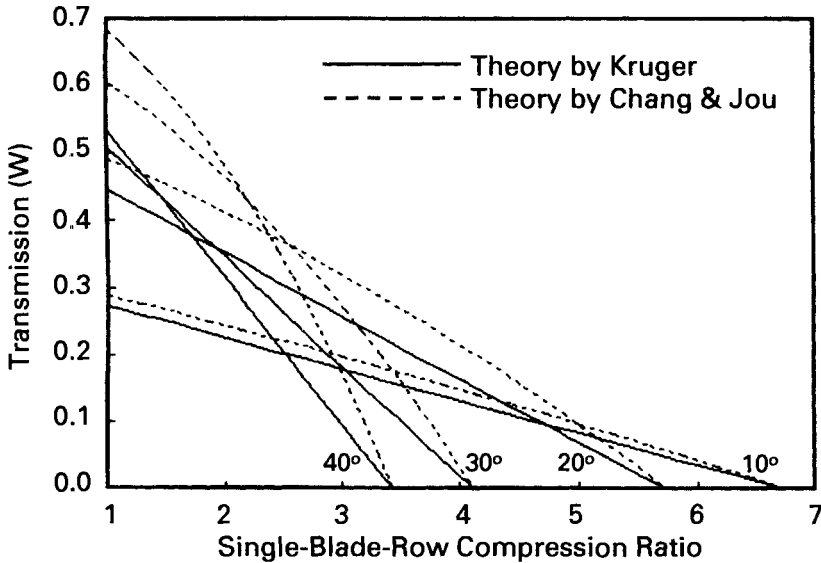


Fig. 11.6 Transmission coefficient versus compression ratio (pressure ratio): Comparison of Kruger's results and Chang-Jou approximate solution for a single blade row with blade speed ratio = 1 and $s/b = 1$. Reprinted with permission from *J. Vac. Sci. Technol. A*, **19**, p. 2900, Y-W. Chang and R-Y. Jou. Copyright 2001, AVS-The Science and Technology Society.

expression for the transmission factor W within the region between these limits. It is complex, so their approximation, valid in the range $0 < s_1 \ll 1$ is given here.

$$W \cong \frac{a_{12} - \left(\frac{n_1}{n_2}\right)a_{21}}{1 - \frac{1}{2}\left(1 + \frac{n_1}{n_2}\right)a_{21} + \frac{1}{2\sqrt{\pi}}\left(\frac{n_2}{n_1} - \frac{n_1}{n_2}\right)a_{21}s_1^{-1}} \quad (11.9)$$

Equation (11.9) is plotted in Fig. 11.6 for a single blade row for compression ratios (pressure ratio n_2/n_1) in the range 1–7. The Chang-Jou theory predicted a higher transmission coefficient than predicted by Kruger; however, it agrees with direct simulation Monte Carlo (DSMC) calculations. The differences between the two models become large when blades of open structure are analyzed. Using blades of closed structure (10°) the two models give similar results. Figure 11.7 illustrates the speed factors for various gases in a commercial turbomolecular pump. At a nitrogen inlet pressure of 0.9 Pa, the rotor is still running at full speed and the gas throughput is 400 Pa-L/s. This is twice the throughput of a nominal 6-in.diameter diffusion pump operating at an inlet pressure of 0.1 Pa.

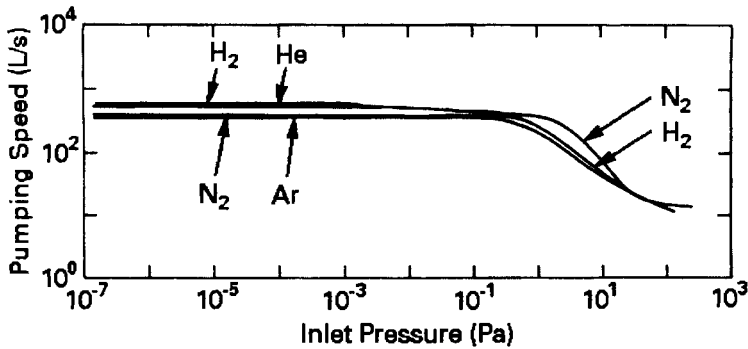


Fig. 11.7 Measured pumping speeds for the Pfeiffer TPU-400 turbomolecular pump. Reprinted with permission from A. Pfeiffer Vakuumtechnik, GmbH, Wetzlar, Germany.

11.3 ULTIMATE PRESSURE

The ultimate pressure of a turbomolecular pump is determined by the compression ratio for light gases and by the amount of outgassing. This is qualitatively similar to a diffusion pump. (See discussion in Section 12.2.) The main difference between the turbomolecular pump and the diffusion pump is the low hydrogen compression ratio in the turbo pump. It is low enough so that the ultimate hydrogen pressure will be determined by $K_{\max}(\text{H}_2)$ and its partial pressure in the foreline. In some very old pumps, which had a water-vapor compression ratio of less than 10^4 , the water-vapor partial pressure may also be compression ratio limited [8]. The partial pressure of all other gases and vapors will be limited by their respective outgassing rates and pumping speeds. During pumping of an unbaked turbomolecular pump, the slow release of water vapor from the blades closest to the inlet may slightly decrease the rate of water removal. The effective compression ratio for water release from the first few blades is much less than K_{\max} .

Henning [9] has shown the forepump oil dominates the partial pressure of hydrogen found in a turbomolecular pump system. The ultimate pressure varied from 2×10^{-7} – 5×10^{-7} Pa as a function of the type of oil in the forepump. Because the turbopump oil has a lower vapor pressure than the mechanical pump oil, it will not contribute so much hydrogen to the background as the forepump oil. Henning and Lotz [10] used perfluoropolyether pump fluid for lubricating both the turbomolecular pump and the forepump in the presence of corrosive gases. Using a mass spectrometer, they observed distinct fluorine and hydrogen peaks. This decomposition occurred because the local heating of the bearings caused the oil temperature to exceed the range of thermal stability. They

concluded from the presence of hydrogen that the ultimate pressure of the pump was not improved with hydrogen-free fluids. They postulated the limiting pressure was caused by the diffusion of hydrogen through the foreline seals.

Ultimate pressures for baked systems between 2×10^{-8} and 5×10^{-9} Pa are possible with high-compression turbomolecular pumps without the assistance in pumping from cryo baffles or titanium sublimation pumps. Hydrogen will constitute more than 99% if the residual gas at the ultimate pressure [8]. Ultimate pressures of order 10^{-7} Pa (10^{-9} Torr) have been achieved with the use of tandem turbomolecular pumps [11].

11.4 TURBOMOLECULAR PUMP DESIGNS

A single blade row is inadequate to serve as a high vacuum pump. Multiple-bladed structures with 8–20 disks will provide adequate compression and speed to make a functional pump. As in the diffusion pump, the stages nearest the high vacuum inlet serve a purpose different from those nearest the outlet. The flow through each stage is constant or, stated another way, the product of speed and pressure is a constant. The blades nearest the inlet are designed to have a high pumping speed and a low compression ratio. The blades nearest the foreline are designed to have a high compression ratio and a low pumping speed. For economic reasons it would be impractical to make each blade differently than its neighbor. A

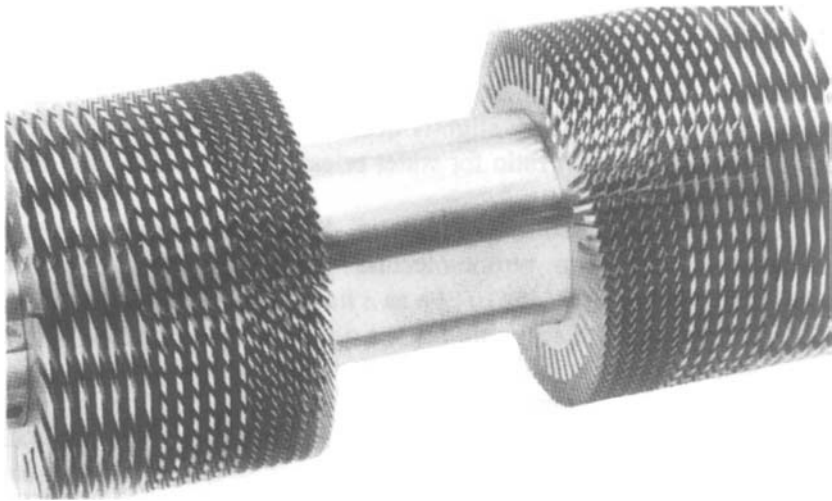


Fig. 11.8 Three-stage rotor from a Pfeiffer TPU-200 turbomolecular pump. Reprinted with permission from A. Pfeiffer Vakuumtechnik, GmbH, Wetzlar, Germany.

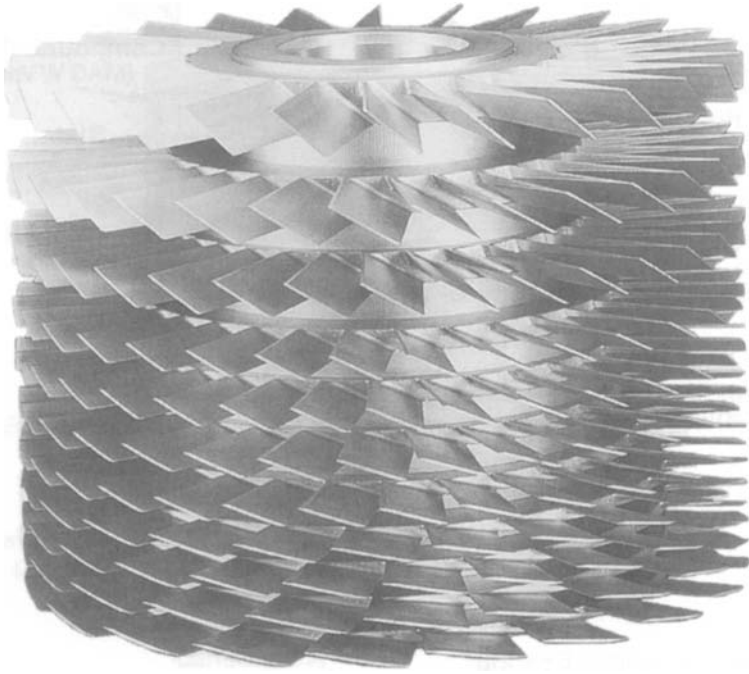


Fig. 11.9 Rotor used in a classical vertical turbomolecular pump. Reprinted with permission from Leybold Vakuum GmbH, Bonner Str. 498, 50968 Köln, Germany.

compromise results in groups of two or three blade types. The blades in each group are designed for a specific speed and compression ratio. Each group of blades may be considered analogous to a diffusion pump jet. The pump designer may trade-off pumping speed and light gas compression ratio by the choice of s/b ratio and ϕ . Pumps exhibiting a large compression ratio for hydrogen use blades that are optically more opaque (s/b , ϕ small) than those designed to maximize the pumping speed (s/b , ϕ large).

Figure 11.8 shows a view of the three-stage rotor used in a horizontal-axis, dual-rotor pump. The rotors are individually abrasive-machined and balanced. The rotor disks are positioned on a cooled hub that is allowed to thermally equilibrate with the disks and hold them rigidly in position. Stator disks are formed in a similar manner, cut into half sections, and mounted stage-by-stage as the rotor is moved into the housing. The rotors used in a classical, vertical-axis pump shown in Fig. 11.9 are machined from a single block of aluminum. In a manner similar to the horizontal turbo design, the compression ratio increases and the speed decreases as gas flows toward the foreline. Turbomolecular pump stator blades are constructed from aluminum alloy stampings [7].

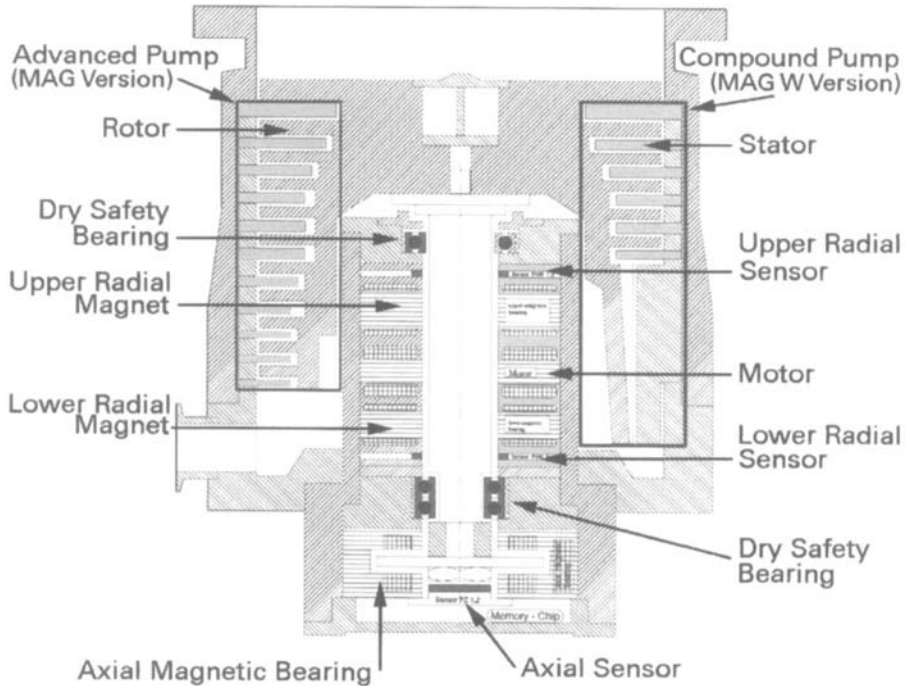


Fig. 11.10 Cross section of a magnetically levitated turbomolecular pump. Reprinted with permission from Leybold Vakuum GmbH, Bonner Str. 498, 50968 Köln, Germany.

Turbomolecular pumps have been built in vertical-axis, single-rotor or horizontal-axis, double-rotor styles. In either configuration the designer is free within limits of material stability to choose the number of stages, blade angle, blade spacing, and blade-to-chord ratios. The horizontal axis pump allows for a somewhat more stable bearing design than does the vertical pump. It is possible to optimize both designs for maximum speed or maximum compression. The single-rotor, vertical-axis pump has little conductance loss between the inlet flange and the rotor, while the horizontal-axis design has a greater conductance loss but pumps from two sides. Henning [8] estimated the pumping speed of a dual-rotor pump to be ~ 1.6 times that of a vertical pump of the same inlet diameter with other factors constant.

Neither style should be subjected to a steady or transient twisting moment by using the inlet flange to bear the load of a heavy work chamber, especially a cantilever load, or the impulse of a heavy flange closure [12]. Improper loading can cause premature bearing failure. All pumps should be suspended from the system by their inlet flanges. The inlet flange should not be used as a mounting platform for a heavy system.

This is usually not a problem for a vertical turbomolecular pump because it looks like a diffusion pump.

The maximum rotational speed is $\sim 80,000$ rpm, or a blade tip velocity of about 500 m/s. These limits are due to bearing tolerances, thermal coefficients of expansion, and material stress limits. Ball bearings are the component subjected to the greatest wear. Oil, either flowing or in a mist, may be used to lubricate and cool bearings. The oil is, in turn, either water- or refrigeration-cooled. Small-diameter bearings are desired to increase the bearing lifetime. Some pumps use grease-packed bearings [13], although they have been shown to be less reliable than oil-lubricated bearings [14]. Magnetically levitated bearings with extremely low wear rates are common; such a pump is illustrated in Fig. 11.10.

11.5 TURBOMOLECULAR DRAG PUMPS

The conventional turbomolecular pump requires a backing pump that can produce exhaust pressures of order $0.1\text{--}1$ Pa ($10^{-3}\text{--}10^{-2}$ Torr). Oil-sealed two-stage rotary mechanical pumps formerly were the pump of choice for this application. In the last decade, cleanliness considerations have dictated

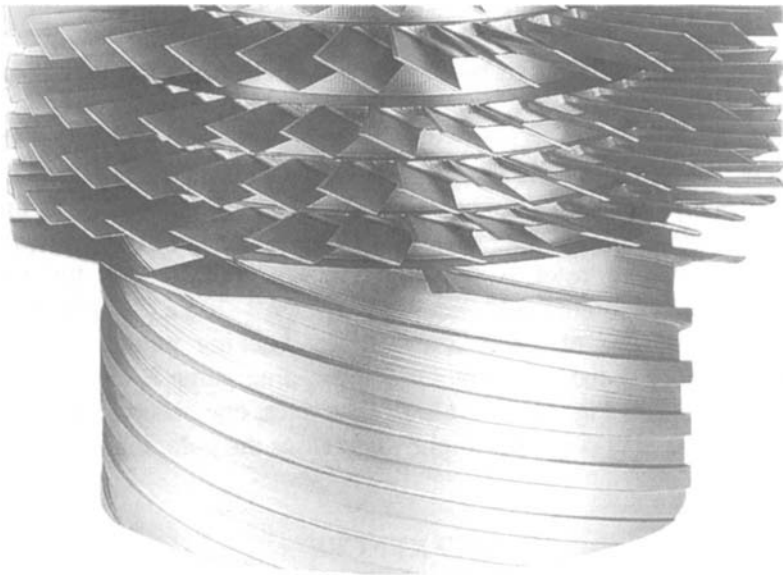


Fig. 11.11 Detail of the Holweck revolving-screw molecular drag stage used in a compound turbo-drag pump. Reprinted with permission from Leybold Vakuum GmbH, Bonner Str. 498, 50968, Köln, Germany.

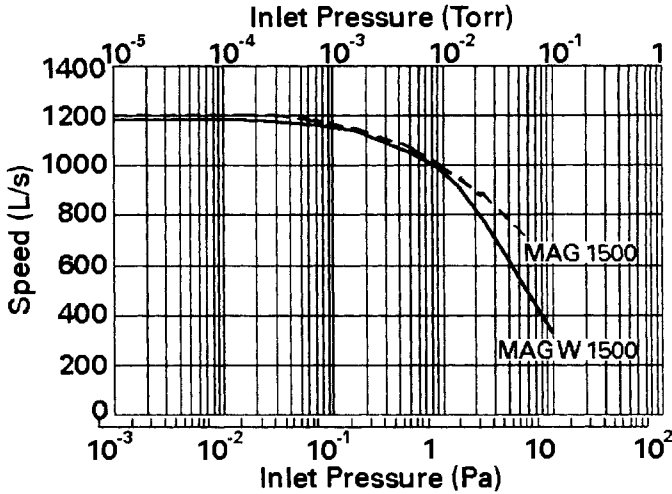


Fig. 11.12 Pumping speeds of a magnetically levitated turbo pump (MAG 1500) and a turbo-drag magnetically levitated turbo pump (MAG W 1500). Reprinted with permission from Leybold Vakuum GmbH, Bonner Str. 498, 50968 Köln, Germany.

the use of completely oil-free pumping systems. Magnetically levitated turbos backed with oil-free mechanical pumps significantly reduce the level of hydrocarbon contamination in turbopumped systems [15]. Many of the dry pumps discussed in Chapter 10 cannot meet the low-pressure requirements for backing a turbo. As a result, molecular drag pump stages have been incorporated on the axis of the turbo after its exhaust, to compress the exiting gas to a pressure compatible with dry pumps such as the screw, scroll, and diaphragm. One common molecular drag pump, the Holweck pump, consists of either a grooved (threaded) rotating cylinder inside a smooth stator cylinder or vice-versa). The design of one integrated turbomolecular drag rotor is illustrated in Fig. 11.11. Such turbo-drag combinations have foreline tolerances in the range 4–20 Pa (30–150 mTorr). This allows the use of small low-cost dry backing pumps. The high vacuum pumping speed of a compound turbo-drag pump is similar to that of a pure turbo. See Fig. 11.12. At high flow rates, one observes some flow limitation in the drag stage that slightly decreases the pumping speed.

REFERENCES

1. W. Becker, *Vakuum Technik*, **7**, 149 (1958).
2. W. Becker, *Vakuum Technik*, **15**, 211 (1966).
3. C. H. Kruger and A. H. Shapiro, *Proc. 2nd. Int. Symp. Rarefied Gas Dynamics*, Berkeley, CA, L. Talbot, Ed., Academic, New York, 1961, pp. 117–140.

4. C. H. Kruger and A. H. Shapiro, *Trans. 7th Natl. Vac. Symp. (1960)*, Pergamon, New York, 1961, pp. 6–12.
5. C. H. Kruger, *The Axial Flow Compressor in the Free-Molecular Range*, Ph.D. Dissertation, Department of Mechanical Engineering, M.I.T., Cambridge, MA, 1960.
6. Yu-Wen Chang and Rong-Yuan Jou, *J. Vac. Sci. Technol. A*, **19**, 2900 (2001).
7. K. H. Mirgel, *J. Vac. Sci. Technol.*, **9**, 408 (1972).
8. J. Henning, *Proc. 6th Int. Vac. Congr., Kyoto, Japan J. Appl. Phys. Suppl. 2*, Pt. 1, 5 (1974).
9. J. Henning, *Vacuum*, **21**, (1971).
10. J. Henning and H. Lotz, *Vacuum*, **27**, 171 (1977).
11. H. Enosawa, C. Urano, T. Kawashima, and M. Yamamoto, *J. Vac. Sci. Technol. A*, **8**, 2768 (1990).
12. K-H Bernhardt, M. Mädler and O. Ganschow, *Vacuum*, **44**, 721 (1993).
13. G. Osterstrom and T. Knecht, *J. Vac. Sci. Technol.*, **16** 746 (1979).
14. M. Heldner and H.-P. Kabelitz, *J. Vac. Sci. Technol. A*, **8**, 2772 (1990).
15. A. Conrad and O Ganschow, *Vacuum*, **44**, 681 (1993).

PROBLEMS

- 11.1 † Describe the operating mechanism of a turbomolecular pump.
- 11.2 Why does a turbomolecular pump need a stator?
- 11.3 A particular turbomolecular pump has a tip velocity of 400 m/s. What is the ratio of average room temperature molecular velocity to blade tip velocity for (a) hydrogen, (b) nitrogen, and (c) xenon molecules? What fraction of the molecules has velocities greater than the blade tip velocity?
- 11.4 † What causes the pumping speed of a turbomolecular pump to fall at its low pressure extreme?
- 11.5 What happens when the critical discharge pressure of a turbomolecular pump is exceeded during operation?
- 11.6 † What is the best place to vent a turbomolecular pump? (a) In the foreline or (b) in the high vacuum chamber?
- 11.7 † When a turbomolecular pump is stopped is it better to (a) continue pumping on it with the forepump to keep it clean or (b) vent it to air with a dry gas?
- 11.8 Qualitatively, what is the relationship between the thermal velocity of a gas and its maximum compression ratio in a turbomolecular pump?
- 11.9 Screens are located in the throat of turbomolecular pumps to prevent objects from damaging the rotor. One pump contains a double mesh screen in the throat. The first mesh is made from 0.005-in.-diameter

wire on 0.025-in. centers, whereas the second mesh is made from 0.02-in.-diameter wire on 0.150-in. centers. The Ho coefficient or transmission coefficient of the pump is $a = 0.24$ without the screen. Calculate the percent reduction in pumping speed.

- 11.10 Figure 11.13 describes the pumping speed versus inlet pressure for two pumps used in series combination: a turbomolecular-drag pump and a screw pump. A gas flow of 300 Pa-L/s is allowed to flow through the two pumps. Under this operating condition, determine (a) the inlet pressure of the turbo-drag pump; (b) the inlet pressure to the screw pump, (c) compression ratio of the turbo-drag pump, (d) the compression ratio of the screw pump.

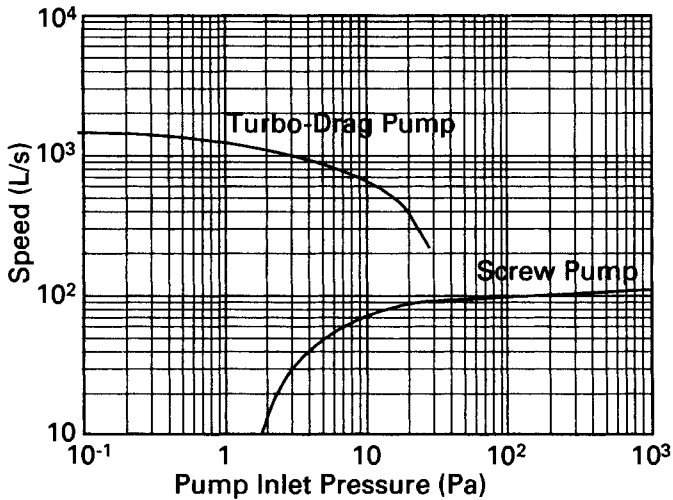


Fig. 11.13 Pumping speed curves for use with Problem 11.10

CHAPTER 12

Diffusion Pumps

The diffusion pump has been a part of vacuum technology for a century. The discovery of low vapor pressure pumping fluids and the ability to control backstreaming soon made it a useful pump [1]. Today, it is still the most widely used high vacuum pump even though ion, cryogenic, and turbomolecular pumps are used for most high-technology applications. Because of its long history, this pump has been the subject of more study and literature than any other high vacuum pump. Its problems are thoroughly understood and its performance is, in some cases, understated. Many excellent articles summarize the pump's properties for practical applications [2–4] and review its operation [1,5–7]. Several texts cover its theory of operation and design [8,9].

Here we review the basic mechanisms of pump operation, pumping speed and throughput, heat effects and backstreaming, baffles, and traps. System problems are treated in later chapters.

12.1 PUMPING MECHANISM

The name “diffusion pump,” first coined by Gaede [10], does not describe the operation of the pump accurately. The diffusion pump is a vapor jet pump, which transports gas by momentum transfer on collision with the vapor stream. A motive fluid such as hydrocarbon oil, an organic liquid, or mercury is heated in the boiler until it vaporizes. The vapors flow up the chimney and out through a series of nozzles. Figure 12.1 sketches a sectional view of a metal-bodied diffusion pump. The nozzles, three in this illustration, direct the vapor stream downward and toward the cooled outer wall where it condenses and returns to the boiler. The vapor flow is supersonic. Gases that diffuse into this supersonic vapor stream are, on average, given a downward momentum and ejected into a region of higher pressure. Modern pumps have several stages of compression—usually three to five for small pumps and up to seven for large pumps.

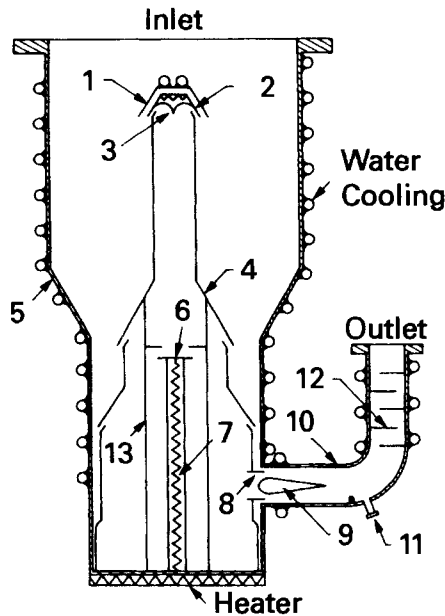


Fig. 12.1 A sectional view of a metal diffusion pump and some of its innovations: (1) Cooled hood for prevention of vapor backstreaming [11,12]; (2) heater for the nozzle's cap to compensate for loss of heat [13]; (3) streamlined surface to avoid turbulence [14]; (4) multiple stages to obtain low pressures [15]; (5) enlarged casing to give larger pumping aperture [16]; (6) baffle to impede the access to the jet of liquid splashed up from the boiler [17]; (7) heater for superheating the vapor [18]; (8) lateral ejector stage [19]; (9) conical body allowing operation against higher forepressures [20]; (10) hot maintained diffuser for oil purification [21] and catchment and drain-off of highly volatile oil components[22]; (12) baffle to reduce oil loss [15]; (13) concentric chimneys that allow oil fractionation [23]. Reprinted with permission from *Vacuum*, 13, p 569, N. A. Florescu. Copyright 1963, Pergamon Press Ltd.

Each stage compresses the gas to a successively higher pressure than the preceding stage as it transports it toward the outlet.

The boiler pressure in a modern diffusion pump is about 200 Pa (2 Torr). Ideally, the pump cannot sustain a pressure drop any larger than this between its inlet and outlet. The practical maximum value of forepressure tolerated by the pump is less than the boiler pressure. This maximum value called the "critical forepressure," ranges from 25–75 Pa (0.2–0.6 Torr) and is dependent on pump design and boiler pressure. The latter number is typical of modern pumps. The diffusion pump cannot eject gas to atmospheric pressure. It must be "backed" by another pump in order to keep the forepressure (exhaust pressure, or foreline pressure) below the critical forepressure. Rotary vane or piston pumps or combinations of rotary and lobe blowers are used as "backing" or "fore" pumps. If the

forepressure exceeds the critical value, all pumping action will cease. The pumping action ceases at high pressures because the directed supersonic vapor stream no longer extends from the jet to the wall, but is ended in a shock front close to the jet [5]. Those vapor molecules beyond the shock front are randomly directed and cannot stop gas molecules from returning to the inlet. As the critical forepressure is exceeded, the inlet pressure will rise sharply and uncontrollably in response to the cessation of pumping. The critical forepressure should never be exceeded. In newer pumps the inlet pressure and the pumping speed will be unaffected by the value of forepressure as long as it is below the critical value and the gas throughput is low. At maximum throughput the critical forepressure will be reduced to about 3/4 of its normal value [2]. The amount of reduction is a function of the pump design, heater power, and pump fluid.

Each stage of the vapor pump has a characteristic speed and pressure drop. Since the jets are in series, the gas flow Q is the same through each stage. The flow, $Q = S\Delta P$, is the product of the speed of the jet times the pressure drop across the jet. The top jet has the largest speed (and the largest aperture) and the lowest pressure drop. The vapor density in the top jet is less than that in the lower jets. Because the gas flow through a series of jets is the same, each successive jet can have a larger pressure drop and a smaller pumping speed. The last jet has the greatest pressure drop. Many pumps use a vapor ejector as the last stage, because it is an efficient gas compressor in this pressure region. The combination of jets and ejector produces a pump with a higher forepressure tolerance than is possible with vapor jets alone. Fractionating pumps [23] have concentric chimneys and boilers with long fluid flow paths that allow light fractions to be preferentially directed to the lower jets after condensation. Degassing of the fluid is accomplished by maintaining a section of the ejector walls at an elevated temperature [21]. Pumps with these and other advances, which use heavy fluids produced by molecular distillation, can pump to 5×10^{-5} Pa (3×10^{-7} Torr) without trapping and $< 5 \times 10^{-9}$ Pa ($< 3 \times 10^{-11}$ Torr) when trapped with liquid nitrogen.

12.2 SPEED-THROUGHPUT CHARACTERISTICS

The four operating regions of the diffusion pump are the constant speed, constant throughput, mechanical pump, and compression ratio regions. They are graphically illustrated in Fig. 12.2. In its normal operating range the diffusion pump is a constant speed device. Its efficiency of pumping gas molecules (the Ho coefficient, or pump capture probability) is about 0.5 for the pump alone, but only about 0.3 when a trap and valve is used. The usual operating range for constant speed is about 10^{-1} Pa to $< 10^{-9}$ Pa

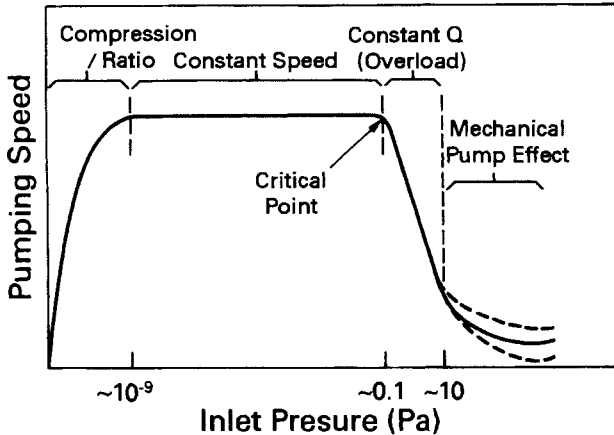


Fig. 12.2 Typical diffusion pump speed curve for a given gas. Four regions are evident: (1) Effect of compression ratio limit; (2) normal operation—constant speed; (3) first jet overloaded—nearly constant throughput; (4) effect of mechanical pump. Reprinted with permission from *Jpn. J. Appl. Phys., Suppl. 2*, Pt. 1, p 25, M. H. Hablani. Copyright 1974, Japanese Journal of Applied Physics.

for most gases. The maximum or limiting inlet pressure is called the “critical inlet pressure” and it corresponds to the point at which the top jet fails. In a 6-in. diffusion pump the top jet becomes unstable at pressures of about 0.1 Pa, the middle jet at pressures of about 3 Pa, and the bottom jet at pressures of about 40 Pa [24].

The gas throughput in the constant speed range is the product of the inlet pressure and the speed of the pump at the inlet flange. It rises linearly with pressure until the critical inlet pressure is reached. Above that pressure the pump throughput is constant until the jets all cease to function. At higher pressures the throughput again increases in accordance with the speed of the backing pump. The maximum usable throughput of the diffusion pump corresponds to the product of the inlet speed and the critical inlet pressure. If that pressure is exceeded, the backstreaming may increase and jet instabilities will appear. These instabilities make pressure control difficult. The maximum throughput should not be exceeded in the steady state, although it often happens for short periods of time during crossover from rough to high vacuum pumping.

Exceeding the critical forepressure in a well-designed pump is usually the result of equipment malfunction, while the critical inlet pressure is easily exceeded by incorrect operation. If the pump is equipped with a sufficiently large forepump, the critical forepressure can still be exceeded if a leak occurs in the foreline, the mechanical pump oil level is too low, the mechanical pump belt is loose, or a section of the diffusion pump

heater is open. The critical inlet pressure can be exceeded by operational error, but otherwise the top jet will continue to pump unless there is a partial heater failure or a large leak.

The speed does not remain constant to extremely low pressures, but it decreases toward zero as shown in the compression ratio region of Fig. 12.2. This curve decreases at low pressures because of the large but finite compression ratio of the diffusion pump jets. The pump whose hypothetical speed curve for one gas is shown in Fig. 12.2 has an ultimate pressure of 10^{-10} Pa. If, at that point, its forepressure were 1 Pa, its compression ratio would be 10^{10} , a value similar to those quoted in the literature. Figure 12.3 shows the air pumping speed for a 6-in. diffusion pump with and without a nitrogen baffle. All diffusion pumps have some small reverse flow of the gas being pumped; and although this reverse flow is exceedingly small for heavy gases, it may be feasible for light gases under certain conditions. Because of their high thermal velocity and small collision cross section, the compression ratio of light gases such as hydrogen and helium is lower than that of heavy gases. Figure 12.4 sketches the relative pumping speeds of several gases and vapors as a function of their inlet pressure, and it illustrates the effect of a low compression ratio for hydrogen. The compression ratio for heavy gases will be about 10^8 – 10^{10} . For light gases it can be small enough (10^3 – 10^6) in some pumps so that a small foreline concentration can be detected at the inlet [1,25]. It is this phenomenon that explains why hydrogen emanating from an ion gauge in the foreline can be detected at the inlet. The operation of one leak detector [26] is based on this principle. The detector is located at the inlet, and the test piece is appended to the foreline. The compression ratio for heavy gases is adequate to produce a low pressure in the detector, while at the same time allowing helium to back-diffuse and be counted.

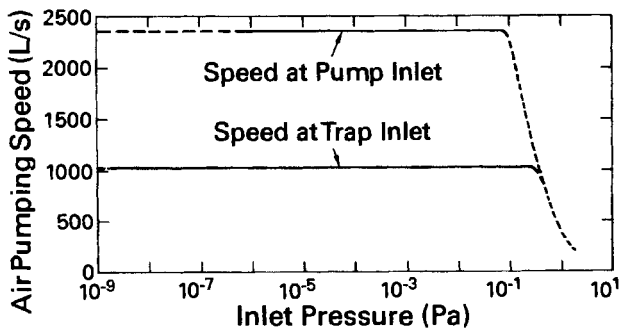


Fig. 12.3 Air pumping speed of the Varian VHS-6, 6-in. diffusion pump with and without a liquid nitrogen trap. Reprinted with permission from Varian Associates, 611 Hansen Way, Palo Alto, CA 94303.

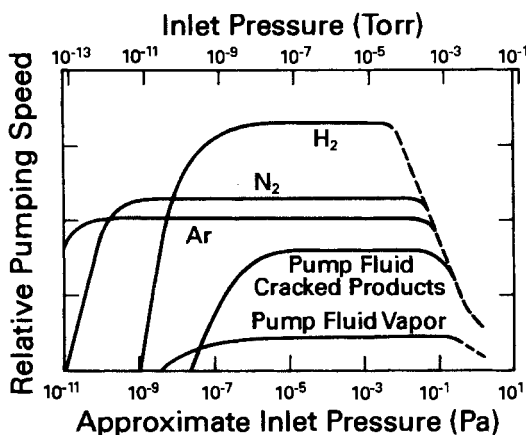


Fig. 12.4 Diffusion pump performance for individual gases. Reprinted with permission from *J. Environ. Sci.*, 5, p. 7, S. G. Bennet and M. H. Hablanian. Copyright 1964, The Institute of Environmental Sciences.

The ultimate or limiting pressure in a diffusion pumped system can be a result of reaching the compression ratio limit or wall outgassing. For the ideal pump with zero outgassing above the top jet and in the work chamber, and using a perfect baffle to collect all oil vapor fragments, the ultimate pressure would be the sum of each of the partial pressures in the foreline divided by their respective compression ratios:

$$P_u = \frac{P_{f1}}{k_1} + \frac{P_{f2}}{k_2} + \frac{P_{f3}}{k_3} \dots \quad (12.1)$$

For the case in which the base pressure of the system is achieved in the pump's constant speed region, the ultimate pressure is the sum of each independent gas flow Q_i , divided by the pumping speed for each gas S_i :

$$P_u = \frac{Q_1}{S_1} + \frac{Q_2}{S_2} + \frac{Q_3}{S_3} \dots \quad (12.2)$$

In practice the ultimate pressure is usually determined by (12.2). In some situations it can be due to gases dissolved in the fluid, the lightest fractions of pump fluid that are released by the trap, or the compression limit. For example, the partial pressure of H_2 and perhaps He may be determined by the compression ratio (12.1). A single pumping speed curve (Fig. 12.2), representative of all gases, cannot be drawn because the pumping speed is not the same for all gases (see Fig. 12.4). The pumping speed is greater for light gases, but not in proportion to $m^{1/2}$ as predicted by the ideal gas law. Usually, He will be pumped about 20% faster than N_2 .

12.3 BOILER HEATING EFFECTS

The effect of boiler heat input variation is summarized concisely in Fig. 12.5. The general trends are that the oil temperature, forepressure tolerance, and throughput increase with boiler power, while pumping speeds decrease at high heat inputs because of the increased density of oil molecules in the vapor stream [7]. It is not possible to optimize the pumping speed for all gases at the same heater power because of the differences in mass and thermal velocity. Each gas reaches maximum speed at a different input power. The pumping speed is a function of the momentum transfer between fluid and gas molecules. Heavy fluid molecules often have lower pumping speeds than light molecules unless the boiler temperature is adjusted. Excessively increasing the boiler temperature also hastens fluid degradation [3]. Pumps can be filled with any fluid; however, some older pumps, especially those designed to work with older fluids, do not provide enough heat input for heavy fluids. The maximum throughput is directly proportional to boiler power. They are dimensionally equivalent; $1000 \text{ Pa-L/s} = 1 \text{ W}$. For pumps of efficient design, this can be as high as 150 Pa-L/s per kW of boiler power [2]. A straight-sided pump with a 200-mm-diameter boiler and throat has the same maximum throughput as a pump with a 200-mm-diameter boiler and an expanded top like the pump shown in Fig. 12.1. The maximum speed of a pump in the high vacuum region is proportional to its inlet area.

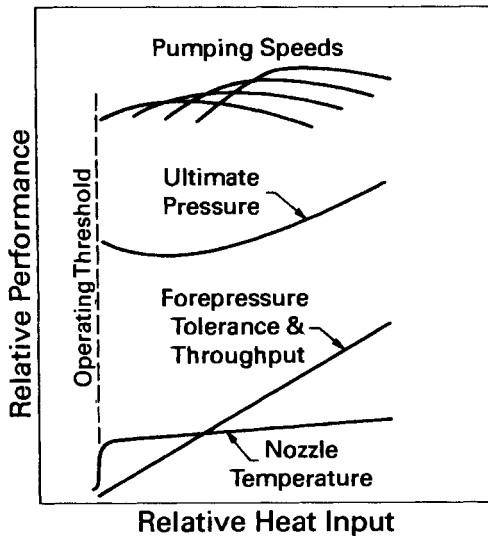


Fig. 12.5 Effect of heat input variations on various diffusion pump parameters. Reprinted with permission from *Jpn. J. Appl. Phys., Suppl. 2*, Pt. 1, p. 25, M. H. Hablanian. Copyright 1974, Japanese Journal of Applied Physics.

12.4 BACKSTREAMING, BAFFLES, AND TRAPS

For the purpose of this discussion, backstreaming is defined as the transport of pumping fluid and its fractions from the pump to the chamber. Hablani [27] properly points out that the discussion of backstreaming must not be limited to the pump but must include the trap, baffle, and ductwork as well because all affect the transfer of pumping fluid vapors from the pump body to the chamber. First, let us consider the contributions from the pump. Five sources of steady-state backstreaming have been identified [12]: (1) Evaporation of fluid condensed on the upper walls of the pump, (2) premature boiling of the condensate before it enters the boiler, (3) the overdivergence of the oil vapor in the top jet, (4) leaks in the jet cap, and (5) evaporation of fluid from the heated lip of the top jet. The backstreaming from (1) can be reduced by the use of low vapor pressure fluids and added trapping over the pump. Most pump designs eliminate sources (2) and (4). The use of a water-cooled cap [1,12] directly over the top jet assembly substantially reduces (3) and (5), which were found to be the major causes of fluid backstreaming. With these precautions the backstreaming can be reduced to $\sim 10^{-3}$ (mg/cm²)/min a short distance above the pump inlet.

Further reduction of the backstreaming is possible by use of a baffle or a trap. The words “trap” and “baffle” are often misused. Operationally, a trap is a pump for condensable vapors, and a baffle is a device that condenses pump fluid vapors and returns the liquid to the pump boiler. Today the two words are often used imprecisely; and when the baffle is cryogenically cooled the distinction disappears. Pump-fluid molecules or fragments may find their way through the trap by creeping along the walls, by colliding with gas molecules, and by reevaporation from surfaces. Creep can be prevented by the use of traps with a creep barrier—a thin membrane extending from the warm, outer wall to the cooled surface [28] or by the use of autophobic fluids such as pentaphenylsilicone or pentaphenylether. Backstreaming due to oil–gas collisions is a linear function of pressure up to the transition region and a function of the trap and pump design. For one 200-mm-diameter diffusion pump and trap combination, the peak value was found to be 3×10^{-6} (mg/cm²)/min at a pressure of 5×10^{-2} Pa [29]. At higher pressures the backstreaming rate was decreased by the flushing action of the gas. In normal operation it traverses this region quickly. The maximum integrated backstreaming rate from oil–gas collisions is small enough so that contamination from this source is of no concern in an unbaked system.

The problem of re-evaporation is subtle. The vapor pressures of diffusion pumps vary widely. See Appendix F.2. The two fluids with the lowest vapor pressures (pentaphenyl silicone and pentaphenylether) have very low room temperature vapor pressures. Some decomposition of the

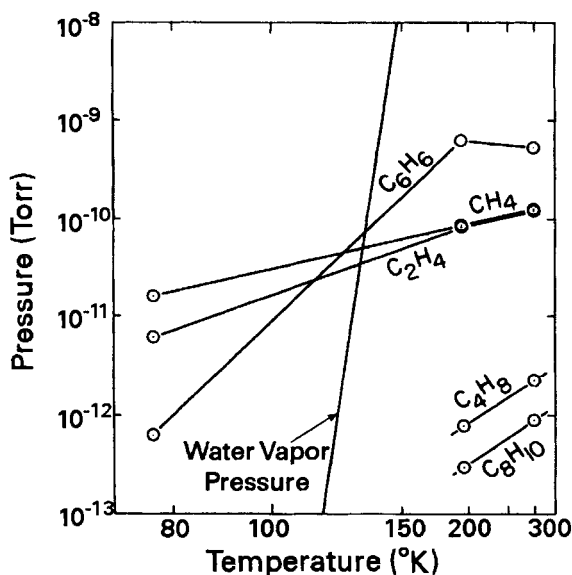


Fig. 12.6 Residual gas analysis of selected mass fragments backstreaming from a diffusion pump filled with DC-705 fluid. Plotted from data reported in *J. Vac. Sci. Technol.*, **2**, p. 293 (1965), C. M. Gosselin and P. J. Bryant.

fluid does occur in the boiler, and light fractions are generated. Residual gases in a DC-705 charged diffusion pump showed backstreaming of light, intermediate, and heavy fragments [30]. See Fig. 12.6. Light fractions (methane, ethane and ethylene) were not effectively trapped even on a liquid-nitrogen-cooled surface because of their high vapor pressures. The very heavy fragments (e.g., C₈H₁₀) were quite effectively trapped with only a water-cooled baffle. The partial pressure of an intermediate weight fragment C₆H₆ was reduced by a factor of 1000, when the trap was cooled from 25°C to -196°C. When using low vapor pressure fluids, such as pentaphenylsilicone or pentaphenylether, the basic operational difference between a liquid nitrogen trap and a cold water baffle is the ability of the liquid nitrogen trap to pump C₆H₆ and to trap, partially, some of the light weight fractions.

The quantitative effects of various trap, baffle, and creep barrier combinations are summarized in Table 12.1 [27]. It was noted that the addition of the chevron water baffle between the liquid nitrogen trap and the pump is not much better than the addition of a piece of straight pipe or elbow of the same length.

The Herrick effect [31] and the fluid burst resulting from the formation and collapse of the top jet are two transient phenomena that cause backstreaming. The Herrick effect is the ejection of frozen fluid droplets

Table 12.1 Diffusion Pump Backstreaming^a

Conditions	Duration of Test (h)	Backstreaming Rate (mg/cm ²)/min
(1) Without baffle	165	1.6×10^{-3}
(2) With liquid nitrogen trap	170	5.3×10^{-6}
(3) Same as (2)	380	6.5×10^{-6}
(4) Item (3) plus water baffle	240	2.8×10^{-7}
(5) Item (4) plus creep barrier	240	8.7×10^{-8}
(6) Same as (5)	337	1.2×10^{-7}

Source: Reprinted with permission from *J. Vac. Sci. Technol.*, 6, p. 225, M. H. Hablanian. Copyright 1969, The American Vacuum Society.

^a Measurements made with a 6-in.-diameter diffusion pump (NRC HS6-1500), DC-705 pump fluid and liquid-nitrogen-cooled collectors.

from the surface of a fluid-covered trap during the initial stages of cooling with liquid nitrogen. These fluid droplets ricochet off the walls and land on samples or fixtures. A well-designed cold cap and water-cooled baffle followed by a continuously operating liquid nitrogen trap will operate for more than a year without collecting excessive amounts of fluid on the trap. The transient backstreaming from the top jet during warm-up and cool-down of the pump is well-documented [12, 19, 32]. Figure 12.7 shows an RGA trace of the parent molecule, $M/z = 446$ of Convalex-10 [32]. The backstreaming decreases as the fluid is cooled and reaches a peak of about

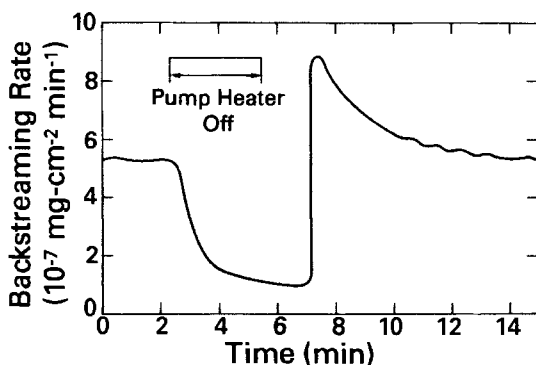


Fig. 12.7 Backstreaming of the parent peak ($M/z = 446$; Convalex-10) over a liquid nitrogen trap during cool-down and start-up of a diffusion pump. Reprinted with permission from *J. Vac. Sci. Technol.*, 9, p. 416, G. Rettinghaus and W. K. Huber. Copyright 1972, The American Vacuum Society.

twice the steady-state rate during heating. A total backstreaming of 6×10^{-4} mg/cm² was measured for a complete start-stop cycle [29]. This backstreaming can be avoided by continuous operation of the diffusion pump or by using the gas-flushing techniques.

By use of high quality, low vapor pressure fluids such as DC-705, Santovac 5, or Convalex 10, and a continuously operating liquid nitrogen trap, the contamination due to pump fluid backstreaming can be made very small. The lowest value of backstreaming shown in Table 12.1 corresponds to a contamination rate of one monolayer per year in a bell jar 500 mm high and 350 mm diameter. This level of organic contamination is below that produced by O-rings and other sources [2]. Fluid backstreaming in a diffusion pump operating at high vacuum is only one source of organic backstreaming. Additional concerns that relate to specific systems are discussed in the Systems chapters.

REFERENCES

1. M. H. Hablanian and J. C. Maliakal, *J. Vac. Sci. Technol.*, **10**, 58 (1973).
2. M. H. Hablanian, *Solid State Technol.*, December 1974, p. 37.
3. M. H. Hablanian, *Proc. 6th Int. Vac. Congr.*, Kyoto, *Japan J. Appl. Phys., Suppl. 2*, Pt. 1, 25 (1974).
4. J. H. Singleton, *J. Phys. E.*, **6**, 685 (1973).
5. N. A. Florescu, *Vacuum*, **10**, 250 (1960).
6. N. A. Florescu, *Vacuum*, **13**, 569 (1963).
7. G. Töth, *Proc. 4th Int. Vac. Congr.*, (1968), Institute of Physics and the Physical Society, London, 300 (1969).
8. S. Dushman, *The Scientific Foundations of Vacuum Technology*, 2nd ed., J. M. Lafferty, Ed., Wiley, New York, 1962, Chapter 3.
9. B. D. Power, *High Vacuum Pumping Equipment*, Reinhold, New York, 1966.
10. W. Gaede, German Pat. 286,404 (filed September 25, 1913).
11. M. Morand, U.S. Pat. 2,508,765 (filed July 27, 1947; priority France, September 25, 1941).
12. B. D. Power and D. J. Crawley, *Vacuum*, **4**, 415, (1954).
13. C. G. Smith, U.S. Pat. 1,674,377 (filed September 4, 1924).
14. W. A. Giepen, U.S. Pat. 2,903,181 (filed June 5, 1956).
15. G. Barrows, Brit. Pat. 475,062 (filed May 12, 1936).
16. J. R. O. Downing, U.S. Pat. 2,386,299 (filed July 3, 1944).
17. B. D. Power, Brit. Pat. 700,978 (filed January 25, 1950).
18. J. R. O. Downing and W. B. Humes, U.S. Pat. 2,386,298 (filed January 30, 1943).
19. R. B. Nelson, U.S. Pat. 2,291,054 (filed August 31, 1939).
20. J. J. Madine, U.S. Pat. 2,366,277 (filed March 18, 1943).
21. N. G. Nöller, G. Reich, and W. Bächler, *Trans. 4th Nat. Symp. Vac. Technol.*, **6**, (1957).
22. B. B. Dayton, U.S. Pat. 2,639,086 (filed November 30, 1951).
23. C. R. Burch and F. E. Bancroft, Brit. Pat. 407,503 (filed January 19, 1933).
24. L. T. Lamont Jr., *J. Vac. Sci. Technol.*, **10**, 251 (1973).
25. S. G. Burnett and M. H. Hablanian, *J. Environ. Sci.*, **5**, 7 (1964).
26. Porta Test® Varian Associates, 611 Hansen Way, Palo Alto, CA 94303.

27. M. H. Hablanian, *J. Vac. Sci. Technol.*, **6**, 265, (1969).
28. N. Milleron, *Trans. 5th Nat. Vac. Symp. (1958)*, Pergamon, New York, 1959, p. 140.
29. G. Rettinghaus and W. K. Huber, *Vacuum*, **24**, 249 (1974).
30. C. M. Gosselin and P. J. Bryant, *J. Vac. Sci. Technol.*, **2**, 293 (1963).
31. M. H. Hablanian and R. F. Herrick, *J. Vac. Technol.*, **8**, 317 (1971).
32. G. Rettinghaus and W. K. Huber, *J. Vac. Sci. Technol.*, **9**, 416 (1972).

PROBLEMS

- 12.1 † Why do diffusion pumps have several stages with different jet-to-wall distances?
- 12.2 † What happens when the critical inlet pressure of a diffusion pump is exceeded during pump operation?
- 12.3 † What happens when the critical forepressure of a diffusion pump is exceeded during pump operation?
- 12.4 A diffusion pump has a maximum inlet speed of 1500 L/s and a maximum inlet pressure of 1.3×10^{-1} Pa. Its critical forepressure is 40 Pa. What is its maximum throughput? What is the minimum pumping speed necessary at the foreline connection to ensure the pump will not exceed the critical forepressure? Would you choose a single-stage or a double-stage vane pump for this application? Why?
- 12.5 Plot the air throughput versus pressure characteristic for the pump whose speed is depicted in Fig. 12.3 with and without the cold trap.
- 12.6 What can happen to a diffusion pump if (a) the cooling water flow is too great, say, 2 g/min through a 6-in. diffusion pump instead of 0.4 g/m, (b) the cooling water temperature is too low, say, 7–10°C, (c) the cooling water has too high a soluble salt content from improper water treatment, (d) the cooling water contains excessive calcium and other insoluble salts (hard water)?
- 12.7 What must be provided to prevent material collected on traps from migrating to the inlet side of a cooled trap during regeneration?
- 12.8 In what pressure range will the gas flow into an 209-mm-diameter diffusion pump be in transition between laminar-viscous and molecular flow?
- 12.9 What will happen if a liquid-nitrogen-cooled trap is warmed for a few hours and then cooled while the high vacuum valve is closed?
- 12.10 Describe qualitatively the sequence in which gases are released when a LN₂ trap coated with O₂, N₂, CO₂, CO, CH₄, and H₂ warms.

CHAPTER 13

Pump Fluids

Organic fluids are used in rotary vane, piston, screw, scroll, lobe, turbomolecular, and diffusion pumps. In a rotary vane or piston pump fluids provide a vacuum seal between the moving surfaces and lubricate and cool the low-speed bearings and sliding surfaces. Screw, scroll, lobe, and turbomolecular pumps use oil or a synthetic fluid to lubricate and cool low-, medium-, or high-speed bearings; however, none of these pumps uses fluid to make the vacuum seal. Diffusion pumps vaporize liquids to form supersonic jets that transfer momentum to gas molecules. Ideally each fluid should be thermally stable, and chemically inert, have a low vapor pressure, and, when necessary, be a good lubricant. Unfortunately every desirable attribute cannot be realized simultaneously so that some compromise is required in formulating or choosing a fluid for any application.

The fluids used in vacuum pumps are highly refined mineral oils and synthetic esters, silicones, ethers, and fluorocarbons. In this chapter we review fluid properties, pump fluid types, selection, and reclamation.

13.1 FLUID PROPERTIES

Vapor pressure and lubricating ability are the two most important properties of a vacuum pump fluid. Low vapor pressure is necessary to avoid oil vapor transport to the vacuum chamber, and mechanical pump fluids need to be good lubricants. In Chapter 18 we discuss rheological properties—absolute and kinematic viscosity and viscosity index. Here we review vapor pressure measurements and other physical and chemical properties of vacuum pump fluids.

13.1.1 Vapor Pressure

Regardless of its other qualities, a pump fluid, lubricant, or additive is of no use if its vapor pressure is so high that it contaminates the working region of the vacuum chamber. A minimum vapor pressure is necessary

and any further reduction will improve performance, simplify trapping and reduce contamination. For example, a mechanical pump fluid should have a vapor pressure less than 0.1 Pa (10^{-3} Torr) at its operating pressure, whereas a diffusion pump requires a fluid whose room temperature vapor pressure is in the range 10^{-3} – 10^{-7} Pa. Most of us will never measure the vapor pressure of a pump fluid, however, we do need to know how, when and if the available data were measured.

Many techniques have been devised for the measurement of oil vapor pressure [1–3]. Knudsen effusion [1,2] is considered to be reliable and accurate, but there is no standard. Fluid is heated to a constant temperature in a partly filled cell with a small orifice. At equilibrium the rate of vaporization from the fluid surface is equal to the rate of arrival. This equilibrium pressure is the vapor pressure. A tiny hole in the top of the cell allows a small fraction of the vapor to effuse from the cell into a vacuum. The surface area of the liquid needs to be at least ten times the area of the hole in order to maintain the liquid at its equilibrium vapor pressure. Also, diameter of the opening must be less than the mean free path of the heated molecules. A typical cell size is 1.2×10^{-2} m in diameter by 4×10^{-3} m high with a 3×10^{-3} -m-diameter orifice. Outside the cell the pressure must be below $\sim 10^{-3}$ Pa to prevent molecules from returning to the opening. If these criteria are met, the vapor pressure can be calculated from (2.9) and (2.13)

$$P = \left(\frac{dm}{dt} \right) \frac{1}{aA} \left(\frac{2\pi kT}{m} \right)^{1/2} \quad (13.1)$$

or

$$P(\text{Pa}) = 2.278 \times 10^4 \left(\frac{dm}{dt} \right) \frac{1}{aA} \left(\frac{T}{M} \right)^{1/2} \quad (13.2)$$

where a is the transmission probability of the orifice. When the orifice thickness is much less than the diameter, $a = 1$; otherwise the appropriate transmission probability must be taken from Table 3.2. The vapor pressure is calculated from the known cell temperature and weight loss (dm/dt). The fractional weight loss is small. For example a 10^{-4} -kg sample of pentaphenyl ether with a molecular weight of 447 and a vapor pressure of 1 Pa at 200°C will lose weight at the rate of 3×10^{-10} kg/s from an effusion orifice of area 7×10^{-6} m². Vapor pressure measurements are made over a range of temperatures corresponding to 0.2–10% weight loss in 600–900 s. The temperature range will be different for each fluid, but in all cases 80–100°C is near the minimum temperature for adequate sensitivity. All data reported below that temperature are extrapolated. The Clapeyron equation

$$\left(\frac{dP}{dT} \right) = \frac{\Delta H}{T\Delta V} \quad (13.3)$$

gives the vapor pressure–temperature relationship for many substances. ΔH is the heat of vaporization of one kilomole of substance, ΔV is the volume change per kilomole during vaporization. When the specific volume of the gas phase is much greater than that of the liquid phase and when ΔH is independent of T , the solution is

$$\log P_v = A - \frac{B}{kT} \quad (13.4)$$

This solution is known as the Clausius-Clapeyron equation. If the heat of vaporization is a constant, B is a constant, and P_v versus $1/kT$ will plot as a straight line for temperatures below about half the critical temperature. Data taken by Hickman [4] on pentaphenyl ether and plotted according to (13.4) are shown in Fig. 13.1. The data were taken over the range 235–370°C. It is most important to recognize that all standard Knudsen cell vapor pressures reported at room and cryogenic temperatures were determined by extrapolation. Laurenson and Troup [5] used a quartz crystal microbalance to measure the vapor flux from a Knudsen cell and measured vapor pressures of mechanical pump fluids to 20°C.

Equation (13.4) is obeyed by fluids, which are single chemical compounds. The pure 5-ring phenyl ether described in Fig. 13.1 is an example of such a fluid. All fluids are not single chemical compounds. Polymers and other mixtures contain molecules of various weights. Polysiloxanes and perfluoropolyether fluids are examples of fluids that contain molecules of similar structure and variable weight. A hydrocarbon mineral oil is an example of a fluid, which has an added complication; it contains three distinct structures. It contains paraffins, naphthenes, and aromatic structures. Each fluid contains a distribution of molecular weights; the published molecular weight is an average.

The concept of vapor pressure has little meaning when applied to polymers with a broad molecular weight distribution such as polysiloxane or polyether. A single chemical compound has a distinct boiling point at a particular pressure. Polymers of broadly varying molecular weights with a large deviation about the mean molecular weight have no unique vapor pressure. The measured vapor pressure is dominated by the vapor pressure of the lower molecular weight fractions. When pump fluid is heated, light fractions preferentially evaporate; the composition of the residual fluid changes slowly and systematically.

Evaporation of light fractions is known to affect vapor pressure measurements [4,5]. If a mixture contains a large fraction of lightweight molecules, as do some polymers, a linear Clausius-Clapeyron equation is not obtained except at high temperatures. Extrapolating these data to low temperatures by means of a straight-line approximation is invalid, because

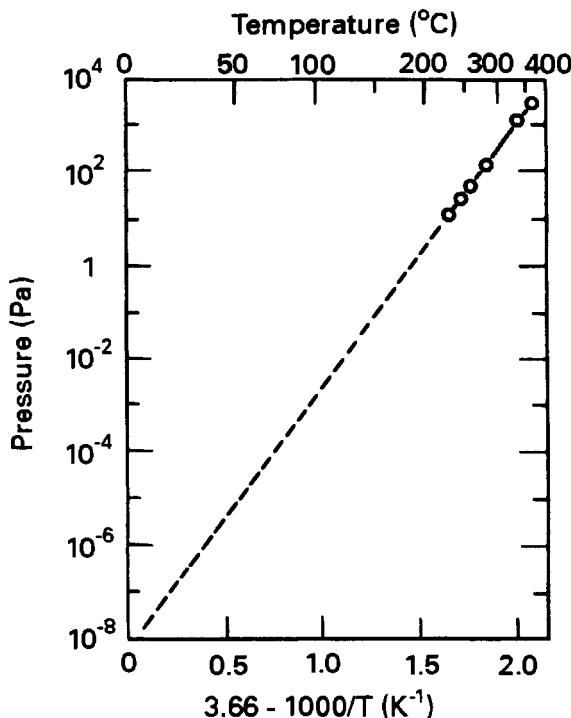


Fig. 13.1 Measured and extrapolated vapor pressure of pentaphenyl ether.

it gives a vapor pressure characteristic of the fluid minus the lightweight impurities. Fractionating diffusion pumps systematically eject the lighter weight fractions to the fore pump. Extrapolating high temperature effusion data from diffusion pump fluids to lower temperatures yields a vapor pressure that is characteristic of the fluid after it has been operated for some time in a fractionating pump, or carefully distilled. Extrapolating the vapor pressures of some mechanical pump fluids to low temperatures is not valid, because the light fractions remain and their vapor pressure is higher than the value predicted by the straight line approximation.

The Knudsen technique has been used to characterize the vapor pressures of pump fluids. Each laboratory has its own procedure. Vapor pressure measurements of vacuum pump fluids have been performed historically by very few investigators and often the one original measurement has been repeatedly republished.

As an alternative to the measurement of vapor pressure, the blank-off pressure in a specific pump is used to characterize commercial pump fluids. The ultimate pressure is dependent on several factors including the pump fluid, boiler power, pump design, and cooling rate. The vapor

pressure and ultimate pressure are not the same, but they do seem to be correlated. The ultimate pressure will usually be within a half an order of magnitude higher than the true vapor pressure [3,4,6–9].

13.1.2 Other Characteristics

Color, pour point, flash and fire points, and gas solubility are properties used to further characterize lubricants and diffusion pump fluids. Color is not directly related to lubricant properties, but it does aid in identification of fluid categories. The color of hydrocarbon pump oils will vary from clear to medium yellow and is characterized by a standard such as the Saybolt color index [10]. Naphthenes are darker than paraffins. Pure straight chain paraffins and most synthetics are transparent, but additives or dyes will cloud or color any fluid.

The pour point is the lowest temperature at which a fluid will flow. Vacuum pump fluids that have been dewaxed behave like Newtonian fluids to very low temperatures. The viscosity at the pour point is of order 10^5 – 10^6 mm²/s [11]. Flash and fire points are, respectively, the temperatures at which a fluid will burn momentarily and continuously in the presence of a flame [12]. The autoignition temperature is the temperature at which the fluid will ignite spontaneously. The ignition properties of organic fluids are a function of the vapor quantity, the surface-to-volume ratio of the test cell, and the spark energy [13]. They are reproducible, but the conditions in the test may not be identical to those in the pump.

The solubility of gas in a liquid obeys Henry's law and is directly proportional to absolute pressure. Gas solubility increases rapidly with fluid viscosity in the 5-to-50-mm²/s range. The increase with viscosity becomes less rapid for 100 mm²/s oils, and then it levels around 2000–3000 mm²/s [14]. The solubility of air in fluids at one atmosphere (percent by volume) was found to be: hydrocarbon oil, 7–10%; phosphate ester, 4–8%; and silicone, 20%. The solubility of individual gases in mineral oil (20°C) is CO₂—80%, N₂—6% and He—2% [15]. Fomblin Y-25 has the following solubility values at 20°C: Air—28%, H₂—8%, He—4%, CO₂—327%, ethylene—122%, while it has a solubility of 350% at 0°C for SF₆ [16]. The solubility of tritium in polyphenyl ether and perfluoropolyether was found to be 8%, and 7% in mineral oil [17]. Dissolved gas is undesirable for several reasons. It increases the time required by a mechanical pump to reach its base pressure and increases its base pressure [15]. High gas solubility can also cause fluid foaming and allow a gas to react with one previously pumped. Dissolved gas reduces oil viscosity, while bubbles in oil increase oil viscosity [18]. High fluid viscosity slows the removal of bubbles, whose size is a function of the interface tension.

13.2 PUMP FLUID TYPES

In this section we review the characteristics of currently used mechanical and diffusion pump fluids. Mechanical pumps first used mercury; soon after, they used mineral oils. Mercury was the first working fluid for diffusion pumps. In 1929 Burch [19] distilled low vapor pressure mineral oils and proposed their use as an alternative to mercury. Later, Hickman [4] distilled synthetic esters and ethers for vacuum use. In the last four decades a host of refined hydrocarbons oils and synthetic fluids have been tried. Not all of them are in use today. Some have been replaced by superior products, have been eliminated for reasons of safety, or were never accepted because they possessed no advantage over existing fluids.

13.2.1 Mineral Oils

The mineral oils used in vacuum pumps are mixtures of paraffin, naphthene and aromatic hydrocarbons. Paraffins, $C_nH_{(2n+2)}$, are straight- or branched-chain hydrocarbon structures containing only single bonds. The high-boiling-point paraffins make excellent lubricants. They are stable at high temperatures, are fluid at low temperatures, have reasonably constant viscosity over a wide temperature range (high viscosity index), and are adhesive enough to remain in place under high shear loads. They are not stable in oxygen at high temperatures. Paraffins have many possible isomers (for example, $C_{10}H_{22}$ has 75), which have differing properties. Aromatic compounds contain phenyl groups with straight- or branched-chain structures. They form sludge at high temperatures and have an undesirably low viscosity index. Naphthenes contain rings and chains with no double bonds. Naphthenes have properties between those of paraffins and aromatics. Carbon analysis shows the typical "paraffin mineral oil" to be composed of approximately 65% paraffin, 30% naphthene, and 5% aromatic hydrocarbons. Carbon analysis gives the weight percent carbon in singly bonded chains. It's not accurate to say that all this carbon is from paraffin structures, because other structures contain some single bonds.

Preparation of a vacuum fluid begins with vacuum distilled base oil that is further purified by solvent extraction and dewaxing [20–22]. The oils supplied to the vacuum fluid distiller are either single cut with one peak in the molecular weight distribution, or blends made from two of the relatively few refined single cuts. These are either a light (30–40 mm²/s), a medium (60–70 mm²/s), or a heavy (100–120 mm²/s) oil.

The oil is further purified by additional distillations. The distillation conditions are chosen to produce fluids of the desired viscosity and vapor pressure. The distilled fluid will have a distribution of molecular weights. Stripping both tars and low-molecular-weight ends produces a single-cut

fluid with a distribution of molecular weights centered about the mean molecular weight. Blending produces a fluid with more than one peak in the molecular weight distribution. Viscosity is inversely proportional to vapor pressure, so the vapor pressure of these broad cuts will differ widely. It is not possible to produce a fluid of extremely low vapor pressure from a blend of two oils with widely differing vapor pressures.

The base oil has characteristics unique to its origin; as a result, all mineral oils are not the same. Not only does the origin determine the paraffin/naphthene/aromatic ratio and the impurities, but it also determines the type of paraffin isomers. For example, the amount of sulfur and other impurities in mineral oil varies with the geographical origin of the crude. For many applications residual sulfur is detrimental, but it does inhibit oxidation [23]. Refiners of the highest-quality, single-cut mineral oils select their base stock from a single source, and they test each lot for uniformity.

We arbitrarily divide mineral oils for vacuum pumps into four grades: mechanical pump, diffusion pump, fully saturated paraffin, and inhibited fluids. The “mechanical pump” grade is, loosely, composed of blended fluids or single-cut fluids that have not been refined to remove light ends and tars. Vapor pressure requirements in a mechanical pump are not as severe as in a diffusion pump. This grade is typically used in mechanical pumps used for rough pumping chambers and backing turbomolecular and diffusion pumps. “Diffusion pump” grade fluids may be characterized as having a single peak in the molecular weight with narrow mass dispersion. The vapor pressure will be the lowest for those cuts with the highest average molecular weight. Hydrocarbon diffusion pump fluids are used in a variety of high vacuum pumping applications, but are not suitable for many ultrahigh vacuum applications.

Fully saturated paraffin oil, or white oil, is made by catalytically hydrogenating paraffin oil. This fluid will be somewhat more stable in the presence of mild corrosive gases than ordinary mineral oil because its lack of dangling bonds reduces its reactivity. White oil is used in mechanical pumps that handle halogens—for example, plasma etching systems.

Dyes are sometimes added to mechanical pump fluids to give them a distinctive color. They serve no functional purpose and may raise the vapor pressure. Most additives have high vapor pressures and are useful for a limited number of applications. Examples are diffusion pumps used for decorative coating and mechanical pumps used for pumping corrosives.

13.2.2 Synthetic Fluids

Mineral oils lack many properties of the ideal fluid. When used in a diffusion pump, their ultimate pressure is unacceptably high for many

applications. They are not stable in oxygen, have some tendency to sludge and foam, and do not offer adequate protection in boundary layer lubrication. Synthetics were developed to overcome the shortcomings of hydrocarbon oils. Fluids with low vapor pressure, high viscosity index, a high degree of oiliness, and chemical inertness have been synthesized.

Esters

Esters are chemicals formed by the reaction of an organic acid and an alcohol. The esters used in vacuum pump fluids all contain the same ester chemical bond, but have differing structures and rather widely varying properties. Sebacate esters are organic esters that were originally developed as jet engine and aircraft instrument lubricants and today used to lubricate turbomolecular pumps. Environmental issues have resulted in the demise of many older ester fluids.

Silicones

The unique character of the silicon–oxygen bond gives similarly unique properties to silicone-based fluids. Silicones, or siloxane polymers, are made up of repeated silicon oxygen groups with silicon bonds to side groups. The type of side groups (methyl, phenyl, alkyl, chloro, etc.) and the number of silicon atoms determine the properties and applications of the fluid. The large size of the silicon atom allows the phenyl and methyl side groups great mobility. The high flexibility of the siloxane chain accounts for the high viscosity index of silicones. As a class, silicones have the highest viscosity index of any fluid. Trisiloxanes and polysiloxanes are two fluids used in vacuum pumps.

Trisiloxanes are widely used diffusion pump fluids. They do not adhere to steel and cannot be used as lubricants in mechanical pumps [24]. They are manufactured by controlled hydrolysis of silanes and addition of phenyl groups, followed by distillation. The first silicone diffusion pump fluids, DC-702 and DC-703 [25], were mixtures of closely related molecular species with similar boiling points. Further separation leads to the

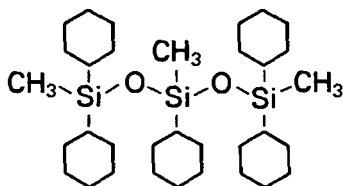


Fig. 13.2 One isomer of pentaphenyltrimethylsiloxane.

isolation of two specific chemical compounds, tetraphenyl tetramethyl trisiloxane, DC 704 [9], and pentaphenyl trimethyl trisiloxane, DC-705 [6]. One possible isomer of pentaphenyl silicone is sketched in Fig. 13.2. DC-705 has one of the lowest vapor pressures of any diffusion pump fluid.

Ethers

An ether may be regarded as a derivative of a water molecule in which the hydrogen has been replaced by alkyl or aryl groups. Polyphenyl ethers were synthesized in an attempt to develop high temperature jet engine lubricants. Hickman [4] was the first to use them as diffusion pump fluids. He found the five-ring phenyl ether (Fig. 13.3) to be stable and have extremely low vapor pressure. Commercially available fluids are mixed meta- and para-isomers of the pentaphenyl ether, which contain trace impurities of the four-ring compound. The four-ring compound has a high vapor pressure, while the six-ring compounds are either solids or glasses. Pentaphenyl ether is very viscous at low temperatures but is stable and has excellent high-temperature lubricating properties. Its wear, friction, and load capacity are in some cases equal to mineral oil [26]. Its chemical stability and low vapor pressure make it an outstanding fluid for critical diffusion pump applications.

Fluorochemicals

Fluorochemical fluids are characterized by their inertness to a wide range of chemical compounds. Large-scale fluorine oil chemistry studies were initiated during the Manhattan project in a search for uranium hexafluoride dilutants, as well as by the Navy in a search for fire-resistant fluids. Partially and fully fluorinated fluids have found use as lubricants for space applications, oxygen compressors, and liquid oxygen systems.

Fluorinated pump fluids, perfluoro alkyl polyethers (perfluoropolyethers or PFPE for short), are currently manufactured by two techniques. Fomblin [16,27] fluids are prepared by the uv-stimulated photooxidation of hexafluoropropylene and oxygen. It is a random copolymer of C_3F_6O and COF_2 with the structure shown in Fig. 13.4a. n ranges from 10-to-40 and is 10–50 times greater than m [28]. Krytox [29,30] fluids are prepared by the

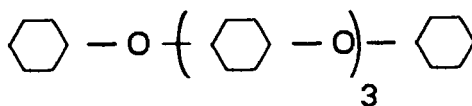


Fig. 13.3 Pentaphenyl ether structure.

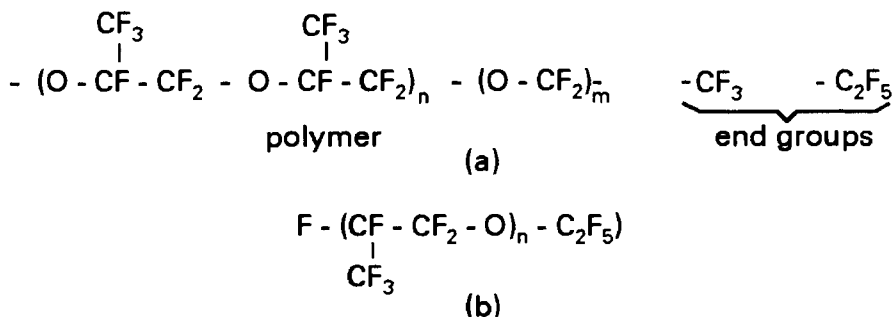


Fig. 13.4 Fluorochemical structures: (a) Fomblin perfluoroalkylpolyether, (b) Krytox perfluoroalkylpolyether.

polymerization of hexafluoropropylene epoxide. Krytox has the structure shown in Fig. 13.4b. It consists of 20–30 repeating $\text{C}_3\text{F}_6\text{O}$ groups.

Raw perfluoropolyethers have a distribution of molecular weights extending as high as 10,000 AMU. They are distilled to yield cuts with average molecular weights in the range 1800–3700 that are suitable for use in mechanical, turbomolecular, and diffusion pumps.

Perfluoropolyethers are stable Lewis bases that react with few chemicals. They should not be placed in contact with ammonia, amines, liquid fluorine, liquid boron trifluoride, or sodium or potassium metal. Laboratory experiments have shown PFPE fluids to decompose when heated sufficiently ($>100^\circ\text{C}$) in the presence of Lewis acids. The trichlorides and trifluorides of aluminum and boron are examples of Lewis acids that may be generated or are used in plasma and reactive ion etching. If heated to a high temperature, Lewis acids act as depolymerization catalysts and cause the release of toxic fragments.

13.3 FLUID SELECTION

In this section we describe typical fluids that are commercially available for use in rotary, lobe, and diffusion pumps. We describe how the pump requirements and possible gas reactions limit the choice of pump fluids. Properties of representative fluids are included.

13.3.1 Rotary Vane, Piston, and Lobe Blower Fluids

Fluids used in vane and piston pumps must provide a vacuum seal between the moving surfaces and lubricate the bearings and sliding surfaces. The fluid in a lobe blower is used to lubricate the gear drive. Fluid assists in

transferring heat from the bearings to the pump surface or cooling jacket in all three pumps. Fluids should not react with process gases or evolve fragments, which could contaminate a process.

The fluid must have a low vapor pressure and be viscous enough to form a film that will fill the gap between the moving surfaces. The viscosity required in a particular pump depends upon the clearances between moving parts, the rotational speed, and the pump operating temperature. Table 13.1 lists typical properties of representative vane, piston, lobe blower, and turbomolecular pump fluids. The viscosity indexes tabulated here were obtained from the manufacturer or calculated from the ASTM standard [31]. Some piston and lobe pumps are machined to fine tolerances, while others are not so closely machined and require a viscous fluid. Viscosity specifications are available from pump manufacturers. Appendixes F.2 to F.4 give vapor pressures and kinematic viscosities.

Interpreting the vapor pressure data is not so easy. Some were taken on a Knudsen cell, some on an isoteniscope, and others by unstated procedures. Manufacturers' vapor pressure data may be taken from the "typical" product, the "worst-case" product, or a sample lot. There can be an order-of-magnitude difference between worst-case and typical data. Each manufacturer needs to be consulted to interpret their published data.

"Mechanical pump" grade mineral oils are satisfactory for routine pumping applications such as backing a diffusion pump or roughing an air-filled chamber. It is common in research and development labs to find "diffusion pump" grade mineral oils used in mechanical pumps. Their use results in a reduced base pressure and less backstreaming, provided that the pump was flushed several times to eliminate all traces of previous fluid. However, they ultimately degrade thermally [30].

Light hydrocarbon fluids are used for cleaning contaminants from mechanical pumps. These fluids are also called flushing fluids. They are simply a light-end by-product from the distillation of ordinary mechanical pump oil. They have a high vapor pressure and are thin (about half the viscosity of normal oils). These light by-products are highly aromatic (high viscosity index) and are good solvents. They clean by causing the pump to run hot. The increased temperature aids in the dissolution of sludge from the pump's interior walls. These fluids simplify periodic maintenance of large mechanical pumps.

For some applications, hydrocarbon oil is totally unsuitable, because it reacts with the process gas. Many corrosive gases will quickly polymerize mineral oil, whereas others will cause its slow decomposition. It is often necessary to use an inert fluid for pumping corrosives. In some applications, inert fluids are required for safety.

Fluorocarbon fluids can be used in vane, piston, and lobe pumps. They have vapor pressures equal to mineral oil and are an excellent choice for

Table 13.1 Properties of Mechanical and Turbomolecular Pump Fluids

Chemical Type	Representative Trade Name	MW (ave)	Sp. Gr. at 25°C	P _v at 20°C (Pa)	Pour Point (°C)	Viscosity Index	Fire Point (°C)
Mineral Oil "Mech. pump"	Balzers P-3 [39]	190	0.88	1×10^{-2}	-16	95	295
	CVC-70/19 [40]	325	0.91	1×10^{-3}	-15	130	250
	Duo-Seal [®] 1407 ^a [41]	450	0.88	—	-6.7	>95	240.6
	Inland 19 [42]	440	0.88	5×10^{-4}	-15	130	244.5
Cleaning fluid	Solvex [®] -10 [40]	250	0.91	8×10^{-2}	-20	-50	220
	Inland FF-10 [42]	—	—	—	—	25	221
Ester Sebacate	Balzers T-11 ^b [39]	416	0.92	5×10^{-4}	-60	130	251
	Leybold HE-500 ^b [43]	430	0.92	2×10^{-3}	-62	130	—
Fluorocarbon PFPE	Fomblin [®] 25/5 ^c [16]	3250	1.9	3×10^{-4}	-35	120	None
	Fomblin [®] 06/6 ^c [16]	1800	1.88	3×10^{-4}	-50	50	None
	Krytox [®] 1514 ^c [29]	3000	1.88	3×10^{-4}	-35	100	None
	Krytox [®] 1506 ^c [29]	2150	1.86	3×10^{-4}	-45	50	None

Source: Reprinted with permission from *J. Vac. Sci. Technol. A*, 2, p 174, J. F. O'Hanlon. Copyright 1984, The American Vacuum Society.

^a Vapor pressure data were taken on a trapped McLeod gauge; data are not representative of the fluid.

^b Contains additives.

^c Recommended by manufacturer for oxygen pumping.

use in a vane pump. PFPE does not oxidize and is completely safe for use when pumping oxygen. It is inert to most corrosive gases. However, corrosive gases can slowly etch the interior of a pump, if the acids they generate are not removed continually. Acid neutralizing, recirculating oil filters are especially important when using PFPE because the fluid is only infrequently changed. Lewis acids are one class of chemicals that can be reactive with PFPE at temperatures over 100°C. Oil temperatures in ballasted or viscous flushed pumps can reach 120°C, and vane tip temperatures can be 100°C higher than the bulk oil temperature under any operating condition. Slow decomposition of PFPE results and a small amount of fluid must be added periodically.

13.3.2 Turbomolecular Pump Fluids

The requirements placed on turbomolecular pump oil are somewhat different from those of mechanical pump oil. Because the bearing loading is not severe, a high-shear-strength, high viscosity oil is not required. In full film lubrication the coefficient of friction is proportional to $\eta U/L$. See Fig. 18.1. High-speed bearings require low-viscosity oil. Although the average fluid temperature is 70°C, spot heating on the bearings can cause decomposition of fluids with poor vapor pressure. To prevent foaming, it is important that the fluid be vacuum-degassed before use.

A light-viscosity mineral oil that has been refined to remove both light ends and tars will work in a turbomolecular pump. The small amount of residual tar is of less concern than hydrogen from light ends, which has a low compression ratio and contributes to the background spectrum.

Sebacate ester, modified by the addition of an antioxidant, a rust inhibitor, a viscosity index improver and extreme pressure additive, is useful for lubricating high-speed turbomolecular pump bearings. PFPE fluids have been used in many turbomolecular pumps. The manufacturer should be consulted to determine if PFPE is compatible with a specific pump and, if so, what viscosity is required. The properties of several turbomolecular pump fluids are given in Table 13.1.

13.3.3 Diffusion Pump Fluids

The ideal diffusion pump fluid should be stable, should have a low vapor pressure, low specific heat, and a low heat of vaporization, and should be safe to handle, dispose of and use. It should not thermally decompose, entrap gas, or react with its surroundings. Unfortunately, no such fluid exists. The properties of the distilled hydrocarbons and synthetic fluids currently used in diffusion pumps are given in Table 13.2. The vapor pressures of diffusion pump fluids are given in Appendix F.3.

The ultimate pressure obtainable with a mineral oil is limited by its decomposition on heating. Several "diffusion pump" grades are manufactured for different applications. Lighter "diffusion pump" cuts (average M.W. 300–450) are used in applications where high pumping speed, moderate pressure, and low cost are most important. These fluids are sometimes used in mechanical pumps. Heavier "diffusion pump" grades (average M.W. > 550) are used to reach low ultimate pressures with reduced backstreaming. Inhibited diffusion pump fluids with improved oxidation resistance are used for operations such as vacuum metallizing. All mineral oils oxidize when exposed to air while they are hot.

Tetraphenyl silicone is extensively used in quick-cycled, unbaked systems because of its moderate cost, low backstreaming, thermal stability, and oxidation resistance. It has a freezing point of 20.5°C. Occasionally, it will be found frozen in an unheated storage area. Pentaphenyl silicone has improved stability and reduced vapor pressure and is used widely in systems that are baked to achieve the lowest ultimate pressures. The ultimate pressure in a diffusion pump charged with tetraphenyl silicone is dependent on purity, in particular on the quantity of low molecular weight impurity [32]. Pentaphenyl silicone is rapidly degraded by BCl_3 [33] and slowly degraded by CF_4 and CCl_4 .

Pentaphenyl ether (PPE) was first suggested by Hickman [4] for vacuum pump use, because of its exceptional stability and low vapor

Table 13.2 Properties of Diffusion Pump Fluids

Chemical Type	Representative Trade Name	MW (ave)	Sp. Gr. at (25°C)	P _v at 25°C (Pa)	Fire Point (°C)	Latent Heat (J/g)	C _p (J/g/°C)	T _{boiler} 100 Pa (°C)
Mineral Oil								
	Apiezon® C [44]	574	0.87	1×10 ⁻⁶	293	217.6	1.92	269
	Balzers-71 [39]	280	0.88	3×10 ⁻⁶	325	—	1.88	180
	Convoil® 20 [40]	400	0.86	5×10 ⁻⁵	258.9	—	—	210
	Invoil® 20 [42]	450	0.88	5×10 ⁻⁵	259	170	1.88	210
Silicone								
Trisiloxane ^b	Dow Corning® 704 [45]	484	1.07	3×10 ⁻⁶	275	220.5	1.72	220
	Dow Corning® 705 [45]	546	1.09	4×10 ⁻⁸	275	215.9	1.76	250
Ether								
PPE ^{a,b}	Convalex 10 [40]	447	1.2	6×10 ⁻⁸	350	205.8	—	275
	Santovac® 5 [46]	447	1.2	6×10 ⁻⁸	350	205.8	1.84 ^c	275
Fluorocarbon								
PFPE ^{a,d}	Fomblin® 25/9 [16]	3400	1.90	3×10 ⁻⁷	None	29.3	1	230
	Krytox® 1625 [29]	3700	1.88	~3×10 ⁻⁷	None	41.8	1	230

Source: Reprinted with permission from *J. Vac. Sci. Technol. A*, 2, p 174, J. F. O'Hanlon. Copyright 1984, The American Vacuum Society.

^a Suitable for use where ion or electron beams could cause polymerization.

^b Excellent oxidation resistance.

^c Four-ring ether.

^d Does not react with oxygen, do not use when pumping Lewis acids.

pressure. Pentaphenyl ether and pentaphenyl silicone have the lowest vapor pressures of any fluid currently available. Explosions could not be induced in DC-705 or pentaphenyl ether in a system pressurized to 1/2 atmosphere [34] with pure oxygen. When using pentaphenyl ether it is absolutely necessary to restrict the cooling water flow so that the ejector stage operates at a wall temperature of 45–50°C. The ejector stage should be warm in all pumps to achieve adequate fluid degassing. However, if the ejector is too cold in a PPE-charged pump, a large fraction of the very viscous fluid will remain on the ejector and inlet walls. Some workers use a slightly larger fluid charge than recommended by the manufacturer to compensate for the fluid that resides on cool walls. PPE is suitable for use in mass spectrometers, leak detectors, residual gas analyzers, electron microscopes, and electron beam mask generation systems, because it does not form an insulating film. It is also the most stable diffusion pump fluid available for pumping corrosive gases. Lewis acids will degrade PPE in diffusion pumps [33].

PFPE fluid is suitable for some diffusion pump applications. From activation energy measurements, decomposition in a diffusion pump at 250°C has been estimated to be 0.009% (Krytox) and 0.14% (Fomblin) in ten years [33]. Fomblin thermally decomposes at the C–C bond to yield equal molar amounts of C₃F₆O, COF₂ and CF₃COF [28,35]. The decomposition of Krytox was reported to be essentially the same, but with

less COF_2 [34]. PFPE decomposes on electron or ion impact into low-molecular-weight radicals and therefore does not form a film; this makes it useful for diffusion pumped electron beam systems. Residual gas analysis has shown the presence of high-molecular-weight fractions up to $M/e = 240$ advising against their use in heavy ion acceleration systems where exchange processes are dangerous [36]. PFPE is extremely stable for pumping all the usual reactive gases such as oxygen except for Lewis acids and fluorinated solvents. Since the boiler operates at temperatures over 200°C , PFPE, a Lewis base reacts and decomposes into toxic vapors. Under no circumstances should diffusion pumps charged with PFPE be used to pump on BCl_3 , AlF_3 , and so on. Pearson et al. [35] report on diffusion pumps charged with Fomblin Y-H VAC 18/8 used for pumping HF and UF_6 . After prolonged use at pressures of 3 Pa, solids of UO_2F_2 and UF_4 deposited, and a dark sulfur-containing colloidal suspension was observed.

Mineral oils and polyphenyl ethers have been shown to be the only fluids stable in pumping tritium [17]. Polyphenylethers were found to be the preferred diffusion pump fluid for pumping tritium, whereas mineral oil was the best choice for mechanical and turbomolecular pump systems. Perfluoropolyether was not satisfactory because of the large quantity of corrosive radiolysis products (HF , F , COF_2) formed while pumping tritium.

The interior of a pump must be thoroughly cleaned before changing fluids. Hydrocarbon oils are easier to remove than silicones, but severely contaminated pumps that use either fluid may be cleaned successively in decahydronaphthalene, acetone, and ethanol. If the pump is relatively clean, acetone and alcohol are usually adequate. Polyphenyl ether is soluble in trichloroethylene and in 1,1,1-trichloroethane, but the latter is less toxic than the former. Pumps charged with PFPE are cleaned with a fluorinated solvent such as trichlorotrifluoroethane or perfluorooctane [37]. If the pump fluid level is low, it is good practice to drain completely and refill rather than add fluid. During operation the light fractions of broad molecular weight fluid are selectively removed and the fluid's viscosity increases slowly with time. Gas bursting may be observed for several days following cleaning and changing fluid. Have patience while waiting for a newly charged pump to reach its ultimate pressure.

Pump boiler power may have to be changed, if the fluid has thermal properties significantly different from those of the fluid for which the pump was designed. Most US pumps are designed to operate with tetra-phenyl siloxane. The heat necessary to maintain the boiler temperature depends upon the heat capacity C and latent heat of vaporization h_v of the new fluid and also depends upon pump heat losses. Calculating their respective heat requirements may allow one to estimate boiler power differences. The heat required to vaporize 1 ml of fluid is $\rho[C(T_{\text{boiler}} - T_{\text{wall}}) + h_v]$. Latent heats and heat capacities of representative fluids are given in Table 13.2.

13.4 RECLAMATION

Reclamation uses procedures such as settling, filtering, adsorption and distillation to remove contamination from pump fluids. Costly fluids can be economically purified, while the cost of reclaiming inexpensive mineral oil is about the same as that of new fluid. Before considering reclaiming, one is advised to consult a firm specializing in reclaiming to determine how fluids should be segregated for shipment and how to specify the quality of the purified fluid. The cleaning procedures vary with the fluid and the type of contamination. The final cost will be dependent on the degree of contamination, the fluid type, and the desired quality of the purified fluid. For example, very low vapor pressure color centers are costly to remove from a silicone fluid, but do not affect pump operation. Therefore, a color specification will increase reclaim cost. The technology and economics of pump fluid reclamation was reviewed by Whitman [38].

REFERENCES

1. G. W. Thomson and D. R. Douslin in: *Techniques of Chemistry*, Vol. 1, A. Weissberger and B. W. Rossiter, Eds., *Physical Methods of Chemistry*, Part 5, Wiley, New York, 1971, p. 74.
2. M. Knudsen, *Ann. Physik*, **28**, 75, 999 (1909); **29**, 179 (1909).
3. J. P. Deville, L. Holland and L. Laurenson, *Proc. 3rd Intl. Congr. Vac. Sci. Technol.*, Pergamon, New York, 1965, p. 153.
4. K. C. D. Hickman, *Trans. 8th. Natl. Symp. on Vac. Technol.*, L. E. Preuss, Ed., Macmillan, New York, 1961, p. 307.
5. L. Laurenson and P. Troup, *J. Vac. Sci. Technol. A*, **8**, 2817 (1990).
6. D. J. Crawley, E. D. Tolmie and A. R. Huntress, *Trans 9th Natl. Vac. Symp. AVS*, Macmillan, New York, 1962, p. 399.
7. G. Rettinghaus and W. K. Huber, *J. Vac. Sci. Technol.*, **9**, 416 (1962).
8. N. T. M. Dennis, B. H. Colwell, L. Laurenson, and J. R. H. Newton, *Vacuum*, **28**, 551 (1978).
9. A. R. Huntress, A. L. Smith, B. D. Power, and N. T. M. Dennis, *Trans. 4th. Natl. Symp. on Vac. Technol.*, W. G. Matheson, Ed., Pergamon, New York, 1957, p. 104.
10. ASTM D-156, *1981 Annual Book of ASTM Standards*, Part 23, American Society for Testing Materials, Philadelphia, 1981, p. 111.
11. H. H. Zuidema, *The Performance of Lubricating Oils*, Reinhold, New York, 1959, p. 30.
12. ASTM D-92, *1981 Annual Book of ASTM Standards*, Part 23, American Society for Testing Materials, Philadelphia, 1981, p. 33.
13. J. M. Kuchta, *Summary of Ignition Properties of Jet Fuels and Other Aircraft Combustible Fluids*, U.S. Bureau of Mines, Pittsburgh Mining and Safety Research Center, AFAPL-TR-75-70, Air Force Aero Propulsion Laboratory, Wright-Patterson Air Force Base, Ohio, Sept., 1975, p. 16.
14. L. Laurenson, Private communication.
15. B. R. F. Kendall, *J. Vac. Sci. Technol.*, **21**, 886 (1982).
16. Montedison USA Inc., 1114 Avenue of the Americas, New York, NY 10036.
17. P. Chastagner, *Selection of Fluids for Tritium Pumping Systems*, 13th Annual Symp. on Applied Vacuum Science and Technology, Clearwater Beach, Florida, Feb. 6, 1984.

18. A. Cameron and C. M. McEttles, *Basic Lubrication Theory*, 3rd ed., Horwood, Chichester, 1980, p. 33.
19. C. R. Burch, *Proc. R. Soc. A*, **123**, 271 (1929).
20. J. R. Davy, *Industrial High Vacuum*, Pitman, London, 1951, p. 109.
21. E. R. Booser, in *Kirk-Othmer Encyclopedia of Chemical Technology*, 3rd ed., 14, M. Grayson and D. Eckroth, Ed., Wiley, New York, 1980, p. 484.
22. H. H. Zuidema, *The Performance of Lubricating Oils*, Reinhold, New York, 1959, p. 177.
23. K. L. Kreuz, *Lubrication*, **56**, 77 (1970).
24. M. J. Fulker, M. A. Baker and L. Laurenson, *Vacuum*, **19**, 555 (1969).
25. A. L. Smith and J. C. Saylor, *Vac. Symp. Trans.*, **31**, 1954.
26. C. L. Mahoney and E. R. Barnum, in *Synthetic Lubricants*, R. C. Gunderson and A. W. Hart, Eds., Reinhold, New York, 1962, p. 402.
27. L. Holland, L. Laurenson, and P. N. Baker, *Vacuum*, **22**, 315 (1972).
28. D. Sianisi, V. Zambeni, R. Fontanelli, and M. Binaghi, *Wear*, **18**, 85 (1971).
29. du Pont and Co., Chemicals and Pigments Department, Wilmington, DE 19898.
30. N. D. Lawson, Perfluoroalkylpolyethers, Report No. A-70020, du Pont, Wilmington, DE, Feb. 1970.
31. ASTM D-2270, *1981 Annual Book of ASTM Standards*, Part 24, American Society for Testing Materials, Philadelphia, 1981, p. 277.
32. D. Petraitis, *Society of Vacuum Coaters, 24th Annual Technical Conf.*, Dearborn, MI, 1981, page 73.
33. H. W. Lehmann, E. Heeb, and K. Frick, *Proc. 3rd. Symp. on Plasma Processing*, 82-6, J. Dieleman, R. G. Frieser and G. S. Mathad, Ed., p. 364 (1982).
34. C. W. Solbrig and W. E. Jamison, *J. Vac. Sci. Technol.*, **2**, 228 (1965).
35. R. K. Pearson, J. A. Happe, G. W. Barton, Jr., LLL Report UCID-19571, Sept. 27, 1982, Lawrence Livermore Laboratory, Livermore, CA.
36. A. Luches and M. R. Perrone, *J. Vac. Sci. Technol.*, **13**, 1097 (1976).
37. L. Laurenson, *Ind. Res. Dev.*, Nov. 1977, p. 61.
38. C. B. Whitman, *J. Vac. Sci. Technol. B*, **5**, 255 (1987).
39. Balzers High Vacuum, Furstentum, Liechtenstein.
40. CVC Products, Inc., 525 Lee Rd, Rochester, NY 14603.
41. Sargent-Welch Co., Vacuum Products Div., 7300 N. Linder Ave., Skokie, IL 60077.
42. IVACO Inc., 35 Howard Avenue, Churchville, NY 14428.
43. Leybold-Heraeus GmbH, Köln, Germany.
44. Edwards High Vacuum, Inc. 3279 Grand Island Blvd. Grand Island, NY 14072.
45. Dow Corning Co., Inc., 2030 Dow Center, Midland, MI 48640.
46. Monsanto, Co., 800 N. Lindbergh Blvd., St. Louis, Mo. 63166.

PROBLEMS

- 13.1 The fluid drained from one rotary vane pump backing a diffusion pump was found to be six parts mineral oil and one part water. Describe the effects of this fluid emulsion on the operation of the diffusion pump and the vane pump. How do you think the water got into the pump? How would you prevent it from recurring?
- 13.2 † (a) What happens to the vapor pressure of a diffusion pump fluid after it has been operated for some time in a fractionating diffusion pump? (b) What happens to mechanical pump fluid after it has been operated in a pump for an extended period of time?

- 13.3 Mineral oil mechanical pump fluid can potentially ignite at $\sim 200^\circ\text{C}$ and an O_2 partial pressure $\sim 20,000$ Pa (155 Torr). This condition can occur within the interstage of a two-stage mechanical pump that is exhausting a chamber filled with O_2 to atmospheric pressure. Why do you think a safety officer demands that a fluorocarbon fluid be used in this pump, although the regulator and flow meter will never allow the chamber pressure to exceed 1 Pa (10^{-2} Torr)?
- 13.4 For the Knudsen cell example given in Chapter 13.1.1 (PPE, 1 Pa, 200°C), calculate (a) the equilibrium number of fluid molecules arriving at and leaving the surface in the Knudsen cell per unit time, (b) the ratio molecules leaving the orifice to those leaving the oil surface per unit time, and (c) the ratio of mean free path of PPE vapor to diameter of the Knudsen cell orifice.
- 13.5 Three pumps are examined. They use, respectively, a saturated white paraffin oil, a silicone, and a perfluoropolyether fluid. All are optically transparent and colorless. How would you identify the three fluids without any sophisticated equipment—for example, with what is available in a typical pump maintenance area? Keep it simple.
- 13.6 What are the effects of operating (a) rotary vane, (b) lobe, and (c) diffusion pumps with too much and too little pump fluid?
- 13.7 † What are the effects of the (a) light ends and (b) the tars in turbomolecular pump diffusion pump fluids?
- 13.8 † How can water vapor be removed from rotary vane pump oil while the pump is operating?
- 13.9 Compare a high-quality mineral oil and tetraphenyl silicone fluid for use in a diffusion pump used for exhausting an unbaked production evaporating system used to deposit aluminum on plastic at 10^{-3} Pa. Give a complete evaluation of the advantages and disadvantages of each fluid.
- 13.10 A 100-mm-diameter diffusion pump charged with DC-704 is used for evacuating CRT's before aluminizing bulb interiors. The bulbs have their faceplates coated with phosphor and lacquer, and the base of their funnels are coated with a carbon-containing dag. During routine maintenance, the pump was removed from the system. There was little fluid in the boiler, but the interior walls of the pump casing were covered with a thick colorless deposit, which could be removed by a knife with some difficulty. Heating the outside of the casing caused the deposit to flow to the boiler. What happened?

CHAPTER 14

Getter and Ion Pumps

Getter and ion pumps are capture pumps. They operate by capturing gas molecules and binding them to a surface. The physical or chemical forces that bind molecules to surfaces are sensitive to the gas species, and all gases are not pumped equally well. As a result, two or more capture processes are usually combined to pump effectively a wide range of active and noble gases.

Getter and ion pumps are often referred to as clean pumps. They are clean in the sense that they do not backstream heavy organic molecules as do diffusion or oil-sealed mechanical pumps; however, they can generate hydrogen, methane, carbon oxides, inert gases, and particles as well. In that sense, entrainment pumps do contaminate. Certain gases will displace other adsorbed gases, and carbon in some metals can react with water vapor when heated to produce methane or carbon oxides. Hydrogen and other gases may be poorly pumped or thermally released from surfaces on which they were sorbed. Capture pumps may produce, or not pump, one or more gas species. The labeling of these gases as contaminants depends on the application.

In this chapter we review the titanium sublimation pump (TSP), the nonevaporable getter pump (NEG), and the ion pump.

14.1 GETTER PUMPS

Many reactive metals rapidly pump large quantities of active gases because they getter (react with) the gases. The gas either reacts to form a surface compound (for example, TiO) or diffuses into the bulk of the getter (as does hydrogen). The pumping speed of a surface getter is determined by the sticking coefficient of the gas on the surface. In a surface getter pump there is little diffusion into the bulk. It is often cooled to enhance the sticking coefficient, and at reduced temperatures, in-diffusion is slow. The pumping speed of bulk getter material is limited by the diffusion of gas through the

surface compounds, so bulk getters are usually operated at elevated temperatures to enhance the dissolution and diffusion of the surface compounds. The titanium sublimation pump is a surface getter pump, and the non evaporable getter pump is a bulk getter pump.

14.1.1 Titanium Sublimation Pumps

Many metals, including molybdenum, niobium, tantalum, zirconium, aluminum, and titanium, are surface getters for active gases. They become the active surface of a vacuum pump when they are deposited on a surface in a thin film layer. Titanium is the choice for commercial pumps because it can be sublimed (changed from the solid to vapor state without being a liquid) at much lower temperatures than most other metals, is inexpensive, and pumps a large number of gases. Figure 14.1 depicts one form of titanium sublimation pump. An alternating current heats the filament, which sublimates the titanium and deposits it on adjacent walls. Pump elements are fabricated with three or four separately heated filaments to extend the time between filament replacements. Active gases are captured on the fresh titanium surface, which is cooled with water or liquid nitrogen. Because heating cannot desorb the pumped gases, a fresh titanium layer must be deposited periodically to ensure continuous pumping. The pumping characteristics of titanium differ for the active gases, the intermediate gases, and the chemically inactive gases. The active gases (carbon oxides, oxygen, water vapor, and acetylene) are pumped with high sticking coefficients. Water dissociates into oxygen and hydrogen, which

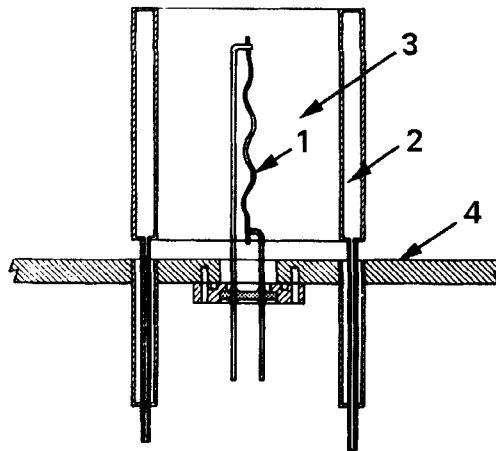


Fig. 14.1 Schematic of a basic titanium sublimation pump. (1) Titanium alloy filament, (2) coolant reservoir, (3) titanium deposit, (4) vacuum wall.

are then pumped separately. The temperature of the film has no major effect on the pumping speed of these gases because the sticking coefficients are generally near unity in the range 77–300 K. The sticking coefficients of the intermediate gases (hydrogen and nitrogen) are low at room temperature but increase at 77 K. After adsorbing, hydrogen will diffuse into the underlying film. The chemically inactive gases such as helium and argon are not pumped at all. Methane has the characteristic of an inactive gas and is only slightly sorbed on titanium at 77 K. Figure 14.2 gives the room temperature sorption characteristics of several active and intermediately active gases [1]. The sticking coefficient is the highest for all gases on a clean film, and for the very active gases it remains so until near saturation.

The replacement of one previously sorbed gas by another gas is important. It does create a memory effect, and it also results in actual sticking coefficients that depend on the nature of the underlying adsorbed gas. Gupta and Leck [1] observed a definite order of preference in gas replacement. Table 14.1 illustrates the order in which active gases replace less active gases. Oxygen, the most active gas, can replace all other gases, whereas all other active gases displace methane, which is bound only by van der Waals forces.

Gas replacement is a major cause of the large differences in measured sticking coefficients, especially when the films were not deposited under

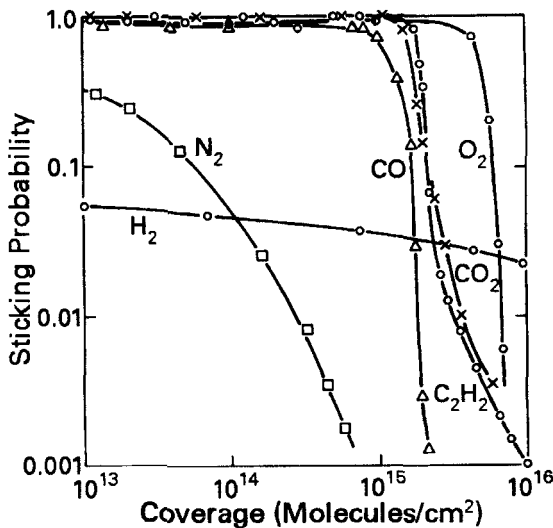


Fig. 14.2 Room-temperature sorption characteristics for pure gases on batch evaporated clean titanium films. Reprinted with permission from *Vacuum*, 25, p. 362, A. K. Gupta and J. H. Leck. Copyright 1975, Pergamon Press, Ltd.

Table 14.1 Order of Preference of Gas Displacement on Titanium Films^a

Pumped Gas	Displaced Gas				
	CH ₄	N ₂	H ₂	CO	O ₂
CH ₄	—	N	N	N	N
N ₂	Y	—	N	N	N
H ₂	Y	Y	—	N	N
CO	Y	Y	Y	—	N
O ₂	Y	Y	Y	Y	—

Source. Reprinted with permission from *Vacuum*, 25, p. 362, A. K. Gupta and J. H. Leck. Copyright 1975, Pergamon Press, Ltd.

^a Y, Yes; N, No.

clean conditions. Harra [2] has reviewed the sticking coefficients and sorption of gases on titanium films measured in several independent studies and tabulated their average values in Table 14.2. These coefficients represent the average of the values obtained in different laboratories and under different conditions. They are probably more representative of those in a typical operating sublimation pump whose history is not known than are those measured under clean conditions.

The TSP operates at pressures below 10^{-1} Pa. Above that pressure, surface compound formation inhibits sublimation. A typical pumping speed curve is sketched in Fig. 14.3. At low pressures there are few collisions between titanium atoms and gas molecules until the titanium atoms reach the surface. At pressures below 10^{-4} Pa, more titanium is sublimed than is needed when the filament is operated continuously. This results in a constant pumping speed that is determined by the surface area of the film and the conductance of any interconnecting tubing. At pressures greater than 10^{-4} Pa, titanium-gas collisions occur before the titanium strikes the surface, and the pumping speed is determined by the rate of titanium sublimation. Gas throughput is proportional to the titanium sublimation rate, therefore the pumping speed will decrease as $1/P$, as shown in Fig. 14.3.

The calculation of the pumping speed in the low-pressure region is not easy to do precisely because of the sticking coefficient uncertainty and the geometry. In molecular flow the pumping speed S of the geometry shown in Fig. 14.1 is given approximately by

Table 14.2 Initial Sticking Coefficient and Quantity Sorbed for Various Gases on Titanium

Gas	Initial Sticking Coefficient		Quantity Sorbed ^a ($\times 10^{15}$ molecules/cm ²)	
	(300 K)	(78 K)	(300 K)	(78K)
H ₂	0.06	0.4	8–230 ^b	7–70
D ₂	0.1	0.2	6–11 ^b	—
H ₂ O	0.5	—	30	—
CO	0.7	0.95	5–23	50–160
N ₂	0.3	0.7	0.3–12	3–60
O ₂	0.8	1.0	24	—
CO ₂	0.5	—	4–24	—
He	0	0		
Ar	0	0		
CH ₄	0	0.05		

Source. Reprinted with permission from *J. Vac. Sci. Technol.*, **13**, p. 471, D. J. Harra. Copyright 1976, The American Vacuum Society.

^a For fresh film thickness of 10^{15} Ti atoms/cm².

^b The quantity of hydrogen or deuterium sorbed at saturation may exceed the number of Ti atoms/cm² in the fresh film through diffusion into the underlying films at 300 K.

$$\frac{1}{S} = \frac{1}{S_i} + \frac{1}{C_a} \quad (14.1)$$

where S_i is the intrinsic speed of the surface and C_a is the conductance of the aperture at the end of the cylindrical surface on which the titanium is deposited. This conductance can be ignored if the film is deposited on the walls of the chamber. If a valve or connecting pipe is used, the appropriate series conductance should be added. The intrinsic speed is approximately

$$S_i (\text{L/s}) = 1000 A \frac{v}{4} s' \quad \blacktriangleright (14.2)$$

where A is the area of the film in units of m², v is the gas velocity in m/s, and s' is the sticking coefficient of the gas. Cooling to 77 K provides little additional pumping speed in pumps whose speed is conductance limited by the geometry.

At high pressures the pumping speed is determined by the rate of titanium sublimation. This theoretical maximum throughput is related to the titanium sublimation rate (TSR) by the relation [3]

$$Q (\text{Pa} \cdot \text{L/s}) = \frac{10^8 V_o \text{TSR (atoms/s)}}{n N_o}$$

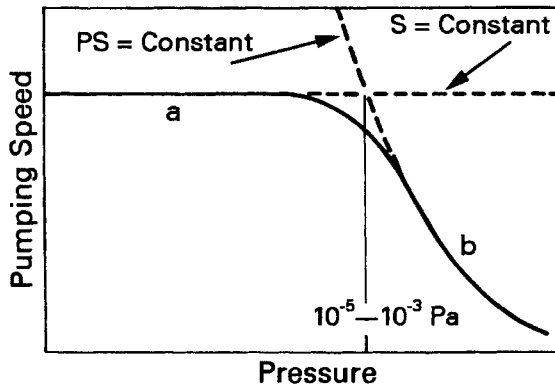


Fig. 14.3 Characteristic pumping speed versus pressure for a TSP: (a) Speed determined by the getter area, sticking coefficient, gas species, and inlet conductance; (b) speed determined by pressure and rate of sublimation.

or

$$Q(\text{Pa} \cdot \text{L/s}) = \frac{10^{-18}}{n} \text{TSR}(\text{atoms/s}) \quad \blacktriangleright (14.3)$$

V_o is the normal specific volume of the gas, N_o is Avogadro's number, and n is the number of titanium atoms that react with each molecule of gas; $n = 1$ for CO and $n = 2$ for N_2 , H_2 , O_2 , and CO_2 [2]. For Ti, (14.3) is

$$Q(\text{Pa} \cdot \text{L/s}) = \frac{1.25 \times 10^{-2}}{n} \text{TSR}(\mu\text{g/s}) \quad (14.4)$$

This theoretical throughput can be reached only when the titanium is fully reacted with the gas. The corresponding pumping speed is obtained by dividing the throughput by the pressure in the pump.

The TSP is used in combination with other pumps that will pump inert gases and methane. Small TSPs are used continuously for short periods to aid in crossover between a sorption pump and an ion pump. Large pumps have been developed for use in conjunction with smaller ion pumps for long-term, high-throughput pumping. The TSP is used intermittently for long periods at low pressures to provide high-speed pumping of reactive gases. At low pressures the film needs to be replaced only periodically to retain the pumping speed. Titanium is sublimed until a fresh film is deposited. The pump is then turned off until the film saturates. Figure 14.4 [3] sketches the pressure rise with decrease in pumping speed as the titanium film saturates in a typical ion-pumped system. P_i is the initial pressure with the ion pump and sublimator operating, and P_f is pressure with only the ion pump operating. Not shown on these curves is the

pressure burst due to gas release from the titanium during sublimation. Hydrogen, methane, and ethane are released from titanium during heating. The methane and ethane result from a reaction between hydrogen and the carbon impurity in the hot filament [1,4]. After sublimation begins hydrogen is pumped. Methane and ethane are marginally pumped on surfaces held at 77 K.

Commercially available TSPs use directly heated filaments, radiantly heated sources, or electron-beam heated sources. The most commonly used source is a directly heated filament with a low-voltage ac power supply. Filaments were first made from titanium twisted with tantalum or tungsten and later from titanium wound over niobium and tantalum wire [5]. Because of thermal contact problems, the sublimation rate proved to be unpredictable. Modern pumps use filaments fabricated from an alloy of 85% Ti and 15% Mo [6–8]. This filament has an even sublimation rate and a long life. A typical filament 15-cm long can be operated at sublimation rates of 30 to 90 $\mu\text{g/s}$. Large TSPs have been constructed with radiantly heated titanium at sublimation rates as high as 150 $\mu\text{g/s}$ [9,10] and with electron-beam-heated, rod-fed sources at sublimation rates ranging from 300 $\mu\text{g/s}$ to 0.15 g/s [11]. Electron-beam-heated sources do not operate

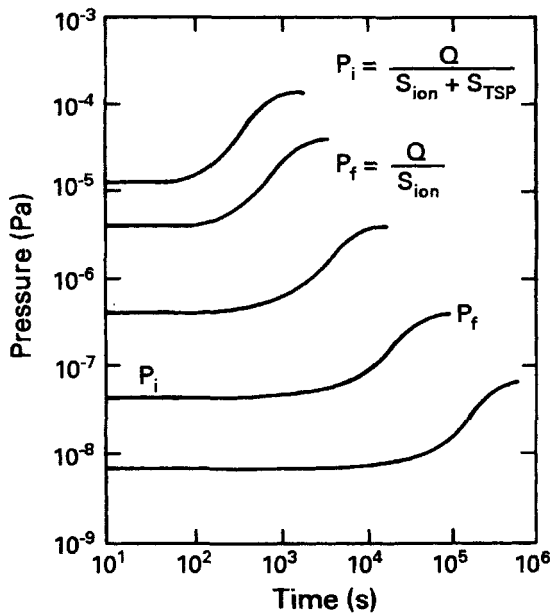


Fig. 14.4 Typical pressure rise due to decrease in pumping speed as a titanium film saturates. Reprinted with permission from General Characteristics of Titanium Sublimation Pumps, B. E. Keitzmann, 1965, Varian Associates, 611 Hansen Way, Palo Alto, CA 94303

well at pressures higher than 10^{-3} Pa and for most applications are too expensive to operate at pressures below 10^{-5} Pa. They serve best as a high-speed pump in the intermediate region. Radiantly heated sources are best for high speed pumping in the very high vacuum region.

14.1.2 Nonevaporable Getter Pumps

A nonevaporable getter (NEG) pumps by surface adsorption followed by bulk diffusion. Its speed for pumping active gases is determined by the gas diffusion rate into the bulk. For this reason, NEG pumps are operated at high temperatures. They do not pump inert gases or methane because these gases do not adsorb on the surface. One effective getter for vacuum use is an alloy of 84% Zr and 16% Al [12–16]. This alloy, when heated to 400°C , has a pumping speed of $\sim 0.3 \text{ L}\cdot\text{s}^{-1}\cdot\text{cm}^{-2}$ (N_2), $\sim 1 \text{ L}\cdot\text{s}^{-1}\cdot\text{cm}^{-2}$ (CO_2 , CO , O_2), and $1.5 \text{ L}\cdot\text{s}^{-1}\cdot\text{cm}^{-2}$ (H_2) [12]. At room temperature H_2 is pumped at about half the speed that it is pumped at 400°C , provided that no oxide or nitride diffusion barriers exist. Other gases are not pumped at room temperature because the surface compounds quickly form diffusion barriers. All gases except hydrogen are pumped as stable compounds and are entrapped permanently [13]. Hydrogen is pumped as a solid solution and may be released by heating above 400°C . The diffusion of carbon monoxide, carbon dioxide, nitrogen and oxygen has been shown to obey a simple parabolic rate law [17]. Cecchi and Knize [18] have shown NEG pump speed to be constant below 10^{-3} Pa and to decrease as $P^{-1/2}$ above 5×10^{-1} Pa.

To operate the Zr-Al getter pump, the chamber is first evacuated to a pressure below 1 Pa, after which the pump is activated by heating to 800°C to allow surface atoms to diffuse within the bulk. The temperature is then reduced to 400°C . The activation step is repeated each time the pump is cooled and released to atmosphere. Another alloy (Zr—70%, V—24.6%, Fe—5.4%) has demonstrated high getter efficiency at room temperature after activation at 500°C [19,20].

NEG pumps have been used as appendage pumps on small systems, as well as primary pumps in large UHV systems, fusion machines and particle accelerators. Appendage pumps equipped with getter cartridges fabricated from a plated steel coated with Zr-Al alloy have pumping speeds as high as 10 to 50 L/s [21]. One getter ion pump package has a combined pumping speed of 1,000 L/s [22]. NEG pumps have a large capacity for pumping hydrogen [16]. The NEG pump has been used in fusion machines [19,23,24], because it can operate without a magnetic field, and it has a high hydrogen pumping speed at room temperature. With the assistance of an ion pump to handle the methane and argon, the NEG can reach base pressures of 10^{-9} Pa. The CERN large positron collider uses 27 km of

linear NEG pump with a speed of 500 L/s per meter of chamber [24]. Getter pumping is also found in Tokamaks to control the density of hydrogen plasmas and remove chemically active impurities. The use of glow discharge cleaning has been shown to have no deleterious effects on the operation of a Zr–Al NEG [25]. Hseuh and Lanni [26] have established a worst-case pressure of less than 3×10^{-9} Pa in an accelerator storage ring using a linear Zr–V–Fe alloy and lumped ion pumps 10 m apart. Getter pumps are now finding other applications, such as for purifying gases used in semiconductor device processing equipment.

14.2 ION PUMPS

The development of the ion pump has made it possible to pump to the ultrahigh vacuum region without concern for heavy organic contamination. This pump exploits a phenomenon formerly considered detrimental to vacuum gauge operation—pumping gases by ions in Bayard-Alpert and Penning gauges. Ions are pumped easily because they are more reactive with surfaces than neutral molecules and if sufficiently energetic can physically embed themselves in the pump walls. If the ions were generated in a simple parallel-plate glow discharge, for example, the pumping mechanism would be restricted to a rather narrow pressure range. Above about 1 Pa the electrons cannot gain enough energy to make an ionizing collision and below about 10^{-1} – 10^{-2} Pa the electron mean free path becomes so long that the electrons collide with a wall before they encounter a gas molecule. Ions can be generated at lower pressures, if the energetic electrons can be constrained from hitting a wall before they collide with a gas molecule. This confinement can be realized with certain combinations of electric and magnetic fields.

The pumping action of a magnetically confined dc discharge was first observed by Penning [27] in 1937, but it was not until two decades later that Hall [28] combined several Penning cells and transformed the phenomenon into a functional pump. Some elemental forms of the (diode) sputter-ion pump are shown in Fig. 14.5 [29]. Each Penning cell is approximately 12 mm in diameter \times 20 mm long with a 4-mm gap between the anode and the cathode. Modern pumps are constructed of modules of cells arranged around the periphery of the vacuum wall with external permanent magnets of 0.1–0.2-T strength and cathode voltages of ~ 5 kV.

The electric fields present in each Penning cell trap the electrons in a potential well between the two cathodes and the axial magnetic field forces the electrons into circular orbits that prevent their reaching the anode. This combination of electric and magnetic fields causes the

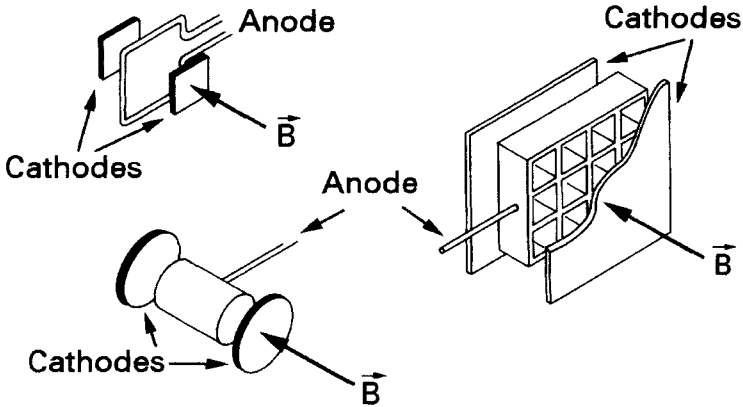


Fig. 14.5 Early forms of the diode sputter-ion pump. (Upper Left) Ring anode cell [27]. (Lower Left) long anode cell [31]; same cell with Ti cathodes [32]. (Right) multicell anode [28]. Reproduced with permission from *Proc. 4th Int. Vac. Cong. (1968)*, p. 325, D. Andrew. Copyright 1969, The Institute of Physics.

electrons to travel long distances in oscillating spiral paths before colliding with the anode and results in a high probability of ionizing collisions with gas molecules. The time from the random entrance of the first electron into the cell until the electron density reaches its steady-state value of $\sim 10^{10}$ electrons/cm³ is inversely proportional to pressure. The starting time of a cell at 10^{-1} Pa is nanoseconds, while at 10^{-9} Pa it is 500 s [30]. The ions produced in these collisions are accelerated toward the cathode, where they collide, sputter away the cathode, and release secondary electrons that in turn are accelerated by the field. Many other processes occur in addition to the processes necessary to sustain the discharge; for example, a large number of low-energy neutral atoms are created by molecular dissociation and some high-energy neutrals are created from energetic ions by charge neutralization as they approach the cathode, collide, and recoil elastically.

The mechanism of pumping in an ion pump is dependent on the nature of the gas being pumped and is based on one or more of the following mechanisms: (1) precipitation or adsorption following molecular dissociation; (2) gettering by freshly sputtered cathode material; (3) surface burial under sputtered cathode material; (4) ion burial following ionization in the discharge; and (5) fast neutral atom burial. (Ions are neutralized by surface charge transfer and reflected to another surface where they are pumped by burial.) Rutherford, Mercer, and Jepsen [33] explained (1)–(4), whereas Jepsen explained the role of elastically scattered neutrals [34]. These mechanisms are illustrated in Fig. 14.6.

Organic gases, active gases, hydrogen, and inert gases are pumped in distinctly different ways. There are a few generalities. Initially, gases tend to be pumped rapidly and their partial pressure decays to a steady state [34–36]. In steady state reemission rates equal pumping rates. This is more pronounced with noble than with active gases. Pumping speeds cannot be uniquely defined for a gas independent of the composition of other gases being pumped simultaneously. The sputter ion pump is capable of reemitting any pumped gas. This reemission or memory effect complicates the interpretation of some experiments. Organic gases are easily pumped by adsorption and precipitation after being dissociated by electron bombardment [33].

Active gases such as oxygen, carbon monoxide, and nitrogen are pumped by reaction with titanium, which is sputtered on the anode surfaces, and by ion burial in the cathode. These gases are easily pumped because they form stable titanium compounds [33].

Hydrogen behaves differently. Its low mass prevents it from sputtering the cathode significantly. It behaves much like it does in a TSP. It is initially pumped by ion burial and neutral adsorption [34,37] and diffuses into the bulk of the titanium and forms a hydride. Sustained pumping of hydrogen at high pressures will cause cathodes to warp [33] and release

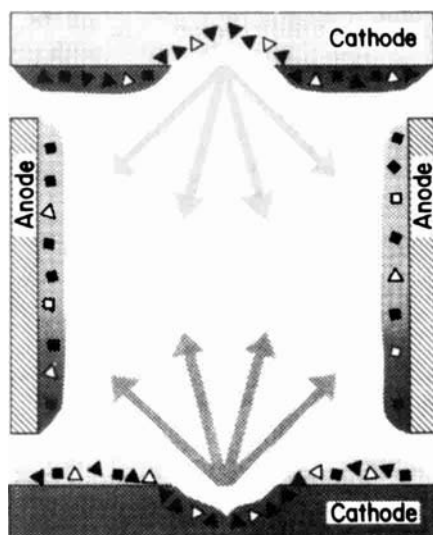


Fig. 14.6 Schematic diagram showing sputter deposition and pumping mechanisms in a Penning cell: ■ Chemically active gases buried as neutral particles; ► chemically active gases ionized before burial; □ inert gases buried as neutral particles; △ inert gases ionized before burial. Reprinted with permission from *Proc. 4th Int. Vac. Congr. (1968)*, p. 325, D. Andrew. Copyright 1969, The Institute of Physics.

gas as they heat. The hydrogen pumping speed does not rate limit unless cathode surfaces are covered with compounds that prevent indiffusion. The pumping of a small amount of an inert gas, say argon, cleans the surfaces and allows continued hydrogen pumping [38], whereas a trace amount of nitrogen will reduce the speed by contaminating the surface [37].

Noble gases are not pumped so efficiently as active gases in a diode pump. They are pumped by ion burial in the cathodes and by reflected neutral burial in the anodes and cathodes. The noble gas pumping on the cathodes is mostly in the area near the anodes where the sputter build-up occurs. Because most of the neutrals are reflected with low energies in the diode pump, their pumping speed in the anode or other cathode is low; for example, argon is pumped only at 1–2% of the active gas speed.

Argon, in particular, suffers from a pumping instability. Periodically the argon pressure will rise as pumped gas is released from the cathodes. Figure 14.7 [29] illustrates some of the geometries that were devised as a solution to the problem of low argon pumping speed and its periodic reemission. Brubaker [39] devised a triode pump with a collector surface that operated at a potential between the anode and cathode (Fig. 14.7a). Its function was to collect low-energy ions that could not sputter. Hamilton [40] showed it worked equally well when the collector surface was held at anode potential (Fig. 14.7b). In the triode pump the argon pumping speeds are as high as 20% of the nitrogen speed. This high speed (high implantation rate) results from the high energy of the neutrals, which are scattered at small angles from the cathode walls with little energy loss.

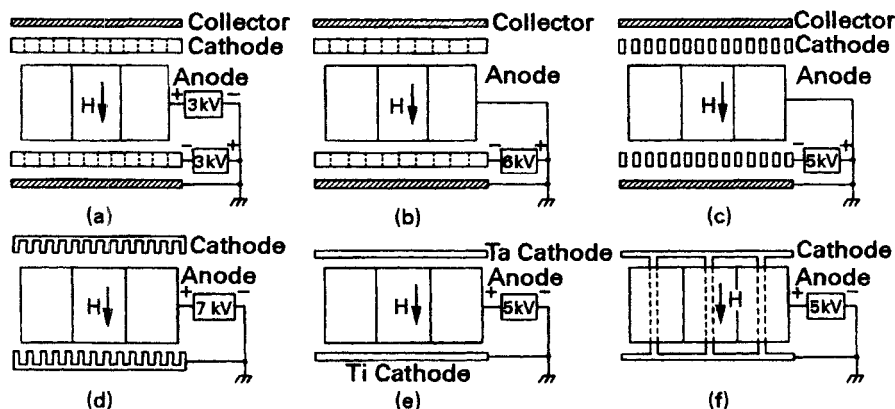


Fig. 14.7 Pump designs for inert gas pumping: (a) The triode pump of Brubaker [39]; (b) triode pump of Hamilton [40]; (c) triode Varian Noble Ion Pump [41]; (d) slotted cathode diode of Jepsen et al. [42]; (e) differential ion pump of Tom and Jones [43]; (f) magnetron pump of Andrew et al. [46]. Reprinted with permission from *Proc. 4th Intl. Vac. Congr.* (1968), p. 325, D. Andrew. Copyright 1969, The Institute of Physics.

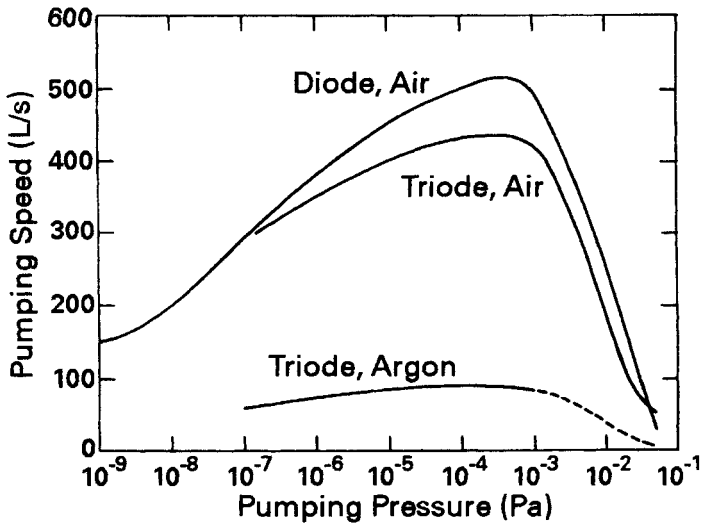


Fig. 14.8 Pumping speeds for air and argon for the 500-L/s Varian diode Vac Ion pump and for the 400-L/s triode Vac Ion pump. Speeds measured at the inlet of the pump. Reprinted with permission from Varian Associates, 611 Hansen Way, Palo Alto, CA 94303.

Sputtering is much more efficient at these small angles than at normal incidence and sputtering of titanium on the collector is more efficient than in the diode pump. The slotted cathode [42] attempts to accomplish this sputtering with one less electrode than the triode (Fig. 14.7d). This pump has an argon pumping speed of 10% of the speed for air. Tom and Jones [43] devised the differential diode ion pump sketched in Fig. 14.7e. A tantalum cathode replaced one titanium cathode. In this manner the recoil energy of the scattered noble gas neutrals, which depends on the relative atomic weight of the cathode material and gas atom, is increased [44,45]. This gives more effective noble gas pumping than in the diode pump. An argon-stable magnetron structure (Fig. 14.7f), was devised by Andrew et al. [46]. The central cathode rod is bombarded by a high flux of ions at oblique angles of incidence. The sputtering of the rod creates a flux that continually coats the cathode plates and the impinging ions and results in a net argon speed of 12% of the air speed [46]. Among the designs discussed here for increasing the argon pumping speed and reducing or eliminating its instability, the triode and differential diode are in most widespread use.

The operating pressure range of the sputter-ion pump extends from 10⁻² to below 10⁻⁸ Pa. Characteristic pumping-speed curves of a diode and a triode pump are shown in Fig. 14.8. If starting is attempted at high pressures, say 1 Pa, a glow discharge will appear and the elements will heat and release hydrogen. As the pressure is reduced, the glow discharge

extinguishes and the speed rapidly increases. At low pressures the speed decreases because the sputtering and ionization processes decrease. The exact shape of a pumping speed curve is a function of the magnetic field intensity, cathode voltage, and cell diameter-to-length ratio. As the pressure decreases, the ionization current decreases. At high pressures, the ion current is approximately proportional to the pressure, and may be used as a gauge. However, at low pressures, there will be no relation between the total ion pump current and the actual pressure. Spurious pump currents prevent the ion current from being used as a gauge at low pressures.

The lifetime of a diode pump is a function of the time necessary to sputter through the cathodes. A typical value is 5000 h at 10^{-3} Pa or 50,000 h at 10^{-4} Pa. The triode, which pumps slightly better than the diode at high pressures, is also easier to start at high pressures and has a lifetime of less than half the diode. In both pumps the life may be shorter due to shorting of the electrodes by loose flakes of titanium.

The sputter ion pump has the advantage of freedom from hydrocarbon contamination and ease of fault protecting but does suffer from the reemission of previously pumped gases, particularly hydrogen, methane, and the noble gases.

REFERENCES

1. A. K. Gupta and J. H. Leck, *Vacuum*, **25**, 362 (1975).
2. D. J. Harra, *J. Vac. Sci. Technol.*, **13**, 471 (1976).
3. B. E. Keitzmann, *General Characteristics of Titanium Sublimation Pumps*, Varian Associates, Palo Alto, CA 94303.
4. L. Holland, L. Laurenson, and P. Allen, *Trans. 8th Natl. Vac. Symp. (1961)*, Pergamon, New York, 1962, p. 208.
5. R. E. Clausing, *Trans. 8th Natl. Vac. Symp. (1961)*, Pergamon, New York, 1962, p. 345.
6. A. A. Kuzmin, *Prib. Tekh. Eksp.* **3**, 497 (1963).
7. G. M. McCracken and N. A. Pashley, *J. Vac. Sci. Technol.*, **3**, 96 (1966).
8. R. W. Lawson and J. W. Woodward, *Vacuum*, **17**, 205 (1967).
9. D. J. Harra and T. W. Snouse, *J. Vac. Sci. Technol.*, **9**, 552 (1972).
10. D. J. Harra, *J. Vac. Sci. Technol.*, **12**, 539 (1975).
11. H. R. Smith, Jr., *J. Vac. Sci. Technol.*, **8**, 286 (1971).
12. P. della Porta, T. Giorgi, S. Origlio, and F. Ricca, *Trans. 8th Natl. Vac. Symp. (1961)*, Pergamon, New York, 1962, p. 229.
13. T. A. Giorgi and F. Ricca, *Nuovo Cimento Suppl.*, **1**, 612 (1963).
14. B. Kindl, *Nuovo Cimento Suppl.*, **1**, 646 (1963).
15. B. Kindl and E. Rabusin, *Nuovo Cimento Suppl.*, **5**, 36 (1967).
16. W. J. Lange, *J. Vac. Sci. Technol.*, **14**, 582 (1977).
17. S. Parkash and P. Vijendran, *Vacuum*, **33**, 295 (1983).
18. J. L. Cecchi and R. J. Knize, *J. Vac. Sci. Technol. A*, **1**, 1276 (1983).
19. C. Boffito, B. Ferrario, P. della Porta, and L. Rosai, *J. Vac. Sci. Technol.*, **18**, 1117 (1981).
20. C. Boffito, B. Ferrario and D. Martelli, *J. Vac. Sci. Technol. A*, **1**, 1279 (1983).
21. P. della Porta and B. Ferrario, *Proc. 4th Int. Vac. Congr. (1968)*, Institute of Physics and the Physical Society, London, **1**, 369 (1968).

22. S.A.E.S. Getters USA, Buffalo, NY.
23. J. S. Moenich, *J. Vac. Sci. Technol.*, **18**, 1114 (1981).
24. C. Benvenuti, *Nuc. Instrum. & Methods*, **205**, 391 (1983).
25. H. F. Dylla, J. L. Cecchi, and M. Ulrickson, *J. Vac. Sci. Technol.*, **18**, 1111, (1981).
26. H. C. Hseuh and C. Lanni, *J. Vac. Sci. Technol. A*, **1**, 1283 (1983).
27. F. M. Penning, *Physica*, **4**, 71 (1937).
28. L. D. Hall, *Rev. Sci. Instrum.*, **29**, 367 (1958).
29. D. Andrew, *Proc. 4th Int. Vac. Congr. (1968)*, Institute of Physics and the Physical Society, London, 1969, p. 325.
30. R. D. Craig, *Vacuum*, **19**, 70 (1969).
31. M. Penning and K. Nienhuis, *Philips Tech. Rev.*, **11**, 116 (1949).
32. A. M. Guerswitch and W. F. Westendorp, *Rev. Sci. Instrum.*, **25**, 389 (1954).
33. S. L. Rutherford, S. L. Mercer, and R. L. Jepsen, *Trans. 7th Natl. Vac. Symp. (1960)*, Pergamon, New York, 1961, p. 380.
34. R. L. Jepsen, *Proc. 4th Intl. Vac. Congr. (1968)*, Institute of Physics and the Physical Society, London, 1969, p. 317.
35. A. Dallos and F. Steinrisser, *J. Vac. Sci. Technol.*, **4**, 6 (1967).
36. A. Dallos, *Vacuum*, **19**, 79 (1969).
37. J. H. Singleton, *J. Vac. Sci. Technol.*, **8**, 275 (1971).
38. J. H. Singleton, *J. Vac. Sci. Technol.*, **6**, 316 (1969).
39. W. M. Brubaker, *6th Natl. Vac. Symp. (1959)*, Pergamon, New York, 1960, p. 302.
40. A. R. Hamilton, *8th Natl. Vac. Sump. (1961)*, **1** Pergamon, New York, 1962, p. 338.
41. Varian Associates, 611 Hansen Way, Palo Alto, CA, 94303.
42. R. L. Jepsen, A. B. Francis, S. L. Rutherford, and B. E. Keitzmann, *7th Natl. Vac. Symp. (1960)*, Pergamon, New York, 1961, p. 45.
43. T. Tom and B. D. Jones, *J. Vac. Sci. Technol.*, **6**, 304 (1969).
44. P. N. Baker and L. Laurenson, *J. Vac. Sci. Technol.*, **9**, 375 (1972).
45. D. R. Denison, *J. Vac. Sci. Technol.*, **14**, 633 (1977). See Reference 1.
46. D. Andrew, D. R. Sethna, and G. F. Weston, *4th Int. Vac. Cong. (1968)*, Institute of Physics and the Physical Society, 1968, p. 337.

PROBLEMS

- 14.1 † Why does a non-evaporable getter (NEG) need to be heated to an activation temperature before being operated as a pump?
- 14.2 † How is a non-evaporable getter restored after it saturates?
- 14.3 † A TSP has an oxygen speed of 3000 L/s on a liquid-nitrogen-cooled surface at 1.33×10^{-4} Pa. How many titanium atoms must strike the pump surface per second per unit area?
- 14.4 Using the average sticking coefficients given in Table 14.2, calculate the room temperature pumping speeds per unit area for oxygen, hydrogen, carbon dioxide and nitrogen.
- 14.5 Calculate the nitrogen pumping speed of the pump shown in Fig. 14.1, assuming that it has a 30-cm diameter inlet, is 30-cm in length, and is cooled with water. Now replace the water with liquid nitrogen and calculate its speed. Why did the speed not increase significantly?

- 14.6 † How should one regenerate a TSP after it has become saturated?
- 14.7 99.99% argon is admitted into a chamber connected to an ion pump. The RGA shows a methane peak, which is 10% of the argon peak. Explain.
- 14.8 † Why are sputter-ion pumps not used for processes that operate in the 10^{-4} -Pa pressure range?
- 14.9 † Why install a grounded screen over an ion pump inlet?
- 14.10† Why is dry nitrogen used as a vent or flush gas in sputter-ion-pumped systems?

CHAPTER 15

Cryogenic Pumps

Cryogenic pumping is the capture of molecules on a cooled surface by weak van der Waals or dispersion forces. In principle, any gas can be pumped, provided that the surface temperature is low enough for arriving molecules to remain on the surface after losing kinetic energy. Cryogenic pumping is a clean form of pumping. The only gas or vapor contaminants are those not pumped, or released from pumped deposits. Unlike the ion pump, the cryopump does not retain condensed and physically adsorbed gases after the pumping surfaces have been warmed. Proper precautions must be taken to vent the pumped gas load.

Cryopumps are used in a wide range of applications and in many forms. Liquid nitrogen-cooled molecular sieve pumps are used as roughing pumps. Liquid nitrogen traps are used between diffusion pumps and chambers to pump oil and water vapor. Liquid nitrogen or liquid helium "cold fingers" are used in high vacuum chambers to augment other pumps. Liquid cryogenics or closed-cycle helium gas refrigerators are used to cool high- and ultra high vacuum cryopumps. Turbomolecular, TSP, or NEG pumps are sometimes appended to cryopumps to improve their pumping speed for hydrogen and deuterium. Cryopumping is the only form of pumping by which extremely large pump speeds (10^7 L/s) can be realized.

Cryogenic pumping is not a new technique. The theory and techniques of pumping on cooled surfaces have been a part of vacuum technology much longer than the helium gas refrigerator; however, knowledge of both is necessary to understand the operation of a He-gas cryopump. Several reviews of cryopumping have been published. Hands [1] reviewed small refrigerator-cooled cryopumps and very large pumps used for fusion experiments. Bentley [2] explained the operation of the Gifford-McMahon refrigerator, and Haefer [3] has discussed the mechanisms of cryogenic pumping, given system calculations, and examples of pumps and applications. Welch [4] has written a comprehensive treatise on capture pumping technology. In this chapter we review the mechanisms of cryocondensation and cryosorption on which all cryogenic pumping is

based; we discuss pumping speed, ultimate pressure and saturation effects, refrigeration techniques, and pump characteristics. We discuss system operation and regeneration techniques in Chapters 20–22. Issues relating to cryopump operation at high flow rates are discussed in Chapter 23.

15.1 Pumping Mechanisms

Low-temperature pumping is based on cryocondensation, cryosorption, and cryotrapping. In Chapter 4 we define the equilibrium or saturated vapor as the pressure at which the flux of vapor particles to the surface equals the flux of particles leaving the surface and entering the vapor phase, provided that all the molecules, solid, liquid, and vapor are at the same temperature. The arriving molecules are attracted to condensation sites on the liquid or solid, where they are held for some residence time after which they vibrate free and desorb into the vapor phase. The vapor pressure and residence time are temperature-dependent. As the temperature is reduced, the vapor pressure is reduced, and the residence time is increased. See, for example, Table 4.1. Tables of vapor pressures of the common gases are given in Appendix B.5. Cryocondensation becomes a useful pumping technique when a surface can be cooled to a temperature at which the vapor pressure is so low and the residence time is so long that the vapor is effectively removed from the system. Liquid nitrogen is a good condenser

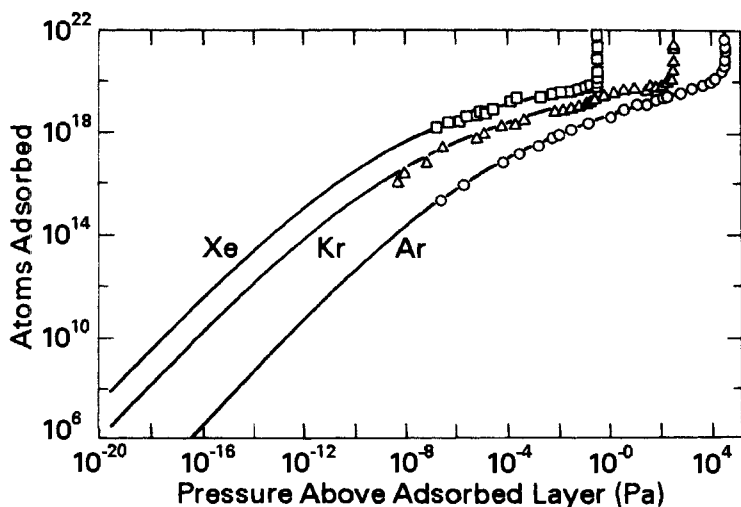


Fig. 15.1 Adsorption isotherms of xenon, krypton, and argon on porous silver adsorbent at 77 K. The lines represent plots of an analytic solution and the points are experimental. Reprinted with permission from *J. Chem., Phys.*, 73, p. 2720, J. P. Hobson. Copyright 1969, The American Chemical Society.

of water vapor, because the vapor pressure of water at 77 K is 10^{-19} Pa. The probability c that an atom will condense on collision with a cold surface is called the condensation coefficient. Condensation coefficients of many gases at reduced temperatures lie between 0.5 and 1.0 [5–7].

Any solid surface has a weak attractive force for at least the first few monolayers of gas or vapor. Figure 15.1 describes a typical relationship between the number of molecules adsorbed and the pressure above the adsorbed gas for Xe, Kr, and Ar on porous silver at 77.4 K [8]. These adsorption isotherms tend toward a slope of one at very low pressures. This shows the number of adsorbed atoms goes to zero linearly with the pressure. The sorption sites become increasingly populated as the pressure increases. The limiting sorption capacity is reached after a few monolayers have been deposited. A typical monolayer can hold about 10^{15} atoms/cm². The actual number depends on the material. The data shown in Fig. 15.1 saturate at 2×10^{19} atoms, because the surface area is larger than 1 cm². At the vapor pressure, condensation begins and the surface layer increases in thickness. The thickness of the solid deposit is limited only by thermal gradients in the solid and by thermal contact with nearby surfaces of different temperatures. The density and thermal conductivity of the solid frost are a function of its formation temperature. It will decrease as the condensation temperature decreases.

A curve similar to Fig. 15.1 may be measured for each temperature of the sorbate. The effect of temperature on the adsorption isotherm is illustrated in Fig. 15.2 for hydrogen on a bed of activated charcoal. Gas adsorption at a given pressure is increased if the temperature is reduced, because the probability of desorption is less than at higher temperatures.

Adsorption is an important phenomenon because it allows a substance to be pumped to a pressure far below its saturated vapor pressure. For gases such as helium, hydrogen, and neon, this is the only mechanism by which pumping takes place. The data in Fig. 15.1 show ultimate pressures ranging from 10^{-1} to 10^{-12} of the saturated pressure. The ultimate pressure is a function of the surface coverage. The surface coverage can be minimized by pumping a small quantity of gas or by the generation of a large surface area with porous sorbents such as charcoal or a zeolite. Adsorption isotherms have been measured for many materials and several data sources are given in reference 8. The adsorbent properties of charcoal and molecular sieve, which are most interesting for cryopumping, have been the subject of considerable investigation [9–17]. In some cases the isotherms do not approach zero with a slope of one, which suggests that the sorbent was not completely equilibrated. Some analytical expressions for adsorption isotherms have been published [8,18,19].

The last mechanism of low-temperature pumping has been given the name cryotrapping [20] and has been studied in some detail [3,20–23].

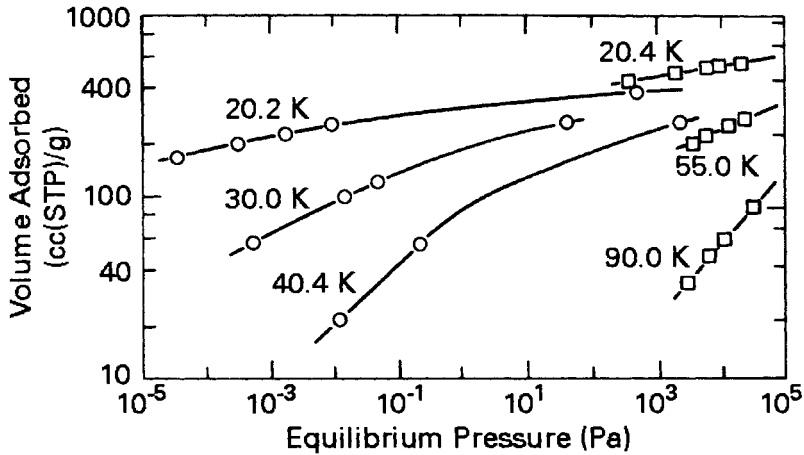


Fig.15.2 Adsorption of hydrogen on coconut charcoal at low pressures. \circ Gareis and Stern [8], \square Van Dingenan and Van Itterbeek [9]. Reprinted with permission from *J. Vac. Sci. Technol.* 2, p. 165, S. A. Stern et al. Copyright 1965, The American Vacuum Society.

Cryotrapping is simply the dynamic sorption of one gas within the porous frozen condensate of another. A gas, which would not normally condense, will sorb if it arrives simultaneously with another condensable gas. Some of the noncondensable gas molecules are adsorbed on the surface of the condensed gas microcrystallites, while others are incorporated within the crystallites [3]. Cryocondensation takes place only between certain pairs of gases. Examples are hydrogen in argon, helium in argon, and hydrogen in carbon monoxide. The cryotrapping of hydrogen in argon is important in sputtering, whereas the pumping of helium in argon is important in fusion work.

Figure 15.3 illustrates the cryotrapping of hydrogen by argon. In this experiment a diffusion pump and a cryosurface pumped in parallel on a known hydrogen gas flow. This resulted in a steady-state hydrogen pressure for zero argon flow whose magnitude was determined by the hydrogen flow rate and diffusion pump speed. As the argon flow was increased, the cryosurface began to pump the hydrogen and reduce its partial pressure. These data show that the efficiency of pumping hydrogen (the hydrogen/argon trapping ratio) is much higher at 5 than at 15 K. At a temperature of more than 23 K, cryotrapping of hydrogen in argon did not occur. The density of the solid argon deposit decreased with condensation temperature; porous argon contained more hydrogen sorption sites than dense argon [22]. Thermal cycling of the argon to a higher temperature irreversibly increased its density and evolved the previously cryotrapped hydrogen.

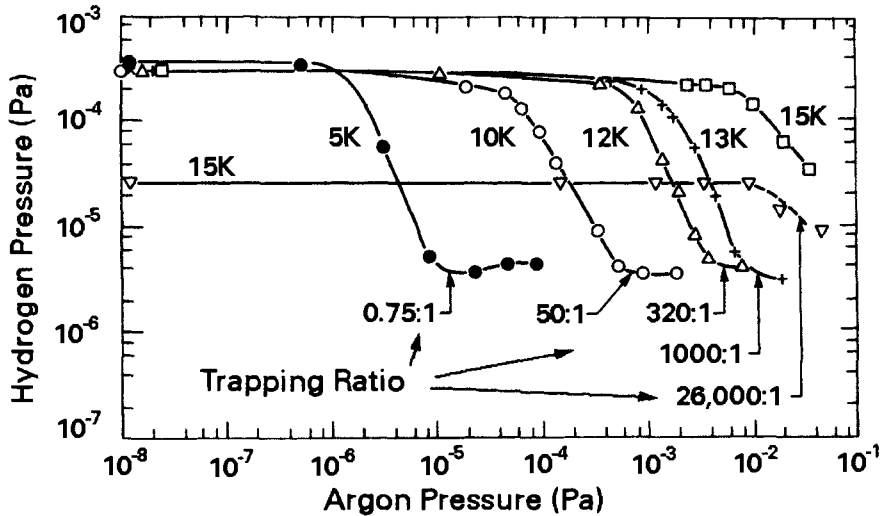


Fig. 15.3 Cryotrapping of hydrogen on solid argon at various temperatures. The drop in hydrogen pressure corresponds to the onset of cryotrapping at a particular argon pressure. Reprinted with permission from *Vacuum*, 17, p. 495, J. Hengevoss and E. A. Trendelenburg. Copyright 1967, Pergamon Press, Ltd.

15.2 SPEED, PRESSURE, AND SATURATION

In Chapters 2, 3, and 7 we outlined kinetic theory and introduced the concepts of gas flow, conductance, and speed. Whenever the temperature in the system is the same everywhere, these ideas can be used to predict the performance of a pump or system. If the temperature varies throughout the system, as it will when a cryopump is used, these notions must be applied with care; some are subject to *misinterpretation*, while others are simply not true. We stated, for example, that the mean-free path was pressure dependent. Strictly speaking, it is particle-density-dependent. The pressure in a closed container will increase if the temperature is increased, but the mean free path will not change because the particle density remains constant. Such a misunderstanding can easily develop because we normally work with constant temperature systems and associate pressure change with particle density change.

The definitions of conductance and speed require the throughput Q to be constant in a series circuit [24]. The throughput is constant only in an isothermal system. See Section 3.2. Throughput has dimensions of energy. In a nonisothermal system, energy is being added to the gas stream as it flows through a warm pipe, and it is removed as it flows through a cool region. Particle flow is constant in a nonisothermal system. It is this concern that

directs us to formulate the behavior of a cryogenic pump in terms of particle flow rather than throughput.

The diagram in Fig. 15.4 describes a chamber with gas at pressure P_c and temperature T_c , connected by area A to a cryogenic pump whose surfaces are cooled to temperature T_s and in which the gas is in thermal equilibrium with the surface. The temperature of the gas in the chamber is assumed to be greater than the gas in the pump. The net flux of particles into the pump is $\Gamma_{net} = \Gamma_{in} - \Gamma_{out}$. This may be written

$$\Gamma_{net} = \frac{An_c v_c}{4} - \frac{An_s v_s}{4} = \frac{AP_c v_c}{4kT_c} - \frac{AP_s v_s}{4kT_s}$$

$$\Gamma_{net} = \frac{AP_c v_c}{4kT_c} \left[1 - \frac{P_s}{P_c} \left(\frac{T_c}{T_s} \right)^{1/2} \right] \quad \blacktriangleright (15.1)$$

In this derivation we have assumed the condensation coefficient is unity. Equation (15.1) may be simplified by observing that the term outside the brackets is Γ_{in} . The maximum particle flow into the pump corresponds to $\Gamma_{out} = 0$, or $\Gamma_{in} = \Gamma_{max}$. Equation (15.1) may be written as

$$\frac{\Gamma_{net}}{\Gamma_{max}} = \left[1 - \frac{P_s}{P_c} \left(\frac{T_c}{T_s} \right)^{1/2} \right] \quad (15.2)$$

Now define

$$P_{ult} = P_s \left(\frac{T_c}{T_s} \right)^{1/2} \quad (15.3)$$

and express (15.2) as

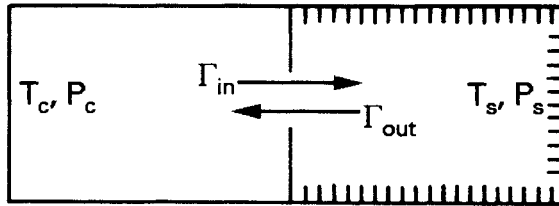


Fig. 15.4 Cryogenic pumping model. The gas in the pump has a temperature T_s equal to the pumping surface and a pressure P_s , which is in equilibrium with the gas condensed or adsorbed on the pumping surface.

$$\frac{\Gamma_{net}}{\Gamma_{max}} = c \left[1 - \frac{P_{ult}}{P_c} \right] \quad \blacktriangleright (15.4)$$

where the condensation coefficient is now included. Equation (15.3) is the thermal transpiration equation (2.37). It relates the ultimate pressure in the chamber of our model P_{ult} to the pressure over the surface. If the pump is a condensation pump, P_s is the saturated vapor pressure. If the pump is a sorption pump, P_s is the pressure obtained from the adsorption isotherm, knowing the fractional surface coverage and temperature of the sorbent.

The ultimate pressure for the cryosorption or cryocondensation pump modeled in Fig. 15.4 can be determined from (15.3) by use of the proper value of P_s . The ultimate pressure for cryocondensation pumping is equal to the saturated vapor pressure multiplied by the thermal transpiration ratio $(T_c/T_s)^{1/2}$. It is a constant during operation of the pump, provided that the temperature of the cryosurface does not change. The ultimate pressure for cryosorption pumping will increase with time because the saturation pressure over the sorbent is a function of the quantity of previously pumped gas. In either case the ultimate pressure in the chamber will be greater than the saturated vapor pressure or adsorption pressure by the transpiration ratio. For $T_c = 300$ K and $T_s = 15$ K the ratio is $P_{ult} = 4.47P_s$.

Equation (15.4) may also be used to characterize the speed of the pump because $\Gamma_{net}/\Gamma_{max}$ is proportional to S_{net}/S_{max} . The pumping speed of a cryocondensation pump is constant and maximum when $P_{ult} \ll P_c$, regardless of the quantity of gas pumped. All gases except H_2 , He, and Ne have a saturated vapor pressure of less than 10–20 Pa at 10 K.

The pumping speed of a cryosorption pumping surface is affected by its prior use, because the saturation pressure of the surface increases as the sites become filled. For high-vapor-pressure gases such as H_2 and He the pumping speed on a molecular sieve at 10–20 K can actually diminish from S_{max} to zero as the clean sorbent gradually becomes saturated with gas during pumping. Figure 15.5 illustrates the expected behavior of speed (linear scale) and ultimate pressure (log scale) as a function of the quantity of gas being pumped (log scale) for both cryosorption and cryocondensation pumping. For both cases the net speed goes to zero as the chamber pressure reaches the ultimate pressure.

The simple model presented here is valid for predicting the performance of a cryogenic pump connected to the chamber by an aperture or pumpingport when all the gas in the pump is cooled to the temperature of the pumping surface. Unfortunately, practical pumps do not meet these criteria. A chamber completely immersed in a liquid cryogen has an ultimate pressure given by P_s ; that is, the gas temperature in (15.3) is $T_c = T_s$. Moore [25] has shown the ultimate pressure in a system consisting of a parallel cryopanel and warm wall to be

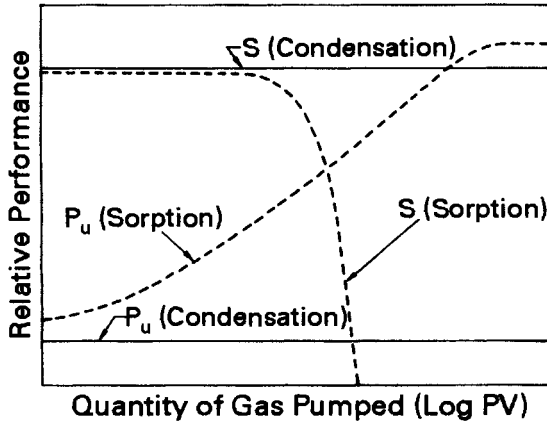


Fig. 15.5 Relative variation of pumping speed and ultimate pressure versus quantity of gas pumped for cryosorption pumping and for cryocondensation pumping.

$$P_{ult} = \frac{P_s}{2} \left[1 + \left(\frac{T_1}{T_2} \right)^{1/2} \right] \quad (15.5)$$

where T_1 is the temperature of the warm wall and T_2 is the panel temperature. Space chambers are constructed with large cryopanel located inside. The gas density and temperature in those pumping systems are neither uniform nor in equilibrium, and the pressure measured depends on the orientation of the gauge [25]. The same is true for a cryogenic pumping unit, which contains surfaces cooled to several different temperatures. The model does not account for the heat carried to the cooled surfaces by the gas or by radiation other than to imply an equal amount of energy must be removed from a cooled surface by the cryogen or refrigerant so that its temperature remain constant. The effects of thermal loading on the pumping surfaces are discussed in Section 15.4. This simple model is sufficient to understand conceptually the speed–pressure relationships for the cryocondensation and cryosorption pumping of individual gases.

In most pumping requirements the pump must adsorb or condense a mixed gas load. Cryotrapping is one instance where the pumping of one gas aids the pumping of another. For example, the pumping speed of hydrogen in the presence of an argon flux may be higher than predicted by cryosorption. Its speed may not decrease to zero when the sorbent is completely covered. Cryosorption pumping of mixed gases may also cause desorption of a previously pumped gas, or reduced adsorption of one of the components of the mixed gas. Water vapor will inhibit the pumping of nitrogen [26], and CO has been shown to replace N_2 and Kr on Pyrex glass

[27]. This is similar to the gas replacement phenomenon for chemisorption that occurs in TSPs; the gas with a small adsorption energy tends to be replaced or be pumped less efficiently than the gas with a large adsorption energy. Hobson [28] and Haefer [3] have reviewed single gas adsorption processes in cryopumps, while Kidnay and Hiza [29] have summarized the literature on mixture isotherms.

15.3 REFRIGERATION TECHNIQUES

Cryogenic pumping surfaces are cooled by direct contact with liquid cryogens, or gases in an expansion cooler. Liquid helium and liquid nitrogen are used to cool surfaces to 4.2 and 77 K, respectively. Other cryogens such as liquid hydrogen, oxygen, and argon are used to obtain different temperatures for specific laboratory experiments. In a liquid-cooled pump heat is removed from the cooled surfaces to an intermittently filled liquid storage reservoir or to a coil through which the liquid cryogen is continuously circulated. In a two-stage closed-cycle gas refrigerator pump, gaseous helium is cooled to two temperature ranges, 10–20 K and 40–80 K. Cryopumping surfaces are attached to these locally cooled regions. Both methods of removing heat, liquid cooling and gas cooling, require mechanical refrigeration but in different ways. Liquid cryogens are most economically produced in large refrigerators at a central location and distributed in vacuum-insulated dewars, while helium gas refrigerators are economical for locally removing the heat load of a small cryogenic pump. The liquid cryogen requirements of a large cryogenic pumped space chamber warrant the installation of a liquifier at the point of use.

Systems using liquid cryogens are often called open-loop systems because the boiling liquid is usually allowed to escape into the atmosphere. This is not necessary; rare gas collection systems have been in use for decades. Helium gas refrigerators are examples of closed-loop systems. Warm gas is returned to the compressor after absorbing heat at low temperatures.

Many thermodynamic cycles have been developed for the achievement of low temperatures [30–33]. Some produce liquid helium or other liquid cryogens, some cool semiconducting and superconducting devices, and others produce refrigeration of useful capacity at temperatures ranging from 100 K to a few degrees above liquid helium temperature. It is the latter class of refrigerators that is used to cool cryogenic pumps. The refrigerator must be reliable, simple, and easy to manufacture and operate. Cycles embodying these attributes have been developed by Gifford and McMahon [32,34–37] and by Longworth [38–40]. These two cycles are

variants of a cycle developed by Solvay [30,33] in 1887. Except for some Stirling cycle machines [41], almost every cryogenic pump in use today is operated on one of these two cycles.

Figure 15.6 illustrates a basic one-stage Gifford-McMahon refrigerator. The helium compressor is located remotely from the expander, and is connected to the expander by two flexible, high-pressure hoses. Within the expander is a cylindrical piston or displacer made from an insulating material. The piston is called a displacer [35] because the regions at each end are connected to give them little pressure difference.

Inside the displacer is a regenerator—a single-channel heat exchanger through which the gas flows at different times in alternate directions. It is tightly packed with a metal of high heat capacity and large surface-area-to-volume ratio. Alloys of lead or copper (or alloys whose heat capacity is high at cryogenic temperatures) in the shape of shot or screen are used to pack the regenerator. In the steady state the regenerator will have a temperature gradient. Ambient-temperature helium entering from the warm end will give heat to the metal, and cold gas entering from the cooler end will absorb heat from the metal. Even though the regenerator is tightly packed, there is not much flow resistance. The regenerator can transfer thermal

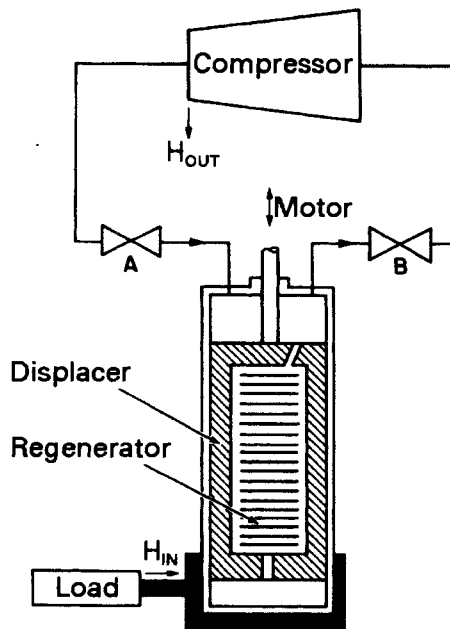


Fig. 15.6 Schematic representation of a single-stage Gifford-McMahon helium gas refrigerator. Adapted with permission from CTI-Cryogenics, Kelvin Park, Waltham, MA 02154.

energy from the incoming to the outgoing helium quickly and with great efficiency.

The operation of the Gifford-McMahon refrigerator can be understood by following the helium through a complete steady-state cycle. High-pressure gas from the outlet of the compressor is admitted to the regenerator through valve A while the displacer is at the extreme lower end of the cylinder. See Fig. 15.6. During the time that valve A is open, the displacer is raised. The incoming gas passes through the cold regenerator and is cooled as it gives heat to the regenerator. At this point in the cycle the gas temperature is about the same as the load. Valve A is then closed before the displacer reaches the top of its stroke. Further movement of the displacer forces the remainder of the gas through the displacer. The exhaust valve B is now opened to allow the helium to expand and cool. The expanding helium has performed work. It is this work of expansion which causes the refrigeration effect. No mechanical work is done since expansion did not occur against a piston. Heat flowing from the load, which is intimately coupled to the lower region of the cylinder walls, warms the helium to a temperature somewhat below that at which it entered the lower cylinder area. As the gas flows upward through the regenerator, it removes heat from the metal and cools it to the temperature at which it was found at the beginning of the cycle. The displacer is now pushed downward to force the remaining gas from the end of the cylinder out through the regenerator where it is exhausted back to the compressor at ambient temperature. A single-stage machine of this design can achieve temperatures in the 30–60 K range.

Lower temperatures can be achieved with two-stage machines. The first, or warm, stage operates in the range 30–100 K, while the second, or cold, stage operates in the range 10–20 K. The exact temperatures depend on the heat load and capacity of each stage. A heat-balance analysis of the refrigeration loss has been performed by Ackermann and Gifford [42]. In the Gifford-McMahon refrigerator the gas is cycled with poppet valves; the valves and the displacer are moved by a motor and all are located on the expander. A Scotch yoke displacer drive is used because it applies no horizontal force to the shaft.

Figure 15.7 illustrates the expander developed by Longsworth [39,40]. As on the Gifford-McMahon refrigerator, the remotely located compressor is connected to the expander by hoses of high-pressure capacity. The helium is cycled in and out of the expansion head through a motor-driven rotary valve. The expander shown here contains a two-stage displacer and two regenerators. The displacer is gas driven instead of motor driven, as in the original Gifford-McMahon cycle. A slack piston is incorporated to improve timing. Surrounding the valve stem is an annular surge volume.

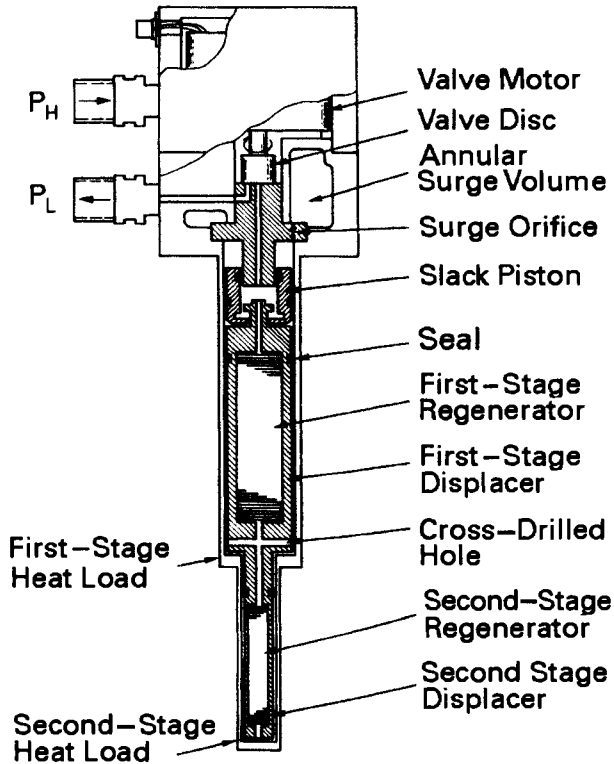


Fig. 15 7 Sectional schematic of the API Model DE-202 expansion head. Reprinted with permission from Air Products and Chemicals, Inc., PA 18105.

This volume is maintained at a pressure intermediate to the supply and exhaust pressures by a capillary tube connected to the regenerator inlet line; it provides the reference pressure for pneumatic operation of the displacer.

In the steady state the operating cycle proceeds as follows [43]: The valve is timed to admit high-pressure helium gas through the stem into the volume below the slack piston and in the regenerators while the displacer is in its lower most position. Because the pressure over the slack pistons is less than the inlet pressure, the piston compresses this gas as it moves upward. The gas bleeds into the surge volume through the surge orifice at a constant rate. The surge orifice is like a dashpot; it controls the speed of the displacer. As the displacer moves upward the high pressure gas flows through the regenerators and is cooled in the process. The inlet valve stops the flow of high-pressure gas just before the displacer reaches the top. This slows the displacer and expands the gas in the displacer. The exhaust valve

opens and the gas in the displacer expands as it is exhausted to the low-pressure side of the compressor. The slack piston moves downward suddenly until it contacts the displacer, after which it moves at constant velocity as gas flows from the surge volume into the space over the slack piston. The expansion of gas in the displacer causes it to cool below the temperature of the regenerator. This is the refrigeration effect. Like the Gifford-McMahon cycle, this cycle does no mechanical work on the displacer because both ends are at the same pressure. The exiting gas removes heat from the regenerator. Before the end of its stroke the displacer is decelerated by closure of the exhaust valve. This completes one cycle of expander operation. Heat is absorbed at two low temperatures and released at a higher temperature.

The compressor used in either of the two Solvay cycle variants is depicted in Fig. 15.8. It uses a reliable oil-lubricated, air-conditioning-type compressor with an inlet pressure of approximately 7×10^5 Pa (100 psig) and an outlet pressure of about 2×10^6 Pa (300 psig). After the gas is compressed, the heat of compression is removed by an air or water after cooler. Oil lubrication can be used without contaminating the cold stages, because it is removed by a two-stage separator and adsorber. Traces of oil, which enter the regenerator, can cause problems. The oil must be cooled before entering the adsorber, as hot oil vapors are not adsorbed on charcoal. It is imperative that the adsorber cartridge be packed tightly and remain cool or it will not adsorb oil vapor.

The most important attribute of small Solvay-type refrigerators is reliability. The low-pressure differential across the seals in the displacers means light pressure loading and long life. Also contributing to long removal life is the use of room-temperature valves, a reliable compressor, and oil techniques. The result is a compact refrigerator that can be isolated

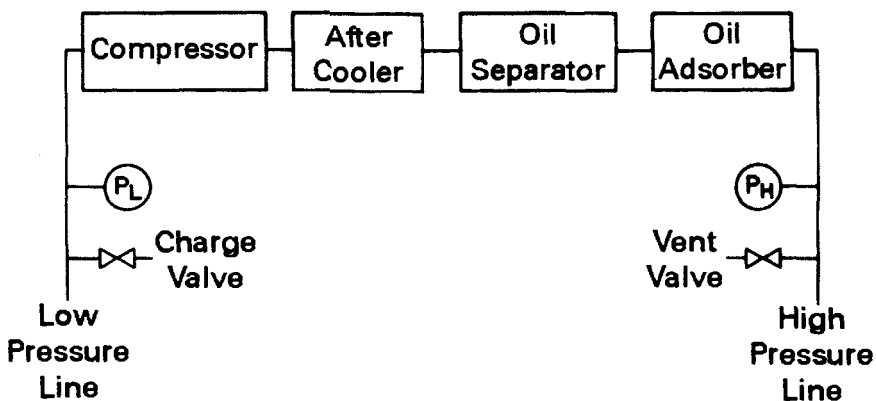


Fig. 15.8 Block diagram of a remotely located helium gas compressor.

from compressor vibration and attached to a vacuum chamber in any attitude.

The coefficient of performance of a refrigerator is defined as the ratio of heat removed to work expended in removing the heat. For an ideal Carnot cycle, the most efficient of all possible cycles, this is [44]

$$\frac{H_{out}}{W_{in}} = \frac{T_1}{T_2 - T_1} \quad (15.6)$$

where heat is being absorbed at T_1 and released at T_2 . For $T_2 = 300$ K a Carnot cycle would require a heat input of 2.9 W to remove 1 W at 77 K and would need a heat input of 14 W to remove 1 W at 20 K. In practice the efficiency of a refrigerator is defined as the ratio of ideal work to actual work. The refrigerators described here have efficiencies of ~ 3 –5% [35,45].

There is interdependence between the refrigeration capacity of the two stages of a cryogenic refrigerator. There is a balance between the heat flow to each stage and the heat removed by each stage. Increasing the load on the warm stage will cause the cold stage to warm slightly also. Each manufacturer will have data on individual compressor performance. The emphasis has been on producing machines with increased capacity in the first stage to isolate radiant heat effectively from the second stage.

15.4 CRYOGENIC PUMP CHARACTERISTICS

In the previous sections we discussed the speed–pressure characteristics of some ideal pumping surfaces. The characteristics of a real cryogenic pump may differ significantly from those ideal cases. A detailed prediction of real pump performance requires a more complete model. The effects of thermal gradients between pumping surfaces and refrigerator, gas and radiant-heat loading, and the geometrical isolation of condensation and sorption stages are three important effects that have not been considered in the ideal model. In the remainder of this section the gas-handling characteristics of rough sorption pumps and refrigerator and liquid-cooled high vacuum pumps are related to the materials, geometry, and heat loading of the pumping surfaces.

15.4.1 Medium Vacuum Sorption Pumps

In the early 1900s Dewar used refrigerated sorption pumping to evacuate an enclosed space. Sorption pumping, as we know it today uses high-capacity artificial zeolite molecular sieves and liquid nitrogen. A unique feature of cryosorption rough pumping is its ability to pump to 10^{-1} Pa without introducing hydrocarbons into the chamber.

A sorption pump designed for rough pumping is illustrated in Fig. 15.9. It consists of an aluminum body that contains many conducting fins and is filled with an adsorbent. A polystyrene foam or metal vacuum Dewar filled with liquid nitrogen surrounds the entire canister. Adsorbent pellets are loosely packed in the canister and do not make good thermal contact with its liquid-nitrogen-cooled walls. To improve the thermal contact pumps with internal arrays of metal fins are constructed. Even so, the interior of the pump is not in equilibrium with the liquid nitrogen bath, especially during pumping.

A common adsorbent is Linde 5A molecular sieve. This sieve, with an average pore diameter of 0.5 nm, exhibits a high capacity for the constituents of air at low pressure. Figure 15.10 illustrates the adsorption isotherms in a pump containing a charge of 1.35 kg of molecular sieve. The adsorptive capacity for nitrogen is quite high in the range 10^{-3} – 10^5 Pa, while the capacity for helium and neon is quite low. Mixed gas isotherms (e.g., neon in air) will show even less pumping capacity for the least active gas (neon), because it will be displaced by any active gas. The pre-adsorption of water vapor will greatly reduce the capacity for all gases; as little as 2 wt.% water vapor is detrimental to pump operation [26]. These isotherms are not valid during dynamic pumping, because the incoming

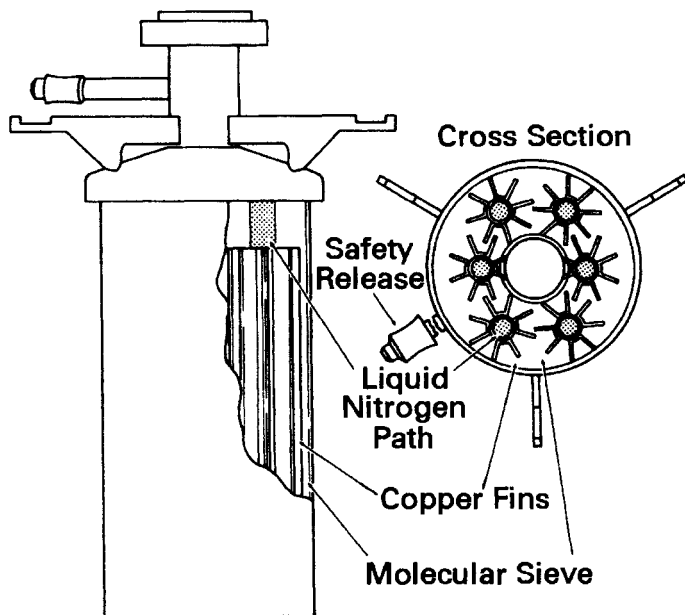


Fig. 15. 9 Typical liquid nitrogen cooled sorption pump. Reprinted with permission from Ultek Division, Perkin-Elmer Corp., Palo Alto, CA 94303.

gas will warm the sieve non-uniformly. They do represent the equilibrium condition of a real pump immersed in a liquid nitrogen bath.

The neon pressure in air is 1.2 Pa, and this limits the ultimate pressure. Figure 15.11 illustrates the time-dependence of the air pressure in a 100 L chamber for single-stage and two-sequential-stage pumping with pumps, each containing 1.35 kg of molecular sieve and pre-chilled at least 15 min. More than 50% of the residual gas present after sorption pumping of air was found to be neon [46]. Staged roughing can reduce the ultimate pressure attainable by sorption pumping with a single pump. In staged roughing, one pump is used, until the chamber pressure reaches approximately 1000 Pa. At that time, the valve connecting that pump to the system is quickly closed and a second pump is connected to the chamber. Figure 15.11 shows the ultimate pressure to be lower and the pumping speed higher than when only one pump was used. The improved pumping characteristic is a result of adsorbate saturation and neon removal. The first pump removed 10^7 Pa-L (99%) of air, including 99% of the neon, while the second removed only 10^5 Pa-L. The ultimate pressure of the second pump is less than the first stage because it pumped a smaller quantity of gas and because most of the neon was swept into the first pump

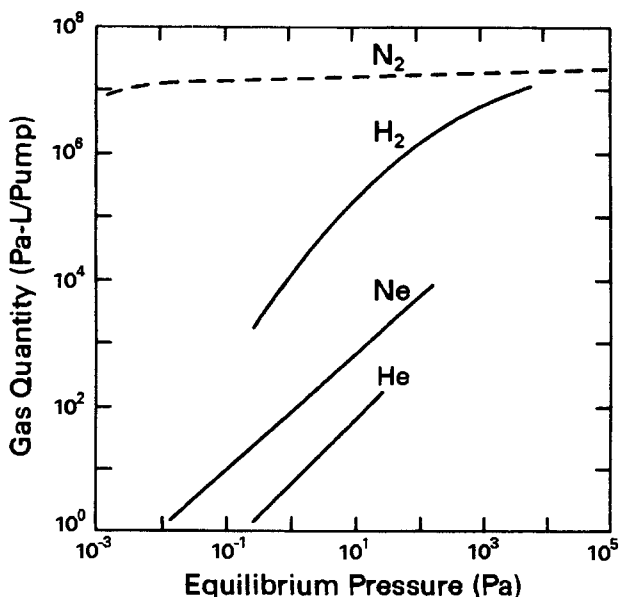


Fig. 15.10 Adsorption isotherms of nitrogen, hydrogen, neon, and helium at 77.3 K in a sorption pump charged with 1.35 kg of molecular sieve. Reprinted with permission from *Cryosorption Pumping*, F. Turner, Varian Report VR-76. Copyright 1973, Varian Associates, 611 Hansen Way, Palo Alto, CA 94303.

by the nitrogen stream and trapped there when the valve closed. The valve needs to be closed quickly at the crossover pressure to prevent back-diffusion of the neon. Alternatively, a carbon vane or water aspirator pump may be used in place of the first sorption roughing stage.

The ultimate pressure attainable with a sorption pump is a function of its history, in particular the bake treatment and the kinds of the gases and vapors. Pressures of an order of 1 Pa are typical. Multistage pumping performance has been characterized by several researchers [46–49], while Dobrozemsky and Moraw [50] have measured sorption pumping speeds for several gases in the pressure range of 10^{-4} – 10^{-1} Pa.

Pumps are normally baked to a temperature of 250°C for about 5 h with a heating mantle or reentrant heating element. Miller [51] measured a water vapor desorption maximum in Linde 5A in the range 137–157°C. All other gases desorb well at room temperature. Baking is required to release water vapor and obtain the full capacity of the sieve.

Each sorption pump has a safety pressure release valve. At no time should the operation of this valve be hindered. Gases will be released when the pump is warmed to atmosphere and when it is baked. A single sorption pump of the size described requires about 5–8 L of liquid nitrogen for initial cooling.

15.4.2 High Vacuum Gas Refrigerator Pumps

A typical high vacuum cryogenic pumping array for a two-stage helium gas refrigerator is depicted in Fig. 15.13. The outer surface is attached to the first (warm, or 80 K) stage and the inner pumping surface is attached to the second (cold or 20 K) stage. Indium gaskets are used to make joints of high thermal conductance. In practice the temperature of the stages is a function of the actual heat load and thermal path. The warm stage pumps water vapor and sometimes CO₂. First stage pumping of CO₂ is a function of the temperature and the partial pressure. The vapor pressure of CO₂ on a 77 K surface is 10^{-6} Pa; CO₂ will be pumped only if its concentration is large enough or the surface temperature is adequately low. The second stage contains a cryocondensation cryosorption pumping surfaces. The cryosorption surface is necessary to pump helium, hydrogen, and neon. It is shielded from the inlet aperture as much as possible to increase the probability that other gases will be condensed on the cryocondensation surface and to prevent direct radiation from an external heat source. Charcoal is the most commonly used sorbent because it can be degassed at room temperature. It has a greater capacity and is less affected by impurities than is molecular sieve. Molecular sieve must be degassed at 250°C, and this is incompatible with the use of indium gaskets.

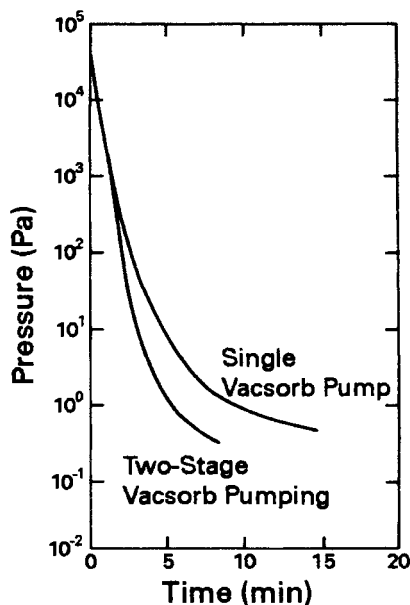


Fig. 15.11 Pumping characteristics of a 100-L, air-filled chamber with (a) one sorption pump and (b) two sequentially staged sorption pumps. Reprinted with permission from *Cryosorption Pumping*, F. Turner, Varian Report VR-76. Copyright 1973, Varian Associates, 611 Hansen Way, Palo Alto, CA 94303.

The temperature of the two pumping surfaces is determined by the total heat flux to the surfaces. Heat is leaked to these surfaces through the expander housing, radiated from high-temperature sources, removed from the incoming gas, and conducted from the warm walls by bouncing gas molecules. Thermal radiation emanates from nearby 300 K surfaces and internal sources such as plasmas, electron-beam guns, and baking mantles. Each condensing molecule releases a quantity of heat equal to its heat of condensation plus its heat capacity. Heat can be conducted from a warm to a cold surface by gas-gas collisions if the pressure is high enough so that $Kn < 1$. In the high vacuum region the radiant flux is much larger than the gas enthalpy or gas conductance. At a pressure of 10^{-4} Pa, a 1000-L/s pump is condensing 0.1 Pa-L/s of nitrogen or a heat load of 0.6 mW. At this pressure, gas conductance can also be ignored.

The radiant heat flow between two concentric spheres or cylinders [52] is given by

$$\frac{H}{A} = \frac{\sigma \epsilon_1 \epsilon_2}{\epsilon_2 + \frac{A_1}{A_2} (1 - \epsilon_2) \epsilon_1} (T_2^4 - T_1^4) \quad \blacktriangleright (15.7)$$

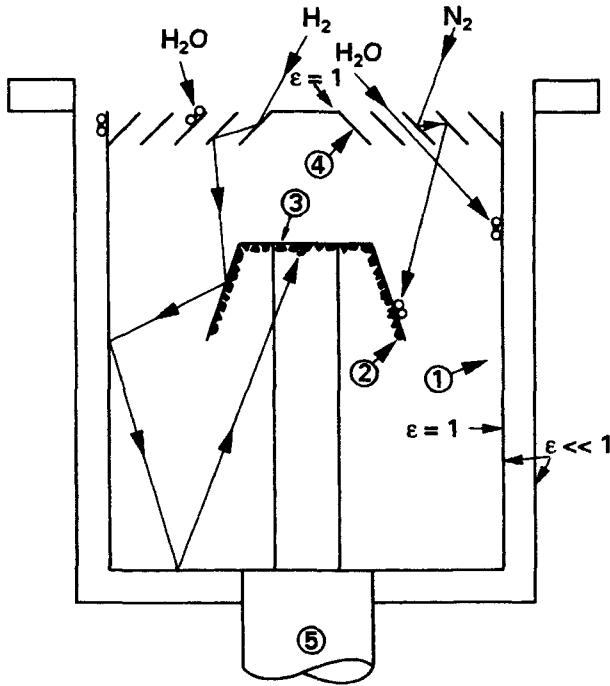


Fig. 15.12 Typical cryogenic pumping array for a two-stage helium gas refrigerator: (1) First-stage array, (2) second-stage cryosorption pump, (3) second-stage cryocondensation pump, (4) chevron baffle, (5) refrigerator head.

where the subscripts 1,2 refer to, respectively, the inner and outer surfaces. If $\epsilon_1 = \epsilon_2 = 1$, the heat flow will be maximum and

$$\frac{H}{A} = \sigma(T_2^4 - T_1^4) \quad (15.8)$$

This yields a heat flow of 457 W/m^2 from the 300 K surface to the 20 K surface. A typical first-stage area of 0.1 m^2 for a small cryogenic pump would then absorb a heat load of 45.7 W . Clearly, this would overload the refrigerator. The radiant heat load is reduced by reducing the emissivities of the inside surface of the vacuum wall and the outside surface of the first stage. If the walls are plated with nickel ($\epsilon = 0.03$) [53], this heat load could be reduced to 0.7 W . Even if these surfaces became contaminated so that $\epsilon_1 = \epsilon_2 = 0.1$, the heat flow would be only 2.4 W .

The first stage isolates the second stage from the radiant heat load and pumps water vapor. Some condensable gas deposits, however, have the property of drastically altering the emissivity of the surface on which they condense. As little as $20 \mu\text{m}$ of water ice on a polished aluminum substrate

at 77 K causes the emissivity to increase from 0.03 to 0.8 [54]. Other data [55] and calculations [56] agree. CO_2 also absorbs thermal energy [55,56].

The two purposes of the first stage—namely pumping water vapor and thermally shielding the second stage—seem contradictory. If the first stage pumps water vapor, its emissivity will rise and it will absorb excess heat and overload the refrigerator. This problem is overcome by keeping the outer wall close to the vacuum wall; the water vapor is now pumped along the upper perimeter of the chevron, the chevron itself, and the interior wall of the first stage. It cannot reach the lower portion of the outside wall. Alternatively, for special cases the exterior may be wrapped with multilayer reflective insulation.

The entrance baffle is designed to prevent radiation from illuminating the second stage. It does this by absorbing radiation in the chevron and allowing transmitted radiation to see the blackened inside wall, where it is absorbed. The entrance baffle also impedes the flow of gases to the second stage. An opaque baffle reduces the radiant loading on the second stage but also reduces the pumping speed for all gases [57]. Good baffle designs are a compromise between radiant heat absorption and pumping speed reduction. One array with an optical transmission of 7×10^{-4} and a molecular transmission of 0.24 was calculated to have the optimum balance between heat adsorption and speed loss [58]. In some pumps the chevrons are painted black; in others they are highly reflective. It matters little because both will soon be “blackened” with water vapor. Figure 15.14 illustrates a cut-away view of one commercial cryogenic pump. Cryopump design problems, including the effect of temperature gradients through the deposit and in the arrays on long-term pump performance, have been reviewed by Hands [59]. Lee and Lee have analyzed the cryopump first-stage array and concluded that a 1-mm-thick oxygen-free electronic (OFE[®]) copper shield resulted in optimum cooling time; if aluminum is used, it should be $1.75\times$ as thick as copper [60].

Approximate pumping-speed calculations can be made for each species if the temperatures and geometry are known; for example, gases pumped on the second stage must first pass through the chevron baffle, where they are cooled. If the effective inlet area, inlet gas temperature, second-stage area, and species are known, the approximate speed and ultimate pressure can be estimated. The pumping speed of a gas in a cryogenic pump is not only related to the size of the inlet flange and refrigeration capacity. It is also dependent on the pumping array (relative sizes of the warm and cold stages), gas species, and history (ice, hydrogen, and helium load). All pumping speeds will fall off near 10^{-1} Pa as the refrigerator becomes overloaded. Because of these effects, it is not possible to draw an illustration analogous to Fig. 12.4, which represents all gas refrigerator-cooled pumps. A representative clean pump of 250-mm-diameter inlet

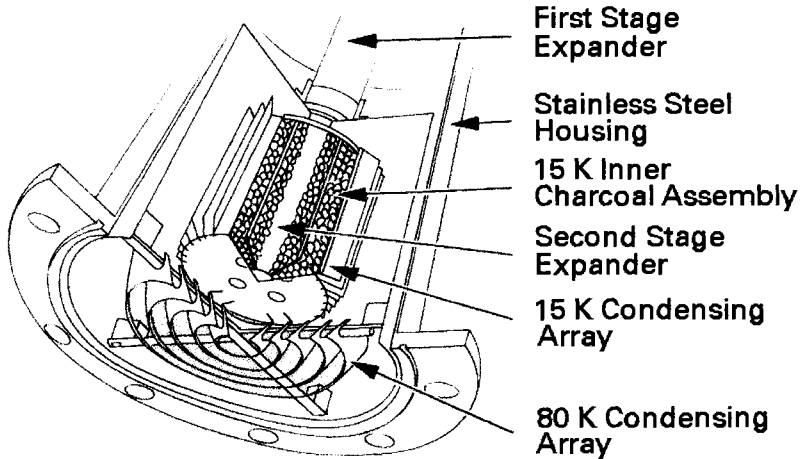


Fig. 15.13 Cutaway view of the Cryo-Torr 8 cryogenic pump. Reprinted with permission from CTI Cryogenics, Kelvin Park, Waltham, MA 02154.

flange diameter might have $S(\text{H}_2) = 4000 \text{ L/s}$; $S(\text{N}_2) = 1200 \text{ L/s}$; $S(\text{Ar}) = 1000 \text{ L/s}$; $S(\text{H}_2) = 1200 \text{ L/s}$; $S(\text{CO}_2) = 900 \text{ L/s}$; and $S(\text{He}) = 700 \text{ L/s}$. The only valid generalization is that helium pumping speed is usually small and has a low saturation value. Hydrogen pumping speeds are larger than those of helium, but will be nil if the sorbent has saturated or its temperature is greater than 20 K.

When the pump becomes saturated, it is shut down while the cryosurfaces warm and the pump is regenerated. (Regeneration techniques are discussed in Chapter 20.) The vaporizing gases exit through the safety valve or manually operated valve, which is connected to a mechanical pump. All cryogenic pumps must have a properly functioning safety release to allow the escape of condensed and adsorbed gases and vapors if the pump fails, is shut-down, or loses power. If there were no safety valve, the pump would become a bomb when warmed.

Recommended practices for measuring the performance and characteristics of closed-loop helium gas refrigerator cryopumps have been published by the American Vacuum Society [61].

15.4.3 High Vacuum Liquid Pumps

Three-stage cryogenic pumps that use liquid helium (4.2 K), gaseous helium boil-off (20 K), and liquid nitrogen are effective in pumping all gases, especially when the molecular sieve is bonded to the third stage [62]. These pumps have been used for pumping large vessels [63–65] and

small vacuum chambers [15,66]. The liquid pump has a higher pumping speed for hydrogen and helium than for a gaseous helium refrigerator because that stage is colder and its temperature is more stable. Additionally, its capacity for pumping He and H₂ is greater due to their increased sticking coefficient at 4.2 K and below [67]. Ultimate pressures of 10⁻¹¹ Pa [63] have been reported. Liquid pumps are individually designed and constructed for large particle beam projects or small laboratory applications.

REFERENCES

1. B. A. Hands, *Vacuum*, **32**, 603, (1892).
2. P. D. Bentley, *Vacuum*, **30**, 145 (1980).
3. R. Haefer, *J. Phys. E: Sci. Instrum.*, **14**, 159 (1981).
4. K. Welch, *Capture Pumping Technology*, Pergamon, Oxford, 1991.
5. J. P. Dawson and J. D. Haygood, *Cryogenics*, **5**, 57 (1965).
6. M. M. Eisenstadt, *J. Vac. Sci. Technol.*, **7**, 479 (1970).
7. R. F. Brown and E. S. Wang, *Adv. Cryog. Eng.* **10**, K. D. Timmerhaus, Ed., Plenum, New York, 1965, p. 283.
8. J. P. Hobson, *J. Phys., Chem.*, **73**, 2720 (1969).
9. P. J. Gareis and S. A. Stern, *Bulletin de l'Institut International du Froid*, Annexe 1966-5, p. 429.
10. W. Van Dingenan and A. Van Itterbeek, *Physica*, **6**, 49 (1939).
11. P. J. Garies, and S. A. Stern, *Cryog. Eng. News*, **26**, 85 (1967).
12. S. A. Stern and F. S. DiPaolo, *J. Vac. Sci. Technol.*, **4**, 347 (1967).
13. G. E. Grenier and S. A. Stern, *J. Vac. Sci. Technol.*, **3**, 334 (1966).
14. A. J. Kidnay, M. J. Hiza and P. F. Dickenson, *Adv. Cryog. Eng.*, **13** K. D. Timmerhaus, Ed., Plenum, New York, 1968, p. 397.
15. R. J. Powers, and R. M. Chambers, *J. Vac. Sci. Technol.*, **8**, 319 (1971).
16. C. Johannes, *Adv. Cryog. Eng.*, **17**, K. D. Timmerhaus, Ed., Plenum, New York, 1972, p. 307.
17. H. J. Halama and J. R. Aggus, *J. Vac. Sci. Technol.*, **11**, 333, (1974).
18. J. P. Hobson, *J. Vac. Sci. Technol.*, **3**, 281 (1966).
19. P. A. Redhead, J. P. Hobson, and E. V. Kornelsen, *The Physical Basis of Ultrahigh Vacuum*, Chapman and Hall, London, 1968, p. 37.
20. R. L. Chuan, Univ. South Calif., Eng. Center Rep. 56-101, 1960.
21. J. Hengevoss and E. A. Trendelenburg, *Vacuum*, **17**, 495 (1967).
22. J. Hengevoss, *J. Vac. Sci. Technol.*, **6**, 58 (1969).
23. J. C. Boissin, J. J. Thibault, and A. Richardt, *Le Vide*, Suppl. 157, 103 (1972).
24. G. Lewin, *J. Vac. Sci. Technol.*, **5**, 75 (1968).
25. R. W. Moore, Jr., *8th Natl. Vac. Symp. (1961)*, **1**, Pergamon, New York, 1962, p. 426.
26. S. A. Stern and F. S. DiPaolo, *J. Vac. Sci. Technol.*, **6**, 941 (1969).
27. Y. Tuzi, M. Kobayashi, and K. Asao, *J. Vac. Sci. Technol.*, **9**, 248 (1972).
28. J. P. Hobson, *J. Vac. Sci. Technol.*, **10**, 73 (1973).
29. J. Kidnay and M. J. Hiza, *Cryogenics*, **10**, 271 (1970).
30. S. C. Collins and R. L. Canaday, *Expansion Machines for Low Temperature Processes*, Oxford University Press, Oxford, 1958.
31. R. Barron, *Cryogenic Systems*, McGraw-Hill, New York, 1966.
32. M. C. Bridwell and J. G. Rodes, *J. Vac. Sci. Technol. A*, **3**, 472 (1985).

33. R. Radebaugh, *Applications of Closed-Cycle Cryocoolers to Small Superconducting Devices*, NBS Special Publication 508, U.S. Department of Commerce, National Bureau of Standards, Washington, DC, 1978, p. 7.
34. W. E. Gifford, Refrigeration Method and Apparatus, U. S. Pat. 2,966,035 (1960).
35. W. E. Gifford and H. O. McMahon, *Prog. Refrig. Sci. Technol.*, **1**, M. Jul and A. Jul, Eds., Pergamon, Oxford, 1960, p. 105.
36. W. E. Gifford, *Prog. Cryog.*, **3**, K. Mendelssohn, Ed., Academic, New York, 1961, p. 49.
37. W. E. Gifford, *Adv. Cryog. Eng.*, **11**, K. D. Timmerhaus, Ed. Plenum, New York, 1966, p. 152.
38. R. C. Longworth, Refrigeration Method and Apparatus, U.S. Pat. 3,620,029, (1971).
39. R. C. Longworth, *Adv. Cryog. Eng.*, **16**, K. D. Timmerhaus, Ed., Plenum, New York, 1971, p. 195.
40. R. C. Longworth, *Adv. Cryog. Eng.*, **23**, K. D. Timmerhaus, Ed., Plenum, New York, 1978, p. 658.
41. For example, Type K-20 Series Cryogenerator, N. V. Philips Gloeilampenfabrieken, Eindhoven, Netherlands.
42. R. A. Ackermann and W. E. Gifford, *Adv. Cryog. Eng.*, **16**, K. D. Timmerhaus, Ed. Plenum, New York, 1971, p. 221.
43. R. C. Longworth, *An Introduction to the Elements of Cryopumping*, K. M. Welch, Ed., American Vacuum Society, p. II-1.
44. F. W. Sears, *An Introduction to Thermodynamics, The Kinetic Theory of Gases and Statistical Mechanics*, Addison-Wesley, Reading, Ma., 1953, p. 84.
45. T. R. Strobridge, *NBS Technical Note 655*, U. S. Department of Commerce, National Bureau of Standards, Washington, D. C., 1974.
46. F. T. Turner and M. Feinleib, *8th Natl. Vac. Symp. (1961)*, **1**, Pergamon, New York, 1962, p. 300.
47. D. Cheng and J. P. Simpson, *Adv. Cryog. Eng.*, **10**, K. D. Timmerhaus, Ed., Plenum, New York, 1965, p. 292.
48. P. Vijendran and C. V. Nair, *Vacuum*, **21**, 159 (1971).
49. F. Turner, Cryosorption Pumping, Varian Report VR-76, Varian Associates, Palo Alto, CA 1973.
50. R. Dobrozemsky and G. Moraw, *Vacuum*, **21**, 587 (1971).
51. H. C. Miller, *J. Vac. Sci. Technol.*, **10**, 859 (1973).
52. R. B. Scott, *Cryogenic Engineering*, Van Nostrand, New York, 1959, p. 147.
53. *Ibid.*, p. 348.
54. R. P. Caren, A. S. Gilcrest, and C. A. Zierman, *Adv. Cryog. Eng.*, **9**, K. D. Timmerhaus, Ed., Plenum, New York, 1964, p. 457.
55. B. C. Moore, *9th Natl. Vac. Symp. (1962)*, Macmillan, New York, 1962, p. 212.
56. S. Tsujimoto, A. Konishi, and T. Kunitomo, *Cryogenics*, **22**, 603 (1982).
57. J. W. Lee and Y. K. Lee, *Vacuum*, **44**, 697 (1993).
58. C. Benvenuti, D. Blechschmidt and G. Passarde, *J. Vac. Sci. Technol.*, **19**, 100 (1981).
59. B. A. Hands, *Vacuum*, **26**, 11, (1976).
60. J. W. Lee and J. Y. Lee, *Vacuum*, **42**, 457 (1991).
61. K. M. Welch, B. Andeen, J. E. de Rijke, C. A. Foster, M. H. Hablanian, R. C. Longworth, W. E. Millikin, Jr., Y. T. Sasaki, and C. Tzemos, *J. Vac. Sci. Technol. A*, **17**, 3081 (1999).
62. H. J. Halama and J. R. Aggus, *J. Vac. Sci. Technol.*, **12**, 532 (1975).
63. C. Benvenuti, *J. Vac. Sci. Technol.*, **11**, 591 (1974).
64. C. Benvenuti and D. Blechschmidt, *Jpn. J. Appl. Phys. Suppl.* **2**, Pt. 1, 77 (1974).
65. H. J. Halama, C. K. Lam and J. A. Bamberger, *J. Vac. Sci. Technol.*, **14**, 1201 (1977).
66. G. Schafer, *Vacuum*, **28**, 399 (1978).
67. C. Day and A. Schwenk-Ferrero, *Vacuum*, **53**, 253 (1999).

PROBLEMS

- 15.1 A cryo pump is regenerated by first removing compressor power, then pumping with a mechanical pump to its base pressure overnight. Is this a good regeneration procedure? If not, why not?
- 15.2 † Describe three ways a cooled surface can pump gases or vapors.
- 15.3 A hydrogen flux is being cryotrapped in an argon flux at a surface temperature of 10 K. A dynamic equilibrium has been reached. The argon 'ice' is warmed to 25 K. Describe qualitatively what happened to the pumping speed and background pressure of hydrogen, when heating the second stage disturbed the equilibrium.
- 15.4 How does a cryosorption pump saturate? What limits the gas quantity pumped on a cryocondensation surface?
- 15.5 A vacuum chamber 40 cm in diameter and 178.25 cm high contains nitrogen gas at STP. How much liquid nitrogen does it take to pump this gas load on a liquid nitrogen cooled molecular sieve whose heat of sorption is 4000 kcal/kg-mole?
- 15.6 A water aspirator pump is sometimes used as an initial roughing pump before operating a sorption pump. It is constructed from a venturi jet of water into which a vacuum inlet is connected. What is the ultimate pressure of this pump?
- 15.7 A small sorption pump containing 1.35 kg of molecular sieve is saturated with 1.2×10^7 Pa-L of nitrogen at a pressure of 10 Pa and a temperature of 77 K. The internal volume of the pump is 2 L. What is the pressure inside an isolated pump when the temperature is raised to 300 K? (Assume the safety valve did not open.)
- 15.8 A spherical Dewar of 50-L capacity is vacuum insulated with a second spherical shell whose radius is 5-cm larger than the Dewar. The emissivity of the outer side of the 50-L Dewar and the inner side of the vacuum jacket are each 0.02. The Dewar is filled with LN₂ at 77.35 K and atmospheric pressure. The Dewar is sealed with a 20-psi (gauge) relief valve. (a) What is the equilibrium temperature of the LN₂ after the pressure rises to that of the relief valve? (b) How long does it take for the LN₂ to reach equilibrium? *Note:* The heat capacity of LN₂ is temperature dependent; assume it to be 57.7 kJ/(kg-mole-K) in the temperature range of interest.
- 15.9 What surface temperatures are required to condense, respectively, water vapor, CO₂, N₂, O₂, and Ar to a pressure of 10^{-4} Pa?
- 15.10 † How is the pumping performance of a helium gas-cooled cryopump dependent on pumping history?

CHAPTER 16

Materials in Vacuum

A superficial examination of a high or ultrahigh vacuum pumping system gives an impression of simplicity: clean, polished metal or glass surfaces, view ports, electrical and motion feedthroughs, piping, and pumps. A close examination reveals that many requirements are placed on materials in vacuum environments and these requirements sometimes conflict. The chamber walls must support a load on $10,335 \text{ kg/m}^2$, a load that is present on the surfaces of all vacuum systems, even those merely roughed to 1000 Pa. Metals must be easy to machine and to join by welding, brazing, soldering or demountable seals. Methods are needed for sealing glasses, ceramics, and other insulators to metals, when optical and electrical feedthroughs are required. The outgassing load from the fixtures of high vacuum chambers and tooling must be reduced to obtain low pressures. High vacuum systems contain a large internal surface, which cannot be baked. Therefore it is essential they be fabricated from materials that can be processed to yield low outgassing rates. Baking is necessary to reduce the outgassing rate and reach the lowest possible pressure in an ultrahigh vacuum system. Baking reduces the maximum stress limit and increases the strain or deformation of stressed parts, and thermal decomposition limits the temperature at which some materials can be baked. The interdependence of cleaning, joining, construction and application need to be clearly understood when choosing materials for use in a vacuum environment.

In this chapter we review the outgassing and structural properties of metals, glasses, ceramics and polymeric materials used in the construction of vacuum equipment. Stainless steel is the dominant material of construction and its structural properties are discussed in some detail. Several older comprehensive papers review the literature of materials for high and ultra high vacuum [1–4]; however, many new results have been obtained in the last decade.

Vaporization, permeation and outgassing are important properties for describing vacuum performance. Vapor pressure limits the useful upper

pressure limit for any material. Desorption from vacuum chamber surfaces provides an additional gas load to the system. Some materials are rather impermeable to gases, whereas others allow certain gases to permeate from the atmospheric side. These effects—collectively referred to as outgassing—limit the ultimate system pressure. In this chapter we review important vacuum related properties of metals, glasses, ceramics, and polymers. Applications of these materials in seals, valves, and other components are discussed in Chapter 17.

16.1 METALS

Metals are used in the chamber and to form its walls. Metals used for vacuum chamber walls should be joinable and sealable and should, have high strength, low permeability to atmospheric gases, low outgassing rate, and low vapor pressure. Metals used within the chamber should have a low outgassing rate and low vapor pressure. Specific vacuum uses, such as filaments, radiation shields, and thermal sinks, will add other constraints. In this section we discuss the vaporization, permeation, and outgassing properties of several metals and some structural properties of aluminum and austenitic stainless steels.

16.1.1 Vaporization

Most metals have a sufficiently low vapor pressure for vacuum use. The vapor pressures of the elemental metals are found in Appendix C.7. Certain metals should not be used in vacuum construction because their vapor pressures are high enough to interfere with normal vacuum baking procedures. Alloys containing zinc, lead, cadmium, selenium, and sulfur, for example, have unsuitably high vapor pressures for vacuum applications. Zinc is a component of brass, cadmium is commonly used to plate screws, and sulfur and selenium are used to make the free machining grades 303S and 303Se stainless steel. These materials should not be used in vacuum system construction. Vapor pressures of the elements are given in Appendix C.6.

16.1.2 Permeability

The permeability, of a gas in a metal is proportional to the product of the gas solubility and the diffusion constant (4.12). Hydrogen is one of the few gases that permeate metals to a measurable extent. Its permeation rate is proportional to the square root of the pressure difference, because it dissociates on adsorption. Figure 16.1 shows the temperature dependence

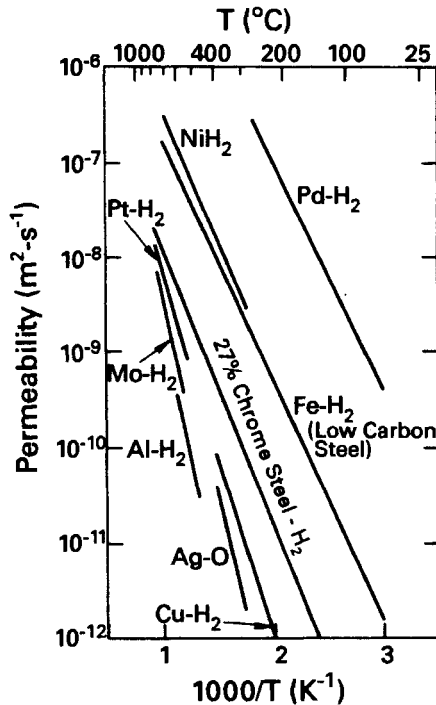


Fig. 16.1 Permeation constant of H_2 through various metals as a function of temperature. Reprinted with permission from *Trans. 8th Natl. Vac. Symp. (1961)*, p. 8, F. J. Norton. Copyright 1962, Pergamon Press, Ltd.

of the permeation constant of hydrogen through several metals. Hydrogen permeation is the least in Al. Other metals through which hydrogen permeates are, in order of increasing permeability, Mo, Ag, Cu, Pt, Fe, Ni, and Pd. The addition of chrome to iron allows the formation of a chrome oxide barrier that reduces the hydrogen permeation rate. The influx will be greater than this value if rusting occurs on the external wall because the reaction of water vapor with iron creates a high local H_2 partial pressure.

Techniques for measuring outgassing are described in Chapter 4. Experimental techniques used to measure the permeation and diffusion constants in solids and have been described elsewhere along with the permeability values of several metals [1].

16.1.3 Outgassing

The gas load in vacuum fixtures and chamber walls is adsorbed on and dissolved in metals. This gas load will affect the performance of high and ultrahigh vacuum systems if it is not removed. Gas is dissolved in a metal

during its initial melting and casting. It consists mainly of hydrogen, oxygen, nitrogen, and carbon oxides. Gas is also physisorbed and chemisorbed on the interior surfaces from exposure to ambient atmosphere. It consists of a large quantity of water vapor, with carbon oxides, oxygen, and some nitrogen. The nature and quantity of the adsorbed layer is also a function of the metal, the gas used to release the system to atmosphere, and the time and extent to which it was exposed to the surrounding air.

In SI the outgassing rate (quantity of gas evolved per unit time per unit surface area) has units of Pa-m/s. Conversion factors are given in Appendix A.3. The pressure in a chamber with net outgassing rate q and area A , when pumped at a speed S , is given by

$$P(\text{Pa}) = 1000 \frac{q(\text{Pa} \cdot \text{m/s})A(\text{m}^2)}{S(\text{L/s})} = \frac{q(\text{Pa} \cdot \text{m/s})A(\text{m}^2)}{S(\text{m}^3/\text{s})} \quad (16.1)$$

The factor of 1000 is included when the pumping speed is expressed in L/s rather than m³/s.

It is important to note that published outgassing, such as given in this chapter and in Appendix C, are net outgassing rates and not true outgassing rates. Hobson described a model of a hollow sphere that was made from the material being measured [5]. q_{net} , the net outgassing rate per unit area of the material, was obtained by properly measuring the flux evolving from the inside of the sphere, Q_T , and dividing it by the area of the sphere A . However, the nonzero pressure inside the sphere indicated there was a flux incident on its surface. For the case where the sticking coefficient $s > 0$, the total or true outgassing rate per unit area of the material was shown to be $q_{\text{true}} = q_{\text{net}} + \Gamma_s$. When $s = 0$, the net outgassing is the same as the true outgassing. In Chapter 4, we noted that measured sticking coefficients of water on stainless steel range from 0.001 to 0.2. Hobson cited examples of a proton storage ring and a space shuttle wake shield where a nonzero sticking coefficient caused a very significant difference in the calculated pressures near the outgassing material.

Dissolved Gas

Release of dissolved gas from inside metals can be eliminated by rendering it immobile, reducing its initial concentration, or erecting a barrier to its passage. Dissolved gas can be rendered immobile by completely immersing a system in liquid helium. At 4.2 K the outdiffusion flux for any gas is so small [(4.3) and (4,5)] that no special precautions need to be taken. The initial concentration can be substantially reduced by vacuum melting, by first degassing parts in a vacuum furnace, or by *insitu* bake of the completed system. A barrier to this outgassing flux can be created by

incorporating a layer of metal such as copper, which has low permeability, or by forming an oxide barrier such as chrome oxide on stainless steel. An oxide barrier to hydrogen diffusion can be formed by an air or oxygen bake or by a multistep chemical treatment such as Diversey [6] cleaning. The latter method leaves some water vapor on the surface. Less thorough cleaning methods are needed after the system has been initially treated. Either glow discharge cleaning or a vacuum bake can be used to clean a chamber after each exposure to ambient. The nature and duration of the cleaning depends on the materials, construction and desired base pressure.

Vacuum melting is an excellent technique for removing dissolved gas under certain conditions. It is expensive and used for specialized applications that require hydrogen and oxygen-free material in small quantities such as certain internal parts and charges for vacuum evaporation hearths.

Vacuum firing of components and subassemblies will effectively remove the dissolved gas load in cleaned and degreased parts. Hydrogen firing is traditionally used for this purpose, because it reduces surface oxides. It has the disadvantage of incorporating considerable gas in the metal at high temperature, which can slowly outdiffuse at low temperature.

Vacuum or inert gas firing is preferred for vacuum components, especially those in ultrahigh vacuum systems. The maximum firing temperatures for several metals are given in Table 16.1. Iron and steel are

**Table 16.1 Firing Temperatures
for Some Common Metals**

Material	Firing Temperature (°C)
Tungsten	1800
Molybdenum ^a	950
Tantalum	1400
Platinum	1000
Copper and alloys ^b	500
Nickel and alloys (Monel, etc.)	750–950
Iron, steel, stainless steel	1000

Source. Reprinted with permission from Vacuum Technology, p. 277, A. Guthrie. Copyright 1963, John Wiley & Sons, New York.

^a Embrittlement takes place at higher temperatures. The maximum firing temperature is 1760°C.

^b Except zinc-bearing alloys, which cannot be vacuum fired at high temperatures because of excessive zinc evaporation.

today not fired at temperatures over 800°C. See Section 21.2.2. Copper and its zinc free alloys are fired at 500°C.

It is important to use oxygen free electronic (OFE[®]) copper, formerly known as OFHC[®] copper, because the copper oxide found in electrolytically tough pitch (ETP) copper will react with hydrogen to form water vapor during baking. The steam will generate voids, which will create porous leaky regions. OFE copper is formed by melting and casting ETP copper under a protective coating of carbon monoxide that reduces copper oxide and prevents contact with atmospheric oxygen.

Based on a single diffusion constant, the time to depletion is $t = d^2/(6D)$ [7]. A 1-h bake of stainless steel at 1000°C would be equivalent to a 2500-h bake at 300°C. Calder and Lewin [8] calculated the time required to reach an outgassing rate of 10^{-13} Pa-m/s for a stainless steel sample 2 mm thick with an initial exposure to 4×10^4 Pa. Their results are shown in Table 16.2 for hydrogen diffusion in stainless steel at temperatures of 300–635°C. This model is valid for high hydrogen outgassing rates in stainless steel. Hydrogen outgassing in UHV chambers is discussed in Chapter 21. Jousten [9] drew different conclusions from vacuum fired 316LN stainless steel. He concluded that the hydrogen outgassing rate decreased with the addition of several 100°C baking cycles, and that the outgassing rate decreased with reduced baking temperature. The lowest observed rate was 5×10^{-12} Pa-m/s (4×10^{-15} Torr-L-s⁻¹-cm⁻²). This result was attributed oxide formation following exposure to humid air. Most likely, this result was due to the large concentration of hydrogen in deep traps that was released after the high temperature bake, but not released after a low temperature bake.

It is not good practice to fire both a screw and the part containing the tapped hole because the screw will bind when it is tightened.

Table 16.2 The Theoretical Time to Reach an Outgassing Rate of 10^{-13} Pa-m/s in Stainless Steel for a single diffusion constant model.

t (s)	D (m ² /s)	T (°C)
10^6 (11 days)	3.5×10^{-12}	300
8.6×10^4 (24 h)	3.8×10^{-11}	420
1.1×10^4 (3 h)	3.0×10^{-10}	570
3.6×10^3 (1 h)	9.0×10^{-10}	635

Source. Reprinted with permission from *Br. J. Appl. Phys.*, **18**, p. 1459, R. Calder and G. Lewin. Copyright 1967, The Institute of Physics.

Surface and Near-Surface Gas

Adsorbed gas may be removed from metal surfaces by thermal desorption, chemical cleaning, or energetic particle bombardment. The procedures used for cleaning metal vacuum system parts depend on the system application. The outgassing rate of unbaked, uncleaned stainless steel is of order 10^{-5} Pa-m/s after 10 h of pumping, depending on its effective surface area. An unbaked system with a 0.5-m^3 work chamber may have as much as 6 m^2 of internal tooling and wall area. If the high vacuum pump has a base plate pumping speed of 2000 L/s, the pressure after 10 h of pumping will be 3×10^{-5} Pa, not a good base pressure for such a system. The outgassing rate of stainless steel must be reduced by a factor of 10–100 over its untreated value to be suitable for high vacuum applications and by a factor of 10^4 – 10^5 for ultrahigh vacuum applications. Unbaked systems with base pressures of $\sim 10^{-6}$ Pa are generally cleaned by chemical or glow discharge cleaning techniques and perhaps a mild bake at temperatures of 40 – 80°C , whereas ultrahigh vacuum chambers are baked to $\sim 150^\circ\text{C}$, or use a form of glow discharge cleaning such as Ar-O_2 or $\text{H}_2\text{-He}$ glow discharge cleaning. Some large collider systems cannot be baked because of their physical size.

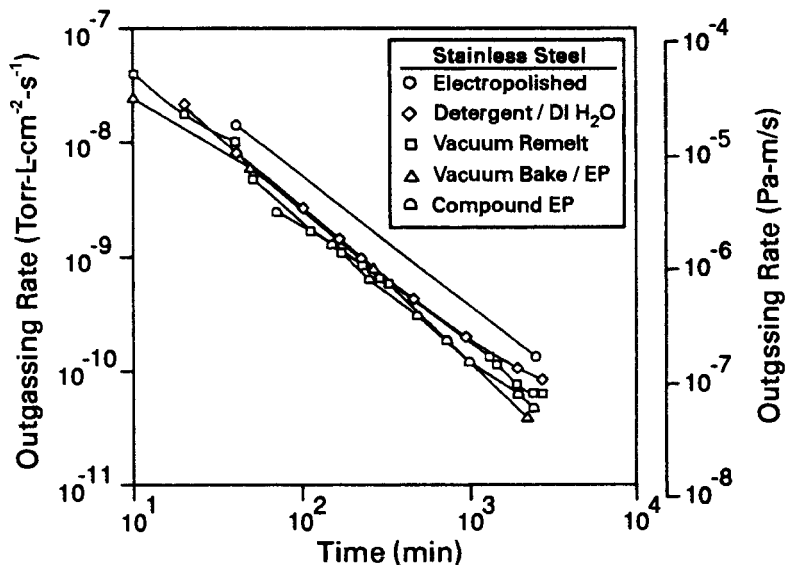


Fig. 16.2 Measured outgassing rates from 304L stainless steel for five different surface cleaning treatments. Reprinted with permission from *J. Vac. Sci. Technol. A*, 11, p. 2623, H. F. Dylla, D. M. Manos, and P. H. LaMarche. Copyright 1993, AVS—The Science and Technology Society.

Dylla et al. have measured the unbaked outgassing rates of 304L stainless steel when prepared by several cleaning methods [10]. Their data, shown in Fig. 16.2, follow the well-reported $1/t$ dependence. All cleaning methods produced nearly identical outgassing rates; differences could be attributable to differences in atmospheric air pre-exposure times [11] and effective surface areas. These experiments found the dominant adsorbed material (>85%) to be water vapor. The 304L pretreatment methods shown in Fig. 16.2 included detergent (Alconox[®]) and DI water, electropolishing, vacuum remelting, vacuum baking/electropolishing, and compound electropolishing. Commercial electropolishing uses phosphoric acid-based solutions. Compound electropolishing refers to a simultaneous mechanical and electropolishing that results in a mirror-like surface with an extremely low surface roughness [12].

Initial surface preparation and cleaning steps such as Blanchard grinding, gross removal by wiping and brushing, high pressure water jets, and immersion in hot (>100°C) perchloroethylene vapor, trichloroethylene, or 1,1,1-trichloroethane often precede detergent cleaning. A number of detergents such as Almeco 18[®] [13] and Almeco P20[®] [14] have been used.

Other chemical cleaning procedures, such as Diversey cleaning, reduce hydrogen outgassing from the near surface region by formation of a chrome-oxide-rich passivation layer. Water vapor was found to be the major outgassing product released from a Diversey cleaned surface [15].

Vacuum baking of stainless steel has been extensively studied because of the wide use it enjoys in vacuum system construction. Nuvolone [16] has systematically compared several of these treatments on 316L stainless steel under identical pre-cleaning and measurement conditions. This work, which is consistent with earlier work, is described in Table 16.3. The lowest outgassing rate was obtained with oxidation in pure oxygen at 2700 Pa. The oxide barrier effectively reduced the hydrogen-outgassing rate. Consistent with recent work, Nuvolone's results show that surfaces cleaned by an 800°C vacuum bake or a 400°C air bake can be stored for long periods before use, provided that they are given a low-temperature bake after assembly.

Reduction of thermal desorption and ultimate pressures have been the main motivator for improved surface cleaning studies; however, the accelerator community requires stringent cleaning to reduce particle-induced outgassing [17]. Glow discharge cleaning has been used for conditioning the beam tubes in the Brookhaven colliding beam accelerator [18] and at the CERN intersecting storage ring [19]. Ar:O₂ plasmas can also remove material by sputtering. In large systems, sputtering is undesirable, because it deposits materials on insulators and windows. Hydrogen glow discharge cleaning has been used at 400 eV. The atomic hydrogen ions therefore have energies no greater than 200 eV, which is

Table 16.3 Outgassing Rates of 316L Stainless Steel After Different Processing Conditions^a

Sample	Surface Treatment	Outgassing Rates (10^{-10} Pa-m/s)				
		H ₂	H ₂ O	CO	Ar	CO ₂
A	Pumped under vacuum for 75 h 50 h vacuum bakeout at 150°C	893 387	573 17	87 6	— —	13. 0.4
B	40 h vacuum bakeout at 300°C	83	0.7	2.2	—	0.01
C	Degassed at 400°C for 20 h in a vacuum furnace (6.5×10^{-7} Pa)	19	0.3	0.44	0.16	0.11
D	Degassed at 800°C for 2 h in a vacuum furnace (6.5×10^{-7} Pa) Exposed to atmosphere for 5 mo, pumped under vacuum for 24 h 20-h vacuum bakeout at 150°C	3.6 — 3.3	— 73 —	0.07 67 0.08	— — —	0.05 13 0.04
E	2 h in air at atmospheric pressure at 400°C Exposed to atmosphere for 5 mo, pumped under vacuum for 24 h 20-h vacuum bakeout at 150°C	17 — 17	— 80 0.75	1.12 69 0.37	— — —	0.4 33 0.17
F	2 h in oxygen at 27,000 Pa at 400°C 20-h vacuum bakeout at 150°	600 5.2	253 0.09	— 0.4	123 0.51	— —
G	2 h in oxygen at 2700 Pa at 400°C 20-h vacuum bakeout at 150°C	— —	20 0.9	13 0.64	8.7 0.45	— —
H	2 h in oxygen at 270 Pa at 400°C 20-h vacuum bakeout at 150°C	— 5.7	16 3.2	52 0.36	19 2	— —

Source. Reprinted with permission from *J. Vac. Sci. Technol.*, 14, 1210, R. Nuvoione. Copyright 1977, The American Vacuum Society.

^a All samples were first degassed in perchloroethylene vapor at 125°C, ultrasonically washed for 1 h in Diversey 708 cleaner at 55°C, rinsed with clean water, and dried.

below sputtering threshold [20]. Desorption of a dilute hydrogen isotope was enhanced by a high constant pressure of hydrogen, and this considerably speeded surface cleaning [21]. See Section 4.3.1. Operators of large systems favor low-temperature cleaning procedures, as they reduce the cost and time to reach ultimate vacuum. Cleaning procedures have been surveyed by the AVS Recommended Practices Committee [22].

Aluminum is also used for construction of large vacuum systems. Traditionally, aluminum has been considered to be a material with a large outgassing rate, due to its thick porous oxide. However, for unbaked chamber use, Fig. 16.3 indicates little difference between samples cleaned with detergent and DI water, machined in ethanol, or extruded in a dry Ar-O₂ ambient TIG or EB welding [11]. This is consistent with the observation that water vapor was the most dominant constituent released from the surface of unbaked aluminum. The outgassing rates from vacuum baked aluminum are as low as those measured from stainless steel.

Although exceedingly low outgassing rates ($<10^{-11}$ Pa·m/s) can be reached after long pumping times in large accelerator systems, a more difficult problem is faced by builders of systems for semiconductor and storage media manufacturing. In these systems, one must reach ultrahigh vacuum conditions within 24–36 h after maintenance, without baking over

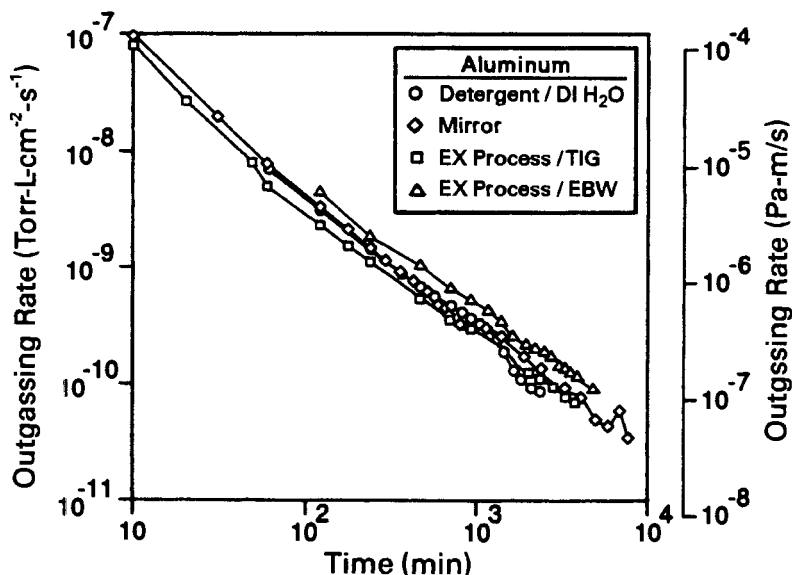


Fig. 16.3 Measured outgassing rates from 6063 aluminum for four different surface cleaning treatments. Reprinted with permission from *J. Vac. Sci. Technol. A*, 11, p. 2623, H. F. Dylla, D. M. Manos, and P. H. LaMarche. Copyright 1993 AVS-The Science and Technology Society.

a temperature of $\sim 80^{\circ}\text{C}$. Thus, the central issue is management of water vapor: its adsorption, residence, and desorption and removal by the pumps. The outgassing data given in Fig. 16.2 and Table 16.3 for stainless steel and in Fig. 16.3, for aluminum are complemented with information in Appendix C.1 and C.2. The ranges of values given in these tables and graphs represent the different conditions under which the samples were prepared and show the differences in measurement techniques.

16.1.4 Structural Metals

Aluminum and stainless steel are the two metals most commonly used in the fabrication of vacuum chambers. Aluminum is inexpensive and easy to fabricate, but hard to join to other metals. It is often used in the fabrication of vacuum collars for glass bell jar systems which are sealed with elastomer O-rings, as well as in some internal fixtures. It is difficult to seal with a metal gasket. Aluminum has been largely bypassed in modern vacuum system construction because of these difficulties. The properties of a few common alloys are given in Table 16.5. Cast tool and jig plate is readily available. It cannot be welded and should never be used in a vacuum system, because it is porous.

Aluminum has been reexamined for use in the construction of chambers for very large high-energy particle accelerators and storage rings [23]. Its high electrical and thermal conductivity and low cost are an asset in the construction of beam tubes. Its residual radioactivity is less than that of stainless steel, because its atomic number is less than that of iron, chrome, or nickel. In this application, explosively bonded aluminum-to-stainless steel sections have been used to make the transition to stainless steel flanges [23]. Ishimaru [24] eliminated stainless steel altogether by designing a system of flanges and bolts of high-strength aluminum alloy for use with aluminum O-rings.

For ordinary laboratory high-vacuum systems, stainless steel is the preferred material. It has high yield strength, is easy to fabricate, and is

Table 16.4 Selected Properties of Common Aluminum Alloys

Alloy	% Alloying Element ^a				Common Forms	TIG Weld	Bend	Vacuum
	Cu	Si	Mg	Cr				
4043	—	5.0	—	—	Weld filler	Yes	Yes	Yes
5052	—	—	2.5	0.25	Sheet, angle, tube	Yes	Yes	Yes
6061	0.25	0.6	1.0	0.2	Sheet, angle, tube	Yes	No	Yes
Cast		Proprietary			Jig plate	No	No	No

^a Welding Alcoa Aluminum, Aluminum Co. of America, Pittsburgh, PA, 1966.

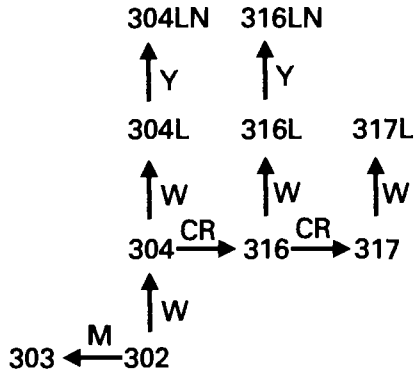


Fig. 16.4 Stainless steels used in vacuum equipment (AISI designation). CR = corrosion resistance, W = ease of welding, Y = yield strength, and M = ease of machining. Reprinted with permission from *Vacuum*, 26, p. 287, C. Geyari. Copyright 1976, Pergamon Press, Ltd.

stable. The stainless steels used in vacuum systems are part of a family of steels characterized by an iron-carbon alloy that contains greater than 13% chrome. The 300 series austenitic steels is used in vacuum and cryogenic work because it is corrosion resistant, easy to weld and nonmagnetic. This series is an “18-8” steel that contains 18% chrome and 8% nickel. To this basic composition additions and changes are made to improve its properties. The low outgassing rate and oxidation resistance of stainless steel is due to the formation of a Cr_2O_3 layer on the surface. Figure 16.4 outlines some of the 300 series alloys and their characteristics. Appendix C.8 contains additional properties and applications of the series.

Types 304 and 316 are the most commonly used grades. Type 303 is easy to machine, but is not used in vacuum systems because it contains either sulfur, phosphorous or selenium. For some applications such as cryogenic vacuum vessels, it is desirable to reduce the thickness of the structural steel walls to reduce heat losses. This can be accomplished without loss of other properties by the use of a nitrogen-bearing alloy such as 304LN or 316LN, or by cold stretching and annealing. The maintenance of corrosion resistance, methods of increasing strength, and reduction of porosity on AISI 300 series stainless steels have been discussed by Geyari [25] and should be thoroughly understood by anyone needing stainless steel for a unique application where it is to be stressed to its limits.

16.2 GLASSES AND CERAMICS

A glass is an inorganic material that solidifies without crystallizing. The common glasses used in vacuum technology are formulated from a silicon

oxide base to which other oxides have been added to produce a product with specific characteristics. Soft glasses are formed by the addition of sodium and calcium oxides (soda-lime glass) or lead oxide (lead glass). Hard glasses are formed by the addition of boric oxide (borosilicate glass). Table 16.5 lists the chemical composition and physical properties of glasses often encountered in vacuum applications.

The physical properties of a glass are best described by the temperature dependence of the viscosity and expansion coefficient. Specific viscosities describe the important properties, because it has no definite melting point. At the strain point ($10^{15.5}$ Pa-s), stresses are relieved in hours. The annealing temperature is defined as a viscosity of 10^{14} Pa-s at which stresses are relieved in minutes. At the softening point the viscosity is about $10^{8.6}$ Pa-s, and the working point corresponds to a viscosity of 10^5 Pa-s. Glass is brittle, and because of its high thermal expansion and low tensile strength it can shatter if unequally heated. Its expansion coefficient is important when selecting the components of a glass-to-glass or glass-to-metal seal.

The viscosity-temperature and thermal expansion characteristics determine the suitability of a glass for a specific application. Borosilicate glasses are used whenever the baking temperature exceeds 350°C , while fused silica is required for temperatures higher than 500°C . The thermal expansion coefficient and strength determine the maximum temperature gradient that a glass can withstand and to what it can be sealed. For example, a borosilicate glass dish can be heated to 400°C in a few minutes, while a large, 1-in.-thick vessel fabricated from lead glass will require 24 h to reach the same temperature. Glasses are used for bell jars, Pirani gauges, U-tube manometers, McLeod gauges, ion gauge tubes, cathode ray tubes, controlled leaks, diffusion furnace liners, view ports, seals, and electrical and thermal insulation.

A ceramic is a polycrystalline, nonmetallic inorganic material formed under heat treatment with or without pressure. Ceramics are mechanically strong and have high dielectric breakdown strength and low vapor pressure. Ceramics include glass bonded crystalline aggregates and single-phase compounds such as oxides, sulfides, nitrides, borides, and carbides. Ceramics contain entrapped gas pores and are not so dense as crystalline materials. Their physical properties improve as their density approaches that of the bulk. Alumina is made with densities that range from about 85% to almost 100% of its bulk density. Most ceramics have a density of about 90% of the bulk. The important physical properties of ceramics are their compression and tensile strength and thermal expansion coefficient. High-density alumina, for example, has a tensile strength 4–5 \times greater than that of glass, and has a compression strength 10 \times greater than its tensile

Table 16.5 Properties of Some Glasses Used in Vacuum Applications

Property	Fused Silica	Pyrex 7740	7720 ^a	Soda 7052 ^a	0080	Lead 0120
Composition						
SiO ₂	100	81	73	65	73	56
B ₂ O ₃		13	15	18		
Na ₂ O		4	4	2	17	4
Al ₂ O ₃		2	2	7	1	2
K ₂ O				3		9
PbO			6			29
LiO				1		
Other				3	9	
Viscosity characteristics						
Strain point °C	956	510	484	436	473	395
Annealing point °C	1084	560	523	480	514	435
Softening point °C	1580	821	755	712	696	630
Working point °C	—	1252	1146	1128	1005	985
Expansion coefficient $\times 10^{-7}/^{\circ}\text{C}$	3.5	35	43	53	105	97
Shock temperature, 1/4-in. plate °C	1000	130	130	100	50	50
Specific gravity	2.20	2.23	2.35	2.27	2.47	3.05

Source. Reprinted with permission from Corning Glass Works, Corning, NY.

^a 7720 glass is used for sealing to tungsten and 7052 glass is used for sealing to Kovar.

strength. The properties of some ceramics are listed in Table 16.6. Alumina is the most commonly used ceramic in applications such as high vacuum feedthroughs and internal electrical standoffs. Machinable glass ceramic also finds wide application in the vacuum industry for fabricating precise and complicated shapes. It is a recrystallized mica ceramic whose machinability is derived from the easy cleavage of the mica crystallites.

Borides and nitrides have found applications in vacuum technology. Evaporation hearths are made from titanium diboride and titanium nitride, alone or in combination. They are available in machinable or pyrolytically deposited form. Forsterite ceramics ($2\text{MgO}:\text{SiO}_2$) are used in applications where low dielectric loss is needed, and beryllia (BeO) is used when high thermal conductivity is necessary. Beryllia must be machined while carefully exhausting the dust, because it is extremely hazardous to breathe. Reviews of ceramics and glasses have been published by Espe [26] and Kohl [27].

Permeation of gas through glasses and ceramics occurs without molecular dissociation. The permeation constant, which is given by (4.12), depends on the molecular diameter of the gas and the microstructure or porosity of the glass or ceramic [28]. Figure 16.5 contains data for the temperature dependence of the permeation rate of He, D₂, Ne, Ar, and O₂ through silicon oxide glasses [1]. With the exception of deuterium and hydrogen, it shows that the permeation rate decreases as the molecular

Table 16.6 Physical Properties of Some Ceramics

Ceramic	Main Body Composition	Expansion Coefficient ($\times 10^{-7}$)	Softening Temperature ($^{\circ}\text{C}$)	Tensile Strength (10^6 kg/m^2)	Specific Gravity
Steatite	MgOSiO_2	70–90	1400	6	2.6
Forsterite	2MgOSiO_2	90–120	1400	7	2.9
Zircon porcelain	ZnO_2SiO_2	30–50	1500	8	3.7
85% alumina	Al_2O_3	50–70	1400	14	3.4
95% alumina	Al_2O_3	50–70	1650	18	3.6
98% alumina	Al_2O_3	50–70	1700	20	3.8
Pyroceram 9696 ^a	Corderite ceramic	57	1250	14 ^b	2.6
Macor 9658 ^a	Fluorophlogopite	94	800	10 ^b	2.52

Source. Reprinted with permission from *Vacuum*, **25**, p. 469, G. F. Weston. Copyright 1975, Pergamon Press, Ltd.

^a Reprinted with permission from Corning Glass Works, Corning, NY.

^b Modulus of rupture.

diameter increases. The measured permeation rate of hydrogen was much larger than predicted because of surface reactions and solubility effects [28]. The permeation of a gas through a glass depends on the size of the pores in relation to the diameter of the diffusing species. Permeation is minor through a crystalline material such as quartz but increases with lattice spacing. The non-network-forming Na_2O , which is added to SiO_2 to form soda glass, plugs these openings (Fig. 16.6) and causes the permeation rate to decrease. Permeation rates for some glasses are given in Fig. 16.7. Shelby [33] has reviewed the diffusion and solubility of gases in glass. The thermal properties and helium permeation of Corning Macor machinable glass ceramic have been reviewed by Altemose and Kacyon [37].

Gases are physically and chemically soluble in molten glass. The gas on the surface of glass is primarily water with some carbon dioxide. Water vapor may exist on glass in layers as thick as 10–50 monolayers [38]. The first bake of glass releases considerable surface water, while the second and succeeding bakes release structural water [39]. See Fig. 16.8. This release of structural water is proportional to $t^{1/2}$ and indicates a diffusion-controlled process [38]. A high temperature bake should completely eliminate outgassing of water from glass, because all the surface water is released in a high temperature bake and the diffusion constant of water vapor is negligible at room temperature. At 25°C , gas evolution from glass is dominated by the permeation of helium. Outgassing rates of some unbaked ceramics and glasses are given in Appendix C.3. In addition, Colwell [40] has tabulated the outgassing rates of more than 80 untreated refractory and electrical insulating materials used in the construction of vacuum furnaces.

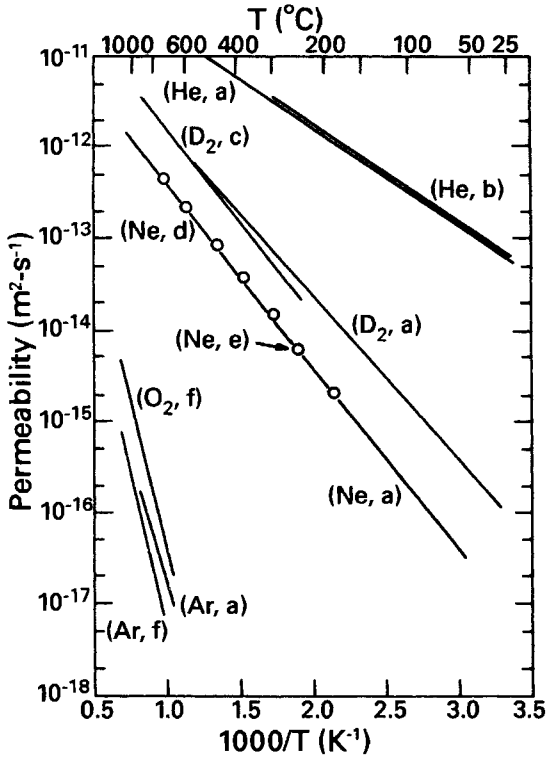


Fig. 16.5 Permeability of He, D₂, Ne, Ar and O₂ through silicon oxide glasses. Data taken from (a) Perkins and Begeal [29]; (b) Swets, Lee, and Frank [30]; (c) Lee [31]; (d) Frank Swets and Lee [32]; (e) Shelby [33]; and (f) Norton [28]. Reprinted with permission from *J. Vac. Sci. Technol.*, 10, p. 543, W. G. Perkins. Copyright 1973, The American Vacuum Society.

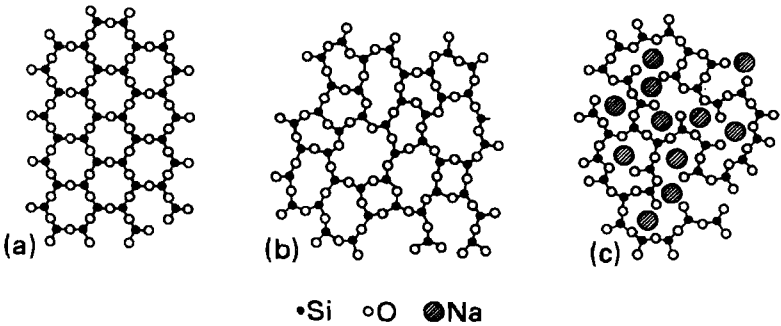


Fig. 16.6 (a) Atomic arrangement in a crystalline material possessing symmetry and periodicity; (b) the atomic arrangement in a glass; (c) the atomic arrangement in a soda glass. Reprinted with permission from the *J. Am. Ceram. Soc.*, 36, p. 90, F. J. Norton. Copyright 1953, The American Ceramic Society.

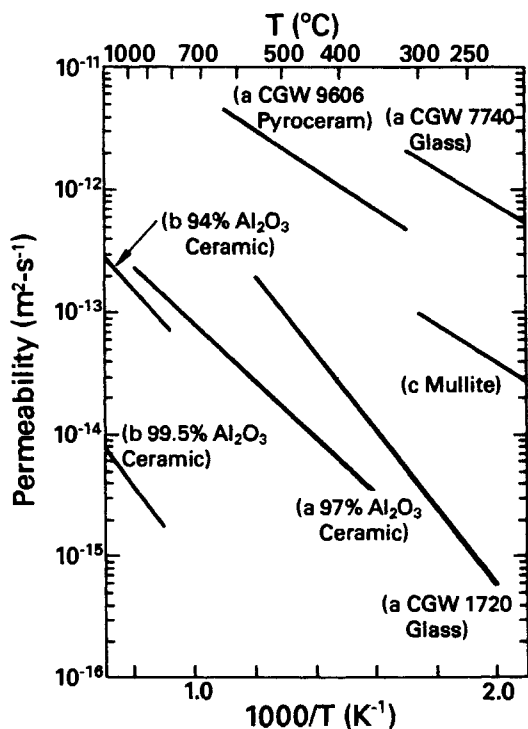


Fig. 16.7 Helium permeability through a number of glasses and ceramics. After Perkins. Data taken from (a) Miller and Shepard [34]; (b) Edwards [35]; (c) Shelby [33]. Reprinted with permission from *J. Vac. Sci. Technol.*, 10, p. 543, W. G. Perkins. Copyright 1973, The American Vacuum Society.

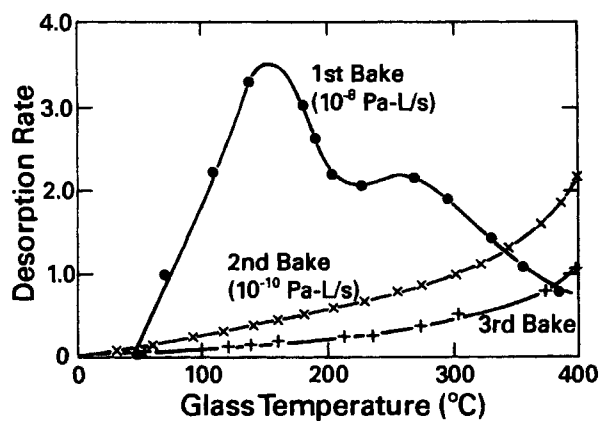


Fig. 16.8 Desorption of water from a Pyrex-glass surface of 180 cm^2 at increasing temperature. Adapted with permission from *Vacuum*, 15, p. 573, K. Erents and G. Carter. Copyright 1965, Pergamon Press, Ltd.

16.3 POLYMERS

Polymeric materials find applications in several areas. The generic, trade and chemical names of common materials are given in Table 16.7. Elastomers such as Buna-N, Viton, Silicone and Kalrez are used to form O-ring gaskets for static, sliding, or rotary seals. Other polymers such as Vespel and Kapton are used for high-voltage vacuum feedthroughs. Mechanical and other properties of elastomers, which are important when these materials are used as seals, are discussed in Chapter 17.

Permeation and outgassing are important physical properties of elastomers. Gases diffuse through voids in the intertwined polymer chains by a thermally activated process. The dimensions of the voids are larger than those in a glass or metal, and as a result the permeation constants are much larger than for those materials. Comparison of the permeation rates of gases through polymers with those for glasses shows that the diffusion process in a polymer is not as sensitive to molecular diameter as it is in a glass. This implies that the diffusion of air and other heavy gases through polymers is a serious problem, while helium is the only gas of any consequence to diffuse through glass. Elastomers will swell when in contact with certain solvents used for cleaning and leak detection. This swelling or increased spacing between molecules results in an increased permeability [2].

Laurenson and Dennis [41] have studied the temperature dependence of gas permeation in three elastomers. Their results, presented in part in Fig. 16.9, have two important conclusions. One is that the change of permeation with temperature is not the same for all gases so that the ratio of permeation

Table 16.7 Generic Trade and Chemical Names of Polymer Materials Frequently Used in Vacuum

Generic	Trade	Chemical
Fluoroelastomer	Viton ^a , Fluorel ^b	Vinylidene fluoride-hexafluoropropylene copolymer
Buna-N (nitrile)		Butadiene-acrylonitrile
Buna-S		Butadiene-styrene copolymer
Neoprene		Chloroprene polymer
Butyl		Isobutylene-isoprene copolymer
Polyurethane	Adiprene ^a	Polyester or polyether di-isocyanate copolymer
Propyl	Nordel ^a	Ethylene-propylene copolymer
Silicone	Silastic ^d	Dimethyl polysiloxane polymer
Perfluoro-elastomer	Kalrez ^a	Tetrafluoroethylene-perfluoromethylvinyl ether copolymer
PTFE	Teflon ^a , Halon ^e	Tetrafluoroethylene polymer
PCTFE	Kel-F ^b	Chlorotrifluoroethylene copolymer
Polyimide	Vespel ^a , Envex ^c	Pyromellitimide polymer

Source. Reprinted with permission from *J. Vac. Sci. Technol.*, 17, p. 330, R. N. Peacock. Copyright 1980, The American Vacuum Society.

^a E. I. du Pont de Nemours and Company.

^b 3-M Company.

^c Rogers Corporation.

^d Dow Corning Corporation.

^e Allied Chemical Company.

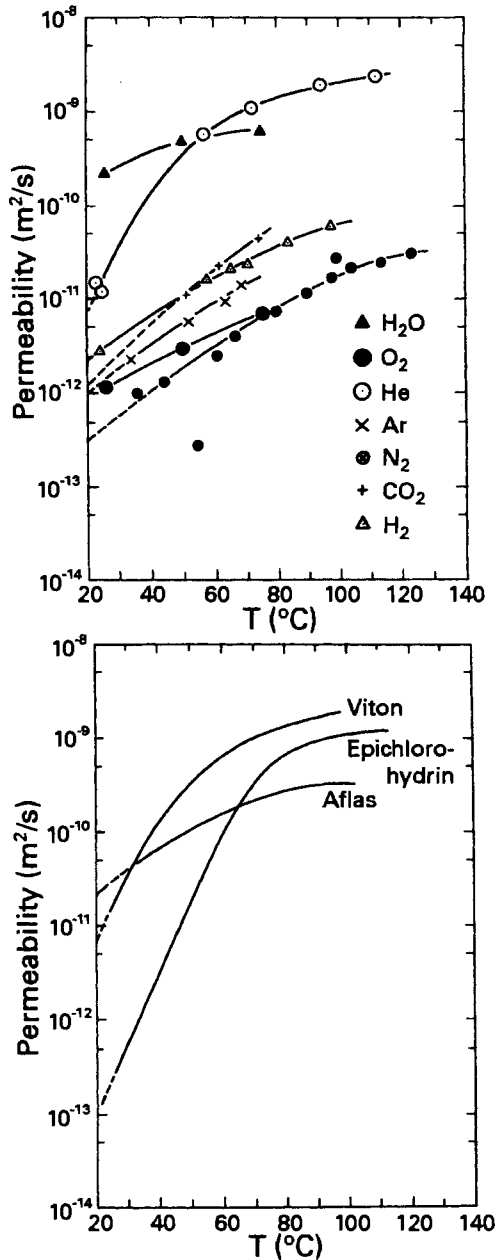


Fig. 16.9 Top: Relation between permeation and temperature for various gases through Viton. Bottom: A comparison of the helium permeability of three elastomers, Viton, Epichlorohydrin, and Aflas, over the range 20–100°C. Reprinted with permission from *J. Vac. Sci. Technol. A*, 3, p. 1707, L. Laurenson and N. T. M. Dennis. Copyright 1985, The American Vacuum Society. The added data for H_2O and O_2 were reported by C. Ma et al., *Journal of the IES*, March/April, 1995, p. 43, using tracer gas measurements in ultrapure N_2 .

constant between two gases at room temperature is not the same at elevated temperature. Second, the change of permeation with temperature for a given gas is not the same in different materials. The material with the lowest permeability to a given gas at room temperature is not necessarily the best material to use at 100°C. Permeation rates for some materials commonly used in vacuum are tabulated in Appendix C.6.

The outgassing of unbaked elastomers has been studied extensively [1, 41–58] and shown to be dominated by the evolution of water vapor. The data in Fig. 16.10 illustrate the time dependence of the outgassing rates of several elastomers. Baking will reduce this gas load, as revealed in the mass scans of Figs. 9.7 and 9.8 taken during the heating of Buna-N and

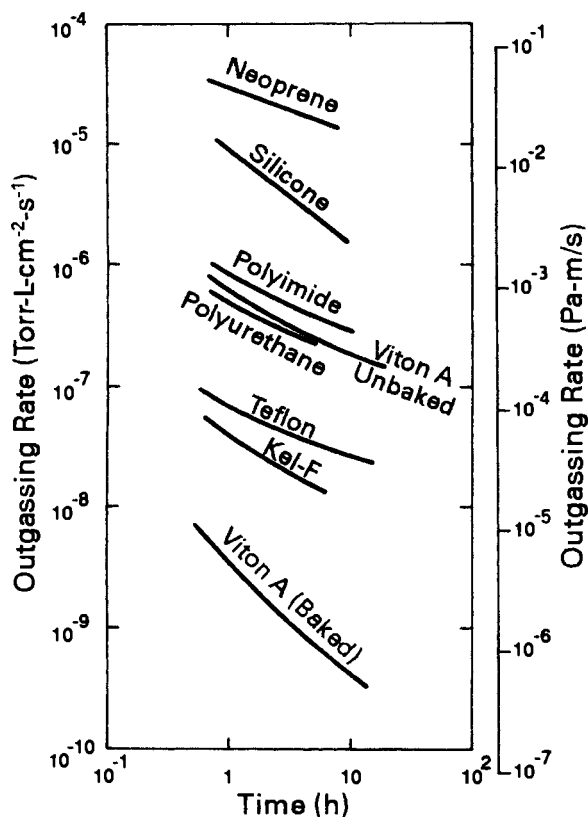


Fig. 16.10 Room-temperature outgassing rates for several polymer materials. The values shown are selected from the literature as typical. The rates decline between one and two decades from one to ten hours of pumping. Moderate baking is even more helpful as a comparison of the two Viton curves shows [45,48,54,55]. Reproduced with permission from *J. Vac. Sci. Technol.*, 17, p. 330, R. N. Peacock. Copyright 1980, The American Vacuum Society.

Viton. These mass scans show that plasticizers, which were added to the polymer before vulcanization, were released as the temperature was increased. Unreacted polymer was also evolved. At a higher temperature, the elastomer began to decompose. de Csernatony [55,56] reviewed the elastomers Kalrez, and the current Viton E60C. Viton E60C appears to be similar in its outgassing to Viton A, while Kalrez has a low outgassing rate and can withstand temperatures up to 275°C.

Outgassing data for elastomers commonly used in vacuum are given in Appendixes C.4 and C.5. Schalla [59] gives data on the outgassing of cellular foams and stranded elastic cords used in the medium vacuum range, whereas Glassford et al. [60,61] have reported the outgassing rates of aluminized mylar and other multilayer insulation materials. Outgassing characteristics of several optically black solar absorbing coatings [62,63], as well as elastomers and carbon foam [59], have been measured.

Sigmond [64] noted that the pertinent outgassing properties were not dominated by the polymer, but by water and by plasticizers and stabilizers of proprietary composition and quantity that were altered from lot to lot without the consumer's knowledge. A volatile organic of mass number 149 was found to be present in ethyl alcohol stored in polyethylene bottles and in samples stored in test tubes closed with plastic caps [64]. This organic vapor turned out to be a fragment of di-butyl-phthalate, a commonly used plasticizer. Because this fragment was easily removed by a 100°C bake, it will contaminate materials stored in plastic bags or boxes or touched by plastic gloves. Parks and co-workers [65] measured the outdiffusion of one plasticizer, 3,5-di-tert-butyl-4-hydroxytoluene (BHT) from polypropylene wafer carrier boxes and found its diffusivity to be $D \text{ (m}^2\text{/s)} = 1855 \exp(-11,986/T)$.

REFERENCES

1. W. G. Perkins, *J. Vac. Sci. Technol.*, **10**, 543 (1973).
2. R. J. Elsey, *Vacuum*, **25**, 299 (1975).
3. R. J. Elsey, *Vacuum*, **25**, 347 (1975).
4. G. F. Weston, *Vacuum*, **25**, 469 (1975).
5. J. P. Hobson, *J. Vac. Sci. Technol.*, **16**, 84 (1979).
6. The Diversy Co., Chicago, IL.
7. W. A. Rogers, R. S. Buritz and D. L. Alpert, *J. Appl. Phys.*, **25**, 868 (1954).
8. R. Calder and G. Lewin, *Brit. J. Appl. Phys.*, **18**, 1459 (1967).
9. K. Jousten, *Vacuum*, **49**, 359 (1998).
10. H. F. Dylla, D. M. Manos, and P. H. LaMarche, *J. Vac. Sci. Technol. A*, **11**, 2623, (1993).
11. M. Li and H. F. Dylla, *J. Vac. Sci. Technol. A*, **11**, 1702 (1993).
12. T. Ohmi, *Microcontamination*, **6**, 49 (1988).
13. C. Benvenuti, G. Canil, P. Chiggiato, P. Collin, R. Cosso, J. Guérin, S. Ilie, D. Latorre, and K. S. Neil, *Vacuum*, **53**, 317 (1999).
14. J. D. Herbert and R. J. Reid, *Vacuum*, **47**, 693 (1996).

15. R. S. Barton and R. P. Govier, *Vacuum*, **20**, 1 (1970).
16. R. Nuvolone, *J. Vac. Sci. Technol.*, **14**, 1210 (1977).
17. H. F. Dylla, *Vacuum*, **47**, 647 (1995).
18. H. C. Hseuh, T. S. Chou, and C. A. Christianson, *J. Vac. Sci. Technol. A*, **3**, 518 (1985).
19. R. Calder, A. Grillot, F. LeNormand and A. Mathewson, *Proc. 7th Intl. Vac. Congr.*, R. Dobrozemsky, Ed., Vienna, 1977, p. 231.
20. Ph. Staib, H. F. Dylla, and S. M. Rossnagel, *J. Vac. Sci. Technol.*, **17**, 291 (1980).
21. R. J. Knize and J. L. Cecchi, *J. Vac. Sci. Technol. A*, **1**, 1273 (1983).
22. Y. T. Sasaki, *J. Vac. Sci. Technol. A*, **9**, 2025 (1990).
23. R. P. Govier and G. M. McCracken, *J. Vac. Sci. Technol.*, **7**, 552 (1970).
24. H. Ishimaru, *J. Vac. Sci. Technol.*, **15**, 1853 (1978).
25. C. Geyari, *Vacuum*, **26**, 287 (1976).
26. W. Espe, *Materials of High Vacuum Technology*, Vol. 2, Pergamon Press, New York, 1966.
27. W. H. Kohl, *Handbook of Materials and Techniques for Vacuum Devices*, Reinhold, New York, 1967.
28. F. J. Norton, *J. Am. Ceram. Soc.*, **36**, 90 (1953).
29. W. G. Perkins and D. R. Begeal, *J. Chem. Phys.*, **54**, 1683 (1971).
30. D. E. Swets, R. W. Lee and R. C. Frank, *J. Chem. Phys.*, **34**, 17 (1961).
31. R. W. Lee, *J. Chem. Phys.*, **38**, 448 (1963).
32. R. C. Frank, D. E. Swets and R. W. Lee, *J. Chem. Phys.*, **35**, 1451 (1961).
33. J. E. Shelby, *Phys. Chem. Glasses*, **13**, 167 (1972).
34. C. F. Miller and R. W. Shepard, *Vacuum*, **11**, 58 (1961).
35. R. H. Edwards, M. S. Thesis, Univ. of Calif., Berkeley, 1966.
36. J. E. Shelby, *Molecular Solubility and Diffusion*, in *Treatise on Materials Science and Technology: Glass II*, Vol. 17, M. Tomozawa and R. H. Doremus, Eds., Academic, New York, 1979.
37. V. O. Altemose and A. R. Kacyon, *J. Vac. Sci. Technol.*, **16**, 951 (1979).
38. B. J. Todd, *J. Appl. Phys.*, **26**, 1238 (1970).
39. K. Erents and G. Carter, *Vacuum*, **15**, 573 (1965).
40. B. H. Colwell, *Vacuum*, **20**, 481 (1970).
41. L. Laurenson and N. T. M. Dennis, *J. Vac. Sci. Technol. A*, **3**, 1707 (1985).
42. R. S. Barton and R. P. Govier, *J. Vac. Sci. Technol.*, **2**, 113 (1965).
43. R. R. Addis, Jr., L. Pensak and N. J. Scott, *Trans. 7th Vac. Symp. (1960)*, Pergamon, New York, 1961, p. 39.
44. R. Geller, *Le Vide*, No. 13, 71, (1958).
45. M. M. Fluk and K. S. Horr, *Trans 9th Vac. Symp. (1962)*, Macmillan, 1963, p. 224.
46. M. Munchhausen and F. J. Schittko, *Vacuum*, **13**, 548 (1963).
47. P. W. Hait, *Vacuum*, **17**, 547 (1967).
48. J. Blears, E. J. Greer and J. Nightengale, *Adv. Vac. Sci. Technol.*, **2**, E. Thomas, Ed., Pergamon, 1960, p. 473.
49. L. de Csernatony, *Vacuum*, **16**, 13 (1966).
50. L. de Csernatony, *Vacuum*, **16**, 129 (1966).
51. L. de Csernatony, *Vacuum*, **16**, 247 (1966).
52. L. de Csernatony, *Vacuum*, **16**, 427 (1966).
53. L. de Csernatony and D. J. Crawley, *Vacuum*, **17**, 55 (1967).
54. T. L. Edwards, J. R. Budge and W. Hauptli, *J. Vac. Sci. Technol.*, **14**, 740 (1977).
55. L. de Csernatony, *Proc. 7th Intl. Vac. Congr. & 3rd Intl. Conf. Solid Surf.*, R. Dobrozemsky, Ed., Vienna, 1977, p. 259.
56. L. de Csernatony, *Vacuum*, **27**, 605 (1977).
57. B. B. Dayton, *1959 Sixth Natl. Symp. on Vac. Technol. Trans.*, Pergamon, New York, 1960, p. 101.

- 58. G. Thieme, *Vacuum*, **17**, 547 (1967).
- 59. C. A. Schalla, *J. Vac. Sci. Technol.*, **17**, 705 (1980).
- 60. P. M. Glassford and C-K. Liu, *J. Vac. Sci. Technol.*, **17**, 696 (1980).
- 61. P. M. Glassford, R. A. Osiecki, and C-K. Liu, *J. Vac. Sci. Technol. A*, **2**(3), 1370 (1984).
- 62. E. D. Erickson, D. D. Berger and B. A. Frazier, *J. Vac. Sci. Technol. A*, **3**, 1711 (1985).
- 63. E. D. Erickson, T. G. Beat, D. D. Berger, and B. A. Frazier, *J. Vac. Sci. Technol. A*, **2**, 206 (1984).
- 64. T. Sigmond, *Vacuum*, **25**, 239 (1975).
- 65. Y-M. Ho, H. G. Parks, and B. Vermere, *Proc. ASCM*, Boston, 30 April 2002. p. 314.

PROBLEMS

- 16.1 Describe the properties of materials which influence (a) the rate of gas evolution from a surface, (b) their use as vacuum vessel walls, and (c) their use within the vacuum environment.
- 16.2 The increased gas load from improperly handled or cleaned metal parts is predominantly a result of (choose two) permeation, desorption, diffusion or evaporation? What other processes will cause gas be evolved from an improperly cleaned or handled elastomer?
- 16.3 What are three ways (other than leaks) by which gas can enter a vacuum system?
- 16.4 What hydrogen flux can be obtained through a leak constructed from a $10,000 \text{ cm}^2$ palladium film 0.02 mm thick held at $T = 400^\circ\text{C}$?
- 16.5 When an arc breakdown occurs in a vacuum switch, dissolved gas will be released from the electrodes at a point where the arc makes contact. Assume that 0.04 g of copper evaporates from the electrodes during a particular arc. Calculate the number of molecules of gas released from the copper, if the copper were contaminated with dissolved gas at a solubility of 1 ppm. Assuming an initial pressure of 10^{-5} Pa, what instantaneous pressure results from this arc in a switch whose interior volume is 1 L?
- 16.6 (a) What is the difference between force and pressure? (b) 50-cm-diameter "Magdeburg hemispheres" are sealed together and exhausted to $P = 2000$ Pa. What is the force (newtons) required to separate the hemispheres? (c) Do high vacuum chambers need to be structurally any stronger than those used in the hemispheres?
- 16.7 A 50-cm-diameter vacuum bell jar is sealed to a base plate with an elastomer L-gasket. The maximum deflection of the center of such a freely mounted circular plate is given by $x(m) = 0.696Pr^4/(Et^3)$, where P is the pressure in Pa, r is the radius, and t is the base plate

thickness in meters. E is the modulus of elasticity. Calculate the base plate thickness required, if it is made from (a) aluminum ($E = 6.9 \times 10^{10}$ Pa), and (b) stainless steel ($E = 1.9 \times 10^{11}$ Pa) such that the maximum deflection of the baseplate in the center is limited to 0.25 mm when the interior of the bell jar is pumped to 10^{-5} Pa.

- 16.8 The maximum shear stress in a freely mounted circular disk is given by $s_m = 1.24Pr^2/t^2$, where P is the uniformly applied pressure in Pa, and s_m is the maximum shear stress in Pa. The maximum stress of a typical piece of borosilicate glass containing scratches and imperfections is about 6.9×10^7 Pa. However, glass exhibits a time-loading effect that reduces its strength when under constant stress for long periods of time. An adequate design load is 6.9×10^6 Pa. Calculate the thickness required for (a) a 2-cm-diameter window and (b) a 20-cm-diameter window on an unbaked high vacuum chamber.
- 16.9 The major concern for the use of plastic materials in unbaked vacuum systems is not vapor pressure but ...
- 16.10 BHT ($C_{15}H_{24}O$), molecular weight 220, is a plasticizer frequently added to polypropylene; it outgasses from polypropylene at room temperature. Assume 10 ppm by weight of BHT is uniformly added to the polymer, and assume $\rho_{\text{polyp}} = \rho_{\text{BHT}} = 0.89$ g/ml. Furthermore, assume a two-dimensional geometry where all the BHT outgassing from one side of a 3-mm-thick, flat polypropylene storage box deposits on the adjacent, closely spaced silicon wafer surface. Calculate the thickness of the BHT contaminant layer on the surface of the silicon wafer after 100-h storage in the polypropylene carrier box at a temperature of 300 K.

Materials

Knowledge of the basic properties of materials from which vacuum systems are fabricated is essential to operate and maintain vacuum systems properly. One of the most troublesome properties of materials used in vacuum applications is gas release from solids at low pressures. Chapter 16 discusses the origins of gas released from metals, glasses, ceramics and polymers commonly used in systems, and it also discusses how it can be removed. Chapter 17 discusses techniques for joining and sealing materials, including valves. Chapter 18 describes lubricants used in vacuum systems. Some details of how hydrogen outgasses in ultraclean systems are discussed in Chapter 21. There is nothing to vacuum, it is all in the packaging.

CHAPTER 17

Joints, Seals, and Valves

In decades past, a discussion of joining and sealing techniques would have been incomplete without a description DeKhotinsky cement, Glyptal, and black wax. The times when valve stems were sealed with string soaked in grease have also passed. Materials technology has advanced to the place where glass-to-metal seals, demountable elastomer and metal-to-metal gaskets, brazed joints, welded joints, valves, and motion feedthroughs are catalog items. Reliable joints, seals, and components are so common that we take them for granted and sometimes contribute to their misuse. Occasionally we use a rubber hose as a flex connector, bake a brass valve, grease an elastomer static seal, bake Viton to an excessively high temperature, try to save money by reusing copper gaskets, or apply "stop leak" to a leaky weld. Singleton [1] remarked that in the early days of vacuum technique, some workers preferred the clear variety of Glyptal so as to hide their mistakes. Today's mistakes can be hidden with a degree of sophistication beneath vacuum epoxy and a coat of paint.

In this chapter we review welded and brazed metal joints, metal, glass and ceramic joints, elastomer and metal sealed flanges, valves, and motion feedthroughs. We emphasize proper selection and use of joining and sealing techniques and not design. Roth has extensively reviewed sealing and joining techniques [2-4].

17.1 PERMANENT JOINTS

Welding, brazing and soldering are used to make permanent joints in vacuum chambers, pumping lines and components. The technique one chooses to use depends on the materials to be joined and on the thermal and vacuum environment to which the parts will be exposed. Welded joints of stainless steel, titanium or aluminum, flame-sealed glass joints, glass-to-metal, and ceramic-to-metal joints are commonly used in high and ultrahigh vacuum system construction.

17.1.1 Welding

Metals can be joined permanently by welding—locally melting—closely mating pieces. Welding of vacuum components is most commonly done by the tungsten inert gas (TIG) process to avoid oxidation. A detailed review of TIG and other welding techniques is given in the American Society of Metals' *Metals Handbook* [5]. TIG welding is not the only technique; plasma-arc and electron-beam welding also can be used. However, these techniques are not as readily available or applicable for all types of joints. TIG welding, also known as heliarc or argon arc welding, is a technique for forming clean, oxide-free, leak-tight joints by flooding the area immediately around the arc with an inert gas, usually argon. TIG welding is used in vacuum fabrication to make joints in materials such as stainless steel, aluminum, nickel, copper, and titanium. It is not suitable for joining alloys with high-melting-point components—for example, brass and certain aluminum or stainless steel alloys. Stainless steel is the most common material used in the construction of high and ultrahigh vacuum vessels. Any 300 series alloy, except 303S and 303Se, is easily welded. It is more difficult to weld aluminum than stainless steel, but a skilled welder can make leak-tight joints. Dissimilar metals also can be welded. Combinations of stainless steel, copper, nickel, and Monel can be joined by TIG welding. Aluminum and stainless can be joined by explosion bonding. The welding of austenitic stainless steels has been reviewed in extensive detail by Rosendahl [6] and Geyari [7].

Figure 17.1 depicts several acceptable vacuum welding techniques. Welding from the vacuum side or through-welding from the atmospheric side, along with welding walls of equal thickness, is basic to good welding practice. It is important for the weld to be clean on its vacuum side. If the weld is made on the atmospheric surface, but does not penetrate completely, a gap may be created, which is impossible to clean. For strength, some joints need to be welded on the atmospheric side as well. If this is necessary it should be a discontinuous weld. See for example, the dashed welds in Fig. 17.1. If the outer weld was continuous and the inner joint was leaky, the leak could not be detected; trapped gas would constitute a slow, “virtual” leak. In small-diameter tubing, the weld cannot be made on the vacuum side. In this case, a through weld will prevent the formation of regions where cleaning solvents can collect. Continuous butt orbital welding is a superior process for joining long lengths of tubing. With this technique the two ends of the tubing are forced together and purged with Ar or Ar-H₂ during welding. Pulsed dc power is applied to a rotating tungsten tip, such that the melt zone completely penetrates the tube weld. A long exhaust tube is necessary to prevent back-diffusion of air (+oxygen). Large pipe can be chemically cleaned following welding.

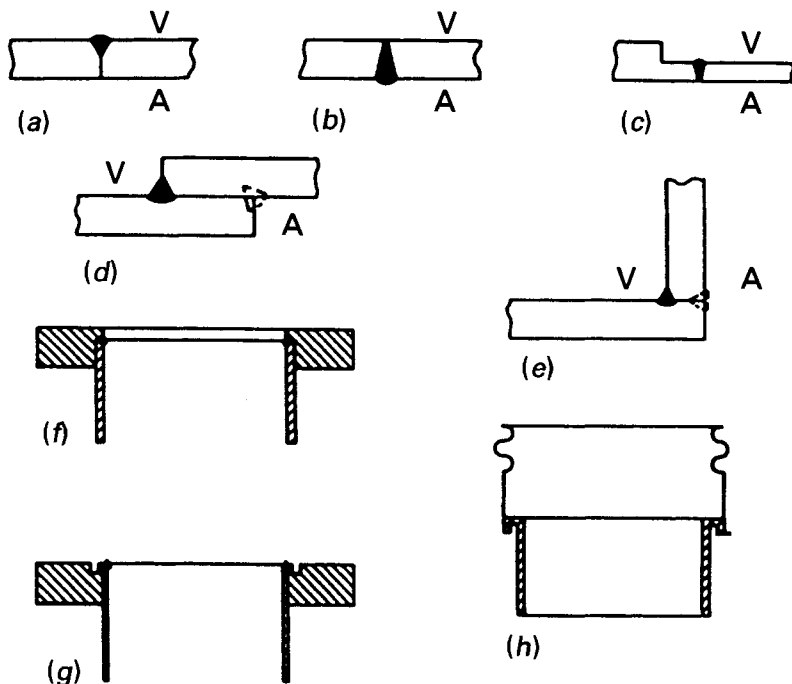


Fig. 17.1 Examples of welded joints: (a) Butt-welded from the vacuum side; (b) through-welded from the atmospheric side; (c) joining parts of unequal thickness; (d) lap weld illustrating proper tack welds on the atmospheric side; (e) corner weld; (f) thick-wall tubing-to-flange weld. The flange is machined so that the bead depth is approximately equal to the wall thickness. (g) Thin-wall tubing-to-flange weld joint showing relief groove; (h) bellows-to-pipe adapter. The right side is shown before welding. The raised lip (0.025 cm high \times 0.035 cm thick) provided filler metal for the weld; a copper heat sink was attached to the bellows end section during welding.

Oxidation can be prevented on the opposite surfaces with an argon flush during welding.

It is also important for the two surfaces to be as equal in thickness as possible. A weld relief groove should be used to match the thickness when welding a flange to a thinner tube. This is particularly important in the welding of thin-wall tubing and bellows. See Fig. 17.1. These two ideas—welding walls of equal thickness and welding from the vacuum side or completely through to the vacuum side—are basic to all properly designed and executed weld joints.

Carbide precipitation and inclusions in ASIA 300 series stainless steels are potentially problems in fabricating vacuum vessels. Carbon that has precipitated at grain boundaries, because of welding or improper cooling after annealing, removes with it a substantial fraction of the chrome from

nearby regions. See Fig. 17.2. The nearby regions then contain less than 13% chrome and are no longer stainless steel. They are subject to corrosion if exposed to a corrosive atmosphere. The formation of microscopic cracks is also a concern for stainless steel subjected to low temperatures. A crack in a carbide-rich zone can cause a leak in a cold trap or cold finger.

Carbide precipitation may be prevented with an alloy containing a low carbon content, a stabilized alloy, or a minimum-heat welding technique. A good solution is the use of low-carbon steel alloys such as 304L and 316L; however, they require more nickel and are more expensive to manufacture than their higher carbon counterparts. Titanium, niobium, and tantalum form carbides more easily than chrome, so an alternative solution is the use of an alloy (321, 347, or 348) stabilized with one of these elements. A minimum heat weld will also reduce the time that the metal weld region spends in the dangerous 500–900°C region. Minimum heat welds are simplified by use of weld relief grooves like those shown in Fig. 17.1. An 18-8 alloy of 0.06% carbon will not precipitate carbides at the grain boundaries if it is cooled from 900°C to 500°C in less than 5 min. As the carbon content is reduced, the steel can remain in the critical temperature region for additional time without carbide precipitation.

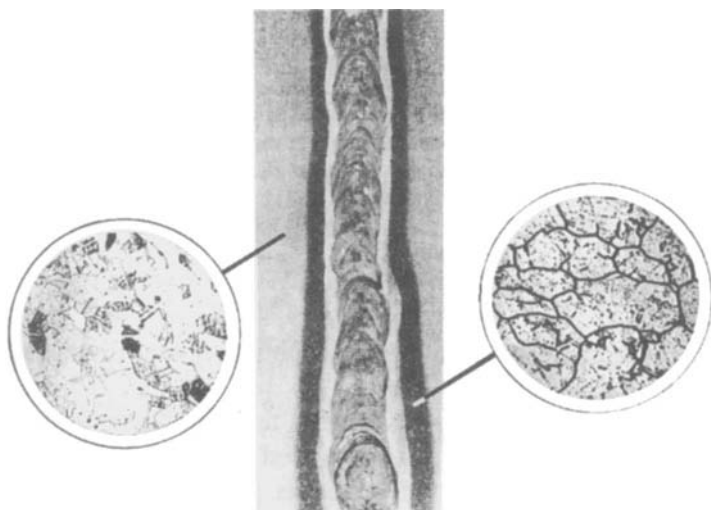


Fig. 17.2 The appearance and location of carbide-rich zones bordering a weld bead in 304 stainless steel. The sample has been etched to make the carbide-rich regions visible. The dark zones on either side of the weld are regions in which the metal cooled from 900°C to 500°C in more than 5 min. The right inset shows a magnified view of the carbide-rich zone. The left inset shows a magnified view of the grain structure of normal annealed 304 stainless steel. Reprinted with permission from *Stainless Steel Fabrication*, Allegheny Ludlum, Pittsburgh. Copyright 1959, Allegheny Ludlum Steel Company.

A most important concern of the ultrahigh vacuum user, and occasionally the high vacuum user, is the proper fabrication and joining of stainless steel components to eliminate leaks through inclusions in the metal. Grease and other impurities mask these minute inclusions, which occur in the process of making steel, until the steel wall is thoroughly baked. At that time tiny leaks will appear. The impurities in a cooling ingot distribute themselves at the top and center. See Fig. 17.3. The portion with the most of the oxide and sulfide impurities is removed before rolling, and any remaining impurities are stretched into long narrow leak paths. The inclusions are in the direction of rolling. It is important to know the inclusion direction when selecting the raw stock from which components are to be made. In particular, inclusions can cause virtual leaks when sheet or tubing is welded on the atmospheric side without full penetration. Figure 17.4 illustrates the origin of leak paths in high vacuum flanges made of plate stock. To avoid such potential leaks, modern flanges are made from bar stock. Also the material is usually forged to break up the long filamentary inclusions and reduce the possibility of such leak paths. For critical applications a section from the each end of the billet will be individually examined before fabrication.

Nonmagnetic steels are used to fabricate some electron-beam and low-cost chambers. One must take care not to use filler welding rods, whose constituents will produce a porous weld.

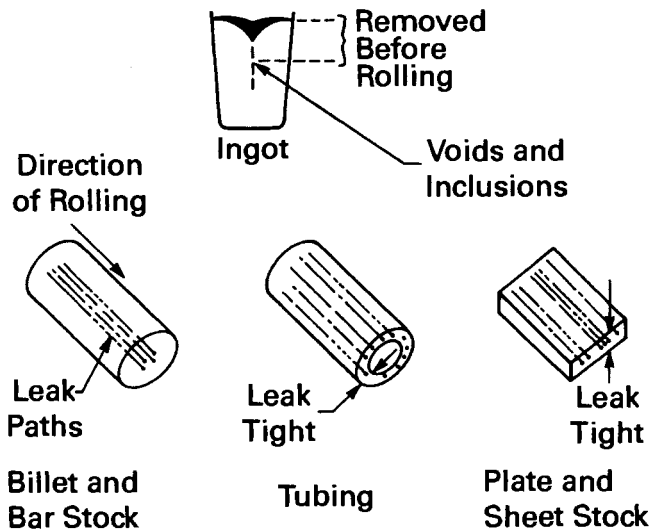


Fig. 17.3 Schematic-inclusions in steel during casting and rolling. Reprinted with permission from Varian Report VR-39, *Stainless Steel for Ultra-high Vacuum Applications*, V. A. Wright, Copyright 1966, Varian Associates, 611 Hansen, Way, Palo Alto, CA.

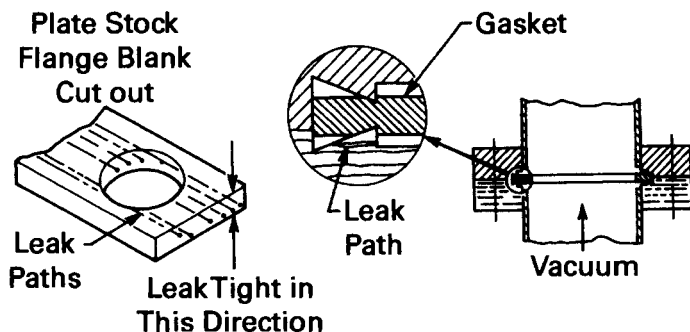


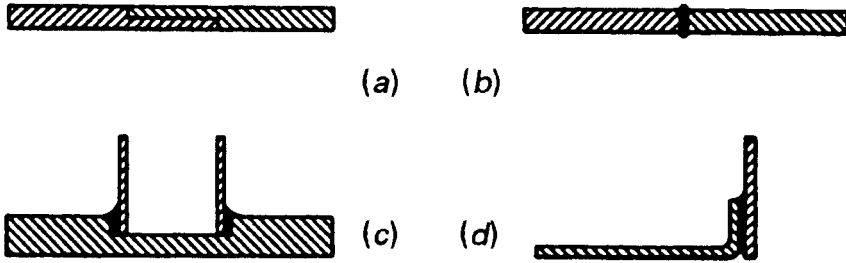
Fig. 17.4 Porosity in high vacuum flanges. Reprinted with permission from Varian Report VR-39, *Stainless Steel for Ultrahigh Vacuum Applications*, V. A. Wright. Copyright 1966, Varian Associates, 611 Hansen Way, Palo Alto, CA.

17.1.2 Soldering and Brazing

Soldering and brazing are techniques for joining metal parts with a filler metal whose melting point is lower than the melting point of the parts to be joined. The definitions of soldering and brazing are not universal. One definition states that brazing is done with fillers whose melting point is greater than 450°C , while soldering uses fillers which melt at lower temperatures. The term "hard soldering" is obsolete. Brazing and soldering are used where alloy or metal combinations cannot be welded, or where warping of parts during welding would produce unacceptable distortion. Soldering is little used in vacuum technique, because low-melting-point solders contain high-vapor-pressure materials, which are unsuitable for use in baked systems. One exception is the use of indium alloy solders for sealing thermocouple feedthroughs.

Furnace brazing in a hydrogen or vacuum ambient is a common method for joining large pieces without introducing thermal stress. Bellows were traditionally brazed to heavier tubing before joints of the type illustrated in Fig. 17.1*h* were developed. Brazing can be done by torch, by dipping, by induction heating, or by heating in a furnace. An excellent review of practical brazing techniques is contained in the pamphlet by Peacock [8].

The parts to be brazed or soldered should be closely machined and have a large area of overlap. The filler has a lower shear stress than the metals being joined, and a large surface is necessary to place the stress on the metal rather than on the filler. The metal parts need to fit uniformly so the filler can flow into the joint by capillary action. Too large a gap will result in voids; the filler will not flow in a gap that is too narrow. Figure 17.5 illustrates proper and improper construction of brazed and soldered joints. The filler should melt at a temperature below the melting point of work.



17.5 Examples of brazed joints: (a) One form of a strong butt-lap joint; (b) a weak butt joint in which the stress is placed on a small filler area; (c) a poor tube-to-flange joint with excessively large clearances; (d) a strong corner joint.

Pure metal and alloy braze fillers are available in a wide range of melting points ranging from -40°C (mercury for cryogenic joints) to 3180°C (rhenium). Several copper-silver and copper-gold alloys with melting points in the range 800 – 1000°C can be used for brazing stainless steel, copper, and other alloys used in the construction of valves, diffusion pump casings, feedthroughs, and internal fixtures. Cu-Ag is a well known braze filler for stainless steel; however, Cu-Au alloys have a low surface tension and readily flow between parts with 0.001 -in. gaps. Tables of braze alloys and applications are found in Kohl [9], the American Welding Society Brazing Manual [10], and the Handy and Harmon Brazing Book [11].

The vapor pressure of some metals is high enough to preclude their use in baked vacuum systems. Older solders are lead-based and brazing alloys with melting points under 700°C contain Pb, Zn, Cd, or P. Such alloys are limited to torch brazing of assemblies that will not be baked. If components containing these elements are baked, the high-vapor-pressure components will vaporize and contaminate the vacuum system. In the same manner, they will contaminate the brazing furnace. In addition to the vapor pressure limitation, there are well-known metal incompatibilities. Au and Al bond to form an intermetallic compound described by the phrase “purple plague.” Au and Ag cannot be used in contact with Hg, and brazing alloys containing Ag cannot be used in contact with Fe-Ni-Co alloys such as Kovar without causing intergranular corrosion.

17.1.3 Joining Glasses and Ceramics

The techniques for joining glasses and ceramics recognize the different expansion coefficient, tensile strength, and shear strength of each material. Glasses have expansion coefficients ranging from $105 \times 10^{-7}/^{\circ}\text{C}$ for soda-lime glass to $3.5 \times 10^{-7}/^{\circ}\text{C}$ for fused quartz. Glasses are weak in tension and

strong in compression; they are weaker than ceramics or metals. Here we review techniques for glass-to-glass seals and for glass- and ceramic-to-metal seals.

Glasses can be fused in a flame, or joined in a furnace by frit or cane solder glass, if their expansion coefficients differ by less than 10%. Frit seals are made with ground solder-glass slurry whose solvent evaporates as the frit melts. Pre-shaped cane glass seals are made from frit or cane solder glass. The parts to be sealed with solder glass are aligned, loaded with a suitable weight, and thermally cycled to the melting temperature of the solder glass. The solder glass and the parts need to have the same expansion coefficient, but the solder-glass melting point must be less than the sealed parts. A review of solder glasses has been published by Takamori [12].

Glass pairs with widely dissimilar expansion coefficients such as quartz and Pyrex, or lead glass and Pyrex, cannot be directly sealed. Such combinations are joined with a graded seal. A graded seal, also known as a step seal, is made by successively joining glasses whose expansion coefficient differs by about 10–15%. Adjacent glasses must also have nearly equal solidification temperatures; otherwise large thermal expansion differences will be frozen in during cooling.

Glasses can be sealed to metals if the metal has the same expansion coefficient as the glass, if the metal holds the glass in compression, or if the metal is very thin so that it can plastically deform. Glass does not adhere directly to metal (except for platinum), but rather to the metal oxide. The metal oxide must be stable and adhere well to the parent metal. Common glass-to-metal seals use matching expansion coefficients. For example, platinum, or an iron–nickel–chrome alloy such as Sealmet 4, seals to lead glass. Tungsten seals to 7720 and 3320 uranium glass, and Kovar seals to 7052 glass. Ring seals are sometimes used where a metal band or ring of appropriate expansion coefficient contracts on cooling to hold the glass in compression. A seal for joining glass to a feathered, deformable copper edge—the Housekeeper seal—has been out of vogue for many years. Today a stainless steel-7052 glass version designed by Benbenek and Hoenig [13] is commercially available. A cross-sectional view is shown in Fig. 17.6a. Construction details, given in the original paper, have been amplified by Rosebury [14]. The direct sealing of glass to stainless steel avoids the corrosion problems associated with the use of iron–nickel–cobalt alloys. Espe [15] describes the alloys used in glass-to-metal seals, while Kohl [9] and Rosebury [14] discuss glass-to-metal seals.

Ceramic-to-metal seals are more easily made and stronger than glass-to-metal seals. Ceramics have high compression strength, so it is not necessary to have as close an expansion coefficient match between ceramic and metal as it is between glass and metal. The high compression strength of a ceramic results in a very rugged seal. Ceramic seals are made by firing a

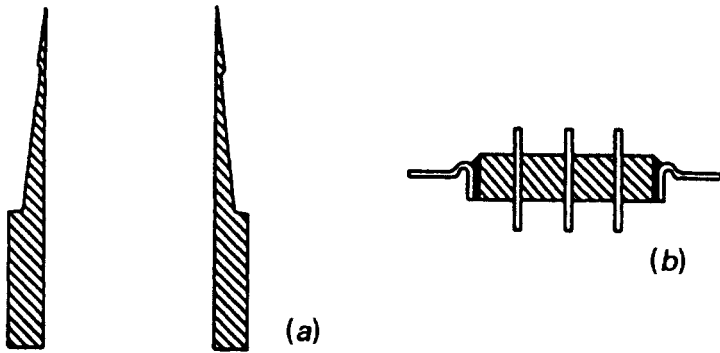


Fig. 17.6 (a) Tapered stainless tubing for fabricating a 7052 or Pyrex glass-to-stainless Housekeeper seal. Reprinted with permission from *Rev. Sci. Instr.*, 31, 460, J. E. Benbenek and R. E. Honig. Copyright 1960, The American Institute of Physics. (b) Ceramic-to-metal seal.

thin layer of refractory metal on the ceramic at high temperatures. The metal is then furnace-brazed to the refractory using filler with a lower melting point than the refractory. For example, alumina is brazed to Kovar via a fired molybdenum paste. See Fig. 17.6b.

17.2 DEMOUNTABLE JOINTS

The most reliable, long-lived connection which can maintain its integrity in vacuum and related environments is a permanent, welded joint. Special purpose welded metal joints can be cut open, and glass can always be cut and reworked. However, most vacuum systems have a requirement for easy access, which cannot be met in this way. Demountable joints are therefore, a practical necessity.

A demountable seal must be designed and constructed to form a leak-tight joint and maintain it until the time it is to be opened. Forming a leak-tight joint requires an initial contact force large enough to make the joined material merge and fill the irregularities in the harder of the two materials. Maintaining the joint requires a force sufficient to overcome the effects of differential expansion and long-term plastic flow. Depending on the relative expansion coefficients of the two materials, a joint may develop an unwanted leak if it is heated or cooled [4]. The restoring force must be maintained by the stored energy in the joint. Stored energy is a fundamental requirement in a demountable seal. (There are one or two cases where two metals form a diffusion joint or bond, and the force can be removed, e.g., copper-steel shear seals; however, they have to be pulled apart.) A joint consists of three components: the seal or gasket material, the

flange pair, and the clamping means. The required energy may be stored in any one of the components or shared between them [8]. In addition to maintaining the seal force, the joint must be able to withstand the thermal, chemical, and radiation environment of the system. It must be constructed from materials whose vacuum properties (vapor pressure, permeation and outgassing rate) are compatible with the vacuum operating range.

Elastomeric compounds are excellent choices for the seal or gasket material. They store elastic energy and conform to fit surface irregularities of the flange. In addition, they are resistant to many chemicals and can be reused. Unfortunately, elastomers have high permeation rates for atmospheric gases and cannot withstand high baking temperatures. For these systems, metal is the only acceptable gasket material. In this section, we review the techniques for demountable joints using both elastomers and metal gaskets. Elastomer gaskets have been reviewed by Peacock [16], while metal seals have been reviewed by Roth [4].

17.2.1 Elastomer Seals

Elastomer seals between metal or glass flanges are made by deforming the elastomer freely between two flat surfaces or confining it in a groove of rectangular, triangular, or dovetail cross section. Elasticity, plasticity, hardness, compression set, seal loading, outgassing, and gas permeation are important attributes of an elastomer seal. A summary of various elastomer seal properties is given in Table 17.1. Elastomers are formed by first grinding the starting polymer, mixing with plasticizers and stabilizers, and vulcanizing it to a state that is largely elastic. The materials are incompressible. That is, any deformation or compression in one direction must be accompanied by motion in another, so that the total volume remains constant. If the compound is completely elastic, it will return to its exact shape after the force has been removed. If it has some degree of plastic behavior it will flow and not return to its original shape. The measure of its shape change is called compression set.

Compression set occurs in an elastomer that has been deformed for a long time. It is more pronounced in elastomers that have been heated, because compression set is strongly temperature-dependent. Figure 17.7 gives comparative compression set data for five elastomers. The time effects of compression set in Kalrez 1050 and Viton A and E-60C are described in Table 17.2. From these data, it might appear that a Kalrez or Viton seal would leak excessively after baking. Peacock [16] comments that many of the problems with compression set in perfluoropolyether may be due to improper groove design. As this material is heated, it expands; expansion can induce excessive compression set if inadequate room for expansion is left in the groove.

Table 17.1 A Summary of Various Mechanical and General Considerations Regarding the Selection of Polymer Seal Materials

Seal Material	Lin. Coeff of Thermal Exp ($\times 10^{-5}/^{\circ}\text{C}$)	Max operating T ($^{\circ}\text{C}$)	Cold flow at T_{op}	Gas Permeation	Wear/ Abrasion Resistance	Prime Seal Appl'n
Fluoroelastomer						
Viton E-60C	16	150	Good	Mod	Good	<i>a</i>
Viton A	16	150	Fair	Mod	Good	<i>a</i>
Buna-N	23	85	Good	Mod	Very good	<i>b</i>
Buna-S	22	75	Good	High	Good	<i>c</i>
Neoprene	24	90	Good	Mod	Very good	<i>d,e</i>
Butyl	19	—	Good	Mod	Good	<i>f</i>
Polyurethane	3–15	90	Poor	Mod	Excellent	<i>g,h</i>
Propyl	19	175	Good	High	Very good	<i>h</i>
Silicone	27	230	Poor	Very high	Poor	<i>i</i>
Perfluoroelastomer	23	275	Poor	—	Excellent	<i>j</i>
Teflon	5–8	280	Very poor	Mod	Excellent	<i>j</i>
Kel-F	4–7	200	Good	Low	Very good	<i>j</i>
Polyimide	5	275	Good	Mod	Very good	<i>j,k</i>

Source. Reprinted with permission from *J. Vac. Sci. Technol.*, 17, 330, R. N. Peacock. Copyright 1980, The American Vacuum Society. (*a*) Generally used vacuum seal; (*b*) best all around low cost; (*c*) little vacuum application; (*d*) oil resistance; (*e*) low cost; (*f*) specific chemical application; (*g*) radiation resistant; (*h*) mechanical properties; (*i*) electrical applications; (*j*) chemical resistance; (*k*) high temperatures.

Adequate seal loading is rarely a problem with an elastomer. However, excessive compression can limit the upper baking temperature, because of thermal expansion. O-rings are typically compressed 15–20% of their diameter. For a nominal 0.318-cm-diameter O-ring of 75 Shore hardness, this translates into a seal force of about 2.7 kg/cm of O-ring length [16]. The initial pressure will be slightly reduced with time as the elastomer undergoes some plastic deformation, but it will not affect the integrity of the vacuum seal. Because sealing is determined by contact pressure, the compressive force, deformation and percentage groove filling must all decrease as the hardness of the O-ring or the expansion coefficient is increased. A chord compression of 20% is typical for Viton O-rings, while Kalrez should not be compressed more than 12%.

O-ring manufacturers can supply tables of groove depths and widths with information for a range of O-ring sizes. Sessink and Verster [17] observed the empirical tabulations from nine sources to vary widely. They found chord compressions up to 38% of the chord diameter and found groove filling ratios (chord cross-section area/groove cross-section area) of 74–102%. In their study, they found the general criterion for high vacuum sealing to be a minimum initial contact pressure of 13 kg/cm² for gaskets in the hardness range 60–75 Shore [17,18]. The tables listed in the various references are not all for the same elastomer. Expansion coefficient,

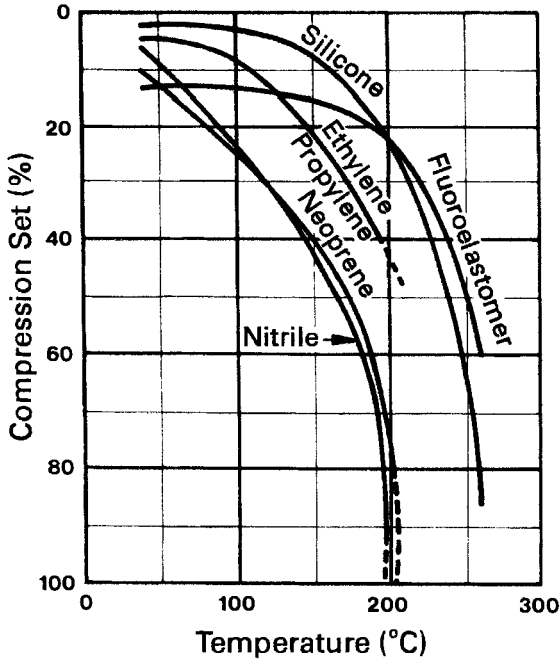


Fig. 17.7 Compression set as a function of temperature measured according to ASTM D-395 (22 h). Reprinted with permission from *J. Vac. Sci. Technol.*, 17, 330, R. N. Peacock. Copyright 1980, The American Vacuum Society.

temperature range and hardness affect the groove depth and width. It is best to obtain a table from an O-ring supplier to verify the groove dimensions for a particular elastomer. Outgassing and permeation data for elastomers are given in Chapter 16 and in Appendix C. Outgassing data are given in Fig. 16.10 and Appendixes C.4 and C.5. Water vapor is the major constituent to degas from unbaked Viton [19].

Permeation data are given in Appendix C.6. Outgassing rates for single, unbaked Viton gaskets of $q = 3.67 \times 10^{-6}/t^{0.41}$ Torr-L/s per linear cm of 5.3-mm-diameter have been measured [20]. This is close to the inverse square root dependence associated with normal permeation. After very long times, this value will stabilize at the steady-state permeation rate. Using both measured permeation constants and measured and empirically determined solubility values, one can construct a plot of the approximate permeation through a single Viton O-ring exposed to atmosphere at room temperature. Figure 17.8 illustrates the air flux through a Viton O-ring assuming that its interior was devoid of gas and that the presence of water vapor—the dominant component—does not affect the solubility of other gases. Note that the time to reach steady state is determined by the diffusion constant,

Table 17.2 Compression set for Viton and Kalrez for various times and temperatures measured per ASTM D-395B

Temperature (°C)	Time (h)	Compression Set (percent)		
		Kalrez 1050	Viton A	Viton E-60C
24	70	20	21	8
100	70	32	—	—
204	70	71	63	13
204	360	—	90	30
204	960	—	—	55
204	7200	—	—	100
232	70	71	—	30
260	70	6	—	—
288	70	74	—	100

Source. Reprinted with permission from *J. Vac. Sci. Technol.*, 17, 330, R. N. Peacock. Copyright 1980, The American Vacuum Society.

whereas the steady-state flux is determined by the product of the diffusion constant and solubility. This calculation illustrates how water dominates the outgassing and permeation of a Viton gasket. de Csernatony [21] observed a 480-fold reduction in the outgassing of an immersed Viton O-ring after a 16-h, 100°C bake; when the O-ring was used as a seal, the reduction was only 6-fold. His measurements illustrate how permeation, and

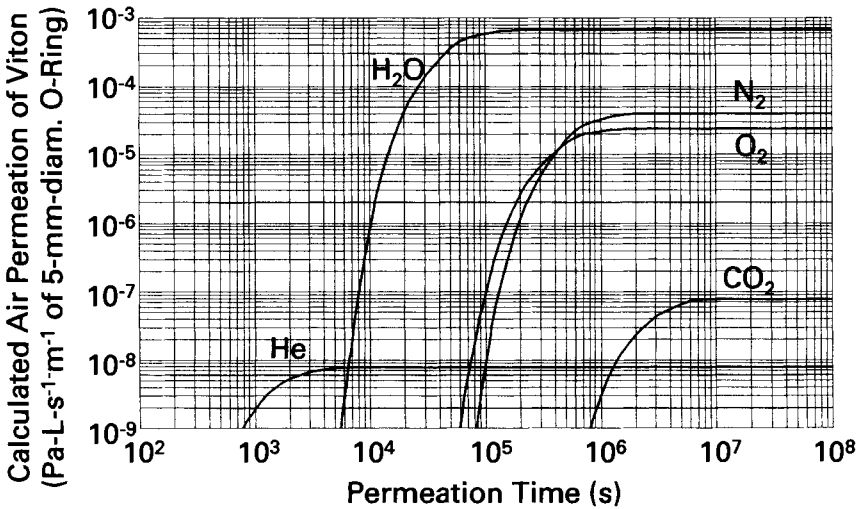


Fig. 17.8 Calculated permeation rates for the components of atmospheric air through Viton at 25°C, using measured permeation constants, and experimental values for solubilities or diffusion constants. These calculations assume no interaction between individual constituents.

not outgassing, dominates the ultimate pressure in a vacuum system containing a large number of O-rings after long pumping times. Gas permeation can limit the time available for leak checking and limit the ultimate pressure in a system containing a large number of O-rings. Laurenson and Dennis [22] have studied the permeation of several gases through uncompressed Viton, Aflas and Epichlorohydrin at several temperatures. Some of their data are presented in Fig. 16.9.

Seal materials are degraded by radiation. Peacock [16] gave a brief review of gamma radiation damage. He noted the trend in elastomers was to become brittle, take a large compression set and increase in hardness after being subjected to high doses of gamma rays. Teflon appeared affected at lower doses than other elastomers, whereas polyimide (e.g. Vespel) withstood considerably more flux than other elastomers. Wheeler and Pepper [23] showed that a high x-ray flux (8×10^6 rad/s) decomposed Teflon into saturated fluorocarbon gases and polymer fragments short enough to desorb from the surface.

Gaskets can be shaped in many ways. Figure 17.9 illustrates several ways that gaskets are used between metal and metal-to-glass joints. The rectangular O-ring groove (17.9a) is a common joint in the United States, while the ISO-KF (kleinflansch) with a centering ring, (17.9b), is the European standard and is now universal. The confined gasket (17.9c) is commercially available and useful, especially on noncircular joints. A half- or full-dovetail groove (17.9d) is especially useful for vertical doors. An L-gasket (17.9e) is freely squeezed between a glass pipe or bell jar and a metal surface. Differentially pumped gaskets (17.9f) are used to reduce permeation between atmosphere and vacuum; they are a viable alternative to metal gaskets for many applications [20].

Cleaning an elastomer by a solvent wash is an ineffective way to reduce outgassing. A simple vacuum bake is most effective. An unbaked Viton O-ring will have an initial outgassing rate of 10^{-3} Pa-m/s. See Appendix C.4. After a 4-h bake at 150°C and 12 h of pumping, this value is reduced to 4×10^{-7} Pa-m/s. Re-exposure to atmosphere will result in increased water outgassing. All elastomers are “sponges” for any gas or vapor to which they have been exposed. This is easily viewed with an RGA, when compressing a gasket in a valve seat; two examples are shown in Fig. 17.23 (Problem 17.9) at the end of this chapter. O-ring grooves need to be carefully cleaned and both groove and ring wiped clean with a lint-free cloth. Grease is not needed to make a static seal between an elastomer and a metal surface. It will cause pressure bursts as trapped gas pockets are released. Occasionally we use grease on a main door seal flange that has become scratched with misuse. Remember to apply the *very thin* coating of grease with lint-free cloth. Finger oils have a very high vapor pressure and they are an unacceptable substitute for grease; wear gloves.

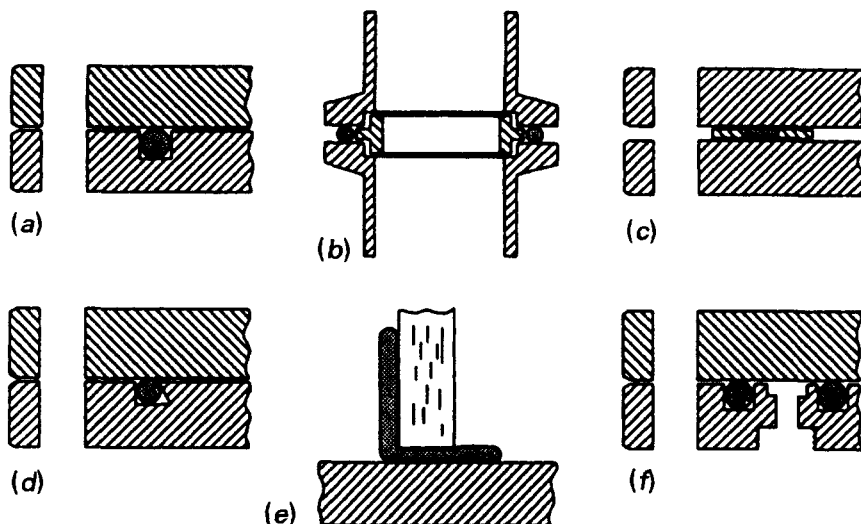


Fig. 17.9 Elastomer seal forms: (a) Rectangular groove, (b) ISO-KF flange with centering ring, (c) confined gasket, (d) dovetail groove, (e) L-gasket, (f) double gasket with differential pumping port.

The most commonly used O-ring elastomers are Buna-N and Viton E-60C. Most of the published data are for Viton A, but it has not been used for many years. Viton E-60C has a lower room-temperature outgassing rate and less compression set than Viton A. Buna-N is used for low cost applications, while Viton is used where a moderate bake and low outgassing are needed. A 200°C bake will release adsorbed gases, unreacted polymer and plasticizers from Viton [16]. It cannot be used at this temperature because of compression set; at higher temperatures it will decompose. Silicone has an unusually high permeation rate; it is infrequently used as a gasket material in very high vacuum systems. It is suitable for some high-temperature vacuum applications. Silicone compounds are formulated for a range of high-temperature applications. Polyimide has a low outgassing rate [24,25], but adsorbs large amounts of water when re-exposed. Hait [26] and Edwards et al. [27] describe flange seals made from thin polyimide films. Elastomer gaskets are widely used in systems that pump to the 10^{-6} -Pa range.

All elastomers shed large quantities of fine particles during normal use. After 20 min agitation in a solution of 1:6 isopropyl alcohol:ultrapure water, particle counts of $1\text{--}2 \times 10^4/\text{cm}^2$ surface area greater than 0.3- μm diameter were measured for Viton, silicone, and nitrile O-rings [28].

17.2.2 Metal Gaskets

The thermal, radiation, outgassing, and permeation properties of elastomers make them unsatisfactory for many seal applications. Metal gaskets must be used in high-quality UHV systems and are often used in high vacuum systems on parts that do not have to be frequently opened to reduce the total outgassing load.

Many metal gasket-flange pairs have been designed. Two designs are illustrated in Figure 17.10. In these flange designs, the gasket is deformed to fill irregularities in the surface of the mating flange. The copper gasket seal has proven to be a popular bakable seal. The most widely used commercial design is the ConFlat [29] flange (17.10a). It consists of two symmetrical flanges each containing a work-hardened knife-edge. The flanges are tightened until they touch and “capture” a section of the copper ring between the knife-edge and the outer shoulder. The copper gasket was designed to contact the outer flange shoulder; however, currently manufactured gaskets are often improperly fabricated with a smaller OD, thus eliminating the force needed to make a proper seal. The knife-edge flange is universal and available in a circular geometry up to 30-cm diameter. Those versions that are fabricated from stainless steel containing an additive to prevent grain growth can be repeatedly baked up to 450°C with excellent reliability. The Helicoflex “Delta” gasket (17.10b) consists of an Inconel spring surrounded by inner and outer linings. The inner Inconel lining distributes the spring force uniformly along the copper sealing lining. Because elastic energy is distributed along the gasket, it is less susceptible to misalignment tolerances and can be used in large sizes.

Large flanges are difficult to keep leak-free, if the knife-edges lose alignment. Knife-edges can become misaligned by differential thermal expansion during normal baking and warping during welding, as shown in Fig. 17.11a [30]. Gaskets are formed from OFE copper, which begins to

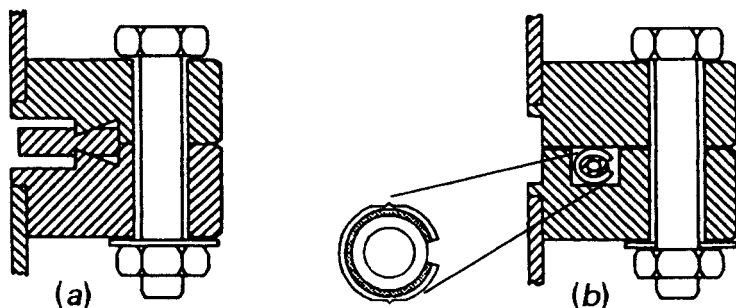


Fig. 17. 10 Metal gasket seals: (a) ConFlat type knife edge seal; (b) Helicoflex Delta seal.

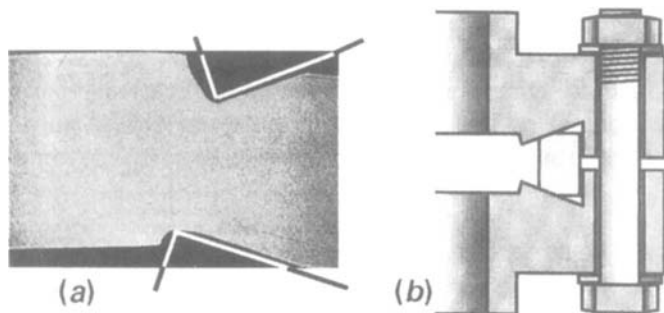


Fig. 17.11 (a) Distortion in a copper gasket caused by uneven thermal expansion of the flange, or weld-induced distortion of the knife-edge flanges. Adapted with permission from *J. Vac. Sci. A*, **5**, 2540, W. Unterlerchner. Copyright 1987, AVS–The Science and Technology Society. (b) A taper gasket designed for use in the ConFlat knife-edge flange; Reprinted with permission from *J. Vac. Sci. Technol. A*, **19**, 2963, S. Kurokouchi, S. Morita and M. Okabe. Copyright 2001, AVS–The Science and Technology Society.

lose hardness at 200°C [30]. Recrystallization begins at 300°C [30]. An alternative design for a copper gasket has been proposed [31,32]. The taper seal gasket illustrated in Fig. 17.11b uses half the sealing force, has no copper inside the knife-edge, and can use a chain clamp instead of bolts [31]. Analysis of the internal forces showed that a large amount of sealing energy in the conventional ConFlat is wasted in the process of pushing the knife-edge into the gasket [32]. This energy generates intense stress in the gasket immediately under the tip of the knife-edge, resulting in stress-induced crystallization and loss of elasticity. Elastic energy storage is necessary to maintain any seal. In an elastomer seal, energy is stored in the gasket. However, the copper gasket cannot store energy, if high stresses induce crystallization. The taper seal gasket contacts the outer flange edge; energy can be stored in gasket and in the bolts or chain clamp.

17.3 VALVES AND MOTION FEEDTHROUGHS

The components used for control, isolation, or motion all use some form of an elastomer or metal seal in combination with a moveable vacuum wall, usually a metal bellows. Valve seals are adaptations of demountable seals described in the previous section. Conductance, leak rate, vacuum range, baking temperature, radiation, or corrosive gas exposure and the need for line-of-sight view in the open position are all variables that influence valve design and selection. Transmitting linear or rotary motion through a vacuum wall is complicated. Dynamic sealing or flexible walls, along with lubrication, are now required. The sealing techniques and materials are also

dependent on the vacuum range, torque, and the rotational speed at which the motion will be transmitted. Weston [33] has extensively reviewed valves and feedthroughs for ultrahigh vacuum applications.

In this section, we review small and large valves, special-purpose valves, and motion feedthroughs. Basic design differences so divide our discussion.

17.3.1 Small Valves

We define a small valve as one in which the throat diameter is less than, say, 6 cm and in which the sealing force is directly applied via a hand lever or screw or a pneumatically operated shaft. Figure 17.12 names the components of a simple, hand-operated, elastomer sealed right-angle valve. Most small valves are right angle, because that is a simple mechanical way of directly applying the sealing force in a direction normal to the valve seat. All valves, small or large, should be constructed from materials whose outgassing load is low enough so that it does not contaminate the process at the operating pressure. We desire the valve to have a maximum conductance for gas flow and to form a leak-tight seal between the plate and the seat and between the stem and the bonnet. We also desire the valve to be reliable and maintenance-free and have a long operating life. The valve design illustrated in Fig. 17.12 is typical of an old-style valve mainly used in roughing lines. Its basic problem, even if made from stainless steel, is its unreliable O-ring stem seal. Today this design is used only in valves designed to release a medium or low vacuum component to atmosphere. In that application, the stem seal is never exposed to vacuum.

In Fig. 17.13a we illustrate a right-angle valve in which the O-ring stem seal has been replaced with a stainless steel bellows. The linear motion needed to open and close the valve is transmitted to the valve plate via the bellows. The only elastomer seals remaining in the valve are static seals. The valve in this illustration is pneumatically driven and can be baked to

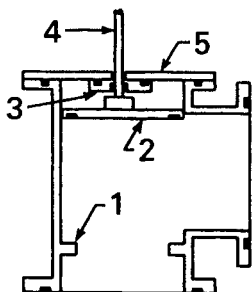


Fig. 17.12 Components of a simple elastomer sealed valve: (1) Valve seat; (2) valve plate; (3) bonnet; (4) stem; (5) stem seal.

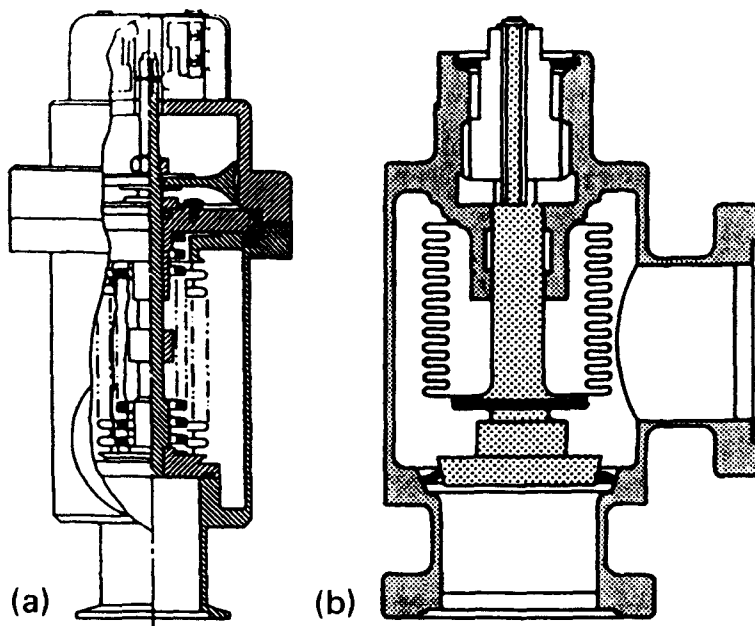


Fig. 17.13 Small right-angle valves: (a) Elastomer-sealed, pneumatically driven valve with a bellows shaft seal. Reprinted with permission of HPS division of MKS Corp., 5330 Sterling Drive, Boulder, CO 80301. (b) All metal valve with metal sealed seat. Reprinted with permission of VAT Inc. 600 W. Cummings Park, Woburn, MA 01801.

150°C in the closed position and to 200°C in the open position. It is used on systems pumped to the 10^{-7} -Pa range. Bellows sealed valves of this type have lifetimes ranging from 20,000 to over 200,000 cycles, and valve plate leak rates of 10^{-12} to 10^{-10} Pa-L/s. A less expensive valve of this type is constructed from brass with a brass bellows and Buna-N seals for non-corrosive applications in the medium vacuum range. Butterfly valves, which operate by rotating a valve plate through 90°, are made with an elastomer O-ring seal on the outer edge of the valve plate. They are available in hand operated versions.

Elastomer seals prevent the use of this valve in UHV systems baked to temperatures over 200°C. An all-metal welded body and metal plate seals are necessary for systems baked at high temperatures. The first all-metal valve was developed by Alpert [34] in the early 1950s. Today, several designs are commercially available. All use some form of copper or gold valve plate and a stainless steel knife-edge seat. Designs with a sapphire valve plate and gold-plated stainless steel seats are also available. The design illustrated in Fig. 17.13b employs a coated steel valve plate and a seat fabricated from a steel with a high elastic limit in the shape of a

conical Belleville washer. The body of this valve is welded, and it is joined to the system by copper knife-edge flanges. Line-of-sight versions of valves such as those illustrated in Fig. 17.13 are available. These valves are constructed by mounting the valve seat at a 45° angle to the connecting tubing. Because of the geometry, a line-of-sight version requires a seat diameter over 1.5 times the pipe diameter. The distance between flanges reduces their conductance to a value less than a right-angle version.

17.3.2 Large Valves

Large valves differ from small valves in several ways. The total required closing force scales with the seal area. For elastomer sealed valves this area is proportional to the O-ring chord diameter and the valve plate diameter. A 5-cm-diameter valve sealed with a 3.2-mm-chord-diameter O-ring requires a total sealing force of 400 Newtons. A 15-cm-diameter valve with a 6-mm-chord diameter O-ring requires about 2000 N, whereas a 30-cm valve with an 8-mm-chord diameter O-ring requires close to 5000 N. If the valve is to remain closed against atmospheric pressure, the body must withstand an even greater force. A 30-cm valve must withstand 7500 N at atmospheric pressure. These forces place stringent design requirements on the valve body. The valve seat must remain flat under these forces at room temperature and while being baked. Direct line of sight transmission through the valve is required for some applications. Physical vapor deposition sources are often isolated by a valve during substrate changing. Particle accelerators and storage rings require clear aperture valves in the beam lines. Multichamber, in-line thin-film deposition systems use large line-of-sight valves, not always circular, to pass wafers between isolated chambers in device processing. Other applications require an isolation valve to have a high open conductance, long life, ease of maintenance, and an ability to be baked. These valves range in sizes to 1.2-m diameter for both high vacuum and UHV.

The most common large valve design is the gate valve. Gate valves are so common that some think they are synonymous with large valves. Gate valves are made in sizes as small as 2 cm; however, they are not the only

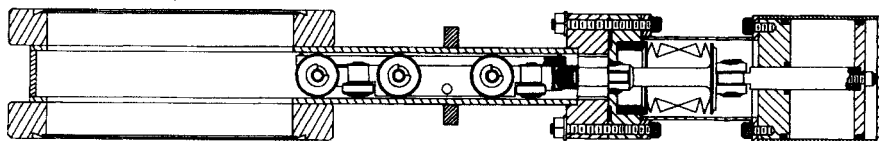


Fig. 17.14 Bellows sealed gate valve. Reproduced with permission from High Vacuum Apparatus, Inc., 1763 Sabre St., Hayward, CA 94545.

large valves. Figure 17.14 illustrates an old-style design. The gate travels horizontally until the valve plate is centered under the seat. Continued translational motion of the shaft causes hinges to move the valve plate upward to a closed position. The bonnet seal is either a grease-packed double O-ring or, in better-quality valves, a bellows. Inexpensive varieties of this design are made with cast aluminum bodies while higher quality versions are made with stainless steel.

A highly reliable valve design is illustrated in Fig. 17.15. In this design the shaft moves the valve plate in and aligns it with the seat. At the end of the valve plate travel, the shaft forces ball bearings out of detents and expands the valve plate against the seat and the backing plate against the valve housing. The use of multiple balls is one advantage of this design. By increasing the number of points at which the force is applied to the seal plate, the wear on each point can be reduced to a low value. These two gate valve designs are available in sizes to 30 cm; however, larger elastomer-sealed gate valves are manufactured. Metal-sealed gate valves are currently available in diameters of 30–40 cm. The reliability of such a valve drops drastically as the diameter increases beyond 30 cm. Baking of a large metal-sealed valve is limited to about 200°C. Large metal-sealed valves have the same problems as large knife-edge flanges.

Other designs use a swinging plate shaped like a Belleville washer, which is forced into position by a wedge pushing on the center, or a coaxial bellows to seat the valve plate against a knife-edge located in the opposite face.

Aluminum-bodied, grease-lubricated valves are acceptable on unbaked systems that pump to 10^{-5} Pa. Stainless steel valves with bellows shaft seals whose moving parts are lubricated with a low-vapor-pressure solid lubricant can be baked to 150°C with the valve closed or 200°C open and can be used on UHV systems. Viton is the most common elastomer used in large valve seals, although others have experimented with polyimide [35]. In all gate valves, elastomer- and metal-sealed, the valve plate must be seated in a direction orthogonal to the drive motion with a force up to several thousand newtons. Moving parts need to be lubricated, and the

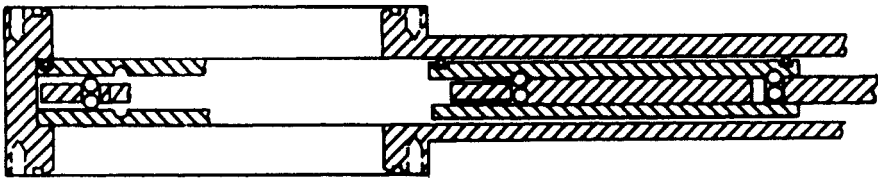


Fig. 17. 15 Sealing concept used in the VAT gate valve. VAT Inc. 600 W. Cummings Park, Woburn, MA 01801.

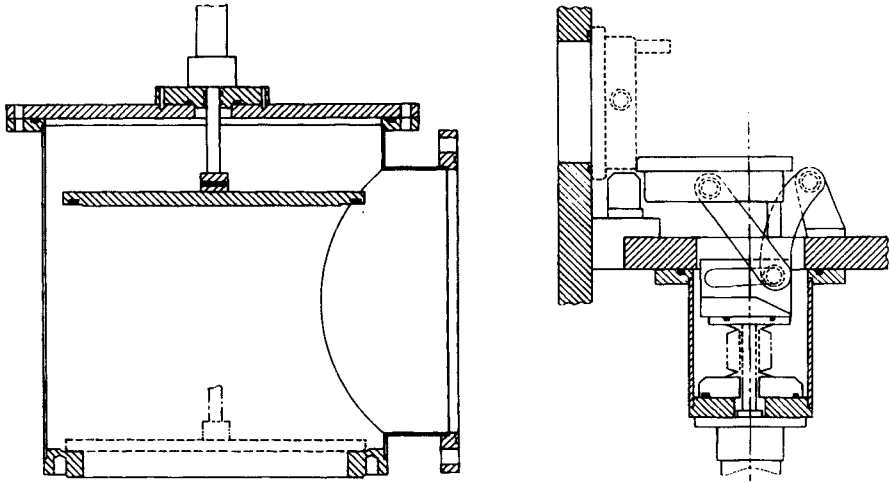


Fig. 17. 16 Poppet (left) and (right) slit valves. Reproduced with permission from CVC Products, Inc. 525 Lee Rd., Rochester, NY.

valve interior needs to be pumped. For these reasons the gate valve is the most complicated piece of machinery in a vacuum system. Stainless steel valves can have plate seal leak rates of order 2×10^{-8} – 2×10^{-9} Pa-L/s, with lifetimes ranging from 10,000 to 50,000 cycles with the typical value on the low side of this range. They can fail by seal leaks, bellows leaks, and wear of moving parts. Bellows failure is the most common problem.

Elastomer-sealed poppet and slit valves are made in large sizes. These styles are illustrated in Fig. 17.16. Poppet valves up to 1.2-m diameter are commercially available. Poppet valves use a simpler mechanism than do gate valves, because the operating force is applied via a large compressed air piston in line with the valve plate motion. The slit valve pivots about an axis parallel to the valve plate surface. These valves are much deeper than a gate valve and their conductance is less. Most large diffusion pumps require an elbow to be connected to a chamber, so the poppet does not reduce the overall conductance as much as we first assume. In some small ion pumped systems, the poppet valve serves both to isolate and baffle the pump entrance. In-line chambers generally cannot be connected closer than needed for a flap valve. Any loss in conductance is more than offset by increased reliability and lower cost. Poppet valves are best used to seal a pump under vacuum while the chamber is vented. In this way the atmospheric pressure forces the valve plate closed. Slit valves are also constructed in rectangular shapes. For example a 5×30 -cm valve might be used on an in-line sputtering system for isolating chambers and load locks. The plates are constructed from stainless steel, use elastomer

gaskets, and are designed for operation in the high vacuum region. Butterfly valves are also fabricated in large diameters.

Large elastomer and metal gasket valves are available for a number of applications, baked and unbaked. They are commercially available in small sizes and custom made in larger diameters. Double-sided all-metal valves have been custom-made [36]. Valves can be purchased with contacts to indicate the full open or closed position. The technology for fabricating large-diameter, all-metal valves that are bakeable to temperatures $> 300^{\circ}\text{C}$ is not simple. Poppet valves are made to fit large diffusion pumps. Special-purpose rectangular slit valves are usually custom-designed for a particular application. As the valve size increases, so does the cost, the probability of failure, maintenance, and difficulty in baking. Ishimaru et al. [37] devised a valve with no elastomer or metal knife-edge seal that can be baked. It makes use of polished metal sealing surfaces that are forced together by compressed air in bellows. The region between is differentially pumped. See Fig. 17.17.

17.3.3 Special-Purpose Valves

The valves described in the previous sections all serve to connect and isolate components of various diameters. There are special cases where we wish to control the conductance between the two chambers with a partially open valve, or control the rate with which gas enters a chamber.

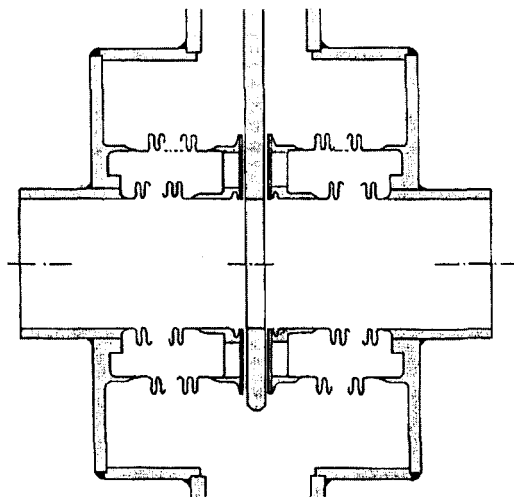


Fig. 17.17 Differentially pumped gate valve. The smooth metal mating surfaces are held together by compressed air. Reproduced with permission from *J. Vac. Sci. Technol. A*, 3, p. 1703, H. Ishimaru et al. Copyright 1985, The American Vacuum Society.

Controlling gas flow in the pressure range 1–10 Pa (10^{-2} – 10^{-1} Torr) is necessary to regulate the pressure in a sputtering or etching chamber. The pressure is regulated with a throttle valve located in the pumping line adjacent to the pump. Typically, the high vacuum pump will be operating at a maximum pressure of, say, 1×10^{-1} Pa (1×10^{-3} Torr), whereas the deposition or etch process may require 3 Pa (2×10^{-2} Torr). The throttle valve can be closed enough to provide this pressure drop. For a chamber using an argon flow of 100 Pa-L/s, this corresponds to a valve conductance of 35 L/s, in contrast to an open conductance of >5000 L/s in the molecular flow region for a 15-cm valve.

The techniques used to throttle gas flow can be simple. For example, a hole in the plate of a gate or butterfly valve. The valve is opened to pump to the base pressure and closed to place the desired throttling conductance in series. This does not allow for adjustment of the closed conductance. Several arrangements have been designed to allow control of the closed conductance. A butterfly valve can close against an external shaft stop. This design and others, which use venetian blinds, rotating pie-shaped segments, or a small iris, are commercially available. Lehmann et al. [38] have designed a large iris valve which has a variable aperture and electronic control. Fifteen-centimeter valves have throttled conductances that are adjustable in the range 1–200 L/s. Throttle valves are typically made with elastomer-sealed flanges and are not bakeable. The operating characteristics of a throttle valve are usually displayed as a plot of conductance versus pressure drop over the range of adjustment. The techniques used to control the closed position of the throttle range from a manual adjustment of the stop setting, to closed-loop pressure control systems in which the error signal from a pressure gauge operates a motor.

Gas flow regulator valves, sometimes called leak valves or metering valves are used to admit controlled quantities of gas from a source external to the vacuum. The external source may be at high pressure (100- to 150-kPa-gauge), at atmospheric pressure, or at a reduced vapor pressure of a supply gas distribution line. The simplest form of metering valve is a needle valve. When it is closed, the needle is seated against a hollow tapered cone of soft metal. Another design used a cylinder in which a fine spiral groove is turned. A screw moves the cylinder inside a hollow mating piece and effectively changes the length of the capillary through which the gas flows. These designs are not bakeable; however, they are commercially available in sizes that span 1–4 decades of flow and cover the range 10^{-3} – 2×10^5 Pa-L/s (10^{-5} – 2×10^3 atm-cc/s). Leak valves in which a sapphire flat is pressed into a metal knife-edge are designed to be baked. A sapphire-metal leak can control flows as low as 10^{-8} Pa-L/s (10^{-6} Torr-L/s). Fixed leaks made from glass capillary tubing are used to calibrate RGAs.

17.3.4 Motion Feedthroughs

Vacuum systems would have few applications if there were no way of transmitting motion to the vacuum environment. Rotary and linear motion are necessary to operate pumps and valves, move samples and sources, open and close shutters, and perform many specialized tasks. Rotary and linear motion feedthroughs are characterized by the torque, the speed at which it is transmitted, and the operating pressure. Rotary and linear feedthroughs for the medium and high vacuum region usually use elastomer seals.

Figure 17.18 depicts two basic forms of dynamic elastomer seal. The rotary seal shown in 17.18a is one form of a simple hand or low-speed rotary seal. In this sketch the O-ring groove is cut into the housing while the shaft contains a retaining ring to prevent linear shaft motion. Alternatively, the O-ring groove may be cut into the shaft. A better version of this feedthrough uses ball bearings on both sides of the O-ring. O-ring manufacturers can provide tables of groove dimensions for these designs using common elastomers. Groove dimensions are somewhat different than those used static seals. Unlike static seals, dynamic O-ring seals need to be greased. The only exception is Teflon. The properties and selection of greases for use in vacuum is discussed in Chapter 18. An improved rotary seal, which can also be used for translation, is shown in Fig. 17.18b. It is a double pumped seal and can be used in the high vacuum range. Replacing machined grooves with sleeves reduces the fabrication cost.

These two elastomer feedthroughs are only two of a large number of elastomer seals. Today it is often easier to substitute a metal seal rather than design a high quality elastomer seal. One exception is for applications which require a high rotational speed and high torque in the very high vacuum or near UHV region where baking may be necessary. For this application a Teflon seal is superior to a greased elastomer. Teflon cold

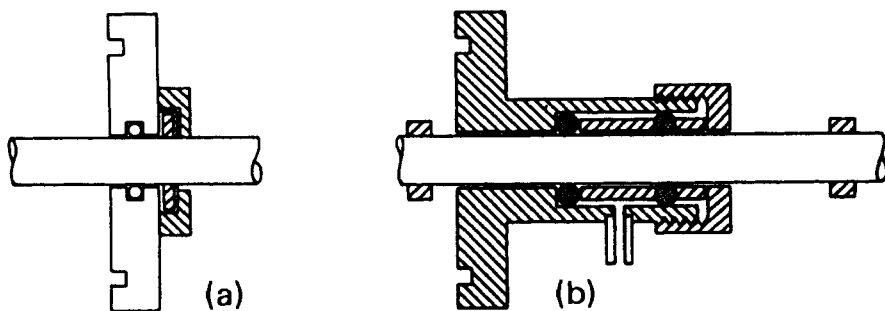


Fig. 17. 18 (a) Rotating and (b) translating elastomer sealed feedthroughs.

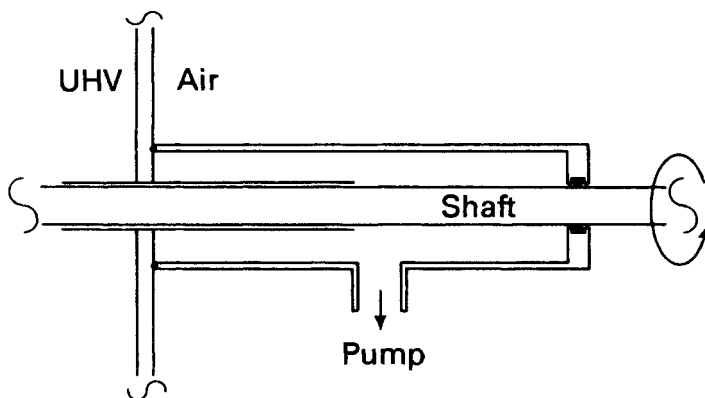


Fig. 17.19 Bakeable differentially pumped motion feedthrough. The inner seal is a low-conductance, differentially-pumped gap between a hollow cylinder and a round shaft. The outer seal could be either an O-ring gasket or a magnetic fluid seal.

flows and must be spring-loaded to avoid leaking. Seal gaskets with a C-shaped cross section have been designed with a special spring located inside the C-ring [39–41]. These seals can be used singly, or in pairs which are differentially pumped and baked to 250°C. They can be rotated at high speed and transmit high torque. Differentially-pumped rotary flange seals have been designed that use two large Teflon C-rings [42]. This design allowed one 15-cm-diameter flange to rotate with respect to another with a dynamic leak rate of 10^{-6} Pa-L/s. Two techniques for transmitting motion through a wall, which do not make use of an elastomer or metal seal, are the differentially pumped seal and the magnetic liquid seal. The differentially pumped seal shown in Fig. 17.19 uses a closely spaced surface to create a low conductance between the vacuum chamber and the differentially pumped chamber. The inner parts of this seal can be baked to high temperature with out any problems.

The magnetic-liquid seal depicted in Fig. 17.20 allows rotary motion to be transmitted on a solid magnetically permeable shaft, by sealing the gap between the housing and the shaft with a magnetic liquid [43–44]. The magnetic liquid consists of a low vapor pressure fluid (e.g. perfluoropolyether) and fine magnetic particles held in suspension with a surfactant. The magnetic lines of force concentrate the magnetic liquid at the ridges machined on the shaft. This seal allows high speed (5000 rpm) and high torque. It is useful in unbaked systems, which are pumped to the 10^{-5} -Pa region, but it does allow air permeation and it may outgas fragments.

Except for the differentially pumped feedthroughs, none of the motion feedthroughs we have described are suitable for the UHV where baking over 100°C is required. For these conditions, all-metal linear and rotary

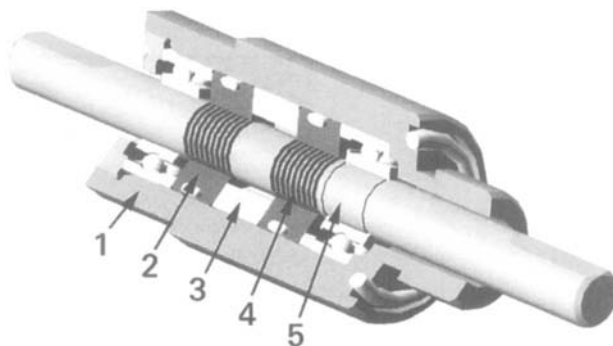


Fig. 17.20 Ferrofluidic® seal: (1) Housing; (2) pole piece; (3) magnet; (4) Ferrofluid; (5) shaft. Reprinted with permission from Ferrotec (USA) Corporation, Nashua, NH 03060.

motion feedthroughs, the differentially pumped feedthrough, or recently designed magnetic couplings are required. Magnetic couplings transmit torque through a thin metal vacuum wall to a magnetic shaft within the vacuum chamber. Magnetic couplings are an excellent way to transmit motion through walls of UHV chambers as long as cooling water or electrical connections are not required. If water or electrical cables must be provided to the rotating assembly, the only purely UHV option is the differentially pumped feedthrough of Fig. 17.19. One example of a magnetic coupling is illustrated in Fig. 17.21. In this assembly, an external motor rotates a magnet that is coupled to a follower located within the ultrahigh vacuum environment. The load is attached to the end of the shaft. Some form of lubrication is required for the follower bearings, and this can be chosen to match the required rotational speeds and loads.

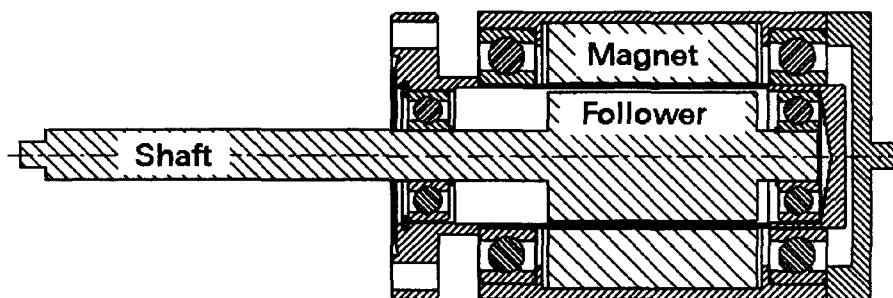


Fig. 17.21 Magnetically coupled UHV feedthrough mounted on a ConFlat flange. An external, rotating magnet couples torque through the stainless steel vacuum wall to a magnetic follower and shaft within the vacuum chamber. Reprinted with permission from Veeco, St. Paul Division, 4900 Constellation Drive, St. Paul, MN 55127.

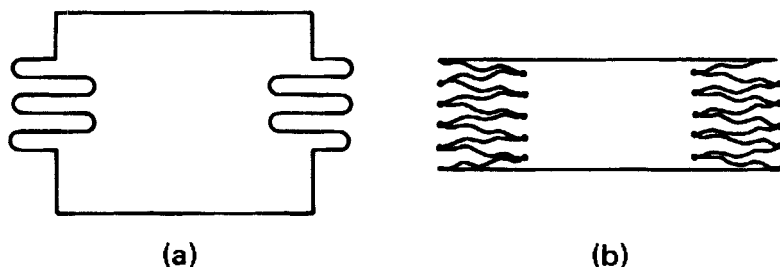


Fig. 17.22 (a) Hydroformed and (b) welded bellows.

Cross-section views of two types of bellows, hydroformed and welded bellows, are shown in Fig. 17.22. Hydroformed bellows are made by hydraulically stretching rolled and welded thin-wall tubing, or deep-drawn thin-wall cups. Welded bellows are made by sequentially welding a series of thin-wall diaphragms. In both designs, 304L, 316L, and 321 are the most commonly used materials for vacuum applications. Welded bellows are more expensive and more flexible than hydroformed bellows; however, fewer convolutions are needed. The limiting extension, compression, and ultimate lifetime of a bellows depend on the stresses encountered at the ends of the stroke. These in turn are dependent on the inner-to-outer radii ratio, material, how much the material has been cold worked, etc. A designer chooses the extension, compression, and the total pitched bellows length to keep the stresses in the bellows below a design value. This design value will be low when long life is a requirement. A few rough generalizations can be made: Bellows are often designed to work only in compression, but work well in both compression and extension. Stroke ratios ranging from 1/3 (extension):2/3 (compression) to 1:1 (extension):(compression) have been used in specific designs. The total stroke length for a bellows used in a vacuum application ranges from 20–33% of the pitched length for hydroformed bellows, to 80% of the pitched length for edge welded bellows.

Hydroformed bellows are adequate for many applications, especially where the bending or compression is small. Edge-welded bellows find many applications where a long stroke is needed in a very short space. Bellows were traditionally furnace-brazed onto a small pipe section for welding onto larger assemblies. Mating pieces machined with heat relief grooves have resulted in elegant pipe joints and valve bodies.

A long bellows section can be used for translational motion as described in Fig. 17.23a. Another solution uses a rotating bellows to drive a lead screw to convert rotary motion outside the chamber into linear motion inside the chamber.

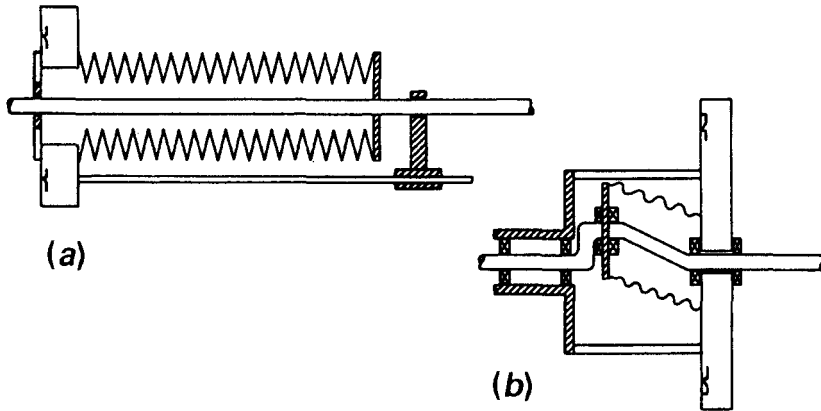


Fig. 17.23 (a) Translating and (b) rotating feedthroughs using metal bellows.

One ingenious solution for transmission motion is shown in Fig. 17.23b. This design illustrates the problems basic to all rotary bellows feedthroughs. Since the shaft is not continuous, it cannot carry a heavy load. Ball bearings are required on both sides of the seal. A variety of metal bellows rotary feedthroughs are commercially available and used frequently in UHV shutters and manipulators for precision movement of small parts, as well as rotation of shutters and substrate holders. Bellows need to be carefully cleaned, but not with solvents, as they are difficult to remove. A vacuum bake is effective. Baking temperatures should not exceed those required for brazing, should it have been used for assembly.

Outgassing has been observed from stainless steel during bending and sliding motion such as that found in sliding vacuum manipulators, motion feedthroughs and valves. Hydrogen was released from the bulk of stainless steel during flexing and while flexed, whereas CH_4 , CO and CO_2 were released from the surface during flexing [45]. Hydrogen and small quantities of CH_4 and CO were observed to desorb from stainless steel during sliding friction in ultrahigh vacuum [46].

REFERENCES

1. J. H. Singleton, *J. Vac. Sci. Technol. A*, **2**, 126 (1984).
2. A. Roth, *Vacuum Sealing Techniques*, Pergamon Press, Oxford, 1966.
3. A. Roth, *J. Vac Sci, Technol.*, **9**, 14, (1972).
4. A. Roth, *J. Vac Sci, Technol.*, **A**, **1**, 211, (1983).
5. *Metals Handbook*, 8th ed., *Welding and Brazing*, 6, American Society for Metals, 1971, p. 113.
6. C. H. Rosendahl, *Sheet Metal Industries*, February 1970, p. 93.
7. C. Geyari, *Vacuum*, **26**, 287 (1976).

8. R. N. Peacock, *Vacuum Joining Techniques*, HPS Corporation, 1898 S. Flatiron Ct. Boulder, CO, 1981.
9. W. H. Kohl, *Handbook of Materials and Techniques for Vacuum Devices*, Reinhold, New York, 1967.
10. American Welding Society, *Brazing Manual*, AWS
11. *Handy and Harmon, Brazing Book*, Handy and Harmon Co., 850 Third Ave. New York, NY, 10022.
12. T. Takamori, *Treatise on Materials Science and Technology: Glass II*, 17, M. Tomozawa and R. H. Doremus, Eds., Academic, New York, 1979, p. 117.
13. J. E. Benbenek and R. E. Honig, *Rev. Sci. Instr.*, **31**, 460, 1960.
14. F. Rosebury, *Handbook of Electron Tube and Vacuum Techniques*, Addison-Wesley, Reading, MA, 1965.
15. W. Espe, *Materials of High Vacuum Technology*, Vol. 2, Pergamon Press, New York, 1966.
16. R. N. Peacock, *J. Vac. Sci. Technol.*, **17**, 330 (1980).
17. B. Sessink and N. Verster, *Vacuum*, **23**, 319 (1973).
18. The relation between International Rubber Hardness Degrees and Young's Modulus is given in ASTM D1415-62T (American Society for Testing Materials, 1916 Race St., Philadelphia, PA 19103) Shore A degrees are approximately IRH degrees. Typical values of Young's modulus are $E = 35, 54$ and 68 kg/cm^2 corresponding to 60, 70, and 75 Shore A degrees.
19. L. de Csernatony, *Vacuum*, **16**, 13 (1966).
20. M. L. Johnson, D. M. Manos, and T. Provost, *J. Vac. Sci. Technol. A*, **15**, 763 (1997).
21. L. de Csernatony, *Vacuum*, **16**, 129 (1966).
22. L. Laurenson and N. T. M. Dennis *J. Vac. Sci. Technol. A*, **3**, 1707 (1985).
23. D. R. Wheeler and S. V. Pepper, *J. Vac. Sci. Technol.*, **20**, 226 (1982).
24. L. de Csernatony, *Proc. 7th Int. Vac. Congr. & 3rd Int. Conf. Solid Surf.*, R. Dobrozemsky, Ed., Vienna, 1977, p. 259.
25. L. de Csernatony, *Vacuum*, **27**, 605 (1977).
26. P. W. Hait, *Vacuum*, **17**, 547 (1967).
27. T. W. Edwards, J. R. Budge and W. Hauptli, *J. Vac. Sci. Technol.*, **14**, 740 (1977).
28. A. M. Arif and J. F. O'Hanlon, unpublished data.
29. W. R. Wheeler and M. Carlson, *Trans. 8th Natl. Vac. Symp., and Proc. 2nd. Int. Congr. Vac. Sci. Technol.*, 1961, Pergamon, New York, 1962, p. 1309.
30. W. Unterlerchner, *J. Vac. Sci. A*, **5**, 2540 (1987).
31. S. Kurokouchi, S. Morita, and M. Okabe, *J. Vac. Sci. Technol. A*, **19**, 2963 (2001).
32. H. Fend, *Vacuum*, **47**, 527 (1996).
33. G. F. Weston, *Vacuum*, **34**, 619 (1984).
34. D. Alpert, *J. Appl. Physics*, **24**, 860 (1953).
35. K. Yokokura and M. Kazawa, *J. Vac. Soc. Japan*, **24**, 399 (1981).
36. C. L. Foerster and D. McCafferty, *J. Vac. Sci. Technol.*, **18**, 997 (1981).
37. H. Ishimaru, T. Kuroda, O. Kaneko, Y. Oka, and K. Sakurai, *J. Vac. Sci. Technol. A*, **3**, 1703 (1985).
38. H. W. Lehmann, B. J. Curtis and R. Fehlman, *Vacuum*, **34**, 679 (1984).
39. BAL-Seal, BAL Engineering Corp., Boulder, CO.
40. Omni-Seal, Aeroquip, Los Angeles, CA.
41. Fluorocarbon Co., Los Angeles, CA.
42. P. J. Silverman, *J. Vac. Sci. Technol. A*, **2**, 76 (1984).
43. R. E. Rosensweig and R. Kaiser, *Office of Adv. Res. and Tech.*, NASA CR 1407, August 1969.
44. K. Raj and M. A. Grayson, *Vacuum*, **31**, 151 (1981).
45. P. Řepa and D. Orálek, *Vacuum*, **53**, 299 (1999).
46. R. A. Nevshupa, J. L. de Segovia, and E. A. Deulin, *Vacuum*, **53**, 295 (1999).

PROBLEMS

- 17.1 † Why is tungsten inert gas welding the commonly used technique for fabricating leak-tight stainless steel or aluminum vacuum joints?
- 17.2 † When through welding (TIG) from the atmospheric side, is it necessary to use a shield gas on the vacuum side?
- 17.3 A 6-mm-diameter tubing is to be furnace brazed to a stainless steel flange with 60% copper–40% gold filler with a melting point of 1010°C. Calculate the diameter of the hole (including tolerance) to be milled in the flange so the parts will have a clearance of less than or equal to 0.05 mm at the brazing temperature.
- 17.4 A 0.5-mm-diameter metal wire with an expansion coefficient of $110 \times 10^{-7}/^{\circ}\text{C}$ is sealed through a glass wall in a perpendicular direction, then cooled to 20°C. The glass expansion coefficient is $100 \times 10^{-7}/^{\circ}\text{C}$. After cooling to 20°C, is the glass near the interface in compression or tension in the: (a) Radial direction, (b) longitudinal direction, and (c) tangential direction?
- 17.5 † What is one fundamental difference between ceramic-to-metal and glass-to-metal joints?
- 17.6 † Describe an effective procedure for cleaning an O-ring. Why not wash an O-ring in acetone?
- 17.7 A groove 4.76 mm wide by 2.38 mm deep has been cut in a flange for use with a Viton O-ring whose cord diameter is 3.53 mm at 20°C. (a) What is the groove filling factor for Viton at 20°C when the flange is closed? (b) What percentage of the groove is filled at 150°C? (c) Your manager wants to bake the apparatus at 275°C and asks you to replace the Viton ring with a Kalrez ring of the same diameter. Is this request reasonable?
- 17.8 Why is it not possible to obtain a good seal on a groove or face which has been polished with abrasive papers, even though the depth of the scratches may be less than those left from machining the groove surface?
- 17.9 The RGA scans depicted in Fig. 17.24 were taken on two occasions when different Viton-sealed valves were closed. Viton absorbs gas from its environment, and when compressed, releases the gas it has absorbed. The nature of the absorbed gas depends on the nature of nearby gas sources. Please identify the gases released in these two unrelated, valve closures. Note that closure B took place near a hot filament ionization gauge.

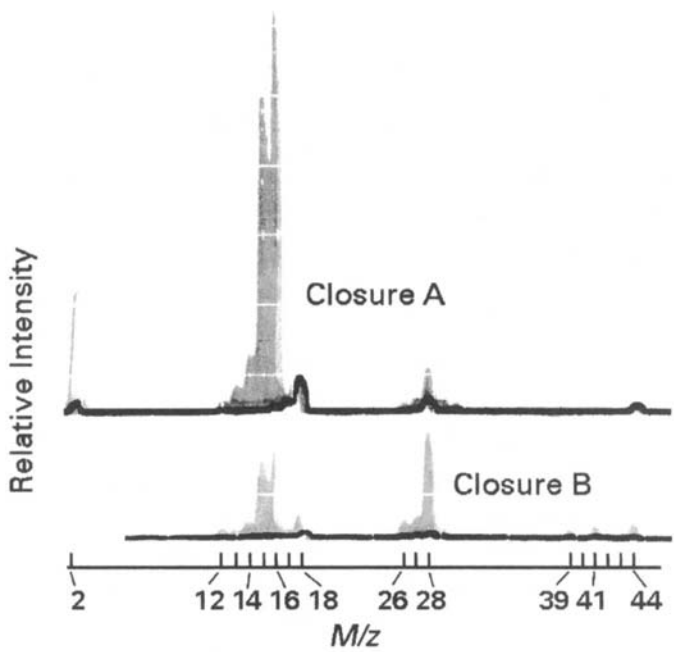


Fig. 17.24 Mass-resolved gas release from two valves with Viton seats during closure of each valve. The black curves are the background; the gray curves are transient gas release.

17.10 A magnetic liquid vacuum seal containing a perfluoropolyether pump fluid and other constituents will allow air to permeate from atmosphere to vacuum. Assume that nitrogen and oxygen are the dominant permeating gases. Assume that each has a diffusion constant of $\sim D = 6 \times 10^{-9} \text{ m}^2/\text{s}$ and a solubility of 0.10. Calculate the total “outgassing” (actually, the permeation gas flux) through the thin ring of fluid for the geometry sketched in Fig. 17.25. Assume the external environment is 1 atmosphere of air at room temperature.

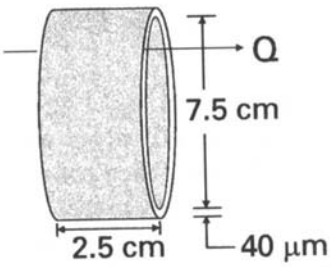


Fig. 17.25

CHAPTER 18

Lubrication

Lubrication is important to vacuum users in oil-lubricated pumps (vane, piston, lobe, and turbomolecular), in moving parts in vacuum (bearings and feedthroughs), and in peripheral applications, such as bolt lubricants. Not all of these applications involve high vacuum, and some take place outside the vacuum environment. Moving parts may be lubricated in vacuum with a liquid film, grease, a dry film, or, in certain cases, no film at all.

Lubricant systems have three components: the materials to be lubricated, the lubricant, and the environment [1]. These three components are interdependent, because surface adhesion and lubrication are not only characteristic of the material and the lubricant, but also of gas interactions. Vacuum is unique, because the gaseous environment has been removed. Lubricants prevent moving surfaces from contact. When surfaces contact, friction occurs and surfaces wear. Friction generates heat, whereas wear destroys material and produces debris. In an atmospheric environment it is the wear, not friction, which is responsible for most problems. In a vacuum environment, friction is a problem. Vacuum eliminates convection cooling, increases lubricant evaporation rates, reduces oxidation of the metals, hastens the onset of cold welding, and alters the size distribution of wear particles.

Earlier papers have reviewed lubrication processes in air or vacuum [2–5]. In this chapter, we review fluid rheology and techniques for vacuum lubrication. In Chapter 13, we discussed their role as pump fluids.

18.1 LUBRICATION PROCESSES

Full-film, elastohydrodynamic, and boundary lubrication are three forms of lubrication. The ratio of the lubricant film thickness to the surface roughness is an important quantity. Lubricant thickness depends on the absolute viscosity η , relative surface velocity U , and the load L . Figure 18.1 (the Stribeck curve) relates these to the coefficient of friction f .

A combination of high absolute viscosity, high relative speed, and low loading results in an oil film whose thickness is much greater than the roughness of either surface. The rapidly moving load rides on an oil wedge. This is called hydrodynamic or full-film lubrication. Viscosity is the most important lubricant property in this regime. Friction can be minimized for a given load or viscosity by the appropriate choice of viscosity.

At some value of low speed, low viscosity, and high loading, irregularities on the two surfaces will contact. This is the boundary lubrication region [2], which can be encountered in pump bearings and vanes during starting and stopping and between slowly sliding surfaces. The relation between friction coefficient f , and surface irregularities is [6]

$$f = s/p \quad (18.1)$$

s is the shear strength and p is the yield pressure of the metal. Both quantities are related to the structure of the material. The coefficient of friction can be reduced by decreasing the shear stress s , or increasing the yield pressure p , by increasing the area over which the force is distributed. In the boundary region the coefficient of friction is determined not only by the manner in which the adjacent surface peaks contact, but by the additives that affect the chemistry of these contacting surfaces.

Intermediate between these two regimes is the elasto-hydrodynamic region, in which oil undergoes a tremendous pressure increase. Its viscosity

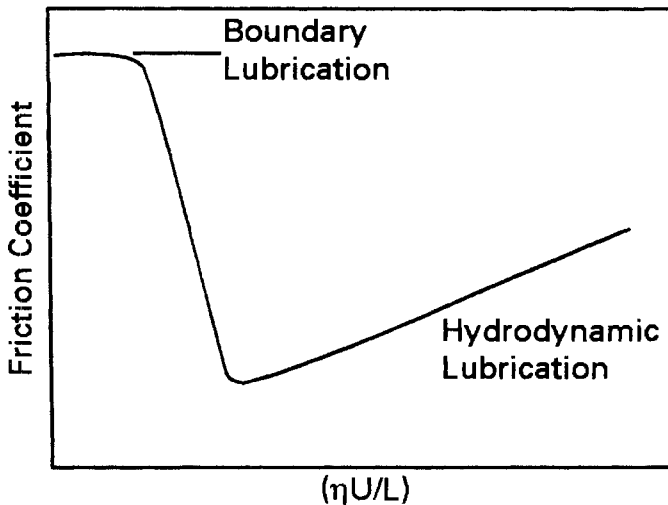


Fig. 18 1 Dependence of friction on viscosity η , relative velocity U , and load L .

increases exponentially and it behaves like a low-shear solid that can deform surface irregularities without contact.

18.2 RHEOLOGY

Rheology is the study of fluid flow. Fluid flow is one physical property of a lubricant, which determines its usefulness for either a vacuum or atmospheric application. Here we discuss absolute viscosity, kinematic viscosity, viscosity index, and techniques by which each can be measured.

18.2.1 Absolute Viscosity

The definition of viscosity was given in (2.21) and is repeated here in a different form.

$$\tau = \eta s' \quad (18.2)$$

τ is the shear stress and s' is the rate of shear. The viscosity of a Newtonian fluid is independent of shear rate. Not all fluids behave in this manner. The viscosity of emulsions like hand cream, grease and some synthetic fluids decreases with increasing shear rate. The decrease is small for the synthetic fluids we use, so η will be considered a constant. The viscosity of grease drops rapidly with shear rate until it approaches the viscosity of the oil from which it is formulated.

The viscosity of a liquid is predominantly a result of cohesive forces between the molecules. Since cohesion decreases with temperature, the viscosity of a liquid decreases on heating. In SI, dynamic viscosity η has units of Pa-s. One mPa-s = 1 centipoise—a handy conversion to remember since the useful literature is tabulated in c.g.s. units. Research instruments measure absolute viscosity of liquids by timing the flow through a long capillary tube under constant head pressure. Such instruments are required for measurement with ASTM and ISO standards. The volume flow rate through the tube (m^3/s) is related to the viscosity by the Poiseuille equation

$$\frac{V}{t} = \frac{\pi d^4 \Delta P}{128 \eta l} \quad (18.3)$$

ΔP is the pressure drop in the tube, d is the diameter, and l is the length of the tube. This equation neglects end effects and is reasonably accurate for long tubes. Engineering instruments attempt to measure absolute viscosity by measuring the torque on an immersed rotating spindle or a rotating cone adjacent to a flat plate. Because the flow is not laminar for low-viscosity liquids, corrections are needed to obtain absolute viscosity [7].

18.2.2 Kinematic Viscosity

Kinematic viscosity ν of a gas or liquid is simply the absolute viscosity divided by the density

$$\nu = \eta/\rho \quad (18.4)$$

In the c.g.s system kinematic viscosity is expressed in units of Stokes. One Stoke = 1 cm²/s. In SI the units are m²/s, but data are usually plotted in mm²/s because 1 cS = 1 mm²/s. Kinematic viscosity, like diffusivity and permeability, is a transport property—observe that all three quantities have dimensions of L^2/T . Kinematic viscosity is measured directly in research instruments by timing the (Poiseuille) flow of a liquid through a long capillary under its own head [8]. Engineering instruments use short tubes or orifices in which the flow is not always laminar, so it is necessary to tabulate factors by which their readings can be converted to kinematic viscosity. Saybolt and Redwood instruments measure the times required for a known quantity of oil with a falling head to flow through short tubes of specific dimensions. The Engler instrument measures the ratio of the times required by equal volumes of oil and water to flow through a particular tube. The Saybolt (U. S.), Redwood (English), and Engler (German) are the most common engineering instruments used for measuring the kinetic viscosity of oils. They are being replaced slowly by long tube instruments to meet SI standards. Appendix F.5 gives the factors for converting Saybolt Universal Seconds (SUS), Redwood No. 1 seconds, and Engler degrees to kinematic units.

The variation of kinetic viscosity with temperature for petroleum oils empirically fits the equation

$$\log(\log(\nu + 0.7)) = A + B \log T \quad (18.5)$$

Measurement of ν at two temperatures, 40°C and 100°C, is adequate for interpolation and extrapolation down to the pour point when plotted according to (18.5). This curve also fits most synthetics except chlorosiloxanes, which show curvature when plotted in this empirical way.

18.2.2 Viscosity Index

Viscosity index V.I., is an empirical way of classifying how kinematic viscosity varies with temperature. It is an arbitrary and purely historical scheme. It recognizes the fact that the (high paraffin content) Pennsylvania oils have a uniformly low change in viscosity with temperature. These oils were arbitrarily assigned a V.I. of 100. Oils from the Gulf (high naphthene

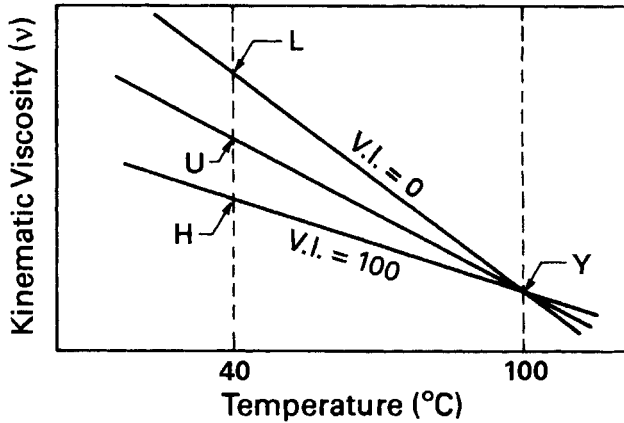


Fig. 18.2 Oil viscosity index.

content) with the greatest viscosity slope were assigned a V.I. of 0. Viscosity Index is calculated from the 40°C and 100°C viscosity values of the unknown oil (*U*), and the tabulated viscosity values of oils of index 0 (*L*) and 100 (*H*). The unknown and the two standards must have the same viscosity at 100°C. See Fig. 18.2. The formulas for calculating V.I. are not stated here because they cannot be used without the extensive tables given in the ASTM standard [9]. Alternatively, V.I. may be obtained from Fig. 18.3. This plot, generated from the ASTM data, greatly simplifies the procedure and yields sufficiently accurate results. The V.I. system was originally intended for use with mineral oils and was modified for use with synthetics. Some synthetics have a negative index, whereas others such as silicones and sebacate esters have indexes over 100%.

18.3 LUBRICATION TECHNIQUES

We can lubricate moving surfaces with liquids—for example, petroleum oils or synthetic fluids, greases, or a variety of solid films such as silver and molybdenum disulfide. The use of these techniques in vacuum gives different results than when they are used in air. Each technique has its own problems when the surrounding gas is removed.

18.3.1 Liquid Lubrication

Petroleum and synthetic fluids are used to lubricate vacuum pumps and moving surfaces in vacuum. In the full-film region, fluid fills the spaces

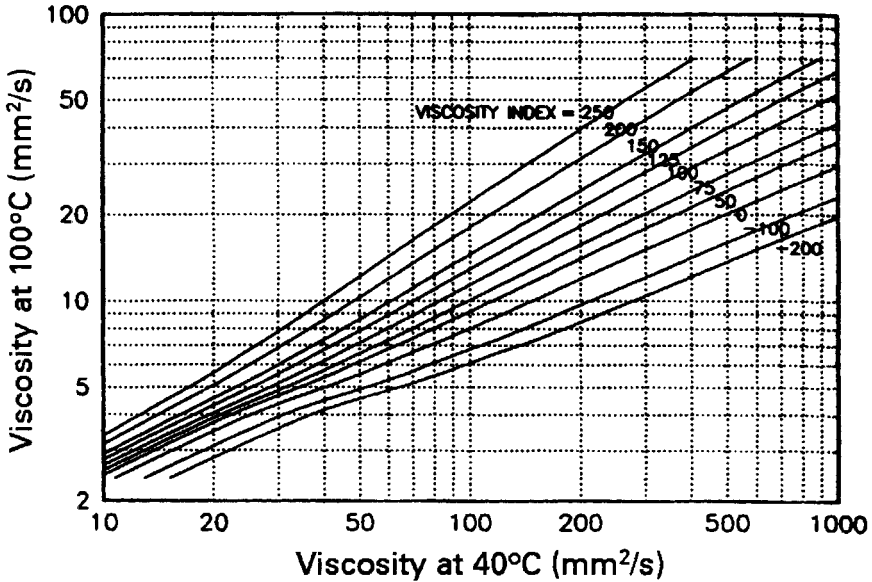


Fig. 18.3 Relation between 40°C and 100°C viscosity for oils of varying viscosity index.

between moving surfaces and keeps them apart. The viscosity should be low enough to allow rotating or sliding motion at the lowest ambient temperature and remain sufficiently high at operating temperature (high viscosity index). The viscosity required for full-film lubrication depends on the operational temperature range and the load. From Fig. 18.1 we see that the ratio of η/L should remain a constant. Therefore, high-viscosity fluids are required for heavy loads. Within a class of fluids, vapor pressure is usually inversely proportional to viscosity. Lubrication in the full-film regime is dependent on the ability of the fluid to adhere to the surface and form a film of adequate shear strength, which will support the bearing load.

Other necessary attributes are adhesion, stability, and heat conductivity. The oil must wet the surface and form a film, which is stable under high shear rate. Shear generates heat, which must be removed to prevent degradation and further viscosity decrease.

Oil adhesion is determined by the strength of the liquid-metal bond. Liquids with unsaturated bonds strongly adhere to or wet metal surfaces. Cohesion is a measure of intermolecular attraction. Oils that are very cohesive do not disperse or spread out rapidly on the surface of a metal. Certain highly cohesive oils such as polyphenyl ether adhere to metals strongly and also form a barrier that prevents creep. The outermost molecules align themselves in such a way that the exposed groups have a

low liquid-metal adhesion. These fluids form a high contact angle with a metal surface and are termed autophobic. Fluids with good adhesion that do not have a resistance to creep will flow and wet a metal surface. Hydrocarbon oils have this property. Except for a fluid like penta-phenyltetramethyl trisiloxane, silicone fluids have high creep rates.

Sliding and rolling surfaces are easily lubricated with liquids for long lifetimes. The simplest liquid lubrication system is a wiped fluid coating. More complex systems can be designed to provide a continuous supply by migration or evaporation from a reservoir. If the fluid has been sufficiently outgassed, it can be used up to the temperature at which the vapor pressure of the fluid is intolerable. Vapor pressures of common fluids used in vacuum are given in Appendixes F.2 and F.3. Polyphenyl ether is a common choice for lubricating hand-operated sliding and rotating surfaces in vacuum. The mechanisms used to supply the lubricant can also cause organic contamination of the vacuum chamber. Contamination can be reduced by choosing oil of sufficiently low vapor pressure or by enclosing the lubricated area with a shroud. A creep barrier will prevent lubricant from creeping along the shaft where it passes through the shroud. PTFE is a hydrocarbon creep barrier, while nylon is a fluorocarbon creep barrier. It may be necessary to cryogenically cool the shroud in the area near the region where the sliding or rotating shaft enters the chamber.

Rolling friction is encountered with ball or roller bearings. A rolling surface looks much like a sliding surface when viewed microscopically, and the effects on viscosity, adhesion, and heat conduction are the same. High-speed ball bearings such as those found on turbomolecular pumps require oil of lower viscosity than is used on slow-speed bearings. Examination of Fig. 18.1 shows that the product ηU needs to remain constant.

Boundary lubrication requires fluids with unique properties, which are usually attained with additives. Sulfur, chlorine, and lead make effective boundary lubricants for steel-on-steel because they form low-shear-stress compounds that are wiped or etched from the high spots. These chemicals function as etchants. Phosphorus functions by forming iron phosphide at hot spots that plastically flows and fills in the asperities. Plastic deformation, like etching, causes the load to be redistributed over an increased area [10]. In both cases the shear strength is reduced, the yield pressure is increased and the friction is reduced according to (18.1).

Oiliness, or lubricity, is an important property of boundary lubricants. It is an imprecise term and cannot be defined quantitatively. It refers to the ability of polar molecules to align themselves in double layers that slide easily over adjacent double layers. Animal fats have a high degree of oiliness, but they do not make acceptable hydrodynamic or boundary lubricants because they are not chemically or thermally stable. Some esters are stable and are used as oiliness additives.

18.3.2 Grease Lubrication

A grease is either a heavy petroleum distillate or, more commonly, a thickened petroleum or synthetic liquid. Petroleum oil can be vacuum distilled to yield wax-like, high-molecular-weight grease (petrolatum) which is uniform in composition. Grease also can be made by the process of gelling or thickening a liquid. Various compounds such as clay, esters, metal soaps, and powdered polytetrafluoroethylene (PTFE) are used to increase the viscosity of oil to the consistency of grease. The oil is either physically entrapped in the thickener, adsorbed on it, or held in place by capillary action [1]. The typical starting material for a thickened grease is an oil whose room-temperature viscosity is about 500 mm²/s. The room-temperature viscosity of a thickened grease is much higher than the base oil at low shear rates, but it drops by a factor of 30 at high shear rates.

Greases are characterized by their chemical type, method of thickening, vapor pressure, service temperature range, reactivity, and consistency. Characteristics of several greases are shown in Table 18.1. The vapor pressure of grease increases with temperature, according to the properties of the oil and the thickener. Laurenson [11,12] has shown the vacuum performance of grease to be dependent on the vapor pressure of the grease and its method of manufacture. He demonstrated that the evaporation rate and quantity of a gelled grease made from hydrocarbon oil or silicone fluid of moderate vapor pressure depended on the total mass of the grease in vacuum, while the evaporation rate of a molecularly distilled grease depended only on the surface area. He attributed this to the fact that the molecularly distilled grease evaporated only from the surface, while the surface oil molecules of a filled grease evaporated from the large effective surface area of the gel. These molecules were replaced by migration from the bulk, as oil feeds a lamp wick. He could not experimentally observe the mass dependence of evaporation rate of filled greases made from very-low-vapor-pressure silicones or perfluoropolyethers (PFPE).

The ASTM penetration test [17] measures the depth in millimeters that a particular cone will penetrate grease in a given time. This is a measure of grease consistency. No. 2 grease with a penetration of 265–295 mm is typically used for low speed bearings. Soft greases are needed for high-speed ball bearings. Each grease types described in Table 18.1 is made in several consistencies.

Grease lubrication is used for long life, low maintenance applications. Grease is often used in low speed ball bearings, rotary feedthroughs, and has been used in turbomolecular pump bearings [18]. Hydrocarbon grease has a characteristically low maximum service temperature. It is rarely much above room temperature for distilled greases, but is higher for filled greases, if the gelling agent is properly chosen. Perfluoropolyether (PFPE)

Table 18.1 Typical Properties of High Vacuum Greases

Trade Name	Chemical Type	Temperature Range (°C)	P_v at 25°C (Pa)	Specific Gravity at 25°C	Penetration ^a (mm)
CVC Celvacene Light [13]	Ester-thickened hydrocarbon	-40-90	10^{-4}	—	150
Apiezon [14] AP 100 Grease	PTFE-thickened hydrocarbon	10-30	10^{-8}	1.042	—
Apiezon [14] L Grease	Distilled hydrocarbon	10-30	10^{-8}	0.896	—
Dow Corning [15] High Vacuum	PTFE-thickened silicone	-40-260	10^{-7}	1.0	<260
Krytox [16] LVP L-10	PTFE-thickened fluorocarbon	-20-200	10^{-13}	1.94	280

^a ASTM D-21.

and silicone fluids have high maximum service temperatures. They are typically formulated from a mixture of fluid and powdered PTFE. Silicone fluids are poor steel-on-steel lubricants, and greases made from them are also poor lubricants unless thickened with a lubricant like PTFE. If a large reservoir of grease is needed, a distilled hydrocarbon, or filled grease made from very-low-vapor-pressure silicone or PFPE fluid, is recommended [11]. If a thin film is adequate, gelled grease may be used. PFPE greases are preferred to silicones where electron bombardment can cause fragmentation. The reaction between greases and elastomers is similar to that for fluids and elastomers shown in Appendix F.1. The gelling agent may cause an additional reaction. Manufacturers can provide information on the reactivity of greases containing proprietary additives.

Bolt lubricants are often used around, but not in vacuum systems. These greases are formulated for the extreme boundary lubrication region. They contain extreme pressure additives such as silver, copper, lead, or molybdenum disulfide. Some base oils and additives used in these greases have high vapor pressures.

18.3.3 Dry Lubrication

The process of lubricating with a solid film is called dry lubrication. In (18.1) we saw that friction can be reduced in the boundary region by increasing the contact area and reducing the shear force of the lubricant. The main advantage of a dry lubricant is its low vapor pressure. Low-vapor-pressure reduces system contamination and allows operation at high temperatures. Solid-film lubricants are useful when loads are extremely high, speeds are low, and surface temperatures are extreme, and the design

must be simplified for maintenance-free long life in vacuum. Dry lubrication is limited by its finite thickness and the debris generated by its sacrificial removal. Dry lubrication failure often results from a local defect and therefore the lifetime of a dry lubricated system is not as predictable as that of a liquid lubricated system in which the lubricant evaporates or migrates in a uniform manner [5].

The desirable properties of a dry lubricant are low vapor pressure, low shear strength, and good adhesion to the base metal. Many solids have been used as dry lubricants. Among them are graphite, sulfides, and selenides of molybdenum and tungsten, gold, silver, and PTFE. It was originally thought the lubricating ability of graphite and other layered solids resulted from their loosely bound layered structure. The weak binding between layers was thought to allow sliding with low shear. This theory was found wanting when it was discovered that graphite was not a good lubricant in vacuum or at high altitude, but only in the presence of water vapor [19]. MoS_2 is a good lubricant in vacuum [20]. The difference in the lubricating ability of these two materials is a result of their differing structure. Graphite consists of a layered structure with a high interlayer binding energy. Contamination from water vapor lowers the binding energy and allows motion with low shear. Molybdenum disulfide films are oriented layers of S–Mo–S with a low binding energy between the adjacent sulfur layers, so contamination is not necessary for low shear sliding [21].

Molybdenum disulfide and tungsten disulfide are the most widely used solid vacuum lubricants. Farr [22] has reviewed its structure and properties as they apply to lubrication. Matthey [23] described how these and other solid films have been used in space hardware. MoS_2 has a very low vapor pressure and can be applied by many techniques including sputtering and spraying. MoS_2 has been deposited by dc sputtering [24] and rf sputtering [25]. Sputter deposited films give satisfactory lubrication but does generate debris [25]. MoS_2 –graphite–sodium silicate coatings on steel have been shown to give good performance and long life [26]. Wear rates of $< 3 \times 10^{-18} \text{ m}^3/(\text{N}\cdot\text{m})$ were observed for spray-gun-coated parts; the wear rates were 100 times larger for MoS_2 films applied in an aerosol. Friction and wear of MoS_2 lubricated steel surfaces has been studied [27]. In the pressure range 10^5 – 10^4 Pa the friction and the wear decreased, because of the removal of water vapor, and remained constant in the pressure range 10^4 – 10 Pa. In the pressure range 10 – 0.1 Pa the friction continued to decrease, while the wear increased greatly. The friction decrease was attributed to the removal of oxygen. The wear increased, because heat could not be dissipated in vacuum. Below 0.1 Pa no further change in wear or friction was observed. O_2 increased the friction by oxidizing MoS_2 to MoO_3 and MoO_2 [27,28].

Soft metals will also lubricate sliding surfaces. Pair hardness, ductility and re-deposition were shown to be important in designing a low-friction,

long-life system [29]. The best gear pair was a silver plated aluminum gear running against a MoS₂-graphite-sodium silicate-coated steel gear. Gold plating stainless steel bolts has proven to be an effective technique for preventing the galling of threads following system baking.

Polytetrafluoroethylene coatings have also been used for vacuum applications. PTFE transfers and re-coats [4]. The long PTFE molecules are oriented parallel to the direction of sliding [3].

Almost anything placed between two moving surfaces will reduce friction and wear. The environment affects the adhesion of a lubricant, its evaporation, oxidation and intercrystalline forces. If we remove all foreign materials, similar metals will instantly cold weld. However, the cold welding of adjacent surfaces can be eliminated with materials of dissimilar lattice constants, such as sapphire balls in stainless steel races [5]. The friction coefficient of this system is higher than a lubricated system.

REFERENCES

1. E. R. Booser, in *Kirk-Othmer Encyclopedia of Chemical Technology*, 3rd ed., 14, M. Grayson and D. Eckroth, Eds., Wiley, New York, 1980, p. 484.
2. N. Tipei, *Theory of Lubrication*, Stanford University Press, 1962, p. 11.
3. D. Tabor, in *Microscopic Aspects of Adhesion and Lubrication*, J. M. Georges, Ed., Tribology Series, Vol. 7, Elsevier, Amsterdam, 1982.
4. D. H. Buckley, *Proc. 6th Intl. Vac. Congr. 1974, Jpn. J. Appl. Phys., Suppl. 2, Pt. 1*, 1974, p. 297.
5. V. R. Friebe and J. T. Hinricks, *J. Vac. Sci. Technol.*, **12**, 551 (1975).
6. F. D. Bowden and D. Tabor, *The Friction and Lubrication of Solids, Part II*, Clarendon Press, 1964.
7. J. R. Van Wazer, J. W. Lyons, K. Y. Kim, and R. E. Colwell, *Viscosity and Flow Measurement*, Interscience, New York, 1963.
8. J. F. Swindells, R. Ullman and H. Mark, in *Technique of Organic Chemistry*, 3rd ed., A. Weissberger, Ed., Vol. 1, Physical Methods of Organic Chemistry, Part 4, Interscience, New York, 1959, p. 689.
9. ASTM D-2270, *1981 Annual Book of ASTM Standards*, Part 24, American Society for Testing Materials, Philadelphia, 1981, p. 277.
10. R. E. Hatton in *Synthetic Lubricants*, R. C. Gunderson and A. W. Hart, Eds., Reinhold, New York, 1962, p. 402.
11. L. Laurensen, *Vacuum*, **27**, 431 (1977)
12. L. Laurensen, *Vacuum*, **30**, 275 (1980)
13. CVC Products Inc., 525 Lee Road, Rochester, NY 14603.
14. Edwards High Vacuum Corp., 3279 Grand Island Blvd., Grand Island, NY 14072.
15. Dow Corning Co, Inc. 2030 Dow Center, Midland, MI 48640.
16. Du Pont and Co. Chemicals and Pigments Department, Wilmington, DE 19898.
17. ASTM D-217, *1981 Annual Book of ASTM Standards*, Part 23, American Society for Testing Materials, Philadelphia, 1981.
18. G. Osterstrom and T. Knecht, *J. Vac. Sci. Technol.*, **16**, 746 (1979).
19. R. H. Savage, *J. Appl. Phys.*, **19**, 1 (1948).
20. J. Haltner, *Wear*, **7**, 102 (1964).
21. P. J. Bryant, P. L. Gutshall and L. H. Taylor, *Wear*, **7**, 118 (1964).

22. J. P. G. Farr, *Wear*, **35**, 1 (1975).
23. R. A. Matthey, *Lubr. Eng. (ASLE)*, **34**, 79 (1978).
24. T. Spavins and J. S. Przybyszewski, J. S. *Deposition of Sputtered Molybdenum Disulfide Films and Friction Characteristics of Such Films in Vacuum*, NASA TDN-4269, December 1969.
25. E. Vest, *Lubr. Engng. (ASLE)*, **34**, 31 (1978).
26. Thomas, *The Friction and Wear Properties of Some Proprietary Molybdenum Disulfide Spray Lubricants in Sliding Contact with Steel*. Report No. ESA CR(P) 1537, European Space Tribology Laboratory, Risley, England, January 1982.
27. G. V. Kurilov, *Soviet Materials Science*, **15**, 381 (1979).
28. M. Matsunaga and T. Nakagawa, *Trans. ASLE*, **19**, 216 (1976).
29. R. E. Kirby, G. J. Collet, and E. L. Garwin, *Proc. 8th Int. Vac. Congr., II*, J. P. Langeron and L. Maurice, Eds., Cannes, France, September, 1980, p. 437.

PROBLEMS

- 18.1 The viscosity of a gas increases with increasing temperature. Why does the viscosity of a liquid decrease with increasing temperature?
- 18.2 A kinetic viscometer reads 40 and 36 mm²/s for two liquids; an absolute viscometer reads 0.04 Pa·s for the same liquids. Explain.
- 18.3 A 10-cm-diameter shaft revolves in a 3-cm-long sleeve bearing at 400 rpm with a radial clearance of 0.01 cm. Find the torque required to overcome the resistance of the oil ($\rho = 0.88$ g/cc, $\nu = 50$ mm²/s).
- 18.4 The viscosity of a substance was found to be 52, 9.2, 3.2, and 1.8 Pa·s at $s' = 10, 100, 1000$, and $10,000$ s⁻¹. Its density is 0.91 g/ml. Plot the kinetic viscosity versus shear rate. What is the material?
- 18.5 How will the vacuum properties of a grease change if the grease is left exposed to the atmosphere? i
- 18.6 Why should grease not be applied with the fingers?
- 18.7 What are three advantages of a synthetic lubricant over paraffin oil?
- 18.8 Why use a solid lubricant instead of a liquid or grease?
- 18.9 Describe the sliding behavior of molybdenum plates, which are placed in vacuum after the following separate treatments: (a) high-temperature hydrogen firing, (b) high-temperature oxidation, and (c) high-temperature baking in hydrogen sulfide.
- 18.10 Describe the lubrication environment in the following applications: (a) shaft bearing in a mechanical pump, (b) a turbomolecular pump bearing, (c) rotating planetary dome roller bearings; unbaked aluminum metallizing system used at 10^{-4} Pa, (d) rotating substrate holder bearing (1 rpm) in a molecular beam epitaxy system. What kind of a metal-lubricant system would you choose for each and why?

CHAPTER 19

Rough Vacuum Pumping

Characterizing vacuum systems during their initial pumping from atmosphere is not a subject of frequent study; however, it is an important phase of the pumping cycle. If the initial pumping is done improperly, it can seriously affect system performance or product quality. No one recipe fits all situations. For accelerator applications, removal of atmospheric gas is but a short part of an extended time at ultrahigh vacuum. For high volume production applications that use load locks to transfer product from atmosphere to vacuum, the load lock pumping and venting times can be a major portion of the brief time the product spends in the process chamber. The significant gas loads released from roll stock and debris collected between cleaning cycles must be considered carefully when specifying roughing pumps and pumping cycles for large coating systems.

How fast should a system be evacuated? To what pressure should it be evacuated? If we pump too slowly, product throughput will be reduced, if we pump too rapidly, water aerosols will form and capital expenditures may increase. If we pump to an unacceptably low pressure, oil-sealed pumps can backstream oil vapors, whereas if we pump to an unacceptably high pressure, the high vacuum pump will not accept the gas load at crossover. Traditionally, these issues were not always discussed in sufficient depth; a one-size-fits all solution was often suggested; however, that no longer applies for the diverse and specialized systems currently used.

Pumping time is dependent on pump and pipe sizes, which in turn affect system cost, return on investment, product cycle time, product quality, and surface contamination. Crossover pressure is a variable that can be adjusted by the operator. If set too low, the product may become contaminated. If set too high, the high vacuum pump may not perform properly. Most importantly, it is a variable that can be changed easily and without consideration of the consequences. The two fundamental questions that we address in this chapter are the rate at which air is pumped during roughing and the condition chosen for crossover from the roughing pump to the high vacuum pump.

19.1 PUMPING RATE

Economics and product quality are the two issues that determine the speed at which atmosphere is removed from the chamber. In general we wish to finish the process as quickly as possible, in a system that was purchased for the lowest possible cost, and without affecting product quality. In some cases these requirements conflict. By understanding vacuum basics, we can best meet the objectives.

19.1.1 Pump Size

Pumping from an initial pressure P_{init} typically atmosphere, to crossover pressure can be modeled by a chamber of volume V connected to a pump of speed S_p , through a conductance C , as depicted in Fig. 19.1. The chamber will be assumed to have an internal outgassing of $Q/S = P_{ult}$ and that will remain approximately constant during the rough pumping cycle. The time dependence of the chamber pressure is described by

$$P_c(t) = (P_{init} - P_{ult}) e^{-\frac{S_c t}{V}} + P_{ult} \quad (19.1)$$

The pumping speed at the chamber exit that is required to reach a desired chamber pressure P_c is dependent on the system volume V , the initial pressure P_{init} , the outgassing rate, and the time specified by the process or customer.

$$S_c = -\frac{V}{t} \ln \left(\frac{P_c - P_{ult}}{P_{init} - P_{ult}} \right) \quad (19.2)$$

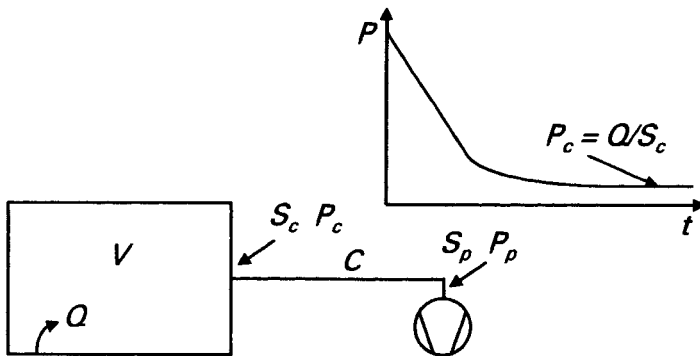


Fig. 19.1 Model for calculating the initial pumping time of a vacuum chamber from atmosphere to crossover. The rough pumping speed used to predict the pressure decrease is the speed measured at the chamber entrance.

Note that the assumed short-term ultimate pressure P_{ult} is the quotient of the outgassing rate and chamber speed that is being calculated $P_{ult} = Q_{og}/S_c$. One must either estimate this correctly or iterate to obtain the solution. For empty chambers, this will be a small quantity; however, when roughing chambers containing large product gas loads e.g., large rolls of paper or plastic, that term is significant. We desire to know the speed at the pump and it can be obtained from

$$\frac{1}{S_p} = \frac{1}{S_c} + \frac{1}{C} \quad (19.3)$$

Assuming we are pumping from atmosphere, the flow is viscous, and therefore C is pressure dependent. The conductance will be large at atmosphere and will decrease as the final pressure is reached. In practice, this means the pumping speed used in (19.1) is pressure-dependent and numerical methods are required to solve the problem exactly. One can obtain a simple approximate solution by assuming the conductance C to have a constant value—its smallest value—the value at the lowest pressure of interest. Using this value of conductance in (19.3) yields a worst-case or largest value of pumping speed required. The actual exhaust time will be less than that calculated with (19.2) and (19.3). The speed of an oil-sealed vane or piston pump can be considered to be constant for all practical purposes, as one rarely operates an oil-sealed pump in its compression-limiting region where the speed drops to zero. Large systems will have compound roughing pumps consisting of perhaps one or more vane or piston pumps and one or more lobe blowers. Small systems may use a scroll pump, screw pump, claw/lobe pump, or vane pump to rough from one atmosphere. The choice of pump depends, in part, on its base pressure.

Speed of roughing is also a consideration. If the pumping time cannot be met economically or quickly with a normal roughing system, an alternative solution can be considered. One such special-purpose roughing system uses one, two, or three sequentially operated pressure dividing tanks configured to remove most of the atmospheric gas in an extremely short time. This design is analogous to that described in Section 15.4.1 for multiple sorption pumps. There are four elements of the load lock cycle. Product is first loaded in the lock, then it is pumped. Next product is transferred to the adjacent process or holding chamber, and lastly the lock is vented to atmosphere. By taking advantage of ballast tanks, as well as the pressure drop produced when the process or holding chamber is opened, the pumping time portion of the load lock cycle can be reduced. During the remaining three parts of the load lock cycle, the ballast tanks can be re-evacuated. In particular situations, this can increase product throughput and profit for a nominal increase in system cost. Because water

aerosols are formed during rapid pumping, this technique cannot be used in sensitive processes, unless aerosol generation is either unimportant or is dealt with by use of internal surfaces spaced close to the product surface. See below.

19.1.2 Aerosol Formation

Water aerosol is formed within a chamber when the pressure is suddenly reduced. The rapidly decreasing pressure causes the temperature to drop and causes the water vapor to become supersaturated. Supersaturated vapor quickly condenses, usually on micrometer- or nanometer-sized dust particles. A numerical simulation showed that water droplets grew to 45 μm diameter in 25 ms at 0.1 atm, and grew to 10 μm in 25 ms at a 1 atm [1]. Growth ceases when the source is depleted. The aerosol droplets collide with surfaces. Nucleating dust and any other atmospheric materials, such as ammonium or sulfur salts [2], remain on the surface after the water droplets evaporate. One may observe the aerosol with a flashlight in a darkened room.

In an isothermal system, the temperature of the gas is held constant by heat flow into the system. In an isentropic system, no heat flows into the system and the gas temperature drops abruptly. Over forty years ago, operators of large space chambers understood that an expanding gas does work on its surroundings, loses energy, and cools. They found that the temperature in the center of these large chambers tended to follow an isentropic expansion [3]. The relation between the pressure drop and temperature drop in an isentropic system is given by

$$\frac{T_{final}}{T_{initial}} = \left(\frac{P_{final}}{P_{initial}} \right)^{\frac{\gamma-1}{\gamma}} \quad (19.4)$$

where γ is the ratio of specific heats of the gas. T and P are, respectively, the absolute temperature and absolute pressure of the gas.

In a real system, the behavior is neither isentropic nor isothermal, but lies somewhere between these two regimes; the temperature will drop, then relax to ambient temperature. A system with a spherical or cubical shape—that is, a system with a small surface-to-volume ratio—will behave more like an adiabatic system; its temperature will drop sharply and take a long time to return to ambient. A system containing many interior walls, with small, local volumes (large surface-to-volume ratio) will transfer heat rapidly to the gas during wall collisions; its gas temperature will drop only slightly and recover rapidly. Systems with high pumping speeds exhibit adiabatic behavior, whereas systems with low pumping speed tend to be isothermal.

Figure 19.2 illustrates the temperature changes recorded by several small-diameter thermocouples during the roughing of a 30-cm-diameter

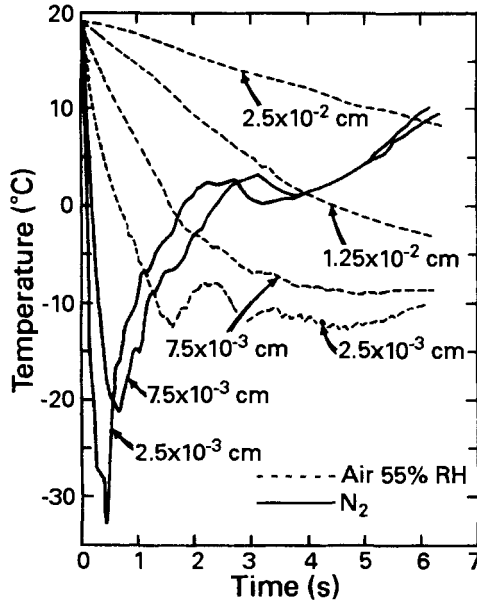


Fig. 19.2 Temperature versus time of fine thermocouples mounted in the center of a vacuum chamber and filled with either nitrogen or air. Reprinted with permission from *J. Vac. Sci. Technol. A*, 9, p. 2802, J. F. O'Hanlon and J-J. Shieh. Copyright 1991, AVS—The Science and Technology Society.

chamber, 30 cm high. The thermocouples were located in the center of the volume; 55% RH air or dry N_2 were individually pumped from atmospheric pressure. Expanding gas does work on its surroundings, cools, and then is warmed as gas-wall collisions transfer heat to the gas. The thermocouples consistently recorded the oscillations shown in Fig. 19.2, when surrounded by air. This was due to the formation of an insulating ice layer on the couples, and turbulent convection currents. Early particle counting measurement suggested that the particles observed during pumping from atmosphere were water droplets, which were formed while the temperature decreased [4].

During cooling, the air becomes supersaturated—that is, the relative humidity exceeds 100%—permitting one of several processes to nucleate an aerosol. Table 19.1 summarizes three critical nucleation processes described by Zhao et al. [2,5]. The presence of submicrometer dust particles will nucleate water condensation at just over 100% RH (critical saturation $S_C = 1$), whereas homogeneous condensation requires a critical saturation of $S_C = 3$ –8. These concepts were first recognized by Sir John Aiken [6] and later used by Charles T. R. Wilson in the development of his cloud chamber [7].

Table 19.1 Critical Saturation Ratio (S_C) for Given Condensation Process and Nuclei^a

Condensation Process	Condensation Nuclei	S_C
Heterogeneous	$\geq 0.1\text{--}0.002\ \mu\text{m}$	1–3
Condensation on ions (singly charged)	Negative ions	4
	Positive ions	6
Homogeneous	Molecular clusters	3–8

^a Reprinted with permission from *Thermal Dynamics and Particle Formation During Vacuum Pump-Down*, Ph.D. Dissertation, University of Minnesota, page 172. Copyright 1990, Jun Zhao.

Since water aerosol can transfer particles from the gas to the surface, it is important to develop a criterion by which supersaturation, and thus particle transport to a surface, can be avoided. This criterion uses a relationship between the initial relative humidity, critical supersaturation S_C , and the degree of isothermal behavior Z . The expression for the Zhao factor [2,5], requires knowledge of the pumping speed and chamber design.

$$Z = \frac{\tau\omega}{\xi} \tag{19.5}$$

ω is the rate of heat flow from the wall; for stainless steel walls and air at STP, $\omega = 0.0673\ \text{m/s}$ [5]. τ is the usual chamber time constant V/S (s). $\xi = V/A$ the chamber volume-to-surface ratio, is given here in units of meters.

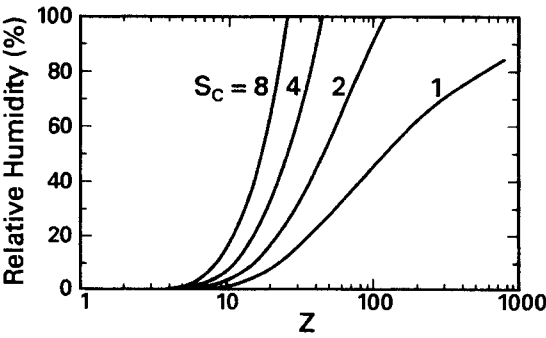


Fig. 19.3 Relationship between relative humidity, critical saturation ratio and the degree to which the chamber is isothermal or adiabatic. An aerosol will not be formed if the intersection of RH and Z lies to the right of a given saturation curve. Reprinted with permission from *Thermal Dynamics and Particle Formation During Vacuum Pump-Down*, Ph.D. Dissertation, University of Minnesota, page 138. Copyright 1990, Jun Zhao.

Figure 19.3 describes the relationship between these variables. It illustrates how the Zhao factor can be used to design an aerosol-free pumping process. First, one must know the initial relative humidity in the chamber to be pumped. Second, one assumes a nucleation mechanism, typically, this is the presence of ultrafine particles on which water can heterogeneously nucleate (the $S_C = 1$ curve in Fig. 19.3). Next, one projects the intersection of the relative humidity and the $S_C = 1$ curve to the horizontal axis and determines the minimum Zhao factor. To prevent heterogeneous nucleation, Z must be greater than the minimum value. If the chamber is known to be free of particles greater than 2- μ m diameter, then negative ions could nucleate particles and one should use the $S_C = 4$ curve to prevent nucleation on ions. (This is the basis of the Wilson Cloud Chamber.)

Zhao's method provides a simple, direct way for designing a chamber and rough pumping speed combination, which will not produce aerosol-induced contamination during initial exhaust from atmosphere. If the chamber design is fixed, reducing the pumping speed may prevent aerosol formation—a process referred to as “soft roughing,” or “slow roughing.” One technique for reducing the roughing speed is based on a valve that opens in two steps. When opened the first step, the roughing begins at a reduced pumping speed. At a reduced pressure, say 0.1 atmosphere, the valve opens completely. This scheme may also be implemented with two valves: one that is the diameter of the roughing line connected in parallel with a small valve containing a choke. Another technique used a valve control algorithm that calculated the critical condensation parameters in real time; the pump throttle valve could then be opened dynamically [9]. This algorithm provided an optimally short roughing time.

If slow roughing adversely affects product throughput, other solutions may be considered. For example, one might purge the chamber with nitrogen to reduce the initial relative humidity; however, low-dew-point N_2 must be used. One might locate the critical surfaces a few millimeters from a chamber wall, such that the conditions of the local volume between the surface and wall met the Zhao criterion. It has been shown that the gas between closely stacked silicon wafers could be exhausted radially at high speed without formation of an aerosol over the wafer surface [8].

19.2 CROSSOVER

System crossover—the point at which the roughing phase is ended and high vacuum phase commences—has been the subject of much oversimplification. The reason for this is straightforward; historically, the overwhelming majority of vacuum systems have been small, say, a volume of a 0.1–.5 m^3 , with a 4-cm-diameter roughing line. Many texts, including

earlier editions of this work, stated that one should not rough a chamber with an oil-sealed mechanical pump below a pressure of circa 10–15 Pa (100–150 mTorr), otherwise oil backstreaming would contaminate the chamber. In reality, there are two criteria that must be met to determine an acceptable crossover. (1): The crossover pressure must be above the pressure at which back-diffusing contaminants from an oil-sealed roughing pump could reach the chamber. (2): The pressure must be below the value at which the high vacuum pump would overload when connected to the chamber gas load. For the prototypical “small” vacuum system, the “100-mTorr rule” is valid, because at that pressure the chamber gas flow or quantity is less than the overload condition of the high vacuum pump.

Widespread use of large vacuum systems in myriad manufacturing applications such as semiconductors, coated paper and plastic films, security, decorative, and architectural glass coating, as well as the introduction of new types of roughing and high vacuum pumps has rendered the “100-mTorr rule” meaningless. Small diffusion-pumped systems are no longer the norm.

Here we review the two relevant issues: oil backstreaming from oil-sealed roughing pumps and the operating condition or property that defines when a diffusion, turbomolecular, cryogenic, or ion pump is overloaded. The physical principle that defines overload is not the same for all pumps.

19.2.1 Oil Backstreaming

Oil backstreaming defines the minimum crossover pressure of an oil-sealed backing pump. Backstreaming of oil vapor been well-studied [10–13]. In one case the backstreaming of oil through a 30-cm-long \times 25-mm-diameter roughing line connected to a 4.5-m³/h rotary vane mechanical pump was found to be small ($\sim 10^{-4}$ mg/min) at high pressures because of the viscous flushing action of the flowing air. At pressures below approximately 15 Pa the viscous flushing action was diminished until at a pressure of 1.3 Pa the backstreaming was 7×10^{-3} mg/min, or 70 times greater than at high pressures [11]. Experimental data for a 9-cm-diameter \times 220-cm-long pipe attached to an oil-sealed mechanical pump are illustrated in Fig. 19.4.

The counterflow diffusion rate of the oil vapor is dependent on a number of variables including the gas flow rate, pressure, pipe diameter, mass of the exhaust gas and, most neglected, the roughing pipe length. Horikoshi and Yamaguchi [12] quantified the back diffusion of molecular contaminants from an oil-sealed pump. They model the backstreamed concentration in the pipe as

$$\frac{N_I(x)}{N_I(0)} = e^{-\frac{x}{L_D}} \quad (19.6)$$

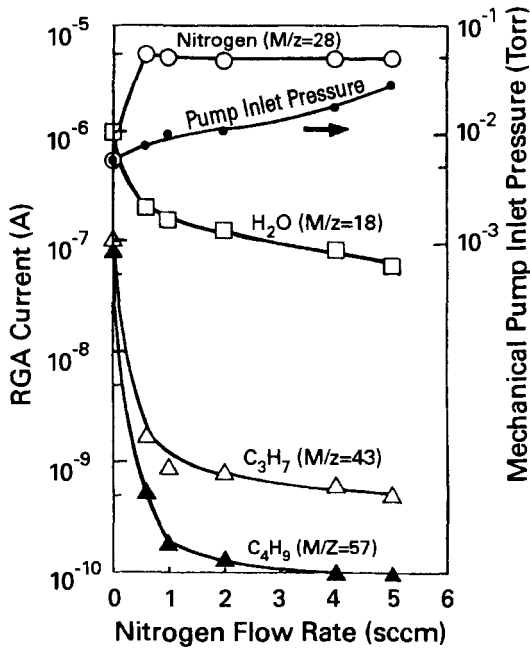


Fig. 19.4 Relation between partial pressures of backstreamed residual gases and the flow rate of nitrogen purge gas. Pipe length = 220 cm, pipe diameter = 9 cm. Reprinted with permission from *J. Vac. Sci. Technology A*, **8**, p. 2764, Y. Tsutsumi, S. Ueda, M. Ikegawa, and J. Kobayashi. Copyright 1990, AVS—The Science and Technology Society.

$N_I(x)$ and $N_I(0)$ are, respectively, the impurity concentrations at distances x and 0 from the pump. L_D is the impurity back diffusion length [12] given by

$$L_D = \frac{D_I \left[1 + \left(\frac{M_I}{M_I + M_G} \right)^N \right] + ND_{I-G}}{Nv_G \left[1 - \left(\frac{M_I}{M_I + M_G} \right)^N \right]} \quad (19.7)$$

D_I and D_{I-G} are the diffusion constants of the impurity molecule, respectively, when its mean free path is greater than the pipe diameter (2.30) and when the carrier gas is in viscous flow (2.35). $N = \lambda_{\text{mol}}/\lambda_{\text{visc}}$, and v_G is the average carrier gas velocity. Figure 19.5 sketches the fraction of a model impurity that would backstream in a 5.4-cm-diameter (2-in.) pipe connected to a 0.008 m³/s (17 cfm) pipe as a function of its internal pressure and length. Argon was used as the model impurity, as it is close in mass to the $M/z=39$ oil fragment; nitrogen was used as the carrier gas. These conditions and a pipe length of 0.5-to-1 m length represent those of the

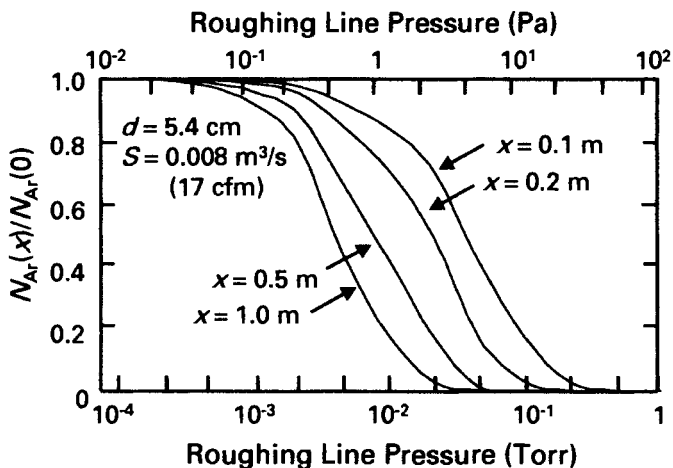


Fig. 19.5 Concentration of a model impurity, argon, counterflowing against a N_2 flow using a relation developed by Horikoshi and Yamaguchi [12].

prototypical “small” vacuum system. The model demonstrates that such a system does not backstream oil when rough pumping is limited to pressures >10 – 15 Pa (100 – 150 mTorr). Note that this model does not account for surface migration. That can be reduced by lining a section of the pipe with a material such as Teflon, which is not wet by mineral oil.

Contamination from the roughing pump may be further reduced by use of a liquid nitrogen [14] or ambient temperature trap and low-vapor-pressure oil. The liquid nitrogen trap with closely spaced surfaces is the most effective, but the most difficult to maintain and consequently infrequently used. Ambient temperature traps do not require constant refrigeration but eventually saturate. Zeolite [15,16], alumina [16–18], and bronze or copper wool have been used for this purpose. Water vapor will soon saturate a Zeolite trap [11,19] and slow the roughing cycle. Zeolite traps can remove more than 99% of the contamination [15], but they generate particles that can drift into valve seats and into the pump and hasten wear. Kendall [20] designed a thermoelectrically cooled (-40°C) zeolite trap, which included a bypass valve to avoid water vapor saturation during the initial portion of the pumping cycle. Catalytic traps [22], which operate on the principle of oxidation and reduction of copper oxide, have been developed [21,22]. Hydrocarbons were oxidized to CO_2 and H_2O in a heated catalyst. The catalyst was regenerated on exposure to air. All traps except LN_2 -cooled traps saturate. Experience has shown that traps are inadequately maintained and provide a false sense of protection.

Santeler [23] developed a gas purge technique to prevent mechanical pump vapors from contaminating a process chamber. The design is shown

in Fig. 19.6. Nitrogen or dry air is admitted to the roughing line at a point near the chamber isolation valve. The flow is adjusted so as to produce a pressure somewhat above that at which oil vapors could backstream, say 10 Pa for the example of the 54-mm-diameter pipe illustrated in Fig. 19.5. When crossover pressure is reached, the roughing valve is closed, and the preset flow prevents oil vapor back flow. Furthermore, it is impossible to pump the chamber below the set pressure.

Oil-free or “dry” roughing pumps do not have the concern of gross oil-vapor backstreaming. However, each has a distinct contamination issue with which to deal. For example, scroll pump users often add a 0.02- μm particle filter in the roughing line at the scroll pump entrance.

19.2.2 Overload Criteria

The crossover condition for a displacement pump is determined by its maximum flow. Cryo pumps have a maximum impulsive heat load, and ion pumps have a maximum pressure above which they will not operate.

Diffusion Pumps

The maximum pressure at which a diffusion pump may be connected to a process chamber corresponds to the point where the *gas flow* from the chamber $Q = d/dt(PV)$, just equals the pump's maximum flow capacity. We noted in Chapter 12 that the rate at which energy is imparted to gas molecules is proportional to the electrical power delivered to the boiler. When the flow capacity of the pump is exceeded, the top jets will fail, because oil-gas scattering destroys the supersonic vapor stream. Continued

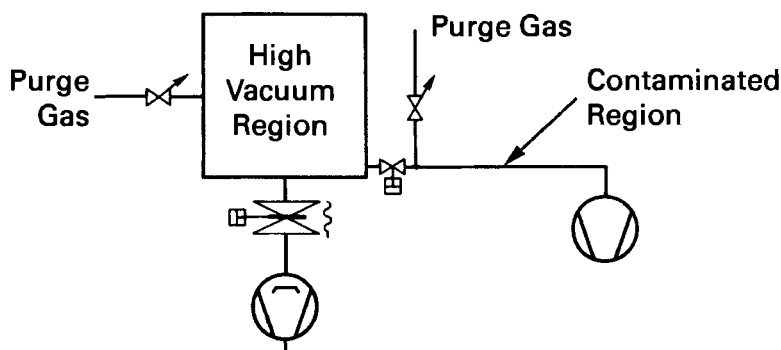


Fig. 19.6 Preventing hydrocarbon contamination from the roughing pump from reaching the process chamber by use of a purge gas. Adapted with permission from *J. Vac. Sci. Technol.*, 8, p. 299, D. J. Santeler. Copyright 1971, The American Vacuum Society.

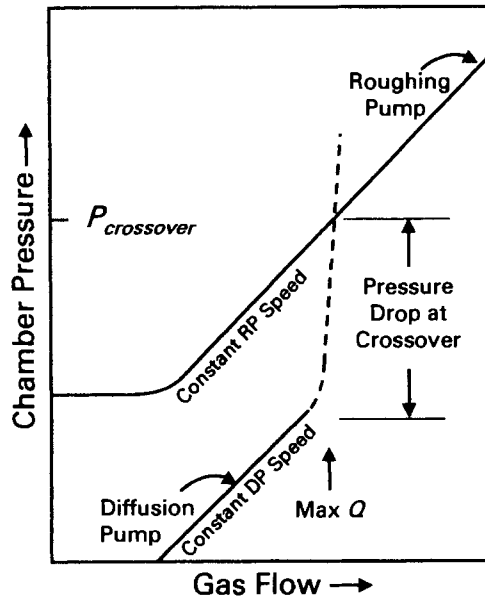


Fig. 19.7 Gas-flow-pressure characteristic of a diffusion pump and roughing pump. Adapted with permission from *J. Vac. Sci. Technol. A*, **10**, p. 2629, M. H. Hablanian. Copyright 1992, AVS—The Science and Technology Society.

increase of the inlet gas flow will cause the lower jets to fail in succession. The pressure–flow characteristics of a diffusion pump and roughing pump are shown in Fig. 19.7. Hablanian noted that the traditional pressure–speed plot masks the dependent variable [24]. The flow–pressure plot reinforces the concept that displacement pumps overload at a limiting gas flow. The sharpness of the flow–pressure behavior in the overload region is related to the safety factor that is used in the jet design. The gradual transition from under- to overloaded operation hides the fact that the top jet has failed and is backstreaming oil. It is best to crossover somewhat below the maximum gas flow (maximum throughput) provided by the pump manufacturer.

The actual gas flow from the chamber can be measured without additional metrology. Figure 19.8 illustrates the necessary measurement procedure. First, one fills the chamber with all product, substrate holders, deposition sources, and so on. Next, one pumps to an intended crossover pressure and quickly closes the roughing system valve. Last, one calculates the gas load released by the chamber $Q = V\Delta P/\Delta t$. This process is repeated for pressures above or below the first attempt until one arrives at a pressure where the loaded chamber outgassing rate is less than the maximum flow capacity of the high vacuum pump. If one knows the outgassing rates of the materials in the chamber and assumes that they are constant during the roughing cycle, the maximum crossover pressure will be

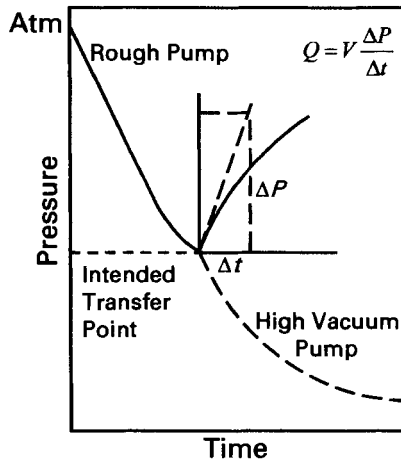


Fig. 19.8 Finding the proper crossover condition by performing a rate of rise measurement. Reprinted with permission from *J. Vac. Sci. Technol. A*, **10**, p. 2629, M. H. Hablani. Copyright 1992, AVS—The Science and Technology Society.

$$P_{crossover, max} = \frac{Q_{max}}{S_{net}} \quad (19.8)$$

where S_{net} is the actual speed of the roughing system at the chamber entrance. When closing the roughing valve and opening the high vacuum valve, the pressure should drop quickly as the ratio of the speeds of high vacuum to roughing pump

$$P_{chamber} (after\ crossover) = \frac{S_{net}}{S_{high\ vacuum}} P_{chamber} (before\ crossover) \quad (19.9)$$

If the pressure does not drop to this value immediately after crossover, then the diffusion pump is operating in its overload region [24]. In such a case, either a lower crossover pressure or a larger diffusion pump would be in order. This subject has been considered in detail by Hablani [25].

Turbomolecular Pumps

Turbomolecular pumps like diffusion pumps, are displacement pumps. They overload at a maximum *gas flow*. However, at overload they behave differently than a diffusion pump. The rotational velocity of the blades will decrease, because the power to the drive motor is constant. Power is the product of rotational velocity and torque. Nesseldreher [26] has observed

gross backstreaming of heavy oil fragments through turbomolecular pumps when their rotational velocity decreased to 40% of maximum. However, most pumps will automatically remove drive power when $\omega < 80\% \omega_{max}$.

The safe maximum crossover pressure corresponds to the maximum gas flow at which the rotational velocity ω just begins to decrease. The speed decrease will not be sudden, because momentum transfer comes from blades whose stages rotate as one. The shape of the overload region is dependent on the staging ratio, or relative sizes of the turbo and roughing pump. Figure 19.9 illustrates this dependence. One can consider the manufacturer's stated value of Q_{max} (the point at which the speed begins to decrease) to be the maximum gas flow. The maximum pressure at crossover is then given by

$$P_{crossover, max} = \frac{Q_{max}}{S_{roughing}} \tag{19.10}$$

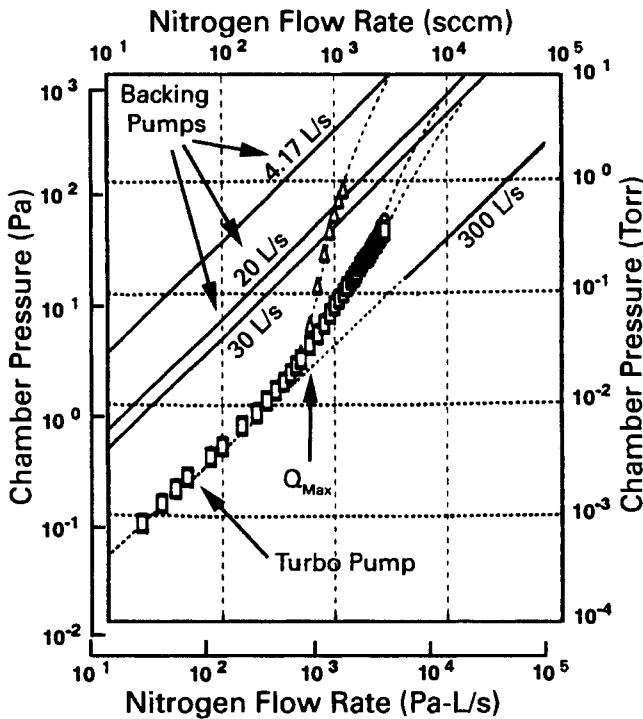


Fig. 19.9 Chamber pressure as a function of gas throughput in a 300-L/s turbomolecular pump, measured individually for backing pumps with speeds of 4.17 L/s, 20 L/s, and 30 L/s. Dotted lines represent measured data. Solid lines are constant pumping-speed lines. Reprinted with permission from *J. Vac. Sci. Technol. A*, **14**, p. 2858, N. Konishi, T. Shibata, and T. Ohmi. Copyright 1996, AVS–The Science and Technology Society.

Using the example in Fig. 19.9, one can see the effect of maximum crossover pressure on the roughing pump size. One must examine the pressure–speed performance characteristic of the roughing pump and ensure that its speed is retained at the lowest pressure—the actual crossover pressure—and not simply at the maximum crossover pressure.

Changing from an oil-sealed roughing pump to an oil-free roughing pump is of no value unless the replacement pump has adequate speed at the crossover pressure. For this reason, oil-free roughing pumps such as screw or scroll pumps are best suited for use with turbo-drag pumps and are not the best choice for use with conventional turbomolecular pumps.

Oil backstreaming of a turbomolecular pump at high values of inlet gas flow is a separate issue and is discussed in Chapter 22. Preventing foreline contamination from reaching the process chamber during power failure, when the rotational velocity decreases to zero, is described in Chapter 20.

Cryogenic Pumps

During crossover, the thermal load from the incoming gas from the chamber will cause the temperature of the two refrigerator stages to increase. The thermal load is proportional to the quantity of the gas impulse and its heat content. The heat capacity of the second (cold) stage is less than that of the first stage; it pumps everything except water vapor. Its temperature increase is a sensitive measure of pump capacity. Note the major distinction between a cryo pump and the displacement pumps discussed previously. Displacement pumps overload at a critical gas flow (Q). Cryo pumps overload at a critical instantaneous gas quantity (PV).

One recommended practice defines cryo pump crossover as the maximum quantity of nitrogen (PV)_{max} that can be condensed in a short time on the second stage of a newly regenerated cryo pump, without the second-stage temperature exceeding 20 K [27]. The relation between this maximum *impulsive heat load* (not gas flow) and the crossover pressure for small pump volumes is given by

$$P_{\text{crossover, max}} \Big|_{\text{unloaded pump}} = \frac{(PV)_{\text{max}}}{V_{\text{chamber}}} \quad (19.11)$$

Measured results for one cryo pump are presented in Fig. 19.10. The first curve in this figure, no loading, shows that this pump has a heat load capacity of $(PV)_{\text{max}} \approx 20 \text{ Pa}\cdot\text{m}^3$ (150 Torr-L). This definition applies to an “unloaded,” or freshly regenerated pump. However, in normal service, the loading increases with time; eventually, the pump must be regenerated. Figure 19.10 illustrates the effect of gas (heat) loading on the second-stage temperature behavior during successive crossovers. As the loading

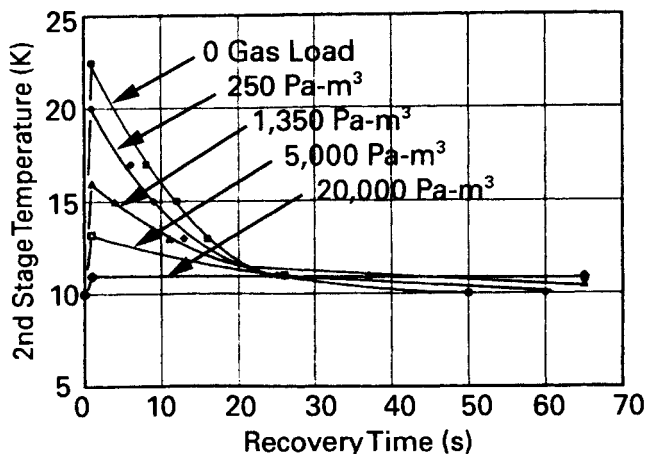


Fig. 19.10 Temperature of the cryopump second stage versus time for five different values of previously pumped nitrogen gas load on the second stage. In each case the nitrogen gas impulse load was $PV = 20 \text{ Pa}\cdot\text{m}^3$ (150 Torr-L or 200 mbar-L) of nitrogen. Reprinted from *Vacuum*, 44, C. Juhnke, H. H. Klein, S. Schreck, U. Timm, H. U. Häfner, M. Mattern-Klosson and H.-J. Mundinger, 717–719, copyright 1993, with permission from Elsevier.

increases, the peak temperature decreases, but the time to recover to base temperature increases [28]. This interrelation between recovery time and accumulated gas load affects the design of cryo-pumped, rapid-cycle load locks. If the required load lock cycle time cannot be met, then either the gas load at crossover must be reduced (reduced crossover pressure) or the refrigeration capacity of the pump must be increased (increased pump size).

The actual crossover pressure must consider the prior gas loading when the system is cycled rapidly. The variable temperature recovery time of the cold stage is a consequence of the rate at which heat in the incoming gas can be removed and transported across the accumulated ice deposit.

Bentley [29] states a rule of thumb for the maximum gas load is $PV_i/W_2 \leq 4 \text{ Pa}\cdot\text{m}^3/\text{W}$ (40 mbar-L/W or 30 Torr-L/W), where W_2 is the refrigeration capacity (watts) of the second stage. If the gas burst is too large, water vapor in the gas burst could reach the adsorbent stage during viscous or transition flow and hinder the pumping of hydrogen and helium.

Ion Pumps

Ion pump crossover must take place below a maximum *pressure*, typically $\sim 10^{-3} \text{ Pa}$. Usually, small ion-pumped systems are rough-pumped with liquid-nitrogen-cooled sorption pumps followed by TSPs. Large systems might be roughed with a turbomolecular pump. As noted in Chapter 14, a plasma will form in an ion pump, if it is ignited at a pressure greater than

$\sim 10^{-3}$ Pa. The heat released by the plasma will warm the electrodes and release adsorbed gas. This causes the pressure to increase additionally, resulting in thermal runaway and a pump that no longer functions.

The crossover-limiting criterion for an ion pump is a maximum pressure. The crossover criterion for turbo and diffusion pumps is a maximum gas flow. For a cryo pump it is maximum impulsive heat load; thus, the maximum crossover pressure of a cryo pump depends on gas heat capacity.

RERERENCES

1. J. Wu, D. W. Cooper, and R. J. Miller, *J. Vac. Sci. Technol. A*, **8**, 1961 (1990).
2. J. Zhao, B. Y. H. Liu, and T. H. Kuehn, *Solid State Techn.*, **33**, 85 (1990).
3. D. J. Santeler, D. W. Jones, D. H. Holkeboer, and F. Pagano, *Vacuum Technology and Space Simulation*, NASA SP-105, National Aeronautics and Space Administration, Washington, DC, 1966. p 80.
4. D. Chen, T. Seidel, S. E. Belinski, and S. Hackwood, *J. Vac. Sci. Technol. A*, **7**, 3105 (1989).
5. J. Zhao, *Thermodynamics and Particle Formation During Vacuum Pump-Down*, Ph.D. Dissertation, University of Minnesota, 1990.
6. John Aitken, *Proc. Royal Society Edinburgh*, **11**, 1880; *Trans. R. Soc. Edinburgh*, **30**, 1880; and *Nature*, **23**, 1880–1881.
7. C. T. R. Wilson, *Proc. R. Soc.*, **86A**, 285 (1911); *Proc. R. Soc.*, **87A**, 277 (1912).
8. J. F. O'Hanlon and J-J Shieh, *J. Vac. Sci. Technol. A*, **9**, 2802 (1991).
9. J. J. Wu, D. W. Copper, R. J. Miller, and J. E. Stern, *Microcontamination*, **8**, 27 (1990).
10. D. W. Jones and C. A. Tsonis, *J. Vac. Sci. Technol.*, **1**, 19 (1964).
11. M. A. Baker, L. Holland, and D. A. G. Stanton, *J. Vac. Sci. Technol.*, **9**, 412 (1972).
12. G. Horikoshi and H. Yamaguchi, *J. Vac. Soc. Japan*, **25**, 161 (1982).
13. Y. Tsutsumi, S. Ueda, M. Ikegawa, and J. Kobayashi, *J. Vac. Sci. Technol. A*, **8**, 2764 (1989).
14. For example, see P. M. Danielson and F. C. Mrazek, *J. Vac. Sci. Technol.*, **6**, 423 (1969).
15. M. J. Fulker, *Vacuum*, **18**, 445 (1968).
16. R. D. Craig, *Vacuum*, **20**, 139 (1970).
17. L. Holland, *Vacuum*, **21**, 45 (1971).
18. M. A. Baker and G. H. Staniforth, *Vacuum*, **18**, 17 (1968).
19. J. H. Singleton, *J. Phys. E.*, **6**, 685 (1973).
20. B. R. F. Kendall, *Vacuum*, **18**, 275 (1968).
21. R. Buhl, *Vak.-Tech.*, **30**, 166, (1981).
22. T. Kraus, F. R. G. Patent No. 1,022,349, Aug. 28, 1956.
23. D. J. Santeler, *J. Vac. Sci. Technol.*, **8**, 299 (1971).
24. M. H. Hablanian, *J. Vac. Sci. Technol. A*, **10**, 2629 (1992).
25. M. H. Hablanian, *High Vacuum Technology: A Practical Guide*, 2nd ed., Marcel Dekker, New York, 1997. Chapter 10.
26. W. Nesseldeher, *Vacuum*, **26**, 281 (1976).
27. PNEUROP: Vacuum Pumps, Acceptance Specifications, Refrigerator Cooled Cryopumps, Part 5, PNRASRCC/5. Frankfurt (1989).
28. C. Juhnke, H. H. Klein, S. Schreck, U. Thimm, H. U. Häfner, M. Mattern-Klosson, and H-J. Mundinger, *Vacuum*, **44**, 717 (1993).
29. P. D. Bentley, *Vacuum*, **30**, 145 (1980).

PROBLEMS

- 19.1 Examine Fig. 10.9, curves C and D, which describe the pressure–speed dependence of a Roots-rotary pump set. Assume that this pump set is connected to a chamber of volume 5 m^3 with a total outgassing rate (walls plus product load) of 100 Pa-L/s . Assume that all pumping lines have a large diameter, are short, and do not significantly reduce the speed of the pump set. Model the pumping speed of the set as two constant-speed segments. One segment from atmosphere until the Roots pump starts and a second for the Roots pump. (a) Calculate and plot the chamber pressure versus pumping time from atmosphere to a final pressure of 1 Pa . (b) Graphically determine the inlet pressure of the rotary pump at the point where the chamber pressure equals 1 Pa .
- 19.2 The nitrogen gas purge technique is illustrated in Fig. 19.6. Assume the mechanical pump has a pumping speed of 17 cfm , and the chamber has a volume of 0.8 m^3 . (a) Calculate the required flow of purge gas. (b) Calculate and plot the chamber pressure versus time from atmosphere to 10 Pa .
- 19.3 A diffusion pumped system consists of a 1-m^3 chamber remotely connected to a 100 cfm roughing pump by a 10-m-long , 100-mm-diameter roughing line. The outgassing rate in the chamber was 2.4 Torr-L/s (mainly water vapor from the product) at maximum crossover pressure. The diffusion pump has a limiting or maximum throughput of 3 Torr-L/s . Assume that the pumping speed of the two-stage mechanical pump is constant for the pressure range of interest. (a) Calculate the time to pump to the maximum crossover pressure. (b) With time, debris collects in the chamber, and increases the outgassing to 4 Torr-L/s . Assume that the initially measured outgassing rate had a time dependence of t^{-1} . Assume the value of 4 Torr-L applied at the initial crossover time calculated in (a). How much longer would the roughing have to operate before reaching maximum crossover pressure?
- 19.4 When crossing over from rough to high vacuum pumping, the pressure in a small chamber will suddenly drop from $\sim 10 \text{ Pa}$ to 10^{-2} Pa when the gate valve is opened. The sudden drop is due mainly to the large pumping speed of the high vacuum pump and, to a small extent, the pressure divider effect of the evacuated volume between the gate valve and the pump entrance. (a) Show qualitatively that a water aerosol can form in the chamber during that brief instant. (b) How did early researchers observe this event?

- 19.5 Figure 19.9 illustrates the measured performance of a 300 L/s turbomolecular pump connected individually to one of three backing pumps. From this graphical data, determine the maximum permissible crossover pressure so that the turbo pump does not overload for mechanical pumps of (a) 4.17 L/s, (b) 20 L/s, (c) 30 L/s.
- 19.6 Assuming that the chamber in Problem 19.3 forms a water aerosol during roughing, comment on the suitability of attempting to reduce the relative humidity in the chamber using nitrogen gas to flush water vapor from the chamber prior to beginning the roughing cycle.
- 19.7 Determine whether a water aerosol will form when the chamber of Problem 19.2 is pumped from atmosphere if the R.H. is 50%. (a) If a water aerosol were found to form, what initial pumping speed would be required to prevent its formation? (b) Alternatively, would flushing the chamber with nitrogen gas be able to reduce the initial relative humidity sufficiently, so that the chamber could be pumped at the same rate?

Pressure dividers are used in some large, specialized vacuum systems to reduce pumping time and increase product throughput and economics. The roughing system, shown in Fig. 19.11, is part of an architectural glass coating system, and is used for Problems 19.8–19.10.

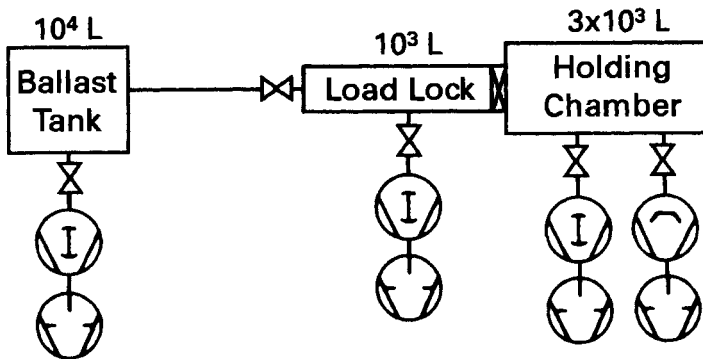


Fig. 19.11

- 19.8 The large ballast tank is first pumped to 6600 Pa (50 Torr). Load lock pumping begins by opening the connecting valve between the ballast tank and the load lock. At this time, the pressure in the lock suddenly drops to an intermediate value. (a) Assuming that the load lock was initially at atmospheric pressure, calculate the intermediate pressure after opening the connecting valve. (The holding tank pass-

- through valve is closed.) (b) The ballast tank valve is then closed and the load lock pumped to a pressure of 13 Pa (100 mTorr) using only the pump set directly attached to the lock. The roughing valve connecting the pump to the lock is next closed and the isolation valve between the lock and the holding chamber is opened. Assuming that the pressure in the holding chamber was 10^{-3} Pa before opening the isolation valve, what is the pressure immediately after the isolation valve is opened, while product is being transferred from the load lock to the holding chamber? (c) If the holding chamber diffusion pump will overload at a gas flow corresponding to 4.7 Pa (35 mTorr), is the pressure reduced sufficiently with the pressure divider effect so that the diffusion pump can be operated without overloading?
- 19.9 This system would not be efficient unless it operated on a rapid cycle. In order for the cycle time to be maintained, each pressure-dividing chamber must be repumped to its original pressure quickly. (a) After the ballast tank has been used, it must be pumped again to its starting pressure of 6600 Pa in 20 s to be ready for the next product cycle. What ballast tank pumping speed is required? (b) After the load lock reaches the intermediate pressure, it must be pumped quickly to 13 Pa (100 mTorr) using the load lock pump set. What pumping speed is required of the load lock pump set, if this is to be done in 8 s?
- 19.10 Rapidly pumping a large chamber may generate a water aerosol. The importance, if any, of water aerosol formation would depend on the nature of the product. Assume for this system a 3-m-long roughing line of 200-mm diameter. Assume that the length and width of the load lock are equal and its internal height is 125-mm. Assume the total internal surface area is $2\times$ the wall area and 50% R.H. (a) Estimate the initial pumping speed of the load lock when it is first connected to the ballast tank. *Hint:* Use the method of Santeler described in Section 3.3.3 to deal with choked flow in a roughing line. (b) Estimate the degree of aerosol formation, based on where this falls on Zhao's saturation curves, assuming nucleation begins on dust particles. (c) For economic reasons the pumping speed and product throughput cannot be reduced. What other options may be realistically considered to reduce water aerosol formation the load lock, assuming that the product consists of very-large-area (~ 100 -in wide \times 144-in. long) glass sheets?

Systems

This group of six chapters focuses on three types of vacuum system used in a number of low- and high-technology industries: systems that will pump to the high and ultrahigh vacuum range, as well as systems that will pump a large gas flow in the medium and low vacuum ranges. One way of viewing these systems is to observe that the end use places emphasis on different facets of the technology. Rough vacuum systems, described in Chapter 19, are used in low-technology applications as well as for load locks in medium- and high-technology applications. In single-chamber high vacuum systems discussed in Chapter 20, large process gas loads and the need for line-of-sight motion of molecules from the hearth to the substrates of batch processes are paramount in determining pumping configuration and chamber design.

The ultraclean vacuum systems described in Chapter 21 are used to keep surfaces free of monomolecular layers of gas contaminants for long periods. The achievement of ultrahigh vacuum pressures is dependent on the careful selection of materials, joining and cleaning techniques, and the choice of pump. Ultraclean vacuum systems have found their way into production lines, as the need for dense, defect-free semiconductor chips and read-write recording heads demanded improvements in processing purity.

The systems described in Chapter 22 are used when high gas flows are required. Because the gas-flow-pressure range is outside that of high vacuum systems, they are throttled or, in some cases, replaced by mechanical pumping systems. These systems, along with some ultraclean systems, often form a single chamber on one of the multichamber systems described in Chapter 23. High-volume production processes, which require near-ultrahigh vacuum conditions, are performed in complex, multichamber systems. These systems provide an ultraclean environment for processing rigid and flexible substrates in random or serial processes sequence.

Chapter 24 reviews the elements of leak detection. Although the leak detector is primarily a measuring instrument, it is used in conjunction with completed systems more than in testing individual components. Its mode of operation is dependent on the pumping system.

CHAPTER 20

High Vacuum Systems

Single-chamber systems capable of producing a high vacuum environment are used for a variety of applications such as the evaporation and condensation of materials to produce thin films. High vacuum pumping packages reviewed in this chapter encompass those that will produce a base pressure of an order of 10^{-6} Pa (10^{-8} Torr), and a process pressure $<10^{-4}$ Pa (10^{-6} Torr). The base pressure of such a system is determined by its pumping speed and chamber outgassing. The pressure will be higher during the process because of the gas load evolved from the source and other heated surfaces. The pumping packages used on high vacuum chambers must have a high enough pumping speed not only to reach the base pressure, but also to maintain the process pressure as well. In addition, systems that are used for production applications should be able to reach this base pressure quickly. These pump packages must pump water rapidly, because it is the most component to remove from an air.

In this chapter we discuss systems with these objectives in mind. We describe the operation of diffusion, turbomolecular, ion, and cryogenic pumped systems, respectively. Included is a procedure for starting, stopping, cycling, and fault protecting each kind of pumping system. We describe problems commonly encountered when using these pumps and conclude with a discussion of high vacuum chamber issues.

20.1 DIFFUSION-PUMPED SYSTEMS

The layout of a small diffusion pumped system is shown in Fig. 20.1. Several accessory items are shown as well. Not every system has or needs all of these additional items, but we show them here to discuss placement and operation. The main parts of this system, the diffusion pump, trap, gate valve, and mechanical pump, form a common high vacuum system.

In less critical applications a water baffle is used. Hablanian [1] measured a backstreaming rate of 5×10^{-6} (mg/cm²)/min for DC-705 fluid

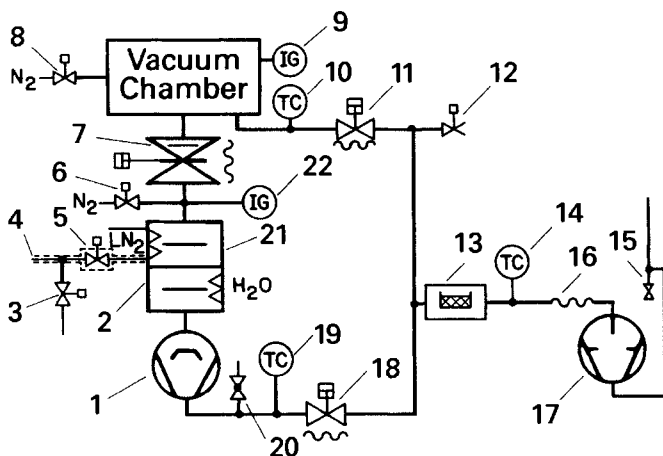


Fig. 20.1 Diffusion pump stack: (1) Diffusion pump, (2) partial water baffle, (3) LN₂ vent valve, (4) LN₂ inlet, (5) LN₂ fill valve, (6) port for gas purging diffusion pump, (7) bellows-sealed high vacuum valve, (8) chamber bleed valve, (9) chamber ionization gauge, (10) chamber thermal conductivity gauge, (11) roughing valve, (12) mechanical pump vent, (13) roughing line trap, (14) roughing line thermal conductivity gauge, (15) sump for collecting condensable vapors, (16) bellows for vibration isolation, (17) mechanical pump, (18) foreline valve, (19) foreline thermal conductivity gauge, (20) leak testing port, (21) liquid nitrogen trap, (22) diffusion pump ionization gauge.

over a 6-in. diffusion pump and simple liquid nitrogen trap. A value of 8×10^{-6} (mg/cm²)/min above a 4-in. diffusion pump baffled with a chevron cooled to 15°C may be calculated from other data [2]. For many processes a cold-water baffle will perform adequately, provided that a pentaphenyl ether or pentaphenyl silicone fluid is used in the pump. As Singleton pointed out, these two fluids are valuable in systems, which are trapped with a less-than-elegant trap [3]. The simplest way to reduce backstreaming in a low-quality system is to use a high-quality fluid.

In critical applications a liquid nitrogen trap and a water- or conduction-cooled cap are used. The liquid nitrogen reservoir is a pump for water vapor and a trap for fluid fragments. A 6-in. diffusion pump stack like the one shown in Fig. 20.1 will have a net pumping speed of 1000 L/s for air at the chamber. A matching liquid nitrogen trap can pump water vapor at speeds up to 4000 L/s. Diffusion pumps, fluids and traps of modern design are capable of reducing backstreaming rates to a level such that organic vapors from other sources may be more prevalent in the chamber.

The arrangement that is shown here for automatically filling the liquid nitrogen trap is convenient, when there is a long vacuum-jacketed supply line that must be chilled each time the trap needs filling. This does not eliminate the need for phase separation on large distribution systems.

Without this arrangement the incoming liquid boils, and the gas quickly warms the trap and releases condensed vapors. To avoid trap warming, a valve is added. When the low-level sensor is activated, the vent valve (#3 in Fig. 20.1) is opened and the warm gas is vented to the atmosphere. A second sensor is placed in the supply line near the vent valve. When cooled by the liquid, it closes the vent valve and opens the fill valve. The controller then performs its normal function. A commercial controller with two-level sense elements (low level and empty) may be modified to perform this function. If the trap is filled from a Dewar with a short length of tubing, this gas bypass operation is not required. Alternatively, we could use a tri-axial delivery pipe in which gas bubbles are automatically vented [4]. If the liquid nitrogen is pressurized when it fills the trap, it will be warmer than 77 K.

Thermal conductivity gauges are located in the work chamber and in the foreline for control and fault protection and in the roughing line to check the mechanical pump blank-off pressure. One ionization gauge is located in the chamber, or on the spool piece adjacent to it, and a second is positioned between the cold trap and the gate valve. Many systems are designed and constructed without a gauge at the latter point, however, it is extremely useful. The most straightforward diagnostic measurement on a diffusion pump is the blank-off pressure, and that measurement can be made only with a gauge located beneath the main valve. Some larger traps are fabricated with an ion gauge port; gate valves with extra piping or ports on the diffusion pump side facilitate easy mounting of the lower ion gauge tube. In general, it is advisable to install the gate valve with its seal plate facing upward to keep the valve interior under vacuum at all times. This reduces the volume and surface area exposed to the atmosphere in each cycle and minimizes the pump-down time. All gauge tubes, both ion and thermal conductivity, should be positioned with their entrances facing downward or to the side to prevent them from becoming traps for debris.

Some other items shown in Fig. 20.1 are not often needed or found on standard systems. A leak-detection port located in the foreline provides the best sensitivity and speed of response for leak detecting the chamber, trap, and diffusion pump. By use of this port a leak detector may be attached while the system is operating. A flow restriction placed on the inlet side of the diffusion pump cooling water coil will save water and increase the oil ejector stage temperature. Roughing traps are often used in diffusion pump systems and, when properly maintained, can reduce the transfer of mechanical pump oil to the chamber. In this system the trap is used as a roughing trap, to prevent mechanical pump fluid from reaching the chamber, and to prevent mechanical pump fluid from reaching the diffusion pump. If the diffusion pump did not contain a fractionating boiler, then mechanical pump oil could migrate to the chamber through the diffusion pump.

20.1.1 System Operation

Let us review the operation of a diffusion-pumped system by studying the sequence of chamber pumping and venting, along with system start-up and shutdown. Assume that the pumps are operating and that the chamber is at atmospheric pressure. The high vacuum and roughing valves are closed. During the chamber rough pumping cycle, the foreline valve is closed and the roughing valve is open. A thermal conductivity gauge, which operates a relay, senses the pressure at which crossover from rough to diffusion pumping occurs. The time constant of a 0- to 150-Pa thermocouple gauge is typically 2 s [5]. In a small system, which has a system roughing time constant much less than the gauge time constant, the pressure will reach a level less than that set on the gauge. This problem is easily corrected by adjusting the set point to a pressure higher than actually desired or by using a pressure switch with a faster time constant. The fact that the gauge reading lags the system pressure can be used as a quick check for leaks or excessive chamber outgassing. When the gauge reaches the desired crossover pressure, the roughing valve closes, the foreline valve opens; a timer usually delays the opening of the high vacuum valve. The thermal conductivity gauge will reach a pressure minimum that is below the set point and will drift upward at a rate determined by the real or virtual leak. If the pressure increases beyond the set point pressure before the timer opens the valve, the sequence may be programmed to abort. If the pressure is below the set point at the end of the timed interval, the high vacuum valve will be programmed to open. The diffusion pump and liquid nitrogen trap will then pump the system to its base pressure. The time required to reach the base pressure is a function of the speed of the diffusion pump and the liquid nitrogen trap, the chamber volume, surface area, and cleanliness. The main species is water and a liquid nitrogen trap pumps water vapor efficiently. Diffusion pumps with expanded tops and oversized liquid nitrogen traps have high pumping speeds for water vapor.

System shutdown begins by closing the high vacuum valve and warming the liquid nitrogen trap, as the diffusion pump removes the evolved gases and vapors. If the trap is allowed to equilibrate with its surroundings naturally, it will take between 4 and 10 h, depending on the trap design. This time can be shortened considerably by flushing dry nitrogen gas through the liquid nitrogen reservoir. When the trap temperature reaches 0°C, the power to the diffusion pump will be turned off. When the pump will be cooled to 50°C, the foreline valve is closed. The mechanical pump is then stopped and vented. Venting of the diffusion pump should be done with the valve located above the trap (#6 in Fig. 20.1). Valve 20 in Fig. 20.1 may be used to vent the pump, but the pump should be cooled to 50°C

or lower and venting should proceed slowly; otherwise the fluid may be forced upward. The diffusion pump should not be vented by opening the foreline valve and allowing air to flow back through the roughing trap and roughing line and into the diffusion pump because this would carry excessive mechanical pump oil vapor into the diffusion pump. Last, cooling water in the diffusion pump should be turned off. If the pump interior is exposed to ambient air when cooled below the dew point, water vapor will condense and contaminate the pump fluid.

Starting a diffusion-pumped system begins by flowing cooling water through the diffusion pump jacket and starting the mechanical pump. After the gas in the roughing line is exhausted to crossover pressure, the foreline valve may be opened and the diffusion pump heater activated. On a system operated by an automatic controller, a preset gauge performs this function. Heating time for a diffusion pump varies from 15 min for a 4-in. or 6-in. pump to 45 min for a 35-in. pump. When starting a diffusion pump, precautions may be taken to prevent the initial backstreaming transient from contaminating the region above the trap before it is cooled. This can be accomplished by precooling the trap or by gas flushing. Not all system controllers activate the liquid nitrogen trap at the same time in the starting cycle. In fact, some controllers leave this as a step to be manually controlled by the operator because a partly cooled trap is preferred when the pump begins to function.

20.1.2 Operating Concerns

The operations sketched in the preceding section did not deal in depth with some of the real and potential problems in diffusion-pumped stacks—problems such as diffusion-pump fluid backstreaming, operation of the trap, and fault protection. Let us consider these here.

Backstreaming is a subject for which many vacuum system users have a limited appreciation. Unfortunately, the definition that states backstreaming is the transfer of diffusion pump fluid from the pump to the chamber is for many a general definition. It is still incorrect when restricted to diffusion pump systems, because mechanical pump oil can be the largest organic contaminant in the work chamber. (See, for example, the mass scans associated with Problem 9.10.)

Diffusion pump fluid backstreaming is controlled by two factors: the diffusion pump, traps, and baffles and system operating procedures. Most important is that the backstreaming from both sources must be reduced to a level that can be tolerated. Methods of reducing fluid contamination from diffusion pumps were discussed in Chapter 12. The diffusion pump should use a high-quality fluid and be baffled by a water-cooled or conduction-cooled cap and a liquid nitrogen trap.

The two most important system-operation concepts for minimizing backstreaming in small systems are to stop roughing at a proper crossover pressure, and to pump through crossover as quickly as possible or use a conductance-limited high vacuum valve. The system will pump through crossover quickly, if the diffusion pump is not operating in its overload region.

The dominant gas load in all unbaked vacuum systems is water vapor. A liquid nitrogen-cooled surface will provide a high pumping speed ($14.5 \text{ L} \cdot \text{s}^{-1} \cdot \text{cm}^2$) for this gas load. The vapor pressure of water at this temperature is about 10^{-19} Pa ; therefore the pumping speed is neither a function of the operating pressure nor sensitive to small surface temperature changes of the trap. However, several gases can evaporate at low pressures or during trap temperature fluctuations. Carbon dioxide is partly condensed; its vapor pressure is 10^{-6} Pa at 77 K . Methane and CO have high vapor pressures and are not condensed. They are adsorbed to some small degree on liquid-nitrogen-cooled surfaces. Two-stage Freon-cooled refrigerators are quite useful for pumping water vapor.

Hengevoss and Huber [6] described the evolution of gases from a liquid nitrogen trap as it slowly warms. CH_4 is first, followed by CO , then CO_2 . Santeler [7] has shown that the evaporation of trapped CO_2 can be eliminated by delaying full cooling of the trap until the system pressure falls below 10^{-3} Pa or by momentarily heating the trap to $135\text{--}150 \text{ K}$ after the system pressure falls below 10^{-6} Pa . Because CO_2 is partly condensed on the trap, it can cause problems. Siebert and Omori [8] have shown how certain liquid nitrogen cooling coil designs with temperature variations of only 1 K allow the release of enough CO_2 to cause total pressure variations of 20% in a system operating in the 10^{-4}-Pa range.

In any vacuum system, faults may occur that could potentially affect equipment performance or product yield. A leak in the foreline, inadequate mechanical pump oil level, or a foreline valve failure could cause the forepressure to exceed the critical value. When the forepressure exceeds the critical value, pump fluid will backstream to the chamber. In addition, many diffusion pump system faults could cause harm to the pumping equipment. Cooling water failure or an inadequate diffusion-pump fluid level will result in excessive fluid temperatures, accompanied by decomposition of some fluids. Certain decomposition products are vapors, whereas others form tar-like substances on the jets and pump body.

Diffusion pumped systems should be equipped with sensors, which will remove power from the system or place it in a standby condition in case of loss of utilities, a leak, loss of cryogen, or loss of pump fluid. Pneumatic and solenoid valves, which leave the system in a safe position during a utility failure, are used on automatically controlled systems. When the compressed air or electrical power fails, all valves except the roughing

Table 20.1 Diffusion Pumped System Operating Concerns

Do	Do Not
Check MP oil level	Exceed DP critical forepressure
Check MP belts	Overload DP in steady state
Measure DP heater power when the system is new	Leave cooling water flowing when system is stopped
Clean roughing trap periodically	Pump O ₂ with improper fluids
Keep cold LN ₂ trap under vacuum	Rough pump in molecular flow

pump vent should close. The roughing pump vent should open to prevent mechanical pump oil from pushing upward into the roughing line. A flow meter may be installed at the outlet (not the inlet) of the diffusion pump cooling water line. The system controller uses the signal from the flow meter to close both high vacuum and foreline valves and to remove power to the diffusion pump. The use of a water filter on the inlet to the diffusion-pump cooling water line will prevent deposits from clogging the line and causing untimely repairs. A thermostatic switch mounted on the outside of the diffusion pump casing performs these tasks; a thermostatic switch mounted on the boiler can detect a low fluid level. The set points on the thermocouple or Pirani gauge controllers are used to signal an automatic controller to close the high vacuum valve in case of a chamber leak and to isolate and remove the power from a diffusion pump with excessively high forepressure. Many liquid nitrogen controllers have low-level alarm sensors, which close the high vacuum valve when the cryogen is exhausted. If not, an insulated thermo switch can be attached to the trap vent line; the boil-off keeps the vent-line temperature below 0°C. Table 20.1 lists some of the concerns with which the operator should be familiar.

This section reviewed several issues relating to the operation and fault protection of diffusion pumped systems. In many cases, diffusion-pump fluid backstreaming results from a utility failure or improper procedure. The easiest way to address these concerns is by fully automatic operation of the system. With automatic control and scheduled maintenance, complete fault protection can be provided and backstreaming minimized to a point at which it is only a small source of organic contamination.

20.2 TURBOMOLECULAR-PUMPED SYSTEMS

Turbomolecular-pumped systems are configured in two ways: with a gate valve, separate roughing line, and foreline, or as a system without valves in which the chamber is roughed through the turbomolecular pump. Figure 20.2 illustrates a system with a gate valve and a separate roughing line.

This system is much like a conventional diffusion pumped system. The entire roughing and foreline section is identical to that found in a diffusion pumped system. The criteria for sizing the forepump are similar to those of a diffusion pump. Diffusion pumps require a forepump whose speed will keep the forepressure below the critical forepressure at maximum throughput. In a turbo-pumped system a forepump of sufficient capacity should be chosen to keep the blades nearest the foreline in molecular flow or just in transition flow at maximum throughput. For classical turbo pumps without drag stages, the maximum steady-state inlet pressure P_{in} is typically 0.5–1.0 Pa and the maximum forepressure P_f is about 30 Pa. Because the throughput is constant, $P_{in}S_{in} = P_fS_f$ or

$$\frac{P_f}{P_{in}} = \frac{S_{in}}{S_f} \quad (20.1)$$

Equation (20.1) states that the staging ratio, or ratio of turbomolecular pump speed to forepump speed, S_{in}/S_f , should be in the range 30–60. A more restrictive condition is placed on forepump size for turbomolecular pumps with low hydrogen compression ratios. A staging ratio of 20:1 is necessary for pumps with maximum compression ratios for $H_2 < 500$, in order to pump H_2 with the same speed as heavy gases.

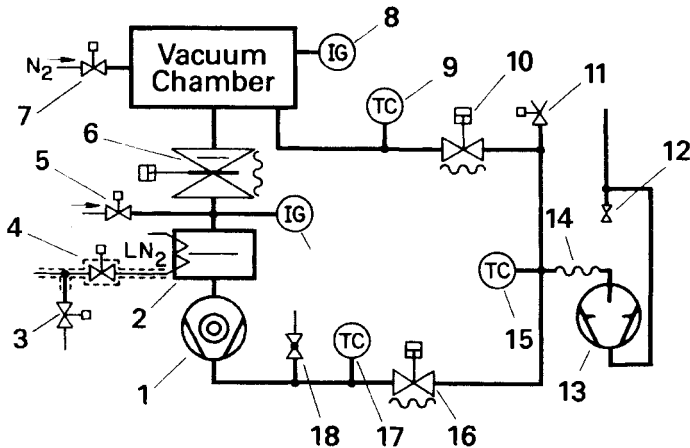


Fig. 20.2 Turbomolecular pump stack with a separate roughing line: (1) Turbomolecular pump, (2) liquid nitrogen trap, (3) LN2 vent valve, (4) LN2 fill valve, (5) turbomolecular pump vent valve, (6) bellows-sealed high vacuum valve, (7) chamber bleed valve, (8) chamber ionization gauge, (9) chamber thermal conductivity gauge, (10) roughing valve, (11) mechanical pump vent valve, (12) sump for collecting condensable vapors, (13) mechanical pump (14) bellows for vibration isolation, (15) mechanical pump thermal conductivity gauge, (16) foreline valve, (17) foreline thermal conductivity gauge, (18) leak testing port, (19) turbomolecular pump ionization gauge.

A conventional liquid nitrogen trap is not required on a turbomolecular pump to stop bearing or mechanical-pump fluid backstreaming. The compression ratios for all but hydrogen, the lightest gas, are high enough so that none will backstream from the foreline side to the high vacuum side, provided that the pump is rotating at rated angular velocity. Oil backstreaming can be eliminated by use of a magnetically levitated turbomolecular-drag pump and dry roughing pump. A liquid nitrogen-cooled surface will not trap the small amount of hydrogen found in the chamber that results from compression limits. Liquid nitrogen may be used to increase the system pumping speed for water vapor. Incorrect as it may seem on first consideration, the optimum place to locate this liquid nitrogen-cooled water vapor pump is directly over the throat of the turbomolecular pump. Alternatively, one could conceive of placing a tee behind the high vacuum valve and attaching the turbomolecular pump to one port and a liquid nitrogen-cooled surface to the other port. The conductance between any two ports of the tee is less than the conductance of a liquid nitrogen trap. A 200-mm-diameter tee, whose length is equal to its inside diameter, has an air conductance between any two ports of 1275 L/s, whereas a low-profile liquid nitrogen trap designed for a 6-in. diffusion pump has a conductance of 1700 L/s. The optimum arrangement for pumping both water and air, each at their highest speed, is a liquid nitrogen trap located between the turbo pump and the high vacuum valve, even though it may convey the erroneous impression that the trap is present to prevent gross hydrocarbon backstreaming. A Meissner trap or water cryo pump will be required in the chamber of any system that has a large water vapor load.

Figure 20.3 depicts a system without a gate valve, in which the chamber is roughed directly through the pump. Because there is no roughing line, the problems associated with roughing line contamination and improper crossover are eliminated. Physically the system becomes simpler. No high vacuum valve is needed and only one ion gauge and thermal conductivity gauge are required. This system must be completely stopped and started each time the chamber is opened to the atmosphere. This makes the use of liquid nitrogen-cooled surfaces awkward, because they must be warmed each time the system is stopped.

Roughing through the turbo pump places a size restriction on the mechanical pump, if the turbomolecular and mechanical pumps are to be started simultaneously. If the mechanical pump is small, it will not exhaust the chamber to the transition region before the turbomolecular pump reaches maximum rotational speed. When this happens, the motor over-current protection circuit will shut down the turbomolecular pump. A properly sized and operated mechanical pump will exhaust the chamber to 20–200 Pa by the time the turbomolecular pump has reached, say, 80% of

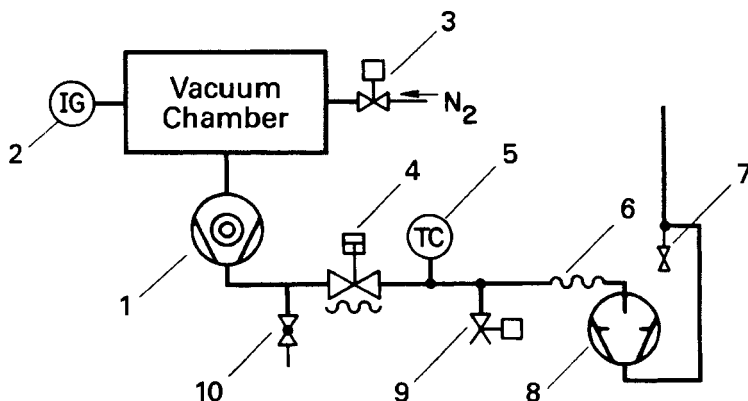


Fig. 20.3 Unvalved turbomolecular pump stack: (1) Turbo pump, (2) chamber ionization gauge, (3) chamber pump and vent valve, (4) mechanical pump isolation valve, (5) foreline and mechanical pump thermal conductivity gauge, (6) bellows for vibration isolation, (7) sump for condensable vapors, (8) mechanical pump, (9) mechanical pump vent.

its rated rotational speed and prevent the backstreaming of the mechanical pump oil. Most turbomolecular pumps are designed with an acceleration time of 5–10 min.

20.2.1 System Operation

The operation of the turbomolecular pumped system with a separate roughing line, shown in Fig. 20.2, is much like that of the diffusion pumped system described in Fig. 20.1. Before rough pumping commences, the high vacuum valve and the roughing valve are closed, while the foreline valve is open. Chamber pump-down begins by closing the foreline valve and opening the roughing valve. As in the diffusion or any other high vacuum system, the rough pumping hardware varies in complexity with chamber size. For 500-L/s or smaller turbomolecular pumps a two-stage rotary vane pump is used; turbo pumps larger than 1000 L/s use a Roots pump backed by a rotary vane pump. At crossover pressure, the roughing valve is closed, and the foreline and high vacuum valves are opened. If the turbo pump is crossed over at a flow less than the maximum throughput, the speed will drop quickly as given in (19.9). Here, as for diffusion pumped systems, the dominant species is water vapor and the pumping rate will be controlled by the speed of the liquid nitrogen trap. If no liquid nitrogen trap is used, this system will pump water vapor somewhat more slowly than an untrapped diffusion pump of the same speed. The large unbaked internal surface area of the pump adsorbs water during the early stages of the high vacuum pump-down cycle and then emits it at lower pressures.

System shutdown begins by closing the high vacuum valve and warming the liquid nitrogen trap, if used, as described in Section 20.1.1. When the trap has equilibrated, the foreline valve is closed and the power to the turbomolecular pump motor is removed. The rotor will now decelerate. Typically, it should take 10 min or more for the rotor to come to a complete stop, but if that were to happen hydrocarbons from the foreline would rapidly diffuse to the region above the pump inlet. To prevent backstreaming of mechanical pump oil vapors and turbomolecular pump lubricating-oil vapors, the pump is vented with a reverse flow of dry gas. Argon or nitrogen, for example, should be admitted at a point above the pump inlet or part way up the rotor stack when the rotor speed has decreased to approximately 50% of maximum rotational speed. The flow should continue until the pump is at atmospheric pressure. This can be properly accomplished by admitting gas through valve 5 (Fig. 20.2). Turbomolecular pumps should not be routinely loaded with atmospheric pressure gas while running at rated speed. It is not good for long-term bearing life. At any time after the foreline valve is closed, the mechanical pump system can be shut off and vented by valve 11 in Fig. 20.2—or, if so equipped, an internal pump vent. The cooling water should be promptly shut off to prevent internal condensation. Tempering the water to just above the dew point may eliminate condensation that may form on outer portions of the pump body during normal operation.

System starting begins by initiating cooling water flow, opening the foreline valve, and simultaneously starting the mechanical and turbo pumps. After the pump accelerates to rated rotational speed, typically within 5–10 min, the liquid nitrogen trap may be filled. At this point the chamber may be pumped as described in the preceding section.

Operation of the system with no gate valve, illustrated in Fig. 20.3, is considerably simplified. Operation begins by opening the cooling water and foreline valves and starting the mechanical and turbomolecular pumps simultaneously. If the rough pump has been chosen to make the chamber roughing cycle equal to the acceleration time, the system will exhaust the chamber to its base pressure without backstreaming foreline oil vapors.

This system is vented and stopped by closing the foreline valve, waiting for the rotor speed to decrease to 50% of maximum rotational speed, and admitting dry gas above the pump throat (valve 3 in Fig. 20.3). The vent valve is closed when the system reaches atmosphere or it will pressurize the chamber. The rough pump is stopped and cooling water halted.

20.2.2 Operating Concerns

Turbomolecular pumped systems share a few problems with diffusion pumped systems and present some that are unique. All are easily soluble.

Nearby amplifiers may pick up electrical or mechanical noise emanating from turbomolecular-pump power supplies. Improper connection of earth and neutral in three-phase supplies may also generate noise. Connecting the ground of each piece of equipment, including the pump, to the ground terminal on the most sensitive amplifier stage and then grounding to earth can eliminate other electrical noise. This is most efficiently done with solid copper strips. Mechanical vibration may be reduced significantly by use of bellows between the pump and chamber.

Turbo pumps must be protected against mechanical damage as well as against the loss of cooling water because the pump is a high-speed device with considerable stored energy. If a large, solid particle enters the rotor or a bearing seizes, serious damage may be done to the pump. The expense of repair could easily exceed that of scraping the varnish from a diffusion pump. Such catastrophes need not occur and do not occur if the most elementary precautions are taken. A splinter shield located at the pump throat adequately protects the rotors and stators from physical damage at some loss in pumping speed; some pumps are available with side entrance ports. Water cooling is used in oil-lubricated or grease-packed bearings. Proper cooling is necessary to remove heat from the bearings and to extend bearing life. Most pumps are manufactured with an internal cooling water thermal sensor so it is generally not necessary to add an external flow sensor. A water-flow restriction may be added to conserve cooling water. Any device with internal cooling water passages requires a clean water supply. Even though filters are used, it is advisable to reverse-flush the pump water lines once or twice a year to remove material that has passed through the filter. If the water supply is unreliable, use a recirculating water cooler. No protection is needed for loss of liquid nitrogen, because it does not serve a protective function; it pumps water vapor.

Turbomolecular pumps will give reliable trouble-free operation if the oil is changed at recommended intervals and they are protected against cooling water failure, power failure, mechanical damage, and excessive torque. This protection is easily and routinely provided with the available technology. Table 20.2 discusses proper turbomolecular pump operation.

Table 20.2 Turbomolecular-Pumped System Operating Concerns

Do	Do Not
Periodically change fluids, if not using dry or levitated pumps	Use undersized forepump
Vent MP to outside exhaust.	Vent cold LN ₂ trap to air
Vent TMP from high vacuum side	Flow cooling water when vented
Keep fore chamber of standard turbo in molecular flow	Run TMP without cooling water fault protection
Check MP oil level	Stop TMP while under vacuum
Check MP belts	Run TMP below maximum rotational speed

20.3 ION-PUMPED SYSTEMS

The sputter-ion pump is the most common of all ion pumps; it is used with a titanium sublimation pump and liquid nitrogen cryo baffle to form a high vacuum-pumping package that is easy to operate and free of heavy hydrocarbon contamination. Invariably it uses a sorption-pumped roughing module that is also free of hydrocarbons.

A typical, small, sputter-ion-pumped system is shown in Fig. 20.4. The TSP and cryocondensation surface may be in the chamber on which sputter-ion pump modules are peripherally located or they may be in separate units as sketched here. Titanium is most effectively sublimed on a water-cooled rather than a liquid nitrogen-cooled surface in a system that is frequently vented to atmosphere. If liquid nitrogen cooling were used, the film on the cooled surface would be composed of alternate layers of titanium compounds and water vapor. Because water vapor is the dominant condensable vapor in rapid-cycle systems, titanium flaking and pressure bursts would frequently result. In frequently cycled systems it is best to separate the two functions and condense water vapor on a liquid nitrogen-cooled surface and titanium on a water-cooled surface.

A two- or three-stage sorption pump is used to rough the system. Alternatively, a gas aspirator, scroll, or carbon vane pump may be used to exhaust the chamber to about 15,000 Pa before sorption pumping. Scroll pumps often require inlet particle filters to prevent backstreaming of particles to the chamber. The gas aspirator requires a high mass flow of nitrogen at high pressure and is noisier and less practical than a carbon vane or scroll pump. Neither pre-roughing pump is necessary, but their use does allow additional sorption cycles between sorption pump bakes. High-capacity modules equivalent to about 10–15 small pumps (10-cm diameter, 25-cm high) are available for roughing large volumes.

If the system is to be cycled frequently, a gate valve should be installed between the high vacuum pumps and the chamber to minimize operation of the ion pump at high pressures. An ion gauge is not needed on the pump side of the gate valve because the ion current is a measure of pressure. A gas-release valve is provided for chamber release to atmosphere. Nitrogen is used for this function because it is easily pumped by the sorption and ion pumps.

20.3.1 System Operation

Evacuation of a small, sputter-ion-pumped chamber begins with sorption pump chilling. Small commercial pumps will equilibrate in 15 min; a cooling time of 30 min is not unreasonable. If the sorption pumps have been saturated by prior use, they must be baked at a temperature of 250°C

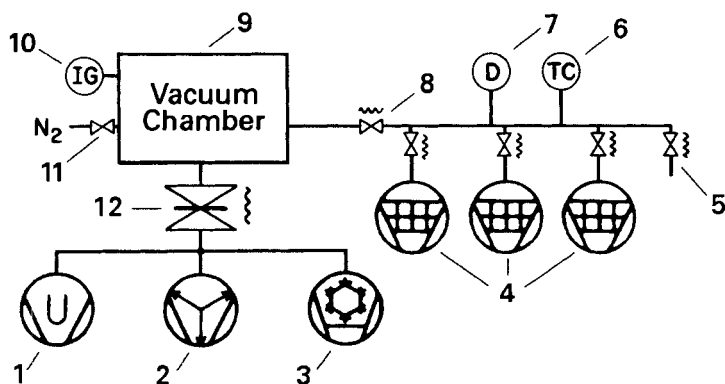


Fig. 20.4 Components of a small sputter-ion-pumped system: (1) Titanium sublimation pump, (2) sputter-ion pump, (3) liquid nitrogen-cooled array for pumping condensable gases, (4) sorption roughing pumps. (5) port for the attachment of a gas aspirator, carbon vane, or scroll roughing pump, (6) thermocouple gauge, (7) diaphragm gauge, (8) roughing valve, (9) work chamber, (10) ionization gauge, (11) chamber release valve, (12) high vacuum valve.

for at least 5 h before they are ready to chill. Pumping on a sorption pump with an oil-sealed mechanical pump is not a good way to speed its regeneration, because oil vapors would backstream and contaminate the sieve. This would permanently destroy the sorption pump sieve. The first stage of a two-stage pump manifold is used to rough to 1000 Pa; the pump is then quickly isolated from the manifold and the second stage is used to pump to 0.4–0.2 Pa. If a three-stage manifold is used, a pressure of 3000–5000 Pa is obtained in the first stage, 15 Pa in the second, and 0.1 Pa in the third. Staged pumping traps the neon that entered the first stage in viscous flow and also reduces the quantity of gas to be pumped by the last stage. Both effects reduce the ultimate pressure. At a pressure of ~ 0.5 Pa continuous sublimation may begin. The sputter-ion pump is started when the chamber pressure reaches 0.05 Pa. The roughing line can be isolated from the system, if the chamber and pump are clean. When the ion pump voltage increases to about 2000 V, its pumping speed will rapidly increase until it reaches its maximum value at about 10^{-3} Pa. Below 10^{-5} Pa, continuous operation of the TSP is not necessary because the sublimation rate of the titanium exceeds the gas flux. As the system pressure decreases, the interval between successive titanium depositions may be increased. When the layer is saturated, the pressure will rise as explained in Fig. 14.4. Timing circuits are available to control the sublimation time and interval between depositions.

A sputter-ion pump, which has been exposed to atmosphere before its operation, will not pump gas as quickly as if it were clean and under

vacuum. Operation of a system previously exposed to air begins with chilling the sorption pumps and water cooling the TSP surfaces. The sorption pumps and TSP are used to rough as described for an operating system. When the sputter-ion pump is started, the system pressure will rise because of electrode outgassing. The solution is to continue pumping with the sorption and TSP until the outgassing load is reduced. If the outgassing is not reduced in a short time, power to the ion pump should be removed to avoid overheating. The outgassing should be reduced, after starting and stopping the sputter-ion pump power supply for a few 5-min cycles. When the pump reaches ~ 2000 V, the roughing line may be isolated from the system and normal operation resumed.

An ion pump is the easiest pump to stop. The high vacuum valve, if any, is closed and the power to the ion pump is removed. The entire system may remain under vacuum until it is needed again. The TSP cooling water should be disconnected if the system is to be vented to atmosphere to prevent condensation on the interior of the system.

20.3.2 Operating Concerns

One advantage of an ion pump is that no fault-protection equipment is needed to prevent damage from a utility failure. Loss of electrical power, cooling water or liquid nitrogen will not harm the pump. Pumping will simply cease, gases will be desorbed from the walls and cryo-baffle and the pressure will rise. If the pressure does not exceed 10^{-1} Pa, the pump can be restarted by applying power to the ion pump.

Of the most severe ion pump concerns is the regurgitation of previously pumped gases, in particular hydrogen. A second concern is large gas loads, which ion pumps do not pump easily. Most of the pumping above 10^{-3} Pa is done by the TSP; at that pressure, filament life is short. Because of their slow pumping speeds, ion pumps are not suited for routine, rapid-cycle use. Table 20.3 details issues relating to their proper operation.

Table 20.3 Sputter-Ion Pump Operating Concerns

Do	Do Not
Operate S-I pump below 10^{-4} Pa in steady state to extend life	Obstruct the safety vent on the sorption pump
Valve S-I pump when releasing chamber to atmosphere	Pump a large quantity of H_2 at high pressure
Clean Ti flakes when replacing filaments	Operate the pump with the high current switch in start mode
Adequately bake sorption pumps	Start the pump at high pressure
Sequentially operate sorption pumps	Leave polystyrene Dewars on pumps while baking

20.4 CRYOGENIC-PUMPED SYSTEMS

The layout of a typical cryo-pumped system driven by a helium gas refrigerator is sketched in Fig. 20.5. As in Fig. 20.1, more valves and other parts are shown than may be necessary. The system requires no forepump, and mechanical pump operation is required only during roughing. A liquid nitrogen trap is not needed for the prevention of backstreaming from the cryogenic pump, but a cryo surface, cold-water baffle, or room-temperature baffle, none of which is shown in the sketch, may be necessary in the chamber to baffle the process heat load. These baffles also reduce the overall system pumping speed. Most cryogenic pumps include a hydrogen vapor-pressure gauge for monitoring the temperature of the second stage. The coarseness of the gauge makes it difficult to read extremely low temperatures. A silicon diode or gold-germanium thermocouple is more accurate than a hydrogen vapor pressure bulb at cold stage temperatures.

20.4.1 System Operation

A roughing pump evacuates the chamber until the crossover. See Section 19.2.2, Overload Condition. At that time the roughing valve is closed and the high vacuum valve is opened. The time required to reach the system base pressure is a function of the history of the cryo pump and its radiation loading, as well as other characteristics of the chamber which affect all pumps. The chamber is cycled to atmosphere in the usual way by closing the high vacuum valve and venting with dry nitrogen gas.

System shutdown begins by closing the high vacuum valve, removing power to the compressor, and equilibrating any liquid nitrogen trap in the chamber or pump with nitrogen gas. When the pump is restarted, it should be regenerated.

20.4.2 Regeneration

The regeneration procedures, which are recommended or available within automatic controllers, make use of various techniques such as external heat, internal heat, pumping, and gas flushing. The object is to remove the captured gases from the pump after the power has been removed. Not all procedures clean the sorbent and pumping surfaces properly. For example, removing the power and warming the refrigerated surfaces will allow water vapor to transfer from the warm stage to the cold stage, and eventually to form a puddle in the bottom of the pump housing. Cryopumps contain a safety relief, but desorbed vapors should not simply be discharged through it when it opens slightly above atmospheric pressure. The regeneration gas

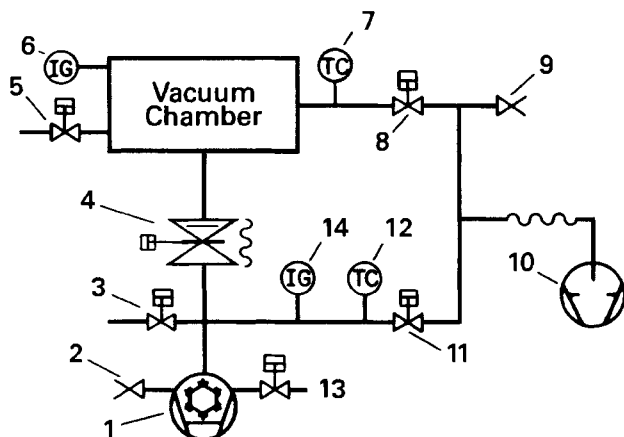


Fig. 20.5 Components of a helium gas refrigerator cryogenic pump stack: (1) Cryopumping surfaces, (2) pressure relief valve, (3) flush gas inlet valve, (4) high vacuum valve, (5) chamber vent valve, (6) ion gauge, (7) thermal conductivity gauge, (8) roughing valve, (9) mechanical pump vent, (10) mechanical pump, (11) roughing valve, (12) thermal conductivity gauge, (13) vent valve, (14) ion gauge.

load should be pumped away in a mechanical pump, but not at pressures at which oil could backstream, if oil-sealed pumps are used. Loading the charcoal with water vapor only increases the cleaning time. Procedures that advocate heating and uncontrolled mechanical pumping or flushing nitrogen 'through the pump', are to be avoided, as are partial regeneration procedures in which argon may be transferred to the charcoal. Charcoal that is loaded with argon will not pump hydrogen at high speed.

One effective procedure consists of directing warm nitrogen purge gas into the cold stage and pumping the exhaust gases with a mechanical pump. The nitrogen gas flow quantity is adjusted to a large enough value to prevent the mechanical pumping line from ever going below a pressure that could cause oil backstreaming, if an oil-sealed pump were used. It is important to remove the heat from the nitrogen purge when the elements reach room temperature or it will delay cooling [9]. It is important that the gas flow is directed at the first stage [10–11] or regeneration times will be considerably lengthened. A second effective procedure uses an electrical heater to warm the second stage charcoal array to 100 K, while room-temperature nitrogen is passed through the pump and exhausted by a pump. Upon reaching 100 K, heater power is removed and it cools to its limiting temperature [12]. Preventing argon transfer to the charcoal from the second stage condensation array, or water vapor transfer from the first stage condensation array is key to any effective regeneration procedure, lest the helium and hydrogen pumping speeds become seriously compromised.

Ice deposits will not cause frequent regeneration in pumps used expressly at high vacuum. Frequent regeneration to remove large argon ice deposits is a concern for pumps used in sputtering systems. Regeneration is required when the power fails or dips for a brief time. Momentary loss of power is a serious concern, especially if the charcoal is saturated with helium. If power is lost for a short time, the helium will be released from the sorbent and will conduct a large amount of heat from the chamber walls to the pumping surfaces. It will serve no purpose to rough the pump to 20 Pa because that is not sufficient to prevent continued conductive heat transfer. A pump will thermally overload after a burst of helium, and require complete regeneration. If power is disconnected long enough for the first stage to release water vapor the vapor will migrate to the charcoal and prevent it from pumping He or H₂, regeneration will be required. For these applications, experience has shown that the mean time between regeneration cycles is determined by external events and not by ice loading.

20.4.3 Operating Concerns

A most important concern is for the magnitude of the heat load on the first stage. In addition to the 300 K radiation from nearby chamber walls, the first stage is subject to thermal radiation from any source such as an electron beam hearth, heater lamp, or sputtering discharge. Heat loads up to 100–150 W, which are possible in many processes, easily exceed the capacity of the 35- to 40-W refrigerator stages. To reduce the incident flux on the first stage, some form of baffling is necessary. The simplest is a reflective, ambient temperature baffle. If that is insufficient, a cooled chevron array may be required. Water or liquid nitrogen may be required for baffle cooling. In many instances the manufacturer is unaware of the details of the process and so cannot provide the correct baffling. It is the user's responsibility to ensure that the process does not thermally overload the pump.

Loss of pumping by power failure or gas overload will not harm the pump. Loss of pumping will delay operation and may destroy a partially completed experiment, but it will not damage the pump. A malfunctioning overpressure relief is about the only way that damage can be done to the operator and pump.

Leaks can develop after regeneration. Charcoal dust that migrates to the O-ring seal in the overpressure relief valve is a common leak source. One may either install a 0.02- μ m-diameter particle filter before the valve, or clean the O-ring during each regeneration cycle with a dry, dust-free wipe.

Cryogenic pumps do not handle all gases equally well. The capacities for pumping helium and hydrogen are much less than for other gases. Some gases are easily pumped, but they do present safety problems.

Table 20.4 Cryogenic Pumping Concerns

Do	Do Not
Crossover at high pressure to avoid backstreaming	Obstruct safety release
Periodically change oil adsorption cartridge	Allow oil to collect on sorbent stage
Regenerate completely with gas purging	Operate an ion gauge within the pump housing
Baffle pumping arrays from heated sources	Concentrate dangerous gases
	Allow carbon dust to deposit on the relief valve O-ring

Because cryo surfaces condense vapors, they can accumulate significant deposits, which, when warmed, could react with one another or air. Some combinations can ignite, so hot filament gauges should never be connected directly to the pump body. Venting flammable or hazardous gases does not lessen the danger of an explosion or reaction. As mentioned in Chapter 15, safety overpressure relief valves are mandatory. These cryo-pump system safety hazards have been reviewed by Lessard [13]. High neutron or gamma radiation will subject polymeric parts to degradation. They are not recommended for such applications [14].

High-purity helium (99.9999%) is required to fill the compressors. Neon is the most common impurity in helium and may condense on the low-temperature stage and lead to seal wear. Table 20.4 summarizes some of the problems in cryogenic pump operation.

20.5 HIGH VACUUM CHAMBERS

All-metal high vacuum chambers are usually fabricated from TIG welded 304 or 316 stainless steel with elastomer sealed flanges. Systems with base pressure requirements of 10^{-2} – 10^{-3} Pa (10^{-4} – 10^{-5} Pa) are often fabricated from epoxy-painted cold-rolled steel. Viton is the preferred gasket material for high-quality systems because of its low permeability. Buna-N is used when cost is a factor and silicone is used in certain high-temperature applications. Any metal, glass, or ceramic whose outgassing rate and vapor pressure is adequately low can be used in the chamber, assuming that it is compatible with other materials and with the thermal cycle. The use of elastomers in the chamber should be approached with more caution. Extreme heat, as well as excited molecules from glow discharge cleaning, sputtering, or ion etching, will decompose materials like polytetrafluoroethylene. Whenever possible, alumina ceramic electrical insulators should be used. Valves with bellows and O-ring stem seals are found on high vacuum chambers. The bellows stem seal is used in locations such as

Table 20.5 General System Operating Concerns

Do	Do Not
Keep a system log; check it frequently	Vent the system with air
Record initial pumping and rate-of-rise data	Vent system while LN ₂ trap or water cryopumps are cold
Record clean RGA spectrum; compare it to later spectra	Outgas ion gauge at $P > 10^{-3}$ Pa
Use clean tools when performing maintenance	Handle fixtures without clean Nylon gloves
	Apply vacuum grease to O-rings unless absolutely necessary

the high vacuum line, foreline, and roughing line, where a vacuum exists on both sides of the seat. Both sides of this valve are leak-tight, but the stem side has a larger internal surface area than the seat side. Valves with O-ring stem seals have a high leak rate and are used only for applications like the chamber air release, where the seat side faces the vacuum. Rubber hose roughing lines or vibration isolation sections should be avoided. Rubber hose deteriorates rapidly. Some general system operating concerns are described in Table 20.5.

20.5.1 Managing Water Vapor

Water vapor alone determines the time required to reach base pressure in an unbaked chamber. This is graphically depicted in two illustrations. The first illustration, Fig. 20.6, demonstrates the relation between the quantity of water to which the inside of the chamber is exposed and the amount of water vapor that is deposited on its surface. These data show that the quantity deposited is directly proportional to the quantity to which the walls are exposed [15]. The second illustration, Fig. 4.5, describes the time required to pump away each of these individual water vapor loads. Together, these two figures clearly demonstrate something that we all know—the longer the system is exposed to atmosphere, the greater will be the time that is required to reach base pressure.

Several methods can be used to reduce the initial water vapor load and thereby minimize the pumping time. Some of these are illustrated in Table 20.6. Nitrogen purging is not nitrogen venting. They have different meanings. Venting to atmosphere with nitrogen means admitting nitrogen gas after the pump valve is closed. Purging with nitrogen means flowing nitrogen gas through the chamber to atmosphere. The effectiveness of a gas purge depends on geometry. Allowing nitrogen purge gas to flow through a chamber and exit via a small-diameter flange will reduce but not eliminate the back-diffusion of atmospheric water vapor. When open, most practical chambers expose large internal surface areas to atmosphere, so alternative

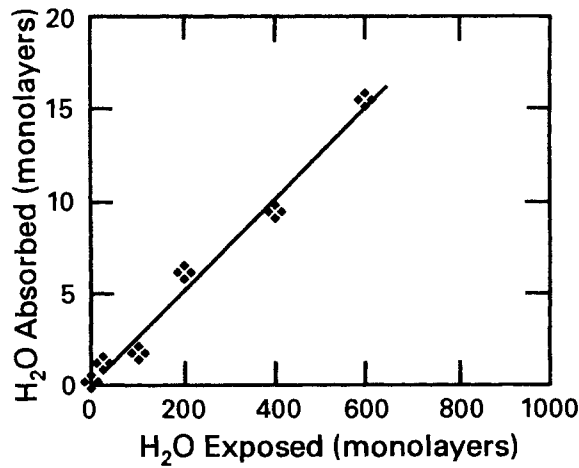


Fig. 20.6 Relation between water vapor exposure and water adsorption on a stainless steel surface. Adapted with permission from *J. Vac. Sci. Technol. A*, 11, p. 1702, M. Li and H. F. Dylla. Copyright 1993, AVS–The Science and Technology Society.

means must be pursued. Heating the exterior walls to ~40° reduces water adsorption. Reducing the time the chamber is exposed to air is the most effective procedure. One can minimize the initial water load by reducing the water vapor flux, exposure time, and adsorption probability.

Once the chamber doors are closed, the options are limited. The initial surface load of water must be removed to the level required to reach process pressure. Some processes allow for chambers to be modestly baked (75–100°C); material heating might affect other processes. Baking reduces residence times and speeds pumping. Mercury lamps can illuminate interior surfaces with photons, which are absorbed in near surface layers. Desorption produced by the light flux results from surface heating; the flux cannot illuminate all interior surfaces uniformly.

Table 20.6 Managing Water Vapor

Do	Do Not
Expose the system to air for the minimum time needed	Leave chiller pumps circulating while open for maintenance
Flush the system with dry nitrogen if this is useful	Leave water cryopumps operational, while open to air
Heat chamber surfaces, while open to atmosphere	Rough pump rapidly and create a water aerosol
Use heating lamps to provide enhanced desorption	Attempt to pump a complex chamber from one flange

REFERENCES

1. M. H. Hablanian, *J. Vac. Sci. Technol.*, **6**, 265 (1969).
2. L. Holland, *Vacuum*, **21**, 45 (1971).
3. J. H. Singleton, *J. Phys. E.*, **6**, 685 (1973).
4. Vacuum Barrier Corp., Woburn, MA 01810.
5. J. M. Benson, *Trans. 8th Natl. Vac. Symp. (1961)*, Vol. 1, Pergamon, New York, 1962, p. 489.
6. J. Hengevoss and W. K. Huber, *Vacuum*, **13**, 1 (1963).
7. D. J. Santeler, *J. Vac. Sci. Technol.*, **8**, 299 (1971).
8. J. F. Seibert and M. Omori, *J. Vac. Sci. Technol.*, **14**, 1307 (1977).
9. R. A. Scholl, *Solid State Technol.*, **187**, Dec. 1983.
10. M. Bridwell and J. G. Rodes, *J. Vac. Sci. Technol. A*, **3**, 472 (1985).
11. R. A. Longworth and G. E. Bonney, *J. Vac. Sci. Technol.*, **21**, 1022 (1982).
12. H-U. Häfner, H-H. Klein, and U. Timm, *Vacuum*, **41**, 1840 (1990).
13. P. H. Lessard, *J. Vac. Sci. Technol. A*, **8**, 2874 (1990).
14. K. M. Welch, *An Introduction to the Elements of Cryopumping*, K. M. Welch, ed., American Vacuum Society, New York, 1975. P. III-20.
15. M. Li and H. F. Dylla, *J. Vac. Sci. Technol. A*, **11**, 1702 (1993).

PROBLEMS

- 20.1 † A diffusion-pumped vacuum system uses electropneumatic valves and is operated by an automatic controller. What operations should the controller be capable of performing if each of the following accidents occurred individually while the system is operating: (a) The ionization gauge tube is carelessly broken; (b) the liquid nitrogen supply is inadvertently valved off at its source, or the dewar runs dry, (c) during an electrical storm the line voltage drops by 30% or fails completely; (d) a water main breaks; (e) the compressed air supply fails, (f) the mechanical pump belt breaks; and (g) a water cooled baffle located directly over a diffusion pump develops a massive leak as a soft-soldered joint in the baffle fails. (h) What transducers should be located on the system to sense these abnormal conditions?
- 20.2 † Chromium films are deposited in a diffusion pumped system. The procedure calls for loading the cleaned glass plates in the chamber, roughing to 2.5 Pa, closing the roughing valve, and opening the gate valve to the liquid-nitrogen-trapped 20-cm-diameter diffusion pump. The chamber is pumped to 5×10^{-5} Pa and the chrome source is outgassed, and chromium is deposited at a rate of 5 nm/s. The diffusion pump is charged with tetraphenyl trisiloxane and the mechanical pump with mineral oil. It is observed that the chromium is not adhering to the entire substrate surface. It is also observed that

- the condition is worse after the system has been opened to atmosphere for routine cleaning. Propose a solution to the problem.
- 20.3 † Water flow sensors are often used to monitor the presence of cooling water flow in turbomolecular pumps. Why should the water flow sensor be installed at the outlet rather than the inlet of a pump? What other sensor could we use instead of a flow sensor?
- 20.4 The 25-cm turbo pump has a 20-cm-diameter valve, whose thickness is 15 cm, in the line between the pump and the chamber. The valve is connected to the pump by means of a 20-cm-diameter tube 15 cm long. An engineer wants to increase the pumping speed at the chamber entrance by replacing the valve and the tube and enlarging the chamber opening so the pumping path is 25-cm-diameter in all components between chamber and pump. The manager doesn't want to spend the money. You are asked to provide a technical evaluation. What do you recommend?
- 20.5 A 10,000-L/s turbopump is connected to the 500-m³/h lobe blower and 100-m³/h rotary vane pump shown in Fig. 10.9. Is this an adequate combination to back the turbo pump for turbo inlet pressures of 0.5 Pa?
- 20.6 Carbon vane pumps are sometimes used to rough pump chambers before starting the sorption pump to reduce the load on the molecular sieve. They will pump to about 10,000 Pa. Given a 50-L chamber and a sorption pump with a capacity of 10⁷ Pa-L of air, how many cycles can we obtain from the sorption pump with and without the use of the carbon vane pump.
- 20.7 † A diffusion pumped system has been retrofitted with a helium gas cryogenic pump. Discuss any problems that might ensue.
- 20.8 A large cryogenically pumped electron-beam lithography system is being started. The steel chamber is 2 m×2 m×0.5 m. The internal surface area of the tooling contains an additional surface area of 8 m². A 3500 L/s cryogenic pump is appended directly to the chamber with a flange of ratio $l/d = 0.05$, and an internal poppet valve. The rough pumping system consists of a 100-cfm lobe blower backed by a 35-cfm rotary vane pump. In order to ensure proper cryopump operation, the pumping stages are regenerated by pumping overnight with the mechanical pump running and with the lobe blower stopped. In the morning the compressor is started. After a few hours of operation the ion gauge reads 1.7×10^{-4} Pa. A rate of rise measurement with the poppet valve closed shows the pressure to rise from 0.01 to 0.035 Pa in 100 s. The hydrogen vapor pressure

thermometer reads 14 K with the poppet valve closed and it rises to 20 K when the valve is opened. You might begin by examining the rate of rise and trying to determine whether there is a leak or this is a normal outgassing load. The operator is concerned because the cold-stage temperature is increasing when the load is applied. Is this concern legitimate?

- 20.9 A small clean stainless steel vacuum system contains a 100-L/s pump and 25 O-rings of 100-mm major diameter \times 6-mm chord diameter. Assume that a reasonable percentage of the O-ring faces the interior of the system, and calculate a typical pressure in the system after 1 h of pumping because of outgassing from the exposed O-ring surface.
- 20.10 The turbo-pumped system in use, similar to that depicted in Fig. 20.2, does not provide an adequately low hydrogen partial pressure in the process chamber. Propose solutions that would not involve replacing the turbo pump.

CHAPTER 21

Ultraclean Vacuum Systems

Treatises on vacuum technology traditionally include a section entitled “ultrahigh vacuum.” For those of us whose interest in vacuum dates to soon after the middle of the last century, that phrase connoted specific construction techniques, components, materials, and procedures, including a 450°C overnight bake. The goal was the achievement of an ultrahigh vacuum environment in which fundamental studies could be performed. Today, such pressures are required for myriad applications ranging from high-energy particle research to the manufacture of magnetic thin-film read-write heads, semiconductor, and opto-electronic devices. Systems have grown in size and complexity. In parallel, technical restrictions have limited the time available to reach ultimate pressure as well as the maximum allowed baking temperatures. Some systems can be baked only to 75–150°C, whereas others, by virtue of their size, cannot be baked at all. All these systems require base pressures in the low 10^{-8} - to 10^{-9} -Pa (10^{-10} - to 10^{-11} -Torr) range. Base pressure requirements will continue to decrease to meet advanced processing needs. Additionally, contamination caused by environmental or process-generated particles as small as 10 nm may affect product yield or the ability to do research.

The term “ultrahigh vacuum” is no longer adequate to describe the requirements demanded by the highest technology applications. Not only must the process or experimental vessel reach the classical ultrahigh vacuum pressure range, but also it be ultraclean, and it must allow translational and rotational motion, electrical power, cooling fluids, and electrical and optical instrumentation signals through its walls without adding contamination. Metrology is not simple. UHV pressure gauges and residual gas analyzers may provide incorrect information, should they be mounted or operated incorrectly; misunderstanding of electron-stimulated desorption can result in inaccurate pressure measurements. The need for distributed pumping to evacuate extremely long, narrow accelerator or beam chambers is well understood; however, the designers of complex production systems with shielded interiors do not yet appreciate that they have a similar problem.

There are many sources and types of contamination in any vacuum system. Gases can desorb from the chamber walls or evolve from a pump. We give here a modified version of a view first proposed by Santeler [1]. Figure 21.1 shows a generalized vacuum system. The total pressure in the system from vacuum chamber sources is composed of the partial pressure of each gas or vapor desorbing from the walls; it is equal to the rate of desorption of that species divided by its pumping speed.

$$P = \sum_i \frac{Q_i}{S_i} \quad \blacktriangleright (21.1)$$

Gases that back diffuse from the pump will contribute to the chamber background pressure

$$P = \sum_i \frac{Q_{pi}}{S_i} \quad (21.2)$$

The total system pressure results from all sources. It is given by

$$P = \sum_i \frac{Q_i}{S_i} + \frac{Q_{pi}}{S_i} \quad (21.3)$$

Santeler's argument states that the first term behaves normally (e.g., as the pumping speed increases, the pressure contribution decreases), but the second term does not behave in a like manner. For example, more hydrogen would backstream from a larger sputter-ion pump. If the backstreamed gas load and the pumping speed were increased in proportion, the base pressure would not change. The result would be an effectively constant base pressure P_o , for a given pump. By this argument (21.3) may be simplified to read

$$P = \sum_i \frac{Q_i}{S_i} + P_o \quad \blacktriangleright (21.4)$$

The production of ultraclean vacuum is therefore concerned with both the pump and chamber. The contamination from the chamber may be reduced by the intelligent choice of materials, fabrication techniques, and operating procedures; the gas load originating in the pump may be reduced by pump design and selection, as well as processing procedures.

This chapter discusses the roles of pumps (turbo, ion, TSP, NEG, and cryo) and chambers (design, materials, and operation) in achieving ultraclean vacuum. The chamber becomes important, because it is more effective to reduce the chamber sources than to increase S beyond certain limits. Pump choice is important, because increasing S will not decrease P_o . Pumps are selected by matching performance with application.

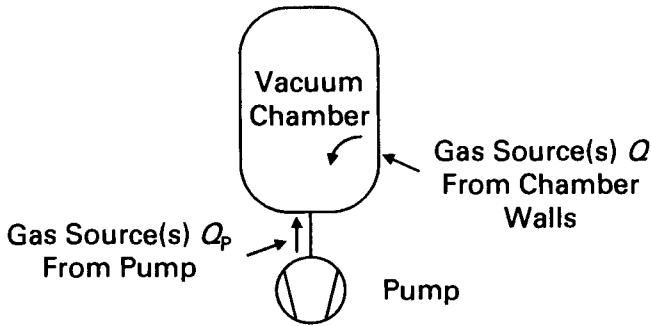


Fig. 21.1 High vacuum pumping schematic.

21.1 ULTRACLEAN PUMPS

Selection of the pumps for an ultraclean vacuum system is important. Equation (21.4) indicates that a clean vacuum pump should reduce pressure by providing high pumping speed (low Q/S) and low backstreaming (low P_o). In addition, the vacuum should be free of particulate contamination. Here backstreaming is defined as the reverse flow of any gas, vapor, or material from the pump. To reduce the contaminant levels, rigorous adherence to exacting pumping procedures is necessary. A refrigerated trap that has been warmed for only a few minutes will release condensed vapors. Although recooling will prevent further contamination, it will take time to repump the vapors that have accidentally been released, especially those that were marginally pumped on cryo surfaces.

Each pump type has its own characteristic class of gases and vapors that it will not pump and that it will generate as impurities. Each pump has its own characteristic particle source. The design and selection of pumps for ultraclean applications is done on an individual basis. There is more than one “best” solution. The remainder of this section reviews the selection and clean operation of some ultraclean configurations.

21.1.1 Turbomolecular Pumps

Turbo pumps can contribute two contaminants to the system; hydrogen and pump fluid vapors. The turbo-pump-generated hydrogen is primarily a result of the pump’s maximum compression ratio and the hydrogen partial pressure in the foreline. Turbo pumps are made with hydrogen compression ratios of 5000–15,000. Putting two turbo pumps in series can further increase the compression ratio for hydrogen. Magnetically levitated turbo pumps are required to eliminate vapors present in turbo pumps using oil-lubricated bearings. The drag stages attached to some pumps provide an

additional way of reducing the hydrogen compression limit. Oil-free scroll or four-stage diaphragm pumps can be used to back turbo-drag pumps. The ultimate pressure may vary within pumps of the same design, because of minute leaks between the stator and housing. The variation in ring-to-wall spacing could be large enough to cause variations in the ultimate pressure of the pump.

Turbomolecular pumps have a large internal surface area and consequently they must be baked, usually into an adjacent turbo pump. Unfortunately the construction of the pump is such that it is not possible to bake it much over 100°C. This bake cycle is necessary to remove the water from the interior of the stator and rotor surfaces. The roughing cycle can contaminate a turbomolecular pumped system just the same as any other system. For this reason, oil-free roughing pumps are required.

21.1.2 Cryogenic Pumps

Helium gas refrigerator pumps are able to reach the ultrahigh vacuum region required for rapid-cycle industrial processing systems. They are often augmented by large area cryo-cooled arrays designed only for pumping water vapor. Hydrogen adsorption isotherms show the greatest capacity at low temperatures. A most important consideration in reaching very low pressures is the isolation of thermal and optical radiation from the cold stage. Baffles have been designed to maximize molecular transmission and minimize photon transmission [2,3]. Gas-refrigerator-cooled pumps cannot be baked above 70–100°C because they use indium gaskets. Turbo pumps are used during the baking cycle. Cryogenic pumps easily pump large amounts of hydrogen, provided that the cold-stage temperature remains at ~20 K. They use no high voltages and generate no hydrocarbons or metal flakes. However, the displacer generates some vibration and the charcoal used on the cold stage sheds dust that can be transported to the chamber. Iwasa and Ito [4] developed a helium gas refrigerator pump using an Er_3Ni heat exchanger with which they were able to reach 3.6 K. Thus, they were able to produce a cryo pump with no dust producing charcoal. Cryo pumps must be carefully damped for use with sensitive surface-analysis equipment such as ESCA or SIMS. The Viton-sealed overpressure relief used in ordinary cryo pumps should be replaced by its single-use, stainless steel foil, knife-relief counterpart.

21.1.3 Sputter-Ion, TSP, and NEG Pumps

Long particle beam lines require distributed pumping. Distributed pumping systems have been designed using continuous strip NEG pumps, in combination with sputter-ion pumps [5]. The distributed NEG pumps

remove all except the noble gases, which are pumped by the sputter-ion pumps. Sputter-ion pumps require baking; they can be baked into the turbo pumps used for system roughing. The main background gas present in a sputter-ion pumped system at low pressures is hydrogen, but small amounts of methane ethane and carbon monoxide are observed.

When used in combination with helium gas cryo pumps, NEG pumps were shown to improve pumping speed of an unbaked chamber and reduce the base pressure of a baked system [6]. NEG pumps have also been used in combination with turbo pumps to produce enhanced pumping of hydrogen and water vapor [7]. Benvenuti et al. [8] have demonstrated that hydrogen, the dominant gas remaining at base pressure, could be pumped with higher speeds by depositing thin-film coatings of nonevaporable getter material on the system walls. Although distributed pumps are necessary to maintain high hydrogen pumping speed at low pressures, TSP have been studied [9,10]. Hydrogen pumping in TSPs is improved if the surfaces are liquid nitrogen-cooled rather than water-cooled. Odaka and Ueda [11] have demonstrated that a 1000°C bake removed large quantities of gaseous impurities from within Ti–Mo filaments. The water vapor load in an ultraclean system is much smaller than it is in an unbaked rapid-cycle system; therefore the sublimed titanium film will not entrap enough water to make titanium flaking a problem. Momose, Saeki, and Ishimaru [12] identified TiO particles generated by ion pumps; they postulated these particles were transported from insulating surfaces within the pump to the chamber by the nitrogen purge gas.

21.2 ULTRACLEAN CHAMBERS

21.2.1 Chambers Materials and Components

AISI grades 304L and 316L are the most frequently used in constructing ultraclean chambers. Stabilized grades such as 321 or 347 contain additives to reduce carbide precipitation; they are acceptable but are expensive. All joints are made by TIG welding or metal gasket flanges; O-rings are not used anywhere in the high vacuum portion of the system, including the high vacuum connection to the pump or trap. In some systems, O-rings are used for internal pass-through valves. After the initial air outdiffuses from these O-rings, they will no longer be a source of residual air contamination. They do shed particles in vast numbers, and they do release process gases from gasket compression during valve closure. See Problem 17.9.

Aluminum, processed by special extrusion or by the EX process, outgasses at the same rate as stainless steel. Ordinary aluminum is covered with a porous, hydrated aluminum oxide over 10 nm thick. This layer

becomes a source for water vapor and therefore is difficult to outgas. The special extrusion process results in a dense aluminum oxide layer of approximately 3-nm thickness; it is achieved by extruding the aluminum in an atmosphere of argon and oxygen [13]. The surface finish on large aluminum components is realized by lathe machining in a vacuum chamber filled with argon and oxygen [14,15]; the resulting oxide is identical in thickness and density to that made by special extrusion. Outgassing rates of 10^{-11} Pa-m/s (10^{-14} Torr-L/s) are achieved with these treatments [16].

High-density alumina is a stable insulator, and it is stronger than quartz or machinable glass ceramic. The properties of this and other materials are discussed in Chapter 16. Metal-to-glass or metal-to-ceramic seals should not be subjected to temperatures higher than 400°C, and sealed copper-gasket flanges should not be baked at temperatures higher than 450°C. Unsealed flanges, however, will tolerate higher temperatures. The flange and knife-edge will suffer some loss of temper during an 800–950°C bake. The exact amount depends on the grade of stainless steels (grain growth retarders) and fabrication steps used in flange construction. Most commercial copper-gasket flanges are forged from grade 304, and some contain trace additives that will retard grain growth during heat treatment. Small grain size is necessary to prevent significant loss of hardness. Not all flanges are forged in the same manner or have the same properties.

It is not recommended that parts be stored in plastic boxes or bags. Polymer storage bags contain plasticizers that readily outdiffuse; see, for example, Problem 16.10. Sulfur from rubber bands will diffuse quickly through the storage bags [17]. Aluminum foil is frequently used to cover open flange faces or to wrap cleaned parts until final assembly. Aluminum foil that has been specifically degreased for vacuum use will not contaminate the cleaned parts. Ordinary household aluminum foil will contaminate the parts with residues of the vegetable-based rolling oil [18]. Precleaned aluminum foil is commercially available.

Internal fixtures held together with screws will have gas trapped between flat surfaces and within and under screw threads. Slotted screws, which allow trapped gases to be vented, should be used within ultraclean chambers. Gold-plated screws, used to secure copper gasket sealed flanges, will prevent galling of threads. Thread galling is a problem with systems that are frequently baked at high temperatures.

Connecting electrical power, instrumentation wiring, process gases and liquids, and cooling fluids through an ultrahigh vacuum wall is not trivial. There are few techniques for accomplishing these objectives. If one requires only linear motion the welded bellows, described in Fig. 17.23a allows motion while maintaining vacuum integrity with a solid metal wall. If rotary motion is required, there are two choices. If no fluids or power are required, the magnetic follower described in Fig. 17.21 is the best solution.

A solid stainless steel interface separates vacuum from atmosphere. If cooling fluids, instrumentation, and electrical power must be provided to a rotating substrate holder, then the differentially pumped rotary motion feedthrough, illustrated in Fig. 17.19, is the only solution. Seals of the ferrofluidic type contain organic liquids that allow air permeation, and thus are not acceptable in the lowest pressure ranges of interest.

Personnel with cleanroom training must construct ultraclean chambers within clean facilities using clean assembly techniques. After pretreatment and fabrication, components, wire, hardware, subassemblies, and all assembly tools are cleaned with a 1:7 mixture of isopropyl alcohol and ultrapure water, before being moved to the assembly cleanroom. Clean tools remain within the assembly area. After assembly and testing is complete, systems are double-wrapped for customer shipment.

21.2.2 Chamber Pumping

The generic pressure–time behavior during pumping is sketched in Fig. 4.10. The volume gas is removed first, followed by surface desorption, outdiffusion from the solid, and, last, permeation through the solid wall. All of these processes except volume gas removal are greatly temperature-dependent. The dominant gas desorbing from the interior surfaces in this portion of the pumping cycle is water vapor. Water vapor will bounce, re-adsorb, and bounce again during the process of being pumped. Eventually, the molecule will reach a pump entrance, where it has a probability of being pumped. Equation (4.16) estimates the residence time of a molecule. This relation predicts that the residence time is dependent on the ratio of chamber wall area to pump entrance area. If the pump entrance area is small (low pumping speed) compared to the total internal area of the system, the residence time will be long. Figures 16.2 and 16.3 show the time dependence of the outgassing rate as the chamber is pumped from atmosphere. The rate is practically independent of surface treatment, because water vapor is the dominant surface contaminant. Multiplying the vertical axis of either of these figures by the internal surface area and dividing by the pumping speed will yield a typical pumping time. Systems are designed to pump from atmosphere to 10^{-7} – 10^{-8} Pa in a specified time, usually in the range 24–48 h.

Designers of particle-beam accelerators learned early that distributed pumping is needed to reach suitably low pressures. Locating a pump at one end of a long, low-conductance tubular chamber would not provide adequate pumping for the entire duct. For that reason these systems are constructed in the form of continuously interconnected extruded parallel tubes of cylindrical or oval cross section. Typically, NEG pumping is provided continuously, with intermittently located ion pumps.

Designers of complex processing chambers with many baffles or internal shields should consider the same concept in attempting to reach low pressures quickly. Consider the diagram in Fig. 21.2. Here we have drawn a generic chamber of rectangular cross section containing two pumps and two internal surfaces. These internal surfaces were added to simulate pumping a complex chamber. The numbers located around the interior were generated by the Monte Carlo technique and represent the number of bounces required by a molecule to reach a pump starting from that location. The number of bounces is dependent on the geometry of the chamber. If one were to install larger pumps at the existing locations, the number of bounces, and hence the time to remove molecules from the distant portion of the chamber, would be altered only marginally. Only by installing an additional pump or two in the upper chamber, can one reduce the pumping time for molecules originating in the upper chamber. Distributed pumping is required to improve the ultimate pressure and time required to reach the base pressure of processing systems containing complex and conductance-limited pumping paths.

Surface preparation methods, treatments and procedures used for reaching pressures in the 10^{-9} Pa (10^{-11}) Torr region have undergone major changes since ultrahigh vacuum pressures were routinely attainable. The original procedures for Diversey cleaning chambers fabricated from 304 stainless steel, followed by a 450°C bake during each pumping cycle, are no longer used. Baking 304L or 316L stainless steel at 800°C in a vacuum furnace is one common prefabrication treatment. Prior to this heat treatment, any surfaces subjected to grinding or similar procedures would have been machined to remove surface damage. After welding and assembly, a number of treatments may be used. One initial treatment involves baking the chamber at 200°C so as to produce an oxide layer on the system interior. After this treatment, the system may or not be baked. Some very large systems cannot be baked at all. In these systems, various

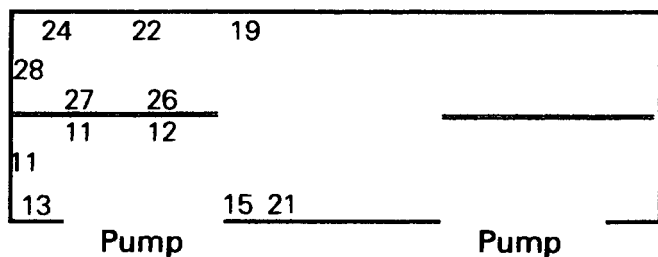


Fig. 21.2 Rectangular chamber containing arbitrary baffles and pumps. The numbers on the interior surface represent the number of bounces required by a molecule originating at that location before it reached a pump entrance.

plasma discharge treatments such as those discussed in Chapter 16 are used to remove adsorbed gases and reduce the ultimate pressure. A chamber bake in the range 75–150°C is a part of the 24- to 48-hour pumping cycle in systems that can be baked.

Unbaked areas of the system can reduce system performance. The area of the system that cannot be baked depends on the pump and the efficiency with which interior surfaces can be baked. An ion pump can be completely baked. A turbomolecular pump and a gas refrigerator cryogenic pump can be baked at approximately 100°C. With the exception of the ion pump, all have some surface that cannot be subjected to a bake at a temperature in excess of 100°C. In some cases, interior surfaces are not completely baked. Consider again the illustration of Fig. 21.2. If the surfaces inside the chamber—shown as a double line—could not be baked, then the residence time of molecules that stick would be significantly longer than the residence time of molecules on the heated surface. Monte Carlo analyses of several chamber configurations show that molecules bounce from heated and unheated surfaces in roughly the proportion of the heated-to-unheated surface area ratio. Since residence time is exponentially reduced with increasing temperature, complete baking of interior surfaces is desirable. UV lamps have been used to assist in this goal. However, they are most useful in applications where large line-of-sight areas can be illuminated.

It was commonly thought that CO and H₂ were the predominant residual gases found in all ultrahigh vacuum systems. The data presented in Fig. 5.15 confirm that CO is an artifact of the hot filament gauge. Hydrogen is the dominant gas remaining at ultrahigh vacuum pressures. The source of this remaining hydrogen outgassing has been the subject of considerable research. Hydrogen is soluble in many metals. Bills [19] noted that there was insufficient atmospheric hydrogen to account for permeation through the bulk of a stainless steel wall, but that other sources, such as the dissociation of water on the chamber exterior, could provide an adequate diffusion source. Redhead [20] has reviewed the status of hydrogen outgassing in ultrahigh vacuum region. In Section 16.3.1 we discussed the diffusion model [21], which assumed hydrogen of one activation energy permeated by a diffusion limited step with zero concentration at the vacuum interface. As Redhead noted, this predicted high outgassing rates well, but did not predict low levels of outgassing. Recently, Moore [22] applied an older recombination model that showed hydrogen atoms must recombine at the surface before desorption. Thus, the concentration of H at the vacuum surface cannot be zero. For low surface coverage the atoms must travel a distance before recombining and recombination becomes the limiting step. Moore solved this problem numerically by matching the diffusive flow of H from the near-surface concentration gradient with the

observed outgassing rates by adjusting the surface recombination coefficient. This concept was used to model hydrogen outgassing from the after-shot dose in a fusion device [23].

A portion of the hydrogen dissolved in stainless steel is trapped at sites such as precipitates and in the Cr-rich phase of stainless steel [24]. These traps have activation energies ranging from 73–180 MJ/kg-mol. Redhead notes that baking at temperatures near 800°C depopulates a large number of hydrogen atoms trapped in these sites, some of which then occupy sites of lower activation energy. For this reason, baking only at a low temperature, say 150°C, may yield lower outgassing rates than by first vacuum firing at 800°C. Additionally, oxygen plays a role in reducing hydrogen outgassing rates. An earlier study [25,26] had shown that the outgassing rate of stainless steel decreased with increasing concentration of Cr in the oxide, but was unchanged with increasing Fe content of the oxide. Thus the oxide can become a hydrogen surface trap. These studies shed light on why the outgassing rate of stainless varies widely with surface treatments such as electropolishing and oxidation.

An experimental technique for reducing hydrogen outgassing makes use of a coating applied to the exterior surface of stainless steel [27]. A 5× reduction in outgassing was achieved, which reportedly resulted from the reduction of the dissociation of water on the exterior stainless steel surface. If this conclusion is verified, it would imply that hydrogen outgassing does not result solely from H within traps, but partly from interstitial permeation. Interstitial H has an activation energy of 56 MJ/kg-mole [25].

21.2.3 Pressure Measurement

The choice of gauge, where to mount it, and how to care for it during baking are relevant issues in ultraclean systems. No gauge tube should be mounted on the base of a system with its entrance facing upward, lest it become a sink for debris. The gauge tube should be kept warmer than the system during cooling after a bake cycle. Gauges and RGA heads should be the last items cooled otherwise they become a small capture pump.

Perhaps the most critical issue is the choice of gauge for measuring extremely low pressures. Hot filament gauges should be operated with emission currents of 10 mA so as to minimize ESD. As we noted in Section 5.2.3, few commercial gauges are available for operation in this region. One can choose between the extractor gauge and the cold cathode gauge. The number of commercially available ultrahigh vacuum gauges is not sufficient to meet future needs. Advanced gauges and RGAs, incorporating the designs of Watanabe [28] for reducing ESD and electrode outgassing will be required.

REFERENCES

1. D. J. Santeler, *J. Vac. Sci. Technol.*, **8**, 299 (1971).
2. C. Benvenuti and D. Blechschmidt, *Jpn. J. Appl. Phys. Suppl. 2*, Pt. 1, 77 (1974).
3. H. J. Halama, and J. R. Aggus, *J. Vac. Sci. Technol.*, **12**, 532 (1975).
4. Y. Iwasa and S. Ito, *Vacuum*, **47**, 675 (1996).
5. C. Benvenuti, *Nucl. Instr. Meth.*, **205**, 391 (1983).
6. R. Giannantonio, M. Succi, and C. Solcia, *J. Vac. Sci. Technol. A*, **15**, 187, (1997).
7. A. Pozzo, C. Boffito and F. Mazza, *Vacuum*, **47**, 783 (1996).
8. C. Benvenuti, J. M. Cazeneuve, F. Ciccoira, A. Santana, V. Johaneck, V. Ruzinov, and J. Fraxedas, *Vacuum*, **53**, 219 (1999).
9. C. Benvenuti and C. Hauer, *Le Vide, Suppl. 2*, **201**, 199 (1980).
10. V. Rao, *Vacuum*, **44**, 519 (1993).
11. K. Odaka and S. Ueda, *Vacuum*, **44**, 713 (1993).
12. T. Momose, H. Saeki, and H. Ishimaru, *Vacuum*, **43**, 189 (1992).
13. H. Ishimaru, *J. Vac. Sci. Technol. A*, **2**, 1170 (1984).
14. J. R. Chen, K. Narushima, M. Miyamoto, and H. Ishimaru, *J. Vac. Sci. Technol. A*, **3**, 2200 (1985).
15. M. Miyamoto, Y. Sumi, S. Komaki, K. Narushima, and H. Ishimaru, *J. Vac. Sci. Technol. A*, **4**, 2515 (1986).
16. H. Ishimaru, *J. Vac. Sci. Technol. A*, **7**, 2439 (1989).
17. T. Sigmond, *Vacuum*, **25**, 239 (1975).
18. V. Rao, *J. Vac. Sci. Technol. A*, **11**, 1714 (1993).
19. D. G. Bills, *J. Vac. Sci. Technol.*, **6**, 166 (1969).
20. P. A. Redhead, *Intl. Workshop on Hydrogen in Mat's. Vac. Sys.*, G. R. Myneni and S. Chattopadhyay, Eds., AIP Conf. Proc. 671, AIP Melville, NY, 2003. p. 243.
21. R. Calder and G. Lewin, *Br. J. Appl. Phys.*, **18**, 1459 (1967)
22. B. C. Moore, *J. Vac. Sci. Technol. A*, **13**, 545 (1995).
23. K. Akaishi, M. Nakasuga, and Y. Funato, *J. Vac. Sci. Technol. A*, **20**, 848 (2002).
24. T. Yoshimura and Y. Ishikawa, *J. Vac. Sci. Technol. A*, **20**, 1450 (2002).
25. Y. Ishikawa, T. Yoshimura, and M. Arai, *Vacuum*, **47**, 701 (1996).
26. K. Okuda and S. Ueda, *Vacuum*, **47**, 689 (1996).
27. C. Dong, P. Mehrotra, and G. R. Myneni, *Intl. Workshop on Hydrogen in Mat. Vac. Sys.*, G. R. Myneni and S. Chattopadhyay, Eds., AIP Conf. Proc. 671, AIP, Melville, NY, 2003. p. 307.
28. F. Watanabe, *J. Vac. Sci. Technol. A*, **20**, 1222 (2002).

PROBLEMS

- 21.1 Table 1.1 classifies the low, medium, high, very high and ultrahigh vacuum ranges. Describe the suitability of the following materials in each range: Brass, cadmium, nickel-plated copper, household aluminum foil used to wrap cleaned parts, aluminum or copper castings, copper sheet, aluminum sheet, quartz, alumina ceramic, Buna-N, Nylon, Teflon, polyimide, and Viton. Assume materials used in the construction of ultrahigh and extreme high vacuum chamber walls might be preprocessed at temperatures as high as 800°C. Assume ultrahigh vacuum chambers may be baked to 75–150°C during routine use.
- 21.2 Why should a pressure gauge be the last item cooled when baking?

- 21.3 A small vacuum chamber with an internal surface of 0.1 m^2 is pumped to its ultimate pressure by a pump of speed 100 L/s . The net outgassing rate of the inner surface is reported to be $3 \times 10^{-11} \text{ Pa-m/s}$. (a) What is the ultimate pressure? (b) If the sticking coefficient of the surface is 0.1 , what is the true outgassing rate of the surface?
- 21.4 A particular vacuum system has a total internal surface area of 50 m^2 and a water pumping speed of $50,000 \text{ L/s}$. Calculate the average number of bounces made by a water molecule at room temperature, during its sojourn to a pump.
- 21.5 Assuming that 20% of the system interior is not baked above room temperature, nor cleaned by any stimulated desorption method, calculate the increase in residence time for the average molecule during baking in the previous problem. (Assume 20% of the molecular bounces land on unbaked, room-temperature surfaces.)
- 21.6 Carefully estimate the outgassing rate of a fingerprint. What compounds are in a fingerprint?
- 21.7 O_2 enters an ion-pumped ultrahigh vacuum system. The pump current increases by $2\times$ and the pressure, as indicated by a Bayard-Alpert gauge, increases $10\times$. What is happening?
- 21.8 † After a rapid system backfill with argon, flakes from a titanium sublimation pump have been blown into the ion pump and the power supply is shorted. What do you do?
- 21.9 (a) Calculate the rate of pressure rise, due to helium in the atmosphere, in a sealed 7740 Pyrex glass system with a wall area of 1 m^2 and a wall thickness of 1 mm which is initially pumped to 10^{-10} Pa . Assume the permeation constant for 7740 glass is $10^{-14} \text{ m}^2/\text{s}$ at 25°C . (b) Calculate the pumping speed necessary to hold the chamber at 10^{-10} Pa , if the permeating helium is the only gas source.
- 21.10 In a surface analysis system samples are introduced through a load lock on a long cylindrical rod. (See Fig. 17.19.) The rod passing through the load lock is isolated at the atmospheric side by an O-ring seal and at the UHV side by a long closely fitting cylinder, which passes through the vacuum wall. Assume the rod diameter is 1 cm , the gap between the rod and cylinder is 0.003 in. , and the cylinder is 8 cm long. (a) Calculate the gas leak into the main chamber through this load lock seal if the base pressure is $1 \times 10^{-8} \text{ Pa}$ in the main chamber and $1 \times 10^{-4} \text{ Pa}$ in the load lock. (b) If the main system pump has a speed of 400 L/s at the chamber, what fraction of its gas load is entering via the concentric seal at the given base pressure?

CHAPTER 22

High Flow Systems

Not all thin-film deposition processes require high or ultrahigh vacuum. Some of the most interesting processes take place in the medium and low vacuum range and require a high gas flow. The pressure–speed ranges for some processes are shown in Fig. 22.1.

Sputter deposition is done in the 0.5- to 10-Pa (10^{-3} - to 10^{-1} -Torr) range. For certain materials sputtering is the preferred deposition technique. Various plasma processes are performed in the range 5–500 Pa (0.01–5 Torr). Plasma deposited films are formed from the reaction of chemical vapors in the glow discharge. Plasma etching and reactive-ion etching are commonly used to pattern thin films. Polymer films are formed from the glow discharge polymerization of a monomer such as styrene. Plasma etching is a simple isotropic chemical etching process that uses chemically active neutrals in the discharge; for example, the plasma decomposes CF_4 and creates fluorine atoms that react with a silicon surface. The pump removes the volatile product SiF_4 . Reactive ion etching is a directional process used for patterning thin-film structures. Its directionality is due to high-energy ions that are accelerated through the plasma sheath toward the surface and enhance the reactivity of the chemically active species with the unmasked portions of a thin film. Because the ion-stimulated reaction proceeds at a rate many times faster than simple plasma etching, the thin film etches downward much faster than laterally. This allows vertical etching of finely resolved lines. Reactive ion etching can be performed over the entire range of pressures used for sputtering and plasma etching. Any differences attributed to pressure are differences in nomenclature rather than theory. Low-pressure chemical vapor deposition (LPCVD) and reduced pressure epitaxy (RPE) are thermal processes that take place at low pressures. The thermal energy is typically provided by induction heating. LPCVD, which is done in the 10- to 100-Pa range, has attracted wide attention. The high diffusivity of the thermally active species at low pressure improves the transport of the vapor throughout the reactor and allows the growth of uniform films on large wafers. Reduced pressure epitaxy takes place in the

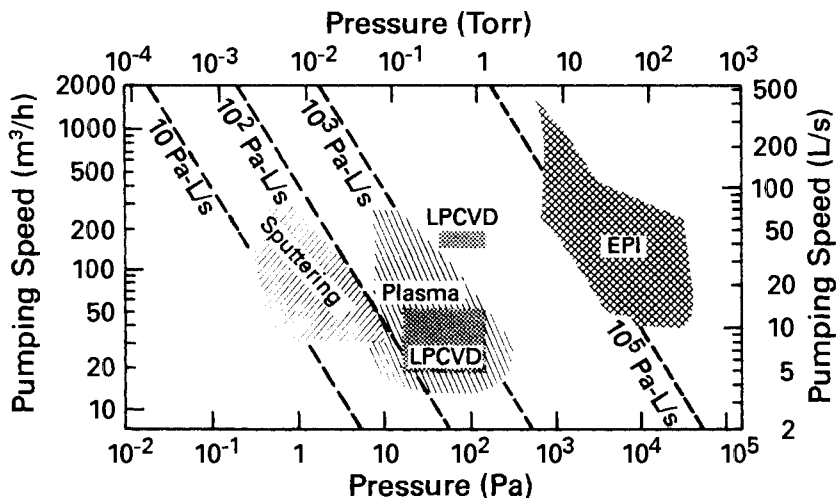


Fig. 22.1 Pressure-speed ranges for some thin-film growth, deposition, and etching processes that require medium to low vacuum and gas flow. Adapted with permission from M. T. Wauk, Applied Materials Inc., 3050 Bowers Avenue, Santa Clara, CA 95051.

500- to 10^5 -Pa pressure range. Epitaxial films grown at reduced pressure are higher in quality and have less autodoping than films grown at atmospheric pressure.

Many processes performed in the medium- or low-vacuum range also require the use of vapors that are toxic, hazardous, or corrosive. Special precautions must be taken in the design, operation, and maintenance of these systems to ensure operator safety and equipment protection. Kumagai [1] describes a generalized approach to handling hazardous gases that both updates and adds content to the earlier AVS Recommended Practice for Pumping Hazardous Gases [2].

Thin-film deposition and etching processes span a pressure and gas flow range that far exceeds the capability of any one pump. The useful pressure for each process is dictated by the process physics. Sputtering cannot commence until the pressure is high enough to initiate a self-sustained glow discharge, but the pressure must be low enough for the sputtered material to reach the anode without suffering a large number of gas collisions. Gas flows ranging from 10 – 10^6 Pa·L/s (0.1 – 10^4 Torr·L/s) are needed for a different purpose in each process. In some processes the high flow dilutes or replenishes the reactant species and simultaneously flushes away the products of reaction and other impurities; in others it mainly serves to flush away impurities.

This chapter describes un-throttled mechanically pumped systems and throttled high vacuum systems. Mechanically pumped systems are used for

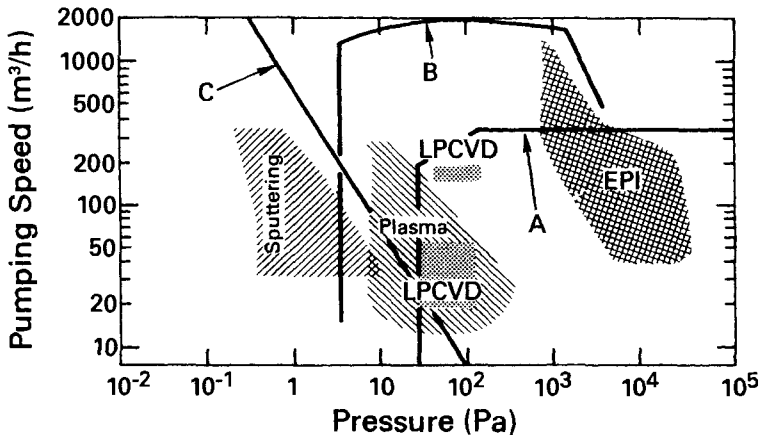


Fig. 22.2 Useful pressure–speed ranges for some pumping systems: (A) rotary mechanical pumps; (B) Roots pump backed by a rotary pump; (C) throttled high vacuum pump. Adapted with permission from M. T. Wauk, Applied Materials, Inc., 3050 Bowers Avenue, Santa Clara, CA 95051.

ion etching, plasma deposition, LPCVD, and RPE. Throttled high vacuum pumps are used mainly for sputtering and ion etching.

22.1 MECHANICALLY PUMPED SYSTEMS

The pressure–speed operating ranges of rotary mechanical pumps, Roots-claw pump combinations, turbo-drag pumps, and throttled high-vacuum pumps differ. Two-stage rotary vane pumps can operate in the sputtering pressure range with less than maximum pumping speed; however, at low pressures they cause backstreaming of oil vapor. Rotary vane pumps are economical to speeds of 200–300 m³/h and provide effective pumping for clean processes in the region delineated by speeds lower than this value and pressures greater than subject to backstreaming. This region is bounded by curve A in Fig. 22.2. Oil-free screw pumps are useful for dusty processes, as they do not contaminate and are little affected by corrosion or particulate contamination. Screw pumps have replaced rotary mechanical pumps for many applications.

For speeds greater than 200–300 m³/h a Roots pump backed by a rotary pump may be used. Again oil backstreaming limits the lowest pressure of operation. At sufficiently low pressures the roughing line would be in free molecular flow and would allow mechanical pump oil to back-diffuse to the Roots pump outlet, creep around the interior surfaces, and enter the process chamber. Oil contamination may be eliminated by bleeding gas

into the roughing line to maintain the Roots outlet at suitably high pressure. The Roots pump has an upper pressure limit of ~ 1000 Pa, which yields the useful operating region outlined in Fig. 22.2B.

Dry pumps using Roots-claw combinations can pump from atmospheric pressure to process pressure without concern for oil contamination. A speed–pressure characteristic for one combination pump is given in Fig. 10.11. These pumps have proven valuable for systems that generate large quantities of dust, such as those producing silicon dioxide from the synthesis of silane and oxygen. The pulsating pressure observed in the exhaust of some dry mechanical pumps can result in enhanced counterdiffusion along the walls of the exhaust pipe. Figure 22.3 illustrates the vortices generated along the pipe walls by the pulsating pressure in an LPCVD pump. Air flows toward the pump during the low-pressure half-cycle in the core. During that time, it becomes entrapped in the vortices, as their layers rotate in opposite directions. On the next half cycle, when the pressure pulse is outward, toward the exit, the air in the vortices moves closer to the pump. Counterdiffusion results from this process of alternately moving toward the pump in one half-cycle, and “hiding” in the vortex currents during the other half-cycle [3]. This enhanced back-diffusion phenomenon is known as Richardson’s annular effect [3,4].

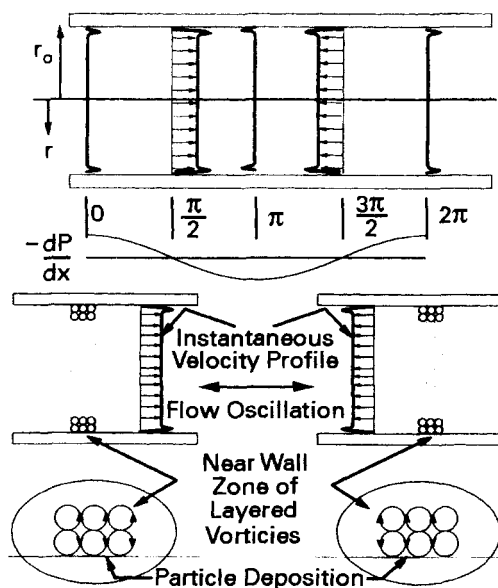


Fig. 22.3 Pressure pulsation within the exhaust of a dry pump. Air can counterdiffuse by alternately flowing in the core toward the pump during the negative half-cycle and remaining within the vortices during the positive half-cycle. Reprinted with permission from *J. Vac. Sci. Technol. B*, **12**, p. 2763. R. A. Abreu, A. D. Troup, and M. K. Sahm. Copyright 1994, AVS—The Science and Technology Society.

22.2 THROTTLED HIGH VACUUM SYSTEMS

The pressure range encompassed by sputtering and other plasma processes is above the operating range of all high vacuum pumps. They can be used with a throttle valve between the pump and the chamber. The throttle valve allows gas to flow from the process chamber to the pump, while keeping the pressure in the pump below its maximum operating pressure.

Turbomolecular and cryogenic pumps will maintain chambers at sputtering pressures when the inlet to each is throttled to a pressure below its respective critical inlet pressure. Figure 22.2C sketches the upper throughput limit of a typical small, throttled high vacuum pump. This section discusses process chambers, as well as the configuration and operation of turbo and cryogenic pumps for sputtering applications. Ion pumps are not considered because of their inability to handle high gas loads; diffusion pumps are no longer used on high-quality etching or deposition systems.

22.2.1 Process Chambers

As we noted in Chapter 21, cleanliness and contamination-free needs force some systems to be designed and constructed according to UHV practice. To reduce overall contamination to the part-per-billion (ppb) level, the ratio of background or chamber contamination to process gas pressure must be kept extremely small. Entrance and exit load locks are used to isolate the environment, and gases of high purity will be delivered to the system through gas distribution systems that will be UHV leak-tight. Many of the gases used in these processes are corrosive, explosive, or poisonous. Designs that focus on UHV construction techniques result in clean systems with reduced maintenance. For example, reduction of moisture levels to the ppb level can reduce the corrosion that results from a reaction with an anhydrous etch gas such as chlorine.

Residual gases pose a greater problem in a sputtering system than in a high vacuum evaporation system, because of enhanced plasma desorption of wall impurities. Electron- and ion-impact desorption efficiently release gases from the chamber walls. They are more effective than a mild bake. If hydrogen is not removed from an argon discharge, the sputtering rate will be reduced [5] and hydrogen will become incorporated in the film [6]. Sputtering discharges with argon or other noble gases can be kept clean by operating the discharge in a static mode with selective pumping or by permitting a large argon flow through the chamber during sputtering. A static discharge is maintained by exhausting the chamber and refilling it with argon to the operating pressure while other gases are selectively removed by an auxiliary pump located within the chamber. The ideal auxiliary pump does not exist. TSPs generate some methane and do not

pump noble gas impurities. NEG pumps have found application, especially for pumping hydrogen. For these reasons, static discharges are not frequently used for sputtering.

Viscous flushing will work only if the gas flows through the active sputtering region and chamber, and if the arrival rate of impurities from the gas source is much less than the desorption rate from the chamber walls. Lamont [7] has pointed out that high throughput alone does not guarantee adequate flushing; it is necessary that the gas stream velocity be large in the region in which the cleaning action is desired. Contamination originating from within the chamber can be reduced with high gas flow. In the high flow limit the lowest possible level of contamination attainable is that of the source gas. In critical applications the source gas is scrubbed by passing it through a titanium sublimation pump. Because of this, there is little point in flushing a small chamber at a rate greater than a few hundred pascal-liters per second with the purest available source gas [8]. Both the source gas cleanliness and the gas flow rate are important to the maintenance of conditions suitable for deposition of pure films.

Gas flushing alone will not adequately clean a chamber. Contamination-free sputtering requires high vacuum pumping to a suitable base pressure [9] followed by pre-sputter cleaning with the discharge operating and with the shutter covering the samples on which a film is to be deposited. The flushing time of a typical small system (< 1 s) implies that a system could be cleaned by pumping to the process pressure and initiating a glow discharge without pumping to high vacuum [10]. Unfortunately, the glow does not clean all surfaces adequately, nor do the surfaces outgas that rapidly. The continued evolution of water vapor from surfaces not exposed to the glow can cause oxygen or hydrogen contamination of deposited films. Most importantly, the only routine way to check for minute leaks in the system without the use of an RGA is to pump to the same low base pressure each time before opening the leak to argon flow. Pre-sputtering cleans by several techniques. If the sputtered material is a getter, it may be allowed to deposit on the chamber walls where it serves as an effective getter pump [11]. The sputtered material also covers adsorbed gases, whereas the discharge cleans surfaces exposed to the glow.

The value of base pressure and the length of pre-sputtering time are process-, equipment-, and material-dependent. No general observations can be made; for example d'Heurle [12] showed that for aluminum films a 10-min pre-sputter cleaning was sufficient, while Blachman [13] required a minimum of 1-h cleaning time for molybdenum. Some material properties are so dependent on film purity that the base pressure and minimum pre-sputtering time are of crucial importance in the repeatable fabrication of uniform, high-quality films. In these systems, contamination concerns require the use of entrance and exit load locks.

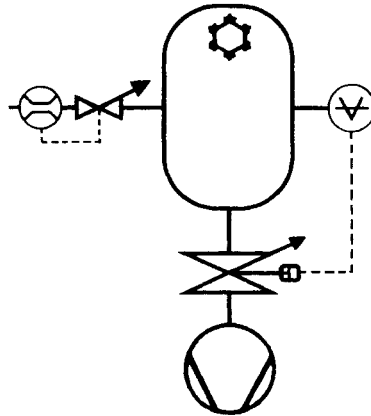


Fig. 22.4 Generic reactive processing chamber illustrating *independent* control of the gas flow and the chamber pressure. The gas flow is regulated by a thermal mass flow controller, while a capacitance manometer measures and maintains the chamber pressure by controlling the throttle valve located between the chamber and the cryo or turbo pump. A cryo panel suitable for pumping water is shown located within the processing chamber. This is often done to improve the water pumping speed and the time required to reach the needed base pressure.

The most basic process control system must control both chamber pressure and the process gas flow. Figure 22.4 illustrates the proper method for controlling these variables. Note that pressure is controlled by the throttle valve, whereas the gas flow is controlled by the mass flow controller. If we were to fix the throttle valve setting, we could change the pressure by changing the gas flow. However, were we to use this procedure, we would be changing two variables (gas flow and pressure) simultaneously. This would make data interpretation difficult, because flow and pressure can change properties of deposited films independently.

22.2.2 Turbo Pumped

A turbo pumped system suitable for high-flow applications must attain an adequate base pressure as well as exhaust a high gas flow at medium vacuum pressures. The two requirements are different but not conflicting. In Chapter 21 we discussed the requirements of a turbo pump for good high vacuum pumping: high compression ratio for light gases, high pumping speed for all gases, and an auxiliary cryo surface for increased water pumping speed. The selection of a pump for a particular application is then made on the basis of pumping speed and compression ratio. Data that describe compression ratio for individual gases are most often available for zero gas flow. These data cannot be used to predict pump

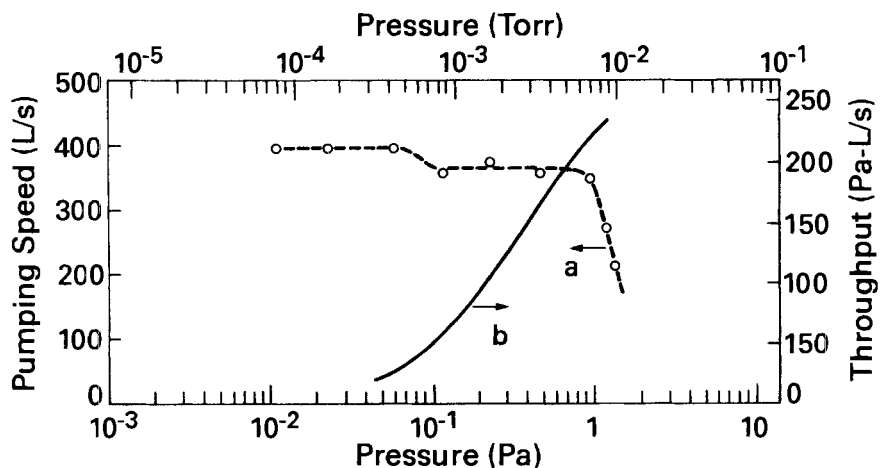


Fig. 22.5 Hydrogen pumping speed (a), and argon throughput (b), as a function of argon inlet pressure in a Balzers 400-L/s turbomolecular pump backed by a $35\text{-m}^3/\text{h}$ rotary vane pump. Reprinted with permission from *J. Vac. Sci. Technol.*, **16**, p. 724, J. F. O'Hanlon. Copyright 1979, The American Vacuum Society.

performance under gas flow. Limited high flow data are available. Some results are presented here.

Figure 22.5 depicts the pumping speed for hydrogen and the argon flow rate as a function of argon gas pressure. The argon flow is the product of the argon pumping speed and the inlet pressure. For this pump the hydrogen speed remained constant for argon inlet pressures ≤ 0.9 Pa (7 mTorr), above which it dropped precipitously. The sudden drop in hydrogen pumping speed corresponded to a similar sharp decrease in the rotational speed of the turbomolecular pump blades in this pump. The exact pressure at which the rotational speed began to decrease is a function of the pumping speed of the forepump. See Fig. 19.9. As the inlet pressure increased, the gas flow in the blades closest to the fore chamber changed from molecular to transition and then to viscous. Near the onset of viscous flow the added frictional drag demanded more torque from the motor; the constant power motor responded by losing speed. The knee of curve A in Fig. 22.5 will move slightly to the right for a forepump larger than the $35\text{-m}^3/\text{h}$ pump used here, and to the left for a smaller forepump. It is important to keep the pump running at full rotational velocity to maintain adequate hydrogen pumping speed. The blades will run at full velocity as long as the inlet pressure is suitably throttled.

Visser [8] has measured the methane compression ratio in a turbo pump during argon flow. His results, shown in Fig. 22.6, quantified the increase in methane compression ratio with increasing argon flow.

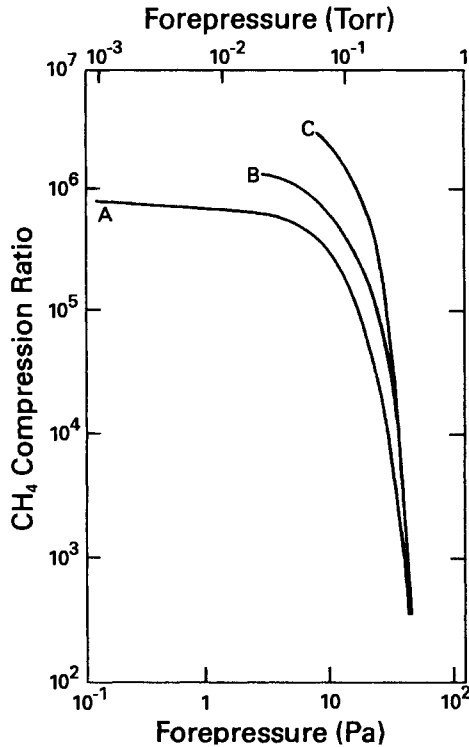


Fig. 22.6 Methane compression ratio as a function of argon gas flow in a Balzers 250 L/s turbomolecular pump. (A) $Q(\text{Ar}) = 0$, (B) $Q(\text{Ar}) = 2 \text{ Pa-L/s}$, (C) $Q(\text{Ar}) = 8 \text{ Pa-L/s}$. Adapted with permission from *Trans. Conference and School on Elements and Techniques and Applications of Sputtering*, Brighton, p. 105 (1971). Courtesy of Materials Research Corp., Orangeburg, NY 10962.

Konishi, Shibata, and Ohmi [14] have shown that the staging ratio (ratio of turbo pump speed to backing pump speed) strongly affect the partial pressure of contaminant gases that originated in the backing pump. Figure 22.7 illustrates the partial pressure of helium challenge gas as measured in the process chamber for a range of nitrogen process gas flow backing pump size. A minimum in the contamination gas (a maximum in its compression) was observed. In molecular flow, the compression ratio for helium is the same as for the condition of no gas flow, as given by the pump manufacturer. As the pump inlet pressure increases, the flow enters the transition region and begins to sweep the helium toward the fore chamber. Eventually, the pressure becomes high enough so that the blades are in viscous flow and the pump's speed decreases. As soon as the rotor velocity begins to decrease, the helium compression ratio decreases. Figure 22.7 demonstrates that process contamination may be reduced by using a

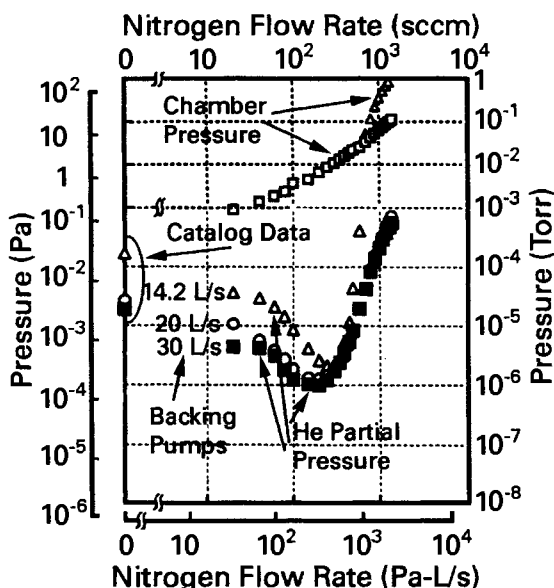


Fig. 22.7 Measured helium partial pressure in the chamber as a function of nitrogen gas flow rate for backing pumps having three different speeds. Helium gas challenge was 200 sccm. Catalog data were calculated from the compression ratios of the TMP. Reprinted with permission from *J. Vac. Sci. Technol. A*, **14**, p. 2958, N. Konishi, T. Shibata and T. Ohmi. Copyright 1996, AVS—The Science and Technology Society.

large backing pump and throttling the turbo pump at least enough to maintain maximum rotor velocity.

Turbo pumps are well-suited for use as a high-flow pump, if it is throttled to keep the blades running at full velocity and is backed by an adequately large mechanical pump. For large turbo pumps (1000 L/s and larger) this will usually mean use of a Roots pump and a suitably large foreline. When operated in this manner, it will have a high pumping speed and a high compression ratio for light gases. The turbo pump thus serves as a one-way baffle for light gases and hydrocarbons, whereas most of the pumping is done by the forepump. The turbomolecular pump is not appropriate for pumping on high-pressure plasma polymer deposition systems because material may deposit on the rotors, unbalance them, and destroy the pump [15]. Alternatively, turbo-drag pumps may be used at higher inlet pressures than pure turbo pumps without throttling.

22.2.3 Cryo Pumped

The cryo pump should be capable of evacuating the chamber to an adequate base pressure and pumping a large gas flow. Chamber outgassing

and the temperature and history of the cold stage determine the ultimate, or base, pressure. In Chapter 15 we discussed how a balance between the refrigeration capacity and the heat loads determined the temperature. Temperature was not the only factor that determined the pumping speed for a gas. It was found to be a function of the nature and quantity of gases previously sorbed.

It was also observed that the heat load carried to the pumping surfaces by the incoming gases under high vacuum conditions (low gas throughput) was insignificant in comparison to the radiant flux. If nitrogen were pumped with a typical two-stage cryo pump, the time to deposit a condensed layer of solid nitrogen 1 mm thick would be about 104 h at a pressure of 10^{-5} Pa [16]. Therefore neither the heat load of the incoming gas nor the resulting solid deposit is a major concern in the high vacuum region. This is not so at high gas flows. As the gas flow to a cryo pump is increased, its pumping speed changes. Figure 22.8 sketches the pressure dependence of the pumping speed over several flow regions. In the free molecular flow region the pumping speed is constant. At somewhat higher pressures the speed increases due to the increased conductance as the gas enters the transition flow region. Under some circumstances this flow will reach a maximum value (choked or critical flow) that is characteristic of the sonic velocity of the gas. At higher pressures the heat conductivity of the gas becomes large and heat from the walls of the chamber will flow to the cooled surfaces by gas transfer. As these surfaces warm, the sticking coefficients decrease and pumping ceases. This behavior has been observed by Dawson and Haygood [17] for CO_2 and by Bland [18] for water vapor. Loss of pumping speed in a practical pump usually occurs at

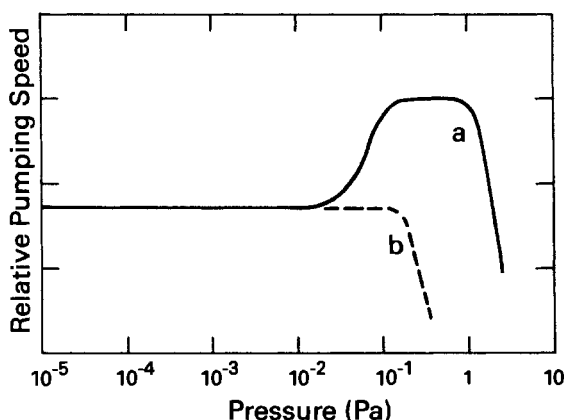


Fig. 22.8 Pressure dependence of cryogenic pumping speed. (a) Free surface, (b) practical baffled pump.

about 0.2–0.4 Pa (1.5–3 mTorr), where the heat loads exceed the capacity of the refrigerator. The pumping speed of a typical pump in the high-pressure region is sketched in Fig. 22.8.

At high throughput, the gas carries most of the heat to the cryo surface. An argon flow of 180 Pa-L/s (1.35 Torr-L/s or 1.8 mbar-L/s) corresponds to an incident heat flux of 1 W on a 20 K surface. For gases such as nitrogen, which have a heat of condensation greater than argon, the heat flux will be proportionately larger. The majority of this heat flux will be absorbed by the cold stage. As an example, consider a two-stage cryo pump with surfaces at 20 and 80 K, respectively, in which the argon collides with the 80 K baffle, passes through the baffle, and finally sticks on the 20 K surface. For each kg-mole of argon that flows into the pump, the expander must remove a total of 13,862 kJ. This value is obtained by taking the difference in enthalpy between 300 and 20 K. See Table 22.1. If all of the argon were cooled to 80 K on impact with the 80 K baffle, a total of 4580 kJ/(kg-mole) would be removed. This value corresponds to 33% of the total heat that is removed during the pumping process. In practice the gas is not cooled to 80 K on impact with the first stage, because the accommodation coefficient is not unity. If, for example, the warm stage had an efficiency of 0.5 for cooling the argon, then 85% of the total heat of the gas would remain to be removed by the 20 K stage. The cold stage removes at least 67% of the heat from argon because its vapor pressure is so low and its heat of condensation is so large. Table 22.1 gives the approximate total enthalpy at the temperatures of the first and second stages of a cryo pump for several gases of interest. The maximum throughput for each gas is determined by the maximum power that can be removed by the stage on which the gas or vapor condenses. The maximum throughput is gas-dependent. CF_4 has a maximum throughput of half the value quoted by the manufacturer for argon. Several other gases used for reactive-ion etching deposit on the 80 K stage and can completely close the baffles and quickly render the pump useless for high vacuum pumping unless it is first regenerated.

At high flow the heat absorbed by the expander will be proportional to the total gas throughput until the pressure is large enough for heat conduction from the walls to be appreciable. Heat conduction from the walls begins at a Knudsen number of 1 and reaches its maximum or high pressure value at $\text{Kn} = 0.01$. This heat flow is added to the heat flow due to heat of condensation but not in a linear manner. Most of the heat delivered by gas conduction flows to the 80 K stage. This added load on the warm stage reduces the refrigeration capacity of the cold stage. For high gas flow applications a cryogenic pump should be designed to minimize the heat load from the walls so that the expander may be most efficiently used to remove the heat of condensation of the incoming gas. For a typical pump

Table 22.1 Enthalpy of Gases Frequently Pumped at High Flow Rates^a

Gas or Vapor	Total Enthalpy kJ/(kg-mole)		
	300 K	80 K	20 K
Ar	13,950	9,370	88
N ₂	15,580	9,190	134
CCl ₄	49,750	2,950	738
CF ₄	26,000	16,000	670
CF ₃ H	30,750	2,678	670
CF ₃ Cl	31,300	20,230	678

^aApproximate total enthalpy at ambient temperature and at the nominal temperatures of the first and second stages of a cryogenic pump for several gases and vapors used in high gas flow applications. The enthalpy is shown in bold for the surface on which the gas or vapor solidifies.

the Knudsen number for air at 0.2 Pa is about 0.3. At this value the heat capacity is a substantial fraction of the high-pressure value, permitting several watts to flow from the chamber walls to the warm stage.

In some high gas flow situations, continued pumping of hydrogen is important but does not always take place. Pumps are designed so that the inner surface of the cold stage is baffled from the warm stage and covered with a layer of activated charcoal. This surface will pump hydrogen, neon, and helium effectively if it is adequately cooled. At 10 K there is adequate sorption capacity for hydrogen on activated charcoal or molecular sieve. Argon will also be pumped on this surface. To avoid or reduce the argon pumping on the inner surface, it is baffled from the remainder of the system. If the baffle is optically dense to keep argon reaching the inner surface, the hydrogen pumping speed will be reduced, and if the baffle is open, the argon will readily pass through, condense on the inner surface, and cover the sorbent with solid argon. All pump designs are a compromise between these two concerns. In a high flow application, however, the sorbent surface will become coated with argon rather quickly, regardless of the nature of the baffling. Once the sorbent becomes coated, cryotrapping is the only mechanism by which hydrogen can be pumped. Hengevoss [19] has shown that the cryotrapping of hydrogen in argon is strongly temperature-dependent. It becomes nil in solid argon for temperatures greater than 20 K. The value of argon throughput, which will keep the second-stage temperature below 20 K, may be below the stated maximum value for a particular pump.

The constraints placed on a cryopump system for high gas flow are considerably different than those placed on pumps used for high vacuum. These systems require a throttle valve to keep the pressure in the cryopump below a value of 0.2–0.4 Pa. The cryo pumps must be able to remove the conductive heat load entering the chamber from the walls. This heat load may be removed by use of a high capacity two-stage gas refrigerator.

Regeneration of a high gas flow system will obviously be more frequent in a pump used for high gas flow than in a pump used for high vacuum, but automatic controllers are available for performing this function on idle time. If a cryopump is used at the design-limit argon throughput, the cold stage will be heated to a temperature at which it will not pump hydrogen or helium; either supplemental pumping or throughput reduction will be necessary to pump these gases. Furthermore, the pump's maximum throughput is dependent on the vapor pressure, specific heat, and heat of sublimation of the gas or vapor being pumped.

Cryogenic pumps also suffer from the phenomenon of overloading. Irreversible warming of a pump can be triggered by a gas burst entering a pump that is running near its throughput limit. It will then cease to pump and require regeneration, because the rate at which heat from this gas burst is entering the cryo pump is greater than the rate at which it can be removed by the refrigerator.

Cryogenic pumping of toxic or explosive gases presents serious safety concerns. If the pump were to suddenly warm, a large quantity of gas could be emptied into the exhaust system. If this gas were toxic, it could overload the exhaust scrubber. If the pump were condensing an explosive gas, operation of an ionization gauge in the pump body during release of the gas would present a serious problem. The ion gauge tube should be located outside the pump body and interlocked so that its filament cannot be operated when gas is being released. A prudent operator would not choose cryogenic pumping for certain gases. These concerns should be understood before cryopumps are chosen for high gas flow applications. Lessard [20] describes the explosion hazards from hydrogen and oxygen, produced by the dissociation of water and entrapped in the cold stage. A potential hydrogen detonation is shown to be a function of the quantity of hydrogen available, which in turn is dependent on the charcoal quantity and the design of the cryo-pump baffles and louvers. Pump manufacturers limit this risk by limiting the quantity of charcoal and thus limiting the quantity of hydrogen that can be adsorbed in the charcoal. Ozone was shown to be a potential risk factor for a small number of system operators. It was concluded that certain rf sputter processes using oxygen could generate O_3 that could be trapped on the cold array. During regeneration it is possible for the ozone to drip from the array in liquid form and detonate from the liquid state with a resulting loud pop or bang [20].

REFERENCES

1. H. Y. Kumagai, *J. Vac. Sci. Technol. A*, **8**, 2865 (1990).
2. J. F. O'Hanlon and D. B. Fraser, *J. Vac. Sci. Technol. A*, **6**, 1226 (1988).
3. R. A. Abreu, A. D. Troup, and M. K. Sahm, *J. Vac. Sci. Technol. B*, **12**, 2763 (1994).
4. E. G. Richardson and E. Tyler, *Proc. Phys Soc. (London)*, **42**, 1 (1929).
5. E. Stern and H. L. Caswell, *J. Vac. Sci. Technol.*, **4**, 128 (1967).
6. J. J. Cuomo, P. A. Leary, D. Yu, W. Reuter, and M. Frisch, *J. Vac. Sci. Technol.*, **16**, 299, (1979).
7. L. T. Lamont, *J. Vac. Sci. Technol.*, **10**, 251 (1973).
8. J. Visser, *Trans. Conference and School on Elements and Techniques and Applications of Sputtering*, Brighton, November 7–9, 1971, p. 105.
9. L. I. Maissel, *Physics of Thin Films*, Vol. 3, G. Hass and R. E. Thun, Eds., Academic, New York, 1966, p 106.
10. G. A. Shirn and W. L. Patterson, *J. Vac. Sci. Technol.*, **7**, 453 (1970).
11. H. C. Theuerer and J. J. Hauser, *Appl. Phys.*, **35**, 554 (1964).
12. F. M. d'Heurle, *Metall. Trans.*, **1**, 625 (1970).
13. G. Blachman, *Metall. Trans.*, **2**, 699 (1971).
14. N. Konishi, T. Shibata, and T. Ohmi, *J. Vac. Sci. Technol. A*, **14**, 2958 (1996).
15. J. Vossen, Dry Etching Seminar, New England Combined Chapter and National Thin Film Division of AVS., October 10–11, 1978, Danvers, MA.
16. G. Davey, *Vacuum*, **26**, 17 (1976).
17. J. P. Dawson and J. D. Haygood, *Cryogenics*, **5**, 57 (1965).
18. M. E. Bland, *Cryogenics*, **15**, 639 (1975).
19. J. Hengevoss, *J. Vac. Sci. Technol.*, **6**, 58 (1969).
20. P. H. Lessard, *J. Vac. Sci. Technol. A*, **8**, 2874 (1990).

PROBLEMS

- 22.1 † Figure 22.4 shows a system with a mass flow controller and a throttle valve. Which valve will independently control the pressure in the chamber? Which valve will independently control the gas flow to the chamber? Why is this arrangement important?
- 22.2 A scientist was observed connecting an ultrapure argon tank to a sputtering system through a 2-meter length of Teflon tubing. Water vapor will permeate Teflon and contaminate the argon gas stream. The Teflon tubing was 6.35 mm in outside diameter with a wall thickness of 1.04 mm. The required argon gas flow was 133 Pa-L/s (1 Torr-L/s). Assume room temperature and a relative humidity of 50%. Calculate the steady-state water vapor contamination in the argon flow to the researcher's sputtering system. The permeation flow through a round tube is given by

$$Q (\text{Pa} \cdot \text{m}^3 / \text{s}) = \frac{2\pi l K_p \Delta P}{\ln(r_o / r_i)}$$

where l is the tube length in meters, r_o and r_i are, respectively, the outer and inner tube radii, K_p is the permeation constant (m^2/s), and ΔP is the pressure differential of the permeating gas (Pa).

- 22.3 The 1500-L/s high vacuum pump on a sputtering system has been replaced with a 3000-L/s cryogenic pump. The operator pumps the system to a predetermined base pressure and initiates the sputtering discharge. Since the pump size has been increased, the system pumps to the base pressure in less time. What fundamental problem will this cause in the performance of the sputtering system?
- 22.4 Given the following: Gas sources, pressure gauges with electrical output, valves with servo-operated controllers, and thermal mass flow sensing elements with electrical outputs. (a) Connect the components to control flows Q_1 and Q_2 of two gases into a chamber such that the majority gas Q_1 controls the total pressure, while the minority constituent remains constant. (b) Connect the equipment in such a way that ratio of the major to minor gas flow remains at a predetermined value, and the system pressure is recorded.
- 22.5 In the problem above, a large burst of gas entered the chamber from wall desorption. Describe qualitatively the transient behavior of (a) the chamber pressure, (b) the flow meter, and (c) the throttle valve.
- 22.6 † How and where would Richardson's annular effect result in the generation of silica dust in an SiO_2 deposition system using silane?
- 22.7 A gas line contains gas flowing at the rate of 10,000 ml/min, and it is leak tight to a level of 10^{-5} T-L/s. (a) What is the contamination of the gas due to the leak? (b) What leak tightness would be required to keep this same contaminant level with only 1 ml/min of gas flow?
- 22.8 Assume we have a sputtering chamber of 100-L volume and internal surface area of 1 m^2 . Assume a normal outgassing rate for clean stainless steel. Determine the argon flow required to maintain the outgassing-generated contaminant level below 1 ppm in the chamber.
- 22.9 Which pump will produce the cleanest vacuum for a sputtering system, a turbo pump or a cryo pump?
- 22.10 In sputtering systems, such as those used to coat roll stock, one brings the sputtering gas supply line inside the small sputtering volume near the drum. In some systems, the internal walls of this volume contain fixed slits through which the gas exits to the pump. The fixed slits have limited conductance and thereby maintain sputtering pressure within the small volume. What difficulty will be encountered with this design?

CHAPTER 23

Multichamber Systems

Multiple chamber systems are economically important in the manufacture of many common consumer products, both low- and high-tech. Coated paper for inkjet and laser printers, computer chips, magnetic storage tape and disks, and coated plastic films for food and anti-static packaging are some items we encounter daily. Other materials fabricated in multichamber systems are used to form component parts of products we may not recognize—products such as retail sales security tags, secure paper currency, thermally efficient home, commercial, and automobile window glass, solar cells, image recording, and active matrix computer displays.

The underlying structure, or substrate, on which films are deposited or patterned, can be either flexible (for example, a roll of plastic film) or rigid, for example (a glass or metal plate or a silicon wafer). In the case of rigid substrates, we can further choose between “in-line” (serial) processing or “cluster” (random) processing. In an in-line system, the products march sequentially through the serial chambers in lock step. In a cluster tool the process sequence for cleaning, etching, deposition, or annealing is chosen by the design of the particular device or product. The same equipment can produce multiple products by altering the process sequence.

The choice of equipment depends on many factors. The product volume, size, allowed defect levels, product yield, and profit margin all influence the cost of manufacturing and the type of system one selects. Low cost consumer products need to be coated rapidly and cheaply; this requires high product throughput in systems with low capital investment. Some high tech products are exceedingly sensitive to cross-contamination from a prior process step; these systems require careful process isolation. No single system design fits all production needs. In this chapter we review some of the issues requiring consideration in order that we understand why products are manufactured in specific systems and how these systems are designed. We review machines for handling flexible and rigid substrates, as well as discuss multichamber pressure reduction techniques for sampling atmospheric pressure gases.

23.1 Flexible Substrates

A large number of consumer products that are manufactured in sheet form require coating. Many polymer films for electrostatic and other packaging, decorative coating, anti-theft and security devices, video tape, capacitors, and heat reflecting and magnetic storage applications, as well as paper for laser and ink jet printing, are economically coated in vacuum deposition systems. These coating processes are only economical, if the material can be deposited at high speeds on large rolls of stock. The machines designed for this purpose are called web coaters. The process, known as semicontinuous coating, is more economical than continuous air-to-air coating, which is only used for certain steel products [1].

The dominant outgassing from the feed stock rolls comes from the ends of the rolls, typically of order 1 m. long and 0.5- to 1-m diameter. The gas load, primarily water vapor, largely originates in the end faces of the feed rolls. Depending on the nature of the material, the total gas load from the feed roll and chamber walls could be as large as 7000–10,000 Pa-L/s (50–70 Torr-L/s). A reasonable deposition pressure for a typical process might be $\sim 10^{-2}$ Pa (10^{-4} Torr). The necessary pumping speed for a single chamber system would therefore be $>10^5$ L/s. Clearly, it would be uneconomical to coat material in a system with such a high capital investment. The equation relating gas flow, pressure, and speed, $S = Q/P$, tells us that low pumping speed is required to remove gas at high pressure. Thus, a two-chamber design in which the feed and winding roll chamber is maintained at a high pressure and in which the deposition chamber is maintained at a low pressure, will be more economical than a single chamber. Figure 23.1a illustrates a two-chamber design. The feed stock is loaded on the upper left spindle. It is threaded around the central drum, then back to the winding roll, where it is stored on the winding roll. Although not shown in Fig. 23.1a, most web coaters contain a glow discharge cleaning apparatus between the feed stock roll and the first slit. This system is designed to remove large amounts of water vapor from the feed material before coating. The inner slits adjacent to the central drum separate the dividing partition and central drum on both sides and both ends of the roll. The entire chamber is constructed in two parts: One part, bounded by the outer slits, contains the rear system wall, deposition tooling, and pumping system connections. The central section containing the three rolls and inner slits can be removed to facilitate loading and unloading feed stock and finished product.

Two separate pumping systems are now required: one to pump the winding chamber and one to pump the deposition chamber. However, the sizes of the pumps are significantly less than those required for a single chamber design. The deposition chamber pump needs to exhaust gas from the deposition process (typically sputter deposition), the outgassing from the

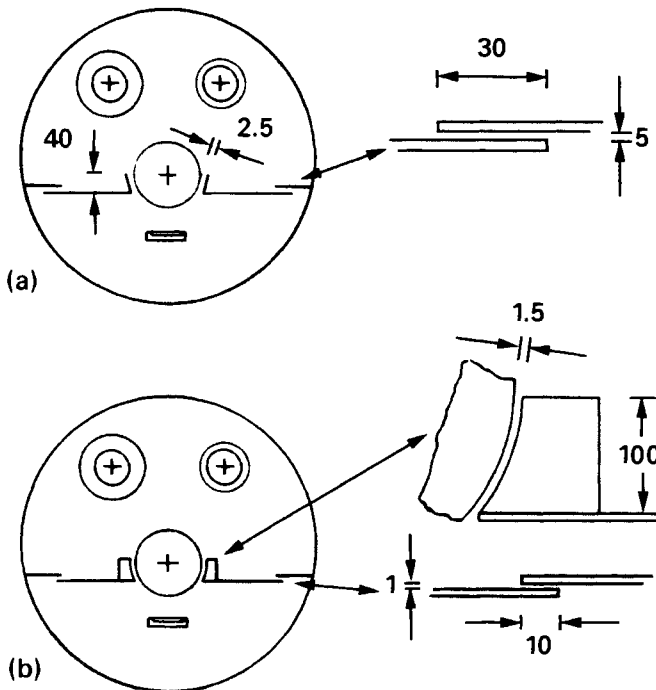


Fig. 23.1 Schematic representation of slit configurations for different two-chamber vacuum web coaters. Reprinted from *Thin Solid Films*, **119**, J. Kieser, W. Schwarz, and W. Wagner, 217–222, copyright 1984, with permission from Elsevier.

deposition chamber walls, and the gas load from the winding chamber that flows through the inner and outer slits. Sophisticated inner slits with reduced spacing have been designed to reduce the gas flow to the deposition chamber; one such design is shown in Fig. 23.1*b*.

The gas flow from the winding chamber to the deposition chamber is primarily water and possibly organic vapors. Demands for reducing the contamination in the deposition chamber necessitate further design changes in the system, shown in Fig. 23.2. In the coating system depicted here a third chamber is used to remove gas at a pressure intermediate to the winding and deposition chambers. With three chambers, one can tolerate increased throughput through the slits, smaller pumps, or lower levels of contamination in the deposition chamber. Pressure in the deposition chamber is the primary web coater design issue [1]; however, overall system cost and deposition cleanliness are also important.

A novel design for multilayer deposition on flexible substrates, Fig. 23.3 was developed by Madan [2]. In this design, the flexible substrate can be transported between a feed roll and winding roll during reactive sputter

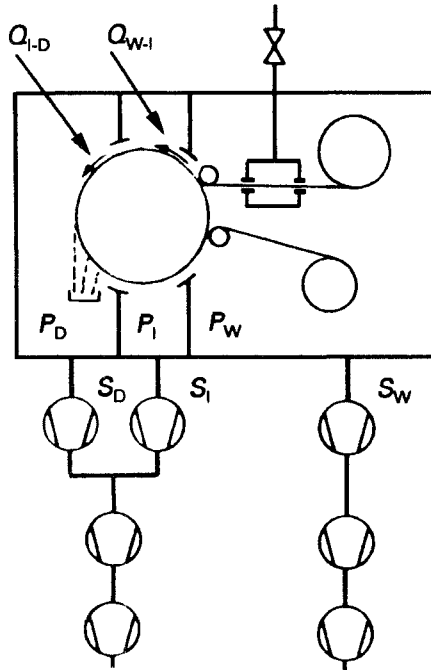


Fig. 23.2 Schematic representation of an advanced vacuum web coater containing an intermediate chamber. The gas flow between the chambers is indicated. A glow discharge unit for pretreatment of the web is shown in the winding chamber. Reprinted from *Thin Solid Films*, 119, J. Kieser, W. Schwarz and W. Wagner, 217–222, copyright 1984, with permission from Elsevier.

deposition. The feed stock can be moved in either direction between left and right rolls. Both rolls are contained within a removable cassette.

Electrical properties of photovoltaic cells and thin-film-transistor displays deposited on flexible substrates, for which this equipment was designed, are extremely sensitive to film deposition process contamination that originated from a previous step. To minimize contamination between two process steps, the cassette, containing either thin stainless steel or a thin plastic substrate, can be removed and transferred between deposition chambers. This design would represent a hybrid inline-cluster system.

23.2. Rigid Substrates

Thin, flexible substrates in roll form are ideally suited for coating in semi-continuous deposition systems. Rigid substrates cannot be handled in the same fashion. Rigid substrates can be coated in either inline systems, or in systems designed in the form of a cluster. In this section we give examples

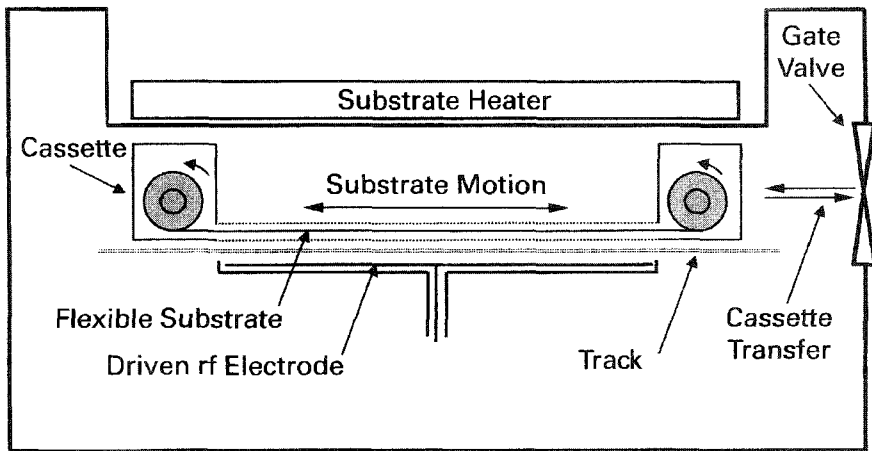


Fig. 23.3 Schematic view of a transportable cassette for holding a rolled, thin, flexible substrate. This cluster-tool configuration has one gate valve. Alternatively, gate valves may be configured at both ends for use in an inline system. U.S. Patent 6,258,408B1. Reprinted with permission of A. Madan, MVSystems Inc. 17301 W. Colfax Ave., Unit 305, Golden, Colorado, 80401.

of both forms of system design. The design of choice depends on the size of the substrate, capital equipment investment, process flexibility, tolerable cross-contamination levels, product throughput, and cost and value added. For extremely high volume, high throughput manufacturing, large inline designs appear to be the most efficient. Cluster designs appear to be most efficient for devices that would require extensive process isolation.

23.2.1 Inline Systems

Inline systems contain integrated atmospheric- or vacuum-based pre-cleaning zones, because operator handling constitutes a large source of contamination. Figure 23-4 illustrates a system containing an atmospheric steam cleaning chamber followed by vacuum drying chambers to eliminate as much water vapor as possible prior to entering the sputter deposition chamber. This system was designed to deposit Cr-Cu-Cr films on ceramic substrates. The substrates were mounted on carriers, which were used for transport through the cleaning, drying and deposition chambers. In this system, argon was used as the sputtering gas. No reactive depositions were required, therefore no isolation chambers were used to separate the individual metal depositions. Adequate cross-contamination reduction could be maintained without intermediate isolation zones, or without slit valves between each metal deposition. The number of series magnetron

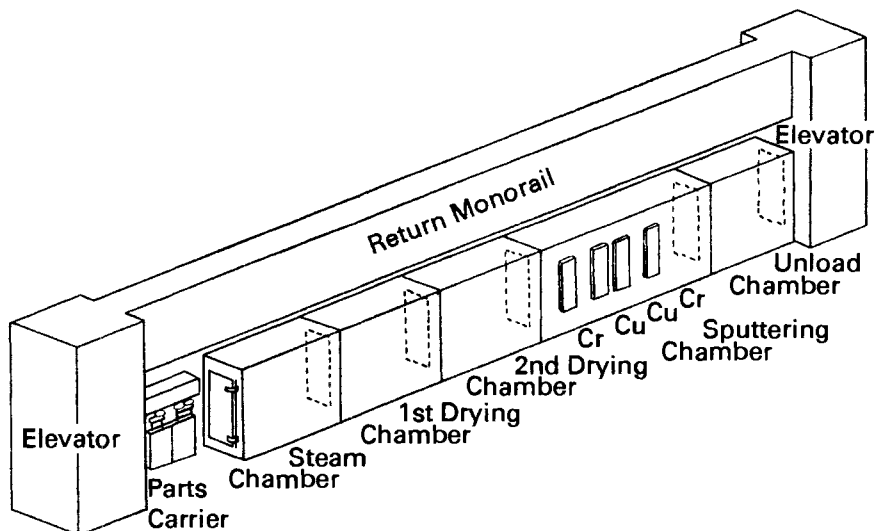


Fig. 23.4 An inline system designed for the deposition of chrome-copper-chrome metallurgy on ceramic substrates. The substrates are steam cleaned and dried before metal deposition. Reprinted with permission from *J. Vac. Sci. Technol. A*, 3, 516, T. Rogelstadt and G. Matarese. Copyright 1985, AVS—The Science and Technology Society.

stages and transport speed can be adjusted to control each layer thickness. This is an example of a straightforward inline system that incorporates pre-cleaning external to vacuum before formation of the metal layers by physical vapor deposition.

When different gas mixtures are required for each film layer, gas cross-contamination can be a problem. Early designs for fabricating thin film solar cells used one deposition chamber to deposit an entire *p-i-n* structure. First a B_2H_6 -doped SiH_4 gas mixture was introduced deposit the *p*-doped silicon layer. Next the intrinsic layer was formed by pyrolysis of SiH_4 . Finally, phosphene was added to the silane to form the *n*-doped silicon layer. Residual diborane caused boron contamination of the intrinsic layer and reduced the sharpness of the *p-i* interface. Residual phosphorous contamination from the last stage also contaminated the boron-doped layer in the next device. An inline design with separate chambers for depositing each layer was shown to reduce gas cross-contamination [3]. See Fig. 23.5. This system contained an entrance load lock, three inline deposition chambers and an exit lock. Each chamber is isolated with a slit valve. One must consider the relative pressures in adjacent chambers when opening the slit valve to transfer a substrate. Some cross-contamination can occur while the slit valve is open.

Separating the process chambers with isolation chambers can further

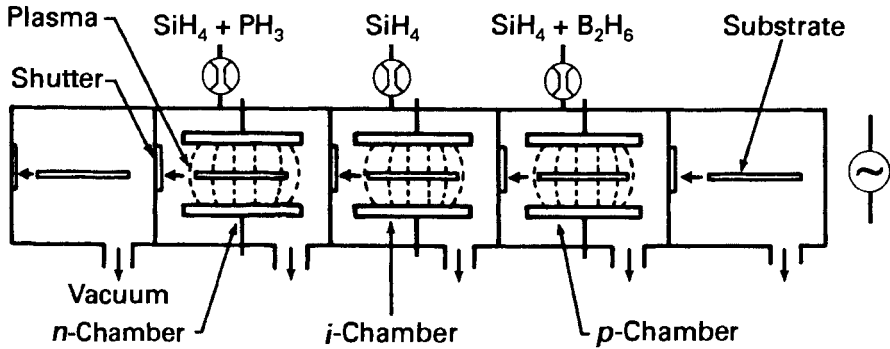


Fig. 23.5 Inline system used for the deposition of *p-i-n* solar cells. This system contained a load and an unload chamber, and separated but not isolated deposition chambers. Reprinted with permission from *Jpn. J. Appl. Phys.*, **21**, 413, Y. Kuwano, M. Ohnishi, S. Tsuda, and Y. Nakashima. Copyright 1982, The Japan Society of Applied Physics.

reduce this cross-contamination problem. Figure 23.6 illustrates one such design. Isolation chambers are used between each process and between entrance and exit locks and process. The isolation chamber between the entrance lock and first process helps to reduce the water vapor impurity on incoming substrates. It may incorporate quartz lamp heating as well as cryo panels to increase the pumping speed for water vapor. The number of deposition modules can be altered to meet the relative film thickness requirements. The isolation module, located between each process chamber, helps to reduce the gas cross-contamination from adjacent processes. Isolation chambers do help to reduce cross-contamination, but proper electrode design and shielding is necessary to reduce particle contamination due to sputter desorption from chamber fittings and walls. Modified opening and closing of slit valves is required to prevent particle generation caused by suddenly opening and closing slit valves.

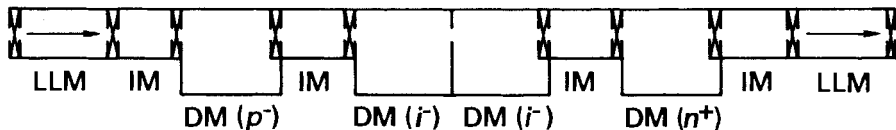


Fig. 23.6 Inline system for the deposition of *p-i-n* solar cells. This system contained isolation modules located between the individual deposition chambers. The isolation modules reduce the cross contamination between deposition chambers. (LLM = load lock module; IM = isolation module; DM = deposition module.) Adjacent chambers are isolated with gate valves. Reprinted with permission from *SPIE*, **706**, 72, A. Madan. Copyright 1986, The Society of Photo-Optical Instrumentation Engineers.

Inline systems are ideally suited for coating large architectural glass plates. A typical system is illustrated in Fig. 23.7. The system is comprised of several zones. First, the plates are washed and then dried. Great care must be taken in the drying process to eliminate as much water vapor as possible. Water will remain, and that must be pumped from the glass surface before it is coated. This is done in the vacuum entry zone. The plates are loaded into the entry lock and pumped rapidly by connecting it to a large, evacuated pressure dividing ballast tank, and then evacuated to about 13 Pa (100 mTorr) with roughing pumps. Next, the valve connecting the load lock and the evacuated (10^{-3} Pa) holding chamber is opened. The entry holding chamber and load lock are relatively sized so that both chambers assume a pressure less than the overload condition of the holding chamber diffusion pumps. Such a roughing sequence is described in Problem 19.8. The valve connecting the load lock and holding chamber is now closed and the system is pumped for a time necessary to remove the remaining water vapor. Dry air may be used to flush the load lock to reduce the initial water vapor load. Cryo pumping installed in both load lock and entry holding chambers will further reduce water vapor partial pressures before the plates are transported to the entry buffer where they await coating. The transport

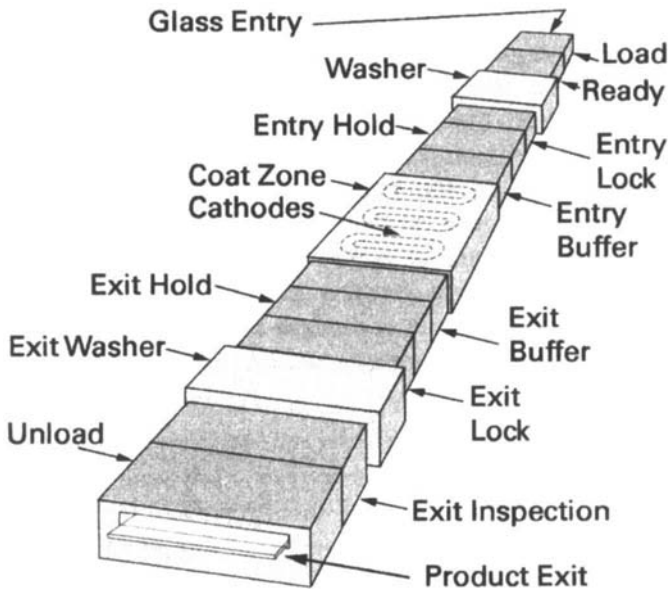


Fig. 23.7 Large double-ended, continuous flow production glass coating system. This system is comprised of load, ready, pre-clean, coat, post-clean, inspection, an unload sections. Reprinted with permission from *Coated Glass Applications and Markets*, p. 21, Russell J. Hill and Steven J. Nadel. Copyright 1999, Von Ardenne Coating Technology, 2700 Maxwell Way, Fairfield, CA, 94533.

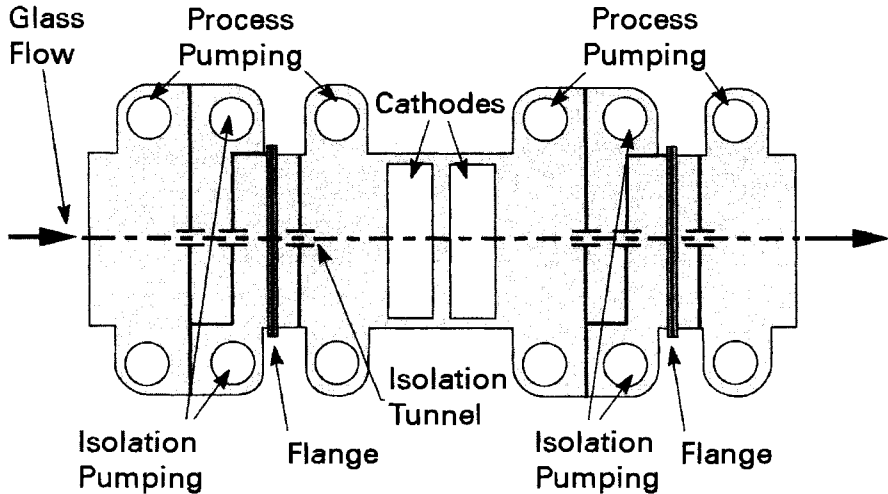


Fig. 23-8 Detail (vertical cross section) showing the method of gas isolation between adjacent process zones in one continuous flow production glass coating system. Each process zone is pumped with four process pumps, whereas each isolation zone is pumped with two pumps. Each isolation pump removes the gas load from the process zone to which it is adjacent. Isolation tunnels limit the gas flow between process zones. Reprinted with permission from *Coated Glass Applications and Markets*, p. 27, Russell J. Hill and Steven J. Nadel. Copyright 1999, Von Ardenne Coating Technology, 2700 Maxwell Way, Fairfield, CA, 94533.

system in the buffer chamber is designed to increase the transport speed of the plates to the speed required within the coating chambers. Note that this system does not use isolation valves to prevent cross-contamination between adjacent sputter deposition targets. Some sputter targets deposit nitrides using argon–nitrogen mixtures and other targets deposit oxides using argon–oxygen mixtures. These gases cannot enter adjacent deposition modules without affecting the optical properties of the deposited films. Isolation is a necessity, but isolation valves cannot be used in a high-speed, continuous transport design. Instead an isolation scheme similar to the one described in Fig. 23.8 is used. The process zones in this system are pumped with four process pumps to handle the large gas flow needed for sputtering. The two isolation zones are each evacuated with a separate pump. Each isolation pump removes the gas load from the process zone to which it is adjacent. Closely spaced plates form isolation tunnels that limit the gas flow from the two process zones. Ideally, the pressure in the two isolation chambers is low enough that the net gas flow through center tunnel in each group of three isolation tunnels should be insignificant. The gap between the top spacer and the upper surface of the glass plates can be adjusted to compensate for the differing incoming product thickness, and thus minimize the gas losses at the isolation slits. The remaining vacuum portion

of this system consists of the exit chambers. Non-vacuum cleaning, inspection, and unloading steps complete the system.

Inline systems are extremely efficient for coating high volumes of large substrates. Deposition chambers can be reconfigured with different cathodes or gases to deposit a range of films with differing solar properties. High product volumes make this an efficient low cost process.

23.2.2 Cluster Systems

Inline systems are not required to achieve isolation and high product quality. Cluster system designs with a central isolation chamber can be viewed in one sense as serial processing wrapped around one isolation chamber. Its single isolation chamber has a distinct cost advantage over large inline systems; however, cluster tools cannot handle the same product throughput or substrate sizes as inline systems. Cluster system designs do have the advantage of random access to process modules. Thus, one could change a layer sequence without refitting or changing a process chamber.

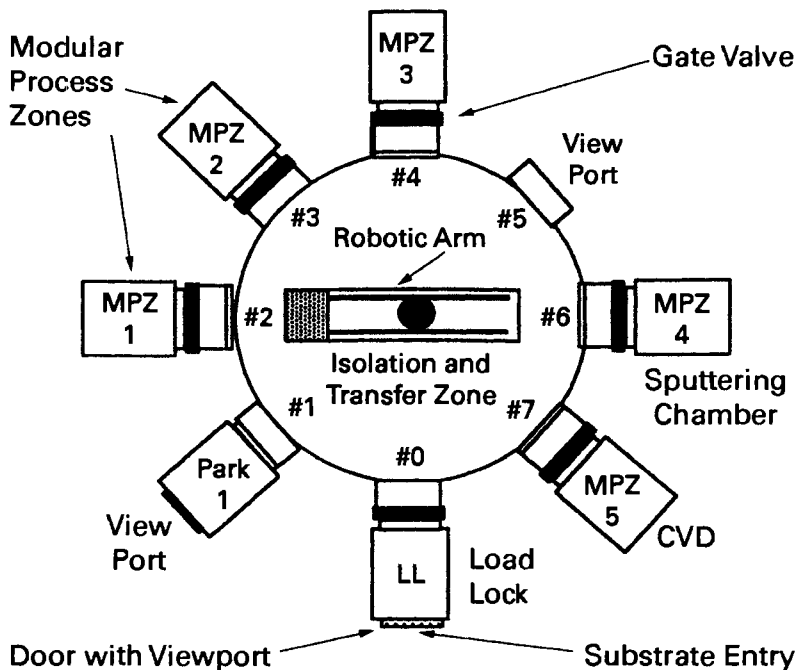


Fig. 23.9 Cluster tool system designed for silicon device fabrication. This system contains a central transfer/isolation chamber, one load-unload chamber, and one auxiliary chamber. The auxiliary chamber can be a buffer or holding chamber. Reprinted with permission from A. Madan, MVSystems Inc. 17301 W. Colfax Ave., Unit 305, Golden, CO, 80401.

One example of a single cluster tool is illustrated in Fig. 23.9. This system contains one load lock through which all substrates are loaded and unloaded. To allow flexibility in substrate movement, one chamber is used to park or store substrates. Each chamber contains a specific process such as reactive sputtering or chemical vapor deposition. The robotic arm is a required feature of all cluster tools and it is used to transfer substrates between process chambers. If needed, a second cluster tool could be connected to the first and provide a greater number of process zones and simultaneous depositions.

The second example of a single cluster tool is depicted in Fig. 23.10. This chamber contains separate exit and entrance load locks. A dual robotic arm, which can access two chambers simultaneously, permits high product throughput. Silicon wafers, for which this system was designed, are loaded externally in ultraclean, isolated cassettes. A separate handling system transfers the incoming 200- or 300-mm-diameter wafers in the cassette to or from their respective unload or load lock. The load and unload chambers contain separate pumping systems capable of pumping each lock to $\sim 10^{-3}$ Pa (10^{-5} Torr). The transfer chamber can be pumped to a

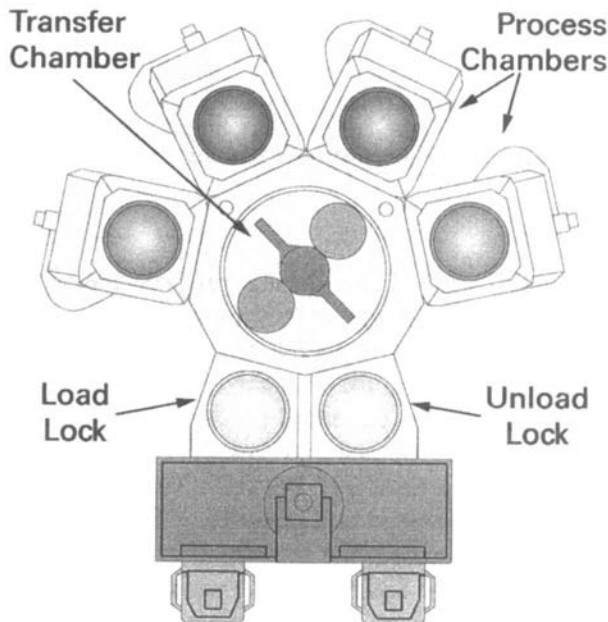


Fig. 23.10 The Dielectric Etch eMax™ Centura® cluster tool designed for processing silicon microelectronic devices. This system contains a central transfer chamber and dual load locks—one used for product load and the second used for product unload. Reprinted with permission from Applied Materials, Inc., 3050 Bowers Ave. Santa Clara, CA 95054.

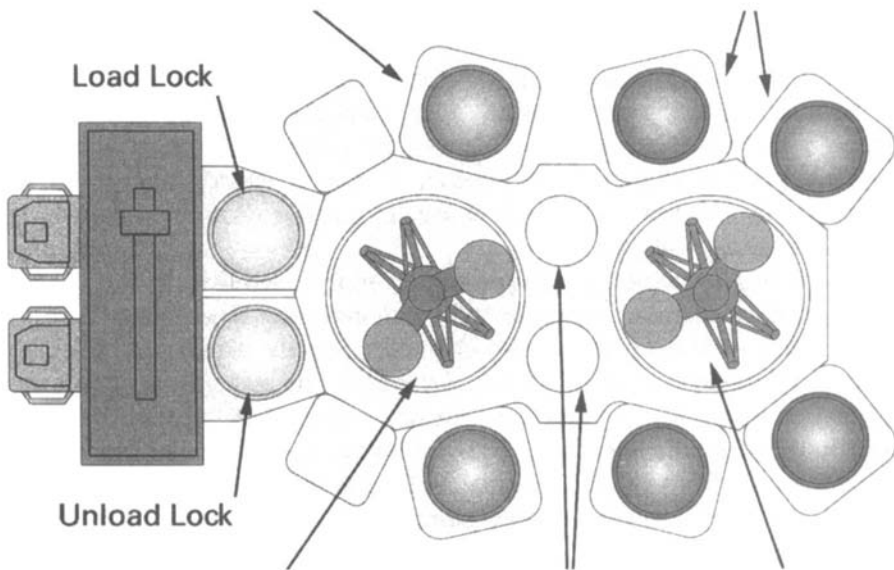


Fig. 23.11 Endura® xP cluster tool system for deposition of metal films. This system contains two transfer chambers and dual load locks. The transfer chambers communicate by means of intermediate locks—one for incoming product and one for outgoing product. Reprinted with permission from Applied Materials, Inc., 3050 Bowers Ave. Santa Clara, CA 95054.

pressure of 10^{-5} Pa (10^{-7} Torr) during product transfer. Each process chamber is isolated from the transfer chamber with a slit gate valve.

A second design of increased complexity, shown in Fig. 23.11, uses two transfer chambers. However, the transfer chambers are not identical and are not designed simply for increased product throughput. In this system, the load/unload locks are pumped to a pressure of 10^{-3} Pa, transfer chamber #1 is pumped to a pressure of 10^{-5} Pa, (10^{-7} Torr) whereas the right-hand #2 transfer chamber is pumped to a pressure of 10^{-6} Pa (10^{-8} Torr). Product wafers are transferred between the transfer chambers through intermediate locks. The intermediate or isolation locks are not pumped, but assume the pressure of the chamber to which they are connected. The purpose of this dual-transfer chamber design is to isolate critical processes from atmospheric contamination. In a single-transfer-chamber system, cross-contamination from the loadlock to the transfer chamber can enter the process chamber. Since the limiting pressure is no less than 10^{-5} Pa, residual water vapor or oxygen desorbing from surfaces can backdiffuse

into adjacent process chambers. Precleaning, which does not demand ultraclean vacuum pressures, is done in the left side. Moving a wafer from transfer chamber #1 to the transfer chamber #2 further reduces the cross-contamination from atmosphere, allowing transfer chamber #2 to attain a reduced base pressure. In turn, this reduces the residual cross-contamination to the critical metal deposition processes. These chambers can be pumped to pressures of order 10^{-7} Pa (10^{-9} Torr) allowing ultraclean metal films to be formed by physical vapor deposition.

Each of the multichamber systems described in this chapter had a different design goal. Some were designed for extremely high product throughput, some for flexibility, and others for high volume manufacturing in an ultraclean environment. Each was designed with the goal of reduced capital cost and reduced unit cost for a specific product. Innovative designers will continue to create new designs that are based on new materials and a thorough understanding of fundamental vacuum principles.

23.3 Instrumentation Systems

Instrumentation systems such as atmospheric pressure ionization mass spectrometers (APIMS) and gas chromatograph–mass spectrometers (GC–MS) have a need for multichamber pumping. In each case, the incoming gas source is at atmospheric pressure. The analyzer chamber cannot operate at this pressure, because the mean free path must be long. In the APIMS, ionization is done in a corona discharge at one atmosphere; however, the mass analysis must be performed at a pressure of order $\leq 10^{-3}$ Pa in order to avoid gas–gas collisions. Typical pressure reducing systems use 2–3 gas expansion chambers. Since a small pump can remove gas rather

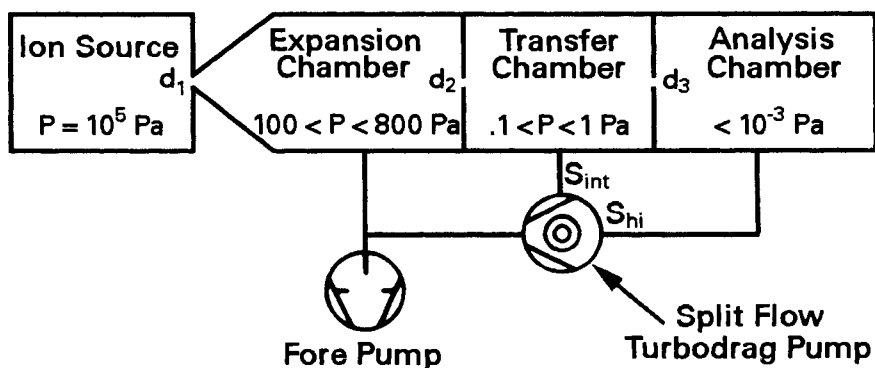


Fig. 23.12 Schematic of a gas sampling system such as might be used on an atmospheric pressure ionization mass spectrometer. Reprinted from *Vacuum*, 47, O. Ganschow and A. Conrad, 757–762, copyright 1996, with permission from Elsevier.

efficiently at high pressures, such a gas sampling system is cost effective, especially when combined with the efficiency of a split-flow turbodrag and single fore pump. An example of such a sampling system is illustrated in Fig. 23.12. Air-to-air coating of steel sheet and wire uses a similar concept where wire or sheet stock passes through slits. Multiple chambers separated by slits are used to reduce the pressure to the central process chambers where the material is cleaned and coated, followed by a reverse sequence of the chambers through which the material exits to atmosphere.

REFERENCES

1. J. Keiser, W. Schwarz, and W. Wagner, *Thin Solid Films*, **119**, 217 (1984).
2. A. Madan, MVS Systems, Inc. 17301 W. Colfax Ave., Unit 305, Golden, CO 80401.
3. Y. Kuwano, M. Ohnishi, S. Tsuda, Y. Nakashima, and N. Nakamura, *Jpn. J. Appl. Phys.*, **21**, 413 (1982).

PROBLEMS

- 23.1 The calculations in this problem refer to the illustration given in Fig. 23.1a. Calculate the high vacuum pumping speeds required for a large production web coater designed for deposition of magnetic recording tape. The rolls are 0.65 m. wide and have a total outgassing rate of 3200 Pa-L/s after a brief pumping time. Proper adhesion requires a glow discharge cleaning step, which adds another 3000 Pa-L/s of gas from the discharge source and surface desorption from the polymer at the operational winding rates. (The glow discharge apparatus is not illustrated in Fig. 23.1, but it is depicted in Fig. 23.2.) A desorption rate of 15 Pa-L/s is measured from a 0.65-m-wide \times 0.5-m-long sample of the polymer, which has been glow discharge cleaned and is exposed to the lower chamber. The gas load from the sputter deposition system is 70 Pa-L/s. The film quality is unacceptable if the pressure in the deposition chamber is $>1 \times 10^{-2}$ Pa. The 2.5-m-diameter mild steel chamber is 1 m deep. It is divided into an upper winding chamber and a lower deposition chamber. Consider the upper and lower parts to have equal internal surface area. The upper half contains a feed roll, a winding roll, and a glow discharge cleaning apparatus. The lower chamber is isolated from the upper chamber by the coating roller and the shelf in the middle. The slits separating the shelf and the drum are described in Fig. 23.1a. They have a total perimeter of 2.2 m along the sides and ends of the center drum. The dimensions of the slits, which separate

- the front of the coater containing the three spindles from the outer walls, are given in Fig. 23.1*a*. They extend a total of 3.2 m along the sides and across the back of the chamber. The following solution sequence is suggested: (a) Tabulate the outgassing loads in the upper and lower chambers. Which gas loads are dominant? Does the outgassing load of the wall have to be known with significant accuracy? (b) Write two coupled equations for the gas flow in and out of the upper and lower chambers. Solve these two equations for the individual high vacuum pumping speeds required at the upper and lower chamber entrances. There are two equations and three unknowns—the speed at the winding chamber, and the speed at the deposition chamber, and the pressure in the winding chamber—your answer will not be unique. *Hint*: Sketch a plot of the calculated upper and lower chamber speeds versus upper chamber pressure. (c) Suggest a pair of pumps for this system. What kind of pumps would you choose for the two chambers?
- 23.2 Solve Problem 23.1, using the slit design given in Fig. 23.1*b*. Assume the same length dimensions for each slit as used for Problem 23.1. If one were to use the same pumping speed for the lower chamber as in Problem 23.1, what would the pressure in the deposition chamber become? Can you translate this into reduced impurity concentration in the sputtering chamber?
- 23.3 What chamber high vacuum pumping speed and high vacuum pump type would be needed if the process were to be done in one chamber with no dividing partition?
- 23.4 Consider the slightly different three-chamber web coater illustrated in Fig. 23.2. Assume the drum slits all have the same conductance as calculated using the dimensions given in Fig. 23.1*b*. Assume a pumping speed in the intermediate chamber of 2500 L/s. Calculate the pump speed needed in the deposition chamber and in the winding chamber. Can the impurity concentration due to gas flow through the slits separating the intermediate and deposition chamber be reduced from the values determined in Problem 23.2?
- 23.5 Examine the inline deposition depicted in Fig. 23.5. (a) Describe the relative pressures that are desired in the load lock and in the first *p*-Si deposition chamber at the time a substrate is transported through the slit valve. (b) Describe the relative pressures desired in each succeeding pair of chambers during substrate transfer. The process gases illustrated show only the active gases; inert gases would also be available either for diluting the silane, or for flushing chambers during wafer transfer.

- 23.6 Examine the inline deposition system depicted in Fig. 23.6. Describe the process conditions during individual substrate transfer that would minimize cross-contamination between adjacent deposition chambers.
- 23.7 Examine the isolation-pumping scheme illustrated in Fig. 23.8 used in a high-speed, large area architectural glass coating system. All isolation “tunnels” or slits are identical. The glass sheets are 100 inches wide (perpendicular to the plane of the page) and 144 in. long; whereas the slits are 104 in. wide. All slits are 8 in. long (parallel to the plane of the page). The gap between the lower slit and the bottom of the glass sheet is 8 mm. The glass is 19 mm thick. The gap between the upper surface of the glass and the upper slit is 22 mm. In a simple nonreactive sputtering application, the argon pressure in the process chamber can range from 2- to 5-mTorr. (a) Calculate the required isolation diffusion pumping speed at the isolation chamber, for an isolation chamber pressure of 10^{-5} Torr. (b) Recalculate the pump speeds if the glass sheet thickness changed to 3.2 mm and the upper slit was not moved. (c) Assuming that the pumping speed at the system is 1/3 of its value at the diffusion pump inlet, what size diffusion pumps would be required? (d) Adjacent 144-in.-long sheets can be spaced as closely as 3 in. from each other on the continuously moving conveyer. Describe the transient condition in the system during the interval when the gap between two sheets passes through the isolation chamber. Can this result in any transient cross-contamination?
- 23.8 Calculate the required diffusion pump speeds at the process chamber, and at the pump for a non-reactive sputtering application using 500 sccm of argon.
- 23.9 What is the purpose of the exit buffer, exit hold and unload locks in the system described in Fig. 23.7? Propose a process sequence with vacuum levels, and so on, for transporting the finished product to the exit inspection zone. What gas might be used for venting? Should it be filtered?
- 23.10 An atmospheric pressure mass spectrometer (APIMS) vacuum system uses a roughing pump ($S = 1.5 \text{ m}^3/\text{h}$) and a split-flow turbo drag pump ($S_{\text{hi}} = 200 \text{ L/s}$, $S_{\text{mt}} = 125 \text{ L/s}$), as shown in Fig. 23.12. Assume that the inlet piping reduces the chamber pumping speeds of the turbo stages to one-half their flange speeds. Calculate the gas flow in each orifice, pipe, and pump inlet, if $P_{\text{expansion}} = 800 \text{ Pa}$, $P_{\text{transfer}} = 1 \text{ Pa}$, and $P_{\text{analysis}} = 10^{-3} \text{ Pa}$. If N_2 is the carrier gas, what are the compression ratios of the inlet and intermediate stages of the turbo? What are the three orifice diameters?

CHAPTER 24

Leak Detection

At some time we will be confronted with a system that does not behave normally—behavior that could be the result of a component malfunction, initial outgassing, or leak. On another occasion we may have to qualify a new system. When and how to hunt for leaks are two useful leak hunting skills. This discussion will focus on how to find leaks, mainly using a mass spectrometer tuned to helium, which permeates fine leaks.

The decision to search for leaks is as important as the method chosen for their detection. Each new component or subassembly should be routinely leak-tested after welding or brazing. However, it is premature to leak-test a new system a few hours after placing it in operation, because its performance does not meet the user's expectations. New systems often pump slowly, because of outgassing from fixtures, seals, and fresh pump fluids. The patient operator will usually wait a few days before criticizing the base pressure. At that time it would be useful to take an RGA scan of the system background or to leak-test the system.

Searching for a leak in an established system is reasonably straightforward, especially when a history of the system is known. A well-documented logbook assists the operator in determining the cause of the poor performance. A logbook should contain information such as the system pressure versus pumping time, base pressure, rate of rise, maintenance history, and a background RGA scan taken under known good performance conditions.

The most sensitive step in the leak-checking procedure is done with a mass spectrometer leak detector (MSLD) or residual gas analyzer (RGA). The MSLD a mass spectrometer permanently tuned to helium at $M/z = 4$ that is attached to a portable unit with a self-contained pumping system. The first all metal leak detector was designed by Prof. A. O. Nier for the Manhattan project [1,2] and had an ultimate sensitivity of 1×10^{-6} sccs (1×10^{-4} Pa-L/s) [1]. By contrast, instruments of this generation have a sensitivity of 10^{-11} sccs (10^{-9} Pa-L/s). This chapter describes the principles of two popular MSLD instruments, the classical forward flow leak detector

and the counter flow detector. The fundamentals of RGA operation were described in Chapter 8, and here we add some leak hunting techniques. The two most important parameters for these instruments are the sensitivity and response time of the measuring instrument. The chapter concludes with hints and procedures for finding leaks.

24.1 INSTRUMENTS

Mass spectrometer leak detectors are configured in two primary styles, forward flow and counter flow. These instruments are normally connected to an evacuated test chamber, which is probed externally with helium. The mass analyzer senses helium permeating a leak. The MSLD inlet may also be connected to a capillary tube or a bypass element, which can sample helium emanating from a pressurized test vessel.

24.1.1 Forward-Flow Leak Detector

The classical forward flow leak detector is sketched in Fig. 24.1. It consists of a small high vacuum pump—formerly a diffusion pump, but currently a turbomolecular pump—a magnetic sector mass filter tuned to $M/z = 4$, a cold trap, a separate mechanical pump, and an arrangement of valves for exhausting the test sample. Some instruments have two mechanical pumps, one for backing the high vacuum pump, and a separate roughing pump for exhausting rather leaky test objects for long times. The test object, which can be either a small assembly or a large vacuum system, is connected to the inlet port, and exhausted. If the object is small, the internal roughing

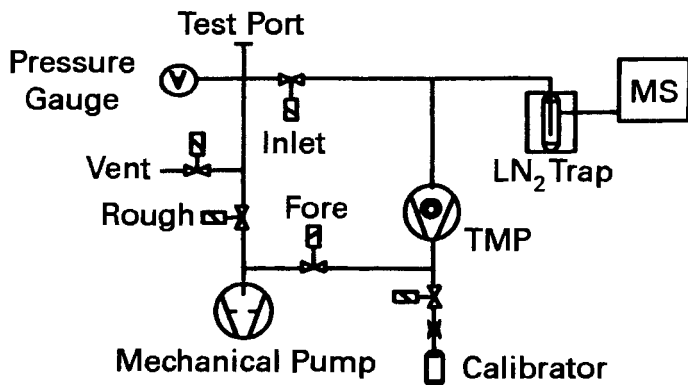


Fig. 24.1 Vacuum circuit of a classical forward flow leak detector. Reprinted from *Vacuum*, 44, W. G. Bley, 627–632, copyright 1993, with permission from Elsevier.

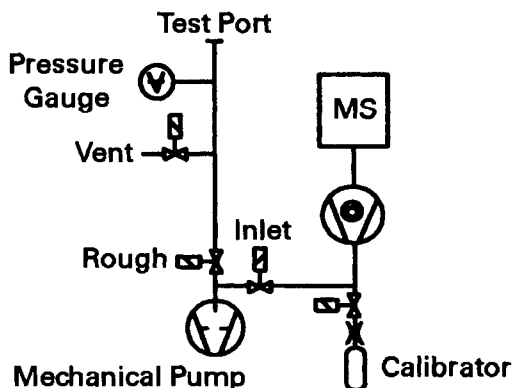


Fig. 24.2 Vacuum circuit of a counter flow leak detector. Reprinted from *Vacuum*, 44, W. G. Bley, 627–632, Copyright 1993, with permission from Elsevier.

pump will suffice; however, if the volume to be tested is large, the system pump will also be needed. After reaching a sufficiently low pressure, the test object is connected to the inlet of the high vacuum pump. Helium sprayed around suspected leak sites will find its way into the high vacuum pump, through the cold trap and into the mass analyzer. A second roughing pump is useful when long times are required to exhaust a test object with large leaks and to prevent excessively high turbo forepressure. The classical leak detector requires a liquid nitrogen trap above the high vacuum pump to prevent diffusion pump fluid from reaching the mass analyzer and to reduce the partial pressure of water and other condensable vapors. Silicone diffusion pump fluids are not recommended for this application, as they leave an insulating deposit on the deflection electrodes.

24.1.2 Counter-Flow Leak Detector

The counter flow leak detector is illustrated in Fig. 24.2. The object to be tested is connected to the foreline of the high vacuum pump; however, the mass filter remains connected to the high vacuum pump inlet. The high vacuum pump used for this application must have a high compression ratio for atmospheric air, but a low compression ratio for helium. This can be accomplished with either a diffusion pump or a turbo pump. Recall that the compression of a diffusion pump jet is exponentially proportional to the oil velocity and the compression of a turbo pump blade is exponentially proportional to the blade tip velocity. Low helium compression can be achieved in a diffusion pump by reducing the number of stages, the heater power, and the pump's height-to-diameter ratio. In a similar manner the rotational speed of the turbo can be decreased, the number of blade rows

can be decreased, and blade angles can be increased. In this manner, the high compression for all gases, except helium, maintains high vacuum in the mass analyzer; however, the low compression for helium allows it to backstream through the turbo or diffusion pump where it is detected.

By isolating the mass filter from the test sample, the need for liquid nitrogen has been eliminated and a truly portable instrument created. The counter-flow concept is the most significant advance in leak detector design, since the invention of the leak detector six decades ago.

24.2 PERFORMANCE

Leak detector performance is primarily dependent on the sensitivity and response time of the instrument, but its overall performance cannot be determined without knowledge of the vacuum system under test.

24.2.1 Sensitivity

Either the RGA or the MSLD is sensitive to a threshold partial pressure of the tracer gas used to probe the leak. In the best case, the minimum detectable partial pressure is the absolute sensitivity of the instrument above the background noise. In a typical operating system a residual background pressure of the tracer gas exists, because it is regurgitated from a pump, back-diffuses through a pump, is released from permeable materials, or is desorbed from a cold trap surface. This residual gas pressure may be considerably greater than the ultimate detectable pressure of the instrument and therefore significantly increase the minimum detectable tracer pressure. The helium leak flux Q_L is related to the helium pressure in the mass spectrometer by $Q_L = P_L S_L$. The sensitivity s , of the forward flow leak detector has been defined as [3]

$$s = \frac{P_L}{Q_L} = \frac{1}{S_L} \quad (24.1)$$

where the given quantities are for helium. In a similar manner, the sensitivity of the counter flow leak detector was shown to be [3]

$$s = \frac{1}{(K_{high\ vac} \cdot S_{fore\ pump})} \quad (24.2)$$

where the compression K is the compression ratio for helium in the high vacuum pump, and S is the helium forepump speed.

As the maximum inlet pressure to either unit is increased, the flow to either the forward flow or counter-flow detector must be throttled, or the

pressure in the mass analyzer will rise above its operating range. Figure 24.3 illustrates how the sensitivity decreases above the throttling pressures for the forward flow and counter flow units. From this figure one sees that the counter-flow unit is more sensitive than the forward-flow unit at high sampling pressures, or leak rates, whereas the forward-flow unit is more sensitive at the lowest possible leak rates. Chew notes that helium retention in commercial mechanical pumps varied widely [4]; for some pumps, pump venting or gas ballast was necessary to remove dissolved helium.

From (24.1) one can see that the maximum detectable sensitivity is reached at zero helium pumping speed. Closing the valve between the system pump and chamber allows the leaking tracer gas to accumulate in the chamber. This is easily accomplished when leak-detecting with an RGA and with MSLD units that are equipped with a valve between the ionizer and self-contained pump. A constant leak will cause the helium partial pressure to increase linearly with time at zero pumping speed. After time t_1 a detector will measure partial pressure P_1 ; the leak flux will be given by $Q = P_1 V/t_1$. This technique for increasing the basic sensitivity is called the accumulation technique. Small volumes may also be tested effectively by isolating them completely from the MSLD. After time t , a connecting valve is opened and the collected quantity of helium is allowed to flow to the MSLD. The minimum leak flux detectable by an RGA or MSLD in normal operation is $\sim 10^{-9}$ Pa-L/s. The accumulation technique has been used to detect leaks as small as 10^{-11} – 10^{-13} Pa-L/s [5,6]. In normal vacuum system operation, leaks less than 10^{-8} Pa-L/s are uncommon [7]; they tend to hydrolyze shut with exposure to atmosphere.

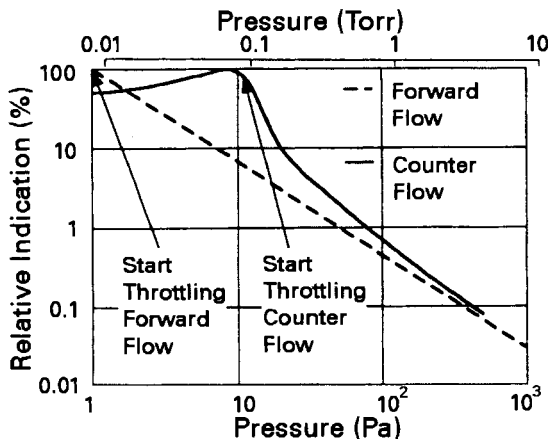


Fig. 24.3 Sensitivity versus pressure for forward-flow and counter-flow leak detectors connected to a pumped vacuum system (10 Pa is the start of throttling the counter-flow leak detector; throttling begins at 1 Pa in the forward flow unit, even when LN_2 is used). Reprinted from *Vacuum*, 44, W. G. Bley, 627–632, copyright 1993, with permission from Elsevier.

24.2.2 Response Time

The maximum sensitivity of the leak detector can be realized only if the tracer gas has had time to reach the steady-state value. For a system of volume V evacuated by a pump of speed S , the pressure change due to a sudden application of a tracer gas to a leak is given by

$$P_{tracer}(t) = P_{tracer}(0)(1 - e^{St/V}) \tag{24.3}$$

where $P_{tracer}(t)$ is the background pressure of the tracer gas. At time zero, the pressure of the tracer gas in the system is $P_{tracer}(0)$. The pressure slowly builds to a steady-state value. Sixty-three percent of the steady-state pressure is reached in a time equal to the system time constant V/S ; five time constants are required to reach 99% of the response. This means that a 100-L system pumped by a leak detector with a speed of 5 L/s will require application of the tracer gas for 20–100 s to realize the maximum sensitivity of the instrument. This is the case when an MSLD is connected to a chamber that has been isolated from the high vacuum pump by a valve. See Fig. 24.4a. Placing pumps in parallel, as illustrated in Fig. 24.4b, can reduce the time constant, but not without loss of sensitivity. If the leak detector can handle the gas load, the fast time constant can be retained in turbomolecular and diffusion pumps without loss of sensitivity by placing the leak detector in the foreline and isolating the mechanical pump from the system by a valve. See Fig. 24.4c. This technique may be used if the gas flow is too large for the leak detector by allowing the leak detector to pump at its maximum flow rate, while pumping the remainder of the gas

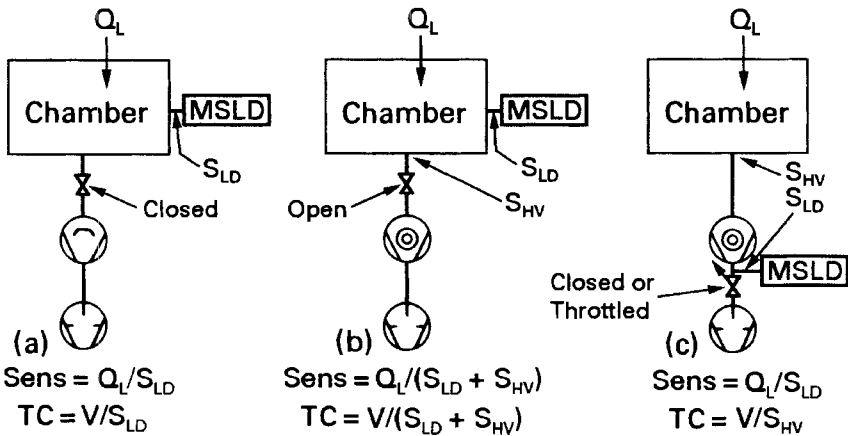


Fig. 24.4 Three techniques for using an MSLD to detect leaks in a vacuum chamber pumped by a diffusion or turbomolecular pump. Methods *a* and *c* have a high sensitivity; methods *b* and *c* have a short response time.

with the forepump. Now, the fast time constant is retained and the sensitivity is reduced only by the ratio of forepump to leak detector flow.

Leak detection in an ion or cryogenic pumped system must be done differently, because they are capture pumps. An ion pump may be helium-leak checked by momentarily removing power to the pump. A cryogenic pump cannot be shut down for leak checking, because the evolved gas load will overload the pump in the MSLD. If the cold stage temperature is increased to 20 K, the helium pumping of the sorbent bed will drop to zero and the leak detector can be operated at its maximum sensitivity. The pump must be equipped with a heating element on the cold-stage for this purpose. If the cold stage is not heated during leak detection, helium will accumulate. Helium will desorb the next time the pump is exposed to air. A sufficient quantity of desorbed helium will thermally short the pump. As we discussed in Chapter 20, no amount of pumping will help; complete regeneration is required. Moraw and Prasol [8] have discussed the optimum conditions for leak detecting large space chambers.

24.2.3 Sampling Pressurized Chambers

The capillary sniffer probe and the bypass sampler are two methods for sampling pressurized containers. It is best to test a system under conditions of normal use. Therefore, gas regulator fittings and gas distribution lines are often tested by internally pressurizing with helium and sniffing for helium escaping to atmosphere. The capillary probe is simply a long probe containing very-small-diameter tube with a porous plug that limits the flow to $\sim 10^{-3}$ sccs (10^{-1} Pa-L/s). The end of the probe is connected to the inlet of the MSLD. Molecular flow through the porous plug enhances the helium flow by a factor of ~ 2 . See equation (2.20). The volume of the tube is sufficiently small to have a response time of ~ 2 s. A bypass sampler operates on an entirely different principle. A sampling probe, illustrated in Fig. 24.5, consists of a long tube connected at one end to a pump with a flow capacity of 1–2 sccs. A small fraction of this flow is pumped into the MSLD through a porous bypass leak. Including the mass separating ability of the porous plug, $\sim 1/1000$ of the helium is sensed by the MSLD. The tube diameter is such that a time constant of a few seconds is maintained.

24.3 LEAK-HUNTING TECHNIQUES

It is not possible to provide a complete list of leak-hunting methods, but it is helpful to review some techniques. A thorough understanding of the system under test is invaluable. The system volume and pumping speed must be known in order to calculate the system time constant.

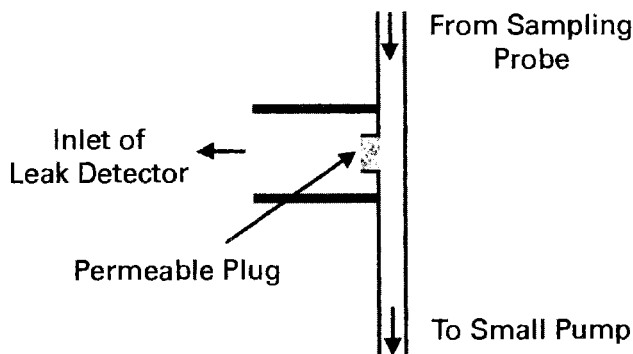


Fig. 24.5 A bypass sampling technique for sniffing He from internally pressurized vessels.

A system that cannot be pumped below the operating range of the roughing pump has a gross leak or a malfunctioning pump. Start at the beginning. First, close all the valves in the system and observe the pressure in the mechanical pump with a thermal conductivity gauge. In a system with no valves, the mechanical pump should be disconnected and connected to a blank flange containing only a thermocouple gauge. Poor pressure at the inlet to the blanked-off roughing pump may be a result of low oil level, oil contamination, or an internal difficulty such as a sticking vane or exhaust valve. A pump used on corrosive gases may be badly etched or contaminated. If the pump is operating properly, sections of the foreline and roughing line can be pumped sequentially and systematically until the leaky section is isolated. Helium may be sprayed around suspected seals and welds, while listening for a change in the pitch of the motor, in the fashion of a child speaking after taking a breath of helium. Alternatively, alcohol sprayed on a leak causes a large upward deflection of a thermal conductivity gauge. Helium sprayed on a leak in a roughing line connected to a sorption pump will show a large pressure increase.

If the system pumps to the high vacuum range, but cannot reach its usual base pressure, there may be a leak. A leak is not the only reason for poor performance. There may also be a faulty high vacuum pump, a leak on the pump side of the gate valve, a contaminated gauge, or considerable outgassing. Next, close the high vacuum gate valve and observe the downstream pressure. A low pressure on the pump side of the gate valve tells us the pump is operating properly. If the blank-off pressure is high, the pump could be leaky or faulty. A leak detector can be attached to the foreline of a diffusion or turbomolecular pump or to a flange adjacent to a cryogenic or ion pump. A valve in the foreline, shown in Fig. 24.4c, allows the leak detector to be attached without removing power from the pumps. When specifying a new system, insist on a valve at this location.

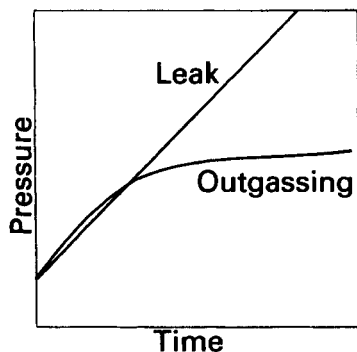


Fig. 24.6 Response of a sealed chamber to a leak and to outgassing from interior walls. Adapted with permission from *Handbook of Vacuum Leak Detection*, N. G. Wilson and L. C. Beavis, Eds. Copyright 1976, The American Vacuum Society.

After the system has been shown to be leak free from the mechanical pump through the top of the high vacuum pump, the gate valve to the chamber may be opened. Poor chamber pressure may result from outgassing, external leaks, or internal leaks. One simple way to distinguish between leaks and outgassing is to examine a plot of the system pressure versus time after closing the high vacuum valve. See Fig. 24.6. A molecular leak causes a linear increase in pressure with time. Outgassing causes the pressure to rise to a steady-state value that is determined by the vapor pressures of the desorbing species. If the system contains an RGA, a quick scan tells us whether the poor performance is due to an atmospheric leak or outgassing, although outgassing of water vapor may be difficult to distinguish from a leak in a water line.

External leak checking with helium should begin at the top of the chamber; only a small helium flow rate is necessary. In some cases it may be necessary to wrap plastic around an area and flush it with nitrogen to prevent helium from entering more than one potential leak site. Alcohol freezes in a small leak and allows adjacent areas to be checked without confusion. The alcohol can be removed with a heat gun. The most obvious places, such as welds and seals should be checked first. Welds and seals are the most common leak sites; however, leaks have been observed in sheet stock used to make flanges or chamber walls. See Chapter 17. Leaks through such voids are usually masked with grease and appear only after baking. The helium background pressure may increase slowly with time when a search is made for small leaks with the MSLD in systems sealed with elastomer O-rings. This pressure rise is due to helium permeation. The permeation time is about 20 min for a typical Viton O-ring. Figure 24.7 illustrates the time required for helium to permeate a gasket at room temperature. Assuming the solubility does not change on heating to 80°C,

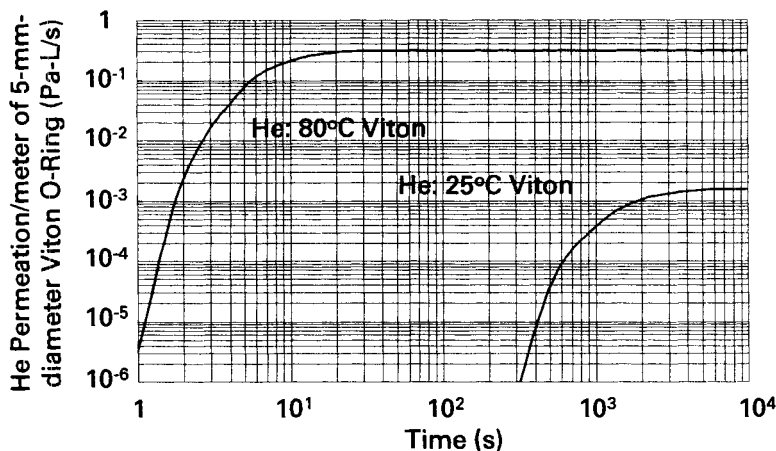


Fig. 24.7 Calculated helium permeation at 25°C and 80°C through a Viton gasket initially containing no helium. The steady-state permeation rates are experimentally measured; the solubility is derived from the measured time to reach equilibrium at room temperature.

the measured helium permeation rates at the two temperatures yield the second curve in Fig. 24.7. There are two messages here. First, do not attempt to leak check the system during baking. Second, helium background from a loaded O-ring will not decrease until it has been pumped from the gaskets. A coffee break may be required before proceeding. Helium may on occasion cause other difficulties. In differentially pumped O-rings, it was observed to collect in sidewall pockets of O-ring grooves; it remained until the flange was loosened [9].

Interior water lines are difficult to check because water may slow the diffusion of helium through the leak. Water lines are best checked by draining, connecting directly to the leak detector, and warming with a heat gun before spraying with helium from the interior of the chamber. If one does not warm with a heat gun, traces of water in the lines will freeze and mask the leak from detection.

Interior leaks in liquid nitrogen traps are quite difficult to locate. Leaks have been observed when LN₂ has been added to the trap, or suspected when large signals at $M/z = 14$ and 28 are observed with an RGA. Trap leaks may be verified by bubbling helium through the liquid nitrogen and looking for its appearance on an RGA or MSLD. The trap will have to be removed from the system and leak checked with an MSLD to pin point the leak. Sometimes the source of a large peak at $M/z = 28$ is not obvious. Nitrogen is often used to release chambers to atmosphere. A through leak in the nitrogen bleed valve cannot be detected by spraying the external walls with helium. Internal valve seat leaks in this line can be located by pumping the nitrogen from a section of this line and replacing it with helium.

RGAs allow the user to determine the state of the system with little additional data. Air leaks and water outgassing are easily differentiated. Air leaks are discerned by the presence of oxygen at $M/z = 32$, except in large TSP systems in which the oxygen pumping speed is so large that the oxygen signal will not be seen, and in baked UHV systems where it is adsorbed on stainless steel walls. Outgassing and water line leaks each can produce a large peak at $M/e = 18$, but they can be distinguished by the rate of rise. The RGA has the added advantage of functioning with tracer gases other than helium. Oxygen is often used for leak checking sputter-ion pumped systems and argon for TSPs. Additional operational hints are given in the AVS leak-detection handbook [10].

The helium mass spectrometer leak detector has been universally accepted for sensitive leak detection of vacuum components and systems. The instrument is most valuable if it has an internal calibration standard and valves for throttling the internal pumping speed (accumulation technique) and the inlet flow (foreline sampling technique). Sampling and sniffing probes are useful for leak checking ultrapure gas delivery lines.

REFERENCES

1. A. Nerkin, *J. Vac. Sci. Technol. A*, **9**, 2036 (1991).
2. A. O. Nier, C. M. Stevens, A. Hustrulid and T. A. Abbott, *J. Appl. Phys.*, **18**, 30 (1947).
3. W. G. Bley, *Vacuum*, **44**, 627 (1993).
4. A. D. Chew, *Vacuum*, **53**, 243 (1999).
5. J. F. O'Hanlon, K. C. Park, A. Reisman, R. Havreluk, and J. G. Cahill, *IBM J. Res. Dev.*, **22**, 613 (1978).
6. F. Watanabe and H. Ishimaru, *J. Vac. Sci. Technol. A*, **8**, 2795 (1990).
7. L. C. Beavis, *Vacuum*, **20**, 233 (1970).
8. M. Moraw and H. Prasol, *Vacuum*, **28**, 63 (1978).
9. M. L. Johnson, D. M. Manos, and T. Provost, *J. Vac. Sci. Technol. A*, **15**, 763 (1997).
10. N. G. Wilson and L. C. Beavis, *Handbook of Leak Detection*, W. R. Bottoms, Ed., American Vacuum Society, New York, 1976.

PROBLEMS

- 24.1 How can gas ballast in a rotary vane pump be used to differentiate between a leak and oil contaminated with a high vapor pressure impurity?
- 24.2 † Why should connecting lines to the leak detector be as short in length and as large in diameter as possible?
- 24.3 Why should you turn off the high voltage (e.g., an rf sputtering power supply or a dc ion pump power supply) before spraying the high-voltage feedthrough on either system with helium?

- 24.4 † When using a MSLD to locate a leak, the helium should be allowed to remain at the leak site until the response (a) increases to its maximum amount or (b) reaches about 4–5 times the background signal level?
- 24.5 † An ultraclean component is leak checked on a counterflow leak detector. (a) Where in the leak detector vacuum circuit is the component attached? (b) Assuming it was leak tight when tested, what must then be done to this ultraclean component before it can be re-mounted on an ultraclean vacuum system?
- 24.6 A combination of a narrow, shallow o-ring groove and a large o-ring diameter, all within tolerances, can lead to trapped gas pockets on the inner and outer diameters at the base of the groove. A measurement of base pressure and/or rate of rise will suggest a leak. Helium leak detecting from the vessel exterior will show no leak even if there is a leak path across the base of the O-ring. How would you modify the flange to eliminate this problem?
- 24.7 Assume the sensitivity of a particular leak detector is 5×10^{-11} sccs. What is the minimum detectable leak that could be detected in a vessel internally pressurized with helium, assuming that the atmosphere contained the normal background concentration of helium, while using (a) a capillary sniffer and (b) a bypass sampler, each having characteristics given in Section 24.2.3.
- 24.8 Figure 24.3 indicates that the sensitivity of the counter-flow leak detector increases slightly, as the inlet pressure rises to the point where it must be throttled. Why does it increase?
- 24.9 Helium is used to internally pressurize a gas line for leak testing. The capillary probe described in Section 24.2.3 is used to sample the closed volume between the nickel gasket and the retaining nut in the all metal tubing seal. The retaining nut with an interior volume of 1 ml, contains two vent holes, one on each side. If the capillary probe is held against one of the leak detection holes, how long would it take for helium exiting a leak in the nut to reach the mass analyzer?
- 24.10 A cryo pumped chamber has a suspiciously high base pressure. All gaskets are helium-leak checked. After considerable searching, the leaking flange is located. It is tightened, the leak disappears, and the pressure drops to an acceptable level. Next an adjoining load lock is evacuated to 1 Pa with a separate pump. The connecting valve to the main cryo pump is then opened. The pressure in the main chamber suddenly rises and the cryo pump quits. Describe what happened. Give a procedure for correcting the situation.

Symbols

Symbol	Quantity	Units
A	Area	m^2
B	Magnetic field strength	T (tesla)
C	Conductance (gas)	L/s
D	Diffusion constant	m^2/s
E_o	Heat transfer	$\text{J}\cdot\text{s}^{-1}\cdot\text{m}^{-2}$
F	Force	N (newton)
G	Electron multiplier gain	
H	Heat flow	J/s
K	Compression ratio (gas)	
K_p	Permeability constant	m^2/s
Kn	Knudsen's number	
K_R	Radiant heat conductivity	$\text{J}\cdot\text{s}^{-1}\cdot\text{m}^{-1}\cdot\text{K}^{-1}$
K_T	Thermal conductivity	$\text{J}\cdot\text{s}^{-1}\cdot\text{m}^{-1}\cdot\text{K}^{-1}$
M	Molecular weight	
N	Number of molecules	
P	Pressure	Pa (pascal)
Q	Gas flow	$\text{Pa}\cdot\text{m}^3/\text{s}$
R	Reynolds' number	
S	Pumping speed	L/s
S''	Gauge sensitivity	Pa^{-1}
T	Absolute temperature	K (kelvin)
U	Average gas stream velocity	m/s
U	Mach number	
V	Volume	m^3
V_a	Acceleration potential	V
V_b	Linear blade velocity	m/s
W	Ho coefficient	
a	Transmission probability	
b	Turbomolecular pump blade chord length	m
c	Condensation coefficient	
c_p	Specific heat at constant pressure	$\text{J}\cdot(\text{kg}\cdot\text{mole})^{-1}\cdot\text{K}^{-1}$
c_v	Specific heat at constant volume	$\text{J}\cdot(\text{kg}\cdot\text{mole})^{-1}\cdot\text{K}^{-1}$

d	Diameter dimension	m
d_o	Molecular diameter	m
d'	Average molecular spacing	m
i_e	Emission current	A
i_p	Plate current	A
l	Length dimension	m
m	Mass of molecule	kg
n	Gas density	m ⁻³
q	Outgassing rate	Pa-m/s
q_k	Permeation rate	Pa-m/s
r	Radius	m
s	Turbomolecular pump blade spacing	m
s_r	Turbomolecular pump blade speed ratio	
u	Local gas stream velocity	m/s
v	Average particle velocity	m/s
Γ	Particle flux	m ⁻² -s ⁻¹
Λ	Free molecular heat conductivity	J-s ⁻¹ -m ⁻² -K ⁻² -Pa ⁻¹
α	Accommodation coefficient	
β	Molecular slip constant	
γ	Ratio c_p/c_v	
ε	Emissivity	
λ	Mean free path	m
η	Dynamic viscosity	Pa-s
ρ	Mass density	kg/m ³
ω	Angular frequency	rad/s
ϕ	Turbomolecular pump blade angle	deg

A User's Guide to Vacuum Technology, 3rd Edition. John F. O'Hanlon
Copyright © 2003 John Wiley & Sons, Inc.
ISBN: 0-471-27052-0

Appendixes

APPENDIX A

Units and Constants

Appendix A.1 Physical Constants

k	Boltzmann's constant	$1.3804 \times 10^{-23} \text{ J/K}$
m_e	Rest mass of electron	$9.108 \times 10^{-31} \text{ kg}$
m_p	Rest mass of proton	$1.672 \times 10^{-27} \text{ kg}$
N_o	Avogadro's number	$6.02252 \times 10^{26} / (\text{kg-mole})$
R	Gas constant	$8314.3 \text{ J-(kg-mole)}^{-1} \text{-K}^{-1}$
V_o	Normal specific volume of an ideal gas	$22.4136 \text{ m}^3 / (\text{kg-mole})$
σ	Stefan-Boltzmann constant	$5.67 \times 10^{-8} \text{ J-s}^{-1} \text{-m}^{-2} \text{-K}^{-4}$

Appendix A.2 SI Base Units

Length	meter	m
Mass	kilogram	kg
Time	second	s
Electric current	ampere	A
Thermodynamic temperature	kelvin	K
Amount of substance	kg-mole	kg-mole

Appendix A.3 Conversion Factors

Conventional unit	→multiply by→	to get SI unit
Mass		
lb	0.45359	kg
Length		
Ångstrom	1.0×10^{-10}	m
micrometer	1.0×10^{-6}	m
mil	0.00254	cm
inch	0.0254	m
foot	0.3048	m
Area		
ft ²	0.0929	m ²
in. ²	6.452	cm ²
ft ²	929.03	cm ²
Volume		
cm ³	0.001	L
in. ³	0.0164	L
gallon (US)	3.7879	L
ft ³	28.3	L
L	1000.0	cm ³
Pressure		
micrometer (Hg)	0.13332	Pa
N/m ²	1.0	Pa
millibar	100.	Pa
Torr	133.32	Pa
inches of Hg	3386.33	Pa
lb/in ²	6895.3	Pa
bar	100,000	Pa
atmosphere	101,323.2	Pa
Conductance or pumping speed		
L/h	0.000277	L/s
L/s	0.001	m ³ /s
L/min	0.0166	L/s
m ³ /h	0.2778	L/s
ft ³ /min	0.4719	L/s
ft ³ /min	1.6987	m ³ /h
Outgassing rate		
(Pa-L)/(m ² -s)	0.001	Pa-m/s
(mbar-L)/(m ² -s)	0.1	Pa-m/s
(Pa-m ³)/(m ² -s)	1.0	Pa-m/s
μL/(cm ² -s)	1.33	Pa-m/s
(Torr-L)/(cm ² -s)	1,333.2	Pa-m/s
to get conventional unit ←	divide by ←	SI unit

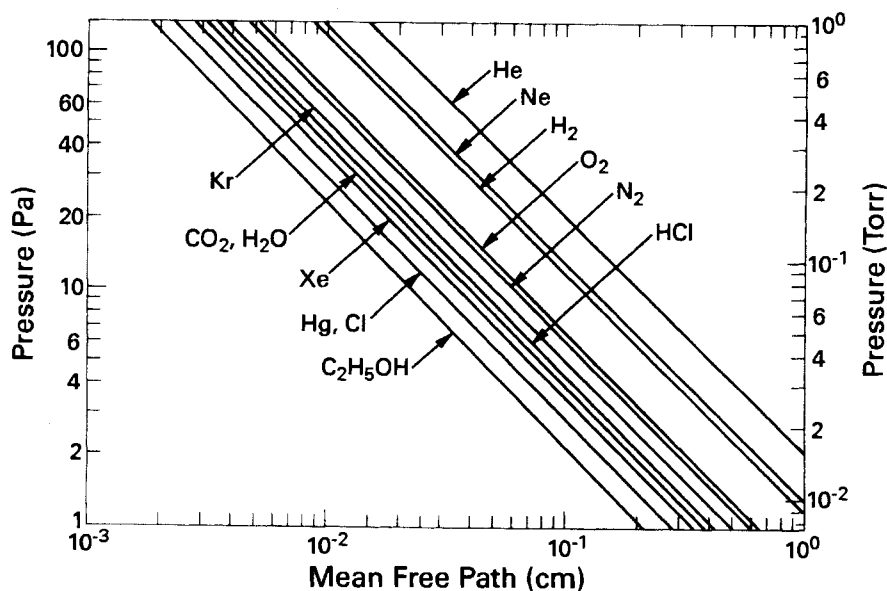
Appendix A.3 (Continued)

Conventional unit	→	multiply by	→	to get SI unit
Gas flow				
molecules/s (at 0°C)		4×10^{-18}		Pa-L/s
Pa-L/s		0.001		Pa-m ³ /s
Torr-L/s		0.133		Pa-m ³ /s
micron - L/s		0.13332		Pa-L/s
standard cc's/min (sccm)		1.69		Pa-L/s
Pa-L/s		3.6		Pa-m ³ /h
atm-cc/s		101.323		Pa-L/s
standard cc's/s (sccs)		101.323		Pa-L/s
Torr-L/s		133.32		Pa-L/s
standard liter/min (slm)		1689		Pa/L/s
(kg-mole)/s (at 0°C)		2.48×10^9		Pa-L/s
Gas permeation constant				
cm ³ gas (STP)-cm thickness/ (cm ² area-s-atmosphere)		0.0001		m ² /s
cm ³ gas (STP)-cm thickness/ (cm ² area-s-Torr)		0.076		m ² /s
Dynamic viscosity				
newton-s/m ²		1		Pa-s
poise		10		Pa-s
Kinematic viscosity				
centistoke		1		mm ² /s
Diffusion constant				
cm ² /s		0.0001		m ² /s
Heat conductivity				
Watt-cm ⁻¹ -K ⁻¹		100		J-s ⁻¹ -m ⁻¹ -K ⁻¹
Specific heat				
J-kg ⁻¹ -K ⁻¹		<i>M</i>		J-(kg-mole) ⁻¹ -K ⁻¹
cal-(g-mole) ⁻¹ -K ⁻¹		4184		J-(kg-mole) ⁻¹ -K ⁻¹
BTU-lb ⁻¹ -°F ⁻¹		4184 <i>M</i>		J-(kg-mole) ⁻¹ -K ⁻¹
Heat capacity				
J/kg		<i>M</i>		J-(kg-mole) ⁻¹
cal-(g-mole) ⁻¹		4184		J-(kg-mole) ⁻¹
BTU/lb		2325.9 <i>M</i>		J-(kg-mole) ⁻¹
Energy, work, or quantity of heat				
ft-lb		1.356		J
kW-h		3.6		MJ
BTU		1055		J
kcal		4184		J
to get conventional unit	←	divide by	←	SI unit

APPENDIX B

Gas Properties

Appendix B.1 Mean Free Paths of Gases as a Function of Pressure^a



Source. Reprinted with permission from *Vacuum Technology*, p. 505, A. Guthrie. Copyright 1963, John Wiley & Sons, New York, 1963.

^a $T = 20^\circ C$.

Appendix B.2 Physical Properties of Gases and Vapors at $T = 0^\circ\text{C}$

Gas	Symbol	MW ^a	Molecular Diameter ^b	Average Velocity ^c	Thermal Cond. ^{a,d}	Dynamic Viscosity ^{a,d}	Diffusion in Air ^{d,e}
			(nm)	(m·s ⁻¹)	(mJ·s ⁻¹ ·K ⁻¹)	(μPa·s)	(10 ⁻⁶ m ² ·s ⁻¹)
Helium	He	4.003	0.218	1197.0	142.0	18.6	58.12
Neon	Ne	20.183	0.259	533.0	45.5	29.73	27.63
Argon	Ar	39.948	0.364	379.0	16.6	20.96	17.09
Krypton	Kr	83.8	0.416	262.0	6.81 ^f	23.27	13.17
Xenon	Xe	131.3	0.485	209.0	4.50 ^g	21.9	10.60
Hydrogen	H ₂	2.016	0.274	1687.0	173.0	8.35	63.4 ^a
Nitrogen	N ₂	28.0134	0.375	453.0	24.0	16.58	18.02
Air		28.966	0.372	445.0	24.0	17.08	18.01
Oxygen	O ₂	31.998	0.361	424.0	24.5	18.9	17.8 ^a
Hydrogen chloride	HCl	36.46	0.446	397.0	12.76	14.25 ^g	14.11
Water vapor	H ₂ O	18.0153	0.46	564.0	24.1i	12.55i	23.9 ^{a,j}
Hydrogen sulfide	H ₂ S	34.08	0.47 ^k	412.0	12.9	11.66	14.62 ^k
Nitric oxide	NO	30.01	0.372 ^k	437.0	23.8	17.8	19.3 ^k
Nitrous oxide	N ₂ O	44.01	0.47 ^k	361.0	15.2	13.5	13.84 ^k
Ammonia	NH ₃	17.03	0.443	581.0	21.9	9.18	17.44
Carbon monoxide	CO	28.01	0.312 ^a	453.0	23.0	16.6	21.49
Carbon dioxide	CO ₂	44.01	0.459	361.0	14.58	13.9	13.9 ^a
Methane	CH ₄	16.4	0.414	592.0	30.6	10.26	18.98
Ethylene	C ₂ H ₄	28.05	0.495	452.0	17.7	9.07	13.37
Ethane	C ₂ H ₆	30.07	0.53	437.0	16.8	8.48	12.14

^a Reprinted with permission from *Handbook of Chemistry and Physics*, 58th ed., R. C. Weast, Ed. Copyright 1977, Chemical Rubber Co., CRC Press, West Palm Beach, FL.

^b Reprinted with permission from *Kinetic Theory of Gases*, E. H. Kennard, p. 149. Copyright 1938, McGraw-Hill, New York.

^c Calculated from Equation (2.2).

^d At atmospheric pressure.

^e Calculated from Equation (2.30).

^f $T = 210\text{ K}$, Reprinted with permission from *Cryogenic and Industrial Gases*, May/June 1975, p. 62. Copyright 1975, Thomas Publishing Co., Cleveland, OH.

^g Footnote e, $T = 240\text{ K}$.

^h $T = 18^\circ\text{C}$.

ⁱ $T = 100^\circ\text{C}$.

^j $T = 8^\circ\text{C}$.

^k Calculated from viscosity data.

Appendix B.3 Cryogenic Properties of Gases

Property	Units	He	H ₂	Ne	N ₂	Ar	O ₂	Xe	CF ₄
nbp liq. ^a	K	4.125	20.27	27.22	77.35	87.29	90.16	164.83	145.16
mp (1 atm) ^b	K		14.01	24.49	63.29	83.95	54.75	161.25	123.16
Density of liquid, nbp ^a	kg/m ³	124.8	70.87	1208	810.0	1410	1140	3058.0	1962.0
Volume of liquid, nbp	(m ³ /kg)×10 ⁻³	8.01	14.1	0.83	1.24	0.709	0.877	0.327	0.597
Volume of gas at 273 K ^a	m ³ /kg	5.602	11.12	1.11	0.79	0.554	0.698	0.169	0.274
Ratio V_{273}^g/V_{nbp}^l		699.4	788.7	1337	637.5	781.5	796.3	516.8	458.3
Heat of vaporization, nbp ^b	kJ/(kg-mole)	95.8	911.0	1740	5580	6502	6812.	12640.	12,000
Heat of fusion, mp ^b	kJ/(kg-mole)	16.75	118.0	338.0	714.0	1120.0	438.0	1812.0	699.0
Spec. heat, c_p^{vap} , 300 K ^b	kJ-(kg-mole) ⁻¹ ·K ⁻¹	20.94 ^c	28.63	20.85	29.08	20.89	29.45	20.85	62.23

^a Reprinted with permission from *Cryogenic and Industrial Gases*, May/June 1975. Copyright 1975, Thomas Publishing Co., Cleveland, OH.

^b Reprinted with permission from *Handbook of Chemistry and Physics*, 58th ed., R. C. Weast, Ed. Copyright 1977, Chemical Rubber Co., CRC Press, West Palm Beach, FL;

^c At -180°C.

Appendix B.4 Gas Conductance and Flow Formulas

Note: In these formulas, pressure is in pascal, volume in m³, length in m, pumping speed in m³/s, gas flow in Pa-m³/s, velocity in m/s, particle density in m⁻³, and temperature in kelvin unless otherwise stated.

Characteristic Numbers

Knudsen's number

$$\text{Kn} = \frac{\lambda}{d}$$
$$\text{Kn} = \frac{6.6}{P(\text{Pa})d(\text{mm})} \quad (\text{air}, 22^\circ\text{C})$$

Reynolds' number

$$\text{R} = \frac{4m}{\pi k T \eta} \frac{Q}{d}$$
$$\text{R} = 8.41 \times 10^{-4} \frac{Q(\text{Pa} \cdot \text{L/s})}{d} \quad (\text{air}, 22^\circ\text{C})$$

Mach number

$$\text{U} = \frac{U}{U_{\text{sound}}} = \frac{4Q}{\pi d^2 P U_{\text{sound}}}$$

Langhaar's number

$$l_e = 0.0568 d \text{R}$$

Quantities from Kinetic Theory

Most probable velocity

$$v_p = (2kT/m)^{1/2}$$

Average velocity

$$v = \left(\frac{8kT}{\pi m} \right)^{1/2} = 1.28 v_p$$
$$v = 463 \text{ m/s} \quad (\text{air}, 22^\circ\text{C})$$

RMS velocity

$$v_{\text{rms}} = (3kT/m)^{1/2}$$

Mean free path, one component gas

$$\lambda = \frac{1}{2^{1/2} \pi d_o^2 n}$$
$$\lambda(\text{cm}) = \frac{0.67}{P(\text{Pa})} \quad \text{or} \quad \lambda(\text{cm}) = \frac{0.005}{P(\text{Torr})} \quad (\text{air}, 22^\circ\text{C})$$

Mean free path, gas *a* in gas *b*

$$\lambda_a = \frac{1}{\left[2^{1/2} \pi n_a d_a^2 \left(1 + \frac{v_b^2}{v_a^2} \right)^{1/2} n_b \frac{\pi}{4} (d_a + d_b)^2 \right]}$$

Particle flux

$$\Gamma = n \left(\frac{kT}{2\pi m} \right)^{1/2}$$

Monolayer formation time

$$t_{ml} = \frac{1}{\Gamma d_o^2} = \frac{4}{n v d_o^2}$$

Ideal gas law

$$P = nkT$$

$$\frac{P_1 V_1}{T_1} = \frac{P_2 V_2}{T_2}$$

Specific heat ratio

$$\gamma \sim 1.4 \text{ (diatomic gas)}$$

$$\gamma \sim 1.667 \text{ (monatomic gas)}$$

$$\gamma \sim 1.333 \text{ (triatomic gas)}$$

Viscosity at normal pressures

$$\eta = \frac{0.499(4mkT)^{1/2}}{\pi^{3/2} d_o^2}$$

Viscosity at reduced pressures (free molecular)

$$\eta_{fm} \text{ (Pa} \cdot \text{s)} = \left(\frac{Pmv}{4kT} \right)$$

Heat conductivity at normal pressures

$$K = \frac{1}{4} (9\gamma - 5) \eta c_v$$

Diffusion constant, gas 1 in gas 2

$$D_{12} = \frac{8 \left(\frac{2kT}{\pi} \right)^{1/2} \left(\frac{1}{m_1} + \frac{1}{m_2} \right)^{1/2}}{3\pi(n_1 + n_2)(d_{o1} + d_{o2})^2}$$

Appendix B.4 (Continued)

Diffusion constant, self-diffusion

$$D_{11} = \frac{4}{3\pi n d_o^2} \left(\frac{kT}{\pi m} \right)^{1/2}$$

Diffusion constant, molecular (Knudsen), pipe of radius r

$$D = \frac{2}{3} r v$$

Speed of sound in a gas

$$U(\text{m/s}) = v \left(\frac{\pi \gamma}{8} \right)^{1/2}$$

Conductance

$$C = \frac{Q}{(P_1 - P_2)}$$

Pumping speed

$$S = \frac{Q}{P}$$

Flow Regimes

<i>Turbulent flow</i>	$R > 2200$
<i>Choked flow</i>	$U = 1$
<i>Viscous flow</i>	$R < 1200$, and $Kn < 0.01$
<i>Poiseuille flow</i>	$U < 1/3$, $R < 1200$, $Kn < 0.01$, and $l_e \ll l$
<i>Molecular flow</i>	$Kn > 1$

Gas Flow Formulas

Continuum flow, thin aperture, any gas

$$Q = AP_1 C' \left(\frac{2\gamma}{\gamma-1} \frac{kT}{m} \right)^{1/2} \left(\frac{P_2}{P_1} \right)^{1/\gamma} \left[1 - \left(\frac{P_2}{P_1} \right)^{(\gamma-1)/\gamma} \right]^{1/2}$$

for $1 > P_2 / P_1 \geq (2/(\gamma+1))^{\gamma/(\gamma-1)}$

Choked flow limit, thin aperture, any gas

$$Q = AP_1 C' \left(\frac{kT}{m} \frac{2\gamma}{\gamma+1} \right)^{1/2} \left(\frac{2}{\gamma+1} \right)^{\gamma/(\gamma-1)}$$

for $P_2 / P_1 \leq (2/(\gamma+1))^{\gamma/(\gamma-1)}$

Continuum flow, thin aperture, air 22 °C

$$Q(\text{Pa} \cdot \text{m}^3 / \text{s}) = 766 A P_1 C' \left(\frac{P_2}{P_1} \right)^{0.714} \left[1 - \left(\frac{P_2}{P_1} \right)^{0.286} \right]^{1/2}$$

for $1 > P_2 / P_1 \geq 0.52$

Choked flow limit, thin aperture, air 22 °C.

$$Q(\text{Pa} \cdot \text{m}^3 / \text{s}) = 200 P_1 A C'$$

for air at 22 °C, when $P_2 / P_1 \leq 0.52$

Viscous flow, long circular tube (Poiseuille)

$$Q = \frac{\pi d^4}{128 \eta l} \frac{(P_1 - P_2)}{2} (P_1 - P_2)$$

Molecular flow:

$$Q(\text{Pa} \cdot \text{m}^3 / \text{s}) = a \frac{v}{4} A (P_1 - P_2)$$

where a is the transmission coefficient and A is the entrance area.

Useful transmission coefficients

Five transmission coefficients for shapes of common interest are given here. Others are found in Fig's. 3.5–3.12.

1. Very thin aperture, length $l \ll$ diameter d

$$a = 1$$

2. Round pipe; any length l , radius r

Use a from Table 3.1 or Fig. 3.5, or use the following expression given by A. S. Berman, *J. Appl. Phys.*, **36**, 3356 (1965). $a = (K_1 - K_2)$. K_1 and K_2 are given by the following formulas with the reduced length $L = l/r$, where l and r are the duct length and radius, respectively.

$$K_1 = 1 + \frac{L^2}{4} - \left(\frac{L}{4} \right) \left[L^2 + 4 \right]^{1/2}$$

$$K_2 = \frac{[(8 - L^2)(L^2 + 4)^{1/2} + L^3 - 16]^{1/2}}{72L(L^2 + 4)^{1/2} - 288 \ln [L + (L^2 + 4)^{1/2}] + 288 \ln 2}$$

Appendix B.4 (Continued)

3. Rectangular pipe, any width-to-thickness ratio (b/h), length l

Use a from Fig. 3.8, or use the following expression calculated from G. L. Saksaganskii, *Molecular Flow in Complex Vacuum Systems*, Gordon and Breach Science Publishers, London, 1988. p. 17.

$$a = c \frac{hb}{l(h+b)}$$

The coefficient c is given by

b/h	0.05	0.1	0.2	0.4	0.6	0.8	1.0
c	1.52	1.44	1.33	1.18	1.12	1.1	1.0

4. Rectangular pipe; thin, slit-like (thickness $h \ll$ width b), any length l

Use a from Table 3.2, or use the following expression given by A. S. Berman, *J. Appl. Phys.*, **36**, 3356 (1965), and erratum **37**, 4509 (1966). $a = (K_1 - K_2)$. K_1 and K_2 are given by the following formulas with the reduced length L , given by $L = l/h$ (length-to-slit spacing).

$$K_1 = \frac{1}{2} \left(1 + (1 + L)^2 - L \right)$$

$$K_2 = \frac{3/2 [L - \ln(L + (L^2 + 1)^{1/2})]^2}{L^3 + 3L^2 + 4 - (L^2 + 4)(L^2 + 1)^{1/2}}$$

5. Annular cylindrical pipe, length l , inner radius r and outer radius r_o

Use a from Fig. 3.6 or use the following formula given by A. S. Berman, *J. Appl. Phys.*, **40**, 4991 (1969).

$$a = \left\{ 1 + L \left[1/2 - A \tan^{-1} \left(\frac{L}{B} \right) \right] \right\}^{-1}$$

$L = l/(r_o - r)$. A and B are given in the formulas below. In these formulas $\sigma = r/r_o$ and has a range $0 < \sigma < 0.9$, and L has a range $0 \leq L \leq 100$.

$$A = \frac{(0.0741 - 0.014\sigma - 0.037\sigma^2)}{(1 - 0.918\sigma + 0.05\sigma^2)}$$

and

$$B = \frac{(5.825 - 2.86\sigma - 1.45\sigma^2)}{(1 + 0.56\sigma - 1.28\sigma^2)}$$

Combining conductances in molecular flow:

1. Parallel

$$C_T = C_1 + C_2 + C_3 + \dots$$

2. Series, isolated

$$\frac{1}{C_T} = \frac{1}{C_1} + \frac{1}{C_2} + \frac{1}{C_3} + \dots$$

3. Series, not isolated, equal entrance and exit areas (Oatley)

$$\frac{1-a}{a} = \frac{1-a_1}{a_1} + \frac{1-a_2}{a_2} + \frac{1-a_3}{a_3} + \dots$$

4. Series, not isolated, unequal entrance and exit areas (Haefer)

$$\frac{1}{A_1} \left(\frac{1-a_{1 \rightarrow n}}{a_{1 \rightarrow n}} \right) = \sum_1^n \frac{1}{A_i} \left(\frac{1-a_i}{a_i} \right) + \sum_1^{n-1} \left(\frac{1}{A_{i+1}} - \frac{1}{A_i} \right) \delta_{i,i+1}$$

where $\delta_{i,i+1} = 1$ for $A_{i+1} < A_i$, and $\delta_{i,i+1} = 0$ for $A_{i+1} \geq A_i$

Transition conductance, Knudsen's method

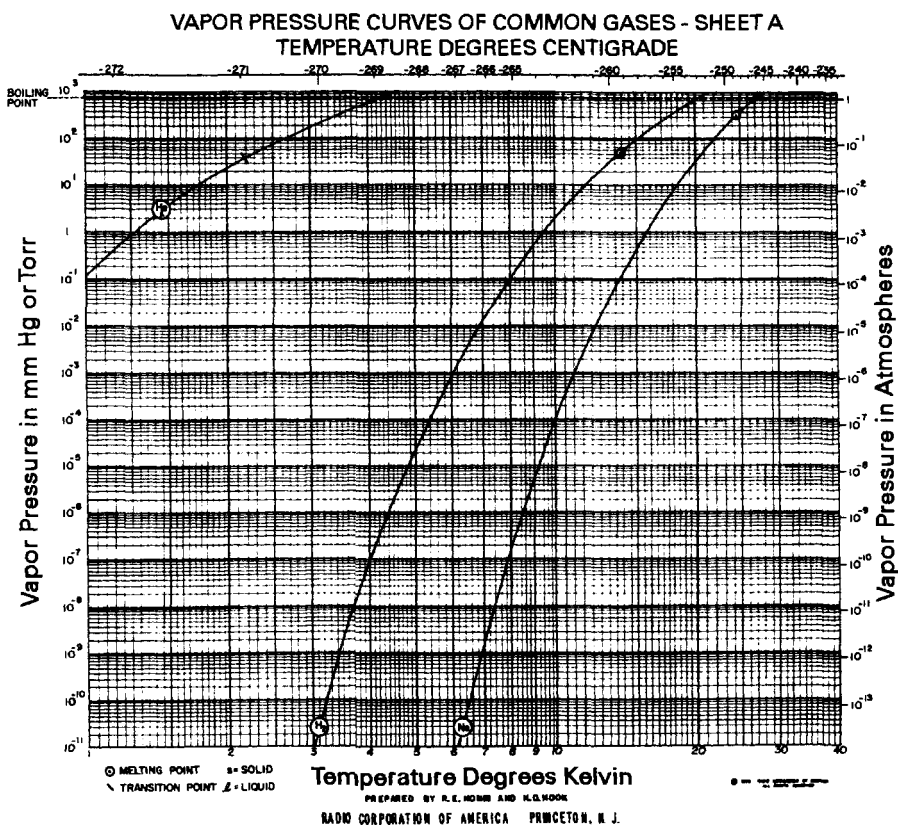
$$C = \frac{Q}{(P_2 - P_1)}$$

$$Q = Q_{\text{viscous}} + Z' Q_{\text{molecular}}$$

where

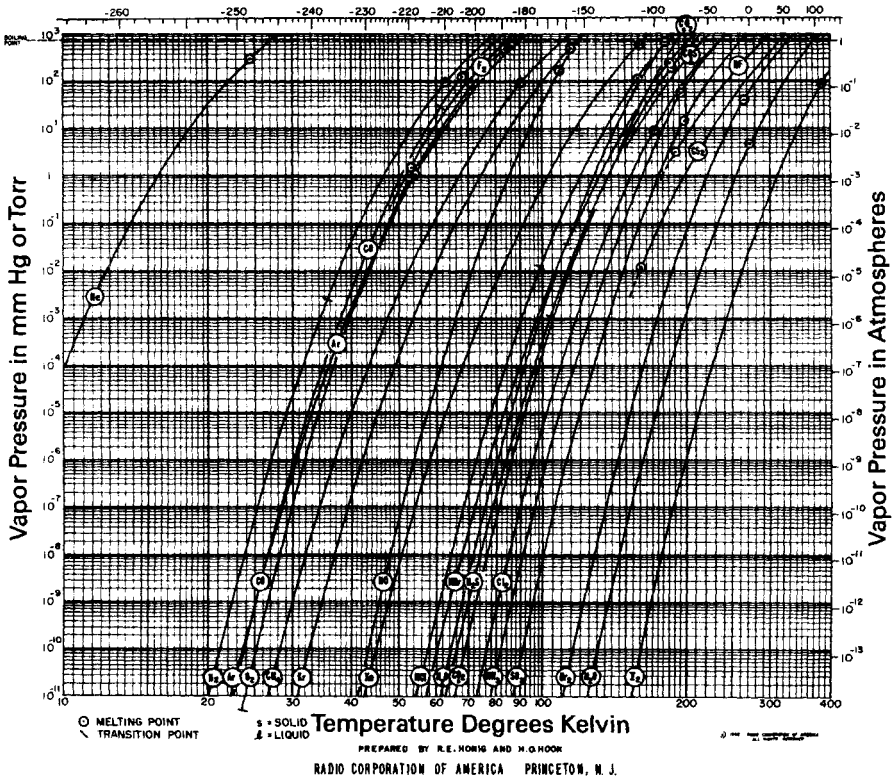
$$Z' = \frac{1 + 2.507 \left(\frac{d}{2\lambda} \right)}{1 + 3.095 \left(\frac{d}{2\lambda} \right)}$$

Appendix B.5 Vapor Pressure Curves of Common Gases



Appendix B.5 (Continued)

VAPOR PRESSURE CURVES OF COMMON GASES - SHEET B TEMPERATURE DEGREES CENTIGRADE



Source. Reprinted with permission from *RCA Review*, **21**, p. 360, Sept. 1960, *Vapor Pressure Data for Some Common Gases*, by R. E. Honig and H. O. Hook. Copyright 1960, RCA Corporation.

Appendix B.6 Appearance of Discharges in Gases and Vapors at Low Pressures

Gas	Negative Glow	Positive Column
Argon	Blue	Violet
Carbon tetrachloride	Light green	Whitish green
Carbon monoxide	Greenish white	White
Carbon dioxide	Blue	White
C ₂ H ₅ OH	—	Whitish
Cadmium	Red	Greenish blue
Hydrogen	Light blue	Pink
Mercury	Whitish yellow	Blue green
Potassium	Green	Green
Krypton	Violet	Yellow pink
Air	Blue	Reddish
Nitrogen	Blue	Red-yellow
Sodium	Whitish	yellow
Oxygen	Yelowish white	Lemon yellow with pink core
Thallium	Green	Green
Xenon	Pale blue	Blue violet

Source. Reprinted with permission from: *Materials for High Vacuum Technology*, Vol. 3, p. 393, W. Espe. Copyright 1968, Pergamon Press.

APPENDIX C

Material Properties

Appendix C.1 Outgassing Rates of Vacuum-Baked Metals

<i>q</i>		
Material	Treatment	(10 ⁻¹¹ Pa-m/s)
Aluminum ^a	15 h at 250°C	53.0
Aluminum ^b	20 h at 100°C	5.3
6061 Aluminum ^c	glow discharge +200°C bake	1.3
Copper ^b	20 h at 100°C	146.0
Copper (OHFC) ^d	24 h at 100°C	2.90
	24 h at 250°C	0.181
Cr (0.5%)—Cu (99.5%) alloy ^d	24 h at 100°C	0.375
	24 h at 250°C	0.357
304 Stainless steel ^a	30 h at 250°C	400.0
Stainless steel ^e	2 h at 850/900°C vacuum furnace	27.0
316L Stainless steel ^f	2 h at 800°C vacuum furnace	46.0
U15C Stainless steel ^g	3 h vacuum furnace 1000°C +25 h in situ vacuum bake at 360°C	2.1

Source. Adapted with permission from *Vacuum*, **25**, p. 347, R. J. Elsey. Copyright 1975, Pergamon Press.

^a J. R. Young, *J. Vac. Sci. Technol.*, **6**, 398 (1969);

^b G. Moraw, *Vacuum*, **24**, 125 (1974);

^c H. J. Halama and J. C. Herrera, *J. Vac. Sci. Technol.*, **13**, 463 (1976);

^d Y. Koyatsu, H. Miki and F. Watanabe, *Vacuum*, **47**, 709 (1996).

^e R. L. Samuel, *Vacuum*, **20**, 295 (1970);

^f R. Nuvolone, *J. Vac. Sci. Technol.*, **14**, 1210 (1977);

^g R. Calder and G. Lewin, *Br. J. Appl. Phys.*, **18**, 1459 (1967).

Appendix C.2 Outgassing Rates of Unbaked Metals¹

Material	q_1 (10 ⁻⁷ Pa-m/s)	α_1	q_{10} (10 ⁻⁷ Pa-m/s)	α_{10}
Aluminum (fresh) ^a	84.0	1.0	8.0	1.0
Aluminum (degassed 24 h) ^a	55.2	3.2	4.08	0.9
Aluminum (3 h in air) ^a	88.6	1.9	6.33	0.9
Aluminum (fresh) ^a	82.6	1.0	4.33	0.9
Aluminum (anodized 2- μ m pores) ^a	3679.0	0.9	429.0	0.9
Aluminum (bright-rolled) ^b	—	—	100.0	1.0
Duraluminum ^b	2266.0	0.75	467.0	0.75
Brass (wave guide) ^b	5332.0	2.0	133.0	1.2
Copper (fresh) ^a	533.0	1.0	55.3	1.0
Copper (mechanically polished) ^a	46.7	1.0	4.75	1.0
Copper, OHFC (fresh) ^a	251.0	1.3	16.8	1.3
Copper, OHFC (mechanically polished) ^a	25.0	1.1	2.17	1.1
Copper, OHFC (20°C) ^c	—	—	0.408	—
Chrome (0.5%)—Copper, OFE (99.5%) ^c	—	—	0.102	—
Gold (wire fresh) ^a	2105.0	2.1	6.8	1.0
Mild steel ^b	7200.0	1.0	667.0	1.0
Mild steel (slightly rusty) ^b	8000.0	3.1	173.0	1.0
Mild steel (chromium-plated polished) ^b	133.0	1.0	12.0	—
Mild steel (aluminum spray coated) ^b	800.0	0.75	133.0	0.75
Steel (chromium-plated fresh) ^a	94.0	1.0	7.7	1.0
Steel (chromium-plated polished) ^a	121.0	1.0	10.7	1.0
Steel (nickel-plated fresh) ^a	56.5	0.9	6.6	0.9
Steel (nickel-plated) ^a	368.0	1.1	3.11	1.1
Steel (chemically nickel-plated fresh) ^a	111.0	1.0	9.4	1.0
Steel (chemically nickel-plated polished) ^a	69.6	1.0	6.13	1.0
Steel (descaled) ^a	4093.0	0.6	3933.0	0.7
Molybdenum ^a	69.0	1.0	4.89	1.0
Stainless steel EN58B (AISI 321) ^b	—	—	19.0	1.6
Stainless steel 19/9/1-electropolished ^d	—	—	2.7	—
-vapor degreased ^d	—	—	1.3	—
-Diversey cleaned ^d	—	—	4.0	—
Stainless steel ^b	2333.0	1.1	280.0	0.75
Stainless steel ^b	1200.0	0.7	267.0	0.75
Stainless steel ICN 472 (fresh) ^a	180.0	0.9	19.6	0.9
Stainless steel ICN 472 (sanded) ^a	110.0	1.2	13.9	0.8
Stainless steel NS22S (mechanically polished) ^a	22.8	0.5	6.1	0.7
Stainless steel NS22S (electropolished) ^a	57.0	1.0	5.7	1.0
Stainless steel ^a	192.0	1.3	18.0	1.9
Zinc ^a	2946.0	1.4	429.0	0.8
Titanium ^a	150.0	0.6	24.5	1.1
Titanium ^a	53.0	1.0	4.91	1.0

Source. Reprinted with permission from *Vacuum*, **25**, p 347, R. J. Elsey. Copyright 1975, Pergamon Press.

¹ $q_n = q_1 t^{-\alpha_n}$, where n is in hours. See Fig. 4.6 for a detailed explanation.

^a A. Schram, *Le Vide*, No. 103, 55 (1963),

^b B. B. Dayton, *Trans. 6th Natl. Vac. Symp. (1959)*, Pergamon Press, New York, 1960, p. 101,

^c Y. Koyatsu, H. Miki, and F. Watanabe, *Vacuum*, **47**, 709 (1996),

^c R. S. Barton and R. P. Govier, *Proc. 4th Int. Vac. Congr. (1968)*, Institute of Physics and the Physical Society, London, 1969, p. 775, and *Vacuum*, **20**, 1 (1970).

Appendix C.3 Outgassing Rates of Ceramics and Glasses^a

Material	q_1 (10^{-7} Pa-m/s)	α_1	q_{10} (10^{-7} Pa-m/s)	α_{10}
Steatite ^b	1200.0	1.0	127.0	—
Pyrophyllite ^c	2667.0	1.0	267.0	—
Pyrex (fresh) ^d	98.0	1.1	7.3	—
Pyrex (1 month in air) ^d	15.5	0.9	2.1	—

Source. Reprinted with permission from *Vacuum*, **25**, p. 347, R. J. Elsey. Copyright 1975, Pergamon Press.

^a $q_n = q_1 t^{-\alpha_n}$, where n is in hours. See Fig. 4.6 for a detailed explanation.

^b R. Geller, *Le Vide*, No. 13, 71 (1958).

^c R. Jaeckel and F. Schittko, quoted by Elsey.

^d B. B. Dayton, *Trans. 6th Natl. Symp. Vac. Technol. (1959)*, Pergamon Press, New York, 1960, p. 101.

Appendix C.4 Outgassing Rates of Elastomers^a

Material	q_1 (10^{-5} Pa-m/s)	α_1	q_4 (10^{-5} Pa-m/s)	α_4
Butyl DR41 ^b	200.0	0.68	53.0	0.64
Neoprene ^b	4000.0	0.4	2400.0	0.4
Perbunan ^b	467.0	0.3	293.0	0.5
Silicone ^c	930.0	—	267.0	—
Viton A (fresh) ^d	152.0	0.8	—	—
Viton A (bake 12 h at 200°C) ^e	—	—	0.027 ^f	—
Polyimide (bake 12 h at 300°C) ^e	—	—	0.005 ^f	—

Source. Adapted with permission from *Vacuum*, **25**, p. 347, R. J. Elsey. Copyright 1975, Pergamon Press.

^a $q_n = q_1 t^{-\alpha_n}$, where n is in hours. See Fig. 4.6 for a detailed explanation.

^b J. Blears, E. J. Greer, and J. Nightengale, *Adv. Vac. Sci. Technol.*, Vol. 2., E. Thomas, Ed., Pergamon Press, 1960, p. 473.

^c D. J. Santeler, et al., *Vacuum Technology and Space Simulation*, NASA SP-105, National Aeronautics and Space Administration, Washington, DC, 1966, p. 219.

^d A. Schram, *Le Vide*, No. 103, 55 (1963).

^e P. Hait, *Vacuum*, **17**, 547 (1967).

^f Pumping time is 12 h.

Appendix C.5 Permeability of Polymeric Materials^a

Material	Permeability (10^{-12} m ² /s)					
	Nitrogen	Oxygen	Hydrogen	Helium	Water Vapor	Carbon Dioxide
PTFE	2.5 ^b	4.78 ^e (25)	20.0 ^b	570.0 ^b	23.6 ^e (25)	—
Perspex	—	—	2.7 ^b	5.7 ^b	—	—
Nylon 31	—	—	0.13 ^b	0.3 ^b	—	—
Neoprene ^c CS2368B	0.21 ^b	1.5 ^b	8.2 ^b	7.9 ^b	—	—
Viton	0.5 ^f (25)	1.14 ^e (25)	8.7 ^f (25)	15 ^f (25)	218 ^e (25)	2.3 ^f (25)
Kapton	0.032 ^c	0.1 ^c	1.2 ^c	2.1 ^c	—	0.2 ^c
Buna-S	4.8 ^d (30)	—	—	—	—	940.0 ^d (30)
Perbunan	0.8 ^d	—	—	—	—	23.0 ^d (30)
Delrin	—	48.0 ^d	—	—	17.0 ^d	92.7 ^d
Kel-F	0.99 ^d (30)	0.46 ^d (30)	—	—	0.22 ^d (25)	—
VespeI	—	0.076 ^e (25)	—	—	31.2 ^e (25)	—
Polyvinylidene chloride (Saran)	0.0007 ^d	0.004 ^d	—	—	1.06 ^d	0.022 ^d
Mylar	0.018 ^g	8.5 ^g	—	1.7 ^g	99 ^g	0.37 ^g
Silicone, dimethyl	210 ^h	450 ^h	495 ^h	263 ^h	28500 ^h	2030 ^h
Kalrez-dry	—	3.11 ^e (25)	—	—	125 ^e (25)	—

^a Measurements made at 23°C unless otherwise noted in parentheses after the value.

^b Reprinted with permission from *Vacuum*, **25**, p. 469, G. F. Weston. Copyright 1975, Pergamon Press. Data derived by Weston from measurements made by Barton reported by J. R. Bailey in *Handbook of Vacuum Physics*, 3, Part 4, Pergamon Press, Oxford, 1964.

^c Reprinted with permission from *J. Vac. Sci. Technol.*, **10**, p. 543, W. G. Perkins. Copyright 1973, The American Vacuum Society.

^d Reprinted with permission from *Vacuum Science and Space Simulation*, D. J. Santeler et al., NASA SP-105, National Aeronautics and Space Administration, Washington, DC, 1966, p. 216.

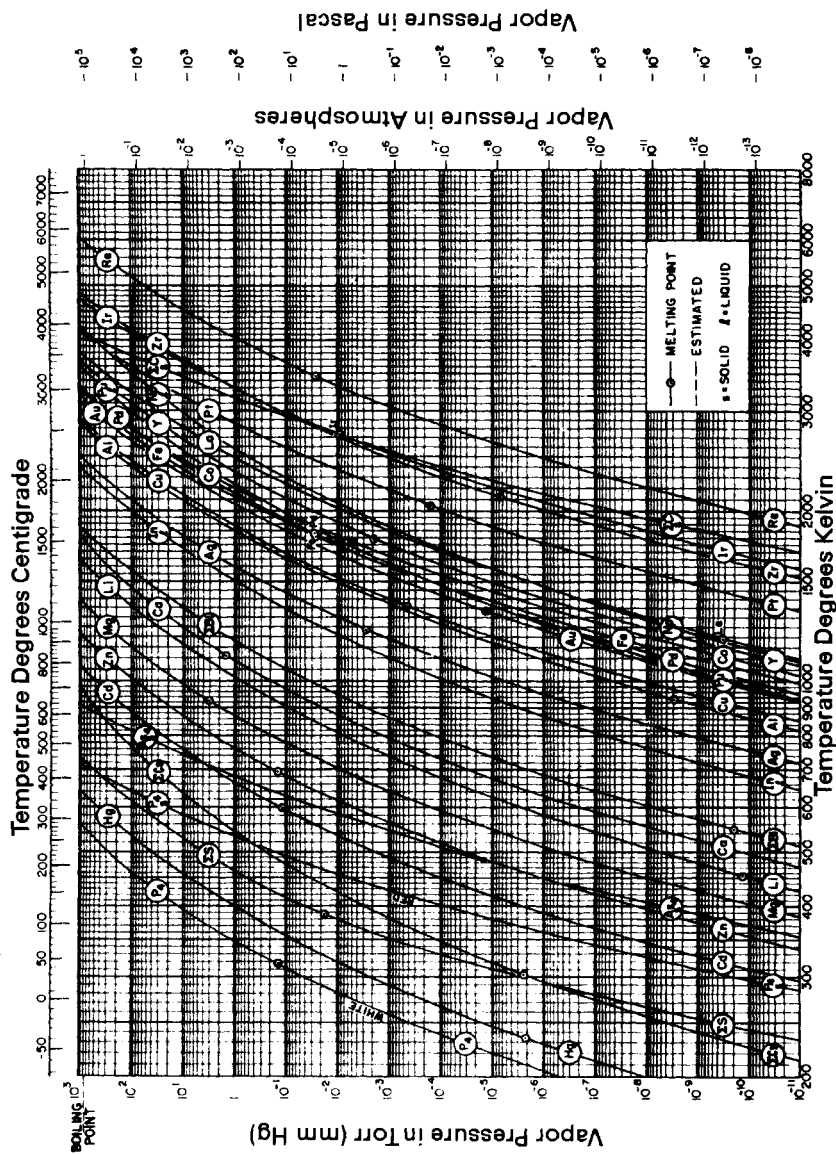
^e Data taken from C. Ma, E. Shero, N. Verma, S. Gilbert, and F. Shadman, *Journal of the IES*, March/April, 1995, p. 43, using tracer gas measurements in an ultrapure nitrogen gas stream.

^f Data taken from L. Laurensen and N. T. M. Dennis, *J. Vac. Sci. Technol. A*, **3**, 1701 (1985). Data at 25°C, from plot in Fig. 16.8, left.

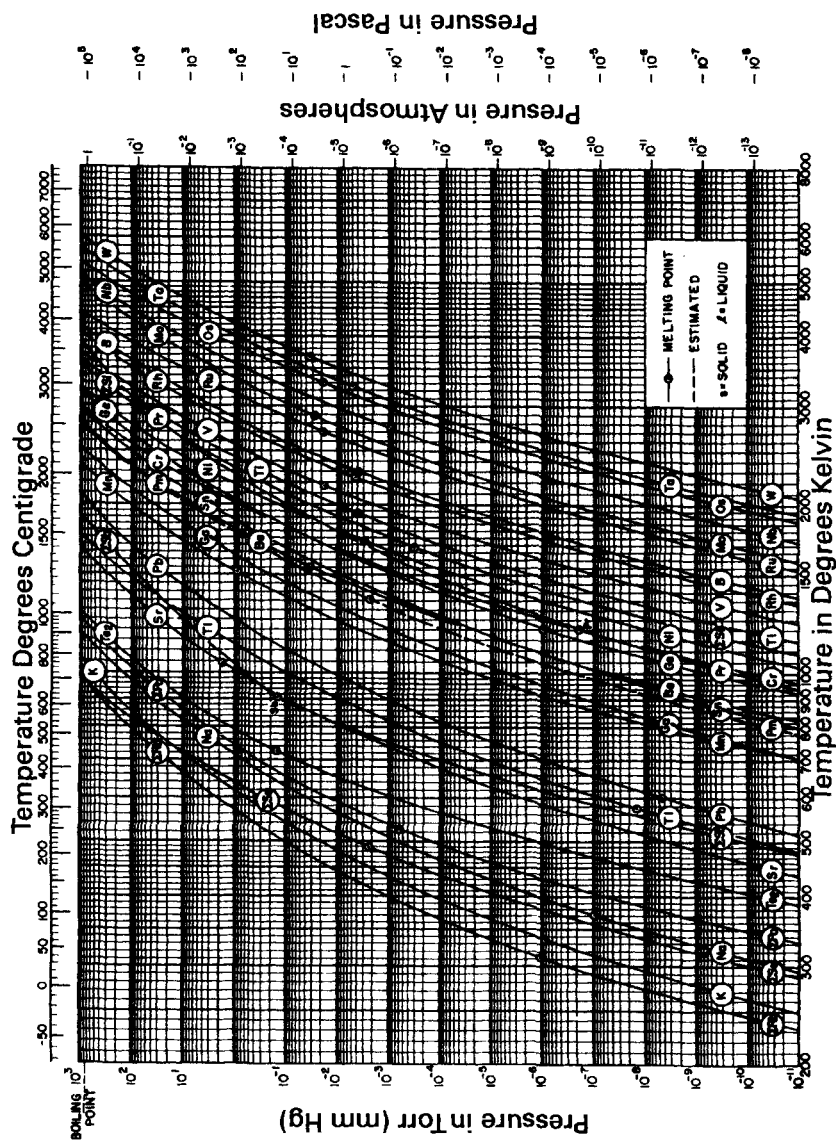
^g Data taken from M. Mapes, H. C. Hseuk, and W. S. Tiang, *J. Vac. Sci. Technol. A*, **12**, 1699 (1994).

^h Data taken from *Introduction to Mass Spectroscopy*, Varian Associates, Palo Alto, 1980, p. 49.

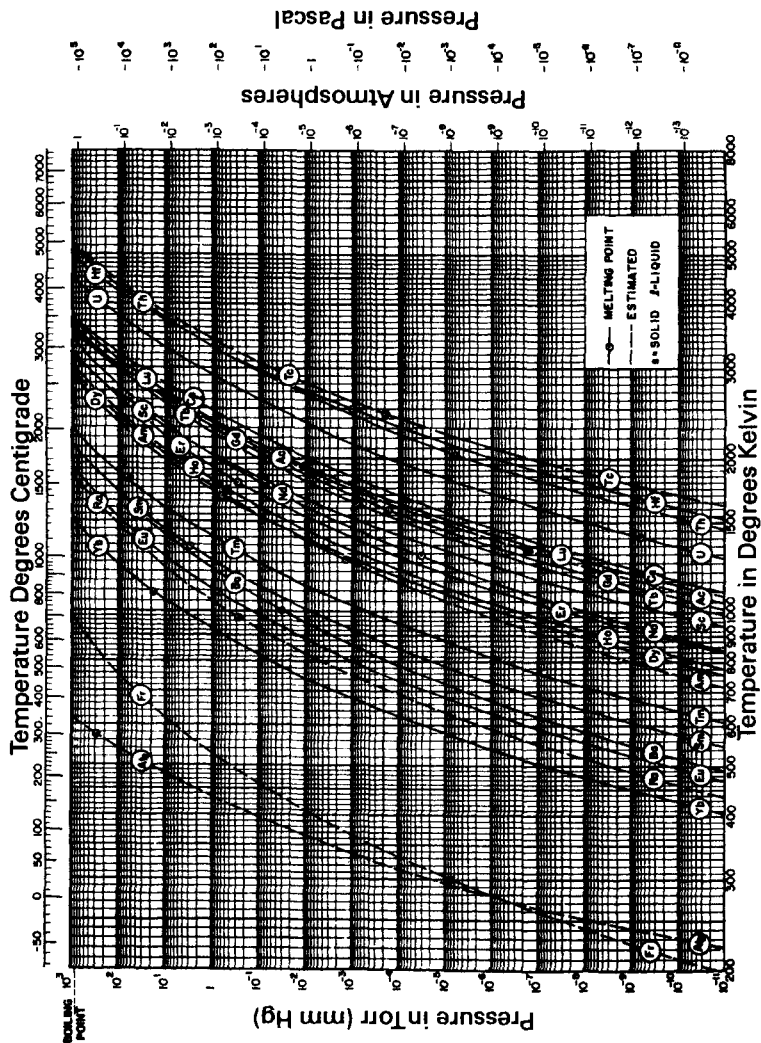
Appendix C.6 Vapor Pressure Curves of the Solid and Liquid Elements—Sheet A



Appendix C.6 Vapor Pressure Curves of the Solid and Liquid Elements—Sheet B



Appendix C.6 Vapor Pressure Curves of the Solid and Liquid Elements—Sheet C



Source. Reprinted with permission from *RCA Review*, 30, p. 285, June 1969, *Vapor Pressure Data for the Solid and Liquid Elements*, by R. E. Hoening and D. A. Kramer. Copyright 1969, RCA Corp.

Appendix C.7 Outgassing Rates of Polymers^a

Material	q_1 (10 ⁻⁵ Pa-m/s)	α_1	q_{10} (10 ⁻⁵ Pa-m/s)	α_{10}
Araldite (molded) ^b	155.0	0.8	47.0	0.8
Araldite D ^c	253.0	0.3	167.0	0.5
Araldite F ^c	200.0	0.5	97.0	0.5
Kel-F ^d	5.0	0.57	2.3	0.53
Methyl Methacrylate ^e	560.0	0.9	187.0	0.57
Mylar (24-h at 95% RH) ^f	307.0	0.75	53.0	—
Nylon ^g	1600.0	0.5	800.0	0.5
Plexiglas ^h	96.1	0.44	36.0	0.44
Plexiglas ^c	413.0	0.4	240.0	0.4
Polyester-glass Laminate ^d	333.0	0.84	107.0	0.81
Polystyrene ^d	2667.0	1.6	267.0	1.6
PTFE ⁱ	40.0	0.45	26.0	0.56
PVC (24-h at 95% RH) ^f	113.0	1.0	2.7	—
Teflon ^h	8.7	0.5	3.3	0.2

Source. Reprinted with permission from *Vacuum*, **25**, p. 347, R. J. Elsey, Copyright 1975, Pergamon Press.

^a $q_n = q_1 t^{-\alpha_1}$, where n is in hours. See Fig. 4.6 for a detailed explanation.

^b A. Schram, *Le Vide*, No. 103, 55 (1963).

^c R. Geller, *Le Vide*, No.13, 71 (1958).

^d B. B. Dayton, CVC Technical Report.

^e J. Blears, E. J. Greer and J. Nightengale, *Adv. Vac. Sci. Technol.*, Vol. 2, E. Thomas, Ed., Pergamon Press, 1960, p. 473.

^f D. J. Santeler, *Trans. 5th Symp. Vac. Tech. (1958)*, Pergamon Press, New York, 1959, p. 1;

^g B. D. Power and D. J. Crawley, *Adv. Vac. Sci. Technol.*, Vol. 1, E. Thomas, Ed., Pergamon Press, New York, 1960, p. 207.

^h G. Thieme, *Vacuum*, **13**, 137 (1963).

ⁱ B. B. Dayton, *Trans. 6th Natl. Vac. Symp. Vac. Technol. (1959)*, Pergamon Press, New York, 1960, p.101.

Performance—Recommended for													
AISI type	General forming		High temperature use	Cryogenic use	Resist carbide precipitation	High yield strength	Non-magnetic at cryogenic temperatures	Free machining	Welding ability	Tensile properties typical, at R. T. annealed		Impact strength at -196°C	Price index
										0.2% proof (yield) kgf mm ²	Ultimate TS kgf mm ²	⁸ Charpy-V J	
302	x								E	22	60	70	100
303S,Se								x	P	22	60		105
304	x		x						E	20	50	70	100
304L	x		x	x					E	18	48	80	115
304N	x		x		x				E	30	55-75	min 63	110
304LN	x		x	x	x	x			E	28	55-75	min 55	125
310	x	x			x	x			G	23	65		210
316	x		x			~			E	22	50		130
316L	x		x	x		~			E	20	45	120	150
316N	x		x		x	x			E	30	60		140
316LN	x		x	x	x	x			E	30	60-80	min 55	160
317	x	x				~			E	24	60		200
321	x	x		x					E	21	50	65	130
347	x	x		x					G	22	50	65	150

Source. Reprinted with permission from *Vacuum*, 26, p. 287, C. Geyari. Copyright 1976, ^a Selection guide for vacuum and cryogenic equipment. X = recommended, P = poor,

Austenitic Stainless Steels^a

Typical Composition, %

C max	Cr	Ni	Mo	N	Others	Description
0.12	17-19	8-10				General purpose. Good resistance to atm. corrosion. Good mechanical properties.
0.15	17-19	8-10			S, Se ≥ 0.15	Free machining type. Good corrosion resistance.
0.08	18-20	8-12				Low C variation of 302. Improved corrosion resistance after welding.
0.03	18-20	8-12				Extra low C prevents carbide precipitation
0.06	18.5	9.5		0.25	Mn 2	Improved mechanical properties.
0.03	18.5	9.5		0.18	Mn 2	Improved mechanical properties. Extra low C prevents carbide precipitation.
0.025	24-26	19-22				High scale resistance. Superior corrosion resistance.
0.08	16-18	10-14	2-3			Very good corrosion resistance in most media.
0.03	16-18	10-14	2-3			Extra low C variation of 316.
0.07	17-18	10-13	2.5-3	0.2	Mn 0.5-2	Improved mechanical properties.
0.03	17.5	13	2.8	0.18	Mn 2	Improved mechanical properties. Extra low C Prevents carbide precipitation.
0.08	18-20	11-15	3-4			Higher alloy content improves creep and corrosion resistance of 316.
0.08	17-19	9-12			Ti ≥ 5×C	Stabilized—Ti prevents carbide precipitation. Improved corrosion resistance after welding.
0.08	17-19	9-13			Nb, Ta ≥ 10×C	Stabilized—Nb, Ta, prevent carbide precip. Improved corrosion resistance after welding.

Pergamon Press.

~ = probable, - should be tested, E = excellent, G = good with precautions.

APPENDIX D

Isotopic Abundances

Element	AMU	Relative Abundance	Element	AMU	Relative Abundance
H	1	99.985	S	32	95.06
	2	0.015		33	0.74
He	3	0.00013		34	4.18
	4	~100.0		36	0.016
Li	6	7.42	Cl	35	75.4
	7	92.58		37	24.6
Be	9	100.0	Ar	36	0.337
B	10	19.78		38	0.063
	11	80.22		40	99.600
C	12	98.892	K	39	93.08
	13	1.108		40	0.0119
N	14	99.63		41	6.91
	15	0.37	Ca	40	96.97
O	16	99.759		42	0.64
	17	0.0374		43	0.145
	18	0.2039		44	2.06
F	19	100.0		46	0.0033
Ne	20	90.92		48	0.185
	21	0.257	Sc	45	100.0
	22	8.82	Ti	46	7.95
Na	23	100.0		47	7.75
				48	73.45
Mg	24	78.60		49	5.51
	25	10.11		50	5.34
	26	11.29	V	50	0.24
Al	27	100.0		51	99.76
Si	28	92.27	Cr	50	4.31
	29	4.68		52	83.76
	30	3.05		53	9.55
P	31	100.0		54	2.38

Appendix D (Continued)

Element	AMU	Relative Abundance	Element	AMU	Relative Abundance
Mn	55	100.0	Zr	90	51.46
Fe	54	5.82		91	11.23
	56	91.66		92	17.11
	57	2.19		94	17.4
	58	0.33		96	2.8
Co	59	100.0	Nb	93	100.0
Ni	58	67.76	Mo	92	15.86
	60	26.16		94	9.12
	61	1.25		95	15.70
	62	3.66		96	16.50
	64	1.16		97	9.45
Cu	63	69.1		98	23.75
	65	30.9		100	9.62
Zn	64	48.89	Ru	96	5.47
	66	27.82		98	1.84
	67	4.14		99	12.77
	68	18.54		100	12.56
	70	0.617		101	17.10
Ga	69	60.2		102	31.70
	71	39.8		104	18.56
Ge	70	20.55	Rh	103	100.0
	72	27.37	Pd	102	0.96
	73	7.67		104	10.97
	74	36.74		105	22.23
	76	7.67		106	27.33
As	75	100.0		108	26.71
Se	74	0.87		110	11.81
	76	9.02	Ag	107	51.82
	77	7.58		109	48.18
	78	23.52	Cd	106	1.22
	80	49.82		108	0.87
	82	9.19		110	12.39
Br	79	50.52		111	12.75
	81	49.48		112	24.07
Kr	78	0.354		113	12.26
	80	2.27		114	28.86
	82	11.56		116	7.85
	83	11.55	In	113	4.23
	84	56.90		115	95.77
	86	17.37	Sn	112	0.95
Rb	85	72.15		114	0.65
	87	27.85		115	0.34
Sr	84	0.56		116	14.24
	86	9.86		117	7.57
	87	7.02		118	24.01
	88	82.56		119	8.58
Y	98	100.0		120	32.97
				122	4.71
				124	5.98

Appendix D (Continued)

Element	AMU	Relative Abundance	Element	AMU	Relative Abundance
Sb	121	57.25	Eu	151	47.77
	123	42.75		153	52.23
Te	120	0.089	Gd	152	0.20
	122	2.46		154	2.15
	123	0.87		155	14.73
	124	4.61		156	20.47
	125	6.99		157	15.68
	126	18.71		158	24.87
	128	31.79		160	21.90
	130	34.49	Tb	159	100.0
I	127	100.0	Dy	156	0.052
Xe	124	0.096		158	0.090
	126	0.090		160	2.294
	128	1.92		161	18.88
	129	26.44		162	25.53
	130	4.08		163	24.97
	131	21.18		164	28.18
	132	26.89	Ho	165	100.0
	134	10.44	Er	162	0.136
	136	8.87		164	1.56
Cs	131	100.0		166	33.41
Ba	130	0.101		167	22.94
	132	0.097		168	27.07
	134	2.42		170	14.88
	135	6.59	Tm	169	100.0
	136	7.81	Yb	168	0.140
	137	11.32		170	3.03
	138	71.66		171	14.31
La	138	0.089		172	21.82
	139	99.911		173	16.13
Ce	136	0.193		174	31.84
	138	0.250		176	12.73
	140	88.48	Lu	175	97.40
	142	11.07		176	2.60
Pr	141	100.0	Hf	174	0.18
Nd	142	27.13		176	5.15
	143	12.20		177	18.39
	144	23.87		178	27.08
	145	8.30		179	13.78
	146	17.18		180	35.44
	148	5.72	Ta	180	0.012
	150	5.62		181	99.988
Sm	144	3.16	W	180	0.135
	147	15.07		182	26.4
	148	11.27		183	14.4
	149	13.84		184	30.6
	150	7.47		186	28.4
	152	26.63	Re	185	37.07
	154	22.53		187	62.93

Appendix D (Continued)

Element	AMU	Relative Abundance	Element	AMU	Relative Abundance
Os	184	0.018		199	16.84
	186	1.59		200	23.13
	187	1.64		201	13.22
	188	13.3		202	29.80
	189	16.1		204	6.85
	190	26.4	Tl	203	29.50
	192	41.0		205	70.50
Ir	191	37.3	Pb	204	1.48
	193	62.7		206	23.6
Pt	190	0.012		207	22.6
	192	0.78		208	52.3
	194	32.8	Bi	209	100.0
	195	33.7		232	100.0
	196	25.4	U	234	0.0057
	198	7.21		235	0.72
Au	197	100.0		238	99.27
Hg	196	0.15			
	198	10.02			

Source. Reprinted with permission from *Mass Spectroscopy for Science and Technology*, F. A. White, p. 339. Copyright 1968, John Wiley & Sons.

APPENDIX E

Cracking Patterns

Appendix E.1 Cracking Patterns of Pump Fluids

AMU	Welch 1407 ^a	Fomblin Y-25 ^b	DC-704 ^c	DC-705 ^c	Octoil-S ^c	Convalex- 10 ^c
18					1.86	
27					14.40	23.20
28			17.19	67.18	8.37	
29				2.56	28.53	23.20
30				3.52	1.10	20.20
31		31.49			1.27	6.00
32			2.15	10.08		
35						
36						6.50
37						
38					0.65	4.20
39				2.22	8.82	14.90
40				4.44	2.21	15.50
41	40			3.59	54.03	31.00
42					17.12	8.30
43	74		2.40	7.69	66.58	29.20
44			1.98	12.47	3.17	50.00
45					1.98	
47		20.67				
50		15.30				5.40
51		27.66	2.61		0.84	11.30
52		2.92				
53	3				3.41	
54					4.34	
55	70		1.31	4.79	54.56	25.60
56	23				22.18	15.50
57	100		2.13		88.20	55.40
59					4.59	
60					2.0	
61						
62						
63						7.70

Appendix E.1 (Continued)

AMU	Welch 1407 ^a	Fomblin Y-25 ^b	DC-704 ^c	DC-705 ^c	Octoil-S ^c	Convalex- 10 ^c
64						8.30
65						7.10
66		2.23				
67	40				4.52	3.60
68	14				4.23	3.00
69	91	100.00		3.59		11.30
70	31	3.39			56.83	18.50
71	83			2.90	46.92	9.50
72					3.14	
73			1.65		2.98	
76						3.40
77	2		2.20			25.60
78	0.7			4.62		4.80
81	22	3.10		1.88	3.80	3.60
82	10				3.91	2.40
83	30			2.90	19.78	11.30
84	12				13.78	4.80
85		2.23		2.05	2.25	
87					1.82	
91		2.03	3.39	3.76		3.00
92						3.60
93	2				1.18	
94	7					3.60
95	3			2.05	2.87	2.40
96	10				2.11	
97		16.37		2.39	10.50	3.00
98					19.87	5.40
100		14.63				
101		14.63			2.00	
108						12.50
112					45.46	
113					25.01	61.30
119		13.88	3.87	3.24		
131		2.36				2.40
135		5.19	20.59	10.26		

^a Data taken on UTI-100B quadrupole with $V_{EE} = -60$ V, only major peaks shown. Reprinted with permission from Uthe Technology Inc., 325 N. Mathilda Avenue, Sunnyvale, CA 94086.

^b Sector data. Adapted with permission from *Vacuum*, 22, p. 315, L. Holland, L. Laurenson, and P. N. Baker. Copyright 1972, Pergamon Press.

^c Sector data. Reprinted with permission from *J. Vac. Sci. Technol.*, 6, p. 871, G. M. Wood, Jr., and R. J. Roenig. Copyright 1969, The American Vacuum Society.

Note. Only peaks up to 135 AMU are shown for the data taken from source c; the largest mass peak (100%) occurs at a higher mass number. The data are *not* renormalized for the range tabulated here.

Appendix E.2 Cracking Patterns of Gases

AMU	Hydrogen ^a H ₂	Helium ^b He	Neon ^b Ne	Carbon Monoxide ^a CO	Nitrogen ^a N ₂	Oxygen ^a O ₂	Argon ^a Ar	Carbon Dioxide ^a CO ₂
1	2.7							
2	100	0.12						
3	0.31							
4		100						
6				0.0008				0.0005
7					0.0006			
8				0.0001		0.0013		0.0005
12				3.5				6.3
13								0.063
14				1.4	9			
15					0.026			
16				1.4		14		16
17						0.0052		
18						0.028	0.071	0.0088
19							0.016	
20			100				5.0	
21			0.33					
22			9.9					0.52
22.5								0.0047
23								0.0012
28				100	100			15
29				1.2	0.71			0.15
30				0.2	0.0014			0.029
32						100		
33						0.074		
34						0.38		
36						0.0023	0.36	
38							0.068	
40							100	
44								100
45								1.2
46								0.38
47								0.0034
48								0.0005

^a Data taken on UTI-100C-02 quadrupole residual gas analyzer. Typical parameters, $V_{EE} = 70$ V, $V_{IE} = 15$ V, $V_{FO} = -20$ V, $I_E = 2.5$ mA, resolution potentiometer = 5.00. Reprinted with permission from Uthe Technology Inc., 325 N. Mathilda Avenue, Sunnyvale, CA 94086.

^b Sector data. Reprinted with permission from E. I. du Pont de Nemours & Co., Wilmington, DE 19898.

Appendix E.3 Cracking Patterns of Common Vapors

AMU	Water Vapor ^a H ₂ O%	Methane ^b CH ₄	Acetylene ^b C ₂ H ₂	Ethylene ^b C ₂ H ₄	Ethane ^b C ₂ H ₆	Cyclo- propane ^b C ₃ H ₆
1	0.1	3.8	3.8	6.4	3.2	1.4
2		0.64	1.2	1.1	0.93	32
3		0.009	0.002	0.022	0.15	0.10
6		0.0003	0.0006	0.0002		
7		0.0013		0.0018		
12		2.1	4.5	2.3	0.47	0.85
13		7.4	7.6	4.0	1.1	1.6
14		15	0.86	8.1	3.4	5.6
14.5					0.24	
15		83			5.7	8.1
16	3.07	100			0.53	2.0
17	27.01	1.3				0.07
18	100					
19	0.19					2.7
19.5						1.3
20						2.3
20.5						0.68
24			7.1	3.2	0.52	0.35
25			23.	12	3.5	2.1
26			100.	61	24.	17
27			2.5	59	33	46
28				100	100	18
29				2.8	21	11
30					24	0.29
31					0.54	
36						1.4
37						11
38						15
39						69
40						30
41						100
42						90
43						18

^a Sector data. Reprinted with permission from E. I. du Pont de Nemours & Co., Wilmington, DE 19898.

^b Quadrupole data, same conditions as given in Appendix E1, footnote *a*. Reprinted with permission from Uthe Technology Inc., 325 N. Mathilda Avenue, Sunnyvale CA 94086.

Appendix E.4 Cracking Patterns of Common Solvents

AMU	Methyl Alcohol ^a	Ethyl Alcohol ^a	Acetone ^a	Isopropyl Alcohol ^a	Trichloroethylene ^a	Gentron-142B ^b
2						3.4
12						2.9
13						3.2
14						9.2
15						16.0
18	1.9	5.5				
19		2.3		6.6		3.3
20						1.7
25						6.5
26		8.3	5.8			17.0
27		23.9	8.0	15.7		4.4
28	6.4	6.9				
29	67.4	23.4	4.3	10.1		
30	0.8	6.0				
31	100	100		5.6		17.0
32	66.7					1.0
35					39.9	5.2
36						1.8
37			2.1		12.8	1.6
38			2.3			0.9
39			3.8	5.7		
41			2.1	6.6		
42		2.9	7.0	4.0		
43		7.6	100	16.6		0.5
45		34.4		100		53.0
46		16.5				3.5
47					25.8	1.1
48						0.5
49						1.4
50						2.9
51						1.9
58			27.1			
59				3.4		
60					64.9	0.6
62					20.9	0.5
63						3.4
64						8.6
65						100.0
66						2.5
87						1.8
95					100.0	
97					63.9	
130					89.8	
132					84.8	
134					26.8	

^a Sector data. Reprinted with permission from VG-Micromass Ltd., 3 Tudor Road, Altringham, Cheshire, TN34-1YQ, England.

^b Quadrupole data, same conditions as given in Appendix E1, footnote *a*. Reprinted with permission from Uthe Technology Inc., 325 N. Mathilda Avenue, Sunnyvale, CA 94086.

Appendix E.5 Cracking Patterns of Semiconductor Dopants^a

AMU	Arsine AsH ₃	Silane SiH ₄	Phosphine PH ₃	Disilane Si ₂ H ₆	Diphosphine P ₂ H ₄	Diborane B ₂ H ₆
1						21.1
2						134.7
3						0.35
10						9.72
11						39.4
12						26.4
13						34.9
14.		0.4				2.23
14.5		0.5				
15		0.4				
15.5		0.1	0.23			
16			0.62			
16.5			0.13			
17			0.48			
20						0.22
21						1.85
22						11.8
23						48.5
24						94.0
25						57.7
26						100.0
27						95.2
28		2				16.7
29		32				
30		100.0				
31		80.	26.7			
32		7.3	100.0			
33		1.5	25.4			
34		0.2	76.7			
56				33		
57				48		
58				82		
59				37		
60				100.0		
61				40		
62				42	100.0	
63				5.7	58.8	
64				4.0	70.6	
65					26.5	
66					1.5	
75	38.5					
76	100.0					
77	28.8					
78	92.3					

^a Quadrupole data, same conditions as given in Appendix E1, footnote *a*. Reprinted with permission from Uthe Technology Inc., 325 N. Mathilda Avenue, Sunnyvale, CA 94086.

APPENDIX F

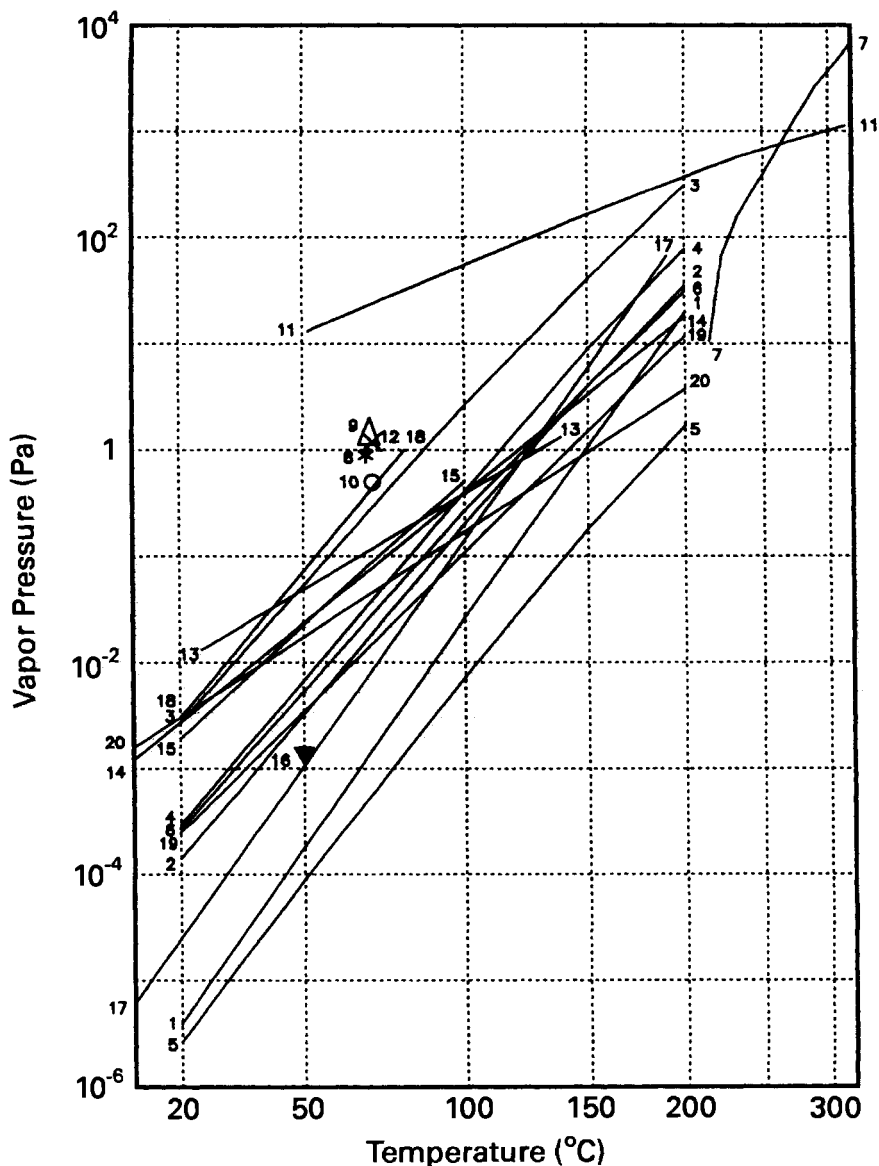
Pump Fluid Properties

Appendix F.1 Compatibility of Elastomers and Pump Fluids

Elastomer	Mineral Oil	Ester	Halo- carbon	Fluoro- carbon	Poly- siloxane
Butyl	No	<100°C	No data	<90°C	No
Buna-N	<100°C	No	<100°C	<90°C	No
Buna-S	No	No	No	No	No
Neoprene	<120°C	No	<120°C	<90°C	No
EPR	Yes	<70°C ^a	Yes	<70°C ^a	No
Silicone	Yes	<175°C	No	<150°C	No
Viton	Yes	<145°C	Yes	<200°C	Yes
Teflon	Yes	<175°C	Yes	<200°C	Yes
Kalrez	Yes	<175°C	Yes	Yes	Yes

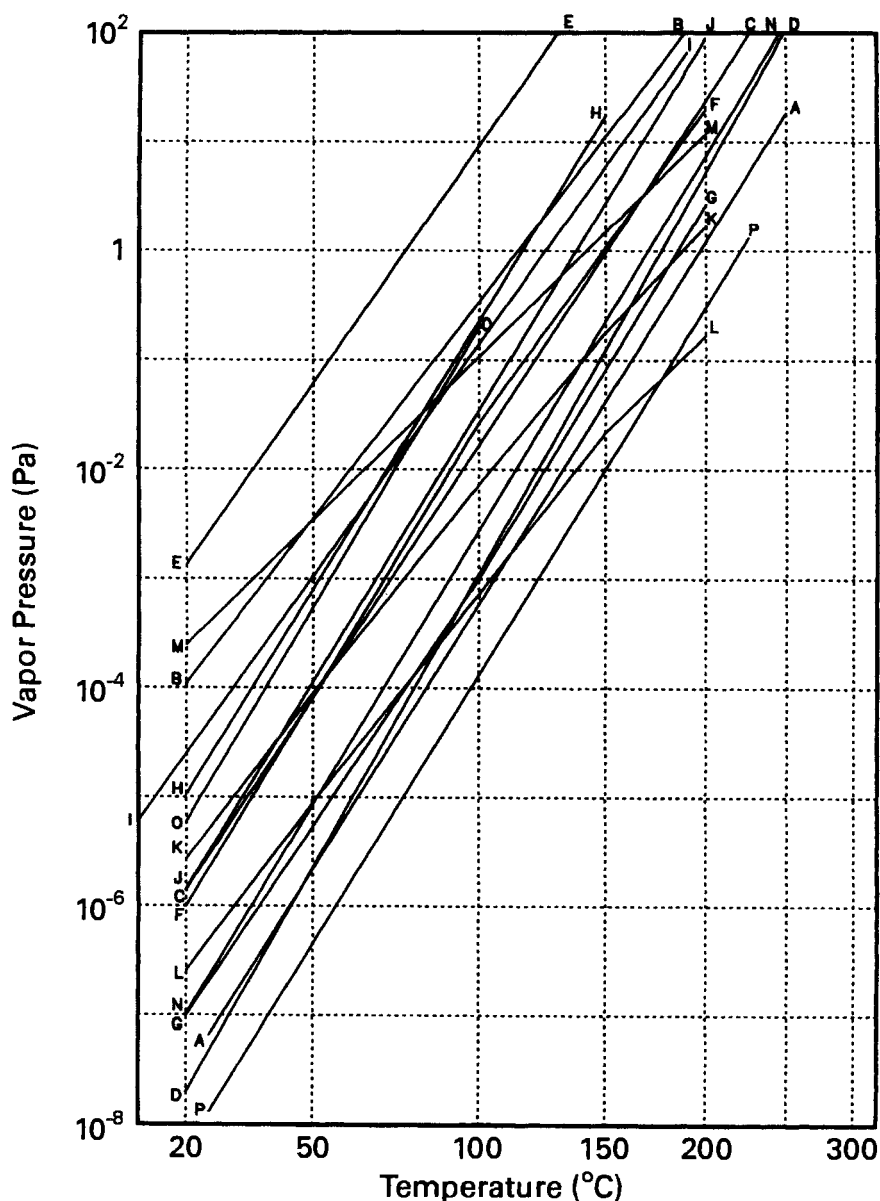
^a No data available for $T > 70^{\circ}\text{C}$.

Appendix F.2 Vapor Pressures of Mechanical Pump Fluids

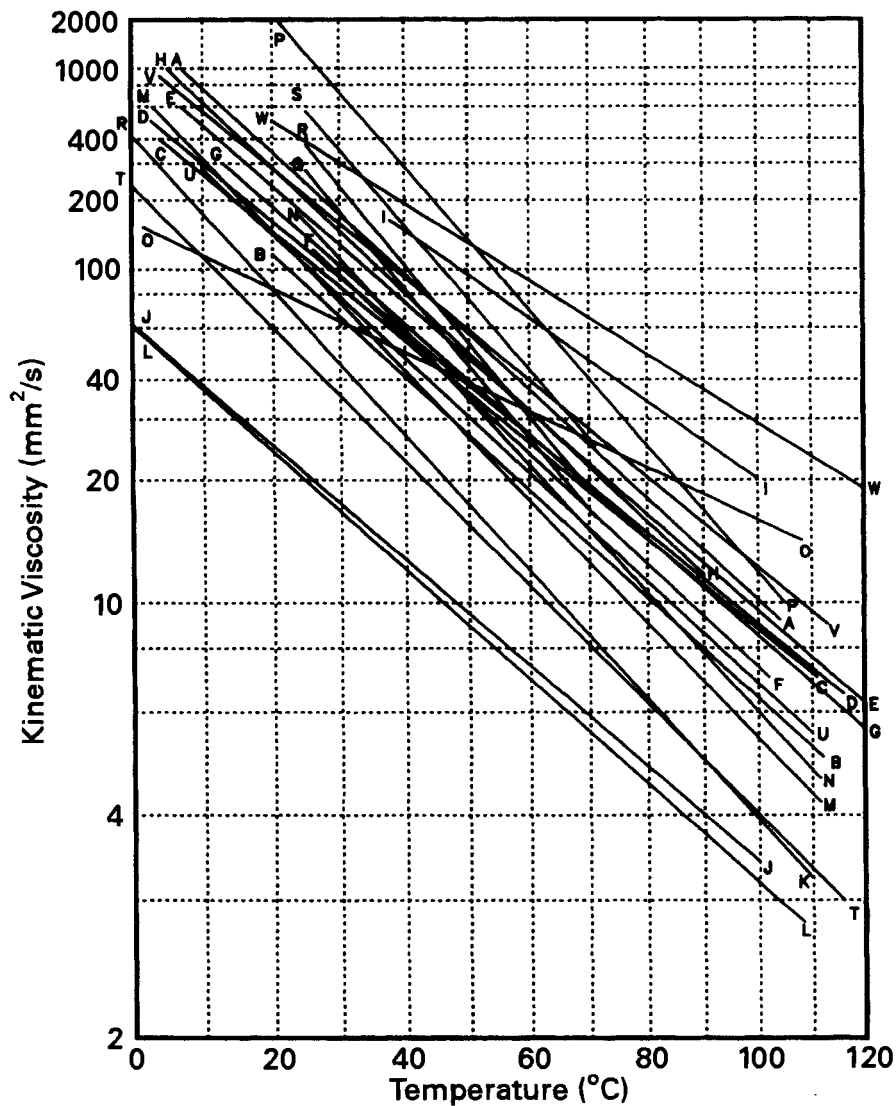


(1) Fomblin Y-H vac 18/8 [1], (2) Fomblin Y-L vac 25/5 [1], (3) Krytox 1525 [2]; (4) Fomblin Y-L vac 06/6 [1]; (5) Krytox 1618 [2]; (6) Krytox 1506, 1514 [2]; (7) Fyrquel-220 [3]; (8) Halovac-100 [4]; (9) Halovac-125 [4]; (10) Halovac-190 [4]; (11) Versilube F-50 [5]; (12) Synlube [6]; (13) Inland-77 [7]; (14) Inland-19 [7]; (15) Balzers P-3 [8]; (16) Welch Duo-Seal 1407 [9]; (17) Convoil-20 [10]; (18) Balzers T-11 [8]; (19) Invoil-20 [7]; (20) Dow Corning FS-1265 [11].

Appendix F.3 Vapor Pressures of Diffusion Pump Fluids



Appendix F.4 Kinematic Viscosity of Pump Fluids



(A) Balzers P-3 [4], Kinney KV-100 [15]; (B) Convoil-20 [10]; (C) Inland-19 [7]; (D) Invoil-20 [7]; (E) Kinney OCR [15], Krytox 1525 and 1625 [2]; (F) Kinney Super X [15]; (G) Welch Duo-Seal 1407 [12], Krytox 1618 [2], Fomblin Y-H vac 18/8 [1]; (H) Inland-77 [7]; (I) Synlube [6]; (J) Balzers T-11 [8]; (K) Octoil [10], Invoil [7]; (L) Octoil-S [10]; (M) Fyrquel-220 [3]; (N) Kinlube 300 [15]; (O) Versilube F-50 [5]; (P) Santovac-5 [12]; (Q) Halovac 100 [4]; (R) Halovac 125 [4]; (S) Halovac 190 [4]; (T) Fomblin Y-L vac 06/6 [1], Krytox 1506 [2]; (U) Fomblin Y-L vac 14/6 [1], Krytox 1514 [2]; (V) Fomblin Y-L vac 25/5, Y-H vac 25/9 [1]; (W) Dow Corning FS-1265 [11]. The fluids grouped under a common heading are not the same, but happen to have similar viscosities.

Appendix F.5 Kinematic Viscosity Conversion Factors

Kinematic Viscosity (mm ² /s)	Saybolt Universal Seconds (SUS)			Redwood Seconds at			Engler Degrees at all Temperatures
	100°F (37.8°C)	130°F (54.4°C)	210°F (98.8°C)	70°F (21.1°C)	140°F (60°C)	210°F (93.3°C)	
5.0	42.3	42.4	42.6	37.9	38.5	38.9	1.40
6.0	45.5	45.6	45.8	40.5	41.0	41.5	1.48
7.0	48.7	48.8	49.0	43.2	43.7	44.2	1.56
8.0	52.0	52.1	52.4	46.0	46.4	46.9	1.65
9.0	55.4	55.5	55.8	48.9	49.1	49.7	1.75
10.0	58.8	58.9	59.2	51.7	52.0	52.6	1.84
12.0	65.9	66.0	66.4	57.9	58.1	58.8	2.02
14.0	73.4	73.5	73.9	64.4	64.6	65.3	2.22
16.0	81.1	81.3	81.7	71.0	71.4	72.2	2.43
18.0	89.2	89.4	89.8	77.9	78.5	79.4	2.64
20.0	97.5	97.7	98.2	85.0	85.8	86.9	2.87
22.0	106.0	106.2	106.7	92.4	93.3	94.5	3.10
24.0	114.6	114.8	115.4	99.9	100.9	102.2	3.34
26.0	123.3	123.5	124.2	107.5	108.6	110.0	3.58
28.0	132.1	132.4	133.0	115.3	116.5	118.0	3.82
30.0	140.9	141.2	141.9	123.1	124.4	126.0	4.07
32.0	149.7	150.0	150.8	131.0	132.3	134.1	4.32
34.0	158.7	159.0	159.8	138.9	140.2	142.2	4.57
36.0	167.7	168.0	168.9	146.9	148.2	150.3	4.83
38.0	176.7	177.0	177.9	155.0	156.2	158.3	5.08
40.0	185.7	186.0	187.0	163.0	164.3	166.7	5.34
42.0	194.7	195.1	196.1	171.0	172.3	175.0	5.59
44.0	203.8	204.2	205.2	179.1	180.4	183.3	5.85
46.0	213.0	213.4	214.5	187.1	188.5	191.7	6.11
48.0	222.2	222.6	223.8	195.2	196.6	200.0	6.37
50.0	231.4	231.8	233.0	203.3	204.7	208.3	6.63
60.0	277.4	277.9	279.3	243.5	245.3	250.0	7.90
70.0	323.4	324.0	325.7	283.9	286.0	291.7	9.21
80.0	369.6	370.3	372.2	323.9	326.6	333.4	10.53
90.0	415.8	416.6	418.7	364.4	367.4	375.0	11.84
100.0a	462.0	462.9	465.2	404.9	408.2	416.7	13.16

^a At higher values use the same ratio as above for 100 mm²/s.

REFERENCES

1. Montedison, USA, Inc., 1114 Ave. of the Americas, New York, NY 10036.
2. Du Pont and Co., Chemicals and Pigments Department, Wilmington, DE 19898.
3. Stauffer Chemical Company, Specialty Chemical Division, Westport, CN 06880.
4. Fluoro-Chem Corporation, 82 Burlews Court, Hackensack, NJ 07601.
5. General Electric Company, Silicone Products Department, Waterford, NY 12188.
6. Synthatron Corp., 50 Intervale Rd., Parsippany, NJ 07054.
7. Inland Vacuum Industries, Inc., 35 Howard Ave., Churchville, NY 14428.
8. Balzers High Vacuum, Furstentum, Liechtenstein.
9. Sargent-Welch Scientific Co., Vacuum Products Division, 7300 N. Linder Ave. Skokie, IL 60077.
10. Veeco, Inc., 525 Lee Rd. Rochester, NY 14603.
11. Dow Corning Company, Inc., 2030 Dow Center, Midland, MI 48640.
12. Monsanto Company, 800 N. Lindbergh Blvd. St. Louis, MO 63166.
13. Varian Associates, Lexington Vacuum Division, 121 Hartwell Ave., Lexington, MA.
14. Edwards High Vacuum, Ltd. Manor Royal, Crawley, West Sussex, England.
15. Kinney Vacuum Co., 3529 Washington St., Boston, MA 02130.

Index

A

Absolute pressure, 14
Accommodation coefficient, 21
Acetone
 cracking pattern, 383
 sensitivity, ion gauge, 97
Activation energy, desorption, 64
Adsorption
 capacity, 265
 isotherms, 264, 266, 278
 pumps, 276
Air
 composition, table, 6
 physical properties, 467
 pressure versus altitude, 7
Air bake, 296
 ultraclean chambers, 411
Alumina, properties, 303, 305
Aluminum
 alloys, properties, 299
 outgassing rate, 298, 478, 479
Amonton's Law, 16
Argon
 atmospheric content, 6
 cracking pattern, 162, 494
 cryogenic properties, 468
 cryogenic pumping, 264
 instability, ion pumping, 258
 isotopic abundance, 488
 physical properties, 467
 sensitivity, ion gauge, 97
 sensitivity, TC gauge, 90
 sorption pumping, 266
Atmospheric gases
 composition, table, 6
 mean free path, 466
Atomic mass unit, definition, 133
Average molecular velocity, 10
 gases, table, 467

Avogadro's law, 16
Avogadro's number, 463

B

Backing pump, 218
Backstreaming
 cryogenic pump, 270, 396
 diffusion pump, 224, 383
 ion pump, 247, 257
 mechanical pump, 366
 through traps, 224, 368
 titanium sublimation, 247, 249
 turbo pump, 371
Baffle
 chevron, trans. prob., 42
 circular plate, trans. prob., 40
 cooling, 224
 definition, 224
Baking
 ceramics, 303
 definition, 194
 glass, 302
 incomplete, 69
 metal, 67, 295
 low temperature, 412
 outgassing rate, 295, 297, 478
 residual gas analysis, 151
 ultraclean procedures,
Bayard-Alpert ion gauge, 96
 accuracy, 100, 105
 nude gauge, 95
 operation, 95
 outgassing, 98, 100
 sensitivity, 97
Bellows,
 seals, 335
 types of, 340
 valves, 331
 welding, 314

Boltzmann's constant, 463

Bourdon gauge, 82

Boyle's law, 15

Brass

outgassing rate, 479

vapor pressure, 290

Brazing, 318

Buna-N

cracking pattern, 170

fluid compatibility, 498

properties, 306, 323

C

Calibration

flow meter, 120

pressure gauge, 104

RGA, 156, 172

Thermocouple gauge, 91

Capacitance manometers, 83

contamination, 85

errors, 86

one-sided transducer, 85

pressure range, 86

two-sided transducer, 84

Carbon dioxide

atmospheric content, 6

cracking pattern, 494

cryogenic pumping, 384

physical properties, 467

sensitivity, ion gauge, 97

sensitivity, RGA, 172

sensitivity, TC gauge, 90

trap desorption, 384

Carbon monoxide

cracking pattern, 163, 494

formation at filament, 101

ion pumping, 249

physical properties, 467

sensitivity, ion gauge, 97

sensitivity, RGA, 172

Ceramics

ceramic-to-metal seals, 319

outgassing rates, 480

permeation rates, 304, 305

properties, 303

Channel electron multiplier, 148

Charles' law, 16

Chemisorption

activation energy, 64

in getter pumps, 254

in sublimation pumps, 248

replacement, 249

Chevron baffle, trans. prob., 42

Choke, 29, 102

Clausing's factor, 35

Claw pump, 193

Cleaning

detergent cleaning, 296

diffusion pumps, 243

Diversey, 296

Electropolishing, 296

glow discharge, 296

vacuum baking, 295

vacuum firing, 293

vapor degreasing, 296

Cold cathode ion gauge

See Ion gauge, cold cathode

Cold trap

high vacuum, 224, 384

mechanical pump, 368

Compressor, helium, 271

Condensable vapor, in:

cold trap, (P) 108, 224, 383

cryogenic pump, 264

rotary vane pump, 186

Condensation coefficient, 251

Conductance, 27

calculations, 33, 39

combinations, 32, 39

complex geometry, 45

conversion factors, 464

definition, 27

molecular flow, 32

orifice, 33

transition flow, 49

viscous flow, 28

Conductivity, heat, 20

Contamination

aluminum foil, 408

cold traps, 224, 368

cryogenic pump, 396, 406

diffusion pump, 224, 384

friction, metal, 341

- ion gauge, gas release, 98
 - ion pump, 258, 393, 407
 - mechanical pump fluid, 239, 368
 - metal, bending, 341
 - non-evaporable getter, 407
 - plastic bags, 408
 - titanium sublimation, flaking, 407
 - turbopump, 247, 249, 405
 - Viton O-ring, squeezing, (P) 344
 - Continuum Flow, 28
 - Conversion factors, 464
 - Copper
 - gasket seal, 328
 - outgassing rate, 478, 479
 - weld distortion, flange, 329
 - Cracking pattern
 - definition, 161
 - gases, 494
 - pump fluids, 492
 - semiconductor dopants, 497
 - solvents, 496
 - stability, 151
 - vapors, 495
 - Cryocondensation, 264
 - Cryogenic pump, 263
 - ion gauge, in, 397
 - limiting capacity, 270
 - liquid pumps, 283
 - maximum speed, 267
 - performance, 283
 - pumping surfaces, 281
 - refrigerator pumps, 271
 - regeneration, 394
 - safety valve, 283
 - sorption, 265
 - throughput, 269
 - trapping, 265, 276
 - ultimate pressure, 270
 - Cryogenic pump applications
 - contamination, 396
 - crossover, 373, 424
 - hazardous gas, 428
 - high gas flow, 424
 - high vacuum, 394
 - operating concerns, 396
 - operating procedures, 394
 - regeneration procedures, 394
 - ultraclean, 406
 - Cryosorption, 265
 - Cryotrapping, 265
- ## D
- Dalton's law, 16
 - Desorption
 - electron impact, 70
 - in cryogenic pumps, 396
 - ion impact, 70
 - thermal, 61
 - Diaphragm gauge, 82
 - Diaphragm pump, 196
 - Diffusion, 21, 58
 - desorption energy, 64
 - during outgassing, 67
 - in gases, 21
 - in solids, 58
 - Diffusion pump, 217
 - backstreaming, 224, 383
 - cleaning, 243
 - critical forepressure, 218
 - critical inlet pressure, 220
 - fluids for, 241
 - maximum speed, 220
 - maximum throughput, 223, 369
 - overload, 369
 - pressure range, 182, 222
 - pumping mechanism, 217
 - traps, 224, 384
 - Diffusion pump applications
 - crossover, 369
 - high vacuum, 379
 - multichamber systems 431
 - operating concerns, 381
 - operating procedures, 382
 - overload criteria, 369
 - Direct gauge, 81
 - Discharge cleaning,
 - Displacement, pump, 181
 - Displacer, 272
 - Dry lubrication, 353
 - dissimilar materials, 354
 - molybdenum disulfide, 354
 - soft metal, 354
 - Dynode, 147, 148

E

Elastomer

- compression, 324, 325
- fluid compatibility, 498
- gaskets, 326
- mechanical properties, 323
- outgassing rates, 308, 485
- permeability, 307, 325, 456, 481
- rotary seals, 337
- static seals, 322

Electron multipliers, 147

- channel, 148
- discrete dynode, 147

Electron-stimulated-desorption

- from surfaces, 70
- in ion gauges, 98, 100

Emissivity

- in cryogenic pumps, 280
- in TC gauges, 87

Enthalpy, gases, low temperature, 427

Errors, pressure measurement

- Bayard-Alpert gauges, 100
- capacitance manometers, 86
- residual gas analyzers, 172
- thermocouple gauges, 88
- UHV gauges, 100

Extractor gauge, 99, 412

F

Faraday cup, 148

Ferrofluidic seal, 339

Filaments

- ion gauge, 98
- RGA, 152

Flaking, in

- sputter-ion pump, 260
- titanium sublimation, 391

Flow meters, 109

- choke, 112
- differential pressure, 114
- mass flow, in, 109
- rotameter, 112
- thermal mass flow, 115

Fluids, pump

- cleaning, 243

color, 233

corrosive applications, 238

cracking pattern, 492

diffusion pump, properties, 241

distillation, 234

elastomer compatibility, 498

esters, 236

ethers, 237

flash point, 233

fluorochemicals, 237

hydrocarbon, 168, 234

mechanical pump, properties, 238, 499, 501

mineral oil, 234

perfluoropolyether, 238

polyphenylether, 237

properties, 498

reclamation, 244

safety, 237, 243

selection, 238

silicone, 169, 236

solubility, 186, 233

trapping, 224, 368

turbo pump, properties, 238, 499, 501

vapor pressure, definition, 229

vapor pressure, diffusion, 500

vapor pressure, mech. & turbo 499

viscosity, 233, 501

Fluorine

dissociation on surface, 164

isotopic abundance, 488

pump fluid reaction, 238

Flux, molecular, 13

Foreline trap, 368

Free-molecular heat flow, 21

Free-molecular viscosity, 21

G

Gas ballast, 186

Gases

appearance in discharges, 477

atmospheric content, 6

conductance formulas, 33, 39, 469

cryogenic properties, 468

mean free path, 466

- physical properties, 467
- transport laws, 15
- vapor pressure tables, 475
- Gas flow, 25
 - choked flow, 29, 112
 - flow meters, 109
 - measuring devices, 110
 - molecular flow, 32
 - transition flow, 49
 - turbulent flow, 28
 - viscous flow, 28
- Gas replacement, 250
- Gaskets
 - copper, 328
 - elastomer, 322
- Gauge, partial pressure
 - See Residual gas analyzers
- Gauges, total pressure, 81
 - accuracy, 100, 105
 - Bayard-Alpert, 96
 - bourdon, 82
 - calibration, 104
 - capacitance manometer, 83
 - classification, 81
 - cold cathode, 103
 - diaphragm, 82
 - indirect gauges, 87
 - inverted magnetron, 103
 - ionization, 94
 - magnetron, 103
 - modulation, 100
 - Pirani, 88
 - pressure ranges, 83
 - thermocouple, 91
- Getter pumps, 247
 - hydrogen capacity, 251
 - nonevaporable, 254
 - speed, 251
 - titanium sublimation, 248
- Glass
 - helium diffusion, 73
 - outgassing rates, 303, 480
 - gas permeation, 304
 - properties, 302
 - sealing, 319
 - viscosity, 301
- Graham's Law, 17

H

- Halogen leak detection, 288
- Heat
 - conductivity, 20
 - conversion factors, 465
 - exchangers, 273
 - radiant, 87, 280
- Helium
 - adsorption isotherm, 266, 278
 - atmospheric content, 6
 - capacity, cryogenic pump, 267
 - cracking pattern, 494
 - cryogenic properties, 468
 - dissolved in oil, 186
 - isotopic abundance, 488
 - leak detector, 283
 - permeation, ceramic, 305
 - permeation, glass, 73, 304
 - permeation, polymers, 307, 325, 456, 481
 - physical properties, 467
 - sensitivity, ion gauge, 97
 - sorption pumping, 277
- Herrick effect, 225
- Ho coefficient, 128, 219
- Hot cathode ionization gauge
 - See Ion gauge, hot cathode
- Hydrocarbon
 - diffusion pump fluid, 168, 234
 - grease, 352
 - mechanical pump fluid, 238, 499, 501
 - trapping, 224, 368
- Hydrogen
 - atmospheric content, 6
 - capacity, cryogenic pump, 267
 - capacity, getter pump, 248, 254
 - capacity, sputter-ion pump, 257
 - cracking pattern, 494
 - isotopic abundance, 488
 - permeation in metals, 73, 291
 - sensitivity, ion gauge, 97

I

- Ice, heat absorption, 281

Indirect gauges, 87

Instability, ion pumps, 258

Ion

collisions at surfaces, 164

mass-to-charge ratio, 133

sources, 134

stimulated desorption, 70

Ion gauge, cold cathode, 103

calibration, 105

magnet configurations, 104

pumping speed, 104

range, 104

Ion gauge, hot cathode, 94

accuracy, 100, 105

Bayard-Alpert, 96

calibration, 105

CO generation, 101

cold trap, (P) 108

controller load (P) 108

degassing, 98

electron-stimulated-desorp. 100

extractor gauge, 99

operation, 95

outgassing, 98

sensitivity, 97

x-ray limit, 100

Ion pump applications

high vacuum systems, 391

operating concerns, 393

ultraclean systems, 406

Ion pumps, 253

diode, 259

lifetime, 260

memory effect, 258

noble gas pumping, 258

triode pump, 259

Ionization, electron impact, 94, 134

Iridium, thoriated, filament, 98, 152

Isotherms, adsorption

argon, 264

helium, 278

hydrogen, 266, 267, 278

krypton, 264

molecular sieve, 278

neon, 278

nitrogen, 278

xenon, 264

J

Jets, diffusion pump, 219

Joints

demountable, 321

permanent, 313

K

Kinematic viscosity, 18

conversion factors, 502

pump fluid, 501

Kinetic theory, 9

Knudsen diffusion, 22

Knudsen's number, 26

L

Latent heats

cryogenic gases, 468

gas cooling, 425

Leak detection, 447

accumulation technique, 285

alcohol, 455

bypass sniffer, 454

counter flow, 449

elastomer gaskets, 455

foreline sampling, 452

forward flow, 448

helium mass spectrometer, 447

pressurized chambers, 453

residual gas analyzer, 457

response time, 450

sensitivity, 450

techniques, 453

time constant, 450

Liquid nitrogen

cooled titanium sublimation, 248

cooled trap, 224, 384

cryogenic pump, 276, 283

properties, 468

Lubrication in vacuum, 345

absolute viscosity, 347

dry, 353

grease, 352

index, 348

kinematic viscosity, 348

- liquid, 349
- processes, 345
- rheology, 347
- solid, 353
- techniques, 349

M

Magnetic sector RGA, 139

Mass flow meter

- See Thermal mass flow meter

Mass spectra

- air, 167
- argon, 162,
- benzene, 169
- Buna-N, 170
- carbon monoxide, 165
- diffusion pumped systems, 141,
42, 146, (P) 180,
- gases, 494
- gauge outgassing, 98
- methane, 162
- mineral oil, 168
- pump fluids, 492
- semiconductor doping gases, 497
- silicone, 169, (P) 344,
- solvents, 496
- vapors, 495
- Viton, 171, (P) 344

Materials, 287, 289

- ceramics, 300
- dissolved gas, 292
- elastomers, 306
- gas efflux, 291, 295, 308, (P) 312
- gas permeation, 304–07
- glass, 300
- metals, 290, 299
- polymers, 306
- vapor pressure tables, 371
- vaporization, 290

Mass flow, 109

Mean free path

- definition, 12
- for various gases, 466

Mechanical pumps

- claw, 193
- diaphragm, 196

- fluids for, 238
- gas ballast, 186
- lobe, 189
- rotary piston, 187
- rotary vane, 183
- screw, 195
- scroll, 194
- traps, 368
- turbodrag, 248
- turbomolecular, 201

Mercury

- brazing alloys, 319
- diffusion pump, 195
- isotopic abundance, 491
- mean free path, 466
- purple plague, 319
- sensitivity, ion gauge, 97
- vapor pressure, 482

Metals

- aluminum, 299
- copper, 294
- metal-to-glass seals, 320
- outgassing rate, 291, 295
- outgassing tables, 498
- stainless steel, 295, 300
- structural properties, 299
- welding, 314

Methane

- atmospheric content, 6
- cracking pattern, 162, 495
- physical properties, 467
- pump fluid degradation, 225, 239
- pumping, titanium sublimation, 253

Molar flow, 109

Molecular flow, 32

- complex structures, 39
- conductance, 32

Molecular sieve

- adsorption isotherms, 278
- sorption capacity, 278

Molecular velocity, 10

Molecular weight, table, 467

Multipliers, electron

- discrete dynode, 147
- channel, 148

Monte Carlo analysis, 38, (P) 55, 410

Motion feedthroughs, 337

N

Neon

- atmospheric content, 6
- cracking pattern, 494
- cryogenic properties, 468
- isotopic abundances, 488
- physical properties, 467
- sensitivity, ion gauge, 97
- sorption pumping, 278

Nickel

- hydrogen permeation, 291
- in stainless steel, 299

Nitrogen

- atmospheric content, 6
- cracking pattern, 494
- cryogenic properties, 468
- ion gauge sensitivity, 97
- isotopic abundance, 488
- physical properties, 467

Non-evaporable getter, 254

Nude ion gauge, 95

O

Oils, pump

- See Fluids, pump

O-rings

- copper, 328
- elastomer, 322

Outgassing

- electron-assisted, 70
- ion gauge, 98, 100
- sputter-ion pumps, 257, 393
- vacuum chambers, 65, 295, 407

Outgassing rate, tables

- ceramics and glasses, 305, 480
- conversion factors, 355
- elastomers, 480
- metals, baked, 478
- metals, unbaked, 66, 479
- polymers, 308, 485

Oxygen

- atmospheric content, 6
- cracking pattern, 494
- cryogenic properties, 468
- isotopic abundance, 488

- physical properties, 467
- sensitivity, ion gauge, 97
- surface dissociation, 164

P

Partial pressure analyzers

- See Residual gas analyzers

Penning gauge, 103

Permeation, 71

- ceramics, 305
- definition, 71
- dissociative, 73
- glasses, 304, 305
- metals, 291, 412
- molecular, 71
- polymers, 307, 481
- units, 73

Physical constants, 463

Physical properties of gases, 467

Physisorption, 63

Pirani gauge, 88

Poiseuille equation, 30

Polymers, 306

- composition, 306
- compression set, 324
- mechanical properties of, 323, 324
- outgassing rates, 308, 485
- permeability, 307, 481

Pressure

- absolute, 14
- conversion factor, 464
- definition, 14
- gauges, See Gauges
- ranges, 4
- units, 14
- vapor, tables, 475, 482, 499, 500

Pump fluids

- See Fluids, pump

Pump, operating procedures

- cryogenic, 394
- diffusion, 379
- sputter-ion, 381
- turbomolecular, 385

Pump, vacuum

- claw, 193
- cryogenic, 263

- diaphragm, 196
 - diffusion, 217
 - fluids, 229
 - getter, 247, 254
 - lobe, 189
 - operating ranges, 182
 - operation, 198
 - rotary piston, 187
 - rotary vane, 183
 - screw, 195
 - scroll, 194
 - sorption, 279
 - sputter-ion, 255
 - staging ratio, (P) 200
 - titanium sublimation, 248
 - turbodrag, 213
 - turbomolecular, 201
 - Pumping speed
 - chamber speed, 127, (P) 131, 132
 - conversion factors, 354
 - definition, 123
 - measurements, 123
 - measurement error, 128
 - time constant, 360
 - water vapor, 126
 - Pumping systems, 357
 - high gas flow, 415
 - high vacuum, 379
 - multichamber, 431
 - overload criteria, 369
 - roughing, 359
 - ultraclean, 403
- Q**
- Quadrupole mass filter, 142
- R**
- Reclamation, pump fluid, 244
 - Reemission, in
 - gauges, 100
 - ion pumps, 258
 - Refrigeration cycle, 271
 - Gifford-McMahon, 273
 - Longworth, 273
 - Solvay, 275
 - Refrigerator, helium gas, 271
 - Regenerator, 272
 - Residual gas analysis, 133, 161
 - at high pressures, 165
 - auxiliary pumps for, 153
 - background noise, 156
 - cracking pattern, definition, 161
 - cracking pattern, tables, 492
 - equipment, 158
 - in high vacuum, 153, 166
 - in leak detectors, 457
 - interpretation of data, 161
 - ion fragments, 164
 - ion molecules reactions, 165
 - isotopic abundance, 488
 - oil contamination, 242
 - qualitative, 166
 - quantitative, 172
 - surface ion release, 164
 - Residual gas analyzers, 133
 - calibration, 156
 - detection, 145
 - differentially-pumped, 154
 - filaments, 154
 - ionizer, closed, 136
 - ionizer, open, 135
 - magnetic sector, 139
 - mass filter, 139
 - mass separation, 139
 - miniature quadrupole, 156
 - mounting, 150
 - quadrupole, 142
 - pressure range, 150
 - resolving power, 145
 - stability, 151
 - Reynolds' number, 26
 - Rhenium, filaments, 152
 - Roots (lobe) pump, 189
 - compression ratio, 190
 - maximum pressure, 191
 - mechanism, 189
 - oil backstreaming, 191
 - pumping speed, 190
 - Rotameter, 112
 - Rotary piston pump, 187
 - mechanism, 187
 - ultimate pressure, 188

Rotary vane pump, 183
 corrosive gas pumping, 238
 dissolved gas, 186, 233
 fluids, 238
 gas ballast, 186
 maintenance, 384
 mechanism, 183
 pumping speed, 182, 185
 Roughing trap, 368

S

Screw pump, 195
 Scroll pump, 194
 Seals
 ceramic-to-metal, 319
 elastomer, 322
 glass-to-metal, 319
 metal gasket, 328
 motion feedthrough, 329
 Secondary emission
 in electron multiplier, 147
 Sensitivity
 capacitance manometer, 86,
 (P) 107
 ion gauge, 97
 residual gas analyzer, 146
 Silicone
 cracking patterns, 492
 elastomer outgassing, 308, 485
 pump fluids, 169, 236
 viscosity, pump fluid, 501
 Soft roughing, 362
 Solubility, gas
 in getter pumps, 254
 in metals, 292
 in pump fluids, 186, 233
 Sorption
 definition, 265
 pump, 276
 staged pumping, 279
 Specific heat, 20
 conversion factors, 465
 Spectra, mass
 See Mass spectra
 Speed, pumping
 See Pumping speed

Spinning rotor gauge, 93
 operation, 93
 stability, 94
 Sputter ion pump
 See Ion pumps
 Stainless steel
 bending outgassing, 339
 carbide precipitation, 315
 forging, 317
 for vacuum construction, 299, 314
 outgassing rates, 295
 selection guide, 486
 vacuum baking, 60, 293
 Stefan-Boltzmann constant, 463
 Sticking coefficient, gas on
 stainless steel, 68
 titanium films, 251
 Sublimation pump, titanium, 248
 mechanism, 248
 rate of sublimation, 250
 use in vacuum system, 391
 Symbols, 459
 System International units, 6, 463
 Systems, vacuum
 aerosol formation, 362
 baking, 60, 295, 411
 cluster tools, 440
 crossover, 367
 cryo pumped, 373, 394, 406
 diffusion pump, 369, 394, 406
 inline, 435
 ion pumped, 374, 391, 406
 managing water vapor, 398, 410
 overload criteria, 369
 split-flow turbo, 446
 throttled high vacuum, 307
 turbo pumped, 371, 385, 405, 421
 ultraclean vacuum, 403

T

Teflon
 cold flow, 322
 cracking, major fragments, 172
 outgassing rate, 308, 485
 Test dome, pumping speed
 high vacuum, 125

- mechanical pump, 124
 - Thermal conductivity gauges, 87
 - accuracy, 92
 - Pirani, 88
 - thermocouple, 91
 - time constant, 382
 - use in systems, 381
 - Thermal desorption
 - from surfaces, 65
 - in ion gauges, 98, 100
 - Thermal mass flow meter, 115
 - calibration, 120
 - correction factor, 118
 - operation, 116
 - technique, 115
 - Thermal transpiration, 22, (P) 107
 - Thoriated iridium, filament, 98
 - Throughput
 - cryogenic pump, 269
 - definition, isothermal, 27
 - diffusion pump, 219, 369
 - flowmeter, 109
 - non-equilibrium, (P) 54, 109
 - turbo pump, 202, 371, 421
 - Time constant
 - system pumping, 360
 - thermocouple gauge, 382
 - Titanium sublimation pump
 - See Sublimation pump, titanium
 - Total pressure gauge
 - See Gauges, total pressure
 - Transition flow, 49
 - Triode
 - ion gauge, 95
 - ion pump, 259
 - Turbomolecular pumps, 201
 - design considerations, 210
 - drag pump, 213
 - fluids for, 240
 - forepump size, 371
 - general speed relation, 207
 - hydrogen pumping, 205
 - magnetically levitated, 212
 - maximum compression ratio, 203
 - maximum flow, 372
 - maximum speed, 206
 - pumping mechanisms, 201
 - speed-compression
 - relationships, 203
 - staging ratio, 371
 - throughput, 202, 371, 421
 - ultimate pressure, 209
 - venting procedures, 389
 - Tungsten, filaments, 98, 152
 - Turbomolecular pump applications
 - differentially-pumped RGA, 153
 - gas sampling, split-flow, 443
 - high vacuum system, 385
 - operating concerns, 389
 - operating procedures, 388
 - throttled operation, 421
 - ultraclean systems, 405
- U**
- Ultimate pressure
 - baking procedures, 60, 295, 411
 - gauges, 99
 - Ultraclean leak detection (P) 458
 - Ultraclean systems, 403
 - Units
 - conversion factors, 464
 - measurement, 6, 463
- V**
- Vacuum
 - bake, 60, 295, 411
 - definition, 3
 - firing, 293
 - isolation, 432, 435, 438
 - load locks, (P) 377, 437
 - pressure ranges, 4
 - Vacuum systems
 - See Systems, vacuum
 - Valves
 - elastomer seated, 330
 - gas release, (P) 344
 - gate, 332
 - metal sealed, 331
 - poppet, 334
 - special purpose, 335
 - Vapor pressure, tables
 - common gases, 475

- elements, 482
- pump fluids, 499
- water vapor, 475

Velocity

- average, 10
- distribution, 10
- molecular, 10
- peak, 10
- rms, 11

Viscosity

- absolute, 18
- conversion factors, 502
- gases, definition, 18
- gases, tables, 467
- greases, oils used in, 353
- index, 348
- kinematic, 348
- pump fluids, 501

Viscous flow, 28**W**

Water flow restrictor, 381

Water vapor

- atmospheric content, 6

- cracking pattern, 495
- physical properties, 467
- vapor pressure, 475

Welding

- carbide precipitation, 315
- inclusions, 317
- joint types, 315
- orbital welding, 314
- tungsten inert gas, 314

X**Xenon**

- atmospheric content, 6
- cryogenic properties, 468
- isotopic abundance, 490
- mean free path, 466
- physical properties, 467
- vapor pressure, 476

X-ray limit, ion gauge, 100

Z

Zeolite, 276

Zirconium alloy getter, 254